NIST Technical Note 1353

U.S. DEPARTMENT OF COMMERCE / National Institute of Standards and Technology

Trapped Ions and Laser Cooling III

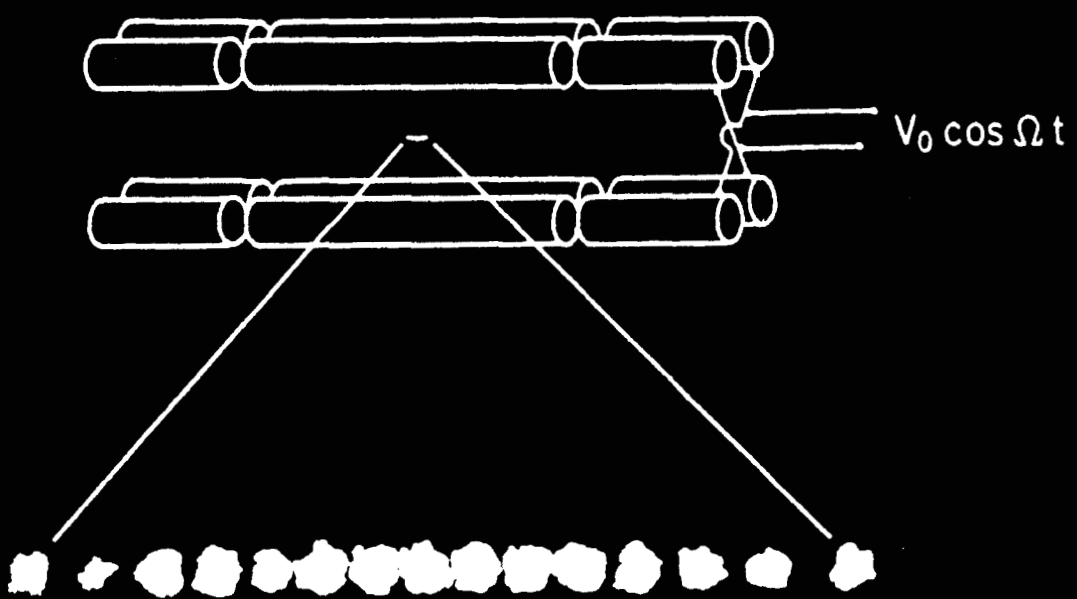

Selected publications of the
Ion Storage Group
Time and Frequency Division
NIST, Boulder, Colorado

Edited by: James C. Bergquist
John J. Bollinger
Wayne M. Itano
David J. Wineland

Trapped Ions and Laser Cooling III

Selected publications of the Ion Storage Group of the Time and Frequency Division

Edited by

James C. Bergquist
John J. Bollinger
Wayne M. Itano
David J. Wineland

Time and Frequency Division
Physics Laboratory
National Institute of Standards and Technology
Boulder, Colorado 80303-3328

Supported in part by
U.S. Office of Naval Research
800 North Quincy
Arlington, Virginia 22217

April 1992

U.S. DEPARTMENT OF COMMERCE, Barbara Hackman Franklin, Secretary
TECHNOLOGY ADMINISTRATION, Robert M. White, Under Secretary for Technology
NATIONAL INSTITUTE OF STANDARDS AND TECHNOLOGY, John W. Lyons, Director

National Institute of Standards and Technology Technical Note
Natl. Inst. Stand. Technol., Tech. Note 1353, 204 pages (April 1992)
CODEN:NTNOEF

U.S. GOVERNMENT PRINTING OFFICE
WASHINGTON: 1992

For sale by the Superintendent of Documents, U.S. Government Printing Office, Washington, DC 20402-9325

PREFACE

This collection of papers represents the work of the Ion Storage Group, Time and Frequency Division, National Institute of Standards and Technology from October 1988 to February 1992. It follows the collections of papers contained in NBS Technical Note 1086, *Trapped Ions and Laser Cooling* (June 1985) and NIST Technical Note 1324 *Trapped Ions and Laser Cooling II* (September 1988). Although the primary goal of this work has been the development of techniques necessary for achieving high resolution spectroscopy, we have also been able to investigate related areas of research.

Papers listed on page vii were published or prepared during the period October 1988 to February 1992 but are not included here. They can be obtained on request. We intend to update this publication periodically to include new work. We hope this collection of papers will be useful to our colleagues in this and related fields.

We acknowledge the important contributions of several colleagues to this collection. In particular, we thank Larry Brewer, Claude Cohen-Tannoudji, Jean Dalibard, Frank Diedrich, Frank Elsner, Sarah Gilbert, Jon Gilligan, Dan Heinzen, Dan Larson, Chuck Manney, Fred Moore, Mark Raizen, and Carl Weimer. We gratefully acknowledge the continued support of the U. S. Office of Naval Research and the support of the Air Force Office of Scientific Research through September 1991.

James C. Bergquist
John J. Bollinger
Wayne M. Itano
David J. Wineland

Boulder, Colorado
March 1992

CONTENTS

FUNDAMENTAL TESTS

NONNEUTRAL PLASMA STUDIES

GENERAL ARTICLES

ADDITIONAL PUBLICATIONS

Reports published or prepared during the period October 1988 to February 1992, but not included in this technical note.

1. "Liquid and Solid Phases of Laser Cooled Ions," S.L. Gilbert, J.C. Bergquist, J.J. Bollinger, W. M. Itano, and D.J. Wineland, in Atomic Physics 11, ed. by S. Haroche, J. C. Gay, and G. Grynberg (World Scientific Press, Singapore, 1989), p. 261.

2. "The Digitized Atom and Optical Pumping," D.J. Wineland, W.M. Itano, J.C. Bergquist and R.G. Hulet, in Atomic Physics 11, ed. by S. Haroche, J.C. Gay, G. Grynberg (World Scientific Press, Singapore, 1989), p. 741.

3. "Progress at NIST Towards Absolute Frequency Standards Using Stored Ions," D. J. Wineland, J. C. Bergquist, J. J. Bollinger, W. M. Itano, D. J. Heinzen, S. L. Gilbert, C. H. Manney, and C. S. Weimer, Proc. 43rd Annual Symposium on Frequency Control, Denver, June 1989, IEEE Catalog no. 89CH2690-6.

4. "Observation of Shell Structures with Ions Stored in Traps," J. J. Bollinger, S. L. Gilbert, and D. J. Wineland, Proc. Workshop on Crystalline Ion Beams, Wertheim, W. Germany, Ed. by R. W. Hasse, I. Hofmann, D. Liese (GSI report GSI-89-10, ISSN 0170-4546), p. 231.

5. "Trapped Atoms and Laser Cooling," D. J. Wineland, "essay" for undergraduate text Physics, by Paul Tipler (Worth, New York, 1991).

6. "Progress at NIST on Absolute Frequency Standards Using Stored Ions," D. J. Wineland, J. C. Bergquist, J. J. Bollinger, W. M. Itano, D. J. Heinzen, S. L. Gilbert, C. H. Manney, M. G. Raizen, and C. S. Weimer, Proc. 4th European Frequency and Time Forum, Neuchatel, March 1990, p. 267.

7. "Liquid and Solid Plasmas," J. J. Bollinger, S. L. Gilbert, D. J. Heinzen, W. M. Itano, and D. J. Wineland, in Atomic Processes in Plasmas, ed. by Y. K. Kim and R. C. Elton, AIP Conference Proceedings 206 (American Institute of Physics, New York, 1990), p. 152.

8. "Test of the Linearity of Quantum Mechanics by RF Spectroscopy of the $^{9}Be^{+}$ Ground State," D. J. Heinzen, J. J. Bollinger, W. M. Itano, S. L. Gilbert, and D. J. Wineland, in Coherence and Quantum Optics, ed. by J. H. Eberly, L. Mandel, and E. Wolf (Plenum, New York, 1990), p. 479.

9. "Trapped Ion Frequency Standards," D. J. Wineland, J. C. Bergquist, J. J. Bollinger, W. M. Itano, D. J. Heinzen, C. H. Manney, F. L. Moore, M. G. Raizen, and C. S. Weimer, Proc. 22nd Ann. Precise Time and Time Interval (PTTI) Applications and Planning Meeting, ed. by R. L. Sydnor (NASA Conf. Publ. 3116, 1991), p. 53.

10. "Atomic Ion Frequency Standards," W. M. Itano, Proc. IEEE 79, 936 (1991).

11. "High Resolution Atomic Spectroscopy of Laser-Cooled Ions," D. J. Wineland, J. C. Bergquist, J. J. Bollinger, W. M. Itano, F. L. Moore, J. M. Gilligan, M. G. Raizen, C. S. Weimer, and C. H. Manney, Proc. Enrico Fermi Summer School on "Laser Manipulation of Atoms and Ions," July 1991, Varenna, Italy, submitted.

12. "Laser Cooling of Trapped Ions," W. M. Itano, J. C. Bergquist, J. J. Bollinger, and D. J. Wineland, ibid.

13. "Ionic Crystals in a Linear Paul Trap," M. G. Raizen, J. M. Gilligan, J. C. Bergquist, W. M. Itano, and D. J. Wineland, Phys. Rev. A, to be published.

14. "Atomic Physics Tests of Nonlinear Quantum Mechanics," J. J. Bollinger, D. J. Heinzen, W. M. Itano, S. L. Gilbert, and D. J. Wineland, Santa Fe Conference on Quantum Measurements, July 1991, to be published.

15. "Single Ion Spectroscopy," J. C. Bergquist, D. J. Wineland, W. M. Itano, F. Diedrich, M. G. Raizen, and F. Elsner, Proc. Soc. Photo-optical Instrumentation Engineers, to be published.

16. "Low Order Modes of an Ion Cloud in a Penning Trap," J. J. Bollinger, D. J. Heinzen, F. L. Moore, W. M. Itano, and D. J. Wineland, Proceedings of the Workshop on Physics with Penning Traps, Lertorpet, Sweden, Physica Scripta, to be published.

Perpendicular laser cooling of a rotating ion plasma in a Penning trap

Wayne M. Itano, L. R. Brewer,* D. J. Larson,† and D. J. Wineland
Time and Frequency Division, National Bureau of Standards, Boulder, Colorado 80303
(Received 13 June 1988)

The steady-state temperature of an ion plasma in a Penning trap, cooled by a laser beam perpendicular to the trap axis, has been calculated and measured. The rotation of the plasma, due to crossed **E** and **B** fields, strongly affects the minimum attainable temperature. This is because the velocity distribution of the ions, as seen by a laser beam intersecting the plasma at some distance from the axis of rotation, is skewed, and this leads to a change in the velocity distribution (and hence temperature) at which a steady state is attained. The calculated temperature is a function of the intensity, frequency, and position of the laser beam, and of the rotation frequency of the plasma. Temperatures of $^9Be^+$ plasmas were measured for a wide range of experimental parameters. The lowest and highest temperatures were approximately 40 mK and 2 K. The measured and calculated temperatures are in agreement.

I. INTRODUCTION

Laser cooling is a method by which radiation pressure is used to reduce the temperature of atoms.[1] It has been demonstrated with free and bound atoms and also with ions confined in Paul and Penning traps. Laser cooling of atoms confined by a harmonic potential has been studied theoretically by many methods.[1] The Paul (radio-frequency) trap uses an oscillating, inhomogeneous electric field to create a harmonic potential for the average motion of an ion.[2,3] However, motion in a Paul trap differs from that in a harmonic trap, since there is a forced oscillation (micromotion) at the frequency of the applied field. The micromotion has not been included in calculations of laser cooling, except by numerical simulation.[4]

In a Penning trap, static electric and magnetic fields confine the ions. In some ways, the Penning trap is more difficult than the Paul trap to treat theoretically. Some of the difficulties arise because the electrostatic potential energy decreases as an ion moves radially outward from the trap axis.[2,3] A magnetic field along the trap axis is required to confine the ions radially. The combined effects of the magnetic field and of the radial electric field lead to a circular $\mathbf{E}\times\mathbf{B}$ drift of the ions about the trap axis. This rotation leads to a basic difference between laser cooling in a Penning trap and in a harmonic trap. It can be shown that conservation of energy and of the axial component of the canonical angular momentum L_z guarantees confinement of the ions.[5] However, external torques, due to collisions with neutral molecules or to asymmetries of the trap fields, change L_z and may cause the ions to move outward radially.[6,7] Thus long-term confinement is not guaranteed even if laser cooling reduces the random motion of the ions. A laser beam of appropriate tuning and spatial profile can be used to apply a torque to the ions in order to prevent this radial drift, while also cooling their random motion.[8] The axial motion in a Penning trap does not suffer from these complications, since the axial well is harmonic, and since there are no axial magnetic forces. A laser beam which is not perpendicular to the trap axis can be used to cool this motion.

The previous theoretical treatment of laser cooling in a Penning trap considered only a single ion.[8] When many ions are confined, the additional electric fields lead to an increased rotation frequency of the ions around the axis, which affects the cooling. Also, detailed calculations were carried out only for the case where the Doppler broadening was much smaller than the natural linewidth of the optical transition. This is often not the case in practice.

Several reports of laser cooling of ions in Penning traps have appeared previously.[9–16] While temperature measurements were reported in all of these references, and Ref. 9 reported a measurement of the cooling rate, in rough agreement with theory, very little has been done in the way of quantitative comparisons of theory and experiment. Simple theoretical calculations yield a predicted minimum temperature $T_{\min}=\hbar\gamma_0/2k_B$, where γ_0 is the radiative linewidth of the atomic transition in angular frequency units and k_B is Boltzmann's constant.[8] This minimum temperature has been approached within about a factor of 10 when the laser beam was perpendicular to the trap axis, and within about a factor of 2 when the cooling laser was not perpendicular to the axis.[15] More typically, the lowest observed temperatures were higher than $T_{\min}$ by two orders of magnitude, and no explanation of this discrepancy has been given.

In this paper we present a calculation of the perpendicular (cyclotron) temperature in a Penning trap for the case in which the cooling laser beam is perpendicular to the trap axis. This geometry is often used experimentally.[9,10,12–14] The calculations are compared to experiments in which temperatures of $^9Be^+$ plasmas were measured for a wide range of experimental conditions. For typical experimental conditions, the minimum perpendicular temperature is found to be much greater than $T_{\min}=\hbar\gamma_0/2k_B$. The reason stems from the condition that the work done by the laser on the ions be zero in the steady state. The rate at which work is done on an ion of velocity **v** by a force **F**, which in this case is parallel to

the direction of propagation of the laser beam, is $\mathbf{F}\cdot\mathbf{v}$. If the laser beam intersects the ion plasma on the side which is receding from the laser due to the rotation of the plasma, $\mathbf{F}\cdot\mathbf{v}$ would tend to be positive. (If it intersects on the other side, the plasma radius expands and there is no steady state.[10]) In order to make the average value $\langle \mathbf{F}\cdot\mathbf{v} \rangle \approx 0$, the frequency of the laser is tuned below resonance, which, because of the Doppler effect, makes $\mathbf{F}$ stronger for ions with $\mathbf{F}\cdot\mathbf{v} < 0$ than for ions with $\mathbf{F}\cdot\mathbf{v} > 0$. In order to get $\langle \mathbf{F}\cdot\mathbf{v} \rangle \approx 0$, due to cancellation between negative and positive contributions to the average, the width of the velocity distribution must have a certain value, which corresponds to a temperature higher than $T_{\min}$.

II. THEORY

A. Simple theory

In this section a simplified theory of perpendicular laser cooling of an ion plasma in a Penning trap is presented. Some of the simplifying assumptions will be modified in the following sections, in order to obtain quantitative predictions that can be compared with experiment.

The trap is assumed to approximate the ideal Penning trap, which consists of a uniform magnetic field $\mathbf{B}=B\hat{\mathbf{z}}$ superimposed on a static electric potential

$$\phi_T(r,z)=\frac{m\omega_z^2}{4q}(2z^2-r^2) , \tag{1}$$

where m and q are the mass and charge of an ion, and ω_z is the frequency of axial motion of a single ion in the trap. The actual frequency of motion of an individual ion is shifted by the presence of the other ions. Here, r and z are the cylindrical coordinates of a point in the trap.

It is assumed that the plasma rotates about the z axis with a uniform angular frequency ω, that is, without shear. The velocity distribution of the ions is assumed to be a Maxwell-Boltzmann distribution superimposed on this uniform rotation. A Maxwell-Boltzmann velocity distribution superimposed on a uniform rotation is a characteristic of a non-neutral plasma in thermal equilibrium in cylindrically symmetric fields.[17,18] If there is shear within the plasma, a resulting frictional force tends to reduce the shear, leading to uniform rotation in the steady state. Approximate uniform rotation of the plasmas has been verified experimentally.[12,15,19,20] The temperatures $T_\perp$ and $T_\parallel$ describe the velocity distributions in the x-y plane in the z direction, and differ because cooling of the z motion occurs only by ion-ion collisions. If there were no relaxation between $T_\perp$ and $T_\parallel$, then $T_\parallel$ would increase without limit, due to heating by photon recoil. We assume that the relaxation is sufficient that $T_\parallel$ reaches a steady value somewhat higher than $T_\perp$. Under the assumptions stated in this section, the calculation of $T_\perp$ does not require any knowledge of $T_\parallel$. If the beam is not perpendicular to the axis, the temperatures depend on the relaxation rate between the perpendicular and parallel kinetic energies, which could be measured by a separate experiment.

A key assumption in the calculation of $T_\perp$ is that, except for the change in energy due to the scattering of photons from the laser, the total (kinetic plus potential) energy of the ion plasma is conserved. This is true to the extent that the plasma is isolated from the rest of the universe and can be described by a time-independent Hamiltonian. These assumptions would be violated by collisions of the ions with neutral atoms or by interactions with time-varying external electric and magnetic fields. In practice, the pressure in the trap and the time-varying fields (due, for example, to thermal radiation or to charges moving on the trap electrodes) can be made low enough that the interaction with the laser is the main source of energy change of the ion system. The rapid heating of the ion plasma that was observed in one experiment after the cooling laser was shut off[21] can be accounted for by a conversion of the electrostatic potential energy of the ions to kinetic energy as the plasma expanded radially.

On the other hand, it is *not* assumed that L_z is conserved in the absence of the torque due to the interaction with the laser. If the trap fields were perfectly axially symmetric, and if the ions were totally isolated from collisions with neutral atoms and the radiation field, then L_z would be conserved. However, static electric or magnetic fields which violate axial symmetry can apply a net torque to the ion plasma and change L_z, even though, being time independent, they cannot transfer energy. In fact, such torques are required in order for the plasma to attain a steady state (a state in which all of the observable properties are constant in time) while the laser beam is applying a finite torque to the plasma. It has been experimentally observed that a steady state can be obtained even when the radial displacement of the laser beam from the trap center is greater than the beam radius. In this case, the torque due to the laser must be balanced by the other external torques. The oscillations that have been observed in the fluorescence of a plasma of laser-cooled Mg^+ ions[13] may be due to the fact that the nature of the external torque is such that the energy and the angular momentum cannot be balanced at the same time, for those experimental conditions.

The calculation of the torque applied by the laser is straightforward.[6] The torque due to static field asymmetries is not well understood in general and is a topic of current experimental[6,7,22–25] and theoretical[26,27] research. In studies of confined electron plasmas, it has been observed that, at sufficiently low pressures, the radial expansion rate, which is a measure of the external torque, is independent of the pressure.[7] The expansion rate decreased when care was taken to reduce asymmetries in the apparatus.[22] Some plasma instabilities which can be driven by static field asymmetries have been studied experimentally.[23,24] No attempt will be made in this article to calculate the external torque. Rather, it is assumed that values of ω and $T_\perp$ that ensure a steady state can be found. The point of the calculation is to determine the value of $T_\perp$ which is consistent with given values of ω and the other parameters. In the experiments, ω and $T_\perp$ were varied by varying the position, intensity, and frequency of the cooling laser beam.

The ion plasma is assumed to interact with a monochromatic laser beam, whose frequency ω_L is close to resonance with a strong optical transition of frequency ω_0. We assume that the upper state of the transition decays only to the ground state. The center of the beam lies in the plane defined by $z=0$, and passes through the point $(x,y,z)=(0,d,0)$, parallel to the x axis (see Fig. 1). The coordinate system is such that, for $d>0$, the rotation of the plasma causes the ions to recede from the laser. The laser intensity is assumed to be so low that saturation of the transition can be neglected. The interaction of the ions with the laser radiation is assumed to consist of a series of photon-scattering events. The events are assumed to occur at random times; hence small effects such as photon antibunching[28–33] are neglected here. The delay between the photon absorption from the laser beam and the subsequent photon emission is neglected. This is justified as long as the natural linewidth of the transition is much greater than the frequencies of motion of the ion. (This case has been called the "weak binding" or "heavy particle" limit.[1]) The change in kinetic energy due to scattering a photon depends on the direction of the emitted photon. The angular distribution of the emitted photons, in a frame moving with the atom, is such that the probability of emission in the direction $\hat{\mathbf{k}}$ is equal to the probability of emission in the direction $-\hat{\mathbf{k}}$. The energy change per scattering event, averaged over all possible emission directions, is then

$$\langle \Delta E_K \rangle = \hbar \mathbf{k}\cdot\mathbf{v} + 2R \ , \tag{2}$$

where $\mathbf{k}$ is the wave vector of the absorbed photon ($|\mathbf{k}|=\omega_L/c$), $\mathbf{v}$ is the velocity of the ion before the scattering event, and the recoil energy $R=(\hbar k)^2/(2m)$ [see Eq. (3) of Ref. 34]. This quantity can be thought of as the time integral for one scattering event, of $\mathbf{F}\cdot\mathbf{v}$, including the average effect of the photon recoil.

The rate of energy change of an ion while it is within the laser beam is equal to the product of the average energy change per photon scattering [Eq. (2)] and the rate of photon scatterings. The rate of photon scatterings (in the low-intensity limit) is

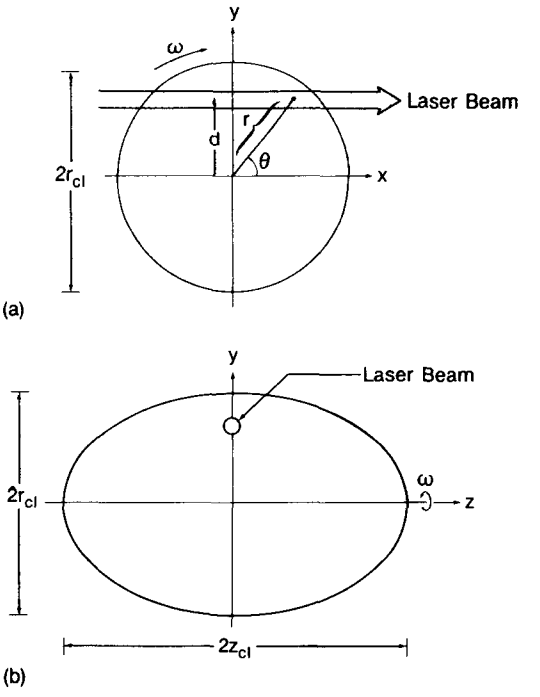

FIG. 1. Diagram showing the laser beam intersecting the ion plasma in (a) the x-y plane and (b) the y-z plane. The laser beam is parallel to the x axis and lies in the $z=0$ plane. Its distance of closest approach to the z axis is d. The direction of the plasma rotation (at angular frequency ω) is indicated.

$$\gamma_L = \frac{I\sigma_0}{\hbar\omega_L}\frac{(\gamma_0/2)^2}{[(\gamma_0/2)^2+\Delta^2]} \ , \tag{3}$$

where I is the light intensity, σ_0 is the scattering cross section at resonance, γ_0 is the natural linewidth of the transition, and $\Delta\equiv\omega_L-\omega_0'-kv_x$ is the detuning of the laser frequency from resonance, taking into account the Doppler shift. Here, $\omega_0'\equiv\omega_0+R/\hbar$ is the resonance absorption frequency of the ion, which is slightly shifted by the recoil term $R/\hbar$. The velocity-averaged rate of energy change of an ion in the beam is

$$\left\langle \frac{dE}{dt} \right\rangle = \frac{I\sigma_0}{\hbar\omega_L}\int_{-\infty}^{+\infty}\frac{(\hbar k v_x+2R)\exp[-(v_x-\omega d)^2/u^2]}{\{1+[(2/\gamma_0)(\omega_L-\omega_0'-kv_x)]^2\}\sqrt{\pi}u}dv_x \ , \tag{4}$$

where $u=(2k_BT_\perp/m)^{1/2}$. Equation (4) is the same as Eq. (7) of Ref. 34, except that the center of the velocity distribution is shifted from $v_x=0$ to ωd due to the uniform rotation of the plasma. The finite width of the beam has been neglected here, but will be included later. Below, we solve Eq. (4) for the steady state given by $\langle dE/dt\rangle=0$.

Equation (4) can be put into a form which is more suitable for computation by expressing the integral in terms of the real and imaginary parts of the complex error function $w(X+iY)$, which can be defined, for $Y>0$, by

$$w(X+iY)=\frac{i}{\pi}\int_{-\infty}^{+\infty}\frac{e^{-t^2}}{X+iY-t}dt \ . \tag{5}$$

The real and imaginary parts of $w(X+iY)$ are

$$\begin{aligned} \mathrm{Re}\,w(X+iY)&=\frac{Y}{\pi}\int_{-\infty}^{+\infty}\frac{e^{-t^2}}{(X-t)^2+Y^2}dt \ , \\ \mathrm{Im}\,w(X+iY)&=\frac{1}{\pi}\int_{-\infty}^{+\infty}\frac{(X-t)e^{-t^2}}{(X-t)^2+Y^2}dt \ . \end{aligned} \tag{6}$$

Tables[35] and methods for the numerical approximation[36] of $w(X+iY)$ have been published.

Let the integration variable in Eq. (4) be changed to $t=(v_x-\omega d)/u$, and let $Y=\gamma_0/(2ku)$ and $X=(\omega_L-\omega_0'-k\omega d)/(ku)$. Then

$$\left\langle \frac{dE}{dt} \right\rangle = \frac{I\sigma_0 Y^2}{\hbar\omega_L\sqrt{\pi}} \int_{-\infty}^{+\infty} \frac{[\hbar k(ut+\omega d)+2R]e^{-t^2}}{Y^2+(X-t)^2}dt \ . \tag{7}$$

Replacing t in the numerator of the integrand by $X-(X-t)$, we have

$$\begin{aligned}\left\langle \frac{dE}{dt} \right\rangle &= \frac{I\sigma_0 kY^2}{\omega_L\sqrt{\pi}} \left[\left[uX+\omega d+\frac{2R}{\hbar k} \right] \int_{-\infty}^{+\infty} \frac{e^{-t^2}}{Y^2+(X-t)^2}dt - u\int_{-\infty}^{+\infty} \frac{(X-t)e^{-t^2}}{Y^2+(X-t)^2}dt \right] \\ &= \frac{I\sigma_0\sqrt{\pi}kY}{\omega_L} \left[\left[uX+\omega d+\frac{\hbar k}{m} \right] \mathrm{Re}w(X+iY) - uY\,\mathrm{Im}w(X+iY) \right] . \end{aligned} \tag{8}$$

If the values of the rotation frequency ω, the spatial offset d, and the laser frequency detuning $(\omega_L-\omega_0')$ are fixed, then $\langle dE/dt\rangle$ is a function only of u, which is a function of $T_\perp$. The steady-state value of $T_\perp$ (if it exists) is found by solving the equation $\langle dE/dt\rangle(T_\perp)=0$ for $T_\perp$. This equation has been investigated numerically, and solutions have been found to exist for $\omega d \geq 0$ and $(\omega_L-\omega_0')<0$. The steady-state value of $T_\perp$ is a function of ω, d, and $\Delta\omega_L \equiv \omega_L-\omega_0'$. Since ω and d occur only in the combination ωd, $T_\perp$ is a function of only two variables, ωd and $\Delta\omega_L$, for a given transition in a given ion. There is no dependence of $T_\perp$ on the intensity I, since it enters the expression for $\langle dE/dt\rangle$ as an overall factor and thus does not change the solution of the equation $\langle dE/dt\rangle(T_\perp)=0$.

Figure 2 shows $T_\perp$ as a function of $\Delta\omega_L$, for $\omega/2\pi=50$ kHz and for several values of d. The values of m, γ_0, and ω_0 are for the $2s\,^2S_{1/2}$ to $2p\,^2P_{3/2}$ [$\lambda=313$ nm, $\gamma_0=(2\pi)19.4$ MHz] transition of $^9Be^+$. For a given value of $\Delta\omega_L$, $T_\perp$ increases as d increases. Hence the lowest temperatures are obtained by keeping d as small as possible. The curve of $T_\perp$ for $d=0$ is the same as what would be obtained for a nonrotating plasma ($\omega=0$), because of the way $T_\perp$ depends on ωd. It attains a minimum value $T_\perp \approx \hbar\gamma_0/2k_B$ for $\Delta\omega_L \approx -\gamma_0/2$, just as predicted by theories developed for free atoms or for atoms trapped in harmonic wells, where rotation does not have to be considered.[1,34]

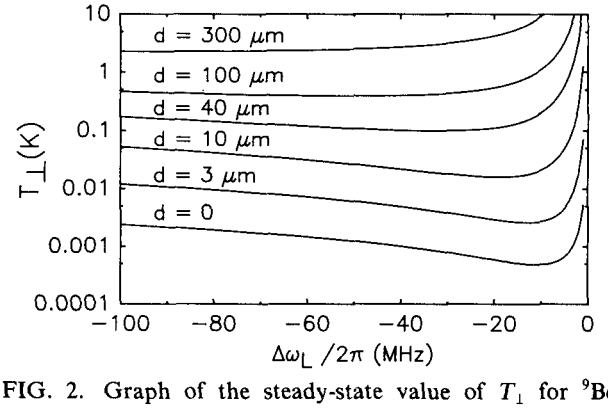

FIG. 2. Graph of the steady-state value of $T_\perp$ for $^9Be^+$ [$\gamma_0=(2\pi)19.4$ MHz, $\lambda=313$ nm] as a function of the laser frequency detuning for several values of the spatial offset d. The rotation frequency $\omega/2\pi$ is 50 kHz. This calculation neglects the finite beam radius and saturation of the optical transition.

We can give a simple explanation for the increase in $T_\perp$ as d increases. In the steady state, $\hbar\mathbf{k}\cdot\mathbf{v}$, averaged over all photon-scattering events, must be negative, in order to balance the $2R$ term in Eq. (2), which is positive. This is done by making $\Delta\omega_L<0$, so that, due to the Doppler shift, there is a preference for ions to scatter photons when $\mathbf{k}\cdot\mathbf{v}<0$. However, for $d>0$, $v_x(\max)$, the most probable value of v_x, is shifted to $v_x(\max)=\omega d>0$, so that $kv_x(\max)>0$. If the width of the v_x distribution, due to the finite value of $T_\perp$, were narrow compared to $v_x(\max)$, this would tend to make the average value of $\hbar\mathbf{k}\cdot\mathbf{v}$ positive. The steady state can come about only when the velocity distribution is wide enough that there is a significant probability for an ion to have $\hbar\mathbf{k}\cdot\mathbf{v}<0$. This corresponds to a higher value of $T_\perp$.

Here we make a few remarks about the motion in the z direction. This motion is affected by the recoil of the photons emitted from the ions and by ion-ion collisions. We have assumed that it eventually reaches a steady state, at some $T_\parallel$, and that there is no additional source of heating or cooling for the z motion. Then Eq. (4) contains all of the contributions to dE/dt, since all of the recoil energy is contained in the term $\hbar\mathbf{k}\cdot\mathbf{v}+2R$, and since the total energy of the ion plasma is conserved in collisions between the ions. Thus Eq. (4) can be used to derive the steady-state value of $T_\perp$, and this value does not depend on the final value of $T_\parallel$.

B. Saturation effects

Equation (4) is valid only in the limit that the laser intensity I is low. To generalize it to arbitrary intensity, the expression for the average scattering rage [Eq. (3)] is replaced by[37]

$$\gamma_L = \frac{I\sigma_0}{\hbar\omega_L} \frac{(\gamma_0/2)^2}{[(\gamma/2)^2+\Delta^2]} \ , \tag{9}$$

where γ is the power-broadened linewidth, given by

$$\gamma = \gamma_0\sqrt{1+2S} \ . \tag{10}$$

The saturation parameter S is related to the intensity by

$$S=\frac{I\sigma_0}{\hbar\omega_0\gamma_0} . \tag{11}$$

As stated previously, we ignore the correlations between photon emissions of an ion, which result in photon antibunching. In more sophisticated treatments of laser cooling, which have not yet been applied to the Penning trap, these correlations lead to a modification of the diffusion constant which enters into the equation that describes the evolution of the distribution function of the ions.[28–33] Javanainen[32] has shown that this correction to the diffusion constant can affect the final temperature of laser-cooled ions in a harmonic trap by as much as 20% at high intensities. It has no effect in the limit of low intensities. We do not include it here, since it would complicate the calculations without greatly increasing the accuracy.

Using the power-broadened line shape [Eq. (9)] in place of the low-intensity line shape [Eq. (3)], we find that the average rate of energy change of an ion in the beam is

$$\left\langle\frac{dE}{dt}\right\rangle=\frac{I\sigma_0\gamma_0^2}{\hbar\omega_L\gamma^2}\int_{-\infty}^{+\infty}\frac{(\hbar k v_x+2R)\exp[-(v_x-\omega d)^2/u^2]}{\{1+[(2/\gamma)(\omega_L-\omega_0'-kv_x)]^2\}\sqrt{\pi}u}dv_x . \tag{12}$$

Aside from an overall multiplicative factor, which does not affect the solution of the equation $\langle dE/dt\rangle(T_\perp)=0$, the only difference between Eq. (12) and Eq. (4) is the replacement of the natural radiative linewidth γ_0 by the power-broadened linewidth γ.

Figure 3 shows $T_\perp$ as a function of $\Delta\omega_L$ for several values of S. The other parameters are $\omega/2\pi=50$ kHz and $d=50$ μm. The lowest temperature for a given frequency detuning is obtained by minimizing S.

C. Finite beam geometry

Up to now, the finite radius of the laser beam has been neglected. In this section we investigate its effect on the steady-state temperature.

The average scattering rate at each point in the plasma depends on the intensity at that point through Eq. (9). Let $n(x,y,z)$ be the time-averaged density (ions per unit volume) at the point (x,y,z). Then the rate of change of the total energy of the ion plasma is

$$\left\langle\frac{dE_{\rm tot}}{dt}\right\rangle=\frac{\sigma_0\gamma_0^2}{\hbar\omega_L}\int_{-\infty}^{+\infty}dx\int_{-\infty}^{+\infty}dy\int_{-\infty}^{+\infty}dz\int_{-\infty}^{+\infty}dv_x I(x,y,z)n(x,y,z)\frac{(\hbar k v_x+2R)\exp[-(v_x-\omega y)^2/u^2]}{\{1+[(2/\gamma)(\omega_L-\omega_0'-kv_x)]^2\}\sqrt{\pi}u\gamma^2} . \tag{13}$$

The linewidth γ is a function of position through its dependence on I, and the fixed spatial offset d of Eq. (4) is replaced by the position variable y.

In the following, we assume that the laser beam is Gaussian, propagates in the $\hat{\mathbf{x}}$ direction, and has its focus at $(x,y,z)=(0,d,0)$. We allow the beam radii w_y and w_z in the radial (y) and axial (z) directions to be different, since this was sometimes the case experimentally. The intensity is then

$$I(y,z)=I_0\exp[-2(y-d)^2/w_y^2-2z^2/w_z^2] , \tag{14}$$

where $I_0=2P/(\pi w_y w_z)$ and where P is the total power in the beam. We neglect the variation of w_y and w_z with x, since, in our experiments, it was small over the size of the plasma. The confocal parameter $b=\pi w^2/\lambda$, which is the distance from the focus at which the beam radius w grows by a factor of $\sqrt{2}$, was typically much greater than the radius of the plasma.

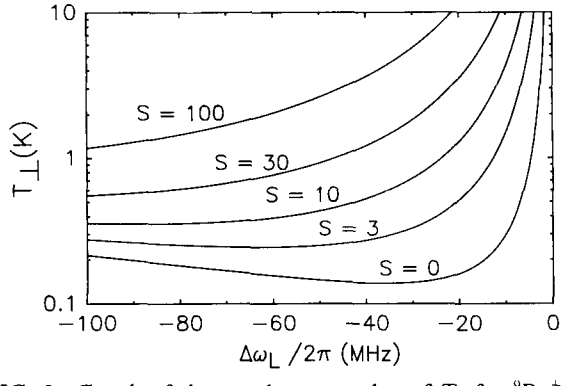

FIG. 3. Graph of the steady-state value of $T_\perp$ for $^9Be^+$ as a function of the laser frequency detuning for several values of the saturation parameter S. The rotation frequency $\omega/2\pi$ is 50 kHz and the spatial offset is 50 μm. This calculation neglects the finite beam radius.

In a continuum model, at low temperatures, the density of a non-neutral plasma is uniform, except for a region on the outer surface whose thickness is on the order of the Debye length.[18] For a non-neutral plasma, the Debye length is defined by[18]

$$\lambda_D\equiv\left[\frac{k_B T}{4\pi n_0 q^2}\right]^{1/2} , \tag{15}$$

where n_0 is the ion density and T is the temperature. For the plasmas studied here, we had $T\leq 2$ K and $n_0\geq 2\times 10^7$ ions/cm^3, so that $\lambda_D\leq 20$ μm. Since the plasmas studied typically had diameters greater than 500

μm, the density can be considered to be uniform. The plasma is a spheroid, whose aspect ratio can be calculated from ω.[6,15] It has been shown theoretically[38] and recently confirmed experimentally[39] that, at very low temperatures, ions in a Penning trap form concentric shells. However, this spatial ordering should have little net effect on the cooling and is ignored here. We assume that the plasma has a uniform density n_0 inside a spheroid of diameter $2r_{cl}$ in the $z=0$ plane and axial extent $2z_{cl}$ and is zero otherwise.

We also assume that the beamwidth is small compared to the plasma dimensions. With these approximations, Eq. (13) is reduced to

$$\left\langle \frac{dE_{\rm tot}}{dt} \right\rangle = \frac{2I_0\sigma_0\gamma_0^2 n_0}{\hbar\omega_L}(r_{cl}^2-d^2)^{1/2}\int_{-\infty}^{+\infty}dy\int_{-\infty}^{+\infty}dz\int_{-\infty}^{+\infty}dv_x \exp[-2(y-d)^2/w_y^2-2z^2/w_z^2] \times \frac{(\hbar k v_x+2R)\exp[-(v_x-\omega y)^2/u^2]}{\{1+[(2/\gamma)(\omega_L-\omega_0'-kv_x)]^2\}\sqrt{\pi}u\gamma^2} . \quad (16)$$

Here, $2(r_{cl}^2-d^2)^{1/2}$ is the length over which the laser beam intersects the plasma. The v_x integration can be expressed in terms of the complex error function, leaving a two-dimensional integration to be done numerically:

$$\left\langle \frac{dE_{\rm tot}}{dt} \right\rangle = \frac{2I_0\sigma_0 n_0\sqrt{\pi}kuY_0^2}{\omega_L}(r_{cl}^2-d^2)^{1/2}\int_{-\infty}^{+\infty}dy\int_{-\infty}^{+\infty}dz \exp[-2(y-d)^2/w_y^2-2z^2/w_z^2] \times \left[\frac{(uX+\omega y+\hbar k/m)}{uY(y,z)}\,{\rm Re}w(X+iY)-{\rm Im}w(X+iY)\right] . \quad (17)$$

Here, $Y_0=\gamma_0/(2ku)$, $X(y)=(\omega_L-\omega_0'-k\omega y)/(ku)$, and $Y(y,z)=\gamma(y,z)/(2ku)$. For a given set of parameters, the equation $\langle dE_{\rm tot}/dt\rangle(T_\perp)=0$ is solved for $T_\perp$. For some ranges of parameters, no solution can be found. This occurs when d is too small relative to w_y, so that the beam has too much intensity on the $y<0$ side of the plasma.

Figure 4 shows $T_\perp$ as a function of $\Delta\omega_L$ for $\omega/2\pi=50$ kHz and for several values of d in the limit of low laser intensity. The beam radii are given by $w_y=w_z=50$ μm. The values of $T_\perp$ calculated from the simple theory of Sec. II A are shown as dashed lines. The effect of the finite beamwidth is to reduce the effective value of d, resulting in a lower value of $T_\perp$. The effect decreases as d increases. For this example, there is a range of values of $\Delta\omega_L$ for which no solution of the equation $\langle dE_{\rm tot}/dt\rangle(T_\perp)=0$ can be found, when d is less than or equal to about 30 μm.

Figure 5 shows the same for a laser power of 50 μW, which is a typical experimental value. This corresponds to a saturation parameter at the center of the beam of $S=3.85$. The effect of saturation is to increase $T_\perp$. This can be seen by comparing the solid curves of Figs. 4 and 5.

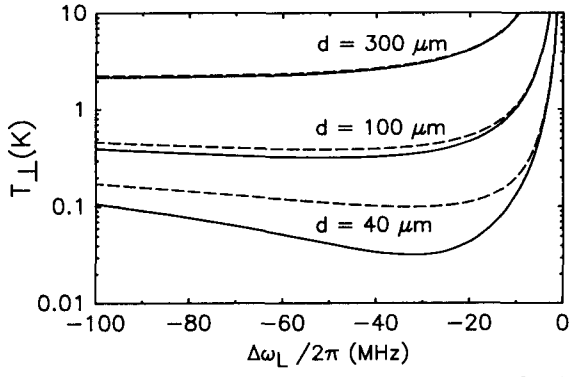

FIG. 4. Graph of the steady-state value of $T_\perp$ for $^9Be^+$ as a function of the laser frequency detuning for several values of d, in the limit of low laser intensity (solid lines). The laser beam is assumed to be Gaussian, with $w_y=w_z=50$ μm. The rotation frequency $\omega/2\pi$ is 50 kHz. The results of the simple theory, which neglects saturation of the optical transition and the finite beam radius, are shown as dashed lines.

III. EXPERIMENT

For the most part, the experimental techniques have been described previously.[12,15] One exception is the abso-

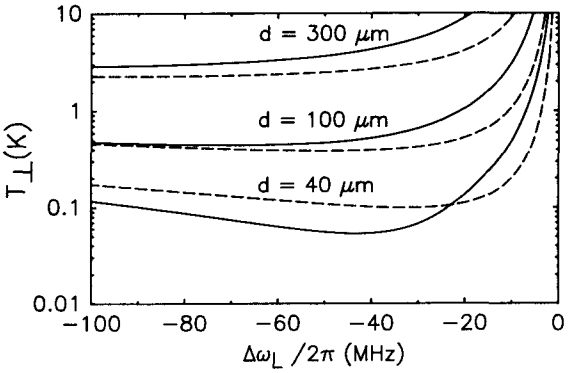

FIG. 5. The same as Fig. 4, except that the laser power is 50 μW. This corresponds to a saturation parameter S at the center of the beam of 3.85.

lute calibration of the laser frequency detuning from resonance $\Delta\omega_L$, which will therefore be described in some detail.

The Penning trap has been described previously.[15,19] It was referred to as trap II in Ref. 15 and has characteristic dimensions $r_0=0.417$ cm and $z_0=0.254$ cm. The operating parameters were $B\approx 1.42$ T [cyclotron frequency $\omega_c\approx(2\pi)2.42$ MHz] and $\omega_z\approx(2\pi)213$ kHz (ring-to-endcap voltage $V_0\approx 1.5$ V). The $^9Be^+$ ions were loaded into the trap by ionizing neutral Be atoms, evaporated from a filament, with an electron beam. The electrons and the neutral Be atoms entered the trap through holes in the endcaps which were centered on the trap symmetry axis.

Two cw single-mode dye lasers were used in the experiment. Both were frequency doubled to 313 nm in a temperature phase-matched rubidium-dihydrogen-phosphate crystal. The two laser beams were directed though the ion plasma, in opposite directions, perpendicular to the magnetic field. The beams passed through 0.25-cm-diam holes on opposite sides of the ring electrode. One of the laser beams, with a power of approximately 50 μW at 313 nm, was used to cool the ions. The other laser beam, which had much lower power at 313 nm (typically less than 1 μW), was used as a probe, inducing changes in the 313-nm resonance fluorescence light from the cooling beam, from which the temperature and rotation frequency could be derived.[12,15] The backscattered resonance fluorescence light in an $f/6$ cone centered on the cooling beam was collected by a mirror (which had a hole to allow passage of the cooling beam) and focused by a system of lenses onto a photomultiplier tube.

The beams were displaced laterally by lenses attached to micrometer-driven stages. The position of the cooling beam relative to the center of the trap was determined by monitoring the intensity transmitted through the trap as the beam was cut off by the edges of the holes in the electrode. The uncertainty in this determination was estimated to be about 13 μm.

The average frequency of the laser beam used for cooling was kept fixed to about 1 MHz by a servolock to a saturated-absorption resonance in molecular iodine. The laser frequency was modulated over a range of about 16 MHz (at 313 nm), in order to obtain the feedback signal necessary for the lock. To simulate this frequency modulation, an additional integration over $\Delta\omega_L$ could be performed. This would improve the accuracy of the calculations only for small values of $\Delta\omega_L$.

An optical double-resonance method described in detail elsewhere[12,15] was used to measure $T_\perp$. The cooling laser was tuned to the $2s\,^2S_{1/2}(m_I=+\frac{3}{2},\ m_J=+\frac{1}{2})$ to $2p\,^2P_{3/2}(m_I=+\frac{3}{2},\ m_J=+\frac{3}{2})$ transition, hereafter called the cycling transition. This yielded a steady fluorescence signal, since this excited-state sublevel always decayed back to the same ground-state sublevel. The weak probe laser was tuned to drive the depopulation transition from the $2s\,^2S_{1/2}(m_I=+\frac{3}{2},\ m_J=+\frac{1}{2})$ sublevel to the $2p\,^2P_{3/2}(m_I=\frac{3}{2},\ m_J=-\frac{1}{2})$ sublevel, which decayed $\frac{2}{3}$ of the time to the $2s\,^2S_{1/2}(m_I=+\frac{3}{2},\ m_J=-\frac{1}{2})$ ground-state sublevel. This sublevel did not fluoresce, since it was far from resonance with either laser. Population in the $2s\,^2S_{1/2}(m_I=+\frac{3}{2},\ m_J=-\frac{1}{2})$ sublevel was transferred back to the $2s\,^2S_{1/2}(m_I=+\frac{3}{2},\ m_J=+\frac{1}{2})$ sublevel in about 1 s by off-resonance optical pumping from the cooling laser.[12,15] The probe laser resonance was observed in

TABLE I. Comparison of calculated and measured values of $T_\perp$ for perpendicular laser cooling of $^9Be^+$ in a Penning trap, for experimentally determined parameters ω, d, $\Delta\omega_L$, P, w_y, and w_z.

$\omega/2\pi$ (kHz)	d (μm)	$\Delta\omega_L/2\pi$ (MHz)	P (μW)	w_y (μm)	w_z (μm)	$T_{\perp\text{calc}}$ (K)	$T_{\perp\text{meas}}$ (K)
67.5	127	−29	30	24	24	$3.0^{+2.7}_{-1.3}$	1.9±0.2
99.7	127	−44	49	82	31	$2.0^{+1.0}_{-0.7}$	1.6±0.3
65.7	127	−44	38	82	31	$0.91^{+0.39}_{-0.30}$	1.27±0.10
35.9	165	−78	30	24	24	$0.82^{+0.16}_{-0.15}$	0.96±0.11
36.7	165	−46	30	24	24	$1.05^{+0.35}_{-0.26}$	0.96±0.11
36.3	165	−61	30	24	24	$0.89^{+0.21}_{-0.18}$	0.91±0.08
38.6	51	−13	30	24	24	$0.62^{+10}_{-0.47}$	0.69±0.07
40.0	127	−46	30	24	24	$0.77^{+0.28}_{-0.20}$	0.61±0.05
32.6	127	−80	30	24	24	$0.49^{+0.10}_{-0.09}$	0.55±0.05
35.9	127	−62	30	24	24	$0.57^{+0.15}_{-0.12}$	0.47±0.05
35.0	89	−29	30	24	24	$0.48^{+0.39}_{-0.18}$	0.27±0.03
28.5	89	−63	30	24	24	$0.24^{+0.06}_{-0.06}$	0.25±0.03
28.1	89	−79	30	24	24	$0.25^{+0.06}_{-0.05}$	0.21±0.03
31.0	89	−45	30	24	24	$0.29^{+0.10}_{-0.09}$	0.20±0.02
29.2	76	−55	49	82	31	$0.087^{+0.046}_{-0.042}$	0.13±0.04
23.1	76	−55	49	82	31	$0.075^{+0.032}_{-0.030}$	0.11±0.05
21.6	51	−79	30	24	24	$0.100^{+0.031}_{-0.029}$	0.097±0.020
38.1	64	−44	38	82	31	$0.044^{+0.067}_{-0.044}$	0.085±0.009
29.4	76	−44	49	82	31	$0.084^{+0.051}_{-0.046}$	0.081±0.011
23.8	51	−46	30	24	24	$0.092^{+0.037}_{-0.033}$	0.080±0.020
17.3	64	−44	38	82	31	$0.037^{+0.019}_{-0.017}$	0.043±0.040

the form of a decrease in the fluorescence from the cycling transition as the probe laser was tuned in frequency. The contribution to the width of this resonance from the Doppler broadening was used to derive $T_\perp$. The optical double-resonance method has the advantage of not greatly perturbing the temperature of the plasma. The rotation frequency ω was measured from the shift in the frequency of the center of the depopulation resonance, due to the Doppler shift, for a given translation of the probe beam in the y direction.[12,15]

The absolute calibration of the cooling laser detuning $\Delta\omega_L$ was made by the following method. The magnetic field was fixed at a particular NMR resonance frequency, and the cooling laser was locked to the iodine signal. The edges of the plasma were located with the probe beam by finding the positions at which the double-resonance signal disappeared.[12,15] The probe beam was then positioned at the center of the plasma and tuned to the cycling transition. At the center of the plasma, $d=0$, so the average Doppler shift due to rotation is zero. The increase in fluorescence as the probe laser was tuned across the cycling transition was observed while the cooling laser kept the plasma at a constant temperature. For this measurement the cooling beam was chopped, and the fluorescence was detected while it was off, in order to reduce the background. The probe laser was then tuned to the frequency at which the peak of the cycling resonance occurred. Some of the radiation from each of the two lasers was combined on the surface of a silicon photodiode by means of a beamsplitter. The beat frequency was measured with a radio-frequency spectrum analyzer. This measurement yielded the value of $\Delta\omega_L/2\pi$ with an uncertainty of about 10 MHz (at 313 nm). The value of $\Delta\omega_L$ at other magnetic fields could be calculated from the known Zeeman shift of the resonance line.

IV. RESULTS

Table I summarizes the results of the measurements. The values of $T_\perp$ calculated from the various experimental parameters are shown in the column labeled $T_{\perp\text{calc}}$. They are in good agreement with the values of $T_\perp$ measured from the Doppler broadening of the optical double resonance, which are shown in the column labeled $T_{\perp\text{meas}}$. This agreement is maintained over a wide range of values of d, ω, and $\Delta\omega_L$. The range of values of $T_\perp$ is from about 0.04 K to about 2 K. All of the parameters that go into the calculation are measured, rather than fitted. The uncertainties in $T_{\perp\text{calc}}$ are due to the uncertainties in the parameters ω, d, $\Delta\omega_L$, P, ω_y, and ω_z. In most cases, the uncertainty in d of about 13 μm makes the largest contribution to the uncertainty in $T_{\perp\text{calc}}$. For small values of $\Delta\omega_L$, the uncertainty in $\Delta\omega_L$ of about $(2\pi)10$ MHz makes the largest contribution. The uncertainty in ω of about 5% and the uncertainties in P, w_y, and w_z of about 20% make relatively minor contributions. Figure 6 is a scatter plot of the measured values $T_{\perp\text{meas}}$ versus the calculated values $T_{\perp\text{calc}}$. The data points lie close to the dashed line, which denotes the condition $T_{\perp\text{meas}}=T_{\perp\text{calc}}$.

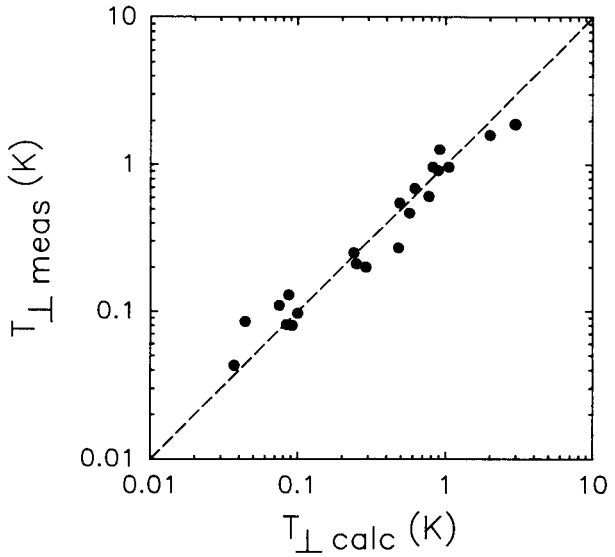

FIG. 6. Scatter plot of measured values of $T_\perp$ (vertical axis) vs calculated values of $T_\perp$ (horizontal axis). The dashed line corresponds to $T_{\perp\text{meas}}=T_{\perp\text{calc}}$.

The observed values of $T_\perp$ are much higher (up to three orders of magnitude) than those predicted by a theory which does not take rotation into account (the $d=0$ curve in Fig. 2). In order to obtain very low temperatures, the cooling laser beam should not be perpendicular to **B**. Low temperatures, approaching the $T_{\min}=\hbar\gamma_0/2k_B$ limit, have been attained for $^9Be^+$ plasmas in Penning traps by supplementing perpendicular cooling with cooling by a beam which was not perpendicular to **B**.[15,39]

A possible configuration for obtaining the lowest possible temperatures is a combination of two laser beams, one to cool the ions and the other to maintain the radial size of the plasma. The strong cooling beam, with a frequency detuning $\Delta\omega_L=-\gamma_0/2$, would be directed along the z axis. If the power in this beam were not too high, then Coulomb coupling between ions would ensure $T_\perp\approx T_\parallel\approx\hbar\gamma_0/2k_B$. The second beam, in the x-y plane, would be positioned to apply a torque to counteract the radial expansion due to external torques and to photon recoil from the cooling beam. The photon-scattering rate from this beam could be made low enough so as not to significantly affect the overall temperature.

ACKNOWLEDGMENTS

We gratefully acknowledge the support of the U.S. Office of Naval Research and the U.S. Air Force Office of Scientific Research. One of us (D.J.L.) acknowledges partial support of the National Science Foundation. We thank J. C. Bergquist, J. J. Bollinger, and S. L. Gilbert for carefully reading the manuscript.

*Present address: L250, Lawrence Livermore National Laboratory, Livermore, CA 94550.

†Permanent address: Department of Physics, University of Virginia, Charlottesville, VA 22901.

[1]For recent reviews of laser cooling, see D. J. Wineland and W. M. Itano, Phys. Today **40**(6), 34 (1987); S. Stenholm, Rev. Mod. Phys. **58**, 699 (1986).

[2]H. G. Dehmelt, Adv. At. Mol. Phys. **3**, 53 (1967).

[3]D. J. Wineland, W. M. Itano, and R. S. Van Dyck, Jr., Adv. At. Mol. Phys. **19**, 135 (1983).

[4]R. Casdorff and R. Blatt, Appl. Phys. B **45**, 175 (1988); J. Hoffnagle, R. G. DeVoe, L. Reyna, and R. G. Brewer, Phys. Rev. Lett. **61**, 255 (1988); R. Blümel, J. M. Chen, E. Peik, W. Quint, W. Schleich, Y. R. Shen, and H. Walther, Nature (London) **334**, 309 (1988).

[5]T. M. O'Neil, Phys. Fluids **23**, 2216 (1980).

[6]D. J. Wineland, J. J. Bollinger, W. M. Itano, and J. D. Prestage, J. Opt. Soc. Am. B **2**, 1721 (1985).

[7]C. F. Driscoll and J. H. Malmberg, Phys. Rev. Lett. **50**, 167 (1983).

[8]W. M. Itano and D. J. Wineland, Phys. Rev. A **25**, 35 (1982).

[9]D. J. Wineland, R. E. Drullinger, and F. L. Walls, Phys. Rev. Lett. **40**, 1639 (1978).

[10]R. E. Drullinger, D. J. Wineland, and J. C. Bergquist, Appl. Phys. **22**, 365 (1980).

[11]D. J. Wineland and W. M. Itano. Phys. Lett. **82A**, 75 (1981).

[12]J. J. Bollinger and D. J. Wineland, Phys. Rev. Lett. **53**, 348 (1984).

[13]R. C. Thompson, G. P. Barwood, and P. Gill, Opt. Acta **33**, 535 (1986); Appl. Phys. B **46**, 87 (1988).

[14]F. Plumelle, M. Desaintfuscien, M. Jardino, and P. Petit, Appl. Phys. B **41**, 183 (1986).

[15]L. R. Brewer, J. D. Prestage, J. J. Bollinger, W. M. Itano, D. J. Larson, and D. J. Wineland, Phys. Rev. A **38**, 859 (1988).

[16]R. G. Hulet, D. J. Wineland, J. C. Bergquist, and W. M. Itano, Phys. Rev. A **37**, 4544 (1988).

[17]R. C. Davidson, *Theory of Nonneutral Plasmas* (Benjamin, Reading, MA, 1974).

[18]T. M. O'Neil and C. F. Driscoll, Phys. Fluids **22**, 266 (1979); S. A. Prasad and T. M. O'Neil, *ibid.* **22**, 278 (1979).

[19]D. J. Larson, J. C. Bergquist, J. J. Bollinger, W. M. Itano, and D. J. Wineland, Phys. Rev. Lett. **57**, 70 (1986).

[20]C. F. Driscoll, J. H. Malmberg, and K. S. Fine, Phys. Rev. Lett. **60**, 1290 (1988).

[21]J. J. Bollinger, J. D. Prestage, W. M. Itano, and D. J. Wineland, Phys. Rev. Lett. **54**, 1000 (1985).

[22]C. F. Driscoll, K. S. Fine, and J. H. Malmberg, Phys. Fluids **29**, 2015 (1986).

[23]D. L. Eggleston, T. M. O'Neil, and J. H. Malmberg, Phys. Rev. Lett. **53**, 982 (1984).

[24]D. L. Eggleston and J. H. Malmberg, Phys. Rev. Lett. **59**, 1675 (1987).

[25]J. Yu, M. Desaintfuscien, and F. Plumelle, in *Laser Spectroscopy VIII*, Vol. 55 of Springer Series in Optical Sciences, edited by W. Persson and S. Svanberg (Springer, Berlin, 1987), p. 75.

[26]J. D. Crawford, T. M. O'Neil, and J. H. Malmberg, Phys. Rev. Lett. **54**, 697 (1985).

[27]J. D. Crawford and T. M. O'Neil, Phys. Fluids **30**, 2076 (1987).

[28]R. J. Cook, Opt. Commun. **35**, 347 (1980).

[29]J. P. Gordon and A. Ashkin, Phys. Rev. A **21**, 1606 (1980).

[30]R. J. Cook, Phys. Rev. A **22**, 1078 (1980).

[31]V. G. Minogin, Zh. Eksp. Teor. Fiz. **79**, 2044 (1980) [Sov. Phys.—JETP **52**, 1032 (1980)].

[32]J. Javanainen, J. Phys. B **14**, 4191 (1981).

[33]S. Stenholm, Phys. Rev. A **27**, 2513 (1983).

[34]D. J. Wineland and W. M. Itano, Phys. Rev. A **20**, 1521 (1979).

[35]V. N. Faddeyeva and N. M. Terent'ev, *Tables of Values of the Function* $w(z)=e^{-z^2}[1+(2i/\sqrt{\pi})\int_0^z e^{t^2}dt]$ *for Complex Argument*, translated by D. G. Fry (Pergamon, New York, 1961); B. D. Fried and S. D. Conte, *The Plasma Dispersion Function* (Academic, New York, 1961).

[36]See, for example, A. K. Hui, B. H. Armstrong, and A. A. Wray, J. Quant. Spectrosc. Radiat. Transfer **19**, 509 (1978); J. Humlíček, *ibid.* **21**, 309 (1979).

[37]See, for example, W. Demtröder, in *Laser Spectroscopy*, Vol. 5 of Springer Series in Chemical Physics, edited by V. I. Goldanskii, R. Gomer, F. P. Schäfer, and J. P. Toennies (Springer, Berlin, 1982), p. 105.

[38]D. H. E. Dubin and T. M. O'Neil, Phys. Rev. Lett. **60**, 511 (1988).

[39]S. L. Gilbert, J. J. Bollinger, and D. J. Wineland, Phys. Rev. Lett. **60**, 2022 (1988).

Laser Cooling to the Zero-Point Energy of Motion

F. Diedrich,[a] J. C. Bergquist, Wayne M. Itano, and D. J. Wineland
Time and Frequency Division, National Institute of Standards and Technology, Boulder, Colorado 80303
(Received 28 July 1988)

A single trapped $^{198}Hg^+$ ion was cooled by scattering laser radiation that was tuned to the resolved lower motional sideband of the narrow $^2S_{1/2}$-$^2D_{5/2}$ transition. The different absorption strengths on the upper and lower sidebands after cooling indicated that the ion was in the ground state of its confining well approximately 95% of the time.

PACS numbers: 32.80.Pj, 32.30.Jc, 35.10.−d

The subject of laser cooling of ions and neutral atoms is currently of great experimental and theoretical interest.[1] It has been applied to high-resolution spectroscopy, low-energy collisions, quantum jumps, and photon antibunching.[2] In all cooling experiments done so far, the oscillation frequency ω_v of the particle in its confining well was less than the linewidth Γ of the cooling transition. This condition also applies to free-atom experiments, where $\omega_v \rightarrow 0$. The lowest temperatures T have been obtained in recent free-atom experiments,[3,4] where kinetic energies near or below that corresponding to the recoil of a single photon from an atom at rest have been achieved ($T \approx 1$ μK). In this Letter we report, for the first time, laser cooling of a single bound atom in the resolved sideband regime $\Gamma \ll \omega_v$. An ion has been cooled so that it occupies the ground state of its confining potential most of the time.

The idea of laser cooling in the resolved sideband regime is as follows[5]: Let the rest frequency of the atom's cooling transition be ω_0. If the atom oscillates at frequency ω_v in its confining well, the atom's absorption and emission spectrum (as viewed in the laboratory) has resolved components at ω_0 and $\omega_0 \pm m\omega_v$ (m an integer). If we irradiate the atom with narrow-band radiation tuned to the first lower sideband at $\omega_0 - \omega_v$, the atom absorbs photons of frequency $\hbar(\omega_0 - \omega_v)$ and reemits photons of average energy $\hbar\omega_0$. Hence, on the average, each scattered photon reduces the atom's vibrational energy by $\hbar\omega_v$, or reduces the atom's vibrational quantum number n_v by 1. In this way, we can obtain $\langle n_v \rangle \ll 1$ and have the atom most of its time in the ground-state level of its confining potential.[6-8] When $\langle n_v \rangle \ll 1$, T is no longer proportional to $\langle n_v \rangle$ but depends logarithmically[7,8] on $\langle n_v \rangle$. The technique of sideband cooling has previously been applied to cool the magnetron motion of trapped electrons with an rf electronic excitation of the axial motion that was coupled to a cooled resistor.[9] The final temperature in this experiment was limited by thermal excitation and the energy of the magnetron motion corresponded to $\langle n_v \rangle \gg 1$. In the experiments described here, we achieve $\langle n_v \rangle \ll 1$ by optical sideband cooling. For our value of ω_v, T was about 50 μK. However, to the extent that the particle is in the ground state of its confining potential (about 95% of the time here) the fundamental limit of laser cooling for a confined particle has been reached.

Our experiments were performed with a single $^{198}Hg^+$ ion stored in a Paul (rf) trap[10,11] which had $\omega_v/2\pi = 2.96$ MHz (see Fig. 1). In order to optimize the cooling, a two-stage process[8] was used. First, the ion was cooled to near the Doppler cooling limit[1] ($T = \hbar\Gamma/2k_B$, where k_B is the Boltzmann constant) by scattering light of wavelength 194 nm on the strong $^2S_{1/2}$-$^2P_{1/2}$ transition [(*A*) in Fig. 1(a)].[12] At the Doppler cooling limit, $\langle n_v \rangle \approx 12$ ($T \simeq 1.7$ mK) for each degree of freedom.[8] In the next stage of cooling, the 194-nm radiation was turned off and the narrow $^2S_{1/2}$-$^2D_{5/2}$ electric quadrupole transition [(*B*) in Fig. 1 (a)] was driven on the first lower sideband frequency $\omega_0 - \omega_v$. Since the natural lifetime of the $^2D_{5/2}$ state limits the maximum scatter rate to approximately $\frac{1}{2}\Gamma(^2D_{5/2}) \approx 6$ photons/s,[10,13] a cooling time of at least 6 s is required to reach $\langle n_v \rangle \simeq 0$ for all degrees of freedom. This time becomes even longer, or cooling is prevented, if external heating is present. Therefore, in order to enhance the sideband cooling rate, the lifetime of the $^2D_{5/2}$ state was shortened by coupling it to the fast decaying $^2P_{3/2}$ state by 398-nm radiation [(*C*) in Fig. 1(a)]. From the $^2P_{3/2}$ state, the ion has high probability

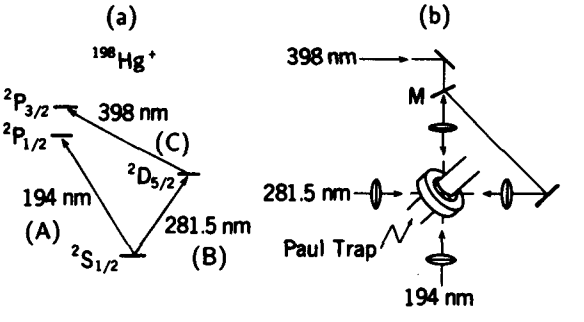

FIG. 1. (a) A simplified energy level scheme of Hg II showing the optical transitions involved in our sideband cooling experiment. (b) The geometrical arrangement of the laser beams. The 194-nm fluorescence is detected normal to the plane of the figure. Mirror *M* reflects 194-nm radiation while transmitting 398-nm radiation.

of rapidly decaying to the ground state. When $\langle n_v \rangle \ll 1$, a quantitative measurement of $\langle n_v \rangle$ from the absorption spectrum becomes very simple. The strength of absorption S_L on the lower sideband is proportional to $\langle n_v \rangle$, while the strength S_U of the upper sideband is proportional to $\langle n_v \rangle + 1$.[8] When $\langle n_v \rangle$ approaches zero, the lower sideband disappears because no more vibrational quanta can be extracted from the ion. If the sideband absorption spectrum is probed with saturating power, the ratio of the strengths of lower to upper sidebands becomes independent of power[14] and directly gives $\langle n_v \rangle$.

To simplify our discussion, we have assumed the trap states and associated wave functions are those of a harmonic potential which is equal to the classical pseudopotential of the rf trap. In the quantum treatment of the rf trap,[15,16] the relevant states are not energy eigenstates because of the time dependence of the potential. However, when the trap drive frequency $\Omega \gg \omega_v$, the atom's optical spectrum and transition matrix elements relevant for cooling closely approximate those for a harmonic potential equal to the classical pseudopotential. The states which represent the cooled ion look like harmonic-oscillator states whose dimensions oscillate with small amplitude at frequency Ω. These states are of the form $\exp[-i\omega_v(n+\frac{1}{2})t]f_n(x,t)$ where the f_n are periodic in time with period $2\pi/\Omega$.[16]

Our trap[10,11] ($r_0 \simeq 466$ μm, $z_0 \simeq 330$ μm) was operated at a trapping field frequency $\Omega/2\pi = 23.189$ MHz. With an rf peak voltage amplitude $V_0 \approx 1.2$ kV and a static potential $U_0 = +71.4$ V applied to the ring electrode, the trap potential was approximately spherical. In order to cool all motional degrees of freedom to near the Doppler cooling limit for the (A) transition, two orthogonal beams of 194-nm radiation, both at an angle of 55° with respect to the trap symmetry (z) axis, were used (Fig. 1). The radiation to drive the (B) transition was derived from a frequency stabilized dye laser ($\lambda = 563$ nm) with a linewidth less than 20 kHz. The output radiation from this narrow-band laser was frequency doubled and focused to as much as 25 W/cm^2 at the position of the ion; this allows strong saturation on the cooling transition. The radiation to drive the (C) transition was derived from a frequency stabilized LD 700 dye laser whose output radiation was frequency doubled and focused to give approximately 1 mW/cm^2 at the position of the ion.

Before the sideband cooling experiment was started, an absorption spectrum of the (B) transition was taken[17] to determine the carrier frequency as well as the sideband frequencies (inset Fig. 2). We made sure that the 282-nm source had equal power at both the upper and lower sideband frequencies. For the sideband cooling and the probing of the absorption spectrum, the following computer-controlled sequence was run repeatedly. First, the 398- and 194-nm radiation were turned on simultaneously for a 20-ms interrogation period. If the 194-nm fluorescence exceeded a preset value during this period, it could be assumed that the ion was laser cooled and cycling between the $^2S_{1/2}$ and the $^2P_{1/2}$ states. This 20-ms interrogation period was repeated until this condition was satisfied. Then the 194-nm radiation was switched off and the 282-nm radiation, tuned to the first lower sideband at $\omega_0 - \omega_v$, was switched on for a cooling time τ_c (typically 200–500 ms). After the 282-nm radiation was switched off, the 398-nm radiation was kept on for a relaxation time τ_r (typically 5 ms) in order to empty the $^2D_{5/2}$ state. After this, the cooled ion was in the electronic ground state and the probing of the absorption spectrum was done as follows: The 282-nm source was switched on at saturating intensity for 10 ms at a frequency corresponding to one point near the upper or lower sideband frequency. After this, the 282-nm beam was switched off and the 194-nm radiation was switched on to see if the ion had made the transition to the $^2D_{5/2}$ state.[11] The result was averaged with the results of previous measurements at the same probe frequency. The frequency of the 282-nm source was stepped to the next value and the cooling and probing cycle was repeated until about 40 cycles for each value of the probe frequency were completed. The results of a typical run are shown in Fig. 2.

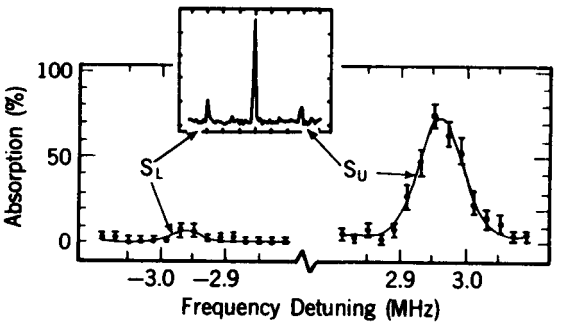

FIG. 2. Absorption spectrum of the $^2S_{1/2}$-$^2D_{5/2}$ electric quadruple transition of $^{198}Hg^+$. The inset spectrum was taken before sideband cooling was applied. It shows the carrier at zero detuning (frequency ω_0) and the first sidebands (at frequencies $\omega_0 - \omega_v$ and $\omega_0 + \omega_v$) generated by the ion's motion in the approximately spherical well. For this spectrum, the bandwidth of the 282-nm radiation was broadened to 120 kHz to reduce the number of required data points and the laser power was reduced in order to avoid saturation. The enlarged part of the figure shows the absorption strength S_L (S_U) on the lower (upper) motional sideband 15 ms after the end of the sideband cooling. Values for S_L and S_U were obtained from Gaussian fits to the data points which are averaged over 41 sweeps.

In order to deduce $\langle n_v \rangle$ for the different motional degrees of freedom, the geometry of our experiment (Fig. 1) has to be considered. The 282-nm beam enters the trap at an angle of 55° with respect to the z axis. The x and y directions were previously determined by the fixed spatial alignment of two simultaneously stored ions,[17] which we take to be along the x axis. From these data, the squares of the projections p_i of unit vectors along the

trap axes onto the 282-nm beam axis are calculated to be $p_x^2 = 0.03$, $p_y^2 = 0.64$, and $p_z^2 = 0.33$. Since we make the differences between the x, y, and z frequencies bigger than $1/\tau_c$, all directions are cooled simultaneously.[8] However, in the analysis, we assume that the probing absorption strength is due only to the ion's motion in the y and z directions. Since the x axis is nearly perpendicular to the 282-nm beam, no meaningful statement abut the energy in this degree of freedom can be made. By neglecting the contribution of the x motion to the sideband strength we overestimate $\langle n_v \rangle$ for the y and z directions. In order to deduce $\langle n_v \rangle$ for the y and z oscillations from our data (Fig. 2), an assumption about the energy distribution between the two directions has to be made. If we assume temperature equilibrium between the y and z degrees of freedom, both contain an energy corresponding to $\langle n_v \rangle = (1 - S_L/S_U)^{-1/2} - 1 = 0.051 \pm 0.012$ quanta. Therefore, for the y and z degrees of freedom, the ion is in the $n_v = 0$ state 95% of the time. The corresponding temperature given by[8] $k_B T = \hbar\omega_v / \ln(1 + 1/\langle n_v \rangle)$ is $T = 47 \pm 3$ μK. For any other energy partition, $\langle n_v \rangle$ and T for one degree of freedom would be less than these values. Independent of the energy distribution, for both degrees of freedom the temperature is much lower than the 194-nm Doppler cooling limit and the ion spends most of its time in the harmonic-oscillator ground-state level.

The theoretical sideband cooling limit[8] gives a value of $\langle n_v \rangle \approx 10^{-6}$. However, since the probing in the experiment is done at saturating power, the measured $\langle n_v \rangle$ corresponds to the energy of the ion at the end of the probing interval, which is typically 15 ms after the end of the sideband cooling, and external heating might have occurred. In order to check for external heating processes, we extended τ_r up to 100 ms and measured S_L/S_U as a function of τ_r. We determined a heating rate (due apparently to pickup of stray noise fields at radio frequencies) of $\langle \dot{n}_v \rangle \approx 6$/s. If we assume the heating is due to thermalization of the ion to room temperature by noise at frequency ω_v, the heating time constant is 95 h.[18] This rate varied slightly with ω_v around $\omega_v = 3$ MHz, but was substantially higher for $\omega_v \lesssim 2.5$ MHz. From these heating data, the measured $\langle n_v \rangle$ is consistent with the theoretical limit at the end of the sideband cooling period. We also measured $\langle n_v \rangle$ for a single degree of freedom directly by changing U_0 to -25 V in order to split the radial and axial sideband frequencies. The 282-nm radiation was tuned so that only the first axial sideband at $\omega_v/2\pi = 4.66$ MHz was cooled and probed. From the results, shown in Fig. 3, we calculate $\langle n_v \rangle = 0.049 \pm 0.045$ at the end of the cooling period, consistent with the theoretical cooling limit. The confinement of the axial motion is given by the spread of the zero-point wave function $z(\text{rms}) \approx 2.4$ nm.

For our data, the uncertainty in the second-order Doppler shift is dominated by the uncertainty in $\langle n_v \rangle$ and

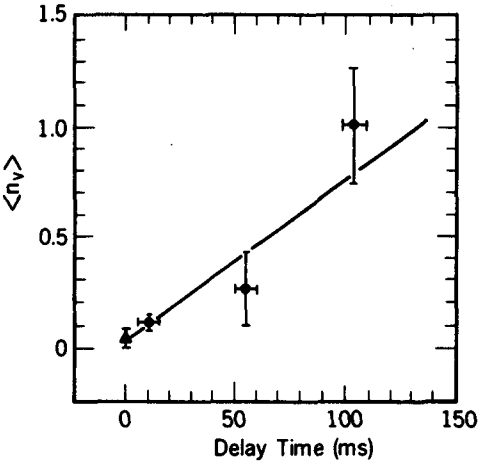

FIG. 3. Vibrational quantum number $\langle n_v \rangle$ for the axial motion ($\omega_v/2\pi = 4.66$ MHz) as a function of time delay between the end of the sideband cooling and probing. A linear extrapolation of the data points (circles) to zero delay time yields $\langle n_v \rangle$ (triangle) consistent with the theoretical expectation.

amounts to $\Delta\nu/\nu < 10^{-20}$ (Ref. 8). It can be made substantially lower by adiabatically lowering the potential well depth after the ion is cooled into the ground state. With our experiment, the absorption of a single quantum of energy at a (tunable) frequency in the MHz range can be detected with an efficiency of nearly 100%. With appropriate coupling to the ion's motion (for example, via one of the endcaps), a similar apparatus could serve as a very sensitive spectrum analyzer. In another possible application, the motion of a trapped charged particle could be damped by coupling it electronically[19] to a second laser-cooled ion in a separate trap, thereby reducing the first charged particle's kinetic energy to near the zero-point energy. Resonant excitation of the first particle's motion could then be detected very sensitively by its influence on the laser-cooled ion. Such a device might be useful in mass spectroscopy.

In summary, we have realized laser cooling in the resolved sideband regime for the first time. The kinetic energy of a trapped atomic ion was reduced to a value where it spent most of its time in the ground-state level of its confining well. To the extent that the ion is in the zero-point energy state of motion, this realizes for the first time the fundamental limit of laser cooling for a bound particle and the ideal of an isolated atomic particle at rest to within the quantum-mechanical limits imposed by the surrounding apparatus.

We acknowledge the support of the U.S. Air Force Office of Scientific Research and the U.S. Office of Naval Research. F. D. thanks the Deutsche Forschungsgemeinschaft for financial support. We thank C. Wieman, J. Bollinger, and J. Helffrich for comments and suggestions on the manuscript. We thank R. Cook and R.

Blümel for helpful discussions on the quantum-mechanical Paul trap.

---

[a]Present address: Max-Planck-Institut für Quantenoptik, Garching, West Germany.

[1]See, for example, S. Stenholm, Rev. Mod. Phys. **58**, 699 (1986); D. J. Wineland and W. M. Itano, Phys. Today **40**, No. 6, 34 (1987), and references therein.

[2]See, for example, *Laser Spectroscopy VII*, edited by T. W. Haench and Y. R. Shen, Springer Series in Optical Sciences Vol. 49 (Springer-Verlag, Berlin, 1987); "Atomic Physics 11," edited by S. Haroche, J. C. Gay, and G. Gynberg (World Scientific, Singapore, to be published).

[3]P. D. Lett, R. N. Watts, C. I. Westbrook, W. D. Phillips, P. L. Gould, and H. J. Metcalf, Phys. Rev. Lett. **61**, 169 (1988).

[4]A. Aspect, E. Arimondo, R. Kaiser, N. Vansteenkiste, and C. Cohen-Tannoudji, Phys. Rev. Lett. **61**, 826 (1988).

[5]D. J. Wineland and H. Dehmelt, Bull. Am. Phys. Soc. **20**, 637 (1975).

[6]W. Neuhauser, M. Hohenstatt, P. Toschek, and H. Dehmelt, Phys. Rev. Lett. **41**, 233 (1978).

[7]D. J. Wineland and W. M. Itano, Phys. Rev. A **20**, 1521 (1979).

[8]D. J. Wineland, W. M. Itano, J. C. Bergquist, and R. G. Hulet, Phys. Rev. A **36**, 2220 (1987).

[9]R. S. Van Dyck, Jr., P. B. Schwinberg, and H. G. Dehmelt, in *New Frontiers in High-Energy Physics*, edited by B. M. Kursunoglu, A. Perlmutter, and L. F. Scott (Plenum, New York, 1978), p. 159.

[10]J. C. Bergquist, D. J. Wineland, W. M. Itano, H. Hemmati, H. U. Daniel, and G. Leuchs, Phys. Rev. Lett. **55**, 1567 (1985).

[11]J. C. Bergquist, W. M. Itano, and D. J. Wineland, Phys. Rev. A **36**, 428 (1987).

[12]H. Hemmati, J. C. Bergquist, and W. M. Itano, Opt. Lett. **8**, 73 (1983).

[13]W. M. Itano, J. C. Bergquist, R. G. Hulet, and D. J. Wineland, Phys. Rev. Lett. **59**, 2732 (1987).

[14]Ref. 8 is in error on this effect of saturation.

[15]R. J. Cook, D. G. Shankland, and A. L. Wells, Phys. Rev. A **31**, 564 (1985).

[16]M. Combescure, Ann. Inst. Henri Poincaré **44**, 293 (1986).

[17]D. J. Wineland, J. C. Bergquist, W. M. Itano, J. J. Bollinger, and C. H. Manney, Phys. Rev. Lett. **59**, 2935 (1987).

[18]The quantity actually measured is the probability, after a time τ_r, of finding the ion in a state with quantum number n_v, where $1 \leq n_v \leq n^* \simeq 10^4$. Strong, discontinuous heating, such as collisions with neutral atoms, would result in $n_v \gg 1$ after each heating event. Hence, a measurement of S_L/S_U vs τ_r would yield a heating rate lower than the actual one. In contrast, a continuous heating process, such as rf noise, would cause $\langle n_v \rangle$ to increase smoothly with time, and the analysis should be valid.

[19]D. J. Wineland and H. G. Dehmelt, J. Appl. Phys. **46**, 919 (1975).

Quantum-limited cooling and detection of radio-frequency oscillations by laser-cooled ions

D. J. Heinzen and D. J. Wineland
Time and Frequency Division, National Institute of Standards and Technology, Boulder, Colorado 80303
(Received 13 March 1990)

A single trapped ion, laser cooled into its quantum ground state of motion, may be used as a very-low-temperature detector of radio-frequency signals applied to the trap end caps. If the signal source is a resonant oscillator of sufficiently high Q, the source may also be placed in its quantum ground state by coupling to the ion. Parametric couplings may be used to cool and detect source modes other than the mode directly coupled to the ion. A theoretical analysis of these cooling and detection processes is presented, and as an example, their application to single trapped electron and proton spectroscopy is examined. Squeezing and low noise detection of one quadrature component of the source oscillation are also discussed. The techniques discussed here may lead to radio-frequency measurements of improved accuracy and sensitivity. Cooling and detection of vibrations of macroscopic oscillators also appear possible.

I. INTRODUCTION

Frequently, measurements depend on the detection of weak signals at radio frequencies. An example to be discussed in this paper is the detection of rf currents in pick-up electrodes induced by charged-particle motion. Weak signals must first be amplified to detectable levels. This amplification may be linear, in which case the fundamental limit to signal detection is set by zero-point fluctuations.[1-5] Alternatively, signals may be amplified by "quantum multiplication," in which an absorbed quantum from the signal-carrying field generates a detectable number of secondary quanta, such as occurs in a photomultiplier tube. In measurements using quantum multiplication,[5-7] there is no fundamental lower limit on noise power. However, the signal acquires shot noise since the absorbed energy is quantized; moreover, phase information is lost.

At radio frequencies, sensitivity at the quantum level cannot be achieved with present techniques. That is, linear rf amplifiers add noise far in excess of the quantum-mechanical minimum;[1-5] also, "quantum multipliers" capable of detecting single rf quanta cannot be constructed with conventional techniques. Essentially, this is due to the smallness of $\hbar\omega/k_B$ (48 μK at $\omega/2\pi=1$ MHz), and to coupling of dissipative elements in the amplifier to thermal reservoirs of temperature $T \gg \hbar\omega/k_B$, which introduces excess thermal noise. Here, $2\pi\hbar$ is Planck's constant, ω is the signal-carrier frequency, and k_B is Boltzmann's constant. The best results have been obtained with a superconducting quantum interference device[8,9] (SQUID) and field-effect-transistor[10,11] (FET) amplifiers, both of which exhibit effective noise temperatures[1-5] $T_{\text{eff}} > 0.1$ K $\gg \hbar\omega/k_B$, that preclude quantum-limited sensitivity.

In order to improve the performance of rf amplifiers, circuit elements with much lower dissipation and noise temperature are required. Such low temperature and dissipation may be achieved in the motion of laser-cooled trapped ions. Recently, a single Hg^+ ion harmonically bound in an rf Paul trap[12,13] has been laser cooled to an extent where it spends most of its time in its zero-point (ground) state of motion.[14] (Although this cooling was demonstrated only for two degrees of freedom of the ion's motion, it can straightforwardly be extended to all three degrees of freedom.) As a by-product of this experiment, single rf quanta absorbed by the ion could be detected with high efficiency. In this paper, we further examine how such a laser-cooled ion can function as a sensitive detector of rf signals applied to the trap electrodes. We examine detection based on both linear amplification and quantum multiplication. For ions which are cooled to temperatures less than $\hbar\omega/k_B$, sensitivity at the quantum level may be achieved.

For such a detector to be useful, the signal source must also have a low noise temperature. Most rf sources do not satisfy this condition, but a source consisting of a resonant oscillator mode of very high Q can be cooled to a very low temperature by coupling to the ion. Examples of such resonant source modes might include modes of a bulk wave resonator such as a piezoelectric crystal, electromagnetic cavity or tuned circuit modes, or an ion confined in another trap. We also show that parametric couplings may be used to cool and detect source modes other than the mode directly coupled to the ion. This may be useful if the desired source mode is not easily coupled out electrically or has a much higher or lower frequency than is convenient to match to the ion's frequency.

Since most rf signals are contaminated by noise far in excess of the quantum-mechanical minimum, we envision the primary applications of these ideas to be the cooling and detection of small excitations of such high-Q oscillators. There are at least two situations in which this is useful. First, the oscillator may be driven by a classical field that is strong (containing many quanta per mode) but couples very weakly to the oscillator. Such couplings might include gravity waves,[15-17] or other weak forces.[16,18] Second, it may be that a precise measurement

of the source oscillator's frequency is desired, and that large amplitudes are undesirable because of anharmonic frequency shifts.

When the source mode is the harmonic oscillation of an ion or ions in a separate trap, this technique of "coupled traps" can provide another means to extend laser cooling to ions which cannot be directly laser cooled. Although sympathetic laser cooling[19] has been successfully applied to ions of the same charge in a Penning trap[19,20] and to small numbers of ions in a Paul trap,[21,22] the coupled trap configuration has the potential advantage that the coupling between different ion species can be easily turned on and off (by changing the resonant mode frequencies) and therefore perturbations between ion species can be avoided.

An interesting application of these ideas may be the cooling and detection of excitations of a single electron or proton (or their antiparticles) confined in an ion trap. We show that these particles can be placed in their quantum-mechanical ground state, and single-quantum excitations to any of the particle's degrees of freedom detected. In addition to the aesthetic appeal of finding such a particle in its ground state, this dramatically reduces perturbations to the particle's frequencies of motion.[23–27] This has important implications for the measurement of the electron g factor,[23,27] electron-positron g-factor ratio[27] and mass ratio,[28] proton-antiproton mass ratio,[29] and mass ratios of other ions.[25,26] In addition, a high-precision determination of the proton g factor (and proton-antiproton g-factor ratio) should be possible with use of this technique; this measurement is very difficult with already proven techniques.

It should also be possible to parametrically drive the ion's motion, resulting in noise-free linear amplification[4] of one of its quadrature amplitudes. Thus, if a signal is present in this quadrature, it can be detected with no added noise. In addition, it should be possible to prepare the laser-cooled ion in a squeezed state[4,30–32] by a nonadiabatic change in the ion trap potential or by a parametric drive. A source consisting of a high-Q oscillator mode may then also be prepared in a squeezed state by coupling to the ion. Thus one of the source mode's quadrature amplitudes may be detected with extremely low noise, limited only by the initial degree of squeezing of the ion.

Because this system is conceptually simple, it could serve as a useful paradigm for quantum measurements. Certain concepts, such as squeezing, can be readily visualized. As a practical matter, we think that these ideas will enable rf measurements to be made with improved accuracy and sensitivity.

This paper is organized as follows. In Sec. II, we begin by discussing signal detection by a single ion, in the simplified case in which the ion trap is driven by a voltage source with added thermal noise. We discuss the detection of a single rf quantum by laser sideband cooling and detection of the ion's motion, and derive expressions for the number of signal-induced and thermally induced quanta. In Sec. III, we extend these results to the case in which the signal source is a high-Q oscillator, showing that cooling and detection at nearly the quantum limit may be achieved by coupling to the ion. Cooling and detection of source modes other than the one directly coupled to the ion via parametric couplings is discussed in Sec. IV. The technique of "coupled-trap spectroscopy," in which the laser-cooled ion is used to cool and detect excitations of a charged particle in a second trap, is introduced in Sec. V. Linear amplification and squeezing of the ion or source oscillator's motion is discussed in Sec. VI. We conclude in Sec. VII.

In Appendices A–C, we further examine the experimental possibilities. A technique for single-quantum detection using Raman transitions is discussed in Appendix A. This technique allows the laser sideband cooling and detection method to be extended to low-mass ions such as $^9Be^+$. This increases the coupling between the source oscillator and the ion, since low-mass ions couple more strongly than high-mass ions. In Appendix B, we analyze an experiment to cool and detect excitations of an electron in a Penning trap with the coupled-trap method. Finally, in Appendix C we examine continuous cooling and the possibility of cooling a mode of a quartz-crystal oscillator.

II. SENSITIVE SIGNAL DETECTION BY A SINGLE ION

We first consider the simplified case in which the ion is driven by a source with purely resistive impedance, as illustrated in Fig. 1. A single ion of charge q_i and mass m_i is confined in a rf trap or Penning trap[12,13,23,27] of end-cap separation d_i. For brevity, we consider the detection of a signal by its influence on the ion's motion along the trap symmetry (z) axis. Similar considerations would apply for detection with motion in the x-y plane using a split-ring electrode. The trapping potential along the z axis is assumed to be harmonic and results in an ion axial oscillation frequency ω_i. We model the source as a voltage source u_s, with dissipation in the source represented by a series resistance R_s at temperature T_s. Associated with the source resistance is a noise voltage source u_{ns}. We also assume that the amplitude and phase of the source u_s is classically well defined, but that the source excites the ion only weakly. This will be a valid assumption if u_s is applied for a very short time or is derived

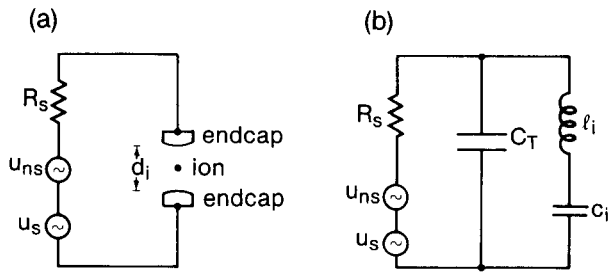

FIG. 1. (a) Single trapped ion driven by a signal source attached to the trap end caps. For simplicity the ring electrode of the ion trap is not shown. (b) Electrical equivalent circuit of the arrangement in (a), where the trapped ion is represented as a series $l_i c_i$ circuit in parallel with the end cap–to–end cap capacitance C_T (Ref. 34).

from a classically strong source which couples very weakly to the ion (due to shielding, for example).

The ion's charge is coupled to the electrical circuit of Fig. 1(a) via the image charges it generates in the end caps. This induced charge is given by[33,34]

$$q_i^{\rm ind}=\frac{\alpha_i q_i z_i}{d_i} , \tag{1}$$

where z_i is the axial displacement of the ion from its equilibrium position, α_i is a geometrical factor of order unity, and we have assumed the rf wavelength is much larger than the trap dimension. (A voltage V applied across the trap end caps generates an electric field $\alpha_i V/d_i$ at the ion. For traps with hyperbolic-shaped electrodes $\alpha_i \simeq 0.8$.[35]) Because the ion is harmonically bound, it can be shown that the ion and its image current are electrically equivalent to a series $l_i c_i$ circuit which shunts the end caps,[34] with

$$l_i=m_i(d_i/\alpha_i q_i)^2 , \tag{2a}$$

$$c_i=(\omega_i^2 l_i)^{-1} . \tag{2b}$$

Additional forces on the ion from the induced charge $q_i^{\rm ind}$ are assumed to be negligible.[34] The circuit of Fig. 1(a) is therefore electrically equivalent to that shown in Fig. 1(b), where C_T is the capacitance between the trap end caps. The effect of the trap capacitance can be neglected if $R_s \ll(\omega_i C_T)^{-1}$; we assume that this is the case in the remainder of this section.

Neglecting the trap capacitance C_T, the circuit of Fig. 1(b) is a driven simple harmonic oscillator, with the resistance R_s and noise source u_{ns} representing the coupling of the circuit to some thermal reservoir. The behavior of such a damped oscillator is described quantum mechanically by[36]

$$\frac{d\hat{a}_i}{dt}=-\left[i\omega_i+\frac{\gamma}{2}\right]\hat{a}_i+\hat{f}_n(t)+f_s(t) , \tag{3a}$$

$$\frac{d\hat{a}_i^{\dagger}}{dt}=\left[i\omega_i-\frac{\gamma}{2}\right]\hat{a}_i^{\dagger}+\hat{f}_n^{\dagger}(t)+f_s^{*}(t) , \tag{3b}$$

where $\hat{a}_i^{\dagger}$ and $\hat{a}_i$ are the creation and annihilation operators for a quantum of oscillation; they are related to the charge $\hat{q}_i^{\rm ind}$ on the capacitor c_i by

$$\hat{q}_i^{\rm ind}=\left[\frac{\hbar}{2\omega_i l_i}\right]^{1/2}(\hat{a}_i^{\dagger}+\hat{a}_i) . \tag{4}$$

Here $\gamma=R_s/l_i$ is the damping rate for the oscillator, and $\hat{f}_n(t)$ and $\hat{f}_n^{\dagger}(t)$ are noise operators, which satisfy[36]

$$\langle\hat{f}_n(t)\rangle=\langle\hat{f}_n^{\dagger}(t)\rangle=0 , \tag{5}$$

$$\langle\hat{f}_n^{\dagger}(t_1)\hat{f}_n(t_2)\rangle=\gamma\bar{n}\delta(t_1-t_2) , \tag{6a}$$

$$\langle\hat{f}_n(t_1)\hat{f}_n^{\dagger}(t_2)\rangle=\gamma(\bar{n}+1)\delta(t_1-t_2) , \tag{6b}$$

where the brackets denote an average over the thermal reservoir states, and

$$\bar{n}=\frac{1}{e^{\hbar\omega_i/k_B T_s}-1} \tag{7}$$

is the number of quanta in the circuit in thermal equilibrium. The effect of the noise voltage source u_{ns} is included via the terms $f_n(t)$ and $f_n^{\dagger}(t)$. The drive is included via the term $f_s(t)$, which is assumed to be classical. For the case of a resonant drive of the form $u_s={\rm Re}(u_{s0}e^{-i\omega_i t})$,

$$f_s=iu_{s0}e^{-i\omega_i t}(8\hbar\omega_i l_i)^{-1/2} .$$

From Eq. (3a), we find that

$$\hat{a}_i(t)=\hat{a}_i(0)e^{-(i\omega_i+\gamma/2)t}+\int_0^t[\hat{f}_n(t_1)+f_s(t_1)]e^{-(i\omega_i+\gamma/2)(t-t_1)}dt_1 , \tag{8}$$

and the corresponding conjugate equation for $\hat{a}^{\dagger}$.

For simplicity, we assume that u_s is a resonant pulse of duration t_m. We find that

$$\hat{a}_i(t_m)=\hat{a}_i(0)e^{-(i\omega_i+\gamma/2)t_m}+\int_0^{t_m}\hat{f}_n(t_1)e^{-(i\omega_i+\gamma/2)(t_m-t_1)}dt_1+\frac{iu_{s0}e^{-i\omega_i t_m}(1-e^{-\gamma t_m/2})}{(2\hbar\omega_i\gamma^2 l_i)^{1/2}} . \tag{9}$$

From Eq. (9) we see that the oscillator's amplitude contains a term proportional to the drive amplitude u_{s0}. This amplitude contribution may be detected directly by a linear parametric amplification technique discussed in Sec. VI.

Alternatively, we may detect the absorbed vibrational quanta. We find that the mean number of quanta $\langle\hat{n}_i\rangle=\langle\hat{a}_i^{\dagger}\hat{a}_i\rangle$ in the circuit at time t_m is given by

$$\langle\hat{n}_i(t_m)\rangle=\langle\hat{n}_i(0)\rangle e^{-\gamma t_m}+\bar{n}(1-e^{-\gamma t_m})+\frac{|u_{s0}|^2}{2\hbar\omega_i\gamma^2 l_i}(1-e^{-\gamma t_m/2})^2 , \tag{10a}$$

where we have neglected possible coherence of the initial state; that is, we assume that $\langle\hat{a}(0)\rangle=\langle\hat{a}^{\dagger}(0)\rangle=0$. The three terms on the right-hand side of Eq. (10a) describe the decay of initial quanta stored in the circuit, the buildup of "blackbody" quanta in the circuit, and the buildup of "signal" quanta. For $t_m \ll\gamma^{-1}$,

$$\langle\hat{n}_i(t_m)\rangle\simeq\langle\hat{n}_i(0)\rangle+\gamma\bar{n}t_m+\frac{|u_{s0}|^2 t_m^2}{8\hbar\omega_i l_i} . \tag{10b}$$

Single-quantum excitations in the circuit representing the ion's motion may be detected via the method outlined in Refs. 14 and 37 and as illustrated in Fig. 2. To summarize the method, we first assume that the ion's internal structure has a ground state $|g\rangle$ which is weakly coupled to an excited state $|w\rangle$, which slowly decays to $|g\rangle$ at a rate γ_w. Also, $|g\rangle$ is strongly coupled to an excited state $|s\rangle$, which rapidly decays to $|g\rangle$ at a rate $\gamma_s \gg\gamma_w$. We assume that $\gamma_w \ll\omega_i$, so that the combined internal-translational quantum states of the ion for levels $|g\rangle$ and $|w\rangle$ consist of well-resolved ladders of states $|g,n_i\rangle$ and $|w,n_i\rangle$, with $n_i=0,1,2,\ldots$. We also assume that $R \ll\hbar\omega_i$, where $R=(\hbar k)^2/2m$ is the recoil energy, with

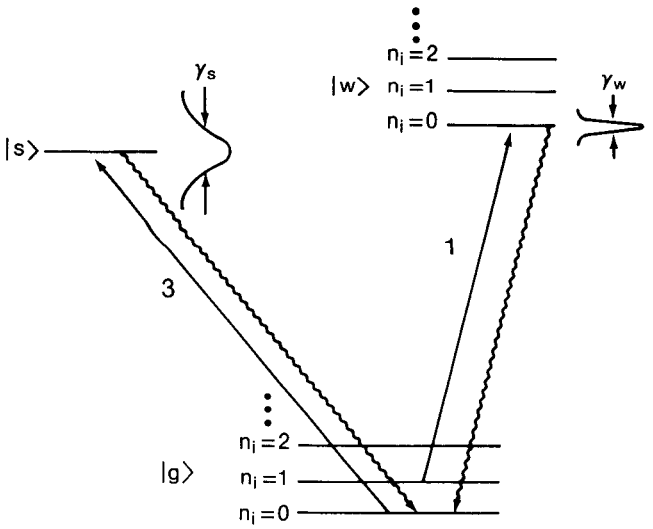

FIG. 2. Sideband cooling and detection of a single trapped ion. The sideband cooling laser (1) is tuned to the first lower sideband of the $|g\rangle \rightarrow |w\rangle$ transition and primarily induces transitions of the type $|g,n_i\rangle \rightarrow |w,n_i-1\rangle$. The detection laser (3) primarily induces transitions of the form $|g,n_i\rangle \rightarrow |s,n_i\rangle$ Observation of the absence of fluorescence from this transition indicates that the ion is in the $|w\rangle$ state. (Dehmelt's electron shelving scheme, Ref. 7.)

k the wave number of the weak transition. The ion is cooled by tuning a laser to the first lower sideband at $\omega_{wg}-\omega_i$, where ω_{wg} is the $|g\rangle \rightarrow |w\rangle$ transition frequency of an atom held at rest. This induces $\Delta n_i=-1$ transitions in the ion, with spontaneous decays back to level $|g\rangle$ occurring predominantly with $\Delta n_i=0$. The ion is therefore optically pumped down the ladder of states until it reaches $n_i=0$ with high probability, at which point it interacts very weakly with the laser.[37-38] A more detailed analysis of the sideband cooling process leads to a limit on $\langle n_i(0)\rangle = f\gamma_w^2/\omega_i^2$, where f is a constant of order unity.[37-38]

Single-quantum excitations from $|g,n_i=0\rangle$ to $|g,n_i=1\rangle$ may be detected by first applying a π pulse[40] of radiation to the $|g,n_i=1\rangle$ to $|w,n_i=0\rangle$ transition. If the ion was initially in the $|g,n_i=1\rangle$ state, it is therefore transferred to the excited state $|w\rangle$, where it remains for a time of order γ_w^{-1}. If it was initially in the $|g,n_i=0\rangle$ state, it remains in the state $|g\rangle$.[14,37] Then a strong pulse of radiation is applied on the $|g\rangle \leftrightarrow |s\rangle$ transition of duration t_d such that $\gamma_s^{-1} \ll t_d \ll \gamma_w^{-1}$. During this time, many photons are scattered and detected if the ion was initially in $|g,n_i=0\rangle$. If it was initially in the state $|g,n_i=1\rangle$, it remains in the state $|w\rangle$ during the time t_d and scatters no photons. High sensitivity of detection of the $|w\rangle$ state is achieved because of the absence of many scattered photons during the time t_D. This is an example of the quantum multiplication provided by "electron shelving" of the ion.[7,41-44] This sideband cooling and detection scheme has recently been demonstrated experimentally.[14] (The work of Ref. 14 differs slightly in that the π pulses on the $|g,n_i=1\rangle$ to $|w,n_i=0\rangle$ transition were not used.)

For this single-quantum detection method to be useful, it is necessary to avoid saturating the detector with thermally induced quanta. Since typically $\bar{n} \gg 1$, this implies that we must have $\gamma t_m < 1/\bar{n} \ll 1$. In this case, the signal-to-background ratio is

$$\left[\frac{S}{B}\right] = \frac{n_s}{\langle \hat{n}_i(0)\rangle + n_{\rm th}} , \tag{11}$$

where $n_s = |u_{s0}|^2 t_m^2/8\hbar\omega_i l_i$ and $n_{\rm th} = \gamma\bar{n}t_m$. The noise will be due to fluctuations (shot noise) in the number of either the signal or background quanta. For example, assume that $\langle \hat{n}_i(0)\rangle$, $n_{\rm th} \ll n_s \ll 1$. Then the noise is dominated by the shot noise of the signal. After N measurement cycles, on the average we detect Nn_s excitations to $n_i=1$, where the rms fluctuations in this number are given by $[Nn_s(1-n_s)]^{1/2} \simeq (Nn_s)^{1/2}$. Therefore the signal-to-noise ratio after N measurements is $(S/N)_N \simeq (Nn_s)^{1/2}$. We note that this shot-noise limitation may be overcome by using the parametric amplification techniques discussed in Sec. VI.

If $n_{\rm th}(t_m)>1$ or $n_s(t_m)>1$, it may be desirable to reduce the interaction time to a time t_m', such that $n_{\rm th}(t_m') \ll 1$ and $n_s(t_m')<1$, although this reduces the ratio $n_s/n_{\rm th}$ by the factor t_m'/t_m. Alternatively, it may be desirable to consider methods to detect final states with $\langle n_i(t_m)\rangle \gg 1$. One method would be to monitor a decrease in fluorescence from the ion due to increased Doppler broadening or to reduced spatial overlap with the exciting laser beam.[24]

Although for simplicity we have considered the ion to be directly driven by a signal source, similar considerations hold when a separate high-Q oscillator is driven by an oscillatory signal and the resulting excitation transferred to the ion for detection, as will be discussed in Sec. III. In this case, the buildup of excitation in the separate oscillator is also described by Eqs. (3)–(10), where γ and $\bar{n}$ now refer to the damping rate and equilibrium number of thermal quanta of the oscillator, and we replace l_i by the oscillator's effective inductance l_s. The oscillating drive need not be electromagnetic; the example of a piezoelectric crystal is discussed in Appendix C. The use of such high-Q oscillators as sensitive detectors of oscillating forces has been discussed in Refs. 15–18.

III. REFRIGERATION AND SENSITIVE DETECTION OF EXCITATION IN A SECOND RESONANT SYSTEM

In this section, we consider a source consisting of a single oscillator mode of sufficiently high Q, such that damping into external reservoirs may be neglected over times of interest. In this case, the source and laser-cooled ion behave simply as a pair of coupled oscillators, and, in the weak damping limit considered here, oscillatory exchange of energy between the two oscillators may be expected. Under these conditions, the ion itself may be used to both cool and detect excitations in the source.

This process may be modeled by the equivalent circuit shown in Fig. 3. As before, l_i and c_i are the effective inductance and capacitance of the trapped ion. The source oscillator may be modeled by a series $l_s c_s$ circuit, with resonant frequency $\omega_s = (l_s c_s)^{-1/2}$. Any parallel source reactance may be included in the capacitance C_T. In gen-

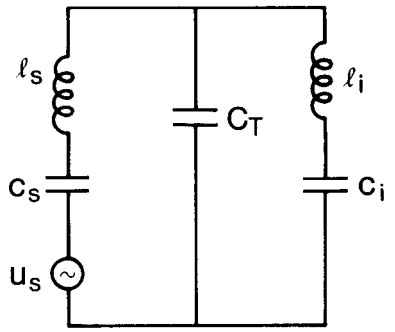

FIG. 3. Equivalent circuit for a single trapped ion coupled to a particular mode of a source oscillator represented by a series $l_s c_s$ circuit.

eral, the source oscillator will in turn be driven by a signal represented here by the voltage source u_s; for the moment, we assume that $u_s=0$.

The Hamiltonian for the circuit of Fig. 3 may be written as

$$H=\hbar\omega_s'(\hat{a}_s^{\dagger}\hat{a}_s+\tfrac{1}{2})+\hbar\omega_i'(\hat{a}_i^{\dagger}\hat{a}_i+\tfrac{1}{2})+(m_i m_s)^{1/2}g^2\hat{x}_s\hat{x}_i \ , \tag{12}$$

where

$$g^2=(l_s l_i C_T^2)^{-1/2} \ , \tag{13}$$

$c_j'=c_j C_T/(c_j+C_T)$, $\omega_j'=(l_j c_j')^{-1/2}$, with $j=s$ or i, and it is assumed that the total charge in the circuit is zero. As usual, we define operators $\hat{p}_j$ and $\hat{x}_j$ in terms of the raising and lowering operators for oscillator j:

$$\hat{x}_j=\left[\frac{\hbar}{2m_j\omega_j'}\right]^{1/2}(\hat{a}_j^{\dagger}+\hat{a}_j) \ , \tag{14a}$$

$$\hat{p}_j=i\left[\frac{\hbar m_j\omega_j'}{2}\right]^{1/2}(\hat{a}_j^{\dagger}-\hat{a}_j) \ . \tag{14b}$$

The "mass" m_j is related to the charge $\hat{q}_j^{\,\mathrm{ind}}$ on the capacitor c_j by $\hat{q}_j^{\,\mathrm{ind}}=(m_j/l_j)^{1/2}\hat{x}_j$. (For an ion's axial oscillation, $m_j\equiv m_i$ is the ion mass.) The Heisenberg equations of motion for $\hat{x}_j$ with the Hamiltonian of Eq. (12) are

$$\frac{d^2\hat{x}_s}{dt^2}+(\omega_s')^2\hat{x}_s=-g^2\left[\frac{m_i}{m_s}\right]^{1/2}\hat{x}_i \ , \tag{15a}$$

$$\frac{d^2\hat{x}_i}{dt^2}+(\omega_i')^2\hat{x}_i=-g^2\left[\frac{m_s}{m_i}\right]^{1/2}\hat{x}_s \ . \tag{15b}$$

The general solution to Eqs. (15) is oscillatory, with frequencies $\omega_{\pm}$ given by

$$\omega_{\pm}^2=\tfrac{1}{2}[(\omega_s')^2+(\omega_i')^2]\pm\tfrac{1}{2}\{[(\omega_s')^2-(\omega_i')^2]^2+4g^4\}^{1/2} \ . \tag{16}$$

We focus here on the case $(|\omega_i'-\omega_s'|\bar{\omega})^{1/2}\ll g\ll\omega_i',\omega_s'$, where $\bar{\omega}=(\omega_++\omega_-)/2\simeq\omega_i'\simeq\omega_s'$. The solutions of Eqs. (15) become

$$\hat{x}_s(t)=\left[\hat{x}_s(0)\cos(\bar{\omega}t)+\frac{\hat{p}_s(0)}{m_s\bar{\omega}}\sin(\bar{\omega}t)\right]\cos(\omega_{\mathrm{ex}}t)+\left[-\hat{x}_i(0)\sin(\bar{\omega}t)+\frac{\hat{p}_i(0)}{m_i\bar{\omega}}\cos(\bar{\omega}t)\right]\times\left[\frac{m_i}{m_s}\right]^{1/2}\sin(\omega_{\mathrm{ex}}t) \ , \tag{17a}$$

$$\hat{x}_i(t)=\left[\hat{x}_i(0)\cos(\bar{\omega}t)+\frac{\hat{p}_i(0)}{m_i\bar{\omega}}\sin(\bar{\omega}t)\right]\cos(\omega_{\mathrm{ex}}t)+\left[-\hat{x}_s(0)\sin(\bar{\omega}t)+\frac{\hat{p}_s(0)}{m_s\bar{\omega}}\cos(\bar{\omega}t)\right]\times\left[\frac{m_s}{m_i}\right]^{1/2}\sin(\omega_{\mathrm{ex}}t) \ , \tag{17b}$$

where

$$\omega_{\mathrm{ex}}=\tfrac{1}{2}(\omega_+-\omega_-)\simeq\frac{\bar{\omega}(c_i'c_s')^{1/2}}{2C_T}\simeq\frac{1}{2\bar{\omega}(l_i l_s)^{1/2}C_T} \ , \tag{18a}$$

and where we define

$$t_{\mathrm{ex}}=\pi/2\omega_{\mathrm{ex}}=\pi\bar{\omega}(l_i l_s)^{1/2}C_T \ . \tag{18b}$$

Equations (17) describe an oscillatory exchange of excitation between the two oscillators. In particular, for time $t\ll t_{\mathrm{ex}}$ we find that

$$\hat{x}_s(t)\simeq\hat{x}_s(0)\cos(\bar{\omega}t)+\frac{\hat{p}_s(0)}{m_s\bar{\omega}}\sin(\bar{\omega}t) \ , \tag{19a}$$

$$\hat{x}_i(t)\simeq\hat{x}_i(0)\cos(\bar{\omega}t)+\frac{\hat{p}_i(0)}{m_i\bar{\omega}}\sin(\bar{\omega}t) \ . \tag{19b}$$

Whereas, for times $|t-t_{\mathrm{ex}}|\ll t_{\mathrm{ex}}$, we find that

$$\hat{x}_s(t)\simeq\left[\frac{m_i}{m_s}\right]^{1/2}\left[\hat{x}_i(0)\cos\left[\bar{\omega}t+\frac{\pi}{2}\right]+\frac{\hat{p}_i(0)}{m_i\bar{\omega}}\sin\left[\bar{\omega}t+\frac{\pi}{2}\right]\right] \ , \tag{20a}$$

$$\hat{x}_i(t)\simeq\left[\frac{m_s}{m_i}\right]^{1/2}\left[\hat{x}_s(0)\cos\left[\bar{\omega}t+\frac{\pi}{2}\right]+\frac{\hat{p}_s(0)}{m_s\bar{\omega}}\sin\left[\bar{\omega}t+\frac{\pi}{2}\right]\right] \ . \tag{20b}$$

At time $t=t_{\mathrm{ex}}$, the $\hat{x}_j$ operators have exactly interchanged values, apart from an amplitude factor and phase shift of $\pi/2$. Further, the $\hat{p}_j$ operators have also interchanged values, apart from an amplitude factor and identical phase shift. It then follows that at time $t\simeq t_{\mathrm{ex}}$, the source and ion oscillators have exactly interchanged wave functions, apart from a phase shift of $\pi/2$. (This may be proved explicitly in the Schrödinger picture.)

This oscillatory exchange between the two oscillators suggests the following scheme for cooling the signal

source, as illustrated in Fig. 4(a). The coupling between the two oscillators may be switched on and off by rapidly (compared with t_{ex}) switching the resonant frequencies of the ion oscillator on or off resonance with the source oscillator. Initially both ion and source are assumed to be hot ($\langle n_s \rangle, \langle n_i \rangle \gg 1$) [Fig. 4(a) (i)]. First, with the oscillators decoupled, the ion is cooled to the zero-point state using sideband cooling [Fig. 4(a) (ii)]. The cooling laser is then turned off, and the ion and source coupling is switched on for a time t_{ex}, at which time the ion's zero-point state has been transferred to the source [Fig. 4(a) (iii)]. Finally, at $t = t_{ex}$ the coupling is switched off, and the ion is again cooled to the zero-point state, leaving both ion and source in the ground state [Fig. 4(a) (iv)]. Because the oscillators may be anharmonic, this may take several such cooling cycles depending on the initial values of $\langle n_s \rangle$ and $\langle n_i \rangle$.

The same idea may be used to detect single-quantum excitations to the source oscillator, as illustrated, in Fig. 4(b). The source and ion are initially cooled into the

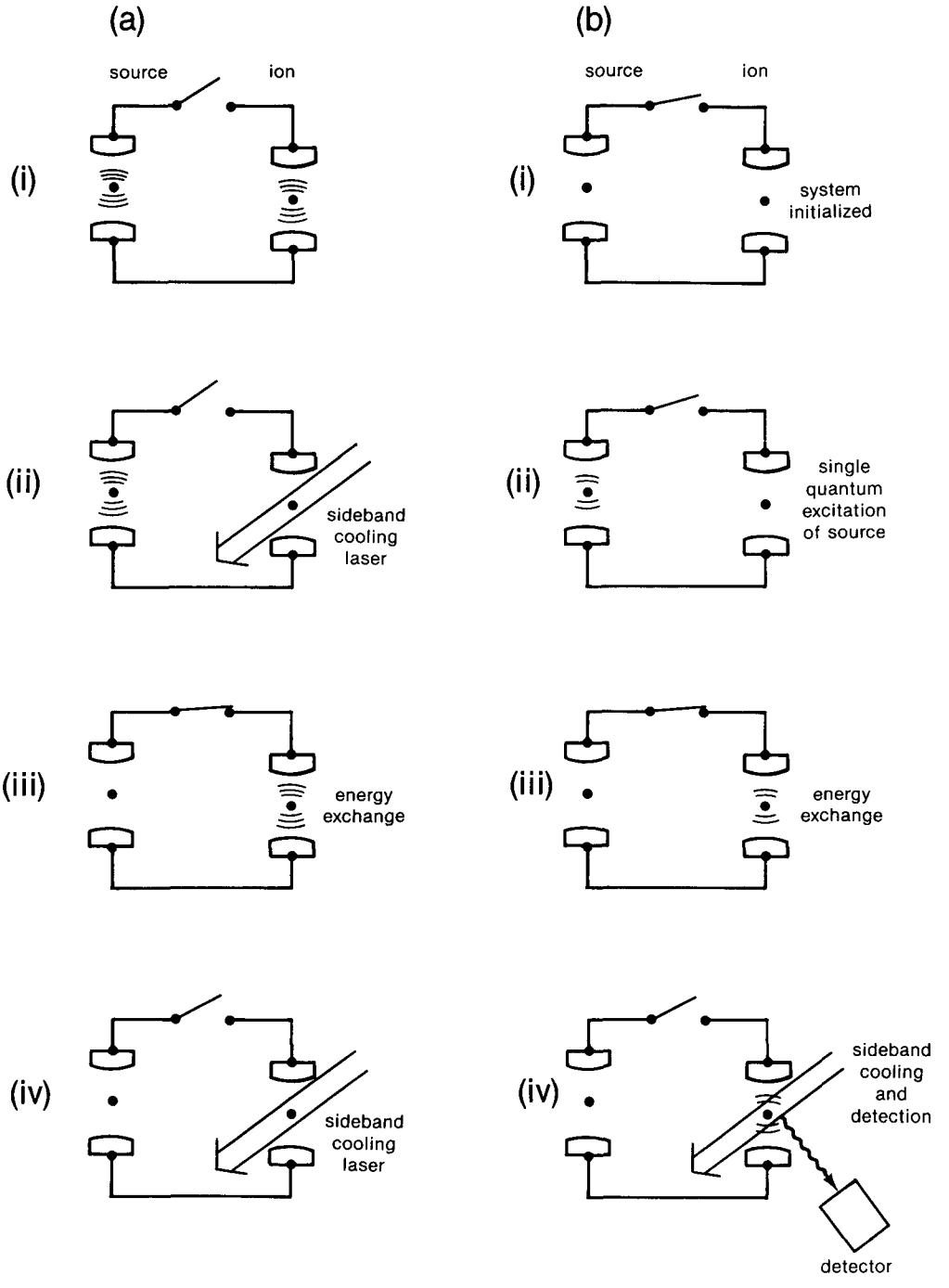

FIG. 4. (a) Cooling of a source to the zero-point state by exchange of energy with an ion which has been laser cooled to the zero-point state. (b) Detecting single-quantum excitations of the source.

zero-point state with the coupling turned off, as in Fig. 4(b) (i). We suppose that the external drive u_s is applied to the source oscillator, which puts at least one quantum of energy into its motion [Fig. 4(b) (ii)]. Then the source and ion are recoupled for a time t_{ex}, resulting in the transfer of the source excitation to the ion [Fig. 4(b) (iii)]. Finally, the excitation of the ion is probed using the sideband method [Fig. 4(b) (iv)].

It should be emphasized that if the signal u_s is continuous and monochromatic, the signal-to-noise ratio is maximized when the source oscillator is driven for times of the order of its relaxation time [see Eqs. (10)]. Then, the source oscillator is contaminated by thermal noise at its equilibrium temperature T_s, and the single-quantum detection technique is not useful. However, this technique should be of advantage whenever the bandwidth of the drive signal is large compared with the source oscillator damping rate. For example, the signal incident on a resonant gravity wave detector may consist of finite duration pulses, rather than a steady drive.[15,16] This technique should also be useful when the signal energy comes from a spin system, which can store only a finite number of quanta (see Sec. V). In each of these cases, the signal-to-noise ratio can be increased by detecting the driven source oscillator's energy against a much lower thermal background.

An additional consideration is that a large source energy may introduce undesirable perturbations to the source. An example, to be discussed further in Sec. V, is the measurement of the cyclotron frequency of a second trapped particle. Most of the important perturbations to the cyclotron frequency, such as anharmonic and relativistic shifts, scale in proportion to the particle energy. Thus, even though a large signal-to-noise ratio is in principle available by applying a large steady drive, the accuracy of the measurement may be degraded by the large energy. The technique described here allows for efficient signal detection at the lowest possible energies, minimizing such perturbations.

The buildup of thermal quanta in an oscillator is described by Eqs. (10). If the present cooling and detection technique is to prove useful, the number of thermally induced quanta $\gamma\bar{n}t_m$ must be less than one, where t_m is the duration of a cooling or measurement cycle. This means that the quality factor $Q=\omega/\gamma$ of the oscillator must satisfy

$$Q>\bar{n}\omega t_m=(kT_s/\hbar)t_m \ , \tag{21}$$

where the equality holds for $kT\gg\hbar\omega$. For example, at $T_s=4.2$ K and $t_m=0.02$ s, we require $Q>10^{10}$. Such high Q's can be achieved in the motion of trapped ions.[12–14] Given the progress that has been made with superconducting cavities and crystal oscillators,[16,17] it may be possible to satisfy inequality (21) for these systems as well. Note that if Q is sufficiently large, the large heat capacity of a macroscopic object such as a crystal oscillator is irrelevant, since only vibrations of a single mode are cooled, not the crystal as a whole.

IV. PARAMETRIC COUPLING OF INTERNAL SOURCE MODES

Parametric coupling of two modes can exchange energy between them with no added noise.[1] Thus the cooling and detection techniques described in the previous section may be extended to other source oscillator modes through parametric couplings. To this end we assume that during a time over which the parametric drive is applied, the Hamiltonian of the source may be written as[1]

$$H=(\hat{a}_1^{\dagger}\hat{a}_1+\tfrac{1}{2})\hbar\omega_1+(\hat{a}_2^{\dagger}\hat{a}_2+\tfrac{1}{2})\hbar\omega_2 +(m_1m_2)^{1/2}g^2\cos(\omega_d t)\hat{x}_1\hat{x}_2 \ , \tag{22}$$

where $\hat{x}_j$ and $\hat{p}_j$ are given by Eqs. (14) with $\omega_j'=\omega_j$, and the third term represents the parametric coupling between two of the source modes, modes 1 and 2, with a frequency ω_d and strength g^2. The parametric drive may be assumed to be classical.[1] It is assumed that the couplings between modes 1 or 2 and all other source modes may be neglected. The Heisenberg equations of motion of $\hat{x}_j$ for the Hamiltonian (22) may be written as

$$\frac{d^2\hat{x}_1}{dt^2}+\omega_1^2\hat{x}_1=-g_1^2\left[\frac{m_2}{m_1}\right]^{1/2}\cos(\omega_d t)\hat{x}_2 \ , \tag{23a}$$

$$\frac{d^2x_2}{dt^2}+\omega_2^2\hat{x}_2=-g_2^2\left[\frac{m_1}{m_2}\right]^{1/2}\cos(\omega_d t)\hat{x}_1 \ , \tag{23b}$$

where, in the present case, $g_1^2=g_2^2=g^2$ (a case where $g_1^2\neq g_2^2$ is treated below). For maximum parametric coupling of the two modes, we require $\omega_d=\omega_1-\omega_2$. Defining new slowly varying operators $\bar{x}_j(t)$ by $\hat{x}_j(t)=\mathrm{Re}[\bar{x}_j(t)e^{i\omega_j t}]$, substituting for $\hat{x}_j$ and ω_d in Eqs. (23), assuming $g\ll\omega_1,\omega_2$, and keeping only secular terms, we find that

$$\frac{d\bar{x}_1}{dt}\simeq\frac{ig_1^2}{4\omega_1}\left[\frac{m_2}{m_1}\right]^{1/2}\bar{x}_2 \ , \tag{24a}$$

$$\frac{d\bar{x}_2}{dt}\simeq\frac{ig_2^2}{4\omega_2}\left[\frac{m_1}{m_2}\right]^{1/2}\bar{x}_1 \ . \tag{24b}$$

Thus noting that $\bar{x}_j(0)=\hat{x}_j(0)-i\hat{p}_j(0)/m_j\omega_j$, we find that the solutions for $\hat{x}_1$ and $\hat{x}_2$ are

$$\hat{x}_1(t)\simeq\left[\hat{x}_1(0)\cos\omega_1 t+\frac{\hat{p}_1(0)}{m_1\omega_1}\sin\omega_1 t\right]\cos\omega_{ex}t +\left[-\hat{x}_2(0)\sin\omega_1 t+\frac{\hat{p}_2(0)}{m_2\omega_2}\cos\omega_1 t\right] \times\left[\frac{m_2\omega_2 g_1^2}{m_1\omega_1 g_2^2}\right]^{1/2}\sin\omega_{ex}t \ , \tag{25a}$$

$$\hat{x}_2(t)\simeq\left[\hat{x}_2(0)\cos\omega_2 t+\frac{\hat{p}_2(0)}{m_2\omega_2}\sin\omega_2 t\right]\cos\omega_{ex}t +\left[-\hat{x}_1(0)\sin\omega_2 t+\frac{\hat{p}_1(0)}{m_1\omega_1}\cos\omega_2 t\right] \times\left[\frac{m_1\omega_1 g_2^2}{m_2\omega_2 g_1^2}\right]^{1/2}\sin\omega_{ex}t \ , \tag{25b}$$

where $\omega_{ex}=g_1g_2/4(\omega_1\omega_2)^{1/2}$.

These equations are essentially the same as Eqs. (17), apart from the factor $(m_i\omega_i/\omega_j\omega_j)^{1/2}$ multiplying the $\sin(\omega_{ex}t)$ terms. Thus the same conclusion may be reached regarding the exchange oscillation: Apart from a phase shift of $\pi/2$, oscillators 1 and 2 exactly exchange wave functions when the drive has been applied for a time $t_{ex}=\pi/2\omega_{ex}$. The factor $(m_i\omega_i/m_j\omega_j)^{1/2}$ normalizes the exchanged wave functions so that the number of quanta are conserved; that is, if $|\psi_1(t=0)\rangle$ has an expansion in terms of the number states of oscillator 1, then $|\psi_2(t=t_{ex})\rangle$ has the same expansion in terms of the number states of oscillator 2, apart from a phase shift.

Equations (25) have important implications for a source coupled to a trapped ion. Suppose that the source is such that only source mode 1 can be efficiently coupled to the ion, but it is desired to measure excitations in source mode 2. Then, according to Eqs. (25), source mode 1 can first be cooled to the $\langle n_1\rangle=0$ state, and this state parametrically transferred to source mode 2, so that $\langle n_2\rangle=0$. We assume that source mode 1 is then recooled to $\langle n_1\rangle=0$. With the parametric drive off, mode 2 may be excited by a signal drive. The excitation in mode 2 may be parametrically transferred to mode 1 and then to the laser-cooled ion for detection. Thus parametric drives may be used to extend the single-quantum detection to source modes other than the one directly coupled to the ion.

V. APPLICATION TO COOLING AND DETECTION OF AN ELECTRON, POSITRON, PROTON, OR ANTIPROTON IN A PENNING TRAP

As an application of the preceding ideas, we consider the measurement of the cyclotron frequency of an electron, a proton or their antiparticles in a Penning trap. The Penning trap consists of a ring electrode and two end-cap electrodes, which to a good approximation produces a potential (in cylindrical coordinates) of the form

$$\phi(\mathbf{r})=\frac{m\omega_z^2}{2q}(z^2-\tfrac{1}{2}r^2)\ , \tag{26}$$

where m, ω_z, and q are the mass, axial frequency, and charge of the trapped particle.[12,13,23,27] Superimposed on the electrostatic potential is a uniform magnetic field $\mathbf{B}=B\hat{z}$, which provides radial confinement of the particle. The Hamiltonian of a single electron in a Penning trap may be written as[23]

$$H_0=(\hat{n}_z+\tfrac{1}{2})\hbar\omega_z+(\hat{n}_c+\tfrac{1}{2})\hbar\omega_c'-(\hat{n}_m+\tfrac{1}{2})\hbar\omega_m+\tfrac{1}{2}\hbar\omega_s\hat{\sigma}_z\ , \tag{27}$$

where $\hat{n}_j=\hat{a}_j^{\dagger}\hat{a}_j$ ($j=z$, c, or m), and

$$\omega_c'=\frac{\omega_c}{2}+\left[\frac{\omega_c^2}{4}-\frac{\omega_z^2}{2}\right]^{1/2}\ , \tag{28a}$$

$$\omega_m=\frac{\omega_c}{2}-\left[\frac{\omega_c^2}{4}-\frac{\omega_z^2}{2}\right]^{1/2}\ . \tag{28b}$$

Here, $\omega_s=(g/2)\omega_c$, with g the electron g factor, $\hat{\sigma}_z$ is the electron's z component of spin, with eigenvalues ±1, and $\omega_c=eB/mc$ is the unperturbed cyclotron frequency of the electron.

The electron has four independent degrees of freedom: an axial oscillation at frequency ω_z, a cyclotron motion (perturbed by the trap electric field) at frequency ω_c', a circular magnetron drift about the z axis at frequency ω_m, and the spin. The magnetron oscillator is inverted, corresponding to the instability of the magnetron motion in the trap.

In terms of the $\hat{a}_j$ and $\hat{a}_j^{\dagger}$, we may also define the operators[45]

$$\hat{z}=\left[\frac{\hbar}{2m\omega_z}\right]^{1/2}(\hat{a}_z^{\dagger}+\hat{a}_z)\ , \tag{29a}$$

$$\hat{p}_z=i\left[\frac{\hbar m\omega_z}{2}\right]^{1/2}(\hat{a}_z^{\dagger}-\hat{a}_z)\ , \tag{29b}$$

$$\hat{\rho}_c=\left[\frac{\hbar}{m\Omega}\right]^{1/2}(\hat{a}_c^{\dagger}+\hat{a}_c)\ , \tag{29c}$$

$$\hat{\pi}_c=i\omega_c'\left[\frac{\hbar m}{\Omega}\right]^{1/2}(\hat{a}_c^{\dagger}-\hat{a}_c)\ , \tag{29d}$$

$$\hat{\rho}_m=\left[\frac{\hbar}{m\Omega}\right]^{1/2}(\hat{a}_m^{\dagger}+\hat{a}_m)\ , \tag{29e}$$

$$\hat{\pi}_m=-i\omega_m\left[\frac{\hbar m}{\Omega}\right]^{1/2}(\hat{a}_m^{\dagger}-\hat{a}_m)\ , \tag{29f}$$

$$\hat{x}=\tfrac{1}{2}(\hat{\rho}_c+\hat{\rho}_m)\ , \tag{29g}$$

$$\hat{y}=\frac{1}{2m}\left[\frac{\hat{\pi}_c}{\omega_c'}+\frac{\hat{\pi}_m}{\omega_m}\right]\ , \tag{29h}$$

where $\Omega=(\omega_c'-\omega_m)/2$.

For reasonable experimental parameters, the electron's cyclotron frequency will lie in the GHz range, while the laser-cooled ion's axial frequency will lie in the MHz range. Therefore the desired cyclotron mode cannot be coupled directly to the ion. In order to cool and detect the electron, we connect the end caps of the electron trap to the end caps of the ion trap and adjust the trap voltages, so that the axial frequency of the electron ω_z equals the axial frequency of the ion ω_i. (We might also consider coupling the electronic axial resonance to the ion's cyclotron resonance by splitting the ion trap's ring electrode.) In this case, the two axial oscillators are equivalent to the circuit of Fig. 3, where $u_s=0$, C_T is the combined capacitance of the two traps in parallel, l_i and c_i are given in Eqs. (2), $l_s=m(d_e/\alpha_e e)^2$, $c_s=(\omega_z^2 l_s)^{-1}$, d_e is the electron end cap separation, and α_e a constant of order unity.[35] Therefore the discussion of Sec. III applies; and it follows that if the ion is prepared in an initial $\langle\hat{n}_i\rangle=0$ state, this state is transferred to the electron's axial oscillation by allowing them to couple freely for a time $t_{ex}=\pi\omega_z(l_s l_i)^{1/2}C_T$. The axial oscillators can be decoupled by rapidly (but adiabatically) changing the ion trap potential, so that $|\omega_i-\omega_z|\gg[\omega_z(l_s l_i)^{1/2}C_T]^{-1}$.

The electron's other two degrees of freedom, the cyclo-

tron and magnetron motion, may each be coupled parametrically to the axial motion in the manner discussed in Sec. IV. This problem has also been considered and demonstrated in the classical regime by Cornell *et al.*[46] We consider an applied field of the form

$$\phi(\mathbf{r})=\frac{E_0}{d}xz\cos\omega_d t \ , \tag{30}$$

with $\mathbf{E}=-\nabla\phi$. Again, the drive may be assumed to be classical.[1] The applied potential gives rise to an additional contribution to the Hamiltonian,

$$H_{\rm int}=\frac{eE_0}{d}\hat{x}\hat{z}\cos\omega_d t \ . \tag{31}$$

The Heisenberg equations of motion of $\hat{\rho}_c$, $\hat{\rho}_m$, and $\hat{z}$ for the total Hamiltonian $H=H_0+H_{\rm int}$ are

$$\frac{d^2\hat{\rho}_c}{dt^2}+(\omega_c')^2\hat{\rho}_c=-\frac{\omega_c' eE_0}{\Omega md}\hat{z}\cos\omega_d t \ , \tag{32a}$$

$$\frac{d^2\hat{\rho}_m}{dt^2}+\omega_m^2\hat{\rho}_m=+\frac{\omega_m eE_0}{\Omega md}\hat{z}\cos\omega_d t \ , \tag{32b}$$

$$\frac{d^2\hat{z}}{dt^2}+\omega_z^2\hat{z}=-\frac{eE_0}{2md}(\hat{\rho}_c+\hat{\rho}_m)\cos\omega_d t \ . \tag{32c}$$

As before, we introduce slowly varying operators by defining $\hat{z}=\mathrm{Re}(\tilde{z}e^{i\omega_z t})$, $\hat{\rho}_c=\mathrm{Re}(\tilde{\rho}_c e^{i\omega_c' t})$, and $\hat{\rho}_m=\mathrm{Re}(\tilde{\rho}_m e^{-i\omega_m t})$. Parametric coupling of the axial and cyclotron motion occurs for $\omega_d=\omega_c'-\omega_z$. Substituting for ω_d, $\hat{z}$, $\hat{\rho}_c$, and $\hat{\rho}_m$ in Eqs. (32), and neglecting nonsecular terms, we find that

$$\frac{d\tilde{\rho}_c}{dt}=\frac{ieE_0}{4m\Omega d}\tilde{z}=\frac{ig_1^2}{4\omega_c'}\tilde{z} \ , \tag{33a}$$

$$\frac{d\tilde{z}}{dt}=\frac{ieE_0}{8m\omega_z d}\tilde{\rho}_c=\frac{ig_2^2}{4\omega_z}\tilde{\rho}_c \ , \tag{33b}$$

$$\frac{d\tilde{\rho}_m}{dt}=0 \ . \tag{33c}$$

Equations (33a) and (33b) are of the form of Eqs. (24), with $\tilde{x}_1\equiv\tilde{\rho}_c$, $\tilde{x}_2\equiv\tilde{z}$, $\omega_1\equiv\omega_c'$, $\omega_2\equiv\omega_z$, $g_1^2=\omega_c' eE_0/\Omega md$, and $g_2^2=eE_0/2md$. Therefore the general solution is of the form of Eqs. (25), where $\hat{p}_1=\hat{\pi}_c$, $\hat{p}_2=\hat{p}_z$, $m_1=m_2=m$, $(\omega_2 g_1^2/\omega_1 g_2^2)^{1/2}=(2\omega_z/\Omega)^{1/2}$, and $\omega_{\rm ex}=(eE_0/4md)(2\Omega\omega_z)^{-1/2}$. Again, the solution is exactly analogous to Eqs. (17), apart from the factor $(2\omega_z/\Omega)^{\pm 1/2}$ multiplying the $\sin\omega_{\rm ex}t$ terms. Thus we find that for $t_{\rm ex}=\pi/2\omega_{ex}$, the axial and cyclotron wave functions have exactly interchanged, apart from a phase shift of $\pi/2$. The factors $(2\omega_z/\Omega)^{\pm 1/2}$ normalize the wave functions, so that the number of quanta are conserved, and so that the exchanged wave functions have the same expansion in a basis of number states, apart from a phase shift.

A drive at $\omega_d=\omega_z+\omega_m$ will couple the axial and magnetron motions. The sum, rather than the difference, of the frequencies appears because of the inversion of the magnetron energy. By again substituting for ω_d, $\hat{\rho}_c$, $\hat{\rho}_m$, and $\hat{z}$ in Eqs. (32) and neglecting nonsecular terms, we get

$$\frac{d\tilde{\rho}_c}{dt}=0 \ . \tag{34a}$$

$$\frac{d\tilde{\rho}_m}{dt}=\frac{ieE_0}{4m\Omega d}\tilde{z}=\frac{ig_1^2}{4\omega_m}\tilde{z} \ , \tag{34b}$$

$$\frac{d\tilde{z}}{dt}=\frac{ieE_0}{8m\omega_z d}\tilde{\rho}_m=\frac{ig_2^2}{4\omega_z}\tilde{\rho}_m \ . \tag{34c}$$

In this case also, Eqs. (34b) and (34c) are of the form of Eqs. (24), with $\tilde{x}_1\equiv\tilde{\rho}_m$, $\tilde{x}_2\equiv\tilde{z}$, $\omega_1\equiv\omega_m$, $\omega_2\equiv\omega_z$, $g_1^2=\omega_m eE_0/\Omega md$, and $g_2^2=eE_0/2md$. The general solution is of the form of Eqs. (25), where $\hat{p}_1=\hat{\pi}_m$, $\hat{p}_2=\hat{p}_z$, $m_1=m_2=m$, $(\omega_2 g_1^2/\omega_1 g_2^2)^{1/2}=(2\omega_z/\Omega)^{1/2}$, $\omega_{\rm ex}=(eE_0/4md)(2\Omega\omega_z)^{-1/2}$, and $\omega_1\equiv-\omega_m$. Again, apart from a phase shift, the axial and magnetron wave functions are exchanged after a time $t_{\rm ex}=\pi/2\omega_{\rm ex}$, with the wave functions normalized so that the number of quanta are conserved.

The electron can be cooled into its $|n_z,n_c,n_m\rangle=|0,0,0\rangle$ ground state, by cooling to $n_z=0$ via coupling to the ion, as illustrated in Fig. 4(a) and by then parametrically driving n_c to zero, recooling to $n_z=0$ again, parametrically driving n_m to zero, and, finally, recooling n_z to zero. Measurements of the electron's cyclotron frequency may be carried out by first applying radiation with a frequency near ω_c' to drive the $|0,0,0\rangle$ to $|0,1,0\rangle$ transition, and then by parametrically exchanging the cyclotron and axial wave functions, as illustrated in Fig. 5. If no transition to the $|0,1,0\rangle$ state occurs after the radiation is applied, the final state of the electron after parametric exchange is $|0,0,0\rangle$; whereas, if a transition to $|0,1,0\rangle$ does occur, the final state of the electron is $|1,0,0\rangle$. The transition may be detected by detecting the presence of a quantum in n_z, by coupling to the ion, as illustrated in Fig. 4(b).

As discussed in Sec. III, the ability to cool and detect single-quantum excitations in this manner does not increase the inherent signal-to-noise ratio of the driven electron, given that a certain amount of damping is present and that a spectrally pure drive is available. Thus

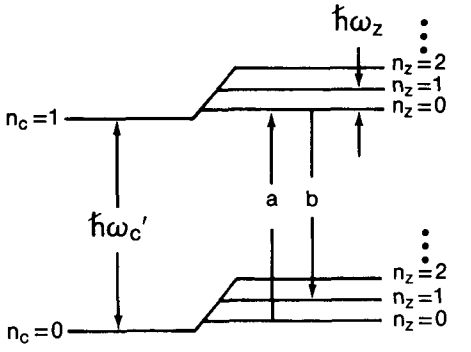

FIG. 5. Lowest electron cyclotron and axial energy levels, illustrating the transfer of a single cyclotron quantum into the axial motion. Only the few lowest cyclotron and axial levels are shown for clarity. (a) $|n_z,n_c\rangle=|0,0\rangle$ to $|0,1\rangle$ transition at ω_c'. (b) $|0,1\rangle$ to $|1,0\rangle$ transition at $\omega_c'-\omega_z$.

one can also achieve an equivalent signal-to-noise ratio by applying a strong continuous drive to the electron's motion, resulting in a large signal power, and by detecting the signal using conventional rf detection.[23] However, this introduces perturbations to the particle's frequencies ω_c', ω_z, and ω_m, making this large signal-to-noise ratio less useful to precision experiments.

For a purely quadratic electric potential and uniform magnetic field, the "true" cyclotron frequency of the particle, in terms of the *measured* frequencies ω_c', ω_z, and ω_m, is given by[23]

$$\omega_c^2=(\omega_c')^2+\omega_z^2+\omega_m^2 \ . \tag{35}$$

This expression remains valid for arbitrary tilt angle of the magnetic field with respect to the trap axis.[23] The most important corrections to Eq. (35) arise from second-order inhomogeneities in the magnetic field, fourth-order corrections to the electric field, and relativistic corrections. (The magnetic- and electric-field inhomogeneities may be parametrized by coefficients B_2 and C_4, respectively.[23]) These corrections are proportional to the particle energies; so accuracy increases as the energies are lowered.

For trapped electron spectroscopy, the B_2 correction has typically been the largest, since a "magnetic bottle" (large B_2) has been deliberately applied for detection purposes.[23,27] However, it should be possible to reduce this, either by use of a "switchable bottle"[47] or by using alternative detection schemes without a magnetic bottle.[48] If such schemes are successful, the most important correction will be the relativistic shift $(\Delta\omega_c/\omega_c)_{\rm rel}=-E_z/2mc^2$, where E_z is the axial energy. (We assume that the cyclotron motion has cooled to $\langle n_c\rangle<1$ by cyclotron radiation, so that relativistic shift due to cyclotron motion may be precisely corrected for, as discussed below.) For $E_z=k_BT$, with $T=4.2$ K, we find that $\Delta\omega/\omega_c=-3.5\times10^{-10}$. Thus electron-positron mass comparisons or g-factor anomaly measurements at or beyond a few parts in 10^{10} will require significantly lower axial temperatures. We note that presently the electron-positron mass ratio has been measured to one part in 10^7,[28] and their anomalies measured to two parts in 10^9.[27]

The character of the systematic corrections changes dramatically when the electron or proton can be cooled to its lowest quantum state. In this case, the resolved quantum level structure of the particle becomes apparent, as was illustrated in Fig. 5, and the perturbations take the form of energy-level shifts.[48] Also, since only single-quantum excitations are observed, the observed resonances will be sharp lines, not broadened by the perturbations. Since the relativistic level structure can be calculated with high precision, the "true" cyclotron frequency can be calculated from the observed level spacings, with well-known corrections taken into account. In fact, this quantum relativistic level structure is of interest in its own right. The relativistic corrections will therefore have essentially no effect on the measurement accuracy in the single-quantum regime.

One of the difficulties associated with mass comparisons[25-28] in the Penning trap is that the magnetic field typically drifts between the loading of one particle and the next. This has limited the accuracy of mass comparisons of atomic ions to a few parts in 10^{10}.[25,26] We envision performing such experiments with a single $^9Be^+$ ion as the detector ion (Appendices A and B). This nearby $^9Be^+$ ion can also serve as a highly accurate magnetometer by measurement of its ground-state electron spin-flip transition frequency, so that such drifts may be corrected for to a high degree. The B_2, C_4, and relativistic corrections are of comparable magnitudes for atomic ions and will limit accuracies to approximately one part in 10^{11} without improved cooling techniques. The present technique provides a means of dramatically lowering these corrections. Mass-ratio comparisons at or beyond a few parts in 10^{12} should be possible.

These techniques may be applied to a measurement of the electron g factor. In this case, the largest systematic effect has been a cavity shift of the cyclotron frequency.[23,49] The uncertainty in this effect could be substantially reduced, however, by choosing electrode shapes which approximate a cylindrical cavity.[49,50] Parameters could be chosen so that this cavity has a lowest-order mode frequency higher than the cyclotron frequency, so that the shift is much smaller and more tractable. The cavity shift effect is less important for the electron-positron g-factor ratio and mass ratio, since it should be the same for both particles. For the mass ratio, the limiting systematic error will most likely be due to an offset of the trap center for the electron compared with that for the positron, due to stray contact potentials. This causes the two particles to see a slightly different magnetic field.[51] We think that the techniques discussed here should allow improved electron-positron mass-ratio and g-factor comparisons. Similar improvements in accuracy should be possible for a direct measurement of the electron g factor, assuming that the cavity shift problem can be adequately addressed.

It should also be possible to make a high-precision measurement of the g factor of the isolated proton or other atomic ions. This measurement has not been carried out using existing techniques of single trapped-particle spectroscopy, because the proton spin and cyclotron magnetic moment are too small to detect the proton-spin flips with magnetic bottle techniques.[23] However, in the technique discussed here, the measurement sensitivity is great enough to detect the spin flips directly, as illustrated in Fig. 6. The proton can be prepared in the $|m_s=+\frac{1}{2},n_c=0\rangle$ state by first preparing it in the $|\pm\frac{1}{2},0\rangle$ state as described earlier, and parametrically driving at $\omega_s-\omega_c'$, where $\omega_s=g_p\mu_NB/\hbar$ is the spin-flip frequency, and μ_N is the nuclear magneton. The proton will either remain in the $|+\frac{1}{2},0\rangle$ state or be driven to the $|+\frac{1}{2},1\rangle$ state. The cyclotron quantum state is exchanged with the axial in an $|n_z=0\rangle$ state, as previously described, leaving the proton in the $|+\frac{1}{2},0\rangle$ state. Spectroscopy of the spin-flip transition at ω_s is carried out by driving the $|+\frac{1}{2},0\rangle\rightarrow|-\frac{1}{2},0\rangle$ transition, followed by a drive at $\omega_s-\omega_c'$, transferring the proton to $|+\frac{1}{2},1\rangle$ if a spin-flip transition occurs, or leaving it in $|+\frac{1}{2},0\rangle$ if a transition does not occur. The cyclotron quantum is then detected

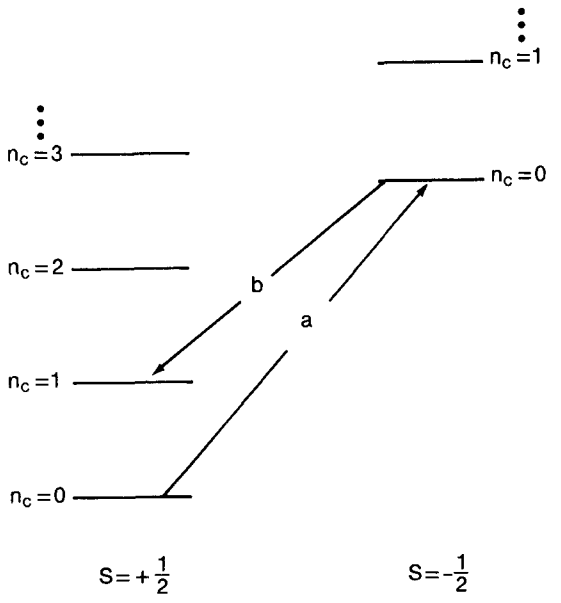

FIG. 6. Lowest proton cyclotron and spin energy levels, illustrating the transfer of proton spin-flip energy into the cyclotron motion. Only the few lowest cyclotron levels are shown for clarity. (a) $|+\frac{1}{2},0\rangle \rightarrow |-\frac{1}{2},0\rangle$ spin-flip transition at ω_s. (b) $|-\frac{1}{2},0\rangle \rightarrow |+\frac{1}{2},1\rangle$ transition at $\omega_s-\omega_c'$.

as described in Fig. 5. In this way, single-quantum spin-flip transitions may be detected and the proton g factor determined by $g_p=2\omega_s/\omega_c$.

The proton g factor enters into the determination of the fundamental constants via the three quantities $g_p/2=\mu_p/\mu_N$, μ_p/μ_B, and m_p/m_e. The two most precisely measured of these quantities determine the third and also appear as auxiliary constants in the least-squares adjustment of the fundamental constants.[52] At present, μ_p/μ_B and m_p/m_e are the most precisely determined, with fractional uncertainties 1×10^{-8} and 2×10^{-8}, respectively.[52] All three of these quantities might be measured with improved accuracy by the techniques discussed here. Also, the proton-antiproton g-factor ratio might be measured with these techniques.

VI. SQUEEZING AND SIGNAL DETECTION BY PARAMETRIC AMPLIFICATION

We have so far described only measurement by quantum multiplication. Linear amplification using a single stored ion is also possible: Degenerate parametric amplification occurs if the ion trap's ring–end-cap voltage is driven at twice the ion's axial resonance frequency.[53] This process can amplify one of the oscillator's two quadrature components with no added noise.[4] The quadrature components $\hat{X}_1$ and $\hat{X}_2$ are defined by[4,30]

$$\hat{a}=(\hat{X}_1+i\hat{X}_2)e^{-i\omega t}\ , \tag{36a}$$

$$\hat{a}^{\dagger}=(\hat{X}_1-i\hat{X}_2)e^{+i\omega t}\ . \tag{36b}$$

In terms of $\hat{X}_1$ and $\hat{X}_2$, the displacement operator $\hat{z}$ may be written as

$$\hat{z}=\left[\frac{2\hbar}{m\omega}\right]^{1/2}(\hat{X}_1\cos\omega t+\hat{X}_2\sin\omega t)\ , \tag{37}$$

so that $\hat{X}_1$ and $\hat{X}_2$ may be identified with the $\cos\omega t$ and $\sin\omega t$ components of the oscillation. $\hat{X}_1$ and $\hat{X}_2$ satisfy the uncertainty relation

$$\Delta\hat{X}_1\Delta\hat{X}_2\geq\tfrac{1}{4}\ , \tag{38}$$

where $\Delta\hat{X}_i\equiv\langle(\Delta\hat{X}_i)^2\rangle^{1/2}$ is the rms fluctuation of $\hat{X}_i$ about its mean. For the vacuum state or for a coherent state, $\Delta\hat{X}_1$ and $\Delta\hat{X}_2$ are equal: $\Delta\hat{X}_1=\Delta\hat{X}_2=\frac{1}{2}$.

Consider the state in which the operators have initial value $\hat{X}_1(t_1)$ and $\hat{X}_2(t_1)$ at time $t=t_1$. Degenerate parametric amplification of this state occurs when an oscillating potential $\mathrm{Re}(Ve^{2i\omega t})$ is applied between the ring and end-cap electrodes of the ion trap, with V a complex constant, $V=|V|e^{i\theta}$. This gives rise to an added potential

$$\phi=\frac{r^2-2z^2}{d_T^2}\mathrm{Re}(Ve^{2i\omega t})\ , \tag{39}$$

where d_T is a characteristic trap dimension. The Hamiltonian describing the axial motion of the ion then becomes

$$H=\hbar\omega(\hat{a}^{\dagger}\hat{a}+\tfrac{1}{2})-\frac{2e\hat{z}^2}{d_T^2}\mathrm{Re}(Ve^{2i\omega t})\ . \tag{40}$$

Neglecting nonsecular terms the Heisenberg equations of motion for $\hat{X}_1$ and $\hat{X}_2$ become

$$\frac{d\hat{X}_1}{dt}=\xi(\hat{X}_2\cos\theta+\hat{X}_1\sin\theta)\ , \tag{41a}$$

$$\frac{d\hat{X}_2}{dt}=\xi(\hat{X}_1\cos\theta-\hat{X}_2\sin\theta)\ , \tag{41b}$$

where $\xi=e|V|/md_T^2\omega$. For $\theta=\pi/2$, Eqs. (41) have the solution

$$\hat{X}_1(t_2)=G^{1/2}\hat{X}_1(t_1)\ , \tag{42a}$$

$$\hat{X}_2(t_2)=G^{-1/2}\hat{X}_2(t_1)\ , \tag{42b}$$

with $G=\exp[2\xi(t_2-t_1)]$. Thus the component $\hat{X}_1$ is amplified by the factor $G^{1/2}$; $\hat{X}_2$ is attenuated by the same factor. Similarly, for $\theta=-\pi/2$, $\hat{X}_2$ is amplified and $\hat{X}_1$ attenuated.

Suppose that a signal X_{1s}, which results from a drive applied from time $t=0$ to t_1, is present in $\hat{X}_1$. We have

$$\hat{X}_1(t_1)=\hat{X}_1(0)+X_{1s}\ . \tag{43}$$

This equation follows from Eq. (8) and the corresponding conjugate equation for $a^{\dagger}(t_1)$, where $X_{1s}=(f_{s0}+f_{s0}^{*})t_1/2$, with $f=f_{s0}e^{-i\omega t}$, and where we assume that $\gamma t_1\ll1$ and that the noise term may be neglected. $\hat{X}_1(t_1)$ may be amplified according to Eqs. (42), giving a signal S and noise N of

$$S=\langle\hat{X}_1(t_2)\rangle^2=GX_{1s}^2\ , \tag{44}$$

$$N=\langle\Delta\hat{X}_1(t_2)^2\rangle=G\langle\Delta\hat{X}_1(0)^2\rangle\ , \tag{45}$$

where we assume that $\langle\hat{X}_1(0)\rangle=0$. For G sufficiently

large, S can be detected with negligible additional noise by monitoring changes in the laser-induced fluorescence of the ion[24] or by detecting the ion's image current with conventional electronics. (For example, in the work of Refs. 26 and 46, the axial amplitudes of single ions are determined with a signal-to-noise ratio greater than unity in a single measurement.) The resulting signal-to-noise ratio S/N is just that of the state before amplification. For an initial vacuum state at $t=0$, $\langle \Delta \hat{X}_1(0)^2 \rangle = \frac{1}{4}$, which gives $S/N = 4X_{1s}^2$.

The fluctuations in the signal quadrature $\hat{X}_1$ may be reduced at the expense of increased fluctuations in quadrature $\hat{X}_2$, by preparing the oscillator in a squeezed state.[4,30] Such a state may be characterized by a wave function (at $t=0$) given by[31]

$$\psi_{sq}(z) = N_{sq} e^{(-1/2)[\beta(m\omega/\hbar)z^2 - 2\beta\delta(2m\omega/\hbar)^{1/2}z]} . \quad (46)$$

Here β is the "squeeze parameter," δ is a coherent amplitude in the $\hat{X}_1$ quadrature and N_{sq} is a normalization factor.

In this state, the variance of $\hat{X}_1$ is decreased by the factor β. Thus the noise is $N_s = 1/4\beta$, and the signal-to-noise ratio $S/N_s = 4\beta X_{1s}^2$, an improvement by the factor β. For $\beta \gg 1$, this implies that a signal energy $\hbar\omega/\beta$, which contains much less than one quantum, may be detected with a signal-to-noise ratio of order unity in a single measurement. Therefore signal detection by degenerate parametric amplification is in principle more sensitive than signal detection by direct measurement of absorbed quanta.

A very direct method of producing the state given by Eq. (46), illustrated in Fig. 7, is to first prepare the ion in the ground state ψ_0' of a well with a different restoring potential $\phi'(z') = m(\omega')^2(z')^2/2q$ $(\omega' > \omega)$ and different origin $\Delta = z - z'$, and then nonadiabatically dropping the potential back to $\phi(z) = m\omega^2 z^2/2q$.[32] This produces the squeezed state

$$\psi_0'(z') = \frac{1}{\pi^{1/4}} e^{(-1/2)(m\omega'/\hbar)(z-\Delta)^2} = \psi_{sq}(z) . \quad (47)$$

This implies that $\beta = \omega'/\omega$, and that $\delta = \Delta(m\omega/2\hbar)^{1/2}$.

A second method of preparing an initially squeezed state is to prepare an initial vacuum state, followed by a parametric drive as in Eqs. (41), with $\theta = -\pi/2$. The variance in the $\hat{X}_1$ quadrature is reduced by a factor G, while that in the $\hat{X}_2$ quadrature is increased by the factor G. The wave function is of the form of Eq. (46) with $\delta = 0$ and $\beta = G$.

Squeezing and detection by degenerate parametric amplification may be extended to source oscillators other than the ion by the methods described in Sec. III. Thus, if the ion is prepared in an initially squeezed state and coupled to a source oscillator as in Fig. 3, after a time t_{ex}, the oscillators have exchanged wave functions; so the source oscillator is prepared in a squeezed state. A signal drive applied to the source generates a source excitation analogous to that described by Eq. (43). The squeezed and driven source oscillator wave function may then be transferred back to the ion, and its $\hat{X}_1$ quadrature amplitude measured by degenerate parametric amplification of the ion's axial motion. In an experiment to measure a very weak force by its excitation of a high-Q oscillator, both quadrature amplitudes may be measured with high sensitivity by using two oscillators, one for each quadrature.[54]

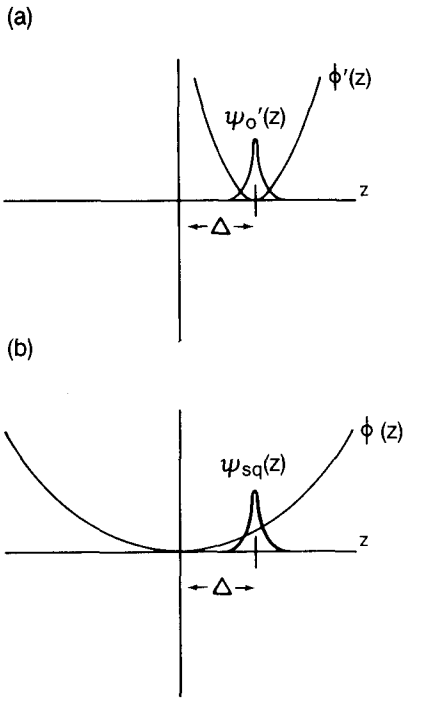

FIG. 7. Preparation of a squeezed state by a nonadiabatic change in the trapping potential. (a) Potential and wave function immediately preceding the potential change where the ion is assumed to be cooled into its ground state of the potential well represented by $\phi'(z)$. (b) Restored potential and squeezed wave function immediately after changing the potential from $\phi'(z)$ to $\phi(z)$.

The buildup of thermal excitation in an oscillator is described by Eq. (9). For $\gamma t_1 \ll 1$, it follows from Eq. (9) and its conjugate that there is a contribution to the variance $\langle \Delta X_1(t_1)^2 \rangle$ of $\gamma(\bar{n} + \frac{1}{2})t_1/2$. Thus, if thermal noise introduced by the coupling of the oscillator to a thermal reservoir is to be negligible, we require $\gamma(\bar{n} + \frac{1}{2})t_1/2 \ll \langle \Delta X_1(0)^2 \rangle = 1/4\beta$. For $\beta = 1$ (no squeezing), this is essentially the same requirement on oscillator Q as the inequality (21); for $\beta > 1$, the oscillator's Q must be still higher by a factor of β.

VII. CONCLUSION

Sensitive detection of signals requires that both signal source and detector exhibit low damping rates, that the source and detector couple efficiently, and that some means is available to cool both source and detector to a temperature of order $\hbar\omega/k_B$. In addition, the detector should provide nearly quantum-limited gain. We have shown that a single laser-cooled trapped ion, coupled to a high-Q source through image currents in the trap electrodes, can provide a realization of such high-sensitivity detection in the rf regime.

Such a detector may have important applications to

precision measurement. We have analyzed one application, the cooling and detection of motions of a second trapped charged particle, and seen that improved accuracy and sensitivity may be expected. These techniques may improve the accuracy of measurements of the electron g factor,[27] electron-positron g-factor ratio,[27] and mass ratio,[28] and can in principle yield the proton g factor and the proton-antiproton mass ratio[29] and g-factor ratio. By extension, these techniques may also find application to measurement of mass or internal degrees of freedom of other atomic or molecular ions. These methods may also prove useful in any experiment requiring very high sensitivity in the rf range or at lower frequencies, such as in gravity wave detection, or detection of very weak forces.[15–18]

Because this kind of experiment is conceptually simple, it may prove useful as a testing ground for topics in quantum measurement theory. For example, studies of squeezed states or quantum limits to signal detection may be carried out this way. The quantum behavior of single trapped particles may also be studied.

An important question is how practical the proposed methods are. This has already been demonstrated to some degree in Ref. 14, and in Appendices A–C we further examine the experimental possibilities. We are currently developing a coupled-trap experiment similar to that described in Appendix B.

ACKNOWLEDGMENTS

We gratefully acknowledge the support of the U.S. Air Force Office of Scientific Research and the Office of Naval Research. We also thank John Bollinger, Wayne Itano, Jim Bergquist, Mark Raizen, Fred Moore, Don McDonald, and John Thomas for comments and suggestions on this manuscript.

APPENDIX A: RAMAN SIDEBAND COOLING AND DETECTION

Most of the experimental techniques discussed in this paper depend on resolved sideband cooling and detection. As described in Sec. II, this requires an ion with the level structure shown in Fig. 2, with easily accessible "weak" ($\gamma_w \ll \omega_z$) and "strong" transitions. Since typically $\omega_z \simeq 1$ MHz, this condition is so far experimentally satisfied only in a few relatively heavy ions, such as Hg^+ (Refs. 14, 32, and 43) or Ba^+ (Refs. 41 and 44) where optical transitions to metastable levels occur. A technique to cool lighter ions is desirable, since this maximizes the coupling between the ion and source.

In this section, we describe how a stimulated Raman transition between two ground-state sublevels (or a ground state and metastable excited state) may serve as the "weak" transition. In this way, sideband cooling may be extended to lighter ions, such as $^9Be^+$, which is the lightest ion which can easily be laser cooled by Doppler cooling.[55,56] Cooling by stimulated Raman transitions has been previously discussed for the case of Ba^+.[57,58]

The general principle of Raman sideband cooling for the axial energy of the ion is illustrated in Fig. 8. We

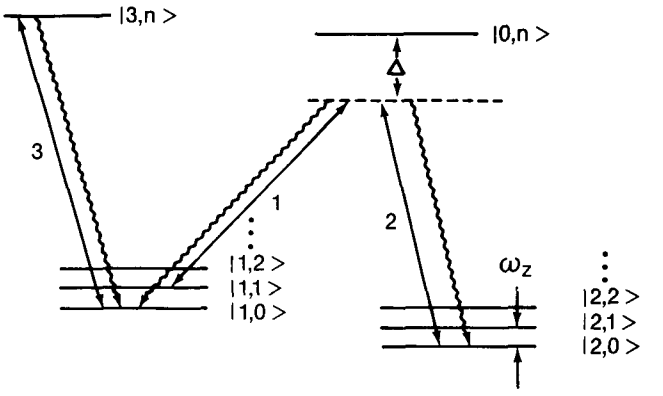

FIG. 8. Energy-level structure for Raman sideband cooling and detection. The Raman cooling transitions are induced by beams 1 and 2; beam 3 is used only for detection of Raman cooling and for Doppler precooling.

consider a four-level system with lower levels $|1\rangle$ and $|2\rangle$ coupled to a common upper level $|0\rangle$. We also assume that level $|1\rangle$ is coupled to an upper level $|3\rangle$, which decays only back to level $|1\rangle$. The $|1\rangle \rightarrow |3\rangle$ transition will serve as the detector of Raman cooling and will also provide Doppler precooling. We denote the combined internal-translational states by $|J,n\rangle$, where J denotes the internal state ($J=0,\ldots,3$) and n the axial harmonic oscillator quantum number. Two classical fields,

$$\mathbf{E}_J = \mathrm{Re}(\mathbf{E}_{0J} e^{i(\mathbf{k}_J \cdot \mathbf{r} - \omega_J t)}), \quad J=1,2 , \tag{A1}$$

couple level $|0\rangle$ to levels $|1\rangle$ and $|2\rangle$, with Rabi frequencies $g_{0J} = |\boldsymbol{\mu}_{0J} \cdot \mathbf{E}_{0J}|/2\hbar$, where $\boldsymbol{\mu}_{0J} = \langle 0|\boldsymbol{\mu}|J\rangle$ is the dipole matrix element between states $|0\rangle$ and $|J\rangle$ ($J=1,2$). The frequencies of the two beams are assumed to be equal to

$$\omega_1 = \omega_{01} - \Delta - \omega_z , \tag{A2a}$$

$$\omega_2 = \omega_{02} - \Delta , \tag{A2b}$$

where ω_{0J} is the transition frequency between states $|0,n\rangle$ and $|J,n\rangle$, and ω_z is the axial oscillation frequency of the ion.

The difference frequency $\omega_1 - \omega_2$ is tuned to the first lower sideband of the $|1\rangle \leftrightarrow |2\rangle$ stimulated Raman transition, inducing primarily $|1,n\rangle \leftrightarrow |2,n-1\rangle$ transitions. For effective cooling, we require that

$$\beta_J = \frac{R_J}{\hbar\omega_z} \ll 1 , \tag{A3}$$

where $R_J = (\hbar k_J)^2/2m$ is the recoil energy for the $|0\rangle \rightarrow |J\rangle$ transition ($J=1,2$). In addition, spontaneous Raman scattering occurs. When $\beta \ll 1$, spontaneous scattering occurs predominantly with $\Delta n = 0$. Thus cooling can occur by means of stimulated Raman transitions $|1,n\rangle \rightarrow |2,n-1\rangle$, followed by spontaneous Raman transitions $|2,n-1\rangle \rightarrow |1,n-1\rangle$.[57] In this case, cooling by stimulated Raman transitions is essentially the same as laser cooling using a narrow optical transition, as illustrated in Fig. 2. In the case of Fig. 2, there is no intermediate level, and the $|J=2\rangle$ level of Fig. 8 is replaced

by the $|w\rangle$ level of Fig. 2. In the case of Fig. 2, the atom is recycled back to the ground state by spontaneous emission $|w\rangle \rightarrow |g\rangle$, rather than by spontaneous Raman transitions $|2,n\rangle \rightarrow |0,n\rangle \rightarrow |1,n\rangle$.

A quantitative description of this cooling process is fairly complex and requires a solution of the density matrix equations for the infinite ladders of states $|J,n\rangle$, $J=0,\ldots,3$; $n=0,\ldots,\infty$. In order for efficient cooling to occur, the atom must make the $|1\rangle \rightarrow |2\rangle$ transition primarily by stimulated Raman scattering, and the $|2\rangle \rightarrow |1\rangle$ transition primarily by spontaneous Raman scattering. One means of accomplishing this with cw excitation is to make $g_{02} \gg g_{01}$.[57] This case has been analyzed by Lindberg and Javanainen,[59] who obtain limiting values of the temperature. In this section, we discuss an alternative method, based on Raman excitation in the transient regime. The analysis of this method is somewhat simpler than the cw case. In addition, this method provides an efficient means of detecting the final temperature.

We first suppose the ion is in the level $|1,n\rangle$, and that both beams are turned on for a time t, where t is sufficiently small that the probability of a spontaneous transition is small. The behavior of the system is adequately described by amplitude equations,

$$\frac{da_{Jn}}{dt} = \frac{-i}{\hbar} \sum_{J',n'} a_{J'n'} e^{i\omega_{JnJ'n'}t} V_{JnJ'n'} - \frac{\gamma_J}{2} a_{Jn} \ . \qquad \text{(A4)}$$

In Eq. (A4), a_{Jn} is the amplitude for the state $|J,n\rangle$, $\hbar\omega_{JnJ'n'}$ is the energy of state $|Jn\rangle$ minus the energy of $|J'n'\rangle$, $V_{JnJ'n'}$ is the matrix element of the perturbation $-\boldsymbol{\mu}\cdot(\mathbf{E}_1+\mathbf{E}_2)$ between states $|J,n\rangle$ and $|J'n'\rangle$, and $\gamma_J=\gamma\delta_{J0}$, where γ is the total spontaneous decay rate of level 0.

If the condition (A3) is satisfied, if $k_J z_0 n^{1/2} \ll 1$, and if

$$|g_{01}| = |g_{02}| \equiv g \ , \qquad \text{(A5a)}$$

$$\Delta \gg \frac{\pi\gamma}{2|\delta k_z| z_0 n^{1/2}} \ , \qquad \text{(A5b)}$$

$$\frac{g^2}{\Delta} \ll \omega_z \ , \qquad \text{(A5c)}$$

then we can show from Eqs. (A4) that for times $t \lesssim 1/\Omega$ only the $|1,n\rangle \leftrightarrow |2,n-1\rangle$ transition is appreciably excited, and that the populations of these two levels are given approximately by

$$P_{1,n} \simeq \cos^2\Omega t \ , \qquad \text{(A6a)}$$

$$P_{2,n-1} \simeq \sin^2\Omega t \ , \qquad \text{(A6b)}$$

where

$$\Omega = \frac{g^2}{\Delta} |\delta k_z| z_0 n^{1/2} \ . \qquad \text{(A7)}$$

Here $\delta k_z = k_{2z} - k_{1z}$ is the difference between the z components of the wave vectors of beams 2 and 1, and $z_0=(\hbar/2m\omega_z)^{1/2}$ is the spread of the zero-point motion of the ion in the axial well. We see that a kind of coherent "Rabi oscillation" between the two lower levels is observed, and that, if the two beams are left on for a time $t_\pi = \pi/2\Omega$, a "Raman π pulse" is obtained, in which the population of level $|1,n\rangle$ is completely transferred to $|2,n-1\rangle$.

The first inequality (A5b) guarantees that the total spontaneous decay probability out of level $|0\rangle$ is small, and the second inequality (A5c) guarantees that the population transferred by stimulated Raman transitions to states other than $|2,n-1\rangle$ state is small. This "Rabi oscillation" is similar to that which has been previously analyzed for a three-level system;[60] our analysis differs in that a minimum of four levels is involved, since the Raman transition proceeds equally through the two excited levels $|0,n\rangle$ and $|0,n-1\rangle$. If $|g_{01}| \neq |g_{02}|$, a coherent population exchange still occurs but with less than 100% efficiency (similar to the three-level case[60]).

The behavior given by Eqs. (A6) indicates that the Raman transition may be used to verify that the ion has been cooled into the state $|1,n\rangle$, with $\langle n\rangle \ll 1$. The two laser beams are pulsed on for a time t_π corresponding to $n=1$. The ion is transferred to the $|2,0\rangle$ state with high probability if it was initially in $|1,1\rangle$; but if it was initially in the state $|1,0\rangle$, it remains there. This behavior is illustrated in Fig. 9, which shows the result of a numerical

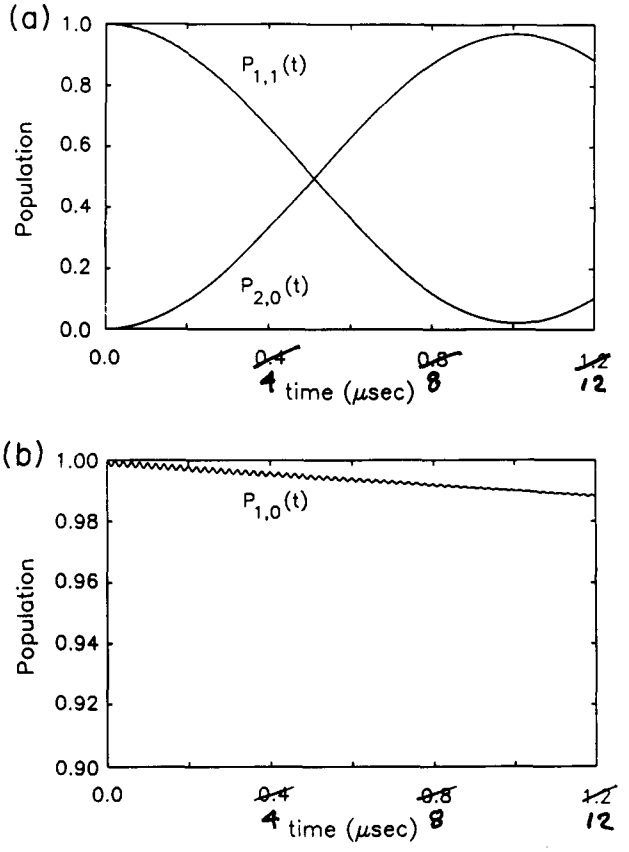

FIG. 9. Level populations for stimulated Raman transitions as functions of time of the states $|J,n\rangle$. Parameters are $|g_{01}|/2\pi = |g_{02}|/2\pi = 40$ MHz, $\Delta/2\pi = 1.5$ GHz, $\omega_z/2\pi = 5$ MHz, and $k_{1z}z_0 = -k_{2z}z_0 = 0.115$. (a) Populations of the $|1,1\rangle$ and $|2,0\rangle$ states, with all population initially in the $|1,1\rangle$ state. (b) Population of the $|1,0\rangle$ state, with all population initially in the $|1,0\rangle$ state.

integration of Eq. (A4). In this simulation, couplings are considered only up to the first order in $k_J z_0 n^{1/2}$, and the basis includes only the $n=0$, 1, and 2 levels of each electronic state. For the parameters indicated in Fig. 9, the $|1,1\rangle \rightarrow |2,0\rangle$ transition is driven with over 97% probability, whereas transitions out of the $|1,0\rangle$ state occur with less than 1% probability. The amplitude equations do not include the repopulation of the ground states due to spontaneous emission from the excited states. For the conditions of Fig. 9, (a) and (b), the integrated decay probability during the time t_π is $(g/\Delta)^2 \gamma t_\pi \approx 0.9\%$. Thus, for the conditions of Fig. 9(b), most of the population loss from the $|1,0\rangle$ state occurs via spontaneous emission, and most of this population returns to the $|1,0\rangle$ state by the end of a cooling cycle, since the probability for the ion to recoil into the $n=1$ state for a single spontaneous scattering event is $\approx \beta \ll 1$ (see discussion below). The presence or absence of the initial $n=1$ quanta may be determined by following the Raman pulse with a pulse of radiation on the $|1\rangle \leftrightarrow |3\rangle$ transition, which here plays the role of the strong transition in a manner analogous to that discussed in Sec. II.

Equations (A6) also suggest one means of cooling the ion. The ion is first precooled by ordinary Doppler cooling[55,56] on the $|1\rangle \rightarrow |3\rangle$ transition to a condition where $\langle n \rangle = n_D = (\gamma_3/\omega_z - 1)/2$.[37] Beams 1 and 2 illuminate the ion, with $|g_{01}| = |g_{02}|$, and beam 1 is chopped on and off, with the initial "on" period adjusted to give a "π pulse" with $n=1$, and the "off" period sufficiently long that the ion returns from state $|2\rangle$ to state $|1\rangle$ by spontaneous Raman scattering with high probability. The ion then is pumped down the ladder of states, losing, on average, approximately one quantum per on-off cycle. (Ramping the pulse length from $t_\pi n_D^{-1/2}$ to t_π would shorten the cooling time.) This may or may not be more efficient than a scheme in which both lasers are left on continuously with $|g_{02}| \gg |g_{01}|$; it has the advantage that the experiment will already be set up in this way for detection purposes, and that the cooling time may readily be estimated. The limiting population of the $n=1$ state will be determined by the probability that an ion in the $|1,0\rangle$ level is promoted into the $|1,1\rangle$ level during one cooling cycle. This can occur by an off-resonant stimulated Raman transition with probability of order $P_{\text{st.R}} = (g^2/\Delta\omega_z)^2$. Also, the ion can reach the $|1,1\rangle$ state by spontaneous Raman transitions, either by directly undergoing the $|1,0\rangle \rightarrow |1,1\rangle$ transition, or by first undergoing the $|1,0\rangle \rightarrow |2,0 \text{ or } 1\rangle$ transition during the beam 1 on period, and then the $|2,0 \text{ or } 1\rangle \rightarrow |1,1\rangle$ transition during the beam 1 off period. Both of these processes occur with a probability of order $P_{\text{sp.R}} = (g/\Delta)^2 \gamma \beta t_\pi$. An ion reaching the $|1,1\rangle$ level returns to the $|1,0\rangle$ level during the following cooling cycle with high probability. Therefore the average population of the $|1,1\rangle$ level is approximately given by the greater of $P_{\text{st.R}}$ or $P_{\text{sp.R}}$. For the example of Fig. 9, $P_{\text{st.R}} = 4.6 \times 10^{-4}$ and $P_{\text{sp.R}} = 3.9 \times 10^{-4}$; so the limiting population of the $n=1$ state is $\sim 10^{-3}$.

In addition to cooling the axial motion, the particle's two transverse degrees of freedom will heat because of recoil. This will not affect the present discussion as long as the transverse motion is not inordinately hot, since the Raman transitions are sensitive only to axial temperature if $\mathbf{k}_1 - \mathbf{k}_2$ is oriented along $\hat{z}$. The transverse temperature may be kept reasonably low by periodic application of Doppler cooling by beam 3, presumably during detection periods. Also, the sideband cooling methods discussed here may easily be extended to the particle's transverse degrees of freedom, so that a very low temperature in three dimensions may be obtained.

The Raman sideband cooling method discussed here may be implemented in the $^9Be^+$ ion.[20] We assume that the $^9Be^+$ ion Zeeman sublevels are split by a strong magnetic field, and that the hyperfine structure may be neglected due to optical pumping[61] into the nuclear spin state $m_I = +\frac{3}{2}$. The levels corresponding to Fig. 8 are

$$|1\rangle \equiv |^2S_{1/2}, m_J = +\tfrac{1}{2}\rangle ,$$

$$|2\rangle \equiv |^2S_{1/2}, m_J = -\tfrac{1}{2}\rangle ,$$

$$|0\rangle \equiv |^2P_{3/2}, m_J = +\tfrac{1}{2}\rangle ,$$

$$|3\rangle \equiv |^2P_{3/2}, m_J = +\tfrac{3}{2}\rangle .$$

The parameters given in Fig. 9 are representative of those which may be obtained with $^9Be^+$ in a Penning trap with a large magnetic field ~ 6 T. For these conditions, $n_D = 2.4$; so only a few Raman cooling cycles are necessary to obtain $\langle n \rangle \ll 1$.

APPENDIX B: EXAMPLE DESIGN PARAMETERS FOR A COUPLED-TRAP EXPERIMENT

In this section we discuss the design of an experiment to cool and detect excitations of an electron in a Penning trap. We assume that a $^9Be^+$ ion is cooled and detected by the Raman sideband method discussed in Appendix A. The electron is assumed to be confined in a Penning trap of end-cap separation d_e, and the ion in a second Penning trap of end-cap separation d_i. We assume that the two traps are arranged in a coaxial fashion, as illustrated in Fig. 10, with a common central end-cap elec-

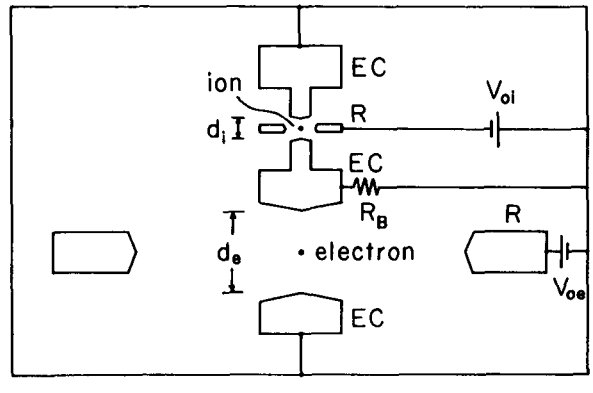

FIG. 10. Coupled-trap experiment: End-cap electrode (*EC*) and ring electrode (*R*). The central end cap is common to the two traps and is connected to the shield by resistor R_B. The trap electrodes and shield (outer boundary) are drawn to scale, with $d_e = 0.4$ cm, and are assumed to have cylindrical symmetry.

trode, and with the two remaining end-cap electrodes connected to an outer conducting shield. The central electrode may be connected to the shield potential via a large resistor and small shunt capacitance, without introducing significant thermal noise or excess capacitance. Potential differences of V_{0e} and V_{0i} are applied between the shield and the electron trap and ion trap ring electrodes, respectively.

We have evaluated the trap design in Fig. 10 numerically, using a modified version of the computer code POISSON.[62] Figure 10 is drawn to scale, and we assume that $d_e=0.4$ cm ($d_i=0.1$ cm). We assume that the trap capacitance C_T is given by its upper limit, which is simply the sum of the capacitances of the central end-cap electrode to all other electrodes and to the shield. We find that

$$C_T \simeq 0.30 \text{ pF} , \tag{B1}$$

$$l_e = m_e(d_e/\alpha_e e)^2 = 905 \text{ H} , \tag{B2}$$

$$l_i = m_i(d_i/\alpha_i e)^2 = 9.86\times 10^5 \text{ H} , \tag{B3}$$

where we calculate that $\alpha_e=0.793$, and $\alpha_i=0.772$. If the traps are placed in a magnetic field of 6 T, then the $^9Be^+$ cyclotron frequency ν_c is 10.2 MHz, and the maximum axial frequency is $\nu_z(\max)=\nu_c/2^{1/2}=7.23$ MHz. We assume that $\nu_z=5$ MHz, which then gives

$$t_{ex} = 2\pi^2 \nu_z (l_e l_i)^{1/2} C_T = 0.88 \text{ s} , \tag{B4}$$

Finally, we calculate that the axial potentials of the two traps are given by

$$V_e(z_e) = 0.563(z_e/d_e)^2 V_{0e} , \tag{B5}$$

$$V_i(z_i) = 1.82(z_i/d_i)^2 V_{0i} , \tag{B6}$$

where z_e and z_i are the electron's and ion's axial displacements from the center of their traps. This implies that an axial oscillation frequency of $\nu_z=5$ MHz is obtained in each trap for $V_{0e}=79.8$ mV, and $V_{0i}=25.5$ V.

The time t_{ex} must be shorter than the time for absorption of one thermal quantum of energy on the axial motion of either the ion or the electron. This seems feasible, since a heating rate of approximately six quanta/s was obtained in the Hg^+ experiments,[14] and this may presumably be improved upon. For single-quantum excitation and detection of the electron's other degrees of freedom, the excitation of that degree of freedom and transfer into the axial motion must be shorter than the time for single-quantum excitation on that degree of freedom due to thermal radiation. The traps must be harmonic and tuned into resonance with each other to an accuracy better than $\Delta\nu_z \simeq 1/2t_{ex}=0.57$ Hz, or a relative accuracy better than 1.1×10^{-7}. This may be difficult but also seems feasible.

APPENDIX C: CONTINUOUS REFRIGERATION

The previous discussions have concentrated on cooling the source modes to the zero-point energy. For some applications, this degree of cooling may not be required and a more modest form of the basic scheme can be employed.

As an example, consider that a cloud of N trapped ions which is laser cooled is used as a refrigerator. For simplicity, we assume that the cooling transition's radiative decay rate γ is larger than the ion's motional frequencies; that is, we are in the Doppler-cooling regime.[55,56] We will consider, as before, the axial motion of the ions, but similar arguments apply to the other degrees of freedom. For this case, Fig. 11 applies where we can determine R_N from the following argument. Near the Doppler-cooling limit, the cooling rate is approximately [see, for example, Eq. (10) of Ref. 39]

$$\frac{dE_z}{dt} = \frac{I\sigma_0}{\hbar\omega_L} R \left[-\frac{2E_z}{\hbar\gamma} + 1 \right] , \tag{C1}$$

where I is the laser beam intensity on the ions, σ_0 is the resonant scattering cross section, ω_L is the laser frequency, E_z is the total axial energy, and I is assumed to be below saturation. We assume that the recoil energy R is such that $R \ll \hbar\gamma$, and that the laser is tuned to $\omega_0-\omega_L \simeq \gamma/2$ for minimum temperature, where ω_0 is the rest frequency of the cooling transition. Equation (C1) applies as long as the Doppler width of the cooling transition is less than the natural width γ. Equation (C1) can be rewritten

$$\frac{d}{dt}(E_z - \hbar\gamma/2) = -\dot{N}_s \frac{2R}{\hbar\gamma}(E_z - \hbar\gamma/2) , \tag{C2}$$

where $\dot{N}_s = I\sigma_0/\hbar\omega_L$ is the resonant scatter rate. ($\dot{N}_s < \gamma$ by the assumption that the laser intensity is below saturation.) The energy decay rate for the equivalent circuit in the left-hand side of Fig. 11 is equal to R_N/l_N; so we make the identification that laser cooling can be represented by a resistor R_N at temperature T_N, where

$$R_N = l_N \dot{N}_s R/(\hbar\gamma/2) , \tag{C3}$$

and where[34] $l_N = l_i/N$, l_i is given in Eq. (2a), and

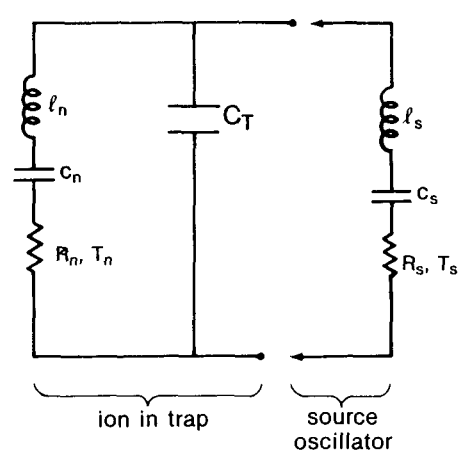

FIG. 11. Use of a cloud of N ions ($l_n=l_i/N$) as a continuous refrigerator to cool a source mode represented by a series $L_sC_sR_s$ circuit The resulting source "temperature" T_s^* is assumed to be given by $\langle i_s^2\rangle l_s/k_B$, where i_s is the total rms current in the inductor l_s.

$T_N=\hbar\gamma/2k_B$ is the Doppler-cooling limit.[55,56] For laser-cooled Be^+ ions as the refrigerator, $\gamma/2\pi=19.4$ MHz assuming laser cooling on the 313-nm first resonance line. Then $R_N\simeq 2.2\times 10^4[\dot{N}_s(s^{-1})/N]\ \Omega$. Since $\dot{N}_s$ can be as high as approximately 10^8/s, extremely large values of resistance at the Doppler-cooling-limit temperature [$T_N(Be^+)\simeq 0.5$ mK] can be obtained.

The main problem in achieving strong damping of source modes is the shunting effect of the trap capacitance C_T. This is not a problem as long as the coupling of the source oscillator mode to external heat sources is weak ($R_s\rightarrow 0$), in which case the source mode comes to the temperature T_N of the cooled ion. This would be a good approximation in the example where the axial motion of an electron is cooled by the axial motion of an ion (Appendix B). In principle, the shunting effects of the trap capacitance can be eliminated by using an inductor in parallel with the trap capacitance. This might be used to advantage in some cases, but the heating effects due to losses in this inductor may outweigh the benefits of the capacitance cancellation.

The refrigerator ions can also be used to cool a mode of a macroscopic oscillator such as a quartz crystal. The equivalent circuit of a quartz-crystal resonator is essentially the same as that of ions in the trap; that is, a series $L_QR_QC_Q$ circuit in parallel with electrode capacitance C_0. To get an idea of the degree of cooling that could be obtained, assume[63] that $L_Q=19.5$ H, $R_Q=65\ \Omega$, $(L_QC_Q)^{-1/2}=2\pi\times 2.5$ MHz, $Q\simeq 5\times 10^6$, and $C_0\simeq 4$ pF. Assuming the same Be^+ trap conditions as in Appendix B, we require $N\simeq l_i/L_Q\simeq 50\,000$ to make $l_N\simeq l_Q$. C_T is in parallel with the much larger quartz-resonator electrode capacitance C_0. Therefore $C_T\rightarrow C_0$ in Fig. 11. Adjusting the laser cooling to make $R_N=1/\omega C_T$, we numerically evaluate the energy in the source mode $\langle i_s^2\rangle L_s$ to be equivalent to a temperature $\langle i_s^2\rangle L_s/k_B\simeq 35$ mK, where we have assumed that $T_s=4.2$ K. Since crystals with much higher Q's (lower values of R_Q) might be obtained, perhaps much lower values of temperature might eventually be reached. For example, Ref. 64 reports a 1-MHz crystal with a Q of 4×10^9 at a temperature of 2 K. If this same Q could be obtained on our example crystal, then $R_s\rightarrow 0.08\ \Omega$, and $\langle i_s^2\rangle L_s/k_B=0.54\ \text{mK}\simeq T_N$.

By use of suitable mechanical transducers and/or of intermediate transfer oscillators, such as quartz crystals, macroscopic oscillators of much larger mass, such as gravitational antennas, may possibly be cooled. Detection of energy changes in these macroscopic resonators can then be detected by the reaction back on the ions as described previously.

[1]W. H. Louisell, A. Yariv, and A. E. Siegman, Phys. Rev. **124**, 1646 (1961).

[2]H. Heffner, Proc. IRE **50**, 1604 (1962).

[3]H. A. Haus and J. A. Mullen, Phys. Rev. **128**, 2407 (1962).

[4]C. M. Caves, Phys. Rev. D **26**, 1817 (1982).

[5]J. Weber, Rev. Mod. Phys. **31**, 681 (1959).

[6]N. Bloembergen, Phys. Rev. Lett. **2**, 84 (1959).

[7]H. Dehmelt, Bull. Am. Phys. Soc. **20**, 60 (1975).

[8]C. Hilbert and J. Clarke, J. Low Temp. Phys. **61**, 263 (1985); M. R. Freeman, R. S. Germain, R. C. Richardson, M. L. Roukes, W. J. Gallagher, and M. B. Ketchen, Appl. Phys. Lett. **48**, 300 (1986).

[9]R. M. Weisskoff, G. P. Lafyatis, K. R. Boyce, E. A. Cornell, R. W. Flanagan, Jr., and D. E. Pritchard, J. Appl. Phys. **63**, 4599 (1988).

[10]M. F. Bocko, Rev. Sci. Instrum. **55**, 256 (1984).

[11]S. R. Jefferts and F. L. Walls, Rev. Sci. Instrum. **60**, 1194 (1989).

[12]H. G. Dehmelt, Adv. At. Mol. Phys. **3**, 53 (1967); **5**, 109 (1969).

[13]D. J. Wineland, Wayne M. Itano, and R. S. VanDyck, Jr., Adv. At. Mol. Phys. **19**, 135 (1983).

[14]F. Diedrich, J. C. Bergquist, Wayne M. Itano, and D. J. Wineland, Phys. Rev. Lett. **62**, 403 (1989).

[15]E. Amaldi and G. Pizzela, in *Relativity, Quanta and Cosmology,* edited by M. Pantaleo and R. De Finis (Johnson Reprint Corp., New York, 1979), Vol. 1, p. 9.

[16]V. B. Braginsky and A. B. Manukin, in *Measurements of Weak Forces in Physics Experiments,* edited by David H. Douglas (University of Chicago Press, Chicago, 1977).

[17]V. B. Braginsky, V. P. Mitrofanov, and V. I. Panov, *Systems with Small Dissipation,* translated by Erast Gliner (University of Chicago Press, Chicago, 1986).

[18]J. E. Moody and F. Wilczek, Phys. Rev. D **30**, 130 (1984).

[19]D. J. Larson, J. C. Bergquist, J. J. Bollinger, Wayne M. Itano, and D. J. Wineland, Phys. Rev. Lett. **57**, 70 (1986).

[20]J. J. Bollinger, D. J. Heinzen, Wayne M. Itano, S. L. Gilbert, and D. J. Wineland, Phys. Rev. Lett. **63**, 1031 (1989).

[21]F. Diedrich (private communication).

[22]D. J. Wineland, Wayne M. Itano, J. C. Bergquist, S. L. Gilbert, J. J. Bollinger, and F. Ascarrunz, in *Non-Neutral Plasma Physics,* Proceedings of the Symposium on Non-Neutral Plasma Physics held at the National Academy of Sciences, 1988, Conf. Proc. No. 175, edited by C. W. Roberson and C. F. Driscoll (AIP, New York, 1988), p. 93.

[23]L. S. Brown and G. Gabrielse, Rev. Mod. Phys. **58**, 233 (1986).

[24]D. J. Wineland, J. J. Bollinger, and Wayne M. Itano, Phys. Rev. Lett. **50**, 628 (1983).

[25]R. S. VanDyck, Jr., F. L. Moore, D. L. Farnham, and P. B. Schwinberg, in *Frequency Standards and Metrology, Proceedings of the Fourth Symposium,* Ancona, Italy, 1988, edited by A. DeMarchi (Springer-Verlag, Berlin, 1989), p. 349.

[26]E. A. Cornell, R. M. Weisskoff, K. R. Boyce, R. W. Flanagan, Jr., G. P. Lafyatis, and D. E. Pritchard, Phys. Rev. Lett. **63**, 1674 (1989).

[27]R. S. Van Dyck, Jr., P. B. Schwinberg, and H. G. Dehmelt, in *New Frontiers in High-Energy Physics,* edited by B. M. Kursunoglu, A. Perlmutter, and L. F. Scott (Plenum, New York, 1978), p. 159; R. S. Van Dyck, Jr., P. B. Schwinberg, and H. G. Dehmelt, Phys. Rev. Lett. **59**, 26 (1987).

[28]P. B. Schwinberg, R. S. VanDyck, Jr., and H. G. Dehmelt, Phys. Lett. **81A**, 119 (1981).

[29]G. Gabrielse, X. Fei, L. A. Orozco, R. L. Tjoelker, J. Haas, H. Kalinowsky, T. A. Trainor, and W. Kells, Phys. Rev. Lett. **63**, 1360 (1989).

[30]D. F. Walls, Nature **306**, 141 (1983), and references therein.

[31]I. Fujiwara and K. Miyoshi, Prog. Theor. Phys. **64**, 715 (1980); W. Schleich and J. A. Wheeler, J. Opt. Soc. Am. B **4**, 1715 (1987).

[32]J. C. Bergquist, F. Diedrich, Wayne M. Itano, and D. J. Wineland, in *Laser Spectroscopy IX*, edited by M. S. Feld, J. E. Thomas, and A. Mooradian (Academic, San Diego, 1989), p. 274.

[33]W. Shockley, J. Appl. Phys. **9**, 635 (1938).

[34]D. J. Wineland and H. G. Dehmelt, J. Appl. Phys. **46**, 919 (1975).

[35]M. A. Philip, F. Gelbard, and S. Arnold, J. Coll. Int. Sci. **91**, 507 (1983); G. Gabrielse, Phys. Rev. A **29**, 462 (1984); E. C. Beaty, Phys. Rev. A **33**, 3645 (1986).

[36]M. Lax, Phys. Rev. **145**, 110 (1966).

[37]D. J. Wineland, Wayne M. Itano, J. C. Bergquist, and R. G. Hulet, Phys. Rev. A **36**, 2220 (1987).

[38]W. Neuhauser, M. Hohenstatt, P. Toschek, and H. Dehmelt, Phys. Rev. Lett. **41**, 233 (1978).

[39]D. J. Wineland and Wayne M. Itano, Phys. Rev. A **20**, 1521 (1979).

[40]L. Allen and J. H. Eberly, *Optical Resonance and Two-Level Atoms* (Wiley, New York, 1975), Sec. 3.2.

[41]W. Nagourney, J. Sandberg, and H. Dehmelt, Phys. Rev. Lett. **56**, 2797 (1986).

[42]D. J. Wineland, J. C. Bergquist, Wayne M. Itano, and R. E. Drullinger, Opt. Lett. **5**, 245 (1980).

[43]J. C. Bergquist, Randall G. Hulet, Wayne M. Itano, and D. J. Wineland, Phys. Rev. Lett. **57**, 1699 (1986).

[44]Th. Sauter, W. Neuhauser, R. Blatt, and P. E. Toschek, Phys. Rev. Lett. **57**, 1696 (1986).

[45]Wayne M. Itano and D. J. Wineland, Phys. Rev. A **25**, 35 (1982).

[46]E. A. Cornell, R. M. Weisskoff, K. R. Boyce, and D. E. Pritchard, Phys. Rev. A **41**, 312 (1990).

[47]R. S. Van Dyck, Jr., F. L. Moore, D. L. Farnham, and P. B. Schwinberg, Rev. Sci. Instrum. **57**, 593 (1986).

[48]H. Dehmelt, Ann. Phys. (Paris) **10**, 777 (1985).

[49]L. S. Brown, G. Gabrielse, J. Tan, and K. C. D. Chan, Phys. Rev. A **37**, 4163 (1988); L. S. Brown, G. Gabrielse, K. Helmerson, and J. Tan, Phys. Rev. Lett. **55**, 44 (1985); L. S. Brown, in *Themes in Contemporary Physics II*, edited by S. Deser and R. J. Finkelstein (World Scientific, Singapore, 1989).

[50]J. Tan and G. Gabrielse, Appl. Phys. Lett. **55**, 2144 (1989).

[51]R. S. VanDyck, Jr., F. L. Moore, D. L. Farnham, and P. B. Schwinberg, Int. J. Mass Spectrom Ion Proc. **66**, 327 (1985).

[52]E. R. Cohen and B. N. Taylor, in *The 1986 Adjustment of the Fundamental Physical Constants*, Report of the CODATA Task Group on Fundamental Constants, CODATA Bulletin No. 63 (Pergamon, Elmsford, NY, 1986).

[53]H. G. Dehmelt and F. L. Walls, Phys. Rev. Lett. **21**, 127 (1968).

[54]V. B. Braginsky, Y. I. Vorontsov, and K. S. Thorne, Science **209**, 547 (1980).

[55]S. Stenholm, Rev. Mod. Phys. **58**, 699 (1986).

[56]D. J. Wineland and W. M. Itano, Phys. Today **40**(6), 34 (1987).

[57]H. Dehmelt, G. Janik, and W. Nagourney, Bull. Am. Phys. Soc. **30**, 111 (1988).

[58]P. E. Toschek and W. Neuhauser, J. Opt. Soc. Am. B **6**, 2220 (1989).

[59]Markus Lindberg and Juha Javanainen, J. Opt. Soc. Am. B **3**, 1008 (1986).

[60]Murray Sargent, III, and Paul Horwitz, Phys. Rev. A **13**, 1962 (1976).

[61]Wayne M. Itano and D. J. Wineland, Phys. Rev. A **24**, 1364 (1981).

[62]Courtesy of R. Wallace and K. C. Dominic Chan, Accelerator Theory and Simulation Group, Los Alamos National Laboratory.

[63]P. Kartaschoff, *Frequency and Time* (Academic, London, 1978), p. 41.

[64]A. G. Smagin, Prib. Tekh. Eksp. **17** (6), 143 (1974).

Sisyphus cooling of a bound atom

D. J. Wineland

Time and Frequency Division, National Institute of Standards and Technology, Boulder, Colorado 80303

J. Dalibard and C. Cohen-Tannoudji

Laboratoire de Spectroscopie Hertzienne de l'Ecole Normale Supérieure, and Collège de France, 24, Rue Lhomond, F-75231 Paris Cedex 05, France

Received May 28, 1991; revised manuscript received September 6, 1991

Cooling that results from optical dipole forces is considered for a bound atom. Through optical pumping, the atom can be made to feel decelerating optical dipole forces more strongly than accelerating optical dipole forces. This effect, which has previously been realized for free atoms, is called Sisyphus cooling. A simple model for a bound atom is examined in order to reveal the basic aspects of cooling and heating when the atom is confined in the Lamb–Dicke regime. Results of semiclassical and quantum treatments show that the minimum energy achieved is near the zero-point energy and can be much lower than the Doppler cooling limit. Two practical examples that approximate the model are briefly examined.

1. INTRODUCTION

Interest in laser-cooled atoms and atomic ions has continued to increase over the past few years. The simplest cooling scheme that has been proposed is called Doppler cooling, in which the atom experiences a damping force owing to spontaneous scattering of light.[1] This cooling applies to a two-level system. That is, it can be explained by a consideration of scattering between a single ground state and a single optically excited state. It leads to minimum temperatures (the Doppler cooling limit) $T_D \approx \hbar\Gamma/2k_B$ when $\hbar\Gamma \gg R$. Here $2\pi\hbar$ is Planck's constant, Γ is the decay rate from the excited state, k_B is Boltzmann's constant, and $R = (\hbar k)^2/2m$ is the recoil energy, where $\lambda = 2\pi/k$ is the wavelength of the exciting radiation and m is the mass of the atom. For strongly allowed (large-Γ) electric dipole transitions in atoms and ions, this leads to temperatures of approximately 1 mK.

In 1988 an important experiment by the group of Phillips at the National Institute of Standards and Technology, Gaithersburg, Maryland,[2] showed that temperatures of laser-cooled sodium atoms were substantially below the minimum temperature predicted theoretically for two-level systems. A theoretical analysis and subsequent experiments[3–8] showed that the new cooling mechanisms responsible for these low temperatures were based on a combination of several effects such as optical pumping between more than one ground-state sublevel, light shifts, and polarization or intensity gradients.

The idea of the new cooling mechanisms is that laser beam electric fields **E** create a polarization **d** in an atom that depends on the ground-state sublevel and on the laser polarization. This dipole interacts with the laser field, and the reactive part of this interaction induces an energy shift of the ground-state sublevels, which varies from one ground-state sublevel to the other. This shift is called the light shift or the ac Stark shift. If the laser intensity or the laser polarization varies in space, these light shifts, which are now position dependent, give rise to a dipole or ponderomotive force equal in magnitude to the gradient of the atomic energy. Optical pumping takes place between the sublevels, so if the laser polarization/intensity varies in space, the relative populations of the ground-state sublevels are also position dependent. For an atom moving arbitrarily slowly in a spatially periodic light field, the averaged force is equal to zero, because the deceleration force experienced by the atom in the ascending parts of the potential curves (associated with the position-dependent light shifts) is offset by the acceleration felt in the descending parts. However, optical pumping takes a finite time to occur (the pumping time τ_P is inversely proportional to the laser intensity I). Therefore, in general, for a moving atom, it is possible to arrange the laser tuning and the polarization/intensity gradients so that the atom has time to run up one of the dipole potential hills (thereby losing kinetic energy) before being optically pumped into another ground-state sublevel where the dipole potential has less effect on the kinetic energy. After a while, the atom is returned by optical pumping (or by some other relaxation mechanism) to the original ground state, and the process is repeated. Since the atom appears to be running up the potential hills more than down, this cooling has been called Sisyphus cooling after the Greek myth[9] (see also Refs. 10 and 11). Cooling that is due to static electric and magnetic fields in combination with optical pumping has also been considered.[12,13]

The Sisyphus cooling mechanism was first introduced for a two-level atom moving in a high-intensity laser standing wave.[9] The required multilevel structure of the atom was then provided by the dressed states of the atom in the strong laser field. However, the time lag appearing between the dressed-state populations of a moving atom and the corresponding populations of an atom at rest is, for a two-level atom, of the order of the radiative lifetime $\tau_R = \Gamma^{-1}$ of the atomic excited state. At low intensity the optical pumping time τ_P for a multilevel atom can be much longer than τ_R. Because of this, the new cooling mechanisms based on optical pumping and light shifts can lead

0740-3224/92/010032-11$05.00

to friction coefficients as high as Sisyphus cooling for two-level atoms but at lower intensity, since, with longer time lags ($\tau_P \gg \tau_R$), smaller velocities can give rise to comparable decelerations.[3]

Doppler cooling exhibits the damping of the spontaneous scattering force, whereas Sisyphus cooling uses the decelerating effect of the dipole force combined with a dissipation of potential energy by spontaneous Raman processes. For completeness, it is useful to identify a third kind of cooling, which may be regarded as due to optical pumping of the atom into a low-energy state that no longer interacts with the laser. Velocity-selective coherent population trapping[8,14] and resolved sideband cooling of trapped ions[15,16] are of this category. In both cases the atoms (ions) are pumped into low-energy states that interact only weakly with the laser. This interaction becomes weaker the smaller the velocity becomes or, in the case of sideband cooling, the narrower the cooling transition is. Related schemes, which put atoms into a low-energy state that no longer interacts (or interacts weakly) with the laser light, have been proposed.[17]

Sisyphus or polarization-gradient cooling[8] has been an important development for cooling and manipulation of atoms. For free atoms Sisyphus cooling gives temperatures down to values where the kinetic energy of the atoms is approximately equal to the depth of the potential wells associated with the position-dependent light shifts. This limit applies down to the point where the dipole well energies are of the order of the recoil energy R, in which case the limiting energy is approximately equal to R.

In this paper we investigate the possibility of extending the Sisyphus cooling mechanism to trapped atoms or ions. We propose a specific scheme and show that it can lead to temperatures much lower than the Doppler limit. Instead of permitting the atom to move freely in space, we assume that the atom is bound to a localized region of space by some external potential. We assume that the intensity gradient is due to a standing-wave laser field. By a localized region of space we mean a region whose spatial extent is much smaller than the wavelength of the cooling laser divided by 2π (e.g., k^{-1}). That is, the atom is confined in the Lamb–Dicke regime. For simplicity of discussion, the atom is assumed to be bound in one dimension by a harmonic well characterized by the oscillation frequency ω_v. The spread of the minimum-energy state is given by $x_0 = (\hbar/2m\omega_v)^{1/2}$, where m is the atomic mass. The spatial extension of the wave functions then scales as x_0, and the condition $x_0 <$ (spatial extent) $\ll 1/k$ is equivalent to $\hbar\omega_v \gg R$. When $R \gg \hbar\omega_v$, the atom, even when it is near its cooling limit, will always sample many peaks and valleys of the standing-wave laser field, and the cooling limit should be adequately described by the theory for free atoms.

For a two-level bound atom the Doppler cooling limit is achieved when the natural width Γ of the optical transition is much larger than the oscillation frequency ω_v[1] and $R/\hbar$. The opposite condition, $\Gamma \ll \omega_v$, corresponds to what is called resolved sideband cooling. In this regime it has been shown[15,16] that it is possible to achieve conditions in which the difference between the minimum energy and the zero-point energy is less than the recoil energy as long as $\omega_v \gg R/\hbar$. (For this case, however, $k_BT > \hbar\Gamma$.) In order to compare Doppler cooling and Sisyphus cooling in the same conditions, we will therefore assume here that $\Gamma \gg \omega_v$. The main result of this paper is that, when $\Gamma \gg \omega_v$ and $\hbar\omega_v \gg R$, Sisyphus cooling leads to minimum temperatures T_s such that $k_BT_s \approx \hbar\omega_v$, whereas Doppler cooling leads to temperatures T_D such that $k_BT_D \approx \hbar\Gamma$, that is, higher than T_s by a factor of Γ/ω_v.

To illustrate the basic ideas, we consider a simple model system, which is described in Section 2. More-complicated cases can be generalized from this example. From a semiclassical treatment (atomic motion treated classically) given in Section 3, we will be able to derive cooling rates and limits. From this treatment we will see that the minimum energies are approximately equal to $\hbar\omega_v$. At these energies we might expect quantum effects of the motion to be important, so we will examine the cooling limits, treating the motion quantum mechanically in Section 4. In Section 5 we briefly compare the cooling rates and limits achieved here with those obtained from Doppler cooling. Although the model was chosen to be simple enough to show the basic effects, in Section 6 we examine a couple of possible experimental examples that closely approximate the simple model.

2. MODEL

A. Atomic Level Structure and Laser Configuration

We consider Sisyphus cooling of a single bound atom. We assume that the atom's internal structure is represented by three levels as shown in Fig. 1. We label these levels g for ground state, e for excited state, and r for reservoir state. We assume that the transition $g \rightarrow e$ is an electric dipole transition excited by a standing-wave laser beam whose frequency ω is tuned above the resonance frequency ω_0 for this transition by an amount δ (where all frequencies are expressed in radians per second). Level e spontaneously decays at rate Γ. It decays to level r with branching fraction β and to level g with branching fraction $1 - \beta$. We assume that the laser's intensity and detuning are such that the fraction of time the atom spends in the excited state is negligible. We assume that level r is transferred back to level g at a rate $R_{r\rightarrow g}=1/T_r$, where the duration of the transfer process is so short ($\ll T_r$) that one can consider the position of the ion as remaining unchanged during the transfer. We assume that the atom is confined to one dimension (the x direction) by a harmonic well U_0 [Fig. 1(b)] characterized by the atom oscillation (or vibration) frequency ω_v. Here, U_0 is assumed to be an external potential that is independent of the laser beam. When the atom spontaneously decays from level e, the direction of photon emission is assumed parallel (or antiparallel) to the atom's motion. We assume that $E_e - E_g \gg |E_r - E_g|$, so that the effect of recoil heating is mathematically simple. These simplifying assumptions will not qualitatively affect the results for other, more complicated cases.

A key element in Sisyphus cooling is that the energies of the dressed states or of the light-shifted ground-state sublevels vary along the direction of the atomic motion. Such a situation will be achieved here if we take a laser intensity that varies linearly with x over the range of atomic motion. We are concerned mainly with the case in which this intensity gradient is due to a laser standing wave along the x direction (see also Appendix A). We then

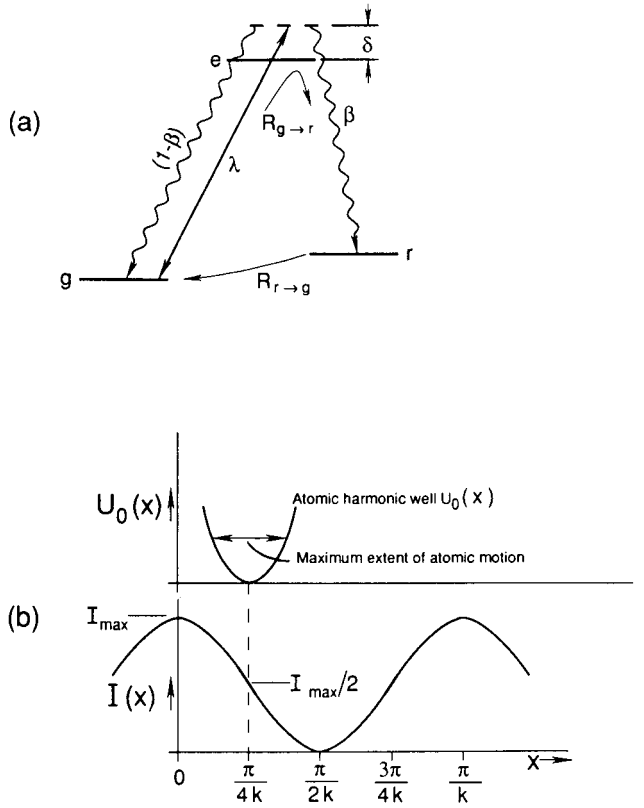

Fig. 1. Model system. (a) The atom has three internal energy levels: g, e, and r. A standing-wave laser beam drives $g \to e$ above its resonance frequency. Level e decays with branching fraction β to level r and with branching fraction $1 - \beta$ to level g. Transfer from level r to g occurs at a rate $R_{r\to g}$. (b) The atom is assumed to be confined by a harmonic well in the x direction. The maximum extent of the atom's motion is assumed to be less than $\lambda/2\pi$ (Lamb–Dicke regime).

write the laser electric field (classically) as

$$\mathbf{E} = (\mathbf{E}_{max}/2)[\cos(kx - \omega t) + \cos(kx + \omega t)]$$
$$= \mathbf{E}_{max} \cos \omega t \cos kx, \quad (1)$$

where x is the atom's position and the wave vector $k = 2\pi/\lambda$, where λ is the laser wavelength. According to Eq. (1), the laser intensity $I(x)$ varies as $\cos^2(kx)$, as shown in Fig. 1(b). Sisyphus cooling will be most efficient when the intensity gradient is a maximum; this occurs at the half-intensity point of the standing wave. Therefore we assume that the atom's average position is near $x = \pi/4k$ [Fig. 1(b)]. The linear variation of the light shift of level g with x over the range of the atom's motion follows from the localization assumption: The extent of the atom's motion is less than $\lambda/2\pi$ (Lamb–Dicke regime).

In this paper we focus on the regime

$$R_{g\to r}, R_{r\to g} \ll \omega_v \ll \Gamma \ll \delta, \quad (2)$$

where $R_{g\to r}$ and $R_{r\to g}$ are, respectively, the rates of transfer from g to r when the atom is in level g and from r to g when the atom is in level r. We also assume that the laser intensity is weak enough to avoid any saturation of the $g \to e$ transition. That is,

$$s \equiv \frac{2\omega_1^2}{4\delta^2 + \Gamma^2} \ll 1. \quad (3)$$

In Eq. (3), s is the saturation parameter and $\omega_1 = \langle e|\mathbf{d}|g\rangle \cdot \mathbf{E}_{max}/\hbar$ is the Rabi frequency. In this low-saturation regime the population of the excited state is small, and we can derive rate equations for the evolution of the lower states r and g.

The condition $\Gamma \ll \delta$ implies that the light shift of g [Eqs. (13) below] is larger than the contribution to the width of this level that is due to the photon scattering rate. The condition $\omega_v \ll \Gamma$ has already been discussed in Section 1 as defining the regime in which the Doppler limit is achieved for a two-level bound atom. In a point of view in which the atomic motion is treated classically (semiclassical approach), the condition $R_{g\to r}, R_{r\to g} \ll \omega_v$ means that the bound atom makes several oscillations in the harmonic binding potential before being transferred from g to r or from r to g. It is then possible to neglect the variation with space of the populations of levels g and r and to consider only their average over an oscillation period. This greatly simplifies the calculation of the rate of variation of the atomic external energy in the semiclassical approach. From a fully quantum point of view, in which the atomic motion is quantized, the condition $R_{g\to r}$, $R_{r\to g} \ll \omega_v$ means that the width of the vibrational levels in the binding potential, owing to the excitation rates from g or r, is smaller than the spacing $\hbar\omega_v$ between these levels. This introduces a similar simplification into the calculations, since it permits a secular approximation to be used. The secular approximation consists in neglecting, in the master equation describing the evolution of the atomic density matrix σ, any coupling between the populations of the vibrational levels and the off-diagonal elements of σ. In this way we can obtain a set of equations involving only the populations of the vibrational levels, which has a simple interpretation in terms of transition rates. This is an example of a situation in which the rate of variation of atomic internal variables ($R_{g\to r}, R_{r\to g}$) is slower than the rate of variation of external variables (ω_v). A similar example was recently studied in connection with the quantization of atomic motion in optical molasses.[18]

B. Qualitative Explanation of the Cooling

For $\delta > 0$, as shown in Fig. 1(a), the electric field of the laser shifts the level g to higher energy. Because $s \ll 1$, the atom is primarily in g or r. When it is in the state g (more precisely, in the dressed state, which contains the larger admixture of g), it is subject to an additional potential energy $U_L(x)$, which is a function of x proportional to the laser intensity. For the conditions of Fig. 1(b) the effect of this potential for the limited range of the atom's motion is to give an additional force in the $+x$ direction.

A crude explanation of the Sisyphus cooling is the following: As the atom oscillates back and forth (with frequency ω_v) in the well $U_0(x)$, it experiences an additional potential hill $U_L(x)$ sloping down toward the $+x$ direction. The atom is more likely to be transferred to level r by spontaneous Raman scattering when it is in regions of higher intensity. Therefore the predominant effect is that, after the atom runs up the laser hill $U_L(x)$ in the $-x$ direction (therefore losing kinetic energy), it is transferred to level r, where $U_L(x) = 0$. After a time of order T_r it is transferred back to level g, where on the average it must run up the hill $U_L(x)$ again before being transferred to level r. This leads to a net cooling effect.

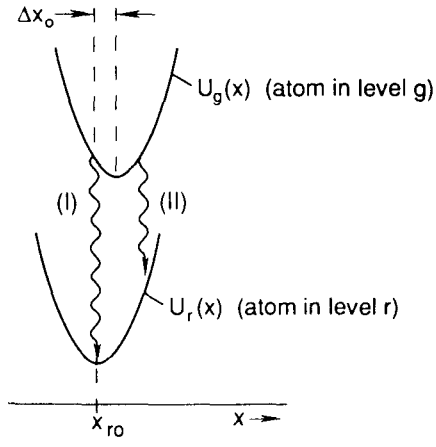

Fig. 2. Qualitative explanation of the cooling. When the atom is in state r, it experiences the confining potential $U_r(x)$, which is unperturbed by the laser fields. When the atom is in level g, the potential well is shifted in the $+x$ direction by the dipole force of the laser. This shifted potential is represented by $U_g(x)$. The laser excitation is assumed to be weak enough that the atom spends a negligible amount of time in level e. Therefore the spontaneous Raman transitions $g \rightarrow e \rightarrow r$ can be represented by transitions between g and r such as those indicated by (I) and (II) in the figure. Process (I) is favored more than process (II) because, when the atom is on the left-hand side of the well U_g, the chance of $g \rightarrow e$ excitation is higher since the laser intensity is higher [see Fig. 1(b)]. Process (I) leads to cooling because the atom drops to a lower part of the well U_r. Process (II) causes heating and, along with the heating resulting from recoil, eventually balances the cooling, resulting in a minimum energy.

A more accurate explanation is the following: When the atom is in the state g, it experiences the combined potential $U_0 + U_L = U_g$, which is a well with frequency ω_v shifted by an amount Δx_0 in the $+x$ direction (upper part of Fig. 2). When the atom oscillates in the $-x$ direction in the well U_g, it is more likely to be transferred to level r by spontaneous Raman scattering because the laser intensity is higher. It can therefore drop into a lower part of the unshifted well $U_r(x) = U_0(x)$, keeping the same position x since the duration Γ^{-1} of the transfer process is much smaller than the oscillation period ω_v^{-1} in the binding potential. It therefore loses potential energy [process (I) of Fig. 2]. After a time of order T_r (which is independent of the position x), the atom is transferred back to level g and the process is repeated. Heating, as illustrated by process (II) in Fig. 2, in which the atom gains potential energy, can also occur but is less favored because the laser intensity is less in the $+x$ direction.

Spontaneous Raman scattering ($g \rightarrow e \rightarrow r$) occurs at a rate proportional to the intensity, which according to Eq. (1) can be expressed as

$$R_{g\rightarrow r} \propto \frac{E_{\max}^2}{2}\cos^2(kx) \simeq I\left(x = \frac{\pi}{4k}\right)\left[1 - 2k\left(x - \frac{\pi}{4k}\right)\right]. \tag{4}$$

The term $-2kxI(x = \pi/4k)$ is responsible for the cooling. The term that is independent of x causes heating because of two effects. First, for each scattering event, photon recoil causes an average increase in energy $2R$.[19] Second, when the atom changes from level g to level r, the well switches from U_g to U_r. As we will see in Section 3, the corresponding potential energy change, when it is averaged over one oscillation period, leads to heating. A similar effect occurs in the transitions from r to g. The balance of the cooling with these sources of heating yields the minimum kinetic energy for the atom. Since $\delta > 0$, there is some additional Doppler or spontaneous force antidamping that tends to increase the atom's energy; this is shown in Subsection 5.B to be negligible for the conditions assumed here.

The cooling is the same when the atom's well is in a region of positive slope [e.g., $x = 3\pi/4k$ in Fig. 1(b)]. The cooling effect goes to zero when the well is centered at points of zero slope [e.g., $x = 0$, $\pi/2k$, and π/k in Fig. 1(b)].

3. SEMICLASSICAL TREATMENT

In this section we treat the external motion of the atom classically. Such treatment, often called semiclassical, is valid if the atomic de Broglie wavelength is small compared with the length scale (the light wavelength λ) over which the field varies.[20] In principle, it should also require that the extension of the atomic wave packet be much larger than the size of the ground state of the confining potential. Actually, we will see that the latter condition can be dropped, and the semiclassical and quantum results are identical even if the atom is mostly in the ground state of the well.

A. Internal Atomic Dynamics

The internal states of the atom are treated quantum mechanically. In the low-intensity domain of interest here [relation (3)], the optical Bloch equations, giving the evolution of the atomic density operator, can be simplified by an adiabatic elimination of the optical coherences (off-diagonal matrix elements of the density operator between ground and excited states). We are then left with a set of rate equations for the populations $\pi_j (j = g, r, e)$ of the atom's three internal levels[20,21]:

$$\dot{\pi}_g = -R_{g\rightarrow e}(x)(\pi_g - \pi_e) + R_{r\rightarrow g}\pi_r + (1 - \beta)\Gamma\pi_e, \tag{5a}$$

$$\dot{\pi}_e = R_{g\rightarrow e}(x)(\pi_g - \pi_e) - \Gamma\pi_e, \tag{5b}$$

$$\dot{\pi}_r = -R_{r\rightarrow g}\pi_r + \beta\Gamma\pi_e, \tag{5c}$$

where

$$R_{g\rightarrow e}(x) = (\Gamma s/2)\cos^2(kx). \tag{6}$$

Since we have assumed that $s \ll 1$, the scatter rate $R_{g\rightarrow e}(x)$ is much smaller than Γ and the population of the excited state, π_e, is small compared with 1. For times long compared with Γ^{-1}, we have therefore approximately

$$\pi_e = \pi_g(s/2)\cos^2(kx), \tag{7}$$

$$\dot{\pi}_g = -R_{g\rightarrow r}(x)\pi_g + R_{r\rightarrow g}\pi_r, \tag{8a}$$

$$\dot{\pi}_r = -\dot{\pi}_g, \tag{8b}$$

where

$$R_{g\rightarrow r}(x) = \beta R_{g\rightarrow e}(x) = \beta(\Gamma s/2)\cos^2(kx). \tag{9}$$

In the limit $R_{r\rightarrow g}, R_{g\rightarrow r} \ll \omega_v$, and when we use $\pi_g + \pi_r \simeq 1$, the steady-state solution of Eqs. (8) is simply

$$\pi_g^{st} = \frac{R_{r\to g}}{\langle R_{g\to r}\rangle + R_{r\to g}}, \tag{10a}$$

$$\pi_r^{st} = \frac{\langle R_{g\to r}\rangle}{\langle R_{g\to r}\rangle + R_{r\to g}}, \tag{10b}$$

where $\langle R_{g\to r}\rangle$ stands for the average of $R_{g\to r}(x)$ over the atom oscillation period for the atom in level g (recall that we have assumed that $R_{r\to g}$ does not depend on x). The time constant τ_{int} for the relaxation of these internal variables is given by

$$1/\tau_{int} = \langle R_{g\to r}\rangle + R_{r\to g}. \tag{11}$$

B. External Atomic Dynamics

When the atom is in level r, or when the atom is in level g in the absence of the laser, the center of the atom's well is denoted x_{r0}. Therefore the atom's harmonic well can be described by

$$U_r(x) = U_0(x) = \tfrac{1}{2}m\omega_v^2(x - x_{r0})^2. \tag{12}$$

When the atom is in level g in the presence of the laser field, the center of the atom's well is shifted by the laser light. Using the dressed-state formalism,[9] we find that the energy of the state g is shifted by an amount

$$U_L(x) = \frac{\hbar}{2}[\omega_1^2\cos^2(kx) + \delta^2]^{1/2} - \frac{\hbar}{2}\delta \simeq U_{L0}\cos^2(kx), \tag{13a}$$

where

$$U_{L0} = \hbar\omega_1^2/4\delta \tag{13b}$$

is the maximum value of U_L. Equations (13) are valid for $\delta \gg \Gamma, \omega_1$. The internal state $|g\rangle$ changes to the dressed state $|g\rangle'$, but $|g\rangle' \simeq |g\rangle$ in the limit $\omega_1 \ll \delta$. The center of the atom's well, x_{g0}, when it is shifted by the dipole potential, corresponds to the spatial minimum of the total potential for the atom in level g:

$$U_g(x) = U_r(x) + U_L(x). \tag{14}$$

Since the cooling will be a maximum where the intensity gradient is maximum, we choose $kx_{r0} = \pi/4$. Assuming that the shift Δx_0 between the two wells is small compared with $\lambda/2\pi$, we linearize $U_L(x)$ around x_{r0} to obtain

$$U_L(x) \simeq U_{L0}/2 - kU_{L0}(x - x_{r0}). \tag{15}$$

The shift Δx_0 is then

$$\Delta x_0 = x_{g0} - x_{r0} = 2\xi(kx_0)x_0, \tag{16a}$$

where

$$\xi = U_{L0}/\hbar\omega_v \tag{16b}$$

and $x_0 = (\hbar/2m\omega_v)^{1/2}$ is the spread of the zero-point wave function in the harmonic well. We show in Subsection 3.D that the minimum kinetic energy is achieved for $U_{L0} \simeq \hbar\omega_v$, that is, for $\xi \simeq 1$. Therefore, since we have assumed the Lamb–Dicke criterion $kx_0 \ll 1$, the shift Δx_0 of the well $U_g(x)$ that is due to the dipole potential is, for minimum kinetic energy, much smaller than x_0 and thus much smaller than $\lambda/2\pi$, as we assumed in deriving Eq. (16a).

C. Cooling Rate

The variation of the external (kinetic + potential) energy E_x can be expressed by the equation

$$\dot{E}_x = \pi_g\langle R_{g\to r}(x)[U_r(x) - U_g(x)]\rangle + \pi_r R_{r\to g}\langle U_g(x) - U_r(x)\rangle + \pi_g\langle R_{g\to e}(x)\rangle 2R. \tag{17}$$

The first two terms stand for the average change in potential energy as the atom goes from g to r and from r to g, respectively. They therefore contain both Sisyphus cooling and the heating that is due to the sudden switching of the wells. Recoil heating for the $g \to r$ transfer is contained in the third term of Eq. (17), and spontaneous force Doppler antidamping (heating) can be neglected (Subsection 5.B). The averages are taken over one oscillation period in the initial potential [$U_g(x)$ for the first term of Eq. (17) and $U_r(x)$ for the second].

As in relation (4), we linearize the rate $R_{g\to r}(x)$ [Eq. (9)] around x_{r0}:

$$R_{g\to r}(x) \simeq \beta(\Gamma s/4)[1 - 2k(x - x_{r0})], \tag{18}$$

and we use the equipartition of energy for the atom oscillating in $U_g(x)$:

$$E_x = 2\left\langle \frac{1}{2}m\omega_v^2(x - x_{g0})^2 \right\rangle. \tag{19}$$

For times long compared with τ_{int}, we then obtain, using Eqs. (10) for π_g and π_r,

$$\dot{E}_x = -(1/\tau_s)(E_x - E_{x0}), \tag{20a}$$

where the steady-state energy E_{x0} is

$$E_{x0} = \frac{m\omega_v^2(\Delta x_0)}{2k} + \frac{R}{k\beta(\Delta x_0)} = \frac{U_{L0}}{2}\left(1 + \frac{1}{\xi^2\beta}\right) = \frac{\hbar\omega_v}{2}\left(\xi + \frac{1}{\xi\beta}\right) \tag{20b}$$

and the Sisyphus cooling time constant τ_s is given by

$$\frac{1}{\tau_s} = \frac{4\langle R_{g\to r}\rangle R_{r\to g}}{\langle R_{g\to r}\rangle + R_{r\to g}}\left(\frac{R}{\hbar\omega_v}\right)\xi. \tag{20c}$$

For the conditions of interest ($\xi \simeq 1, R/\hbar\omega_v \ll 1$), one can check that $\tau_s \gg \tau_{int}$.

D. Cooling Limit

In steady state the atom's external energy is reduced to E_{x0} [Eq. (20b)]. E_{x0} is minimized when the laser intensity is adjusted to make $\xi \equiv U_{L0}/\hbar\omega_v = \beta^{-1/2}$, in which case

$$E_{x0}^{min} = \hbar\omega_v/\sqrt{\beta} = U_{L0}. \tag{21}$$

From the second expression in Eq. (21) the minimum external energy is equal to the depth of the wells created by the standing-wave laser beam. This agrees with the result of Sisyphus cooling of free atoms.[8] When $\beta \simeq 1$, this predicts an energy near the zero-point energy for the ion in its well. In such a situation we might question the validity of this approach, which treats the atomic motion classically. Therefore it will be useful to compare the cooling limit derived here with the results from a quantum-mechanical treatment of the atom's motion.

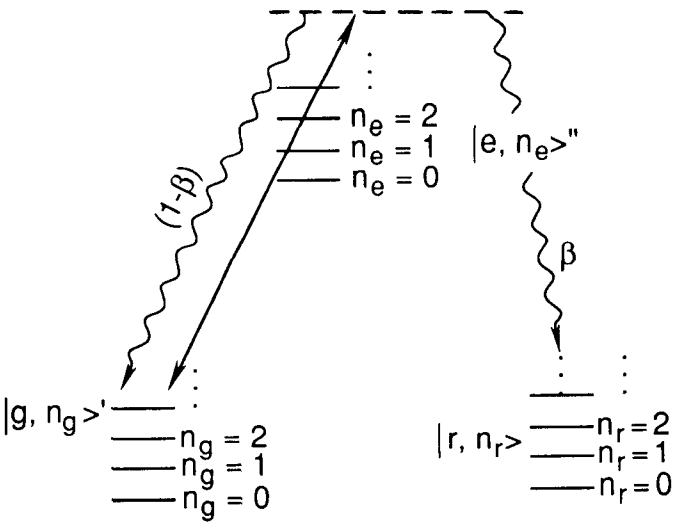

Fig. 3. Diagram for the cooling when the motion is quantized. Each electronic state has a sublevel structure of harmonic-oscillator levels labeled by the quantum numbers n_j, where $j = g$, e, or r. Cooling is represented by scattering processes of the form $n_g \rightarrow n_e \rightarrow n_r$, where $n_r < n_g$. This may be viewed as due to spontaneous Raman scattering off states $|g, n_g\rangle'$ and $|e, n_e\rangle''$, which are dressed by the laser.

4. QUANTUM TREATMENT

A. Transition Rates

In this section we treat the atom's motion in its well quantum mechanically. We describe the cooling process as shown in Fig. 3, where laser photons undergo spontaneous scattering from the dressed states, which now include the perturbed harmonic-oscillator states (denoted by primes and double primes).

Cooling results from spontaneous Raman scattering processes of the form $|g, n_g\rangle' \rightarrow |e, n_e\rangle'' \rightarrow |r, n_r\rangle$, where $n_r < n_g$. States $|g, n_g\rangle'$ and $|e, n_e\rangle''$ are assumed to be dressed by the standing-wave laser field. We can calculate the cooling and the cooling limit as was done in Ref. 19. For practical purposes the cooling rate is adequately represented by the semiclassical treatment of Subsection 3.C. Here we are interested primarily in the cooling limit, since the semiclassical treatment predicts a minimum energy approximately equal to $\hbar\omega_v$. We can calculate the minimum energy, using Eq. (27) of Ref. 19. It will be more instructive, however, to calculate the rates for each process $n_g \rightarrow n_r$ separately. According to Ref. 19, these rates can be written as

$$\Gamma_{g,n_g\rightarrow r,n_r} = C\left|\sum_{n_e} \frac{\langle n_r|\exp(-i\mathbf{k}_s\cdot\mathbf{X}|n_e\rangle''\{\langle n_e|''\}f(X)\,|n_g\rangle'}{\delta - (E_{n_e} - E_{n_g})/\hbar + i\Gamma/2}\right|^2, \tag{22}$$

where C is a factor that includes the laser intensity (at the position $x = \pi/4k$) and matrix elements for the $g \rightarrow e$ transition, $\mathbf{X}$ is the atomic position operator, and $\mathbf{k}_s$ is the wave vector for the scattered photon. For simplicity we will assume the scattered photon to be in either the $+x$ or the $-x$ direction, so that $\mathbf{k}_s \cdot \mathbf{X} = \pm kX$. $f(X)$ is a function representing the x dependence of the laser's electric field amplitude near $x = \pi/4k$; from Eq. (1), $f(X) \simeq 1 - k(X - x_{r0})$. E_{n_e} and E_{n_g} are the energies of the individual harmonic-oscillator levels for the excited and ground states, respectively. The sum is performed over all possible excited harmonic-oscillator states.

Since we have assumed that $\delta \gg \omega_v$, the denominator in the sum in Eq. (22) can be approximated by δ. This amounts to neglecting Doppler antidamping; the validity of this approximation is discussed in Subsection 5.B. With this approximation and the closure relation over the states $|n_e\rangle''$, Eq. (22) simplifies to

$$\Gamma_{g,n_g\rightarrow r,n_r} = \beta(C/\delta^2)|\langle n_r|\exp(-i\mathbf{k}_s\cdot\mathbf{X})f(X)\,|n_g\rangle'|^2. \tag{23}$$

When $\beta \neq 1$, we must also consider scattering directly back to the ground state from the excited state. These direct rates give rise to additional recoil heating for the $g \rightarrow e \rightarrow g$ scattering process:

$$\Gamma_{g,n_g\rightarrow g,n_g^*} = (1-\beta)(C/\delta^2)|\{\langle n_g^*|'\}\exp(-i\mathbf{k}_s\cdot\mathbf{X})f(X)\,|n_g\rangle'|^2, \tag{24}$$

where n_g^* is the final harmonic-oscillator state in the direct scattering process. Finally, we must consider the change in harmonic-oscillator energy levels in the transitions $r \rightarrow g$. As in the semiclassical treatment, this leads to a heating resulting from the sudden switching of the harmonic well (even without any spatial variation of the transfer rate $R_{r\rightarrow g}$). This process is described by the rate

$$\Gamma_{r,n_r\rightarrow g,n_g} = C'|\{\langle n_g|'\}1|n_r\rangle|^2, \tag{25}$$

where C' is a constant characterizing the rate of the $r \rightarrow g$ process. In Subsection 4.D these rates will be used in a master equation for the populations of the harmonic-oscillator levels. Before that is discussed, two preliminary steps are required. First we must find an expression for the perturbed harmonic-oscillator wave functions. Then we will obtain simple expressions for the rates in Eqs. (23)–(25).

B. Dressed Harmonic-Oscillator Wave Functions

As we discussed in Section 1, the dipole force acts uniformly over the extent of the wave functions of interest in the Lamb–Dicke limit. Therefore the effect of this dipole force is simply to shift the center of the harmonic-oscillator well for the g state to $x_{r0} + \Delta x_0$, the value calculated semiclassically. (This can be explicitly verified by the use of second-order perturbation theory to dress the wave functions.) The wave functions $|n_g\rangle'$ are simply obtained by using the spatial translation operator

$$|n_g\rangle' = \exp(-i\Delta x_0 P_x/\hbar)\,|n_g\rangle, \tag{26}$$

where P_x is the x component of the atomic momentum operator.

In the following, we will require both the position and momentum operators X and P_x in terms of raising and lowering operators $a^\dagger$ and a:

$$X = x_0(a^\dagger + a), \tag{27}$$

$$P_x = ix_0 m\omega_v(a^\dagger - a). \tag{28}$$

C. Evaluation of the Rates

Using Eq. (26) in Eqs. (23)–(25), we find that

$$\Gamma_{g,n_g\rightarrow r,n_r} = \beta(C/\delta^2)|\langle n_r|A_1|n_g\rangle|^2, \tag{29a}$$

$$\Gamma_{g,n_g\rightarrow g,n_g^*} = (1-\beta)(C/\delta^2)|\langle n_g^*|A_2|n_g\rangle|^2, \tag{29b}$$

$$\Gamma_{r,n_r\rightarrow g,n_g} = C'|\langle n_g|A_3|n_r\rangle|^2, \tag{29c}$$

where

$$A_1 = \exp(-ik_sX)f(X)\exp(-i\Delta x_0 P_x/\hbar), \tag{30a}$$

$$A_2 = \exp(i\Delta x_0 P_x/\hbar)\exp(-ik_sX)f(X)\exp(-i\Delta x_0 P_x/\hbar), \tag{30b}$$

$$A_3 = \exp(-i\Delta x_0 P_x/\hbar) \tag{30c}$$

and where $k_s = \pm k$, depending on the direction of the spontaneously emitted photon (assumed to be along the $+x$ or the $-x$ direction).

We now replace the position and momentum operators X and P_x in A_1, A_2, and A_3 by their expressions in terms of a and $a^\dagger$ [Eqs. (27) and (28)]. It is convenient to change the origin of the x axis to x_{r0}, in which case $f(X) = 1 - kX$. Since $kx_0(n+1)^{1/2} \ll 1$ (Lamb–Dicke criterion), we keep only terms in first order in kx_0a or $kx_0a^\dagger$. This gives

$$A_1 \simeq 1 - kx_0[a^\dagger(1 - \xi + ik_s/k) + a(1 + \xi + ik_s/k)], \tag{31a}$$

$$A_2 \simeq 1 - kx_0(a^\dagger + a)(1 + ik_s/k), \tag{31b}$$

$$A_3 \simeq 1 + \xi kx_0(a - a^\dagger). \tag{31c}$$

Therefore, in the Lamb–Dicke limit, the important rates are those for which the vibrational quantum number changes by 1, and we have

$$\Gamma_{g,n\to r,n} = \beta\frac{C}{\delta^2} \equiv R_{g\to r}, \tag{32a}$$

$$\Gamma_{g,n\to r,n+1} = R_{g\to r}(kx_0)^2(n+1)[1 + (1-\xi)^2], \tag{32b}$$

$$\Gamma_{g,n\to r,n-1} = R_{g\to r}(kx_0)^2 n[1 + (1+\xi)^2], \tag{32c}$$

$$\Gamma_{r,n\to g,n} = C' \equiv R_{r\to g}, \tag{32d}$$

$$\Gamma_{r,n\to g,n+1} = R_{r\to g}(kx_0)^2(n+1)\xi^2 = \left(\frac{n+1}{n}\right)\Gamma_{r,n\to g,n-1}, \tag{32e}$$

$$\Gamma_{g,n\to g,n+1} = \frac{1-\beta}{\beta}R_{g\to r}2(kx_0)^2(n+1) = \left(\frac{n+1}{n}\right)\Gamma_{g,n\to g,n-1}. \tag{32f}$$

D. Rate Equations and Cooling Limit

A master equation for the populations takes the form

$$\dot{\pi}_{g,n} = \sum_{n'=n-1}^{n+1}\sum_{i=g,r}(-\Gamma_{g,n\to i,n'}\pi_{g,n} + \Gamma_{i,n'\to g,n}\pi_{i,n'}), \tag{33a}$$

$$\dot{\pi}_{r,n} = \sum_{n'=n-1}^{n+1}(-\Gamma_{r,n\to g,n'}\pi_{r,n} + \Gamma_{g,n'\to r,n}\pi_{g,n'}), \tag{33b}$$

where $\pi_{g,n}$ denotes the population with internal state g and external state n, etc. As expected, in steady state these equations show, after a little algebra, that the total population going from n to $n+1$ is equal to the total population going from $n+1$ to n. That is,

$$(\Gamma_{g,n\to r,n+1} + \Gamma_{g,n\to g,n+1})\pi_{g,n} + \Gamma_{r,n\to g,n+1}\pi_{r,n} = (\Gamma_{g,n+1\to r,n} + \Gamma_{g,n+1\to g,n})\pi_{g,n+1} + \Gamma_{r,n+1\to g,n}\pi_{r,n+1}. \tag{34}$$

In order to exploit this result, we now look for an approximate expression for $\pi_{g,n}$ and $\pi_{r,n}$ as a function of the total population of level n ($\pi_n = \pi_{g,n} + \pi_{r,n}$). Equations (33), written for steady state, give a relation between $\pi_{g,n}$, $\pi_{r,n}$, $\pi_{g,n\pm1}$, and $\pi_{r,n\pm1}$. If we assume that ξ is not large compared with 1 and recall that $kx_0(n+1)^{1/2} \ll 1$, then Eqs. (32) and (33) give $\Gamma_{g,n\to r,n}\pi_{g,n}/\Gamma_{r,n\to g,n}\pi_{r,n} \simeq 1 + 0[(n+1)(kx_0)^2]$, so

$$\pi_{gn} \simeq \frac{\Gamma_{r,n\to g,n}}{\Gamma_{g,n\to r,n} + \Gamma_{r,n\to g,n}}\pi_n, \tag{35a}$$

$$\pi_{rn} \simeq \frac{\Gamma_{g,n\to r,n}}{\Gamma_{g,n\to r,n} + \Gamma_{r,n\to g,n}}\pi_n. \tag{35b}$$

Substituting relations (35) into Eq. (34) and using Eqs. (32), we obtain

$$\frac{\pi_{n+1}}{\pi_n} = \frac{1 + \beta\xi(\xi-1)}{1 + \beta\xi(\xi+1)}, \tag{36}$$

where we have neglected terms of order $(n+1)(kx_0)^2$ and higher. For $\xi \ll 1$, we have $\pi_{n+1}/\pi_n \to 1$. π_{n+1}/π_n is minimized for $\xi = U_{L0}/\hbar\omega_v = \beta^{-1/2}$, in which case

$$\left(\frac{\pi_{n+1}}{\pi_n}\right)_{\min} = \frac{2 - \sqrt{\beta}}{2 + \sqrt{\beta}}. \tag{37}$$

Since, according to Eq. (36), π_{n+1}/π_n is independent of n, we can write

$$\frac{\pi_{n+1}}{\pi_n} = \exp\left(-\frac{\hbar\omega_v}{k_BT}\right), \tag{38}$$

which shows that the system reaches a thermodynamic equilibrium. For such a thermodynamic equilibrium, $\langle n_v\rangle = [\exp(\hbar\omega_v/k_BT) - 1]^{-1}$, in which case

$$\langle n_v\rangle = [1 + \beta\xi(\xi-1)]/2\beta\xi. \tag{39}$$

This is minimized for $\xi = \beta^{-1/2}$, in which case

$$\langle n_v\rangle = \beta^{-1/2} - 1/2. \tag{40}$$

This corresponds to a minimum energy

$$E_{x0}^{\min} = \hbar\omega_v(\langle n_v\rangle + 1/2) = \hbar\omega_v\beta^{-1/2}, \tag{41}$$

in agreement with the semiclassical answer [Eq. (21)]. This remarkable agreement between the semiclassical and quantum theories can be interpreted in the following way. The motion of a quantum particle in a harmonic well is governed by the same basic equations as those for the classical motion. (This is particularly clear in the Wigner function approach and is a particular feature of the harmonic potential.) Consequently, the only place where Planck's constant plays a role in the problem here is in the recoil heating, where $R = \hbar^2k^2/2m$, and this recoil is handled in the same way in both treatments. Therefore it should not be surprising that both approaches lead to the same minimum energy, even though this energy is close to the zero-point energy in the quantum well.

5. DISCUSSION

A. Cooling Rate

It is interesting to compare the rate for the Sisyphus cooling discussed here with the rate for Doppler cooling. Doppler cooling can be represented in Fig. 1 by the con-

ditions $\beta = 0$ and $\delta < 0$. The rate for Doppler cooling has been calculated by many authors; for example, from Eq. (19a) of Ref. 22 the cooling rate is

$$\tau_D^{-1} = -2R_{SD}\hbar k^2\delta_D\{m[(\Gamma/2)^2 + \delta_D^2]\}^{-1}, \quad (42)$$

where R_{SD} is the total scattering rate, the subscripts D stand for Doppler cooling, and the intensity is assumed to be below saturation ($s \ll 1$). For minimum temperature using Doppler cooling, we want $\delta_D = -\Gamma/2$. For this case,

$$\tau_D^{-1} = 4R_{SD}R/\hbar\Gamma. \quad (43)$$

According to Eq. (20c), assuming, for example, that $R_{r\to g} \gg \langle R_{g\to r}\rangle$ (that is, $\pi_g \approx 1$), the ratio of rates for Sisyphus cooling and Doppler cooling is

$$\frac{\tau_s^{-1}}{\tau_D^{-1}} = \left(\frac{\Gamma}{\omega_v}\right)\left(\frac{\langle R_{g\to r}\rangle}{R_{SD}}\right)\xi. \quad (44)$$

Therefore, for the minimum-temperature case ($\xi \approx 1$), the ratio of Sisyphus cooling to Doppler cooling is approximately given by the ratio $(\Gamma/\omega_v)(\langle R_{g\to r}\rangle/R_{SD})$. For $\langle R_{g\to r}\rangle/R_{SD} \approx 1$, Sisyphus cooling is faster by Γ/ω_v.

Comparing the Sisyphus cooling rate with the cooling rate in the resolved sideband limit[15,16,19] is not so straightforward because the conditions in which each applies are different. For efficient sideband cooling (in a two-level atom), we want $\delta = -\omega_v$ and $\Gamma \ll \omega_v$, and these conditions are incompatible with relation (2). Therefore a comparison of cooling rates depends on the specific atomic system considered. The practical advantages of one cooling scheme over the other will also depend on the specific system investigated; this will depend, for example, on the availability and the ease of operation of the required lasers.

B. Contribution of Doppler Antidamping in Sisyphus Cooling

For the model considered here ($\delta > 0$), Doppler cooling is turned into an antidamping term. We can use Eq. (42) to check that this heating effect can be neglected compared with Sisyphus cooling. For the situation of interest here ($\delta \gg \Gamma$), we have

$$\tau_D^{-1} = \left(\frac{4\pi_g\langle R_{g\to r}\rangle}{\beta}\right)\frac{R}{\hbar\delta} = \left(\frac{4}{\beta}\right)\left(\frac{\langle R_{g\to r}\rangle R_{r\to g}}{\langle R_{g\to r}\rangle + R_{r\to g}}\right)\left(\frac{R}{\hbar\delta}\right). \quad (45)$$

By comparing with Eq. (20c), we find that

$$\frac{\tau_D^{-1}}{\tau_S^{-1}} = \left(\frac{1}{\beta\xi}\right)\frac{\omega_v}{\delta} \ll 1. \quad (46)$$

Therefore we may neglect the effects of Doppler antidamping compared with Sisyphus cooling except when $\beta \ll 1$.

C. Cooling Limit

The minimum energy for Doppler cooling is $\hbar\Gamma/2$. Therefore, according to Eq. (21) or (41), the minimum energy for Sisyphus cooling will be smaller than that for Doppler cooling by the approximate ratio $\omega_v/\Gamma \ll 1$. Consequently, the Sisyphus cooling rate is more efficient (at low temperatures, where the Lamb–Dicke criterion is satisfied) and the Sisyphus cooling limit is smaller than that for Doppler cooling. The minimum energy for sideband cooling and Sisyphus cooling is approximately the same, since the ion can be cooled to near the zero-point energy ($\hbar\omega_v/2$) in either case. However, for some applications it may be desirable to cool to $\langle n_v\rangle \ll 1$, in which case sideband cooling appears to be the appropriate choice.

6. POSSIBLE EXPERIMENTAL CONFIGURATIONS

To give an idea of how Sisyphus cooling might be employed, we consider the example of a single, trapped $^{24}Mg^+$ ion in a magnetic field **B**. To make the problem tractable, we will consider only the cooling of one degree of freedom, namely, the axial oscillation in a Paul rf trap or a Penning trap. To be consistent with the notation above, we call this the x degree of freedom. We will also make the simplifying assumption that the scattering rate for cooling the other degrees of freedom is adjusted so that, on the average, the recoil heating of the axial degree of freedom appears to be due only to reemission along the $+x$ or the $-x$ direction from the laser that cools the axial degree of freedom. This is consistent with the assumption made in the calculations of Sections 3 and 4.

The relevant internal energy levels are shown in Fig. 4(a). We assume that a linearly polarized standing-

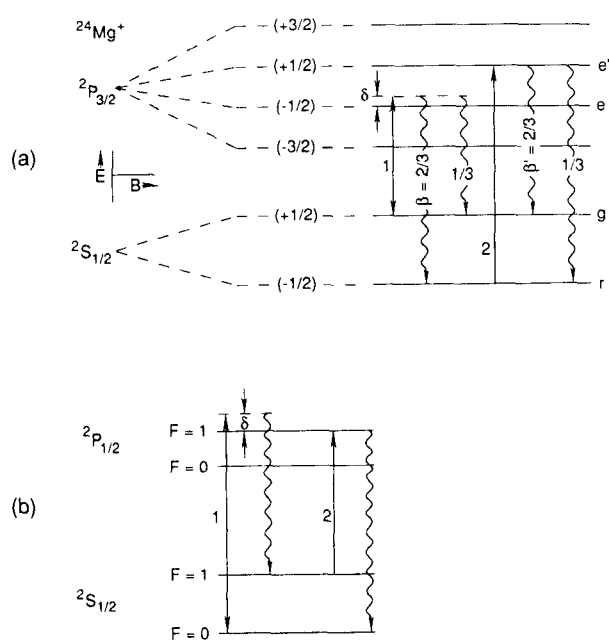

Fig. 4. The cooling described in the text could be approximately realized by a trapped $^{24}Mg^+$ ion in a magnetic field. A specific case is illustrated for the levels labeled g, e, and r in (a). Transfer from level r to level g could be realized with microwave radiation tuned to the $r \to g$ transition. This transfer could also be accomplished by spontaneous Raman transitions $r \to e' \to g$ by using a traveling-wave laser beam (laser 2 in the figure) tuned to the $r \to e'$ transition. In this case additional recoil heating must be accounted for (see the text). Another case that would apply to an ion or an atom with an outer unpaired electron and a spin 1/2 nucleus (and no intermediate electronic states) is shown in (b). Here the magnetic field is assumed to be small enough that the Zeeman structure is unresolved. Transfer from r to g through spontaneous Raman transitions (laser 2) is indicated in the figure.

wave laser beam (**k** vectors parallel and antiparallel to **x**) is tuned above the $^2S_{1/2}(m_J = +1/2) \rightarrow {}^2P_{3/2}(m_J = -1/2)$ transition frequency by an amount δ [laser 1 in Fig. 4(a)]. We assume that **B** (parallel to **x**) is large enough that $\hbar\delta \ll 2\mu_B B/3$, where μ_B is the Bohr magneton. This ensures that there will be negligible excitation on transitions other than those of interest. One situation for approximate realization of the cooling limit described in Subsections 3.D and 4.D is the following: First we leave laser 1 on long enough that the ion is pumped to level r with high probability [from Fig. 4(a), $\beta = 2/3$]. We then turn laser 1 off and transfer ions from level r to g with a microwave π pulse. (To accomplish the transfer, we need not as-sume that the duration of the π pulse is less than ω_v^{-1}.) Laser 1 is then turned on again, and the process is repeated. When laser 1 is turned back on, we assume that it is accomplished in a time long compared with ω_v^{-1} but short compared with $R_{g\rightarrow r}^{-1}$, so n_g is unchanged as $|g\rangle$ becomes dressed. As far as the cooling limit goes, this situation is actually somewhat better than the model that we have assumed in Section 2 because we avoid the heating resulting from well switching in the $r \rightarrow g$ transition. Mathematically, this amounts to setting $A_3 = 1$ in Eq. (29c). In this case the steady-state energy would be given by $\langle n_v\rangle = [2 + \beta\xi(\xi - 2)]/4\beta\xi$. This would be minimized for $\xi = (2/\beta)^{1/2}$, in which case $\langle n_v\rangle_{\min} = (2\beta)^{-1/2} - \frac{1}{2}$. For $\beta = 2/3$, $\langle n_v\rangle_{\min} \simeq 0.37$.

Experimentally, it might be easier to accomplish the $r \rightarrow g$ transfer with a second, traveling-wave laser beam tuned near the $^2S_{1/2}(m_J = -1/2) \rightarrow {}^2P_{3/2}(m_J = +1/2)$ transition [laser 2 in Fig. 4(a)]. (Additional cooling could be obtained with a second, standing-wave laser beam, but this would be more difficult to arrange experimentally.) The $r \rightarrow g$ transfer is then accomplished by spontaneous Raman scattering with probability $\beta' = 2/3$ for each scattering event from laser 2. This basic scheme could also be realized on $^2S_{1/2} \rightarrow {}^2P_{1/2}$ transitions in $^{24}Mg^+$ or other ions (atoms) with similar energy-level structure.

Using laser 2 will lead to a slightly higher minimum energy than our model predicts because of the additional recoil heating in the $r \rightarrow g$ transfer. To account for this heating properly, we must modify Eq. (17). Therefore we write

$$\dot{E}_x' = \dot{E}_x + \pi_r R_{r\rightarrow e'}(2R), \tag{47}$$

where $\dot{E}_x$ is given by Eq. (17), $R_{r\rightarrow e'}$ is the excitation rate from r to e' [e' is the $^2P_{3/2}(m_J = +1/2)$ level] that is due to the second laser, and $R_{r\rightarrow g} = 2R_{r\rightarrow e'}/3$. In steady state this amounts to doubling the recoil heating term in Eq. (17). For this case, $E_{x0} = \hbar\omega_v(\xi + 3/\xi)/2$, which is minimized for $\xi = \sqrt{3}$, yielding $E_{x0} = \sqrt{3}\,\hbar\omega_v$ or $\langle n_v\rangle = \sqrt{3} - 1/2 \simeq 1.23$.

For $^{24}Mg^+$ we take $\Gamma/2\pi = 43.0$ MHz and $\lambda = 279.64$ nm. If we assume that $\omega_v/2\pi = 2$ MHz, the conditions of relation (2) are reasonably satisfied for $\delta/2\pi = 1$ GHz and $\omega_1/2\pi = 0.118$ GHz (obtained from $\xi = \sqrt{3}$), in which case $R_{g\rightarrow e} \simeq 4.68 \times 10^5\ s^{-1}$. For these conditions and laser 2 adjusted to make $R_{r\rightarrow e'} = R_{g\rightarrow e}$, we have $\tau_s = 17.4\ \mu s$. For the transitions of interest the resonant cross section is $\lambda^2/4\pi$. If laser 2 is tuned to resonance the required intensity is 5.34 mW/cm^2. For one of the beams in the standing-wave laser beam, we require an intensity of 5.78 W/cm^2. To satisfy the condition $\hbar\delta \ll 2\mu_B/3$ we require that $B \gg 0.107T$. The effective temperature of the ion is given by

$$T = \hbar\omega_v/[k_B \ln(1 + \langle n_v\rangle^{-1})]. \tag{48}$$

For $\langle n_v\rangle \simeq 1.23$, $T \simeq 0.16$ mK. For the same transition the Doppler cooling limit is $\langle n_v\rangle \simeq 10$, corresponding to $T \simeq 1$ mK. For $\langle n_v\rangle < 1$, Eq. (48) shows that the temperature is only logarithmically dependent on $\langle n_v\rangle$. To achieve lower temperatures, we require ω_v to be lower, but if we make ω_v too low, we violate the condition $kx_0 \ll 1$ (in the example above, $kx_0 \simeq 0.23$).

Another scheme that might be used to cool an ion in a rf trap in a low magnetic field is illustrated in Fig. 4(b). This would work for $^{199}Hg^+$ ions, for example. Laser 1 provides the Sisyphus cooling, and laser 2 [or microwave radiation between the $^2S_{1/2}$ ($F = 0$) and ($F = 1$) levels] provides the repumping into level g. Similar schemes exist in other ions or atoms.

Experimentally, it may be difficult to make the center of the atom's well coincide with the point of maximum intensity gradient. One way around this problem for the standing-wave configuration would be to permit the standing wave to run over the center of the atom's position. This could be accomplished by the construction of a moving standing wave composed of two counterpropagating laser beams separated by frequency ω_m. When $R_{g\rightarrow r} \ll \omega_m \ll \omega_v$, the above expressions hold, with the magnitude of the intensity gradient replaced by its value averaged over the standing wave.

7. SUMMARY

We have examined Sisyphus cooling for a bound atom for the condition in which the radiative linewidth Γ is much larger than the oscillation frequency ω_v of the atom in its well. We have studied the strong-binding limit, which is given by the condition that the recoil energy be much less than the zero-point energy of the atom in the well. We have examined the cooling, using a simple three-level model for the internal states of the atom. We have assumed that the atom is confined in one dimension and cooled by a standing-wave laser beam. This model can be generalized to more-complicated cases. Since the minimum energies are near the zero-point energy of the atom in its well, we have examined the cooling limit, treating the atom's motion both classically and quantum mechanically. Within the approximations of the model the cooling limits are found to be the same.

We found that the minimum energy of the atom occurs when the depth of the dipole potential well created by the standing wave is approximately equal to the zero-point energy of the atom. In this case the minimum energy of the atom is given by the condition that the mean occupation number $\langle n_v\rangle$ of the atom in its well be approximately equal to 1. If we compare Sisyphus cooling with Doppler cooling, which operates on the same type of broad transition ($\Gamma \gg \omega_v$), we find that Sisyphus cooling is much more efficient for both the cooling rate (as long as we are in the Lamb–Dicke limit) and the cooling limit. Sisyphus cool

ing leads to a temperature nearly as low as that resulting from sideband cooling without the requirement of a narrow atomic transition. We have briefly examined experimental examples that assume atomic ions stored in traps. The same ideas should apply, however, for neutral atoms confined by magnetic traps, optical dipole traps, etc.

APPENDIX A: COOLING IN OTHER INTENSITY GRADIENTS

In the main text we have treated Sisyphus cooling in a standing-wave laser beam. The main ingredient in the cooling is that the atom experiences an intensity gradient along its direction of motion. Therefore it is useful to consider cooling in a more general intensity gradient. The cooling treatment of Section 4 applies, except that we must replace k in relations (4) and (15), Eq. (16a), and relation (18) by $[dI/dx_i]/2I$ evaluated at the equilibrium position of the ion, $x_i(0)$. If we define

$$\zeta = \frac{1}{k}\left|\frac{[dI/dx_i]_{x_i(0)}}{2I[x_i(0)]}\right|, \tag{A1}$$

then we find that the cooling rate is equal to the cooling rate of Eqs. (20) multiplied by ζ^2, and the cooling limit (from the condition $\dot{E}_x = 0$) is given by

$$E_{x_0} = U_{L_0}\frac{1 + 1/\xi^2\zeta^2\beta}{2}. \tag{A2}$$

This limiting energy is minimized for $\xi = (2/\beta\zeta^2)^{1/2}$, in which case

$$E_{x_0}^{\min} = \hbar\omega_v/\zeta\sqrt{\beta}. \tag{A3}$$

As an example, consider cooling in the intensity gradient of a focused traveling-wave Gaussian laser beam whose intensity in the direction transverse to the axis of the beam is given by $I(x_i) = I_0 \exp(-2x_i^2/w_0^2)$, where w_0 is the beam waist. If we assume that the atom is nominally localized to the position where $I[x_i(0)] = I_0/2$, then $x_i(0) = \pm[(\ln 2)/2]^{1/2}w_0$. For this condition, $\zeta = [(\ln 2)/2\pi^2]^{1/2}(\lambda/w_0)$. For a given ω_v, the cooling rate is reduced by the factor ζ^2, and the minimum energy is increased by the factor ζ^{-1}. However, in certain experiments this cooling might still be useful, because the region over which this intensity gradient is linear is larger and a standing-wave laser beam is not required. Therefore the condition $\hbar\omega_v \gg R$ need not be satisfied. On the other hand, the minimum achievable energy is larger than the recoil energy. This can be shown with the fact that the relative variation of $I(x)$ over the spatial distribution corresponding to Eq. (A3) should remain much less than 1.

ACKNOWLEDGMENTS

D. J. Wineland thanks the U.S. Office of Naval Research and the U.S. Air Force Office of Scientific Research for support. J. Dalibard warmly thanks the National Institute of Standards, Gaithersburg, for hospitality and partial support for the period during which this research was completed. He also acknowledges financial help from Direction des Recherches, Etudes et Techniques. We thank W. M. Itano and W. D. Phillips for helpful suggestions on the manuscript.

The Laboratoire de Spectroscopie Hertzienne de l'Ecole Normale Supérieure is associated with the Centre National de la Recherche Scientifique and the Université Pierre et Marie Curie.

REFERENCES AND NOTES

1. For a review of early experiments and theory see W. D. Phillips, ed., *Laser Cooled and Trapped Atoms,* Vol. 8 of Progress in Quantum Electronics (Pergamon, Oxford, 1984); P. Meystre and S. Stenholm, eds. feature on the mechanical effects of light, J. Opt. Soc. Am. **2,** 1705 (1985); S. Stenholm, Rev. Mod. Phys., **58,** 699 (1986); D. J. Wineland and W. M. Itano, Phys. Today **40**(6), 34 (1987).
2. P. Lett, R. Watts, C. Westbrook, W. D. Phillips, P. Gould, and H. Metcalf, Phys. Rev. Lett. **61,** 169 (1988).
3. J. Dalibard, C. Salomon, A. Aspect, E. Arimondo, R. Kaiser, N. Vansteenkiste, and C. Cohen-Tannoudji, in *Atomic Physics 11,* S. Haroche, J. C. Gay, and G. Grynberg, eds. (World Scientific, Singapore, 1989), p. 199; J. Dalibard and C. Cohen-Tannoudji, J. Opt. Soc. Am. B **6,** 2023 (1989).
4. S. Chu, D. S. Weiss, Y. Shevy, and P. J. Ungar, in *Atomic Physics 11,* S. Haroche, J. C. Gay, and G. Grynberg, eds. (World Scientific, Singapore, 1989), p. 636; P. J. Ungar, D. S. Weiss, E. Riis, and S. Chu, J. Opt. Soc. Am. B **6,** 2058 (1989); D. S. Weiss, E. Riis, Y. Shevy, P. J. Ungar, and S. Chu, J. Opt. Soc. Am. B **6,** 2072 (1989).
5. P. D. Lett, W. D. Phillips, S. L. Rolston, C. E. Tanner, R. N. Watts, and C. I. Westbrook, J. Opt. Soc. Am. B **6,** 2084 (1989).
6. B. Sheehy, S-Q. Shang, P. van der Straten, S. Hatamian, and H. Metcalf, Phys. Rev. Lett. **64,** 858 (1990); S-Q. Shang, B. Sheehy, P. van der Straten, and H. Metcalf, Phys. Rev. Lett. **65,** 317 (1990).
7. See S. Chu and C. Wieman, eds., feature on laser cooling and trapping of atoms, J. Opt. Soc. Am. B **6,** 2109 (1990); L. Moi, S. Gozzini, C. Gabbanini, E. Arimondo, and F. Strumia, eds., *Light Induced Kinetic Effects on Atoms, Ions, and Molecules* (ETS Editrice, Pisa, 1991).
8. C. Cohen-Tannoudji and W. D. Phillips, Phys. Today **43**(10), 33 (1990).
9. J. Dalibard and C. Cohen-Tannoudji, J. Opt. Soc. Am. B **2,** 1707 (1985).
10. A. P. Kazantsev, Zh. Eksp. Teor. Fiz. **66,** 1599 (1974) [Sov. Phys. JETP **39,** 784 (1974)]; A. P. Kazantsev, V. S. Smirnov, G. I. Surdutovitch, D. O. Chudesnikov, and V. P. Yakovlev, J. Opt. Soc. Am. B **2,** 1731 (1985).
11. V. G. Minogin and O. T. Serimaa, Opt. Commun. **30,** 123 (1977).
12. T. Breeden and H. Metcalf, Phys. Rev. Lett. **47,** 1726 (1981).
13. D. Pritchard, Phys. Rev. Lett. **51,** 1336 (1983).
14. A. Aspect, E. Arimondo, R. Kaiser, N. Vansteenkiste, and C. Cohen-Tannoudji, Phys. Rev. Lett. **61,** 826 (1988); J. Opt. Soc. Am. B **6,** 2112 (1989).
15. F. Diedrich, J. C. Bergquist, W. M. Itano, and D. J. Wineland, Phys. Rev. Lett. **62,** 403 (1989); W. Neuhauser, M. Hohenstatt, P. Toschek, and H. Dehmelt, Phys. Rev. Lett. **41,** 233 (1978); D. J. Wineland, W. M. Itano, J. C. Bergquist, and R. G. Hulet, Phys. Rev. A **36,** 2220 (1987).
16. Sideband cooling in the resolved sideband limit could also be obtained by using stimulated Raman scattering. See, for example, M. Lindberg and J. Javanainen, J. Opt. Soc. Am. B **3,** 1008 (1986); H. Dehmelt, G. Janik, and W. Nagourney, Bull. Am. Phys. Soc. **30,** 111 (1988); P. E. Toschek and W. Neuhauser, J. Opt. Soc. Am B **6,** 2220 (1989); D. J. Heinzen and D. J. Wineland, Phys. Rev. A **42,** 2977 (1990).
17. T. V. Zueva and V. G. Minogin, Sov. Tech. Phys. Lett. **7,** 411 (1981); L. Moi, Opt. Commun. **50,** 349 (1984); J. Liang and C. Fabre, Opt. Commun. **59,** 131 (1986); D. E. Pritchard, K. Helmerson, V. S. Bagnato, G. P. Lafyatis, and

A. G. Martin, in *Laser Spectroscopy VIII,* W. Persson and S. Svanberg, eds. (Springer-Verlag, Berlin, 1987), p. 68; J. Hoffnagle, Opt. Lett. **13,** 102 (1988); H. Wallis and W. Ertmer, J. Opt. Soc. Am. B **6,** 2211 (1989).
18. Y. Castin and J. Dalibard, Europhys. Lett. **16,** 761 (1991).
19. D. J. Wineland and W. M. Itano, Phys. Rev. A **20,** 1521 (1979).
20. S. Stenholm, *Foundations of Laser Spectroscopy* (Wiley, New York, 1984).
21. These results may be derived from more-general density matrix treatments. See, for example, Ref. 20 and V. S. Letokhov and V. P. Chebotayev, *Nonlinear Laser Spectroscopy* (Springer-Verlag, Berlin, 1977).
22. W. M. Itano and D. J. Wineland, Phys. Rev. A **25,** 35 (1982).

Hg^+ Single Ion Spectroscopy*

J.C. Bergquist, F. Diedrich,† Wayne M. Itano, and D.J. Wineland
Time and Frequency Division
National Institute of Standards and Technology
Boulder, CO 80303, USA

Introduction

A single ion in an electromagnetic trap can be localized in a small volume and held for a long period of time. A trapped ion also can be isolated from collisions and other perturbations and laser cooled to low temperatures. By monitoring the presence or absence of fluorescence from a strongly allowed transition, one can detect each transition to a metastable state. These characteristics make it possible to study the spectrum of a single ion with great precision. The vibrational energy states of the bound ion are quantized. We have used laser-sideband-cooling to drive the ion to the lowest energy level of the harmonic well of the trap.

Experiment

A mercury atom that is ionized by a weak electron beam is captured in the harmonic well created by an rf potential applied between the electrodes of a miniature Paul trap (1,2). The ring electrode has an inner diameter of about 900 μm and is placed symmetrically between two endcap electrodes that are separated by about 650 μm. The frequency of the rf potential is about 21 MHz. Its amplitude can be varied up to 1.2 kV. The classical motion of the ion consists of a small-amplitude oscillation, at the frequency of the applied rf potential, superimposed on a larger-amplitude harmonic motion, called the secular motion. The frequencies of the secular motion depend on the strength of the rf field (and any static field applied to the electrodes) and were typically 1-4 MHz. The ion is laser cooled to a few millikelvins by a few microwatts of 194 nm cw laser radiation (3) that is frequency tuned below the $5d^{10}6s\ ^2S_{1/2}$ - $5d^{10}6p\ ^2P_{1/2}$ first resonance line (1,4). In order to cool all motional degrees of freedom to near the Doppler cooling limit ($T = \hbar\gamma/2k_B \simeq 1.7$ mK) the 194 nm radiation irradiates the ion from 2 orthogonal directions, both of which are at an angle of 55° with respect to the symmetry (z) axis of the trap. The 282 nm radiation that drives the narrow $5d^{10}6s\ ^2S_{1/2}$ - $5d^96s^2\ ^2D_{5/2}$ transition is obtained by frequency-doubling the radiation from a narrowband cw ring dye laser. In the long term, the laser is either stabilized by FM optical heterodyne spectroscopy to a saturated absorption hyperfine component in $^{129}I_2$ (5) or directly to a stable high finesse reference cavity (6). The frequency of the laser is scanned by an acousto-optic modulator that is driven by a computer controlled synthesizer. Up to a few microwatts of 282 nm radiation could be focussed onto the ion in a direction counterpropagating with one of the 194 nm light beams.

Optical-optical double resonance (electron shelving) (1,2,4,7-11) with a net quantum amplification in excess of 100 at 10 ms is used to detect transitions driven by the 282 nm laser to the metastable $^2D_{5/2}$ state. The fluorescence from the laser-cooled ion is constant when it is cycling between the $^2S_{1/2}$ and $^2P_{1/2}$ states and zero when it is in the metastable $^2D_{5/2}$ state (1,4,7,8). Thus the $^2S_{1/2}$ - $^2D_{5/2}$ resonance

†Present address Gsänger Optoelektronik GmbH, Planegg,
Federal Republic of Germany

spectrum is obtained by first probing the S-D transition at a particular frequency near 282 nm, then turning off the 282 nm radiation, turning on the 194 nm radiation, and looking for 194 nm fluorescence. The two radiation fields are alternately applied to avoid light shifts and broadening of the narrow S-D transition. The absence of 194 nm fluorescence indicates that a transition into the metastable D state has occurred; its presence indicates that the ion has remained in the ground state. The 282 nm frequency is then stepped and the measurement cycle repeated. Each new result at a particular 282 nm frequency is averaged with the previous measurements at that frequency. The normalization of the signal is 1 for each measurement of high fluorescence and 0 for each measurement of no fluorescence. The high fluorescence level makes it possible to determine the state of the atom with almost no ambiguity in a few milliseconds. Thus, it is easy to reach the quantum noise limit of a single atomic absorber (1). Figure 1 shows the signal from an 8 MHz scan of the 282 nm laser through a Zeeman component of the S-D transition in $^{198}Hg^{+}$ (1). The Doppler-free central feature (carrier) and the motional sidebands due to the secular motion of the cold ion are fully resolved (12,13). The number and strength of the sidebands are a direct measure of the amplitude of the ion's motion and of its temperature.

In Fig. 2, we show a high resolution scan through the Doppler-free resonance of the $^{2}S_{\frac{1}{2}}(F = 0, m_F = 0) - {}^{2}D_{5/2}(F = 2, m_F = 0)$ transition in $^{199}Hg^{+}$ which is first-order field independent at a magnetic field $B \approx 0$. The full width at half maximum (FWHM) is approximately 86 Hz at 563 nm (172 Hz at 282 nm). This corresponds to a fractional resolution of better than 2×10^{-13} ($Q \approx 5\times10^{12}$). For this trace the laser was spectrally narrowed by locking to a mechanically, acoustically and thermally quiet reference cavity that had a finesse of about 60,000. The

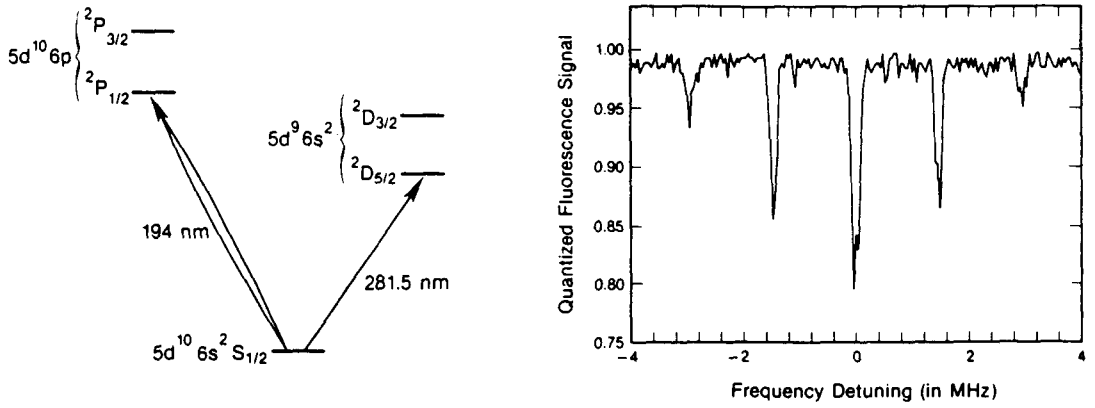

Fig. 1. On the left is a simplified energy-level diagram for $^{198}Hg^{+}$. The 282 nm transition can be observed by monitoring the 194 nm fluorescence. If the ion makes a transition from the $^{2}S_{\frac{1}{2}}$ to the $^{2}D_{5/2}$ level the 194 nm fluorescence disappears. For the figure on the right, the relative detuning from line center is plotted in frequency units at 282 nm. On the vertical axis is plotted the probability that the 194 nm fluorescence is on immediately after the 282 nm pulse. The Doppler-free recoilless-absorption-resonance or carrier (central feature) can provide a reference for an optical frequency standard. (From Ref. 1)

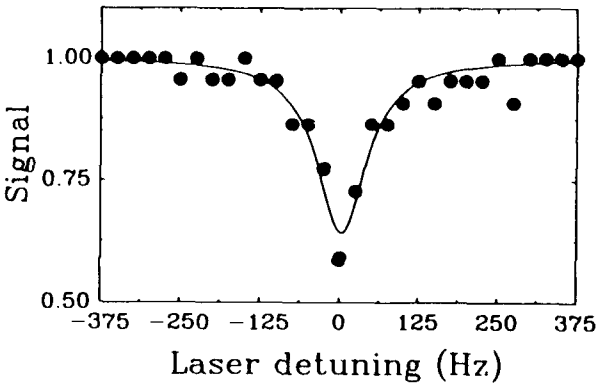

Fig. 2. High resolution scan through the Doppler-free resonance of the $^2S_{\frac{1}{2}}(F = 0, m_F = 0)$ - $^2D_{5/2}(F = 2, m_F = 0)$ transition in a single laser cooled $^{199}Hg^+$ ion. A frequency doubled and stabilized 563 nm laser ($\nu \approx 5\times10^{14}$ Hz) is stepped through the resonance in 25 Hz increments. The full width at half maximum is about 86 Hz. The integration time per point is about 0.5 s.

frequency of the laser fluctuates less than 50 mHz relative to this reference cavity. This is determined from the measurement of the noise in the error signal. The actual frequency fluctuations of the laser are governed by the stability of the mechanically and thermally isolated reference cavity (6). The natural linewidth of the S - D transition is approximately 1.7 Hz (2). The measured linewidth in Fig. 2 is likely limited by low frequency fluctuations in the length of the stable reference cavity (14). Better mechanical isolation of the reference cavity might permit us to reach the 1.7 Hz resolution limit.

The possibility of cooling the Hg^+ ion further, to the zero point energy of motion, is intriguing for several reasons. Cooling so that the average occupational number $\langle n_v \rangle$ for the motional energy of the bound atom is zero is a fundamental limit to laser-cooling for any bound particle (1,15) and forces a quantum mechanical treatment of the atom-trap system. Driving a single atom in a macroscopic trap to the zero point energy of motion exploits the benign environment near the center of an rf trap. Finally, if an ion is prepared in the lowest vibrational state, experiments such as squeezing the atom's position and momentum can be demonstrated (16).

In a rigorous treatment of the ion-trap system, stationary states do not exist since the trapping potential is time dependent. However, quasi-stationary states, obtained by solving for the eigenvalues of the Floquet operator, do exist (17,18). That these states correspond closely to the stationary states of the pseudo-potential of the rf trap is verified by the spectrum shown in Fig. 1. The carrier (at frequency ω_0) results from transitions in which the vibrational quasi-energy is unchanged. The upper and lower sidebands, spaced by multiples of the secular frequencies ($\omega_0 \pm n\omega_v$), correspond to transitions which increase or decrease the quasi-energy. Recently, we have cooled a single $^{198}Hg^+$ ion to the lowest vibrational state ($n_v = 0$) by a method called optical sideband cooling (15). First, the ion was laser-cooled to a few millikelvins by radiation scattered from the strong transition at 194 nm. This reduced the vibrational quantum number to a mean value of $\langle n_v \rangle \approx 12$. The secular frequency was about 3 MHz. Laser radiation tuned to the frequency of the first lower vibrational sideband (at frequency $\omega_0 - \omega_v$) of the narrow S-D transition was then applied to the ion. For each photon re-emitted at the unshifted carrier frequency, the vibrational energy was reduced by $\hbar\omega_v$. After the sideband cooling, laser radiation of saturating intensity was applied at the lower sideband frequency.

Absence of absorption indicated that the ion was in the $n_v = 0$ state. The ion was found to be in the $n_v = 0$ state about 95% of the time.

Starting from the ground vibrational state ($n_v = 0$), the absorption of a single quantum of energy at a frequency corresponding to the secular vibrational frequency (ω_v) would raise n_v by one unit. This could be detected with an efficiency of nearly 100%. Also, it should be possible to produce squeezed states (16) of the atom's motion from the zero point energy state by a sudden, non-adiabatic weakening (and, in general, shifting) of the trap potential or by driving the atomic motion parametrically at $2\,\omega_v$. If after some time the atom could then be returned to the $n_v = 0$ state by reversing the above procedures, the zero point energy state could be detected by the absence of the lower sideband.

We acknowledge the support of the U.S. Air Force Office of Scientific Research and the U.S. Office of Naval Research. F. Diedrich thanks the Deutsche Forschungsgemeinschaft for financial support.

References

1. J.C. Bergquist, W.M. Itano, and D.J. Wineland, Phys. Rev. A 36, 428 (1987).
2. J.C. Bergquist, D.J. Wineland, W.M. Itano, H. Hemmati, H.-U. Daniel, and G. Leuchs, Phys. Rev. Lett. 55, 1567 (1985).
3. H. Hemmati, J.C. Bergquist, and W.M. Itano, Opt. Lett. 8, 73 (1983).
4. J.C. Bergquist, R.G. Hulet, W.M. Itano, and D.J. Wineland, Phys. Rev. Lett. 57, 1699 (1986).
5. J.L. Hall, L. Hollberg, T. Baer, and H.G. Robinson, Appl. Phys. Lett. 39, 680 (1981).
6. J. Hough, D. Hils, M.D. Rayman, Ma L.-S., L. Hollberg, and J.L. Hall, Appl. Phys. B 33, 179 (1984).
7. W. Nagourney, J. Sandberg, and H. Dehmelt, Phys. Rev. Lett. 56, 2797 (1986).
8. T. Sauter, W. Neuhauser, R. Blatt, and P.E. Toschek, Phys. Rev. Lett. 57, 1696 (1986).
9. D.J. Wineland, J.C. Bergquist, W.M. Itano, and R.E. Drullinger, Opt. Lett. 5, 245 (1980); D.J. Wineland and W.M. Itano, Phys. Lett. 82A, 75 (1981).
10. H. Dehmelt, J. Phys. (Paris) Colloq. 42, C8-299 (1981).
11. H. Dehmelt, Bull. Am. Phys. Soc. 20, 60 (1975).
12. R.H. Dicke, Phys. Rev. 89, 472 (1953).
13. D.J. Wineland and W.M. Itano, Phys. Rev. A 20, 1521 (1979).
14. D. Hils and J.L. Hall, in Frequency Standards and Metrology, edited by A. DeMarchi (Springer-Verlag, Berlin, Heidelberg, 1989) p. 162.
15. F. Diedrich, J.C. Bergquist, W.M. Itano, and D.J. Wineland, Phys. Rev. Lett. 62, 403 (1989).
16. J.C. Bergquist, F. Diedrich, W.M. Itano and D.J. Wineland, in Frequency Standards and Metrology, edited by A. DeMarchi (Springer-Verlag, Berlin, Heidelberg, 1989) p. 287.
17. R.J. Cook, D.G. Shankland, and A.L. Wells, Phys. Rev. A 31, 564 (1985).
18. M. Combescure, Ann. Inst. Henri Poincaré 44, 293 (1986).

Frequency Standards in the Optical Spectrum*

*D.J. Wineland, J.C. Bergquist, W.M. Itano, F. Diedrich**, and C.S. Weimer*
National Bureau of Standards, Boulder, CO 80303, USA

1. Introduction

A long standing problem of spectroscopic measurements in the optical region of the spectrum has been the difficulty of obtaining accurate frequency reference standards to which spectral measurements can be compared. As will be discussed in this symposium on the hydrogen atom, this affects the value of the Rydberg constant as derived from optical measurements in hydrogen. As the experiments on hydrogen improve, the need for better reference points becomes more acute.

In this paper, we address two aspects of this general problem. First, we discuss the problem of frequency standards in the optical spectrum. (An analogue in the microwave region of the spectrum is the cesium beam frequency standard.) If one or a few of these reference frequencies can be accurately calibrated (perhaps by a frequency synthesis chain[1]) then it may be possible to compare optical spectra to these standards. As an example of the precision that might be achieved, we discuss only optical standards based on stored ions. Second, we discuss the problem of frequency comparison of unknown frequencies to the standards. Here we primarily restrict discussion to generation of wideband frequency "combs".

2. Optical Frequency Standards

One way an optical standard could be provided is by harmonic multiplication of a microwave frequency standard in a synthesis chain. By use of this technique, a laser at 88 THz (3.39 μm) has been made phase coherent with a microwave oscillator.[1] The best optical frequency standards may be made by locking a local oscillator (laser) to an atomic or molecular resonance line. State-of-the-art accuracies are characterized by measurements on methane stabilized He-Ne lasers in which reproducibilities in the 10^{-13} range have

* Supported by the U.S. Air Force Office of Scientific Research and the U.S. Office of Naval Research. Contribution of the U.S. National Bureau of Standards; not subject to U.S. Copyright.

** Supported by the DFG.

The Hydrogen Atom Editors: G.F. Bassani · M. Inguscio · T.W. Hänsch

been reported.[1] There are many other schemes for optical frequency standards.[1-3] Here, we will only discuss possibilities with single stored ions in order to give an idea of what stabilities and accuracies might be achieved.

3a. Single Ions

The use of single trapped ions as optical frequency standards was suggested by Dehmelt[4] in 1973. Since that time, demonstrations of laser cooling,[5] 100% detection efficiency,[6-8] and lasers with sub-Hz resolution,[1,9] have increased confidence that a single-ion frequency standard is viable. As an example, we summarize the current status[10] and discuss future prospects using single Hg^+ ions. Similar experiments using different kinds of ions have been reported at Seattle,[4,6] and Hamburg,[7,11] and other labs are initiating experiments.

In the NBS work, the transition of interest for a frequency standard is the Hg^+ $5d^{10}6s\ ^2S_{\frac{1}{2}} \rightarrow 5d^9 6s^2\ ^2D_{5/2}$ quadrupole transition at 281.5 nm shown in Fig. 1. The $^2D_{5/2}$ level has a lifetime of 86 ms, corresponding to a natural width of 1.8 Hz. Use of the single photon quadrupole transition has an advantage over two-photon Doppler free transitions[12] because ac Stark shifts are negligible.

A mercury atom that was ionized by a weak electron beam was captured in a miniature Paul (radio frequency) trap that has internal dimensions of $r_o \cong 466$ μm and $z_o \cong 330$ μm. The rf trapping frequency was 21.07 MHz with a peak voltage amplitude of about 730 V. The ion was laser cooled by a few microwatts of cw laser radiation that was frequency tuned below the $6s\ ^2S_{\frac{1}{2}} - 6p\ ^2P_{\frac{1}{2}}$ electric dipole transition near 194 nm. When the Hg^+ ion was cold and the 194 nm radiation had sufficient intensity to saturate the strongly allowed S-P transition, 2×10^8 photons/s were scattered. With our collection efficiency, this corresponded to an observed peak count rate of about $10^5\ s^{-1}$ against a background of less than $50\ s^{-1}$.

Optical-optical double-resonance utilizing quantum amplification[4,6-8] was used to detect transitions of the ion driven by the 281.5 nm laser to the metastable $^2D_{5/2}$ state. This method makes use of the fact that the 194 nm fluorescence intensity level is bistable; high when the ion is cycling between the S and P states (the "on" state) and nearly zero when it is in the metastable D state (the "off" state). The fluorescence intensity in the on state is high enough that the state of the atom can be determined in a few milliseconds with nearly 100% efficiency. The full measurement cycle was as follows: A series of measurements of the 194 nm fluorescence was made, using

a counter with a 10-ms integration period. As soon as the counter reading per measurement period was high enough to indicate that the ion was in the on

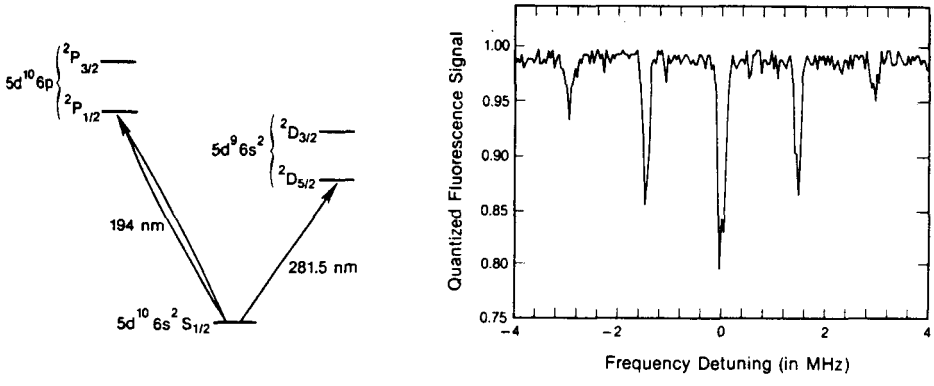

Fig. 1. On the left is a simplified energy-level diagram for $^{198}Hg^+$. The 281.5 nm quadrupole "clock" transition can be observed by monitoring the 194 nm fluorescence. If the ion has made a transition from the $^2S_{\frac{1}{2}}$ to the $^2D_{5/2}$ level the 194 nm flourescence disappears. For the figure on the right, on the horizontal axis is plotted the relative detuning from line center in frequency units at 281.5 nm. On the vertical axis is plotted the probability that the fluorescence from the 6s $^2S_{\frac{1}{2}}$ - 6p $^2P_{\frac{1}{2}}$ first resonance transition, excited by laser radiation at 194 nm, is on immediately after the 281.5 nm pulse. The electric-quadrupole-allowed S-D transition and the first-resonance S-P transition are probed sequentially in order to avoid light shifts and broadening of the narrow S-D transition. The recoilless absorption resonance or carrier (central feature) can provide a reference for an optical frequency standard. (From ref. 11)

state, the 194-nm radiation was shut off and the 281.5 nm radiation was pulsed on for 20 ms. Then, the 194 nm radiation was turned on again, and the counter was read. If the reading was low enough to indicate that the ion had made a transition to the $^2D_{5/2}$ state (the off state), the signal was defined to be 0. Otherwise, it was defined to be 1. The 281.5 nm laser frequency was then stepped, and the cycle was repeated. As the 281.5 nm laser frequency was swept back and forth through the resonance, the quantized measurement of the fluorescence signal at each frequency step was averaged with the previous measurements made at that same frequency. Since we could

detect the state of the ion with nearly 100% efficiency, there was essentially no instrumental noise in the measurement process. Occasionally, while the 194 nm radiation was on, the ion decayed from the $^2P_{\frac{1}{2}}$ state to the metastable $^2D_{3/2}$ state rather than directly to the ground state.[13] This process led to a background rate of false transitions which was minimized by the quantized data-collecting method described above and by decreasing the 194 nm fluorescence level thereby decreasing the $^2P_{\frac{1}{2}}$-$^2D_{3/2}$ decay rate. Neglecting decay to the $^2D_{3/2}$ level, the quantized measurement scheme removes any contribution to the signal base line due to intensity variations in the 194-nm source. The 281.5 and 194 nm radiation were chopped so that they were never on at the same time. This eliminated shifts and broadening of the narrow 281.5-nm resonance due to the 194 nm radiation.

Figure 1 shows the signal from an 8 MHz scan of the 281.5 nm laser through a Zeeman component of the ion. The central feature or "carrier" can be the reference for an optical frequency standard. The laser could be servoed to this resonance by probing on both sides of the resonance to develop an error signal which forces the average frequency of the laser to the center of the resonance. Two primary requirements for good performance are: (1) immunity from and ability to characterize systematic frequency shifts (accuracy) and (2) sufficient signal-to-noise ratio and line Q to reach the accuracy level in a reasonable length of time (stability).

3b. Stability

If we make the simplifying assumption that the time-domain Ramsey method is used to interrogate the clock transition, then the frequency stability (two-sample Allan variance[14]) is given as[15]

$$\sigma_y(\tau) \equiv [\langle(\langle\omega_k\rangle_\tau - \langle\omega_{k+1}\rangle_\tau)^2\rangle_k/2\omega_0^2]^{\frac{1}{2}} = (2\omega_0^2 T_R \tau)^{-\frac{1}{2}} . \qquad (1)$$

In this expression, $\langle\omega_k\rangle_\tau$ is the kth measurement of the frequency of the locked oscillator averaged over time τ, $\langle\ \rangle_k$ denotes an average over many measurements, ω_0 is the nominal frequency of the clock transition, and T_R is the interrogation time between pulses in the Ramsey method. Thus $\sigma_y(\tau)$ is a measurement of the rms fluctuations of the average frequency between adjacent measurements of duration τ. Eq. 1 assumes that optical state preparation (cooling and optical pumping) and fluorescence detection takes a time much less than T_R. We have also assumed $T_R \ll \tau(D_{5/2})$ and that the frequency of the 281.5 nm laser changes by much less than $(2T_R)^{-1}$ in time T_R. For our Hg^+ example, assuming T_R = 25 ms, $\sigma_y(\tau) \cong 7 \times 10^{-16}\tau^{-\frac{1}{2}}$. Therefore, at averaging

times of 1 s, the measurement imprecision on a single ion should be on the order of 1 part in 10^{15} or 1 Hz. Even better performance is expected on ions with narrower linewidths. To realize such stabilities, very narrow, tunable lasers are required but this technology is now available.[9]

3c. Accuracy

The advantage of single ions over other experimental configurations is the relative immunity from systematic frequency shifts. Laser cooling gives the lowest second order Doppler shifts for single (as opposed to many) trapped ions.[16] In the Doppler cooling limit,[5] the magnitude of the second order Doppler shift for Hg^+ ions in an rf trap is fractionally 2.4×10^{-18}. Laser cooling to the zero point energy, which has recently been achieved,[17] gives even smaller shifts. One must also account for all perturbing influences on the ion's internal structure.[4,18] For example, one must consider the perturbations due to static and time varying multipole interactions for electric, magnetic, and gravitational fields. These include atom trapping field interactions, collisions with neutral atoms, ac Stark shifts due to laser beams, stray electric and magnetic fields, gravitational red shifts, etc.

For the $^2S_{\frac{1}{2}} \rightarrow {}^2D_{5/2}$ quadrupole transition in Hg^+, the limiting accuracy may be due to the uncertainty in the interaction of the $^2D_{5/2}$ atomic quadrupole moment with static electric fields of quadrupole symmetry.[4,18] The interaction with the quadrupolar electric fields of the trap can be calibrated since they affect the ion oscillation frequencies of the trap in a known way. More difficult to control are the effects due to patch fields or stray charge build up. Shifts may be on the order of 0.1 Hz. We can significantly reduce the uncertainty due to these shifts, however, by taking the mean quadrupole transition frequency for three mutually orthogonal orientations of a quantizing magnetic field. In this case, the mean quadrupole shift is zero. For the $^1S_0 \rightarrow {}^3P_0$ transitions of the group IIIA ions, such shifts are absent.[4]

Although experimental verification is still lacking, it would appear that single ion optical frequency standards will eventually yield extremely high performance. Accuracies and stabilities better than 1 part in 10^{15} seem quite feasible; eventually they could exceed 1 part in 10^{18}.

4. Frequency Comparison

To appreciate the problem of frequency comparison in the optical region of the spectrum one needs only to plot the electromagnetic spectrum on a linear

frequency scale. The number (and spectral density) of accurate optical frequency standards is very small to begin with; this is to be compared with the situation in the microwave spectrum (and below) where commercially available synthesizers provide state-of-the-art precision at any frequency.

A laser whose frequency is unknown can be compared to a reference laser by heterodyne methods to high precision.[1] Beat frequency measurements up to 2.5 THz in the visible spectrum have already been made.[19] An alternative to simple heterodyne schemes is harmonic mixing by use of synthesis chains.[1] Here, the unknown laser frequency is compared (via heterodyne methods) to a harmonic of some well known reference line such as the methane stabilized He-Ne laser at 3.39 μm.[1]

Comparisons can also be made by wavelength methods. These have the advantage that two lasers of quite different frequency can be compared but are currently limited in accuracy to about the 10^{-10} to 10^{-11} range.[20]

For high accuracy comparison, heterodyne detection and synthesis chains are proven methods but have not been demonstrated in the visible yet. Moreover, since they are somewhat cumbersome and their coverage in the optical spectrum somewhat sparse, it is useful to pursue alternative methods.

5a. Wideband Comb Generation

Precise frequencies relative to a frequency standard (at frequency ω_0) can be provided by comb generation. If we amplitude or frequency modulate (at frequency Ω) a source at the standard frequency, then spectral components at frequencies $\omega_0 \pm n\Omega$ (n an integer) are generated. If n and Ω are chosen so that $\omega_0 + n\Omega \cong \omega$(unknown) then ω(unknown) can be precisely determined by heterodyne methods. The challenge is to make $(n\Omega)$ very large.

5b. Amplitude Modulation

As a specific example, let

$$A(t) = \sin(\omega_0 t + \varphi)\, f(t), \qquad (2)$$

where f(t) is periodic with period $2\pi/\Omega$. We will assume f(t) is an even function and near t = 0, has the form

$$f(t) \cong \exp[-(t/\tau)^2] \qquad \left(-\frac{\pi}{\Omega} < t < \frac{\pi}{\Omega}\right), \qquad (3)$$

where we also assume $\tau \ll 2\pi/\Omega$. (See Fig. 2) Expanding A(t) in a Fourier series, we find

$$A(t) \cong \frac{\Omega\tau}{2\sqrt{\pi}} \left\{ \sin(\omega_0 t+\varphi) + \sum_{n=1}^{\infty} \exp(-(n\Omega\tau/2)^2)\ (\sin[(\omega_0+n\Omega)t+\varphi_0] + \sin[(\omega_0-n\Omega)t + \varphi_0]) \right\}. \quad (4)$$

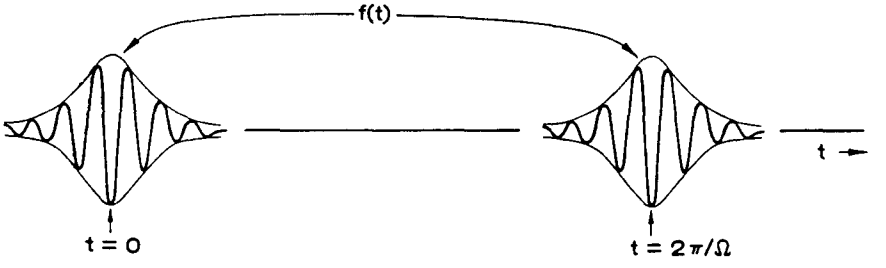

Fig. 2. A sine-wave carrier (frequency ω_0) is assumed to be periodically amplitude modulated at frequency Ω with a Gaussian envelope. Exact frequency division (ω_0/Ω = integer) is obtained if the phase of the carrier is fixed to the phase of the modulation envelope.

To make the spectral component at $\omega_0 \pm n\Omega$ as large as possible we want $n\Omega\tau/2$ close to unity. For harmonic generation, $\omega_0 = \Omega$. For either harmonic generation or comb generation around a high frequency ω_0, the comb bandwidth is approximately equal to $1/\tau$. High order multiplication to the visible or large bandwidth combs in the visible are difficult to achieve for two reasons: (1) it is difficult to make τ small enough and (2) the modulator must be sufficiently broadband to pass the fundamental and its harmonics or sidebands.

We remark that Fig. 2 is characteristic of the output of a mode locked laser[21] or a free electron laser with pulsed input electron beam.[22] Mode-locked lasers have already been suggested as devices for frequency translation in the optical spectrum.[21]

5c. Frequency Modulation

Consider sine wave modulation of a carrier at frequency ω_0:

$$A(t) = A_0 \sin[\omega_0 t + \frac{\Delta\omega}{\Omega} \sin\Omega t + \varphi]$$
$$= A_0 \sum_{n=-\infty}^{\infty} J_n(\frac{\Delta\omega}{\Omega}) \sin[(\omega_0 + n\Omega)t + \varphi], \quad (5)$$

where $\Delta\omega$ is the frequency swing. Assume we are interested in the spectral component at a particular (large) value of n. We make the substitution $\Delta\omega/\Omega = n\beta$, and will limit ourselves to the case where $\beta < 1$. From Meissel's formula[23] for $J_n(n\beta)$, for large n and $\beta < 1$, we can write

$$J_n(n\beta) \cong \left[\frac{\beta e^{(1-\beta^2)^{\frac{1}{2}}}}{1+(1-\beta^2)^{\frac{1}{2}}}\right]^n [2\pi n(1-\beta^2)^{\frac{1}{2}}]^{-\frac{1}{2}} . \quad (6)$$

We can make the spectral component at $\omega_0 + n\Omega$ reasonably large by making β close to unity or the modulation index $\Delta\omega/\Omega$ close to n. This is the primary practical problem for n large.

6a. Frequency Division

Using amplitude or frequency modulation of a carrier at frequency ω_0, we can achieve exact frequency division if we make sidebands of the carrier to such low frequency that we can force the condition $\omega_0 - n\Omega = (n+2)\Omega - \omega_0 = \Omega$ so that $\omega_0/\Omega = n+1$. For example, if we examine Fig. 2, we can achieve exact frequency division by any means which locks the phase of the carrier to the phase of the amplitude modulation; that is, the undulations of the carrier do not "slip" under the envelope of the amplitude modulation. A divider based on these principles would be quite useful if Ω is in the microwave region (or below) where precise frequency synthesis is possible. Since Ω and n could be freely chosen, any value of ω_0 could be measured in a single device.

6b. Single Electron Frequency Divider

The required extreme amplitude or frequency modulation might be accomplished with the interaction of an electromagnetic wave (at frequency ω_0) with a single electron oscillating at frequency Ω. For example, Ω might be the cyclotron frequency of the electron in a magnetic field.

As originally proposed,[24] extreme amplitude modulation of the electromagnetic wave (at the site of the electron) could be accomplished by

focussing the wave with a fast lens or slow wave structure (miniature waveguide) onto a portion of the electron's cyclotron orbit. The energy coupled into the electron at frequency $\omega_0-n\Omega = (n+2)\Omega-\omega_0 = \Omega$ is balanced by synchrotron radiation and phase locking can occur. Lens focussing requires the electron to be relativistic, $\gamma \equiv (1-(v/c)^2)^{-\frac{1}{2}} \geq 2$ to achieve a significant coupling[24] (v = electron speed, c = speed of light). Use of a slow wave structure would allow use of lower energy electrons.

Driving the electron could also be accomplished using an inverse synchrotron radiation geometry.[25] Here, a collimated laser beam is made to coincide with a tangent to the electron's orbit. We require the electron to be relativistic to achieve a significant interaction. If the laser beam waist is made much larger than the electron orbit dimensions, then we have the case of extreme frequency modulation of a plane wave as first analyzed by Kaplan.[26] Here, the electric field at the site of the electron is given by Eqs. 5 and 6 with $\beta = v/c$. Again, we require the electron to be somewhat relativistic to make J_n and J_{n+2} sufficiently large ($\omega_0-n\Omega = \Omega$).

In all cases above, the center of the electron's orbit (in the plane of the orbit) must be held within $\lambda\!\!\!^{-}(= c/\omega_0)$. A specific scheme for accomplishing this is discussed in Ref. 24. At NBS we have initiated a project along these lines. At first, low order division ($n < 10$) where ω_0 and Ω are both microwave frequencies will be tried. Aside from the practical application discussed here, such an experiment is interesting in terms of the fundamental nonlinear interactions of simple elementary systems.

We thank L. Hollberg and D. Jennings for helpful comments on the manuscript.

1. D.A. Jennings, K.M. Evenson, and D.J. Knight, Proc. IEEE 74, 168 (1986); S.N. Bagaev and V.P. Chebotayev, Usp. Fiz. Nauk 148, 143 (1986) (Sov. Phys. Usp. 29, 82 (1986)), and references therein.
2. Proc. Fourth Symp. Freq. Standards and Metrology, Ed. A. DeMarchi, Ancona, Italy, Sept. 1988 (Springer-Verlag, Heidelberg) to be published.
3. Proc. Third Symp. Freq. Standards and Metrology, J. de Physique, Vol. 42, Colloque C-8, 1981.
4. H.G. Dehmelt, Bull. Am. Phys. Soc. 18, 1521 (1973) and 20, 60 (1975); H.G. Dehmelt, IEEE Trans. Instrum. Meas. IM-31, 83 (1982); H.G. Dehmelt, in Advances in Laser Spectroscopy, Ed. by F.T. Arecchi, F.S. Strumia, and H. Walther, (Plenum, New York, 1983), p. 153.

5. See for example, D.J. Wineland and W.M. Itano, Phys. Today, 40, no. 6, p. 34 (1987), and references therein.
6. W. Nagourney, J. Sandberg, H. Dehmelt, Phys. Rev. Lett. 56, 2797 (1986).
7. T. Sauter, W. Neuhauser, R. Blatt, P.E. Toschek, Phys. Rev. Lett. 57, 1696 (1986).
8. J.C. Bergquist, R.G. Hulet, W.M. Itano, D.J. Wineland, Phys. Rev. Lett., 57, 1699 (1986).
9. J.L. Hall, D. Hils, C. Salomon, and J.M. Chartier, in Laser Spectroscopy VIII, ed. by W. Persson and S. Svanberg, (Springer, Berlin Heidelberg, 1987) p. 376.
10. J.C. Bergquist, W.M. Itano, D.J. Wineland, Phys. Rev. A36, 428 (1987).
11. P.E. Toschek, in Tendances Actuelles en Physique Atomique, Les Houches, Session 38, G. Grynberg and R. Stora, eds., (North-Holland, 1984) p. 381.
12. J.C. Bergquist, D.J. Wineland, W.M. Itano, H. Hemmati, H.U. Daniel, G. Leuchs, Phys. Rev. Lett. 55, 1567 (1985).
13. W.M. Itano, J.C. Bergquist, R.G. Hulet and D.J. Wineland, Phys. Rev. Lett. 59, 2732 (1987).
14. J.A. Barnes, A.R. Chi, L.S. Cutler, D.J. Healey, D.B. Leeson, T.E. McGunigal, J.A. Mullen, Jr., W.L. Smith, R.L. Sydnor, R.F.C. Vessot, and G.M.R. Winkler, IEEE Trans. Instrum. Meas. IM-20, 105 (1971).
15. D.J. Wineland, W.M. Itano, J.C. Bergquist and F.L. Walls, in Proceedings of the Thiry-fifth Annual Symposium on Frequency Control (1981), p. 602 (copies available from Electronics Industry Assn., 2001 "Eye" St., N.W. Washington, D.C. 20006).
16. D.J. Wineland, in Precision Measurement and Fundamental Constants II, Natl. Bur. Stand. (U.S.) Special Publ. No. 617, edited by B.N. Taylor and W.D. Phillips, (U.S. GPO, Washington, D.C., 1984), p. 83.
17. F. Diedrich, J.C. Bergquist, W.M. Itano, D.J. Wineland, to be published.
18. D.J. Wineland, Science 226, 395 (1984), and references therein.
19. R.E. Drullinger, K.M. Evenson, D.A. Jennings, F.R. Petersen, J.C. Bergquist, L. Burkins, and H.U. Daniel, Appl. Phys. Lett. 42, 137 (1983).
20. R.G. DeVoe, C. Fabre, K. Jungmann, J. Hoffnagle, and R.G. Brewer, Phys. Rev. A37, 1802 (1988).
21. S.R. Bramwell, D.M. Kane, and A.I. Ferguson, Opt. Commun. 56, 12 (1985); J.A. Valdmanis, R.L. Fork, and J.P. Gordon, Opt. Lett. 10, 131 (1985); see also D.M. Kane, S.R. Bramwell, and A.I. Ferguson, Appl. Phys. B39, 171 (1986).

22. S. Penner et al., in Proc. 9th Int. F.E.L. Conf., Williamsburg, VA, 1987, to be published.
23. G.N. Watson, Theory of Bessel functions (Cambridge Press, 1952), p. 227.
24. D.J. Wineland, J. Appl. Phys. 50, 2528 (1979); J.C. Bergquist, D.J. Wineland, Natl. Bur. Stand. (U.S.), Tech Note 1086, (U.S. G.P.O., 1985) p. TN-30.
25. R.H. Pantell and J.A. Edighoffer, J. Appl. Phys. 51, 1905 (1980).
26. A.E. Kaplan, Optics Lett. 12, 489 (1987).

Progress at NIST Toward Absolute Frequency Standards Using Stored Ions

D. J. WINELAND, J. C. BERGQUIST, J. J. BOLLINGER, W. M. ITANO, D. J. HEINZEN, S. L. GILBERT, C. H. MANNEY, AND M. G. RAIZEN

Abstract—**Experiments at NIST, whose goal is to realize frequency standards of high accuracy using stored ions, are briefly summarized. In one experiment, an RF oscillator is locked to a nuclear spin-flip hyperfine transition (frequency $\simeq 3.03 \times 10^8$ Hz) in $^9Be^+$ ions that are stored in a Penning trap and sympathetically laser-cooled. Stability is better than $3 \times 10^{-12}\,\tau^{-(1/2)}$ and uncertainty in Doppler shifts is estimated to be less than 5×10^{-15}. In a second experiment, a stable laser is used to probe an electric quadrupole transition (frequency $\simeq 1.07 \times 10^{15}$ Hz) in a single laser-cooled $^{199}Hg^+$ ion stored in a Paul trap. The measured Q value of this transition is approximately 10^{13}. Future possible experiments are also discussed.**

INTRODUCTION

ONE GOAL of the ion storage group at NIST (formerly the National Bureau of Standards) has been to realize a stored ion frequency standard whose absolute inaccuracy is less than 1 part in 10^{14}. Primary design considerations in these experiments have been influenced by the assumptions that 1) for many ions in the trap, the uncertainty in the measurement of the second-order Doppler shift will be the largest contribution to inaccuracy and 2) the magnitude of the second-order Doppler shift decreases as the number of ions in the trap decreases.

These assumptions are supported both by experiments and theoretical analysis [1]–[6]. For a given number of ions N in the trap the second-order Doppler shift is minimized when the secular motion in the Paul trap [2]–[5] or the cyclotron and axial motion in the Penning trap [1]–[3] are reduced by some means to negligible values (for example, by the use of buffer gas collisions [4] or laser cooling [6], [7]). For the Paul trap, the second-order Doppler shift is then dominated by the velocity in the RF micromotion [1]–[5]. The basic idea is as follows: in the quadrupole Paul trap the RF micromotion velocity increases with the distance of the ion from the center of the trap. As the number of trapped ions increases, space charge repulsion holds ions farther from the center of the trap thereby increasing the ion's micromotion speed and second-order Doppler shift. For a spherical cloud of ions, the number of ions N is proportional to the fractional second-order Doppler shift, averaged over the cloud, $\langle \Delta\nu_{D2}/\nu_0 \rangle$ [2]–[4]:

$$N = -2.16 \times 10^{16}\, r_{cl} M \langle \Delta\nu_{D2}/\nu_0 \rangle / Z^2 \quad \text{(RF trap)} \tag{1}$$

where r_{cl} is the cloud radius in centimeters, M is the ion mass in atomic mass units and Z is ion charge in units of the proton charge. The number of ions for a given second-order Doppler shift can be increased by using a nonspherical ion cloud geometry in an elongated trap [5]. However, the basic idea still holds that as the number of ions increases so does $|\langle \Delta\nu_{D2}/\nu_0 \rangle|$. The second order Doppler shift is minimized for a single ion [6] or for more than one ion in a trap with linear geometry (discussed below).

In the Penning trap, when the cyclotron and axial kinetic energies are reduced to small values, the second order Doppler shift is dominated by the velocity in the rotation of the ion cloud. In this case, N and $\langle \Delta\nu_{D2}/\nu_0 \rangle$ are related by [1]–[3]

$$N = 3.10 \times 10^{13}\, B \langle -\Delta\nu_{D2}/\nu_0 \rangle^{1/2} \cdot z_{cl}(r_{cl} - r_c')/Z \,\text{(Penning trap)} \tag{2}$$

where B is the trap magnetic field strength in teslas, $2z_{cl}$ and r_{cl} are the cloud height and radius in centimeters, $r_c' = (5\langle -\Delta\nu_{D2}/\nu_0 \rangle)^{1/2} c/\Omega_c$ (Ω_c is the ion's cyclotron frequency and c is the speed of light), and Z is the ion charge in units of proton charge. Equations (1) and (2) are valid for one species of ion in the trap.

Therefore, for both traps, $|\langle \Delta\nu_{D2}/\nu_0 \rangle|$ increases as N increases and we are faced with a compromise in design. For good signal-to-noise ratio (SNR) and therefore good frequency stability, we desire large N. However this increases $|\langle \Delta\nu_{D2}/\nu_0 \rangle|$ and therefore decreases accuracy because of our inability to measure precisely the velocity distributions needed to determine $\langle \Delta\nu_{D2}/\nu_0 \rangle$. This tradeoff between stability and accuracy has resulted in different approaches. In the work of one group [4], [8], a stored $^{199}Hg^+$ ion standard with excellent stability has been realized. In these experiments $N \simeq 2 \times 10^6$ and $\langle \Delta\nu_{D2}/\nu_0 \rangle \simeq -2 \times 10^{-12}$, so an accuracy of 10^{-14} would require a knowledge of $\langle v^2 \rangle$ to 0.5% precision. This problem can be reduced in the elongated trap geometry of [5] but, in-

Manuscript received February 1, 1990; revised May 28, 1990; accepted May 31, 1990. This paper is based on a paper by the authors in *Proc. 43rd Annu. Symp. Freq. Contr.*, Denver, June 1989, pp. 143–150, (IEEE Cat. no. 89CH2690-6, NO Nov. 1989).

The authors are with the National Institute of Standards and Technology, Time and Frequency Division, Mail Code 576, Boulder, CO 80303.

IEEE Log Number 9038497.

dependent of the trap geometry, the accuracy can generally be improved by using smaller numbers.

At NIST the primary goal of stored-ion frequency standard work has been high accuracy. The preceding arguments have forced us to use small numbers of ions (approximately 10^4 or less) that are laser-cooled. The loss in short-term stability due to reduced numbers can be partially regained by going to very long interrogation times. These trade-offs are apparent from the expression for stability if we assume the Ramsey method of interrogation and assume 100% detection efficiency. For these conditions [3],

$$\sigma_y(\tau) = (\tau N T_R \omega_0^2)^{-(1/2)} \quad (\tau > T_R) \qquad (3)$$

where τ is the averaging time, T_R is the Ramsey interrogation time and ω_0 is the clock transition frequency (in radians per second). From this expression, we also see the importance of making ω_0 large.

Of course, to achieve high accuracy, we must also account for the perturbations due to static and time-varying multipole interactions for electric, magnetic, and gravitational fields. These include atom-trap field interactions, collisions, shifts due to uncontrolled electric and magnetic fields, and gravitational red shifts. However for more than one ion in the trap, the dominant uncertainty appears to be caused by the uncertainty in the second-order Doppler shift.

Below, we briefly discuss experiments at NIST on stored-ion frequency standards. More detailed accounts are forthcoming.

$^9Be^+$ Hyperfine Clock

In this experiment, an oscillator has been locked to the $(m_I = -1/2, m_J = 1/2) \leftrightarrow (-3/2, 1/2)$ nuclear spin-flip hyperfine "clock" transition ($\omega_o/2\pi \cong 303$ MHz) in the ground state of $^9Be^+$ (Fig. 1). The basic idea of this experiment has been described previously [9]–[12]; the current experiment works as follows [12]: Between 5000 and 10 000 $^9Be^+$ ions and 50 000 to 150 000 $^{26}Mg^+$ ions were simultaneously stored in a cylindrical Penning trap [12] with $B \cong 0.8194$ T under conditions of high vacuum ($\lesssim 10^{-8}$ Pa). At a magnetic field B of 0.8194 T the clock transition depends only quadratically on magnetic field fluctuations, and therefore the accuracy is not limited by field fluctuations. To minimize second order Doppler shifts of the clock transition, the $^9Be^+$ ions were cooled to less than 250 mK in the following manner: The $^{26}Mg^+$ ions were directly laser-cooled and compressed by a narrow-band (~ 1 MHz) laser radiation source at 280 nm. The $^9Be^+$ ions were then sympathetically cooled [13] by their Coulomb interaction with the cold Mg^+ ions (see Appendix I). A narrow-band 313-nm radiation source was used to optically pump and detect the $^9Be^+$ ions [9]–[12]. With the 313-nm source tuned to the $2s\ ^2S_{1/2}(m_I = 3/2, m_J = 1/2)$ to $2p\ ^2P_{3/2}(3/2, 3/2)$ transition, 94% of the $^9Be^+$ ions were optically pumped into the $2s\ ^2S_{1/2}(3/2, 1/2)$ ground state. The 313-nm source was then turned off to avoid optical pumping and ac Stark shifts while the clock transition was driven.

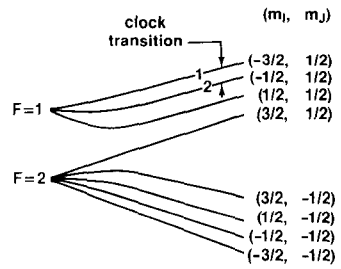

Fig. 1. Hyperfine energy levels (not drawn to scale) of the $^9Be^+$ $2s\ ^2S_{1/2}$ ground state as a function of magnetic field. At $B = 0.8194$ T the 303 MHz clock transition is independent of magnetic field to first order.

The clock transition was detected by the following method: After the 313-nm source was turned off, the ions in the $(3/2, 1/2)$ state were transferred to the $(1/2, 1/2)$ state and then to the $(-1/2, 1/2)$ state by two successive RF π pulses. Each pulse was 0.2 s long and was resonant with the appropriate transition frequency (around 321 MHz and 311 MHz respectively). The clock transition was then driven by Ramsey's method of separated oscillatory fields in the time domain with RF pulses of about 1-s duration and a free precession time on the order of 100 s. This transferred some of the ions from the $(-1/2, 1/2)$ state to the $(-3/2, 1/2)$ state. Those ions remaining in the $(-1/2, 1/2)$ state were then transferred back to the $(3/2, 1/2)$ state by reversing the order of the two RF π pulses. The 313-nm source was then turned back on, and the population of ions in the $(-3/2, 1/2)$ state was registered as a decrease in the $^9Be^+$ fluorescence, relative to the steady-state fluorescence, during the first second that the 313-nm source was on. (The optical repumping time of the ions from the $(-3/2, 1/2)$ state to the $(3/2, 1/2)$ state was about 10 s.) The sympathetic cooling of the $^9Be^+$ ions by the continuously cooled Mg^+ ions is necessary if long interrogation times are to be used, since otherwise the $^9Be^+$ ions would slowly heat up while the 313-nm laser is off [11].

The Ramsey signal was used to steer the frequency of a synthesized RF source [9]–[12]. Ramsey signal measurements were taken near the frequencies corresponding to the half minimum points on both sides of the center frequency. The difference in the measured signal strengths on either side of the line center was used to electronically steer the average frequency of the synthesizer to ω_0. Most runs were taken with a commercial cesium beam clock (fractional frequency stability $\sigma_y(\tau) \simeq 6 \times 10^{-12}\ \tau^{-(1/2)}$ for measurement time τ in seconds) as the reference oscillator, but a few runs were taken with a passive hydrogen maser ($\sigma_y(\tau) \simeq 2\text{–}3 \times 10^{-12}\ \tau^{-(1/2)}$) as the reference oscillator. Stabilities of the $^9Be^+$ clock are measured to be better than $3 \times 10^{-12}\ \tau^{-(1/2)}$ for the number of ions used, which is within a factor of 4 of the theoretical maximum stability given by (3). The systematic offset of our measurement due to the second-order Doppler frequency shift was dominated by the velocity in the rotation motion

of the ions about the trap axis. This shift was measured to be $(-1.2 \pm 0.5) \times 10^{-14}$.

An apparent pressure shift with an unexpectedly large value was discovered when the background gas pressure was increased. The background gas pressure could be increased by moving the magnet of the sputter ion pump that evacuated the trap region so that it overlapped fewer pumping cells and reduced the pumping speed. (We checked to make sure the magnetic field at the site of the ions was not disturbed.) The composition of the gas was not known since the pressure was measured with a Bayard-Alpert gauge. However, when the vacuum vessel containing the trap was initially evacuated the dominant background gases were H_2 and He as determined by a quadrupole mass analyzer. Therefore we expect that the background gas during the frequency standard measurements was either H_2 or He, or both. If the background gas was dominated by He, the fractional pressure shift was measured to be about -3×10^{-6} Pa^{-1}; if the background was dominated by H_2, the pressure shift was measured to be about -9×10^{-6} Pa^{-1}. Atomic ion hyperfine pressure shifts for He have previously been measured in $^{137}Ba^+$ [14] and in $^{199}Hg^+$ [8] to be 5×10^{-11} Pa^{-1} and 4×10^{-11} Pa^{-1} respectively. The authors of [14] show that the charge induced multipole interaction between the Ba^+ and the noble gas atoms used in that study should give an important contribution to the pressure shift. Since this interaction depends primarily on the polarizability of the neutral we would expect that the pressure shift for He atoms on $^9Be^+$ ions would not be significantly different than that for Ba^+ or Hg^+. Similarly, since the polarizability of H_2 is midway between Ar and Ne, we might expect the pressure shift for H_2 on Be^+ to be near those for Ar and Ne on Ba^+, which were measured to be -6×10^{-10} Pa^{-1} and -6×10^{-9} Pa^{-1} respectively.

The apparent large discrepancy between our data and other measured pressure shifts is not understood at this time. One possible explanation is suggested by studies [15] of radiative association of C^+ with H_2 to form CH_2^+. In the models of this process, it is assumed that the H_2 can stick to the C^+ for a long enough time to allow the C^+–H_2 complex to radiatively stabilize. This sticking is possible because the collision energy can be taken up by the internal degrees of freedom in the H_2 molecule. The sticking time can be orders of magnitude longer than the interaction time during a simple elastic collision. If a similar sticking mechanism is active in H_2–Be^+ collisions, it may account for the apparent large pressure shift. One way to check this hypothesis is to measure the pressure shifts of Be^+ on Ne and Ar, where the sticking would not be expected to occur, and on H_2 or other polyatomic gases, where sticking might occur.

The uncertainty in this apparent pressure shift will probably limit the accuracy of the current $^9Be^+$ clock measurements to around 1 part in 10^{13}. However, we hope to more fully understand the shift before stating a final uncertainty. We are also continuing to search for other causes of systematic errors such as electronic offsets. However, we feel the accuracy could be improved beyond 5 parts in 10^{15} in the future. If the apparent collisional shift is real, it may be necessary to use liquid He cryopumping to reduce the background pressure.

Hg^+ Optical Clock

The velocity in the micromotion for an ion in a quadrupole RF trap is proportional to the distance of the ion from the center of the trap. For two or more laser-cooled ions in the trap, the Coulomb repulsion between ions holds them away from the trap center, and the second-order Doppler shift is dominated by the velocity of micromotion. However, a single ion can be held near the trap center if sufficiently cooled. In this case the kinetic energy in the micromotion can be equal to that of the secular motion [2], [3], [16], [17]. If the ion is laser-cooled, resulting Doppler shifts can be extremely small; uncertainties can be less than 1 part in 10^{20} in some cases [17], [18]. However with $N = 1$, stability is marginal unless we make ω_0 high enough (see 3). One way to accomplish this is to let ω_0 correspond to an optical transition. Dehmelt suggested this idea in 1973 [6]. The reasons that a clock based on an optical transition in an ion has not been realized yet are: 1) it took several years to isolate and manipulate single ions in the traps; 2) local oscillators (lasers) with the desired spectral purity are still not available; and 3) accurate comparison of laser and microwave frequencies is extremely difficult and remains an important problem. Nevertheless the potential accuracy of single-ion optical frequency standards is extremely high [6], [19] ($\simeq 10^{-18}$) so it is important to pursue this research.

At NIST we have investigated the use of the $5d^{10}6s\ ^2S_{1/2} \rightarrow 5d^96s^2\ ^2D_{5/2}$ electric quadrupole transition ($\omega_0/2\pi \simeq 1.07 \times 10^{15}$ Hz) in $^{198}Hg^+$ (see Fig. 2) as an optical frequency standard [20]. The single mercury ion is confined in a miniature RF trap that has internal dimensions of $r_o \cong 466$ μm and $z_o \cong 330$ μm [20], [21]. The amplitude of the trapping field (frequency $\Omega/2\pi \cong 21$–23 MHz) can be varied to a peak of 1.2 kV. The ion is laser-cooled to a few millikelvins by a few microwatts of CW laser radiation that is tuned below the $^2S_{1/2}$–$^2P_{1/2}$ first resonance line near 194 nm. In order to cool all motional degrees of freedom to near the Doppler cooling limit [7] ($T = \hbar\gamma/2k_B \cong 1.7$ mK) the 194 nm radiation irradiates the ion from 2 orthogonal directions, both of which are at an angle of 55° with respect to the symmetry (z) axis of the trap. The 282-nm radiation that drives the narrow $^2S_{1/2}$–$^2D_{5/2}$ transition is obtained by frequency-doubling the radiation from a narrowband CW ring-dye laser. The frequency of the laser is stabilized by locking it to a stable Fabry-Perot cavity. The frequency of the laser is scanned by an acoustooptic modulator that is driven by a computer controlled synthesizer. Up to a few microwatts of 282 nm radiation could be focussed onto the ion in a direction counterpropagating with one of the 194-nm light beams.

Optical-optical double resonance was used to detect transitions driven by the 282-nm laser from the ion's $^2S_{1/2}$ ground state to the metastable $^2D_{5/2}$ state [20], [21]. The

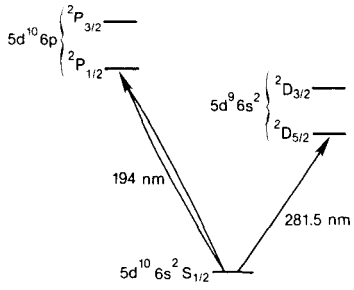

Fig. 2. Simplified optical energy-level diagram for Hg^+. The lifetime of the $^2D_{5/2}$ level is about 0.1 s, which would give a linewidth of approximately 2 Hz on the electric quadrupole $^2S_{1/2} \rightarrow {}^2D_{5/2}$ transition. By observing the presence of or lack of fluorescence from the $^2S_{1/2} \rightarrow {}^2P_{1/2}$ transition, the quadrupole "clock" transition can be detected with 100% efficiency.

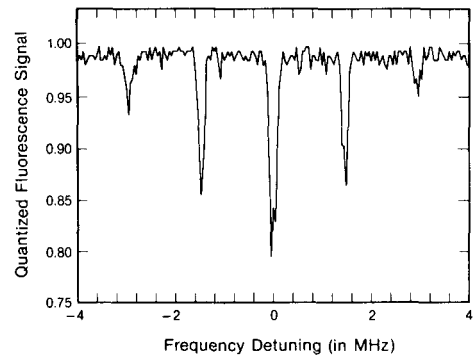

Fig. 3. Quantized signal showing the electric-quadrupole-allowed $5d^{10}6s\ ^2S_{1/2}(m_J = -1/2) \rightarrow 5d^9 6s^2\ ^2D_{5/2}(m_J = 1/2)$ transition in a single, laser-cooled $^{198}Hg^+$ ion. On the horizontal axis is plotted the relative detuning from line center in frequency units at 282 nm. On the vertical axis is plotted the probability that the fluorescence from the $6s\ ^2S_{1/2}$-$6p\ ^2P_{1/2}$ first resonance transition, excited by laser radiation at 194 nm, is on. The electric-quadrupole-allowed *S–D* transition and the first-resonance *S–P* transition are probed sequentially to avoid light shifts and broadening of the narrow *S–D* transition. Clearly resolved are the recoilless absorption resonance (carrier) and the Doppler sidebands due to the residual secular motion of the laser-cooled ion. Each point is the average of 230 measurement cycles (from [21]).

194-nm fluorescence rate from the laser-cooled ion is high when the ion is cycling between the $^2S_{1/2}$ and $^2P_{1/2}$ states (Fig. 2) and nearly zero when the ion is in the metastable $^2D_{5/2}$ state. The $^2S_{1/2}$–$^2D_{5/2}$ resonance spectrum was obtained by probing the *S–D* transition at a particular frequency for the 282-nm radiation for 20 ms, then turning off the 282-nm radiation and turning on the 194-nm radiation to look for the presence or absence of scattered photons at 194 nm. (The two radiation fields are alternately applied to avoid light shifts and broadening of the narrow *S–D* transition by the 194-nm radiation.) If there was no fluorescence at 194 nm, a transition into the metastable *D* state had occurred; the presence of 194-nm fluorescence indicated that the ion was in the ground state and no transition was recorded for this frequency of the 282-nm laser. The frequency of the 282-nm radiation was then stepped and the measurement cycle repeated. As the frequency was swept back and forth each new result at a particular frequency of the 282-nm radiation was averaged with the previous measurements at that frequency. Normalization (or digitization) of the signal was obtained by assigning a 1 to each measurement of high fluorescence and a 0 to each measurement of no fluorescence. The high fluorescence level made it possible to determine the state of the atom with almost no ambiguity in a few milliseconds. Thus, it is possible to reach the shot noise limit imposed by the single atomic absorber [21].

The quantized fluorescence signal obtained from an 8 MHz scan of the 282-nm laser through the $^2S_{1/2}(m_J = -1/2) \rightarrow {}^2D_{5/2}(m_J = 1/2)$ Zeeman component of the electric quadrupole transition in $^{198}Hg^+$ is shown in Fig. 3. The recoilless-absorption resonance (carrier) and the motional sidebands due to the secular motion in the harmonic well of the RF trap are completely resolved [21].

To avoid broadening of the quadrupole transition due to magnetic field fluctuations, we have recently [22] performed the same experiment on the $^2S_{1/2}(F = 0, m_F = 0) \rightarrow {}^2D_{5/2}(F = 2, m_F = 0)$ transition in $^{199}Hg^+$, which becomes field independent as $B \rightarrow 0$. The carrier is now observed with a linewidth $\Delta\nu \leq 100$ Hz (limited by laser spectral purity), which gives a line Q of about 10^{13}, the highest reported in atomic or molecular spectroscopy. Current efforts are devoted to improving the 282-nm laser spectral purity by locking it to a more stable reference cavity. If the laser's spectral purity can be made high enough, then when the laser is locked to the ion transition, stabilities are anticipated to be better than $10^{-15}\ \tau^{-(1/2)}$ and accuracies could be 1 part in 10^{18} or better [1], [3], [6], [17]–[21].

Future Penning Trap Experiments

The $^9Be^+$ ion experiments have the primary disadvantage that ω_0 is relatively low and the resulting frequency stabilities are modest. We might hope to substitute $^{201}Hg^+$ ions in place of the $^9Be^+$ ions because $^{201}Hg^+$ has a higher frequency clock transition ($\omega_0/2\pi \cong 26$ GHz), which is field independent at $B = 0.534\ T$ [1]. However two disadvantages compared to the $^9Be^+$ case arise: (1) If the Hg^+ is sympathetically cooled by lighter ions such as Mg^+ or Cd^+ it will reside in an annulus surrounding the lighter ions [13]; this makes the second-order Doppler shift larger for a given density and number of ions. (2) $^9Be^+$ and $^{25}Mg^+$ have simple optical pumping schemes whereby a single laser frequency can be used to optically pump into a single ground state sublevel [10]. For $^{201}Hg^+$ or $^{199}Hg^+$ in a strong field (required for a Penning trap) optical pumping schemes would require auxiliary laser lines at 194 nm and microwave oscillators to manipulate the ground state sublevels [1]; the simple optical pumping schemes as in the case of $^9Be^+$ and $^{25}Mg^+$ do not appear possible. $^{199}Hg^+$ in a Penning trap would provide a very interesting system when magnets of high enough field strength become available. For example, the $(m_I = 1/2, m_J = 1/2) \leftrightarrow (-1/2, 1/2)$ hyperfine transition in the ground state of $^{199}Hg^+$ ($\omega_0/2\pi \simeq 20.9$ GHz) is field independent at $B = 43.9\ T$. At present, we must await the required magnet.

TABLE I
EXPECTED FREQUENCY STABILITIES FOR VARIOUS IONS OF INTEREST FOR FREQUENCY STANDARDS

$M_1(u)$	$M_2(u)$	ω_0	$B(T)$	ξ	$\lvert\Delta\nu_{D2}/\nu_0\rvert$	b_1	z_{cl}(cm)	N_1	T^*	$\sigma_y(1\text{ s})$ ($T_R = 100$ s)
9(Be^+)	26(Mg^+)	303 MHz[10]	0.8194	0.1	10^{-15}	125 μm	0.5	6630	65 mK	6.45×10^{-13}
9(Be^+)	26(Mg^+)	303 MHz[10]	0.8194	0.01	10^{-15}	1.25 mm	0.5	67400	65 mK	2.02×10^{-13}
67(Zn^+)	113(Cd^+)	1 GHz[23]	8	0.1	10^{-15}	56 μm	0.5	28500	484 mK	9.44×10^{-14}
67(Zn^+)	113(Cd^+)	1 GHz[23]	8	0.01	10^{-15}	560 μm	0.5	292000	484 mK	2.94×10^{-14}
199(Hg^+)	203(Tl^+)	20.9 GHz	43.9	0.01	10^{-16}	58 μm	0.5	52400	144 mK	3.51×10^{-15}
201(Hg^+)	203(Tl^+)	25.9 GHz[1]	0.534	0.1	10^{-15}	1.48 mm	0.5	50100	1.45 K	2.75×10^{-15}
201(Hg^+)	203(Tl^+)	25.9 GHz[1]	0.534	0.01	10^{-15}	1.48 cm	0.5	524000	1.45 K	8.49×10^{-16}
201(Hg^+)	203(Tl^+)	7.73 GHz[1]	3.91	0.1	10^{-15}	204 μm	0.5	50100	1.45 K	9.21×10^{-15}
201(Hg^+)	203(Tl^+)	7.73 GHz[1]	3.91	0.01	10^{-15}	2.04 mm	0.5	524000	1.45 K	2.85×10^{-15}

[a]The ions are assumed to be confined in a Penning trap and sympathetically cooled. M_1 is the mass of the "clock" ion in atomic mass units (u), M_2 is the mass of the ion that is directly laser cooled and sympathetically cools M_1. For all cases $M_1 < M_2$ so that the cloud geometry of Fig. 5 applies. The clock frequency ω_0 is assumed to be "field independent" as for the $^9Be^+$ case described in the text. This choice determines the magnetic field. From the magnetic field B and an assumed value of ξ (6), the density of species 1 can be determined from (5). If we desire a certain value of the second order Doppler shift $\langle \Delta\nu_{D2}/\nu_0 \rangle$, we then determine a value of the cloud radius b_1 and the ion number (7) for an assumed value of z_{cl}. From (3), we then determine $\sigma_y(\tau)$ assuming $T_R = 100$ s for the Ramsey interrogation time. We refer to $\sigma_y(1\text{ s})$ for convenience. T^* is the temperature at which the second order Doppler shift from the axial and cyclotron motion would be equal to the value listed in the table. Therefore we have implicitly assumed the temperature of the cyclotron and axial motion is much less than T^*. From this, we see the importance of laser cooling.

Within the limits imposed by today's technology, an experiment similar to the $^9Be^+$ experiment but with better expected performance might be provided by $^{67}Zn^+$ ions [23]. The clock transition could be the ($m_I = /2$, $m_J = 1/2$) $\leftrightarrow$ (3/2, 1/2) transition ($\omega_0/2\pi \simeq 1$ GHz), which is field independent at $B \simeq 8$ T. Some other examples are summarized in Table I. Similar schemes are possible with ions such as Ba^+ but optical pumping is complicated.

FUTURE PAUL TRAP EXPERIMENTS

The advantage of the Paul trap is that a magnetic field is not required for trapping. This allows us to be rid of a cumbersome magnet and allows use of transitions that are field independent at $B = 0$. The primary disadvantage is that up to the present time it has been impossible to laser-cool very many ions ($N > 100$). As discussed above, the use of small numbers may not be a limitation if ω_0 can be made big enough. This is the basic philosophy behind the single-ion optical frequency standards. Even for $\omega_0/2\pi = 40.5$ GHz ($^{199}Hg^+$) and $N = 1$, from (3) we can expect [3] $\sigma_y(\tau) = 3.9 \times 10^{-13}\ \tau^{-(1/2)}$ when $T_R = 100$ s. Because the second-order Doppler shift is expected to be so small for single ions, it is perhaps useful to look at this case a little more closely.

The main advantage of using a single ion in an RF trap is that the kinetic energy of micromotion can be on the order of the secular motion energy. For a single $^{199}Hg^+$ ion cooled to the Doppler-cooling limit [21], the second-order Doppler shift would be [3] $\langle \Delta\nu_{D2}/\nu_0 \rangle = -2.3 \times 10^{-18}$. In a quadrupole ion trap, two or more ions in the trap are pushed from the center of the trap by the mutual Coulomb repulsion and the second-order Doppler shift is higher [2]. Consider the trap shown in Fig. 4. This design is essentially the same as that described by Prestage *et al.* [5] and Dehmelt [24]. In the trap of Fig. 4, the RF electric fields are transverse to the trap axis for the entire z extent of the trap. If a single string of ions is trapped along the z axis, then the kinetic energy of micromotion is about

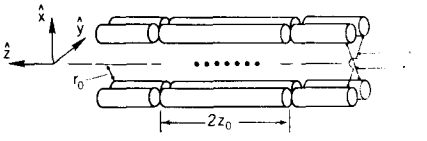

Fig. 4. Linear trap configuration. The alternating RF voltage $V_o \cos \Omega t$ is assumed to be applied to diagonally opposing electrodes as shown. We assume the end portions of the electrodes are long enough that the resulting RF potential at the position of the ions is independent of z, so that the RF electric fields are parallel to the x-y plane. To trap ions along z, we assume the center four electrodes are at static ground potential and the two sets of four electrodes on either end are at a static potential U_o ($U_o > 0$ to trap positive ions). The average position of the ions could be made to coincide with the RF electric field null by applying slightly different static potentials to the four central rods to correct for contact potential offsets etc. This geometry would allow laser beams to be directed along the z axis. Such a trap might also be useful for studing fundamental atom-radiation interactions such as the statistics of fluorescence from or the interaction of a cavity with two or more well localized atoms.

equal to the kinetic energy in the secular motion. Therefore, the fractional second-order Doppler shift could be as low as $5kT/2mc^2$. This is 5/6 of the value for a quadrupole RF trap [2] because of the absence of RF micromotion along the z direction. At the Doppler-cooling limit, this gives $\Delta\nu_{D2}/\nu_0 \simeq -2 \times 10^{-18}$ for all Hg^+ ions in the string.

Use of the trap of Fig. 4 would allow $N >> 1$ giving good stability and still yield a small second-order Doppler shift. For the experimentally achievable conditions of Appendix II, $N = 50$ ions could be stored along the z axis like "beads on a string" with ion spacings of approximately 5 μm. With this spacing each ion could be independently detected by using an image detector [25], [26], [39]. Therefore each ion could be treated as an independent atomic clock where the clock transition could be detected with 100% efficiency [21]. From (3), for $T_R = 100$ s and $\omega_0/2\pi = 40.5$ GHz ($^{199}Hg^+$) the frequency stability of this clock "ensemble" would be $\sigma_y(\tau) = 5.5 \times 10^{-14}\ \tau^{-(1/2)}$. For these long interrogation times, sympathetic cooling might be required to avoid heating while

the Hg^+ optical pumping laser was turned off to avoid light shifts during the Ramsey period. The ions used to cool the Hg^+ ions would also find a position in the string of ions along the z axis. Arrays of traps have also been proposed previously [27]. These trap arrays would have the same advantages as above for increasing N and minimizing the second-order Doppler shift.

For optical spectroscopy, lasers with high spectral purity are required (see the following). This is the current limitation to reaching the natural linewidth resolution in the NIST Hg^+ experiments. In future experiments, the laser can be locked to the ion resonance line in a manner similar to that described for the $^9Be^+$ hyperfine transition. That is, the clock transition is alternately probed on either side of the resonance (at the frequencies near maximum slope). After several measurements an error signal is built up which is used to servo the average frequency of the laser to the center of the clock resonance. A partial test of this lock can be made by briefly interrupting this servo, probing a portion of the clock resonance line (while assuming that the center of the clock resonance is given by the most recent servo measurements), and then returning to servo operation. This process is repeated until a resonance line similar to that of Fig. 3 is obtained. This, of course, does not test for a slow drift in the ion resonance frequency, but should be a fairly good test of the ability to servo the laser to the clock transition.

The main systematic error for the Hg^+ optical experiment may ultimately be the uncertainty in the shift of clock transition from static electric fields of quadrupole symmetry such as those caused by static potentials applied to the trap electrodes [6]. The basic idea is that the D state of the clock transition has a quadrupole moment that can interact with static fields of quadrupole symmetry to give a shift that must then be measured. Although troublesome, it should be possible to remove this offset from a clock calibration to about the same precision as the measurement precision [3]. Dehmelt has pointed out the advantage of the singly ionized group IIIA atoms in this respect [6]; the interesting clock transitions in these ions are the $^1S_0 \rightarrow {}^3P_0$ intercombination lines that are not shifted by static quadrupole electric fields. However, at low magnetic field these transitions have magnetic field dependence on the order of the nuclear Zeeman effect. Therefore careful control of the magnetic field would be required [6]. At higher fields, field-independent transitions could be used to advantage [28]. A linear trap or trap arrays could be used to increase SNR as described previously. For clock transitions involving a state with a quadrupole moment, such as for Hg^+, the mutual Coulomb interaction between ions would cause an additional quadrupole frequency shift that must be taken into account [29]. For the group IIIA ions, this shift would be absent.

Lasers and Laser Metrology

For optical frequency standards and spectroscopy experiments, the most outstanding current problem is that of local oscillator (laser) spectral purity. Lasers that are locked to reference cavities have been shown to track the cavity frequency to precisions of much less than 1 Hz [30]. The problem then remains that the length of the cavity and therefore the frequency of the laser are modulated by acoustic noise with deviations typically much greater than 1 Hz. It is desired to make this reference cavity stable enough (frequency deviations less than the linewidth of the optical transition) over the attack time of the servo used to lock the laser to the ion line.

A more general problem is that of cost, power requirements, and complexity of the lasers required for optical pumping and laser cooling. At present, most experiments use near-ultraviolet laser lines provided by gas laser pumped dye lasers that are frequency doubled or summed to give a few microwatts at wavelengths corresponding to certain transitions in various ions. However, this technology may simplify in the coming years. Partly because of efforts by the optoelectronics industry, it is not unreasonable to think that such lasers will be replaced by cheap, high-efficiency solid-state lasers. This is already happening at near-infrared wavelengths where diode lasers are used to optically pump and laser-cool neutral cesium and rubidium atoms.

Finally, we call attention to the problem of frequency metrology that is important in the generation of time from optical frequency standards. The technology to connect the microwave region of the spectrum to the optical spectrum through the use of synthesis chains exists [31]. Other schemes have been proposed and are being worked on [32], [33], [40]. However, this metrology problem is significant and simpler schemes would help realize the full benefits of optical frequency standards.

Appendix I
Sympathetically Cooled Ions in a Penning Trap

An approximate model of a two species ion plasma in a Penning trap is shown in Fig. 5. To make the problem tractable, we will assume that the species of spectroscopic interest is of lighter mass (species 1) and therefore resides inside species 2, which is directly laser-cooled. The case where species 2 is sympathetically cooled by species 1 [13] could be treated in a similar manner. If we assume $N_1 \ll N_2$, we can approximate the species 1 ions by a cylinder of radius b_1, and height $2z_{cl}$. If we can assume that the cyclotron and axial motion of the ions have been cooled to negligible values, the second-order Doppler shift averaged over ions of species 1 is due to the velocity of cloud rotation and is given by

$$\langle \Delta\nu_{D2}/\nu_0 \rangle = -\omega^2 b_1^2/4c^2, \tag{4}$$

where ω is the rotation frequency and c is the speed of light. The density of species 1 is

$$n_1 = m_1\omega(\Omega_1 - \omega)/2\pi q_1^2 \tag{5}$$

where m_1, Ω_1, and q_1, are the mass, cyclotron angular frequency and charge of species 1 [34], [35]. An experimentally useful parameter to characterize the density of spe-

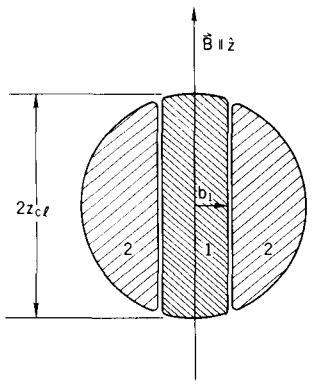

Fig. 5. Approximate model for a sympathetically cooled ion sample in a Penning trap. We assume $q_1/m_1 > q_2/m_2$ so that species 1 (which is the "clock" species) is approximated by a uniform density column of height $2z_{cl}$ and radius b_1. Species 2 is assumed to be continuously laser cooled and by the Coulomb interaction continuously cools species 1. All ions are assumed to be in thermal equilibrium and therefore co-rotate about the z axis at frequency ω. The second order Doppler shift of species 1 is assumed to be dominated by the velocity in this rotation.

cies 2 is the parameter

$$\xi = 2\omega/\Omega_2 \tag{6}$$

where Ω_2 is the cyclotron frequency of species 2. ξ is the ratio of the rotation frequency ω to the maximum allowable rotation frequency $\Omega_2/2$ given by the Brillouin density [34], [35].

From (4)–(6), and the formula $N_1 = 2\pi b_1^2 z_{cl} n_1$, we have

$$N_1 = 8m_2c^2z_{cl}(1 - \xi m_1q_2/2m_2q_1)\langle -\Delta\nu_{D2}/\nu_0\rangle/\xi q_1q_2 \tag{7}$$

where m_2 and q_2 are the mass and charge of ions of species 2. From these expressions and (3) applied to species 1, we can generate the parameters of Table I. Accuracy of 10^{-15} with reasonable stability seems possible. Of course the local oscillator spectral purity must be good enough to reach these conditions. The $^{199}Hg^+$ example is not now realistic due to the lack of a suitable magnet.

Appendix II
Linear Paul Trap

To describe the trapping from ponderomotive fields we assume that near the trap axis, the time varying potential has the form

$$\phi = \frac{V_0(x^2 - y^2)}{2R^2}\cos\Omega t \tag{8}$$

where R is approximately equal to the dimension r_0 indicated in Fig. 4. ($R = r_0$ if the electrode surfaces lie along equipotentials of (8).) If Ω is high enough (defined in the following) this results in the harmonic pseudopotential well in the radial direction:

$$\phi_p = \frac{qV_0^2}{4m\Omega^2R^4}(x^2 + y^2) = \frac{m}{2q}\omega_r^2(x^2 + y^2) \tag{9}$$

where $\omega_r \equiv qV_0/(\sqrt{2}\, m\Omega R^2)$ is the single-ion oscillation frequency in the radial direction. Expression (9) is expected to be fairly accurate when $\Omega >> \omega_r$, which is the condition for Ω being large enough.

For the static potential due to voltage U_0 applied to the end sections, we will make the approximation that, near the center of the trap, this potential is given by

$$\phi_s = kU_0(z^2 - (x^2 + y^2)/2)$$
$$= \frac{m}{2q}\omega_z^2(z^2 - (x^2 + y^2)/2) \tag{10}$$

where k is a geometric factor and ω_z is the z oscillation frequency for a single ion in the trap. Equation (10) represents the lowest order term in the expansion of the static potential for the electrode configuration of Fig. 4 with the bias assumed. If the length of the central rods is long compared to their spacing, then higher-order terms in the expansion become more important so that the static potential changes significantly only near the point of separation between the end and center sections. For simplicity, we will assume that the length of the central rods is approximately equal to the rod spacing and that the extent of the ion sample is small compared to R so that (10) should be a reasonable approximation to the actual potential.

The addition of this static potential weakens the strength of the pseudopotential well in the radial direction so that the total potential in the radial direction is given by

$$\phi_r = \frac{m}{2q}(\omega_r^2 - \omega_z^2/2)(x^2 + y^2) = \frac{m}{2q}(\omega_r'^2)(x^2 + y^2) \tag{11}$$

where ω_r' is the single ion radial oscillation frequency for the combined potentials.

A possible advantage of such a linear trap may be for laser-cooling large numbers of ions in an RF trap. As has been noted in recent papers [36], [37], the RF micromotion in a quadrupole Paul trap perturbs the ion's spectrum and can inhibit laser-cooling. This may be one of the main reasons large numbers of ions in an RF trap have not been laser cooled. If a cooling laser is directed along the z axis of the trap in Fig. 4, the ion's spectrum is not perturbed by micromotion and laser cooling should occur according to the simple theory [38], [41] if RF heating is not too severe.

"Beads on a String"

The most interesting case for accurate spectroscopy is when all ions are confined along the z axis. To analyze this case, first assume that ω_r' is large enough to make the ions lie along the z axis. Then, for a given N and ω_z, we minimize the total ion potential to obtain z_i, for $i = (1, \cdots, N)$. From the z_i we can then find a condition on ω_r' to insure all ions stay along the z axis.

For ions pinned on the z axis, the total ion potential

energy is

$$q\phi_T = \frac{m}{2}\omega_z^2 \sum_i^N z_i^2 + q^2 \sum_{i<j}^N |z_i - z_j|^{-1} \qquad (12)$$

Using a computer, we have minimized ϕ_T as a function of ion positions for various experimental parameters. Near $z = 0$ (trap center), the ions are closest together and fairly regularly spaced. The closer the spacing, the higher ω_r' must be to maintain all ions on the z axis.

To find the condition on ω_r', consider an infinite string of ions with equal spacing d along the z axis. If one ion is displaced a distance $\delta x (<< d)$ from the z axis, it experiences a force away from the z axis of strength

$$F_x = \left(2 \sum_{n=1}^{\infty} n^{-3}\right) \frac{q^2}{d^3} \delta x = (2.404) \frac{q^2}{d^3} \delta x. \qquad (13)$$

If we have only 5 ions spaced by d the analogous force on the center ion is given by (13) with the numerical factor equal to 2.250 rather than 2.404. Therefore even if the ions are only approximately evenly spaced, (13) will be a good estimate of F_x for a particular ion if we take d to be the mean of the spacing to the nearest neighbor ions. For the ions to be stably trapped on the z axis, we want the pseudopotential force inward to be larger than the force outward as expressed by (13). From (11) and (13) we therefore require that

$$(\omega_r')^2 > 2.404\, q^2/md^3 \qquad (14)$$

or $\omega_r'/2\pi > 91.9\,(Md^3)^{-(1/2)}$ where M is the ion mass in atomic mass units, d is the spacing in micrometers, and $\omega_r'/2\pi$ is in megahertz.

As an example, for $N = 50$, $\omega_z/2\pi = 50$ kHz, and $M = 199$ ($^{199}Hg^+$ ions), the computer calculation gave an overall string length of 266 μm. The spacings of adjacent pairs of ions in μm, starting from the outermost pair of ions on one end and ending with the center pair are: 10.48, 8.46, 7.43, 6.77, 6.30, 5.95, 5.68, 5.46, 5.28, 5.12, 4.99, 4.88, 4.79, 4.71, 4.64, 4.58, 4.53, 4.48, 4.45, 4.42, 4.39, 4.37, 4.36, 4.35, 4.35. Using $d = 4.35$ μm, we find from (14), $\omega_r'/2\pi > 718$ kHz, $\omega_r/2\pi > 719$ kHz. If $R = 0.75$ mm and $\Omega/2\pi = 5$ MHz, then we require $V_o > 233$ V.

ACKNOWLEDGMENT

The authors gratefully acknowledge the continued support of the Office of Naval Research and the Air Force Office of Scientific Research. The authors thank R. Drullinger, H. Robinson, and M. Young for helpful comments on the manuscript.

REFERENCES

[1] D. J. Wineland, W. M. Itano, J. C. Bergquist, and F. L. Walls, *Proc. 35th Annu. Symp. Freq. Contr.*, Philadelphia, PA, May 1981, pp. 602-611. (Copies available from: Annual Frequency Control Symposium, c/o Electronic Industries Assoc., 2001 Eye St., Washington, DC, 20006.)

[2] D. J. Wineland, "Precision Measurement and Fundamental Constants II," B. N. Taylor and W. D. Phillips, Eds. National Bureau of Standards (U.S.) Spec. Publ. 617 1984, pp. 83-92.

[3] D. J. Wineland, W. M. Itano, J. C. Bergquist, J. J. Bollinger, F. Diedrich, and S. L. Gilbert, in Frequency Standards and Metrology, *Proc. 4th Symp.*, A. DeMarchi, Ed. Berlin: Springer-Verlag, 1989, p. 71-77.

[4] L. S. Cutler, R. P. Giffard, and M. D. McGuire, *Appl. Phys.*, B36, 137, pp. 137-142, 1985; L. S. Cutler, C. A. Flory, R. P. Giffard, and M. D. McGuire, *Appl. Phys.*, vol. B39, pp. 251-259, 1986.

[5] J. Prestage, G. J. Dick, and L. Maleki, *J. Appl. Phys.*, vol. 66, pp. 1013-1017, 1989.

[6] H. G. Dehmelt, *IEEE Trans. Instrum. Meas.*, vol. IM-31, pp. 83-87, 1982, and references therein.

[7] D. J. Wineland and W. M. Itano, *Physics Today*, vol. 40, no. 6, pp. 34-40, 1987.

[8] L. S. Cutler, R. P. Giffard, and M. D. McGuire, *Proc. 37th Annu. Symp. Freq. Contr.*, 1983, pp. 32-36, (copies available from IEEE, 445 Hoes Lane, Piscataway, NJ 08854).

[9] J. J. Bollinger, S. L. Gilbert, W. M. Itano, and D. J. Wineland, in *Frequency Standards and Metrology, Proc. 4th Symp.*, A. DeMarchi, Ed. Berlin: Springer-Verlag, 1989, pp. 319-325.

[10] J. J. Bollinger, W. M. Itano, and D. J. Wineland, *Proc. 37th Annu. Symp. Freq. Contr.*, 1983, pp. 37-41 (copies available from IEEE, 445 Hoes Lane, Piscataway, NJ 08854).

[11] J. J. Bollinger, J. D. Prestage, W. M. Itano, and D. J. Wineland, *Phys. Rev. Lett.*, vol. 54, pp. 1000-1003, 1985.

[12] J. J. Bollinger, D. J. Heinzen, W. M. Itano, S. L. Gilbert, and D. J. Wineland, *Phys. Rev. Lett.*, vol. 63, pp. 1031-1034, 1989.

[13] D. J. Larson, J. C. Bergquist, J. J. Bollinger, W. M. Itano, and D. J. Wineland, *Phys. Rev. Lett.*, vol. 57, pp. 70-73, 1986.

[14] J. Vetter, M. Stuke, and E. W. Weber, *Z. Phys.*, vol. A273, pp. 129-135, 1975.

[15] E. Herbst, *Astrophys. J.*, vol. 252, pp. 810-813, 1982, and references therein.

[16] H. G. Dehmelt, *Adv. At. Mol. Phys.*, vol. 3, pp. 53-72, 1967.

[17] D. J. Wineland, W. M. Itano, J. C. Bergquist, and R. G. Hulet, *Phys. Rev.*, vol. A36, pp. 2220-2232, 1987.

[18] F. Diedrich, J. C. Bergquist, W. M. Itano, and D. J. Wineland, *Phys. Rev. Lett.*, vol. 62, pp. 403-406, 1989.

[19] D. J. Wineland, *Science*, vol. 226, pp. 395-400, 1985.

[20] J. C. Bergquist, F. Diedrich, W. M. Itano, and D. J. Wineland, in *Frequency Standards and Metrology, Proc. 4th Symp.*, A. DeMarchi, Ed. Berlin: Springer-Verlag, pp. 287-292.

[21] J. C. Bergquist, W. M. Itano, and D. J. Wineland, *Phys. Rev.*, vol. A36, pp. 428-430, 1987.

[22] J. C. Bergquist, F. Diedrich, W. M. Itano, and D. J. Wineland, in *Laser Spectroscopy IX*, M. S. Feld, J. E. Thomas, and A. Mooradian, Eds. San Diego, Academic, 1989, pp. 274-277.

[23] W. M. Itano and D. J. Wineland, *Bull. Am. Phys. Soc.*, vol. 24, p. 1185 (1979).

[24] H. G. Dehmelt, in *Frequency Standards and Metrology, Proc. 4th Symp.*, A. DeMarchi, Ed. Berlin: Springer-Verlag, 1989, p. 286.

[25] D. J. Wineland, W. M. Itano, J. C. Bergquist, S. L. Gilbert, J. J. Bollinger, and F. Ascarrunz, in "Non-neutral plasma physics," C. W. Roberson and C. F. Driscoll, Ed. *A.I.P. Conf. Proc.*, vol. 175, Amer. Inst. of Physics, New York, 1988, pp. 93-108.

[26] R. Blümel, J. M. Chen, F. Diedrich, E. Peik, W. Quint, W. Schleich, Y. R. Shen, and H. Walther, in *Atomic Physics*, vol. 11, S. Haroche, J. C. Gay and G. Grynberg, Eds. Singapore: World Scientific, 1989, pp. 243-259.

[27] F. G. Major, *J. de Physique (Lettres)*, vol. 38, pp. L-221-L-225, 1977.

[28] D. J. Wineland and W. M. Itano, *Bull. Am. Phys. Soc.*, vol. 27, p. 864, 1982.

[29] D. J. Wineland, W. M. Itano, J. C. Bergquist, J. J. Bollinger, and J. D. Prestage, *Ann. Phys. Fr.*, vol. 10, pp. 737-748, 1985.

[30] D. Hils and J. L. Hall, in *Frequency Standards and Metrology, Proc. 4th Symp.*, A. DeMarchi, Ed. Berlin: Springer-Verlag, 1989, pp. 162-173.

[31] See, for example, *Frequency Standards and Metrology, Proc. 4th Symp.*, A. DeMarchi, Ed. Berlin: Springer-Verlag, 1989.

[32] D. J. Wineland, J. C. Bergquist, W. M. Itano, F. Diedrich, and C. S. Weimer, in *The Hydrogen Atom*, G. F. Bassani, M. Inguscio, and T. W. Hänsch, Eds. Berlin: Springer-Verlag, 1989, pp. 123-133.

[33] H. R. Telle, D. Meschede, and T. W. Hänsch, *Optics Lett.*, vol. 15, pp. 532-534, 1990.

[34] T. M. O'Neil, *Phys. Fluids*, vol. 24, pp. 1447-1451, 1981.

[35] L. R. Brewer, J. D. Prestage, J. J. Bollinger, W. M. Itano, D. J. Larson, and D. J. Wineland, *Phys. Rev.*, vol. A38, pp. 859-873, 1988.
[36] R. G. DeVoe, J. Hoffnagle, R. G. Brewer, *Phys. Rev.*, vol. A39, pp. 4362-4365, 1989.
[37] R. Blümel, C. Kappler, W. Quint, and H. Walther, *Phys. Rev.*, vol. A40, pp. 808-823, 1989.
[38] D. J. Wineland and W. M. Itano, *Phys. Rev.*, vol. A20, pp. 1521-1540, 1979.
[39] W. M. Itano, J. C. Bergquist, and D. J. Wineland, in *Proc. Workshop on Crystalline Ion Beams*, Wertheim, West Germany, R. W. Hasse, I. Hofmann, D. Liese, Eds., (GSI rep. GSI-89-10, ISSN 0170-4546), pp. 241-254.
[40] T. W. Hänsch, in *The Hydrogen Atom*, G. F. Bassani, M. Inguscio, and T. W. Hänsch, Eds. Berlin: Springer-Verlag, 1989, pp. 93-102.
[41] W. M. Itano and D. J. Wineland, *Phys. Rev.*, vol. A36, pp. 35-54, 1982.

D. J. Wineland, photograph and biography not available at time of publication.

J. C. Bergquist, photograph and biography not available at time of publication.

J. J. Bollinger, photograph and biography not available at time of publication.

W. M. Itano, photograph and biography not available at time of publication.

D. J. Heinzen, photograph and biography not available at time of publication.

S. L. Gilbert, photograph and biography not available at time of publication.

C. H. Manney, photograph and biography not available at time of publication.

M. G. Raizen, photograph and biography not available at time of publication.

A 303-MHz Frequency Standard Based on Trapped Be^+ Ions

J. J. Bollinger, D. J. Heinzen, W. M. Itano, S. L. Gilbert, and D. J. Wineland

Abstract—**A 303-MHz hyperfine transition in the ground state of $^9Be^+$ was used as a basis of a frequency standard. The ions were stored in a Penning ion trap. Linewidths as narrow as 900 μHz were obtained. The frequency stability was measured to be better than $3 \times 10^{-12}\tau^{-1/2}$. The inaccuracy in the second-order Doppler shift was reduced to 5 parts in 10^{15} by laser cooling. An apparent pressure shift with an unexpectedly large value was discovered which limits the accuracy of the current experiment to approximately 1 part in 10^{13}.**

I. Introducton

ION TRAPS provide the confinement with low perturbations necessary for improved frequency standards. For a microwave (or RF) frequency standard, typically many ions are stored in a trap in order to increase the signal-to-noise ratio and obtain good frequency stability. With many ions in a trap, the second-order Doppler shift is one of the largest systematic contributions to the inaccuracy of the standard [1]-[6]. In frequency standards which aim at high accuracy, the technique of laser cooling can be used to reduce the second-order Doppler shift to an acceptable level [1]-[3]. In this paper we investigated the use of Be^+ ions stored in a Penning trap to make a microwave (or RF) frequency standard with high accuracy. Be^+ is technically easy to trap and laser cool and, therefore, is a good candidate for investigating the use of stored ions as a microwave frequency standard. Other ions with even higher potential line Q's are discussed in [3].

Fig. 1 shows the energy level structure of the ground state of $^9Be^+$ as a function of the trap magnetic field B. At $B \simeq 0.8194$ T, the transition between levels 1 and 2, called the clock transition, depends only quadratically on magnetic field fluctuations and is, therefore, a suitable transition for a frequency standard. In this experiment, an oscillator is locked to this clock transition. The basic idea of this experiment has been described previously [7]-[10]. A description of the current experiment [10] is given below.

II. Experimental Technique

Between 5000 and 10 000 $^9Be^+$ ions and 50 000 to 150 000 $^{26}Mg^+$ ions were stored simultaneously in a cylindrical Penning trap [11] with $B \simeq 0.8194$ T under conditions of high vacuum ($\simeq 10^{-8}$ Pa). In order to minimize second-order Doppler shifts of the clock transition, the $^9Be^+$ ions were cooled to less than 250 mK by the following method. The $^{26}Mg^+$ ions were directly laser cooled and compressed by a narrow-band (~ 1 MHz) radiation source at 280 nm. The $^9Be^+$ ions were then sympathetically cooled [12] by their Coulomb interaction with the cold Mg^+ ions. A narrow-band 313-nm radiation source was used to optically pump and detect the $^9Be^+$ ions [13], [14]. Lenses were used to image the $^9Be^+$ fluorescence onto the photocathode of a photon-counting imaging detector. The overall detection efficiency was $\sim 2 \times 10^{-4}$. With the 313-nm source tuned to the $2s^2S_{1/2}(m_I = 3/2, m_J = 1/2)$ to $2p^2P_{3/2}(3/2, 3/2)$ transition, 94% of the $^9Be^+$ ions were optically pumped into the $2s^2S_{1/2}(3/2, 1/2)$ ground state. The 313-nm source was then turned off to avoid further optical pumping and ac Stark shifts. The sympathetic cooling of the $^9Be^+$ ions by the Mg^+ ions provided a steady cooling source independent of the 313-nm radiation and therefore permitted the use of long transition times.

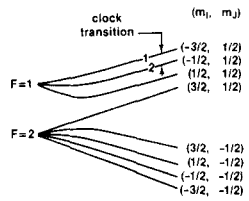

Fig. 1. Hyperfine energy levels (not drawn to scale) of the $^9Be^+$ $2s\ ^2S_{1/2}$ ground state as a function of magnetic field. At $B = 0.8194$ T the 303-MHz clock transition is independent of magnetic field to first order.

The clock transition was detected by the following method. After the 313-nm source was turned off, the ions in the $(3/2, 1/2)$ state were transferred to the $(1/2, 1/2)$ state and then to the $(-1/2, 1/2)$ state by two successive RF π pulses. Each pulse was 0.2-s long and resonant with the appropriate transition frequency (around 321 and 311 MHz, respectively). The clock transition was then driven by Ramsey's method of separated oscillatory fields with RF pulses of about 1-s duration and a free-precession time on the order of 100 s. Free-precession periods as long as 550 s were also used. This procedure transferred some of the ions from the $(-1/2, 1/2)$ state to the $(-3/2, 1/2)$ state. Those ions remaining in the $(-1/2, 1/2)$ state were then transferred back to the $(3/2, 1/2)$ state by reversing the order of the two RF π pulses. The 313-nm source was then turned back on, and the population of ions in the $(-3/2, 1/2)$ state was registered as a decrease in the $^9Be^+$ fluorescence, relative to the steady-state fluorescence, during the first second that the 313-nm source was on. The time for optical pumping from the $(-3/2, 1/2)$ state to the $(3/2, 1/2)$ state was approximately 10 s. After each measurement the system was reinitialized by leaving the 313-nm laser on for about 25 s.

III. Results

Fig. 2 shows the Ramsey signal obtained with a 550-s free precession period. The 900-μHz linewidth gives a line Q of 3.4

Manuscript received June 13, 1990; revised October 4, 1990. This work was supported by the Office of Naval Research and by the Air Force Office of Scientific Research.

The authors are with the National Institute of Standards and Technology, Boulder, CO 80303.

IEEE Log Number 9042018.

0018-9456/91/0400-0126$01.00 © 1991 IEEE

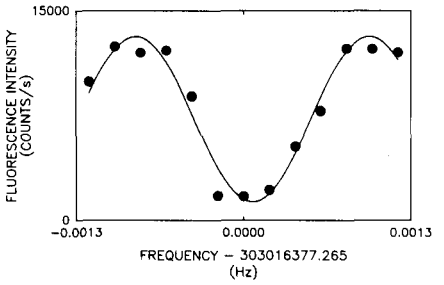

Fig. 2. Ramsey signal of the clock transition for a 550-s free precession period. The data are the result of one sweep (that is, one measurement per point). The sweep width is 2.4 mHz and the frequency interval between points is 0.2 mHz. The dots are experimental and the curve is a least-squares fit.

$\times 10^{11}$. Ramsey signals obtained with a 100-s free precession period were used to servo the frequency of a synthesized RF source [7]–[10]. Measurements were taken near the frequencies corresponding to the half minimum points on both sides of the center frequency. The difference in the measured signal strengths on either side of the line center was used by a computer to servo the average frequency of the synthesizer to the clock transition frequency. Most runs were taken with a commercial cesium beam clock (fractional frequency stability $\sigma_y(\tau) \simeq 6 \times 10^{-12}\tau^{-1/2}$ for measurement time τ in seconds) as the reference oscillator for the synthesizer, but a few runs were taken with a passive hydrogen maser ($\sigma_y(\tau) \simeq 2 - 3 \times 10^{-12}\ \tau^{-1/2}$) as the reference oscillator. The stability of the $^9Be^+$ clock was measured to be better than $3 \times 10^{-12}\ \tau^{-1/2}$ for 10^3 s $\leq \tau \leq 10^4$ s, which is within a factor of 4 of the theoretical limiting stability for the number of ions used [3]. For $\tau \geq 10^6$ s the frequency stability was apparently limited by the pressure shift discussed below to $\sim 3 \times 10^{-14}$. The largest contribution to the second order Doppler shift was due to the $\vec{E} \times \vec{B}$ rotation of the ions about the axis of the trap. The rotation frequency and ion cloud radius were measured by using a weak laser beam to probe the ion cloud [13]. The fractional second-order Doppler shift was calculated to be $(-1.2 \pm 0.5) \times 10^{-14}$.

An apparent pressure shift more than three orders of magnitude larger than expected was discovered when the background gas pressure was increased. The background gas pressure could be increased by moving the magnet of the sputter ion pump which evacuated the trap region so that it overlapped fewer pumping cells and reduced the pumping speed. (We checked to make sure the magnetic field at the site of the ions was not disturbed. In addition, the shape and apparent temperature of the ion cloud could be monitored immediately before and after the Ramsey interrogation period from the image of the ion fluorescence. The increased background gas had a negligible effect on the cloud shape and temperature.) The composition of the gas was not known since the pressure was measured with a Bayard-Alpert gauge. However, when the vacuum vessel containing the trap was initially evacuated, the dominant background gases were H_2 and He. If the background gas was dominated by He, the fractional pressure shift was about $-3 \times 10^{-6}\ Pa^{-1}$; if the background was dominated by H_2, the pressure shift was about $-9 \times 10^{-6}\ Pa^{-1}$. Atomic ion hyperfine pressure shifts due to He have previously been measured in $^{137}Ba^+$ [15] and in $^{199}Hg^+$ [16] to be $5 \times 10^{-11}\ Pa^{-1}$ and $4 \times 10^{-11}\ Pa^{-1}$, respectively. Vetter *et al.* [15] show that the long-range charge-induced interaction between the Ba^+ and the noble gas atoms gives one of the largest contributions to the pressure shift. Since this interaction depends primarily on the polarizability of the neutral atom we would expect that the pressure shift for He atoms on $^9Be^+$ ions would not be significantly different than that for Ba^+ or Hg^+. Similarly, since the polarizability of H_2 is midway between Ar and Ne, we might expect the pressure shift for H_2 on Be^+ to be near those for Ar and Ne on Ba^+, which were measured to be $-6 \times 10^{-9}\ Pa^{-1}$ and $-6 \times 10^{-10}\ Pa^{-1}$, respectively [15].

The apparent large discrepancy between our data and other measured pressure shifts is not understood at this time. One possible explanation is suggested by studies [17] of radiative association of C^+ with H_2 to form CH_2^+. In the models of this process, it is assumed that the H_2 can stick to the C^+ for a long enough time to allow the $C^+ - H_2$ complex to radiatively stabilize. This sticking is possible because the collision energy can be taken up by the internal degrees of freedom in the H_2 molecule. The sticking time can be orders of magnitude longer than the interaction time during a simple elastic collision. If a similar sticking mechanism is active in $H_2 - Be^+$ collisions, it may account for the apparent large pressure shift. We plan to check this hypothesis by measuring the pressure shifts of Be^+ on Ne and Ar, where the sticking would not be expected to occur, and on H_2, where sticking might occur.

If the apparent collisional shift is real, the background pressure of 10^{-8} Pa in this trap will limit the accuracy of the Be^+ clock to about 1 part in 10^{13}. We are continuing to search for other causes of systematic error such as electronic offsets. We feel the accuracy could be improved beyond 5 parts in 10^{15} in the future. It may be necessary to use liquid He cryopumping to reduce the background pressure.

ACKNOWLEDGMENT

The authors thank F. Moore and J. Wells for carefully reading the manuscript.

REFERENCES

[1] D. J. Wineland, W. M. Itano, J. C. Bergquist, and F. L. Walls, "Proposed stored $^{201}Hg^+$ ion frequency standards," in *Proc. 35th Ann. Symp. Freq. Control*, Philadelphia, PA, pp. 602–611, 1981.

[2] D. J. Wineland, W. M. Itano, J. C. Bergquist, J. J. Bollinger, F. Diedrich, and S. L. Gilbert, "High accuracy spectroscopy of stored ions," in *Proc. 4th Symp. Frequency Standards and Metrology*, (Ed. A. DeMarchi) Ancona, Italy, pp. 71–77, 1989.

[3] D. J. Wineland *et al.*, "Progress at NIST towards absolute frequency standards using stored ions," *IEEE Trans. Ultrason. Ferroelec. Freq. Contr.*, vol. 37, pp. 515–523, 1990.

[4] M. Jardino, F. Plumelle, M. Desaintfuscien, and J. L. Duchene,

"Experimental determination of the energy of stored ions from the side-bands in their microwave spectrum," in *Proc. 38th Ann. Symp. Freq. Control*, pp. 431-434, 1984.

[5] L. S. Cutler, C. A. Flory, R. P. Giffard, and M. D. McGuire, "Doppler effects due to thermal macromotion of ions in an RF quadrupole trap," *Appl. Phys. B.*, vol. 39, pp. 251-259, 1986.

[6] J. D. Prestage, G. J. Dick, and L. Maleki, "New ion trap for frequency standard applications," *J. Appl. Phys.*, vol. 66, pp. 1013-1017, 1989.

[7] J. J. Bollinger, S. L. Gilbert, W. M. Itano, and D. J. Wineland, "Frequency standards utilizing Penning traps," in *Proc. 4th Symp. Frequency Standards and Metrology*, (Ed. A. DeMarchi) Ancona, Italy, pp. 319-325, 1989.

[8] J. J. Bollinger, W. M. Itano, and D. J. Wineland, "Laser cooled $^{9}Be^{+}$ Accurate Clock," in *Proc. 37th Ann. Symp. Freq. Contr.*, pp. 37-41, 1983.

[9] J. J. Bollinger, J. D. Prestage, W. M. Itano, and D. J. Wineland, "Laser-cooled-atomic frequency standard," *Phys. Rev. Lett.*, vol. 54, pp. 1000-1003, 1985.

[10] J. J. Bollinger, D. J. Heinzen, W. M. Itano, S. L. Gilbert, and D. J. Wineland, "Test of the linearity of quantum mechanics by RF spectroscopy of the $^{9}Be^{+}$ ground state," *Phys. Rev. Lett.*, vol. 63, pp. 1031-1034, 1989.

[11] S. L. Gilbert, J. J. Bollinger, and D. J. Wineland, "Shell-structure phase of magnetically confined strongly coupled plasmas," *Phys. Rev. Lett.*, vol. 60, pp. 2022-2025, 1988.

[12] D. J. Larson, J. C. Bergquist, J. J. Bollinger, W. M. Itano, and D. J. Wineland, "Sympathetic cooling of trapped ions: A laser-cooled two species nonneutral ion plasma," *Phys. Rev. Lett.*, vol. 57, pp. 70-73, 1986.

[13] L. R. Brewer, J. D. Prestage, J. J. Bollinger, W. M. Itano, D. J. Larson, and D. J. Wineland, "Static properties of a non-neutral $^{9}Be^{+}$ – ion plasma," *Phys. Rev.* vol. A38, pp. 859-873, 1988.

[14] W. M. Itano and D. J. Wineland, "Precision measurement of the ground-state hyperfine constant of $^{25}Mg^{+}$," *Phys. Rev.*, vol. A24, pp. 1364-1373, 1981.

[15] J. Vetter, M. Stuke, and E. W. Weber, "Hyperfine density shifts of $^{137}Ba^{+}$ ions in noble gas buffers," *Z. Phys.*, vol. A273, pp. 129-135, 1975.

[16] L. S. Cutler, R. P. Giffard, and M. D. McGuire, "Mercury-199 trapped ion frequency standard," in *Proc. 37th Ann. Symp. Freq. Contr.*, pp. 32-36, 1983.

[17] E. Herbst, "A reinvestigation of the rate of the $C^{+} + H_2$ radiative association reaction," *Astrophys. J.*, vol. 252, pp. 810-813, 1982, and references therein.

LIGHT INDUCED KINETIC EFFECTS ON ATOMS, IONS AND MOLECULES
eds. Moi L., Gozzini S., Gabbanini C., Arimondo E., Strumia F., 1991, ETS Editrice,Pisa

SINGLE ION OPTICAL SPECTROSCOPY*

J.C. Bergquist, Wayne M. Itano, Frank Elsner†, M.G. Raizen and D.J. Wineland

Time and Frequency Division
National Institute of Standards and Technology
Boulder, Colorado 80303, U.S.A.

ABSTRACT

A single $^{199}Hg^{+}$ ion is confined in a miniature rf trap and is laser-cooled to nearly 0.001 K. We have studied the spectrum of the narrow $5d^{10}6s\ ^2S_{1/2}$ - $5d^96s^2\ ^2D_{5/2}$ electric-quadrupole-allowed transition near 282 nm and obtain a linewidth below 80 Hz (FWHM). The measured lifetime of the metastable $^2D_{5/2}$ state gives a natural linewidth limit for this transition of 1.8 Hz. The narrow linewidth, the ability to detect transitions with unit probability, and the small perturbations of a single laser-cooled ion make it an attractive candidate for an optical frequency standard. Our present resolution is limited by the spectral purity of the frequency-doubled dye laser at 563 nm. Optical heterodyne measurements between two laser beams locked to independent, high-finesse cavities give a beat note of less than 40 Hz (FWHM at 563 nm) that is dominated by noise in the frequency range from 0 to 10 Hz. This is caused by the insufficient isolation of the cavities from mechanical vibrations in this frequency range. Better isolation methods intended to improve the laser linewidth to about 1 Hz or less are being investigated. A linear Paul trap, in which it would be possible to trap and cool many ions unperturbed by rf micromotion, is being tested.

EXPERIMENT

The ion trapping and laser-cooling have been described elsewhere[1,2]. A ^{199}Hg atom is ionized and trapped in the harmonic pseudopotential well created by an rf potential applied between the electrodes of a miniature Paul trap. The separation between the endcap electrodes ($2z_0$) is about 650 μm. The frequency of the rf potential is about 21 MHz. Its amplitude can be varied up to 1.2 kV resulting in a secular frequency of up to 4 MHz. The ion is laser cooled to a few millikelvins by a few microwatts of radiation from two 194 nm sources. One source induces transitions from the $5d^{10}6s\ ^2S_{1/2}(F=1)$ to the $5d^{10}6p\ ^2P_{1/2}(F=0)$ level. This is essentially a two

level system suitable for laser-cooling, except for weak off-resonance pumping into the $^2S_{\frac{1}{2}}(F=0)$ state. The second 194 nm source, tuned to the $^2S_{\frac{1}{2}}(F=0)$ to $^2P_{\frac{1}{2}}(F=1)$ transition, returns the ion to the ground state F=1 hyperfine level. The frequency separation between the two radiation sources is equal to the sum of the ground and excited state hyperfine splittings (about 47 GHz). The complication of two-laser cooling is dictated by the hyperfine structure of $^{199}Hg^+$. An isotope with hyperfine structure is required in order to have a first-order field-independent clock transition near $B \simeq 0$. The two 194 nm beams are made collinear and irradiate the ion at an angle of 55° with respect to the symmetry (z) axis of the trap. In this way, all motional degrees of freedom are cooled to near the Doppler cooling limit of 1.7 mK. 194 nm fluorescence from the ion, collected in a solid angle of about $5 \times 10^{-3} \times 4\pi$ sr, is detected with an efficiency of 10% to give a peak count rate on resonance of about 25 000 s^{-1}.

The 282 nm radiation that drives the narrow $5d^{10}6s\ ^2S_{\frac{1}{2}} - 5d^9 6s^2\ ^2D_{5/2}$ transition is obtained by frequency-doubling the radiation from a cw dye laser that is stabilized to a Fabry-Perot cavity with finesse[3] $F \simeq 60\ 000$. Prior to being frequency doubled, the 563 nm radiation is passed through an acousto-optic modulator so that its frequency can be tuned through the S-D resonance. Since the Zerodur[4] reference cavity contracts at a nearly constant rate of 3.3 Hz/s[5], the acousto-optic modulator is driven by a frequency obtained by summing the rf output of two synthesizers. The frequency of one synthesizer sweeps opposite to the cavity drift; the frequency of the second synthesizer is stepped back and forth through the S-D resonance. The 282 nm laser and the two-frequency 194 nm source are turned on and off sequentially using shutters and the acousto-optic modulator. This prevents any broadening of the narrow S-D transition due to the 194 nm radiation. Optical-optical double resonance[1,6] (electron shelving)[7] is used to detect <u>each</u> transition made to the metastable D state as a function of the frequency of the 282 nm laser. At the beginning of each cycle, both 194 nm lasers irradiate the ion. The fluorescence counts in a 10 ms period must exceed a minimum threshold (typically 20 counts) before the interrogation sequence can continue. The 194 nm beams irradiate the ion for sequential 10 ms periods until the threshold is met. Then the 194 nm radiation tuned to the $^2S_{\frac{1}{2}}(F=0) - {}^2P_{\frac{1}{2}}(F=1)$ transition is chopped off for 5 ms. During this time the 194 nm radiation tuned to the $^2S_{\frac{1}{2}}(F=1) - {}^2P_{\frac{1}{2}}(F=0)$ transition optically

pumps the ion into the $^2S_{1/2}(F=0)$ ground state. Then this 194 nm source is turned off. One millisecond later, the 282 nm radiation, tuned to a frequency resonant or nearly resonant with the $^2S_{1/2}(F=0, m_F=0)$ - $^2D_{5/2}(F=2, m_F=0)$ transition irradiates the ion for an interrogation period that was varied up to as long as 15 ms. At the end of this period, the 282 nm radiation was turned off and both 194 nm sources were turned on. Another 10 ms detection period was used to determine whether a transition to the D state had been made (fluorescence counts > threshold, no; fluorescence counts < threshold, yes). The result was recorded as a 1 or 0 (no or yes) and averaged with the previous results at this frequency. Then the frequency of the 282 nm radiation was stepped and the measurement cycle repeated.

Since the frequency drift of the 282 nm laser depended not only on the reference cavity contraction rate, but also on small pressure and temperature changes, on laser power variations, etc.[8,9], we locked the frequency of the laser to the narrow S-D transition to remove any long term frequency drifts. To do this, we modified the measurement cycle to include a lock cycle. We began each measurement cycle by stepping the frequency of the 282 nm radiation to near the half maximum on each side of the resonance N times (N varied from 8 to 32). At each step, we probed for 5 ms, and then looked for any transition with the electron-shelving technique. We averaged the N results from each side of the resonance line, took the difference and corrected the frequency of the synthesizer drifting against the cavity. The gain of this lock needed to be properly adjusted to avoid adding frequency noise to the laser. In this way, variations in the frequency of the 282 nm laser for time periods exceeding a few seconds were reduced.

In Fig. 1, we show the spectrum obtained by scanning in this drift-free way through the Doppler-free resonance of the $^2S_{1/2}(F=0, m_F=0)$ - $^2D_{5/2}(F=2, m_F=0)$ transition. The lineshape shown is the result of 138 consecutive scans. The probe period was 15 ms and the step size was 15 Hz at 563 nm (30 Hz at 282 nm). The resonance shows a clearly resolved triplet with the linewidth of each component less than 40 Hz (< 80 Hz at 282 nm). We first thought that the triplet structure might be due to 60 Hz modulation of the frequency of the 563 nm laser either due to grounding problems, line pickup or inadequate servo gain. However, when the radiation from two independently stabilized laser beams were heterodyned

together (see next section), the 60 Hz modulation index was far too small to account for the sideband structure observed on the S-D resonance. In addition, the frequency separation of the peaks is nearer to 50 Hz, not 60 Hz. We now think that, most likely, the triplet structure is caused by Rabi power broadening. The 282 nm radiation is focussed to a spot size of about 25 μm; therefore, on resonance, fewer than 10^6 photons/s (< 1 picowatt) will saturate the transition. Below the data is a theoretical lineshape calculated for an ion at rest, for no broadening due to collisions or laser bandwidth, for a pulse length of 15 ms and for sufficient power at resonance to give a 3.5 π-pulse. Qualitatively the figures compare well. The fluctuations from measurement cycle to measurement cycle in the quantum-occupation-number of the ion in the harmonic well of the trap cause variations in the transition probability of the ion. This, and the finite laser linewidth, likely cause the general broadening and weakening of the signal. We will investigate the lineshape and the effects of power broadening in more detail in future experiments.

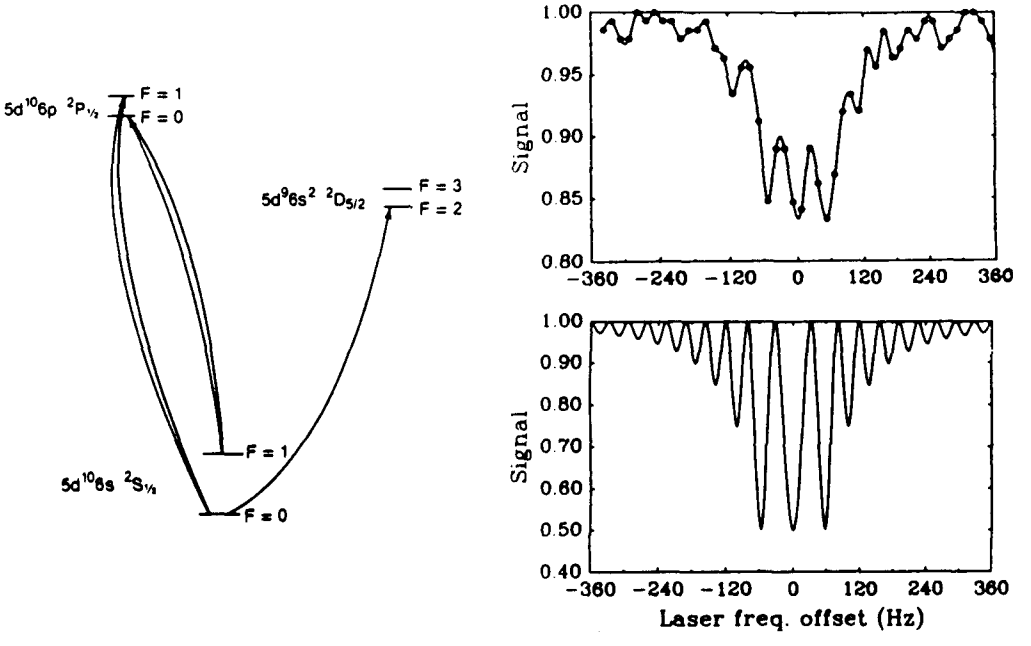

Figure 1. On the left is a simplified energy-level diagram for $^{199}Hg^+$ at zero field. Shown in the upper figure on the right is the power-broadened lineshape obtained by scanning through the Doppler-free resonance of the $^2S_{\frac{1}{2}}(F=0,\ m_F=0)$ - $^2D_{5/2}(F=2,\ m_F=0)$ transition in a single laser cooled $^{199}Hg^+$ ion. A 563 nm laser that is stabilized to a high finesse reference cavity, which in turn is long-term stabilized to the ion, is frequency doubled and stepped through the resonance for 138 consecutive sweeps. The

step size is 15 Hz at 563 nm (30 Hz at 282 nm). The lower-right figure shows the lineshape calculated for conditions similar to the experimental conditions for the upper figure, except that the ion is assumed to have zero temperature and the laser is assumed to have zero linewidth.

REFERENCE CAVITY STABILITY

To simplify the study of the performance of a laser locked to a reference cavity against external perturbations, we constructed a second Zerodur reference cavity. This study was carried out by heterodyning the light from laser beams locked to the two independent cavities and analyzing the fluctuations in the power spectrum of the beat frequency. Each laser beam was locked to its reference cavity using the reflection sideband technique discussed in detail by Drever et al.[8] In attempting to narrow the 563 nm laser to the order of 1 Hz or less, great care must be taken in the electrical and optical set-up. Many of the techniques and subtle difficulties are treated in earlier papers by Hough et al.[9] and by Salomon et al.[10] The optical and electrical problems limit the laser linewidth in our work at or below the 1 Hz level; the dominant contribution to the laser linewidth is the length stability of the reference cavities.[10-12] Some aspects of our stabilized laser systems and efforts made to isolate the cavities from external perturbations will be summarized here.[13]

Each cavity is constructed with a Zerodur[4] cylindrical spacer that has a diameter of 10.2 cm with a 1 cm holed bored down the axis. The mirrors are highly polished Zerodur[4] substrates that are coated to give high finesse and good efficiency and then optically contacted to the polished ends of the spacer. The cavities are suspended by two thin molybdenum wires inside an aluminum vacuum vessel that has an inner diameter of 26.7 cm. The wires were slung around the spacers at the nodal positions for the lowest order bending mode (about L/5 from each end where L is the cavity length) and attached to the walls of the vacuum vessel by small clamps. The two wires open into a symmetric "V" at each end; with opening angles of about 10° at one end and about 15° at the other end. This allowed free movement of the cavities along the direction of their axis. The damping of this motion was primarily into the aluminum housing and from there into the table and padding used for isolation. The aluminum vacuum vessels were thermally insulated and temperature controlled to the order of a few mK. The temperature coefficient of our Zerodur[4] spacers was approximately $6 \times 10^{-9}/^{\circ}C$ near room temperature. The thermal time

constant from the walls of the evacuated aluminum housing to the spacers was on the order of 1 day. Low pressure was maintained in each vacuum vessel by an ion pump that was directly attached to the vessel. The pressure in one vessel was about 8×10^{-9} Torr (1.1×10^{-6} Pa) but only 2×10^{-7} Torr (2.7×10^{-5} Pa) in the second system. This is marginally adequate, since 10% pressure fluctuations in the second system would cause frequency fluctuations of a few Hz to the laser stabilized to its cavity from changes in the index of refraction.

The length of one Zerodur[4)] rod results in a free spectral range of 562 MHz while the other gives 622 MHz. The finesse of the longer cavity is 60 000 and the transmission efficiency on resonance exceeds 23%. The shorter cavity has a finesse of 90 000 and an efficiency of about 27%. (Two Fabry-Perot cavities have been constructed from ULE[4)] spacers that are about 10 cm long by about 7.6 cm in diameter. Both cavities have a measured finesse that exceeds 130 000. The frequencies of the mechanical resonances of these shorter, stiffer bars will be about a factor of 3 higher than the Zerodur bars. In general, if the frequencies of the mechanical vibrations are high enough, the clock transition can be probed by the "unperturbed" carrier of the laser spectrum.) The aluminum vacuum vessels rested on Viton[4)] rubber strips attached to V-blocks made of aluminum. The V-blocks were secured to a rigid plexiglass[4)] plate. Each reference cavity system was mounted on separate optical tables that (initially) consisted of surface plates damped into sand. The sand box sat on soft rubber pads and cinder block legs in one case and on low-pressure inner tubes and cinder block legs in the second. Noise vibrations on the floor and on the table tops were monitored with sensitive seismometers. Some isolation from mechanical vibrations at frequencies above 5 Hz was achieved for both table tops.

For heterodyning purposes a small fraction of the frequency stabilized light from each cavity was combined on a beam splitter and detected with a fast diode. The heterodyned signal was amplified and analyzed with two spectrum analyzers used in tandem. This allowed us not only to look directly at the beat note but also to Fourier analyze the noise terms that contribute to its linewidth. The first analyzer could be used to observe the beat signal or as a frequency discriminator. As a discriminator, the scan was stopped and the analyzer was used as a tunable rf receiver with a variable bandwidth. The center frequency was shifted so that the

heterodyne signal lay at the 3 dB point of the response curve. The bandwidth was adjusted so that the frequency excursions of the beat signal were much less than the bandwidth. This produced a one-to-one map of frequency excursions to voltage excursions whose Fourier power spectrum could be analyzed in the second, low-frequency (0-100 kHz) spectrum analyzer. This allowed us to study the nature and origin of the vibrational noise that contributes to the linewidth of the stabilized laser.

The width of the heterodyne signal between the two stabilized lasers was less than 40 Hz. The noise power spectrum revealed that low frequency fluctuations in the range from near 0 to 30 Hz dominated this linewidth. The vibrational noise spectrum measured by the seismometers on the table tops matched the largest noise components of the beat note. The frequencies of the pendulum motion of the suspended cavities were about 1.4 Hz and 1.48 Hz which gave FM at these frequencies. There were also bright features in both the laser and the seismometer power spectra that came from floor motion at 14.6 Hz, 18.9 Hz and at 29.2 Hz. These all had enough power to contribute to the beat note linewidth. When the pendulum motions of the bars were quiet, the integral of the nearly featureless noise power spectrum from ~ 0 Hz to 10 Hz most strongly contaminated the spectral purity of the lasers. Some, if not all of this noise was mechanical in origin, but it was not clear how it coupled to the suspended cavity. To help elucidate the connection, we drove the table tops in either the horizontal or vertical direction with a small loudspeaker connected to an audio signal generator. The motion of the speaker diaphragm was coupled to the table by a rod glued to the diaphragm and gently loaded against the table. The table could be driven at frequencies from a few Hz to about 500 Hz with enough power to be 40 dB above any background noise term. When the loudspeaker drove the table in the horizontal plane in a direction parallel to the axis of the cavity, the isolation of the suspended cavity was sufficiently good that the beat signal showed no evidence of the perturbation even at the high drive levels. However when the drive was applied vertically at a level barely perceptible above the vertical background noise, the heterodyne signal revealed added noise power at the drive frequency. The stiff support in the vertical direction strongly coupled vertical motion into effective cavity length changes. The sensitivity of the Fabry-Perot cavity to vertical motion was orders of magnitude higher than for horizontal motion parallel to the cavity axis.

For practical reasons, we were unable to drive the table in the horizontal plane in a direction perpendicular to the cavity axis.

In order to improve the vertical isolation, one table was suspended just above the floor with latex-rubber tubing attached to the ceiling. The resonance frequencies for both the vertical motion and the horizontal pendulum motion of the suspended table were near 0.33 Hz. These were damped to the floor with two small dabs of grease. The linewidth of the heterodyne signal between the laser radiation stabilized to the cavity supported on this table and the laser radiation stabilized to the cavity supported on the best sandbox table dropped from 40 Hz to less than 20 Hz. The Fourier noise power spectrum from 0-10 Hz is shown in Fig. 2. The beatnote linewidth obtained by integrating the power spectrum is about 15 Hz. We suspect that the laser stabilized to the cavity on the sandbox table is the dominant contributor to the width of the heterodyne signal since the vibrational noise measured on this table is greater. Current efforts are devoted to measuring the narrow S-D transition in $^{199}Hg^{+}$ using the laser stabilized to the cavity on the suspended table. A linear rf Paul trap [14-17] has been constructed and is also being tested. With this trap it is possible to store and laser-cool many ions which gives a better signal-to-noise ratio (thereby better stability), but it is still possible to have a small second-order Doppler shift.

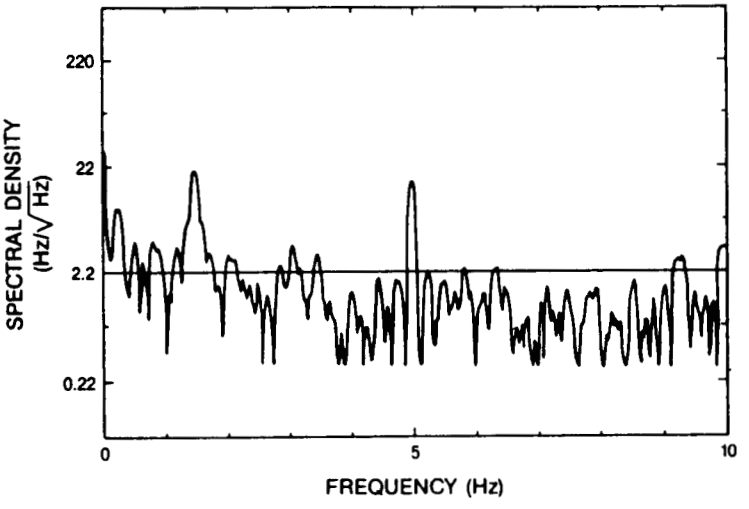

Figure 2. Fourier noise-power spectrum of laser heterodyne signal.

We acknowledge the support of the Air Force Office of Scientific Research and of the Office of Naval Research.

†Present address: Universität Hamburg, D-2000 Hamburg, Federal Republic of Germany.

REFERENCES

1. Bergquist, J. C., Itano, W. M. and Wineland, D. J., Phys. Rev. A36, 428 (1987).
2. Bergquist, J. C., Wineland, D. J., Itano, W. M., Hemmati, H., Daniel, H. -U. and Leuchs, G., Phys. Rev. Lett. 55, 1567 (1985).
3. Bergquist, J. C., Diedrich, F., Itano, W. M. and Wineland, D. J., in Laser Spectroscopy IX, ed. by M. S. Feld, J. E. Thomas, and A. Mooradian (Academic Press, San Diego, 1989) p. 274.
4. Mention of specific trade names is for purposes of technical communication alone and does not imply endorsement by N.I.S.T.
5. Bayer-Helms, F., Darnedde, H. and Exner, G., Metrologia 21, 49 (1985).
6. Wineland, D. J., Bergquist, J. C., Itano, W. M. and Drullinger, R. E., Opt. Lett. 5, 245 (1980); Wineland, D. J. and Itano, W. M., Phys. Lett. 82A, 75 (1981).
7. Dehmelt, H., Bull Am. Phys. Soc. 20 60 (1975); Dehmelt, H., J. Phys. (Paris) Colloq. 42, C8-299 (1981).
8. Drever, R. W. P., Hall, J. L., Kowalski, F. V., Hough, J., Ford, G. M., Munley, A. J. and Ward, H., Appl. Phys. B31, 97 (1983).
9. Hough, J., Hils, D., Rayman, M. D., L. -S., Ma, Hollberg, L. and Hall, J. L., Appl. Phys. B33, 179 (1984).
10. Salomon, Ch., Hils, D. and Hall, J. L., J. Opt. Soc. Am. B5, 1576 (1988).
11. Bergquist, J. C., Diedrich, F., Itano, W. M. and Wineland, D. J., in Frequency Standards and Metrology, ed. by A. DeMarchi (Springer-Verlag, Berlin, Heidelberg, 1989) p. 287.
12. Hils, D. and Hall, J. L., ibid, p. 162.
13. Bergquist, J. C., Elsner, F., Raizen, M. G., Itano, W. M. and Wineland, D. J., in preparation.
14. Prestage, J., Dick, G. J. and Maleki, L., J. Appl. Phys. 66, 1013 (1989).
15. Dehmelt, H. G., in Frequency Standards and Metrology, ed. by A. DeMarchi (Springer-Verlag, Berlin, Heidelberg, 1989) p. 286.
16. Wineland, D. J., Bergquist, J. C., Bollinger, J. J., Itano, W. M., Heinzen, D. J., Gilbert, S. L., Manney, C. H. and Raizen, M. G., to be published in I.E.E.E. Trans. on Ultrasonics, Ferroelectrics, and Frequency Control.
17. Walther, H., in these proceedings.

JOURNAL OF MODERN OPTICS, 1992, VOL. 39, NO. 2, 233–242

Linear trap for high-accuracy spectroscopy of stored ions†

M. G. RAIZEN‡, J. M. GILLIGAN,
J. C. BERGQUIST, W. M. ITANO and
D. J. WINELAND

Time and Frequency Division, National Institute of Standards and Technology, Boulder, Colorado 80303, USA

(*Received 3 July 1991; revision received 23 September 1991*)

Abstract. In a linear r.f. Paul trap, 'crystallized' structures of laser-cooled $^{199}Hg^{+}$ ions are observed. The ground-state hyperfine transition at 40·5 GHz is observed in microwave–optical double-resonance spectroscopy. Future prospects are also discussed.

1. Introduction

Trapping and cooling of large numbers of ions, each confined to much less than a wavelength of an atomic transition (the Lamb–Dicke regime), is of great interest for high-accuracy spectroscopy, improved frequency standards, and atom–radiation field experiments. In a quadrupole r.f. Paul trap, the kinetic energy of a single trapped ion is on the order of the secular energy, and confinment of a single ion to the Lamb–Dicke regime for an optical transition has been successfully demonstrated [1, 2]. For a single $^{199}Hg^{+}$ ion laser-cooled to the Doppler limit [3], the fractional second-order Doppler shift is $\langle \Delta\nu_{D2}/\nu_0 \rangle = -2{\cdot}3 \times 10^{-18}$ [4]. However, two or more ions in the trap are pushed by their mutual Coulomb repulsion from the centre of the trap, which leads to relatively large micromotion associated with the non-zero r.f. field and limits laser cooling and the achievable confinement [5–7].

The linear trap design is descended from a race-track-configuration r.f. trap, first used by Drees and Paul for short-term confinement of an electron-ion plasma [8] and later by Church for longer confinement of atomic ions [9]. Race-track traps consist of quadrupole r.f. electrodes, similar to those used in mass filters, bent to form a closed path. Charged particles feel a force toward the axis of the quadrupole and follow trajectories that carry them around the path formed by the trap electrodes. Dehmelt first suggested using a string of ions in a linear trap to suppress the second-order Doppler shift [10]. In race-track traps, the ions are usually free to move along the axis of the trap, but to satisfy the Lamb–Dicke criterion it is necessary to fix the position of each ion in this direction as well as in the radial direction. The linear trap described here uses a static electric field to confine the ions in the axial direction. Using a static field allows us to fix the axial positions of the ions, but sacrifices the race-track trap's ability to confine both positive and negative charges simultaneously. The static field also weakens the radial confinement, as will be discussed below.

‡ Present address: Department of Physics, University of Texas at Austin, Austin, Texas 78712, U.S.A.

0950-0340/92 $3·00

Prestage *et al.* [11] have trapped a cloud of $^{199}Hg^+$ ions elongated along the axis of a linear trap and have demonstrated a $^{199}Hg^+$ frequency standard with excellent frequency stability. Crystallized strings of laser-cooled $^{24}Mg^+$ ions have been observed in a race-track trap at the Max Planck Institute for Quantum Optics [12]. In our group at the National Institute of Standards and Technology (NIST), we have constructed a linear r.f. trap and have observed simple 'crystallized' linear structures of up to tens of $^{199}Hg^+$ ions [13]. By varying the axial well depth, we have also observed more complex structures.

In the next section we describe the principle of the linear trap and present the results of numerical simulations of ion configurations. We then describe our trap and present images of trapped 'crystallized' structures of ions. We next present preliminary observations of the 40·5 GHz ground-state hyperfine transition of $^{199}Hg^+$ using microwave–optical double-resonance spectroscopy with a trapped string of ions and discuss the potential for a microwave frequency standard. We conclude with a discussion of future experiments and prospects.

2. Linear trap, theory

Consider the trap shown in figure 1. The r.f. electric fields are transverse to the trap axis for the entire axial extent of the centre segment of the trap. We assume that near the trap axis the time varying potential is

$$\phi = \frac{V_0(x^2 - y^2)}{2R^2} \cos \Omega t, \tag{1}$$

where R is approximately equal to the distance from the axis to the surface of the trap electrodes. For sufficiently high drive frequency Ω this results in a harmonic pseudopotential well in the radial direction of the form

$$\phi_p = \frac{qV_0^2}{4m\Omega^2 R^4}(x^2 + y^2) = \frac{m}{2q}\omega_r^2(x^2 + y^2), \tag{2}$$

where $\omega_r \equiv qV_0/(\sqrt{2}m\Omega R^2)$ is the oscillation frequency in the radial direction. The confinement in the radial direction is identical to that of a quadrupole mass analyser [14].

To provide confinement along the axis of the trap, a static voltage U_0 is applied to the end sections. Determining the potential in the trap due to this static potential on

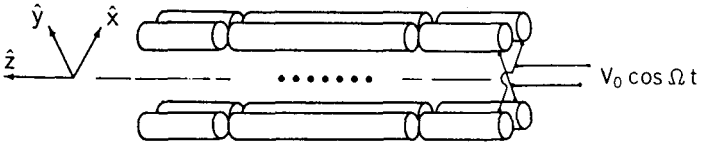

Figure 1. Linear trap configuration. An alternating r.f. voltage $V_0 \cos \Omega t$ is applied to diagonally opposite electrodes as shown. The segments of each rod are capacitively coupled so that each one can be biased at a different static potential, yet remain at the same r.f. potential. We assume that the end segments of the electrodes are long enough so that in the centre section of the trap the r.f. electric fields are parallel to the xy plane. To trap ions along z we assume the centre four electrodes are at static ground potential and the two sets of four electrodes on either end are at a static potential U_0 ($U_0 > 0$ to trap positive ions).

the electrodes would require a full three-dimensional calculation, which is beyond the scope of the present work. However, near the centre of the trap, the static potential can be approximated by

$$\phi_s = kU_0[z^2 - (x^2+y^2)/2] = \frac{m}{2q}\omega_z^2[z^2 - (x^2+y^2)/2], \tag{3}$$

where $\omega_z \equiv (2kqU_0/m)^{1/2}$ is the axial oscillation frequency in the trap and k is a geometric factor. The potential well in the radial direction is weakened by the addition of the static potential, and is given by

$$\phi_r = \frac{m}{2q}(\omega_r^2 - \omega_z^2/2)(x^2+y^2) = \frac{m}{2q}(\omega_r')^2(x^2+y^2), \tag{4}$$

where ω_r' is the radial oscillation frequency in the presence of the static potential and pseudopotential.

The kinetic energy in the micromotion of a string of ions trapped along the z axis can be about equal to the kinetic energy in the secular motion. At the Doppler cooling limit, the fractional second order Doppler shift can then be as low as $-2{\cdot}3 \times 10^{-18}$ for *all* the Hg^+ ions in the string [4]. We have performed numerical simulations to find ion configurations in a linear trap as a function of the number of ions and the radial and axial secular frequencies [15]. This calculation found the equilibrium positions of the ions by minimizing the potential energy, assuming harmonic potentials in the radial and axial directions and Coulomb repulsion between the ions.

The simplest configuration of ions is a linear string, which is obtained when the radial well is much deeper than the axial well. A computer simulation of eight ions in a string is shown in figure 2. The ions can be pushed into planar or three-dimensional configurations by increasing the axial well depth relative to that of the radial well. In figure 3 a planar zig–zag structure of 11 ions is shown. Such configurations are closely related to structures predicted for cold ions in storage rings [16].

3. Linear trap, experiment

The linear trap constructed in our group at NIST follows a geometry similar to the outline of figure 1. This design ensures that the r.f. fields are transverse to the trap axis. The trap dimensions are: rod diameters 1·6 mm, distance of the rod centres from the z axis of the trap 1·55 mm, and the axial centre trapping section 2·5 mm. The

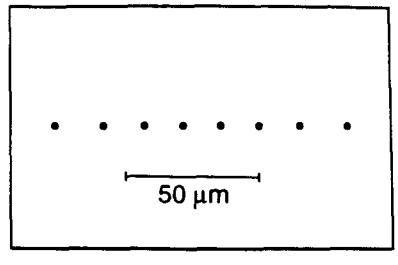

Figure 2. Numerical simulation of a crystallized string of eight $^{199}Hg^+$ ions for secular frequencies $\omega_r'/2\pi = 435$ kHz, $\omega_z/2\pi = 41{\cdot}7$ kHz. These secular frequencies were obtained by scaling secular frequencies measured under different conditions to the potentials applied to the trap when figure 5 was acquired.

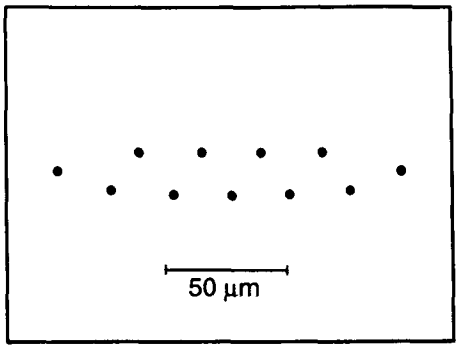

Figure 3. Numerical simulation of a crystallized zig–zag structure of 11 $^{199}Hg^{+}$ ions. An asymmetry in the two radial directions (x, y) was assumed, pinning the structure in the weaker of the two wells, and the projection is at 45° from the plane of the structure. The secular frequencies are $\omega_x'/2\pi = 77$ kHz, $\omega_y'/2\pi = 92{\cdot}4$ kHz, and $\omega_z/2\pi = 31$ kHz. These secular frequencies were obtained by scaling measured frequencies to the potentials applied when figure 6 was acquired and increasing ω_y' by 20% *ad hoc* to make the results agree with figure 6.

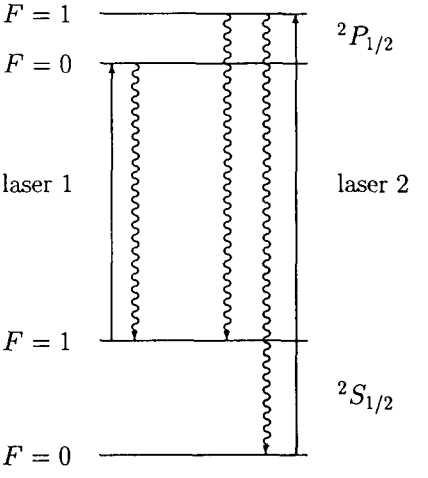

Figure 4. Energy level structure for the $^2S_{1/2}$ and $^2P_{1/2}$ levels of $^{199}Hg^{+}$ near zero magnetic field. The $^2S_{1/2}(F=0)-(F=1)$ hyperfine splitting is 40·5 GHz, and the $^2P_{1/2}(F=0)-(F=1)$ hyperfine splitting is 6·9 GHz. The intervals are not drawn to scale. Lasers 1 and 2 are used for cooling, optical pumping, and detection as described in the text.

radial size of the trap was chosen to permit Hg^{+} ions to be confined near the Lamb–Dicke regime for an optical transition by a 12·7 MHz r.f. drive with a voltage amplitude V_0 of approximately 700 V. In the work so far, amplitudes V_0 of up to 350 V were used. Axial confinement is achieved with a static voltage of typically 1 V or less. $^{199}Hg^{+}$ ions are loaded into the trap by leaking neutral ^{199}Hg (isotopic purity 91%) into the vacuum chamber to a pressure of approximately 10^{-6} Pa and then ionizing some of these atoms in the trap with electrons from a field emission point. After the trap is loaded, the chamber is evacuated to a pressure of approximately 10^{-8} Pa. The ions are laser-cooled by a few microwatts of c.w. laser radiation at 194 nm [2].

Due to the hyperfine structure of $^{199}Hg^+$, optical pumping must be considered in the laser cooling scheme. In figure 4 we show the hyperfine levels for the $^2S_{1/2}$ and $^2P_{1/2}$ states of $^{199}Hg^+$ in zero magnetic field. Two lasers at 194 nm are required. The ions are both cooled and detected using a laser (laser 1 in figure 4) that is tuned slightly below the resonant frequency of the optical transition $^2S_{1/2}(F=1) \rightarrow {}^2P_{1/2}(F=0)$. This is a 'cycling transition' since the ions that are excited to the $^2P_{1/2}(F=0)$ level can decay only to the $^2S_{1/2}(F=1)$ level according to dipole selection rules. The ions are detected by collecting photons scattered in this transition. Laser 1 can also weakly excite the $^2S_{1/2}(F=1) \rightarrow {}^2P_{1/2}(F=1)$ optical transition (it is detuned 6·9 GHz from this resonance, whose natural linewidth is $\gamma/2\pi = 70$ MHz). From the $^2P_{1/2}(F=1)$ level the ions can then decay to the $^2S_{1/2}(F=0)$ level. By itself, laser 1 would optically pump the ions into the $^2S_{1/2}(F=0)$ level, which would spoil the laser cooling. To prevent this, we have a second laser (laser 2 in figure 4), that is offset 47·4 GHz to the blue of laser 1 in order to repump the ions from the $^2S_{1/2}(F=0)$ level back to the $^2S_{1/2}(F=1)$ level. In addition to the above considerations, we must prevent optical pumping into the $^2S_{1/2}(F=1, m_F=\pm 1)$ levels. We do this by applying a magnetic field of about 5×10^{-4} T (5 G) at approximately 45° to the electric field vector of the 194 nm radiation.

To cool both the radial and axial motion of the ions, we direct the laser beam through the trap at an angle of approximately 9° to the trap axis. Fluorescence emitted perpendicular to the axis of the trap is collected by a fast lens system, which images it with a magnification of 22 onto an imaging photon detector. The secular frequencies of the trap are measured by applying a drive to the trap electrodes and observing a drop in the fluorescence (due to strong excitation of the secular motion of the ions) as the drive sweeps through resonance [17]. These measurements permit a quantitative comparison between the observed ion configurations and the numerical simulations described earlier. The secular frequencies were measured for several different r.f. and static voltages and had the correct functional dependence on the voltages. The unperturbed radial secular frequency ω_r was proportional to the r.f. voltage and the axial secular frequency ω_z was proportional to the square root of the static voltage. For very small axial voltage (less than 100 mV) the effects of local contact potentials can come into play, making it difficult to characterize the axial well depth. By changing the loading conditions (that is, by changing the neutral Hg background pressure and the duration and intensity of the field emission), we can trap different numbers of $^{199}Hg^+$ ions and have resolved as many as 33 ions in a string and as few as a single ion. To crystallize and resolve significantly longer strings, higher laser power and improved imaging optics will probably be required. Another limitation may be our ability to cancel the effects of local patch potentials over the entire axial extent of the string. In the present trap, static offsets can be independently applied to three of the four trapping rods to compensate for such potentials, but as the string of ions approaches the radial size of the trap (750 μm), these potentials may vary over the length of the string. In this case, we expect the static compensation to be less effective. In addition, we can apply a different static voltage to each end to translate the entire structure along the axis.

Two representative pictures of crystallized structures are shown in figures 5 and 6. In figure 5, eight ions in a string are clearly resolved. Figure 6 shows a structure of 11 ions (10 $^{199}Hg^+$ ions and one impurity ion). This structure was obtained by lowering the r.f. voltage on the trap for a fixed static voltage. Both ion configurations are in close agreement with the numerical simulations shown in figure 2 and in figure

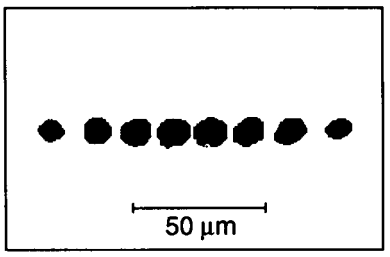

Figure 5. Image of crystallized string of eight $^{199}Hg^{+}$ ions. The potentials applied to the trap when this image was acquired were used as input for the numerical simulation shown in figure 2.

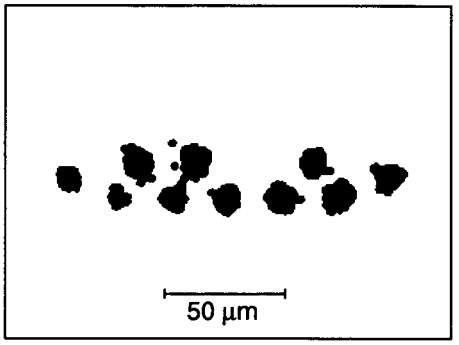

Figure 6. Image of a crystallized structure of ten $^{199}Hg^{+}$ ions and one impurity ion. The potentials applied to the trap when this image was acquired were used as input for the numerical simulation shown in figure 3.

3, which used secular frequencies that corresponded to the trap conditions for figures 5 and 6, respectively. These values were obtained by scaling secular frequencies measured under different trap conditions to the potentials applied to the trap when figures 5 and 6 were acquired. In order for the numerical simulation shown in figure 3 to agree with the ion configuration of figure 6 it was necessary to assume an azimuthal asymmetry in the radial potential sufficient to force the ions into a plane. The source of this asymmetry is not known, but it may be due to differences in contact potentials or static electric charges on the electrodes. For a large number of ions and a weak axial well, more complicated two and three-dimensional structures are seen. Such structures are closely related to the structures predicted for cold ions in storage rings [16]. A systematic and quantitative study of these two and three-dimensional crystallized structures will require eliminating the azimuthal asymmetry or characterizing it more completely.

4. Microwave–optical double-resonance

A string of cold ions is of great interest for high-resolution spectroscopy and improved frequency standards. With imaging techniques, each ion can be treated as an independent atomic clock, which is detected with 100% efficiency (using Dehmelt's 'electron shelving' technique [2, 18, 19]). We assume that the Ramsey separated field method is used in the time domain to interrogate the clock transition at frequency ω_0 (in rad s^{-1}). In this method, excitation of the clock transition is by

two phase-coherent pulses of radiation, each of duration ΔT_R, separated by a time T_R. We assume that $\Delta T_R \ll T_R$. By probing the clock transition on each side of the Ramsey peak, we can obtain an error signal to drive the average frequency to ω_0. The frequency stability for the locked oscillator as characterized by the two-sample Allan variance [20] is

$$\sigma_y(\tau) = (\tau N T_R \omega_0^2)^{-1/2}, \qquad (\tau > T_R), \tag{5}$$

where τ is the averaging time and N is the number of atoms. This expression shows that there is an advantage in using large N, ω_0, T_R, and τ. The trap environment can enable long interrogation times T_R. To achieve high accuracy, we must minimize and account for external perturbations due to electric, magnetic, and gravitational fields. These include ion–trap and ion–ion interactions, collisions with neutral background atoms, external magnetic and electric fields, and gravitational red shifts. For a microwave transition on a cold string of $^{199}Hg^+$ ions, the uncertainty could eventually be as small as the uncertainty of the second-order Doppler shift. At the Doppler limit of laser cooling, the fractional second order Doppler shift of $^{199}Hg^+$ is $-2{\cdot}3 \times 10^{-18}$ [4]. To realize this small Doppler shift it will be necessary that the equilibrium radial position of the ions coincide exactly with the line along which the r.f. trapping fields vanish. Otherwise, the micromotion will cause the second-order Doppler shifts to be much larger. The contributions of other effects, such as Stark shifts due to neighbouring ions, are discussed in [21, 22].

This potential for very high accuracy has led us to investigate the possibility of a microwave frequency standard based on the 40·5 GHz ground-state hyperfine splitting of $^{199}Hg^+$ with a trapped and laser-cooled string of ions. This transition is independent of the magnetic field to first order at zero field. For a Ramsey interrogation time of $T_R = 100$ s and $\omega_0/2\pi = 40{\cdot}5$ GHz, the frequency stability of a clock 'ensemble' of $N = 50$ ions would be $\sigma_y(\tau) = 5{\cdot}5 \times 10^{-14} \tau^{-1/2}$.

As a first step toward this goal we have recently detected the 40·5 GHz ground-state hyperfine transition of a string of $^{199}Hg^+$ ions by microwave–optical double-resonance. For this preliminary measurement the total fluorescence of the whole string of ions was measured. This meant that the measurement was sensitive to noise arising from intensity and frequency fluctuations in the cooling/detecting laser, so the stability figure given by equation (5) is not applicable.

To describe the measurement sequence we rely on the discussion of laser cooling and optical pumping given in the previous section and on figure 4. As described above, when the lasers are on, it is necessary to apply a magnetic field to prevent optical pumping into the ($F=1$, $m_F = \pm 1$) levels of the ground-state. However, to avoid second-order Zeeman shifts of the $(F=1)-(F=0)$ ground-state hyperfine interval, we wanted to have zero magnetic field during the measurement. To this end, we used two sets of Helmholtz coils. One set cancelled the ambient field and the second set applied a field of about 5×10^{-4} T (5 G) to prevent optical pumping. With the second set of coils switched off, the residual magnetic field near the trap was measured to be approximately $1{\cdot}6 \times 10^{-5}$ T (0·16 G). The sequence of the measurement is as follows:

(*a*) Lasers 1 and 2 and the magnetic field are all initially on to laser-cool the ions.
(*b*) Laser 2 is turned off and the ions are optically pumped by laser 1 into the $F=0$ ground-state.

(*c*) Both lasers are turned off, the second set of Helmholtz coils are switched off, bringing the magnetic field near zero. The $^2S_{1/2}(F=0)\rightarrow{}^2S_{1/2}(F=1)$ hyperfine transition near 40·5 GHz is driven using the Ramsey method with two microwave pulses, each of duration ΔT_R and separated by a time T_R. ΔT_R and the microwave power are adjusted to be close to values that give a $\pi/2$ pulse at the resonant frequency.

(*d*) The magnetic field is switched back to the value at step (*a*), laser 1 is turned on, and we measure flurorescence from the ions. The fluorescence is proportional to the number of ions (driven by the microwaves) that have made the transition to the $^2S_{1/2}(F=1)$ state.

At the end of this sequence, the frequency of the microwave source is stepped, and the sequence is repeated. The results of many such scans are averaged together. The results of such a measurement, made with eight ions and $T_R = 1{\cdot}8$ s, is shown in figure 7. The line centre and linewidth were determined from a least-squares fit of a cosine function to the central lobe of the observed Ramsey spectrum. For the signal-to-noise ratio of this spectrum, the difference between a cosine function and an exact Ramsey profile is insignificant. The measured linewidth is 251 ± 6 mHz, which gives

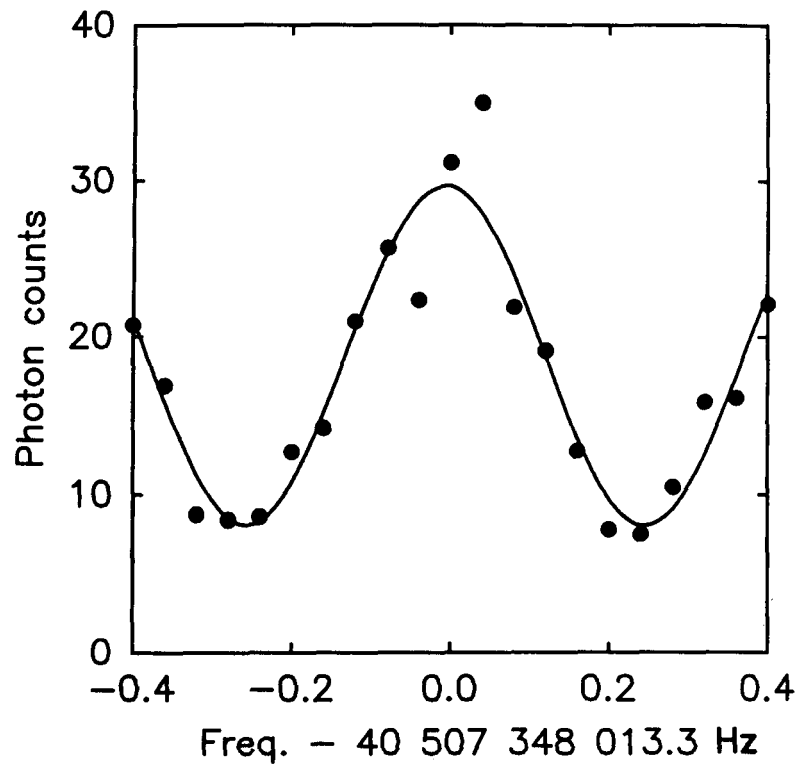

Figure 7. Microwave–optical double-resonance of the $^2S_{1/2}(F=0)\rightarrow{}^2S_{1/2}(F=1)$ hyperfine splitting of $^{199}Hg^+$ at 40·5 GHz. Shown is the central peak of a Ramsey resonance with the measurement sequence as described in the text, taken with a linear string of eight ions. The circles represent data; the solid line is a cosine function fit to the data using the least-squares criterion. For this measurement $T_R = 1{\cdot}8$ s, $\Delta T_R = 130$ ms, and each point is the average of 27 measurements. Including time for cooling, pumping and detection, each measurement cycle takes about 3 s.

a fractional resolution of $6{\cdot}2 \times 10^{-12}$. The theoretical linewidth for the pulse duration and free precession times used in this measurement is 254 mHz, in good agreement with the data.

For future experiments, in which the individual ions will be monitored separately, the fluorescence detection efficiency must be high enough that when laser 1 is turned on, enough photons will be detected that we can be sure whether each ion has or has not made the microwave transition. The number of photons scattered by an ion before it is pumped into the $^2S_{1/2}(F=0)$ level is approximately equal to the square of the ratio of 6·9 GHz (the detuning of laser 1 from the $^2S_{1/2}(F=1) \rightarrow {}^2P_{1/2}$ $(F=1)$ transition) to 35 MHz (half the radiative linewidth). This gives about 40 000 photons if laser 1 is resonant with the $^2S_{1/2}(F=1) \rightarrow {}^2P_{1/2}(F=0)$ transition. Therefore, the detection efficiency must be significantly better than the inverse of this number which is 3×10^{-5}. If this condition is met, it should be possible to detect the microwave transitions in each ion with nearly 100% efficiency. We have measured the detection efficiency of the present apparatus to be near 10^{-4}, which is marginally acceptable.

5. Future prospects

To reach the very high accuracy which should be possible with such a clock, it will be advantageous to use longer interrogation times. To reduce heating caused by collisions with background neutral atoms during the interrogation time, cryogenic pumping or sympathetic cooling [23] will most likely be required. Although in our preliminary measurements the total fluorescence from the entire string was measured, it appears possible to measure the fluorescence from each ion individually. It is then a data handling problem to route the counts from each ion to the correct 'bin' in the servo electronics.

Beyond the applications to high-accuracy spectroscopy, confining a string of ions so that each is in the Lamb–Dicke regime should make it possible to perform interesting experiments in fundamental physics such as studies of interference, cavity QED, collective behavior, and the fundamental quantum noise in the measurement of a transition in a single atom.

Acknowledgments

We gratefully acknowledge the support of the U.S. Office of Naval Research and and the Air Force Office of Scientific Research. We thank F. Moore and H. Robinson for helpful suggestions on the manuscript.

References

[1] Janik, G., Nagourney, W., and Dehmelt, H., 1985, *J. opt. Soc. Am.* B, **2,** 1251.
[2] Bergquist, J. C., Itano, W. M., and Wineland, D. J., 1987, *Phys. Rev.* A, **36,** 428.
[3] Itano, W. M., and Wineland, D. J., 1982, *Phys. Rev.* A, **25,** 35; Wineland, D. J., and Itano, W. M., 1987, *Phys. Today,* **40** (6), 34.
[4] Wineland, D. J., Itano, W. M., Bergquist, J. C., and Hulet, R. G., 1987, *Phys. Rev.* A, **36,** 2220; Wineland, D. J., Itano, W. M., Bergquist, J. C., Bollinger, J. J., Diedrich, F., and Gilbert, S. L., 1989, *Frequency Standards and Metrology,* Proceedings of the fourth Symposium, edited by A. DeMarchi (Berlin: Springer-Verlag), pp. 71–77.
[5] Wineland, D. J., 1984, *Precision Measurement and Fundamental Constants II,* edited by B. N. Taylor and W. D. Phillips (National Bureau of Standards (U.S.) Spec. Publ. 617), p. 83.
[6] DeVoe, R. G., Hoffnagle, J., and Brewer, R. G., 1989, *Phys. Rev.* A, **39,** 4362.

[7] BLÜMEL, R., KAPPLER, C., QUINT, W., and WALTHER, H., 1989, *Phys. Rev.* A, **40,** 808.
[8] DREES, J., and PAUL, W., 1964, *Z. Phys.*, **180,** 340.
[9] CHURCH, D. A., 1969, *J. appl. Phys.*, **40,** 3127.
[10] DEHMELT, H. G., 1989, *Frequency Standards and Metrology*, Proceedings of the fourth Symposium, edited by A. DeMarchi (Berlin: Springer-Verlag), p. 286.
[11] PRESTAGE, J. D., DICK, G. J., and MALEKI, L., 1989, *J. appl. Phys.*, **66,** 1013; PRESTAGE, J. D., DICK, G. J., and MALEKI, L., 1991, *I.E.E.E. Trans. Instrum. Meas.*, **40,** 132.
[12] WALTHER, H., 1991, *Light Induced Kinetic Effects on Atoms, Ions and Molecules*, Proceedings Workshop Elba Island, Italy May 2–5, 1990, edited by L. Moi *et al.* (Pisa: ETS Editrice), p. 261; BIRKL, G., KASSNER, S., QUINT, W., and WALTHER, H., Max Planck Institute for Quantum Optics, private communication.
[13] RAIZEN, M. G., BERGQUIST, J. C., ITANO, W. M., and WINELAND, D. J., 1991, *Conference on Quantum Electronics and Laser Science*, Talk QWE3, Baltimore, MD.
[14] PAUL, W., REINHARD, H. P., and VON ZAHN, U., 1958, *Z. Phys.*, **152,** 143.
[15] WINELAND, D. J., BERGQUIST, J. C., BOLLINGER, J. J., ITANO, W. M., HEIZEN, D. J., GILBERT, S. L., MANNEY, C. H., and RAIZEN, M. G., 1990, *I.E.E.E. Trans. Ultrasonics, Ferroelectrics, and Frequency Control*, **37,** 515; ITANO, W. M., BERGQUIST, J. C., and WINELAND, D. J., *Proceedings of Crystalline Ion Beams*, Wertheim, W. Germany, edited by R. W. Hasse, I. Hofmann and D. Liese (GSI report GSI-89-10, ISSN 0170-4546), p. 241.
[16] HASSE, R. W., and SCHIFFER, J. P., 1990, *Ann. Phys. N.Y.*, **203,** 419; HASSE, R. W., and SCHIFER, J. P., *Proceedings of Workshop on Crystalline Ion Beams*, Wertheim, W. Germany, edited by R. W. Hasse, I. Hofmann and D. Liese (GSI report GSI-89-10, ISSN 0170-4546), p. 33; HABS, D., *Ibid.*, p. 43.
[17] WINELAND, D. J., BOLLINGER, J. J., and ITANO, W. M., 1983, *Phys. Rev. Lett.*, **50,** 628.
[18] NAGOURNEY, W., SANDBERG, J., and DEHMELT, H., 1986, *Phys. Rev. Lett.*, **56,** 2797.
[19] SAUTER, TH., NEUHAUSER, W., BLATT, R., and TOSCHEK, P. E., 1986, *Phys. Rev. Lett.*, **57,** 1696; SAUTER, TH., BLATT, R., NEUHAUSER, W., and TOSCHEK, P. E., 1986, *Optics Commun.*, **60,** 287.
[20] BARNES, J. A., CHI, A. R., CUTLER, L. S., HEALEY, D. J., LEESON, D. B., MCGUNIGAL, T. E., MULLEN, J. A., JR., SMITH, W. L., SNYDOR, R. L., VESSOT, R. F. C., and WINKLER, G. M. R., 1971, *I.E.E.E. Trans. Instrum. Meas.*, **20,** 105.
[21] ITANO, W. M., LEWIS, L. L., and WINELAND, D. J., 1982, *Phys. Rev.* A, **25,** 1233.
[22] WINELAND, D. J., ITANO, W. M., BERGQUIST, J. C., BOLLINGER, J. J., and PRESTAGE, J. D., 1985, *Ann. Phys.* (Paris) **10,** 737.
[23] LARSON, D. J., BERGQUIST, J. C., BOLLINGER, J. J., ITANO, W. M., and WINELAND, D. J., 1986, *Phys. Rev. Lett.*, **57,** 70.

PHYSICAL REVIEW

LETTERS

VOLUME 63 4 SEPTEMBER 1989 NUMBER 10

Test of the Linearity of Quantum Mechanics by rf Spectroscopy of the $^9Be^+$ Ground State

J. J. Bollinger, D. J. Heinzen, Wayne M. Itano, S. L. Gilbert, and D. J. Wineland

National Institute of Standards and Technology, Boulder, Colorado 80303

(Received 15 May 1989)

A hyperfine transition in the ground state of $^9Be^+$ was used to test a nonlinear generalization of quantum mechanics recently formulated by Weinberg. We searched for a dependence of the frequency of a coherent superposition of two hyperfine states on the populations of the states. We are able to set a limit of 4×10^{-27} on the fraction of binding energy per nucleon of the $^9Be^+$ nucleus that could be due to nonlinear corrections to quantum mechanics.

PACS numbers: 03.65.Bz, 06.30.Ft, 32.30.Bv

Since the 1920s, quantum mechanics has passed numerous tests as illustrated by the agreement between the predictions of specific quantum-mechanical theories and experimental measurements. For example, the measured energy levels of the hydrogen atom are in excellent agreement with the predictions of quantum-mechanical theory. However, this could be regarded as a test of the accuracy of the Hamiltonian rather than a test of quantum mechanics itself. It should be possible to test the basic framework of quantum mechanics independently of and more precisely than any particular quantum-mechanical theory. Recently, Weinberg[1,2] has formulated a general framework for introducing nonlinear corrections to quantum mechanics which enables such a test. He has suggested that a sensitive way to search for possible nonlinearities is to look for a change in a transition frequency as the wave function of a system changes between initial and final states. Monochromatic radiation used to drive the transition would therefore not stay in resonance throughout the entire transition. If the transition can be driven experimentally in time T, then the maximum frequency shift due to the nonlinearity must be on the order of $1/T$. Because nuclear magnetic resonance transitions in $^9Be^+$ have been observed with T as long as 1 s, Weinberg sets a limit of $\sim10^{-15}$ eV on the magnitude of any such nonlinear corrections to the energy of the ^9Be nucleus. In this Letter we report an experiment which improves this limit by 5 orders of magnitude.

In the formalism developed in Refs. 1 and 2, the equation which describes the time evolution of the wave function $\psi(t)$ is nonlinear and derivable from a Hamiltonian function $h(\psi,\psi^*)$. For a discrete system, it takes the form

$$i\hbar\frac{d\psi_k}{dt}=\frac{\partial h(\psi,\psi^*)}{\partial\psi_k^*}, \tag{1}$$

where ψ_k is the amplitude of state k. In general, h is not a bilinear function of ψ and ψ^* as in ordinary quantum mechanics, but the property of homogeneity $[h(\lambda\psi,\psi^*)=h(\psi,\lambda\psi^*)=\lambda h(\psi,\psi^*)$ for any complex $\lambda]$ is retained. Homogeneity guarantees that if $\psi(t)$ is a solution of Eq. (1) then $\lambda\psi(t)$ is also a solution representing the same physical state. Homogeneity ensures the proper treatment of physically separated systems and distinguishes this formalism from previous nonlinear generalizations[3,4] and tests[5,6] of quantum mechanics.

Consider a two-level system which in the absence of nonlinear corrections has eigenvalues E_k, $k=1,2$. Because any nonlinear corrections to quantum mechanics are expected to be small, it is reasonable to write the Hamiltonian function as the sum of the bilinear term $h_0(\psi,\psi^*)=\sum_{k=1,2}E_k\psi_k^*\psi_k$ of ordinary quantum me-

chanics and a term $h_{nl}(\psi,\psi^*)$ that is not bilinear and contains the small nonlinear corrections. A form of h_{nl} appropriate for the work discussed here is $h_{nl}=n\bar{h}(a)$, where $n\equiv|\psi_1|^2+|\psi_2|^2$, $a\equiv|\psi_2|^2/n$, and $\bar{h}$ is a real function.[1,2] The nonlinear time-dependent Schrödinger equation then takes the form

$$i\hbar\frac{d\psi_1}{dt}=\left[E_1+\bar{h}-a\frac{d\bar{h}}{da}\right]\psi_1\equiv\hbar\omega_1(a)\psi_1,$$

$$i\hbar\frac{d\psi_2}{dt}=\left[E_2+\bar{h}+(1-a)\frac{d\bar{h}}{da}\right]\psi_2\equiv\hbar\omega_2(a)\psi_2,$$

which has solutions

$$\psi_k(t)=c_k e^{-i\omega_k(a)t},\quad k=1,2, \tag{2}$$

where a and the c_k's can be parametrized by $c_1=\sin(\theta/2)$ and $c_2=a^{1/2}=\cos(\theta/2)$. The relative phase of the two components of the wave function (specifically, the time dependence of the coherence $\psi_1\psi_2^*$) evolves with a frequency

$$\omega_p\equiv\omega_1(a)-\omega_2(a)=\omega_0-(d\bar{h}/da)/\hbar,$$

where $\omega_0=(E_1-E_2)/\hbar$ is the atomic transition frequency in the absence of nonlinearities. A two-level system is mathematically equivalent to a spin-$\frac{1}{2}$ system in an external, uniform magnetic field, where θ is the angle by which the spin is tipped with respect to the magnetic field and ω_p is the precession frequency of the spin about the magnetic field.[7] In the language of the equivalent spin-$\frac{1}{2}$ system, the effect of the nonlinear correction $d\bar{h}/da$ is to create a dependence of the precession frequency ω_p on the tipping angle θ between the spin and the magnetic field.

We searched for a θ dependence of the precession frequency of the $(m_I,m_J)=(-\frac{1}{2},+\frac{1}{2})\rightarrow(-\frac{3}{2},+\frac{1}{2})$ hyperfine transition at $\sim$303 MHz in the ground state of $^9Be^+$ (see Fig. 1). At a magnetic field B of 0.8194 T, this transition, referred to as the clock transition, depends only quadratically on magnetic field fluctuations. With $\psi_1\equiv\psi(-\frac{3}{2},+\frac{1}{2})$ and $\psi_2\equiv(-\frac{1}{2},+\frac{1}{2})$ the simplest nonbilinear addition to the Hamiltonian function of the free $^9Be^+$ nucleus for the two states is[1,2]

$$\bar{h}(a)=2\epsilon a^2, \tag{3}$$

where ϵ is a measure of the strength of the nonlinear correction. This gives rise to a dependence of ω_p on θ of

$$\omega_p=\omega_0-4(\epsilon/\hbar)\cos^2(\theta/2). \tag{4}$$

This discussion assumes that the $^9Be^+$ nuclear spin is decoupled from the valence electron spin and therefore the $(-\frac{1}{2},\frac{1}{2})$ and $(-\frac{3}{2},\frac{1}{2})$ states are pure (m_I,m_J) states. At a magnetic field of 0.8194 T these states have a 0.02 to 0.03 amplitude admixture of $m_J=-\frac{1}{2}$ states. This creates small corrections to Eqs. (3) and (4) which we neglect.

Between 5000 and 10000 $^9Be^+$ ions and 50000 to 150000 $^{26}Mg^+$ ions were simultaneously stored in a cylindrical Penning trap[8] with $B\simeq0.8194$ T under conditions of high vacuum ($\lesssim10^{-8}$ Pa). To minimize second-order Doppler shifts of the clock transition, the $^9Be^+$ ions were cooled to less than 250 mK. The $^{26}Mg^+$ ions were directly laser cooled and compressed by a narrow-band ($\sim$1 MHz) radiation source at 280 nm.[9] The $^9Be^+$ ions were then sympathetically cooled[10] by their Coulomb interaction with the cold Mg^+ ions. A narrow-band 313-nm radiation source was used to optically pump and detect the $^9Be^+$ ions.[11,12] With the 313-nm source tuned to the $2s\,^2S_{1/2}(m_I=\frac{3}{2},m_J=\frac{1}{2})$ to $2p\,^2P_{3/2}(\frac{3}{2},\frac{3}{2})$ transition, 94% of the $^9Be^+$ ions were optically pumped into the $2s\,^2S_{1/2}(\frac{3}{2},\frac{1}{2})$ ground state.[11,12] The 313-nm source was then turned off to avoid optical pumping and ac Stark shifts. The sympathetic cooling of the $^9Be^+$ ions by the Mg^+ ions provided a steady cooling source independent of the 313-nm radiation and therefore permitted the use of long transition times.

The clock transition was detected by the following method. After the 313-nm source was turned off, the ions in the $(\frac{3}{2},\frac{1}{2})$ state were transferred to the $(\frac{1}{2},\frac{1}{2})$ state and then to the $(-\frac{1}{2},\frac{1}{2})$ state by two successive rf π pulses. Each pulse was 0.2 s long and resonant with the appropriate transition frequency (around 321 and 311 MHz, respectively). The clock transition was then driven by Ramsey's method of separated oscillatory fields[13] with rf pulses of about 1-s duration and a free-precession time on the order of 100 s. This transferred some of the ions from the $(-\frac{1}{2},\frac{1}{2})$ state to the $(-\frac{3}{2},\frac{1}{2})$ state. Those ions remaining in the $(-\frac{1}{2},\frac{1}{2})$ state were then transferred back to the $(\frac{3}{2},\frac{1}{2})$ state by reversing the order of the two rf π pulses. The 313-nm source was then turned back on, and the population of ions in the $(-\frac{3}{2},\frac{1}{2})$ state was registered as a decrease in the $^9Be^+$ fluorescence, relative to the steady-state fluorescence, during the first second that the 313-nm source was on. [The optical repumping time of the ions from the $(-\frac{3}{2},\frac{1}{2})$ state to the $(\frac{3}{2},\frac{1}{2})$ state was an or-

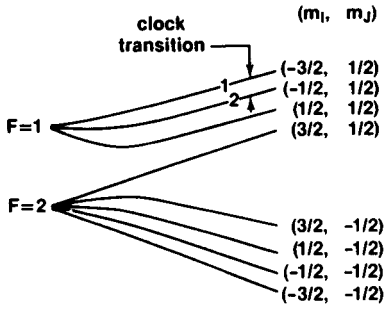

FIG. 1. Hyperfine energy levels (not drawn to scale) of the $^9Be^+$ $2s\,^2S_{1/2}$ ground state as a function of magnetic field. At $B=0.8194$ T the 303-MHz clock transition is independent of magnetic field to first order.

der of magnitude longer than this.]

For the test of nonlinearities, Ramsey's method with unequal rf pulses was used to drive the clock transition and measure ω_p for different values of θ. First an rf θ pulse of duration τ_θ was applied. This prepared the ions into a coherent superposition of the $(-\frac{1}{2},\frac{1}{2})$ and $(-\frac{3}{2},\frac{1}{2})$ states given by Eq. (2) for a particular value of θ. The value of θ was determined from $\theta=(\tau_\theta,\tau_\pi)\pi$, where τ_π was the length of time to drive a π pulse at the same rf power. After the rf θ pulse, the ions freely precessed for a time T. This was followed by an rf $\pi/2$ pulse coherent with the first pulse which completed the Ramsey excitation. In the limit that $T\gg\tau_\theta,\tau_{\pi/2}$, the Ramsey line shape [specifically, the number of ions remaining in the $(-\frac{1}{2},\frac{1}{2})$ state as a function of the rf frequency ω in the Ramsey excitation] is proportional to

$$1-\sin\theta\cos\{[\omega-\omega_p(\theta)]T\},$$

where $\omega_p(\theta)$ is given by Eq. (4). The center frequency of the Ramsey line shape is the precession frequency $\omega_p(\theta)$. Figure 2 shows a Ramsey signal obtained with $T=150$ s and $\theta=\pi/2$.

The Ramsey signal was used to steer the frequency of a synthesized rf source.[11] Ramsey-signal measurements were taken near both of the full-width-at-half-maximum frequencies $\omega_+\equiv2\pi\nu_+$ and $\omega_-\equiv2\pi\nu_-$, where ν_+ and ν_- are indicated in Fig. 2. The difference in the measured signal strengths on either side of the line center was used to electronically steer the average frequency of the synthesizer to $\omega_p(\theta)$. Eight pairs of measurements were taken with an angle $\theta_A=1.02$ rad followed by eight pairs of measurements with an angle $\theta_B=2.12$ rad. This pattern was repeated for the length of an entire run as indicated in Fig. 3. The average frequency of the synthesizer for $\theta=\theta_A$ was then subtracted from the average frequency of the synthesizer for $\theta=\theta_B$. Run lengths varied between 4 and 10 h. The uncertainty was due to the frequency instability of the reference oscillator used with the synthesizer. Most runs were taken with a commercial cesium beam clock [fractional frequency stability[14] $\sigma_y(\tau)\sim6\times10^{-12}\tau^{-1/2}$ for measurement time τ in seconds] as the reference oscillator. For a limited time we had access to a passive hydrogen maser[15] [$\sigma_y(\tau)\sim(2\text{-}3)\times10^{-12}\tau^{-1/2}$] and a few runs were taken with the passive hydrogen maser as the reference oscillator.

Runs were taken with free-precession periods of $T=30$, 60, and 100 s and rf pulse lengths of $\tau_A=0.65\tau_{\pi/2}$, $\tau_B=1.35\tau_{\pi/2}$ with $\tau_{\pi/2}=0.5$, 1, and 2 s. A weighted average of the synthesizer frequency differences for $\theta=\theta_A$ and $\theta=\theta_B$ from 25 runs is 2.7(6.0) μHz. The uncertainty (in parentheses) is the external error calculated from the scatter of the 25 measurements from the weighted average and is in good agreement with the internal error of 5.7 μHz calculated from the uncertainties of each of the 25 runs. The time constant of the servo would have decreased the apparent size of a real frequency difference by 28%. This results in a possible dependence of the precession frequency on θ of $[\omega_p(\theta_B)-\omega_p(\theta_A)]/2\pi=3.8(8.3)$ μHz and from Eq. (4) a value for the parameter ϵ of

$$\epsilon/2\pi\hbar=1.8(4.0)\ \mu\text{Hz}. \tag{5}$$

The error is a 1 standard deviation uncertainty. A few runs were also taken with $\theta=\pi/2$. The frequency $\omega_p(\pi/2)/2\pi$ was compared with the frequencies $\omega_p(\theta_A)/2\pi$ and $\omega_p(\theta_B)/2\pi$ for runs taken within a few days of each other. The standard deviation of the frequencies from their average was 6 μHz, consistent with the 7-μHz uncertainty of the frequencies. The $\theta=\pi/2$ runs do not improve the limit of Eq. (5) on a possible correction to ω_p linear in a, but in general can be used to help place limits

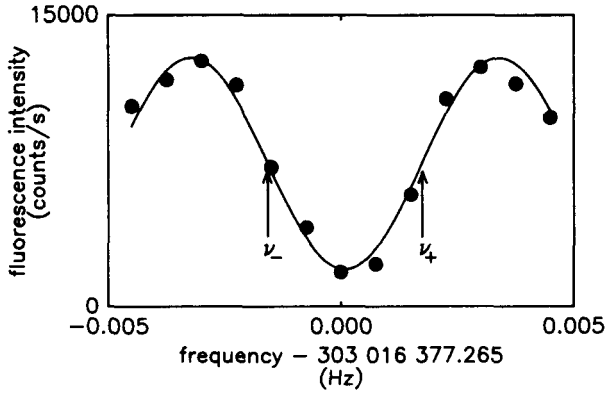

FIG. 2. Ramsey signal of the clock transition with $T=150$ s and $\theta=\pi/2$. The data are the result of one sweep (that is, one measurement per point). The sweep width is 9 mHz and the frequency interval between points is 0.750 mHz. The dots are experimental and the curve is a least-squares fit. The signal-to-noise ratio is limited by the frequency stability of the reference oscillator. The full-width-at-half-maximum frequencies are indicated by ν_+ and ν_-.

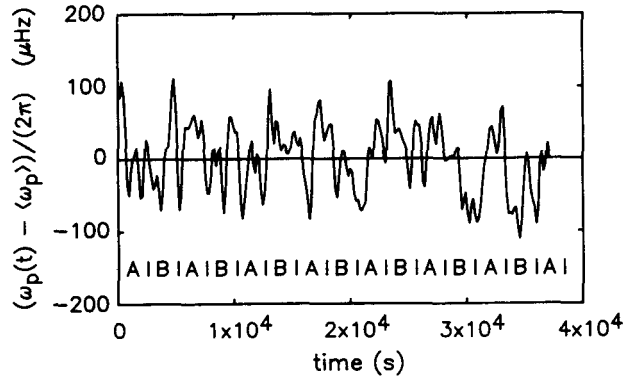

FIG. 3. $^9Be^+$ precession frequency $\omega_p(t)$, referred to a passive hydrogen maser, as a function of time for a single run with $T=100$ s. The periods A (B) during which the initial Rabi pulse created a mixed state with angle $\theta_A=1.02$ rad ($\theta_B=2.12$ rad) are indicated.

on a more complicated form for $\bar{h}(a)$.

Equation (5) sets an upper limit of $|\epsilon| < 2.4\times10^{-20}$ eV (5.8 μHz) for a nonlinear contribution to the $^9Be^+$ nuclear Hamiltonian. This is less than 4 parts in 10^{27} of the binding energy per nucleon of the $^9Be^+$ nucleus and improves the limit set in Ref. 1 by roughly 5 orders of magnitude. The limit on $|\epsilon|$ is also 5 orders of magnitude smaller than experimental limits placed by neutron interferometry[5,6] on $|b|$, where b is the coefficient of a logarithmic addition $-b\psi(\mathbf{x})\ln|\psi(\mathbf{x})|^2$ to the one-particle Schrödinger equation. However, this nonlinearity does not satisfy the property of homogeneity and therefore these experiments[5,6] test for a nonlinearity which does not satisfy the requirements of the framework developed by Weinberg. Our experimental result is limited by statistics due to the frequency instability of the reference oscillator. The largest known systematic error of our measurement of $\omega_p(\theta)$ is the second-order Doppler (time dilation) frequency shift due to the temperature and $\mathbf{E}\times\mathbf{B}$ rotation of the ions in the trap.[11] Its size is less than 3 μHz (1×10^{-14}). We believe it can be held constant to significantly better than 10% over the time required to make a frequency difference measurement. With a better reference oscillator or a second $^9Be^+$ clock, it should therefore be possible to improve our limit on $|\epsilon|$ by more than an order of magnitude. Improvements on this measurement may also be possible using nuclear magnetic resonance techniques on neutral atoms.[16,17]

We gratefully acknowledge the support of the U.S. Air Force Office of Scientific Research and the U.S. Office of Naval Research. We thank S. Weinberg for a number of helpful discussions clarifying the theory, and J. C. Bergquist and S. R. Lundeen for their comments on the manuscript.

[1]S. Weinberg, Phys. Rev. Lett. **62**, 485 (1989).

[2]S. Weinberg, Ann. Phys. (N.Y.) **194**, 336 (1989).

[3]I. Bialynicki-Birula and J. Mycielski, Ann. Phys. (N.Y.) **100**, 62 (1976).

[4]A. Shimony, Phys. Rev. A **20**, 394 (1979).

[5]C. G. Shull, D. K. Atwood, J. Arthur, and M. A. Horne, Phys. Rev. Lett. **44**, 765 (1980).

[6]R. Gahler, A. G. Klein, and A. Zeilinger, Phys. Rev. A **23**, 1611 (1981).

[7]R. P. Feynman, F. L. Vernon, Jr., and R. W. Hellwarth, J. Appl. Phys. **28**, 49 (1957).

[8]S. L. Gilbert, J. J. Bollinger, and D. J. Wineland, Phys. Rev. Lett. **60**, 2022 (1988).

[9]W. M. Itano and D. J. Wineland, Phys. Rev. A **24**, 1364 (1981); W. M. Itano, L. R. Brewer, D. J. Larson, and D. J. Wineland, Phys. Rev. A **38**, 5698 (1988).

[10]D. J. Larson, J. C. Bergquist, J. J. Bollinger, W. M. Itano, and D. J. Wineland, Phys. Rev. Lett. **57**, 70 (1986).

[11]J. J. Bollinger, J. D. Prestage, W. M. Itano, and D. J. Wineland, Phys. Rev. Lett. **54**, 1000 (1985).

[12]L. R. Brewer, J. D. Prestage, J. J. Bollinger, W. M. Itano, D. J. Larson, and D. J. Wineland, Phys. Rev. A **38**, 859 (1988).

[13]N. F. Ramsey, *Molecular Beams* (Oxford Univ. Press, London, 1956).

[14]$\sigma_y^2(\tau) = \langle [f_{i+1}(\tau) - f_i(\tau)]^2/2\bar{f}^2 \rangle$, where $f_i(\tau)$ is the ith measurement of the frequency over a measurement time interval τ, the brackets denote an average over all measurements, and $\bar{f} = \langle f_i \rangle$. See J. A. Barnes *et al.*, IEEE Trans. Instrum. Meas. **20**, 105 (1971).

[15]F. L. Walls, IEEE Trans. Instrum. Meas. **36**, 596 (1987).

[16]S. K. Lamoreaux, J. P. Jacobs, B. R. Heckel, F. J. Raab, and E. N. Fortson, Phys. Rev. A **39**, 1082 (1989).

[17]T. E. Chupp, E. R. Oteiza, J. M. Richardson, and T. R. White, Phys. Rev. A **38**, 3998 (1988).

QUANTUM OPTICS OF SINGLE, TRAPPED IONS*

Wayne M. Itano, J.C. Bergquist, F. Diedrich,† and D.J. Wineland

Time and Frequency Division
National Institute of Standards and Technology
Boulder, CO 80303

INTRODUCTION

Single ions in ion traps can be localized in small volumes and held for long periods of time. This makes it easier to observe certain nonclassical properties of the electromagnetic field, such as photon antibunching and sub-Poissonian photon statistics, which are reduced when large numbers of atoms are present. Such properties can be observed in atomic beams so dilute that the probability of having more than one atom in the observation volume is low.[1,2] Trapped ions can be studied for much longer times. This makes it possible, for example, to observe repeated quantum jumps of the *same* atom.[3-5] When there are only a few (or one) ions in the trap, their number can be known and kept fixed. Thus, sub-Poissonian photon statistics can be observed[6,7] *without* the time gating which is necessary with atomic beams.[2] Another advantage of trapped ions is that, thanks to their isolation from collisions and other perturbations, they can be laser-cooled to low temperatures and studied spectroscopically with great precision. A single ion has even been cooled to the ground energy level of the harmonic well of the trap, so its motion must be treated quantum mechanically.[8]

EXPERIMENT

Hg^+ ions were confined in a Paul trap that consists of a toroidal ring electrode, with an inner diameter slightly less than 1 mm, and two endcap electrodes, which are placed symmetrically on opposite sides of the hole through the ring.[9] A combination of static and rf potentials applied between the electrodes effectively creates a three-dimensional harmonic well. The classical motion consists of a small-amplitude oscillation, at the frequency of the applied rf potential, superimposed on a large-amplitude, harmonic motion, called the secular motion. The frequencies of the secular motion were 1–4 MHz.

A cw, tunable 194 nm radiation source[10] with a power of about 5 μW was used to excite the $^2S_{1/2}$ to $^2P_{1/2}$ first resonance line of Hg^+. In order to cool the ions, the frequency of the 194 nm source was tuned slightly lower than the atomic resonance. The radiation pressure force increases when the ion's velocity is opposed to the direction of 194 nm propagation, because the Doppler shift brings the light frequency closer to resonance. This form of laser cooling is called Doppler cooling. The 194 nm fluorescence

†Present address: Gsänger Optoelektronik GmbH, Planegg, Federal Republic of Germany.

Coherence and Quantum Optics VI
Edited by J. H. Eberly *et al.*
Plenum Press, New York, 1990

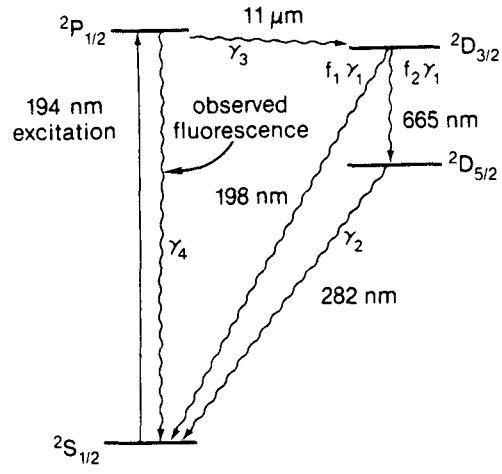

Figure 1 The lowest four energy levels of Hg^+.

from a single, cooled ion was easily observed. The photon detection efficiency was about 5×10^{-4}. Approximately 50 000 photons/s from a single ion were detected with a photomultiplier tube.

QUANTUM JUMPS

Quantum jumps of single, trapped ions have been observed in Ba^+,[3,4] Hg^+,[5] and Mg^+.[11] In this context, the term "quantum jump" refers to a sudden change in the fluorescence intensity when the atom makes a transition to or from a metastable level. We have observed photon antibunching and sub-Poissonian statistics in the system shown in Fig. 1. Measurements of the radiative decay rates were reported previously.[7] The 194 nm source drives the Hg^+ ion from the ground $^2S_{1/2}$ level to the $^2P_{1/2}$ level, which decays at a rate of 4×10^8 s^{-1}. Usually, the ion decays back to the ground state, emitting a 194 nm photon. However, about once in 10^7 times, it decays instead to the metastable $^2D_{3/2}$ level, and emits an 11 μm photon. The $^2D_{3/2}$ level decays with a total rate of $\gamma_1 = 109 \pm 5$ s^{-1}. It decays directly to the ground state with probability $f_1 = 0.491 \pm 0.015$ and to the metastable $^2D_{5/2}$ level with probability $f_2 = 1 - f_1$. The $^2D_{5/2}$ level decays to the ground state at a rate $\gamma_2 = 11.6 \pm 0.4$ s^{-1}.

Figure 2 shows the 194 nm fluorescence from a single Hg^+ ion as a function of time. When the ion makes transitions between the $^2S_{1/2}$ level and the $^2P_{1/2}$ level, the fluorescence has a high, steady level. When the ion makes a transition (quantum jump) to the $^2D_{3/2}$ level and emits an 11 μm photon, the fluorescence drops to the background level. When the ion returns to the ground state, the fluorescence goes back to the high level. We call the sudden drops in fluorescence "on-to-off" quantum jumps and the sudden increases "off-to-on" quantum jumps.

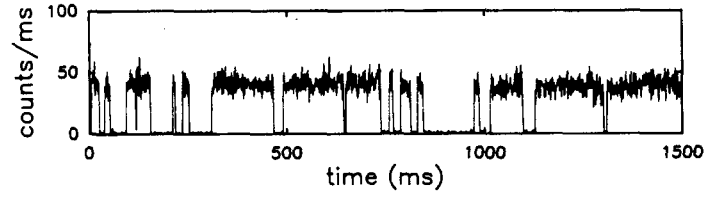

Figure 2. 194 nm fluorescence of a single Hg^+ ion as a function of time.

Table 1. Table of observed and calculated values of $Np(n)$ and Q. Values of $Np(n)$ and Q for Poissonian distributions having the same $\langle n \rangle$ are shown for comparison.

		$p(n)$								Q
	$n =$	0	1	2	3	4	5	6	7	
1-ion	Obs.	350	785	572	222	58	12	0	1	-0.253 ± 0.025
	Calc.	360.3	771.5	568.3	228.2	59.2	10.9	1.5	0.2	-0.243
	Poiss.	470.5	680.9	492.6	237.6	86.0	24.9	6.0	1.2	0.000
2-ion	Obs.	796	1503	1118	445	99	35	2	2	-0.194 ± 0.019
	Calc.	775.0	1558.1	1077.1	436.8	122.3	25.8	4.3	0.6	-0.198
	Poiss.	969.0	1373.8	973.9	460.2	163.1	46.3	10.9	2.2	0.000

Let $g^{(2)}(\tau)$ be the normalized intensity correlation function of the 11 μm field generated by the radiative decay from the $^2P_{1/2}$ level to the $^2D_{3/2}$ level. Reference 7 used a solution of the density-matrix equations of the four-level atomic system, valid for times long compared to the lifetime of the $^2P_{1/2}$ level, to show that

$$g^{(2)}(\tau) = 1 - C_+ e^{-\gamma_+ \tau} - C_- e^{-\gamma_- \tau}, \tag{1}$$

where

$$\gamma_\pm \equiv \frac{1}{2}\{(\gamma_0 + \gamma_1 + \gamma_2) \pm [(\gamma_0 + \gamma_1 + \gamma_2)^2 - 4f_2\gamma_0\gamma_1 - 4\gamma_1\gamma_2 - 4\gamma_0\gamma_2]^{\frac{1}{2}}\}, \tag{2}$$

$$C_\pm \equiv \pm\gamma_\mp(f_1\gamma_\pm - \gamma_2)/[\gamma_2(\gamma_+ - \gamma_-)]. \tag{3}$$

Here, γ_0 is the transition rate from the "on" to the "off" state. It depends on the intensity and frequency detuning of the 194 nm source. Since $g^{(2)}(\tau) \to 0$ as $\tau \to 0$, the 11 μm light is antibunched. The calculated and measured $g^{(2)}(\tau)$ are in good agreement [see Fig. 2(a) of Ref. 7]. Photon antibunching was also observed with two Hg^+ ions separated by about 3 μm.[7] The observed $g^{(2)}(\tau)$ was consistent with the assumption that the two ions were independent.

Given $g^{(2)}(\tau)$, we can compute the complete photon counting distribution. Let $p(m)$ be the probability that m, 11 μm photons are emitted in an interval of length T. It can be shown that

$$p(m) = \frac{1}{m!}\sum_{r=0}^{\infty}\frac{(-1)^r}{r!}\langle n^{(m+r)}\rangle, \tag{4}$$

where the rth factorial moment of n is defined for $r = 1, 2, 3\ldots$, by

$$\langle n^{(r)}\rangle \equiv \langle n(n-1)\ldots(n-r+1)\rangle \equiv \sum_{n=0}^{\infty} n(n-1)\ldots(n-r+1)p(n) \tag{5}$$

and $\langle n^{(0)}\rangle = 1$.[13] With the assumption that the ion loses memory of its previous history after each 11 μm photon emission, the factorial moments are given by

$$\langle n^{(r)}\rangle = \langle\hat{I}\rangle^r r! \int_0^T dt_r \ldots \int_0^{t_2} dt_1\, g^{(2)}(t_r - t_{r-1})\ldots g^{(2)}(t_2 - t_1), \quad r = 2, 3, \ldots,$$

$$\langle n^{(1)}\rangle = \langle n\rangle = \langle\hat{I}\rangle T, \qquad \langle n^{(0)}\rangle = 1, \tag{6}$$

where $\langle\hat{I}\rangle$ is the average number of 11 μm photons emitted per unit of time.[13] The normalized second factorial moment Q is given by Eq. (11a) of Ref. 13. This parameter measures the departure of the variance of a distribution from that of a Poissonian distribution. Negative values of Q indicate sub-Poissonian statistics.

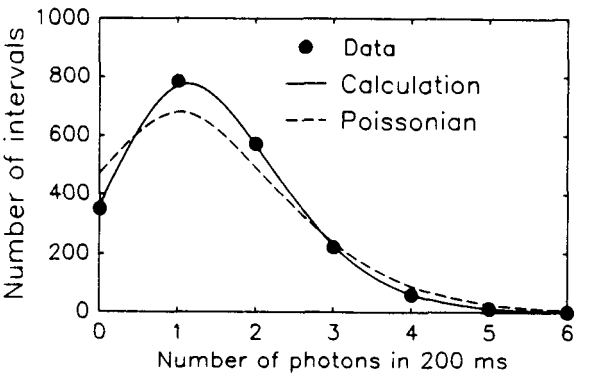

Figure 3. Observed and calculated photon count distributions. The uncertainties are less than or approximately equal to the radii of the dots. A Poissonian distribution is shown for comparison.

Observed and calculated values of $Np(n)$ and Q for one and two ions are shown in Table 1. Here, $Np(n)$ is the number of intervals in which n photons were detected, where N is the total number of intervals. For the one-ion data, $N = 2000$, $T = 200$ ms, $\gamma_0 = 12.55\ \mathrm{s}^{-1}$. For the two-ion data, $N = 4000$, $T = 100$ ms, $\gamma_0 = 12.1\ \mathrm{s}^{-1}$. The observed and calculated values are in good agreement with each other and clearly differ from the values for a Poissonian distribution. The statistical uncertainties of $Np(n)$ are approximately the square roots of the measured values. The values of Q depend on the value of T. For example, Q was measured to be -0.242 ± 0.025 for $T = 200$ ms.[7] Values of $p(n)$ were calculated by computing $\langle n^{(r)} \rangle$ for $r = 0, \ldots, 11$ from Eq. (6) and using Eq. (4). Figure 3 shows the observed and calculated values of $Np(n)$ for one ion. The dots represent the experimental data. The solid line is a smooth curve connecting the calculated values.

If the atom loses all memory after each quantum jump, then the lengths of successive intervals between jumps should show no correlation. Let $T_1, T_2, \ldots, T_n$ be the successive intervals between off-to-on or on-to-off quantum jumps. A nonrandom pattern in the scatter plot of T_n vs T_{n+1} would be an indication that the seemingly random sequence of quantum jumps was actually governed by a low-dimensional chaotic attractor. Such patterns have been observed, for example, in the time sequence of drips from a leaky faucet.[14] Plots of T_n vs T_{n+1} for both the off-to-on and the on-to-off quantum jumps are shown in Fig. 4. No nonrandom structure is apparent.

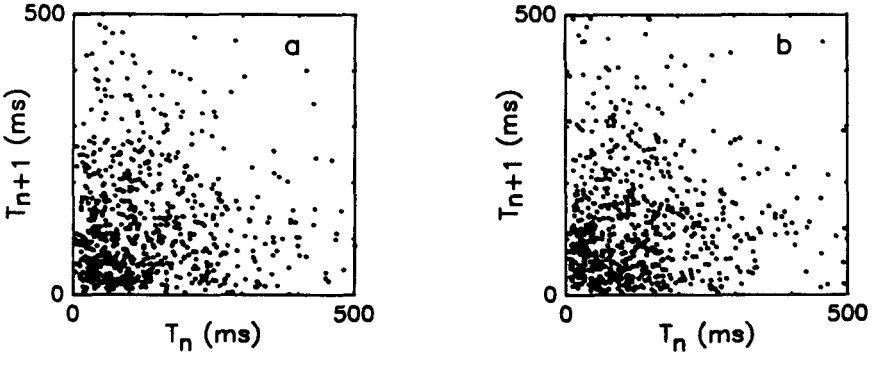

Figure 4. Scatter plot of T_{n+1} vs T_n, where T_n is the nth interval between successive (a) on-to-off quantum jumps and (b) off-to-on quantum jumps.

QUANTUM HARMONIC OSCILLATOR

The wavefunctions of a single charged particle in a Paul trap have been calculated in Refs. 15 and 16. Since the Hamiltonian is time dependent, stationary states do not exist. However, quasi-stationary states, obtained by solving for the eigenvalues of the Floquet operator, do exist. They correspond in some sense to the stationary states of the secular harmonic oscillator potential.

The absorption spectrum of a narrow optical resonance of an ion in a Paul trap consists of an unshifted carrier, surrounded by discrete motional sidebands. The sidebands are spaced by multiples and combinations of the secular frequencies. We have observed these sidebands in the absorption spectrum of the $^2S_{1/2}$-to-$^2D_{5/2}$ transition of a single trapped Hg^+ ion.[9] The carrier results from transitions in which the vibrational quasi-energy is unchanged. The upper and lower sidebands correspond to transitions which increase or decrease the quasi-energy.

Recently, we have cooled a single Hg^+ ion almost to the lowest ($n_v = 0$) vibrational quasi-energy state, by a method called sideband cooling.[8] First, the ion was Doppler cooled to about 2 mK with the $^2S_{1/2}$-to-$^2P_{1/2}$ transition, so that the mean value of n_v was about 12 at a secular frequency of 2.96 MHz. Laser radiation tuned to the first lower sideband of the narrow $^2S_{1/2}$-to-$^2D_{5/2}$ transition was then applied to the ion, lowering n_v by one for each photon absorbed. After the sideband cooling period, laser radiation of saturating intensity was applied at the lower sideband frequency. Absence of absorption, detected by optical double resonance,[9] indicated that the ion was in the $n_v = 0$ state. The ion was found to be in the ($n_v = 0$) state about 95% of the time.

Starting from the $n_v = 0$ state, other quantum harmonic oscillator states could be prepared by manipulation of the electric potentials applied to the trap. A coherent state could be prepared by quickly shifting the static potential of one endcap relative to the other, thus shifting the center of the potential well. A squeezed state could be prepared by shifting the static potential on both of the endcaps relative to the ring.

Acknowledgments

We wish to acknowledge the generous support of the Air Force Office of Scientific Research and the Office of Naval Research.

REFERENCES

1. H. J. Kimble, M. Dagenais, and L. Mandel, Phys. Rev. Lett. **39**, 691 (1977); M. Dagenais and L. Mandel, Phys. Rev. A **18**, 2217 (1978).
2. R. Short and L. Mandel, Phys. Rev. Lett. **51**, 384 (1983).
3. W. Nagourney, J. Sandberg, and H. Dehmelt, Phys. Rev. Lett. **56**, 2797 (1986).
4. Th. Sauter, W. Neuhauser, R. Blatt, and P. E. Toschek, Phys. Rev. Lett. **57**, 1696 (1986).
5. J. C. Bergquist, R. G. Hulet, W. M. Itano, and D. J. Wineland, Phys. Rev. Lett. **57**, 1699 (1986).
6. F. Diedrich and H. Walther, Phys. Rev. Lett. **58**, 203 (1987).
7. W. M. Itano, J. C. Bergquist, and D. J. Wineland, Phys. Rev. A **38**, 559 (1988).
8. F. Diedrich, J. C. Bergquist, W. M. Itano, and D. J. Wineland, Phys. Rev. Lett. **62**, 403 (1989).
9. J. C. Bergquist, W. M. Itano, and D. J. Wineland, Phys. Rev. A **36**, 428 (1987).
10. H. Hemmati, J. C. Bergquist, and W. M. Itano, Opt. Lett. **8**, 73 (1983).
11. R. G. Hulet, D. J. Wineland, J. C. Bergquist, and W. M. Itano, Phys. Rev. A **37**, 4544 (1988).
12. W. M. Itano, J. C. Bergquist, R. G. Hulet, and D. J. Wineland, Phys. Rev. Lett. **59**, 2732 (1987).
13. L. Mandel, Opt. Lett. **4**, 205 (1979).
14. P. Martien, S. C. Pope, P. L. Scott, and R. S. Shaw, Phys. Lett. **110A**, 399 (1985).
15. R. J. Cook, D. G. Shankland, and A. L. Wells, Phys. Rev. A **31**, 564 (1985).
16. M. Combescure, Ann. Inst. Henri Poincaré **44**, 293 (1986).

Quantum Zeno effect

Wayne M. Itano, D. J. Heinzen, J. J. Bollinger, and D. J. Wineland
Time and Frequency Division, National Institute of Standards and Technology, Boulder, Colorado 80303
(Received 12 October 1989)

The quantum Zeno effect is the inhibition of transitions between quantum states by frequent measurements of the state. The inhibition arises because the measurement causes a collapse (reduction) of the wave function. If the time between measurements is short enough, the wave function usually collapses back to the initial state. We have observed this effect in an rf transition between two $^9Be^+$ ground-state hyperfine levels. The ions were confined in a Penning trap and laser cooled. Short pulses of light, applied at the same time as the rf field, made the measurements. If an ion was in one state, it scattered a few photons; if it was in the other, it scattered no photons. In the latter case the wave-function collapse was due to a null measurement. Good agreement was found with calculations.

I. INTRODUCTION

The quantum Zeno effect (or paradox) is the inhibition of transitions between quantum states by frequent measurements.[1-7] Misra and Sudarshan[1] were the first to call the effect by that name, but closely related work was done much earlier.[8]

Consider the decay of an unstable state, such as an unstable particle. An observation that the state has not decayed causes a collapse (reduction) of the wave function to the undecayed state. The probability that the state decays after this collapse grows quadratically with time, for short enough times. Suppose n measurements, spaced in time by T/n, are made. The probability that the state will survive for a time T goes to 1 in the limit $n \rightarrow \infty$. Hence, Misra and Sudarshan argued, a continuously observed state can never decay.[1] This effect is difficult to observe in spontaneous decay because the interval during which the probability grows quadratically is very short compared to the time required to make a measurement. Ghirardi *et al.*[3] have shown, by general arguments based on the time-energy uncertainty relations, that the dependence of the lifetime on the frequency of measurements, although present in principle, would be extremely difficult to observe. Deviations from an exponential decay law, expected theoretically for very short and very long times, have not yet been observed experimentally.[9]

The term "quantum Zeno effect" is applied also to the inhibition of *induced* transitions by frequent measurements. This effect can easily be observed experimentally, in contrast to the inhibition of spontaneous transitions. Consider a system made up of two levels, labeled 1 and 2. Assume that the system can be driven from level 1 to level 2 by applying a resonant perturbation for a given length of time. Assume that it is possible to make measurements of the state of the system, which project the system into one of the two levels, and which take a negligible amount of time. If the system is initially in level 1, and we make n equally spaced measurements while the perturbation is applied, the probability of finding the system in level 2 at the end of the period decreases as n increases. Various cases of this type have been examined theoretically.[10-12]

II. THEORY

Cook[12] proposed an experiment on a single, trapped ion to demonstrate the quantum Zeno effect on an induced transition. Trapped ions provide very clean systems for testing calculations of the dynamics of quantum transitions. They can be observed for long periods, free from perturbations and relaxations. Their levels can be manipulated easily with rf and optical fields.

In Cook's proposed experiment, the ion was assumed to have the level structure shown in Fig. 1. Level 1 is the ground state. Level 2 is an excited metastable state. Spontaneous decay from level 2 to level 1 is assumed to be negligible. If the ion is in level 1 at time $\tau = 0$, and a perturbation having the resonance frequency $(E_2 - E_1)/\hbar$ is applied, a coherent superposition state is created. Let P_1 and P_2 be the probabilities for the ion to be in levels 1 and 2. Then $P_2(\tau) = \sin^2(\Omega\tau/2)$

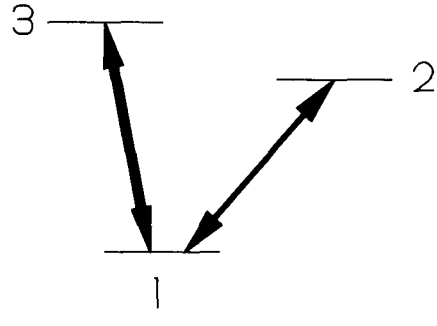

FIG. 1. Energy-level diagram for Cook's proposed demonstration of the quantum Zeno effect.

TN-98

and $P_1(\tau) = \cos^2(\Omega\tau/2)$, where Ω, the Rabi frequency, is proportional to the amplitude of the applied field. If a measurement of the state of the ion is made after a short time, such that $\Omega\tau \ll 1$, then $P_1(\tau) \approx 1$ and $P_2(\tau) \approx \frac{1}{4}\Omega^2\tau^2 \ll 1$. If, instead, the ion starts out in level 2, the situation is reversed, so that $P_2(\tau) \approx 1$ and $P_1(\tau) \approx \frac{1}{4}\Omega^2\tau^2$.

Assume that level 3 is connected by a strongly allowed transition to level 1 and that it can decay *only* to level 1. The state measurement is carried out by driving the $1 \rightarrow 3$ transition with an optical pulse. This pulse causes a collapse of the wave function. The wave function of the ion is projected by the measurement into level 1 or 2 with probabilities equal to the squares of the wave-function amplitudes for being in level 1 or 2. If the ion is projected into level 1 at the beginning of the pulse, it cycles between level 1 and level 3, and emits a series of photons until the pulse is turned off. If it is projected into level 2, it scatters no photons. The latter case is an example of what Porrati and Putterman have called a wave-function collapse due to a null measurement.[13] That is, the *absence* of scattered photons when the optical pulse is applied is enough to cause a collapse of the wave function to level 2. The pulse must be long enough so that an ion in level 1 would have time to scatter a few photons. It does not matter whether a switched-on detector capable of detecting the photons is actually present. The state of the ion is recorded in the electromagnetic field. The measurement (and the subsequent wave-function collapse) takes place after the field has interacted with the ion for a sufficient amount of time.[12,14] If a measurement finds the ion to be in level 1, the ion returns to level 1 after the end of the measurement, within a time approximately equal to the lifetime of level 3. If a measurement finds the ion to be in level 2, the ion never leaves that level during the measurement. If this measurement is followed immediately by a second one, the result will *almost* always be the same. Thus the optical pulses make nearly ideal, nondestructive measurements. However, since a finite time is required to make a measurement, the wave function can evolve between measurements. Therefore, it is possible for the result of the second measurement to differ from that of the first.

Cook's proposed experiment was to drive the $1 \rightarrow 2$ transition with an on-resonance π pulse (a square pulse of duration $T = \pi/\Omega$) while simultaneously applying a series of short measurement pulses. The duration of a measurement pulse was assumed to be much less than the time between pulses. Suppose the ion is in level 1 at time $\tau = 0$. The π pulse is then applied. Without the measurement pulses, the probability $P_2(T)$ to be in level 2 at $\tau = T$ is 1. Let n measurement pulses be applied at times $\tau = kT/n = k\pi/(n\Omega)$, where $k = 1, \ldots, n$. The level populations at the end of the π pulse are easily calculated with the use of the vector representation of a two-level system.[15] The equations simplify if we transform to a coordinate system in which the rotating component of the rf perturbation is stationary. (We ignore the counter-rotating component.) The system is described by a vector $\mathbf{R} \equiv (R_1, R_2, R_3)$, whose components can be expressed in terms of the density matrix ρ:

$$\begin{aligned} R_1 &\equiv \rho_{12} + \rho_{21}, \\ R_2 &\equiv i(\rho_{12} - \rho_{21}), \\ R_3 &\equiv \rho_{22} - \rho_{11} \equiv P_2 - P_1. \end{aligned} \tag{1}$$

The equation of motion for $\mathbf{R}$ is

$$d\mathbf{R}/dt = \boldsymbol{\omega} \times \mathbf{R}, \tag{2}$$

where $\boldsymbol{\omega} = (\Omega, 0, 0)$. The geometrical interpretation of Eq. (2) is that $\mathbf{R}$ precesses about $\boldsymbol{\omega}$ with fixed magnitude and angular velocity $|\boldsymbol{\omega}| = \Omega$. At $\tau = 0$, $\mathbf{R} = (0, 0, -1)$. Just before the first measurement pulse at $\tau = \pi/(n\Omega)$,

$$\begin{aligned} \mathbf{R} &= [0, \sin(\Omega\tau), -\cos(\Omega\tau)] \\ &= [0, \sin(\pi/n), -\cos(\pi/n)]. \end{aligned} \tag{3}$$

The measurement pulse projects an ion into level 1 or 2. Its effect on the density matrix, which corresponds to an ensemble average, is to set the coherences (ρ_{12} and ρ_{21}) to zero, while leaving the populations (ρ_{22} and ρ_{11}) unchanged. Hence, R_1 and R_2 are set to zero, while R_3 remains unchanged:

$$\mathbf{R} = [0, 0, -\cos(\pi/n)]. \tag{4}$$

Thus, at $\tau = \pi/(n\Omega)$, just after the first measurement pulse, $\mathbf{R}$ is the same as it was at $\tau = 0$, except that its magnitude has been decreased by a factor of $\cos(\pi/n)$. After the second measurement $[\tau = 2\pi/(n\Omega)]$, $|\mathbf{R}|$ is decreased by another factor of $\cos(\pi/n)$. This follows from the fact that Eq. (2) is linear with respect to $\mathbf{R}$. After n measurements, $(\tau = \pi/\Omega)$,

$$\mathbf{R}(T) = [0, 0, -\cos^n(\pi/n)]. \tag{5}$$

We use Eq. (1) to express P_2 in terms of R_3:

$$\begin{aligned} P_2 &= R_3 + P_1 = R_3 + (1 - P_2) \\ &= \tfrac{1}{2}(1 + R_3). \end{aligned} \tag{6}$$

In deriving Eq. (6), we used the conservation of probability for a closed two-level system: $P_1 + P_2 = 1$. Substituting the value of $R_3(T)$ from Eq. (5) into Eq. (6), we have

$$P_2(T) = \tfrac{1}{2}[1 - \cos^n(\pi/n)]. \tag{7}$$

It can be shown from Eq. (7) that $P_2(T)$ decreases monotonically toward zero as n goes to infinity. For large n,[12]

$$P_2(T) \approx \tfrac{1}{2}[1 - \exp(-\tfrac{1}{2}\pi^2/n)]. \tag{8}$$

Equation (8) was derived from Eq. (7) by expanding $\cos(\pi/n)$ in a power series and using

$$\lim_{n\to\infty}(1 - x/n)^n = e^{-x}. \tag{9}$$

III. EXPERIMENT

Our experiment is very similar to that proposed by Cook. Levels 1 and 2 are the $(m_I, m_J)=(\frac{3}{2},\frac{1}{2})$ and $(\frac{1}{2},\frac{1}{2})$ hyperfine sublevels in the ground $2s\,^2S_{1/2}$ state of $^9Be^+$ (see Fig. 2). These levels are separated by 320.7 MHz at the magnetic field used in the experiment ($B \approx 0.8194$ T). Level 3 is the $(m_I = \frac{3}{2}, m_J = \frac{3}{2})$ sublevel of the $2p\,^2P_{3/2}$ state, which decays only to level 1. Spontaneous decay from level 2 to level 1 is negligible.

The experimental apparatus has been described previously.[16–18] About 5000 $^9Be^+$ ions were stored in a cylindrical Penning trap. The pressure in the trap was about 10^{-8} Pa. The storage time of the ions in the trap was several hours. A frequency-doubled cw dye laser generated 313-nm radiation to drive the $1 \rightarrow 3$ transition in order to optically pump, detect, and laser cool the $^9Be^+$ ions. The 313-nm fluorescence from the ions was detected by an imaging photon-counting detector.[16] About 100 000 $^{26}Mg^+$ ions were confined together with the $^9Be^+$ ions. The $^{26}Mg^+$ ions were laser-cooled by 280-nm radiation from a frequency-doubled cw dye laser. The $^9Be^+$ were kept cold ($\lesssim$250 mK) by long-range Coulomb collisions with the $^{26}Mg^+$ ions even when they were not directly laser-cooled by the 313-nm source.[19]

The polarization of the 313-nm beam was perpendicular to the magnetic field. When the 313-nm radiation was nearly resonant with the $1 \rightarrow 3$ transition and no rf field was applied, about $\frac{16}{17}$ of the population was optically pumped to the $(\frac{3}{2},\frac{1}{2})$ ground-state sublevel (level 1).[20–22] The remaining population was in the $(\frac{3}{2},-\frac{1}{2})$ sublevel. When the 313-nm radiation was on continuously, the populations approached the steady state with a time constant of about 1 s.

The measurement sequence for the $1 \rightarrow 2$ transition was as follows: The 313-nm radiation was left on for about 5 s to prepare most of the $^9Be^+$ ions in level 1 and to empty level 2. The 313-nm radiation was then turned off. The 320.7-MHz rf field was turned on for $T = 256$ ms. Its frequency and amplitude were adjusted to make this an on-resonance π pulse. During the rf pulse, n pulses of length $\tau_p = 2.4$ ms and wavelength 313 nm were applied, where n was 1, 2, 4, 8, 16, 32, or 64. The pulses were long enough to collapse each ion's wave function without causing significant optical pumping. The delay from the beginning of the rf pulse to the beginning of the first 313-nm pulse was $(T/n - 1.3)$ ms. The time between the beginning of one 313-nm pulse and the beginning of the next one was T/n.

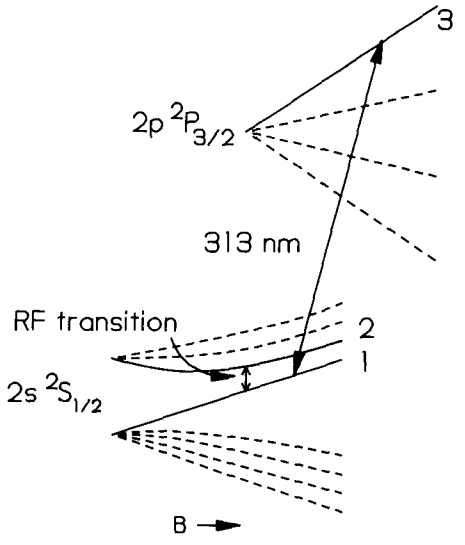

FIG. 2. Diagram of the energy levels of $^9Be^+$ in a magnetic field B. The states labeled 1, 2, and 3 correspond to those in Fig. 1 .

After the end of the rf π pulse, the 313-nm radiation was turned on and left on to prepare the state. The number of photons counted in the first 100 ms was recorded. This signal was roughly proportional to the number of ions remaining in level 1. However, background counts, counter deadtime, and optical pumping during the 100 ms cause deviations from this proportionality. In order to calibrate the signal, known level populations were created by applying rf pulses of lengths $\tau = 0, 32, 64, \ldots, 544$ ms. The population of level 1 (per ion in the subsystem made up of levels 1 and 2) was then given by $\cos^2(\Omega\tau/2)$. From these data, the precise value of Ω and also the calibration of the signal as a function of the population of level 1 were obtained. The deviations of the calibration points from a smooth curve gave an indication of the measurement errors.

The 313-nm radiation was turned on and off with an electromechanical shutter that had a rise or fall time of about 0.2 ms. The 320.7-MHz rf field was turned on and off with a semiconductor diode switch, which had a switching time of about 150 ns and an on-to-off ratio of about 75 dB. The 280-nm beam was left on continuously. The measurement sequence was the same for the $2 \rightarrow 1$ transition, except that first an rf π pulse, free from 313-nm pulses, transferred the level 1 population to level 2 immediately after the 313-nm radiation was shut off.

The $1 \rightarrow 2$ transition frequency decreases by 22 Hz for a 1-μT increase in B. If the transition frequency shifts by more than a small fraction of $1/T \approx 4$ Hz, the observed transition probabilities will deviate significantly from the calculated ones. The center frequency of the $1 \rightarrow 2$ resonance was measured before and after each run. If the frequency shifted by more than about 0.1 Hz, the data from that run were not used. Drift of the magnetic field was the main obstacle to increasing T. Relaxations of the ground-state hyperfine levels are very weak when the 313-nm radiation is not applied. This was shown in studies of the $(m_I, m_J)=(-\frac{1}{2},\frac{1}{2})$ to $(-\frac{3}{2},\frac{1}{2})$ transition. The derivative of this transition frequency with respect to B goes to zero at $B \approx 0.8194$ T. At this value of B, weak relaxation processes due, for example, to collisions or to the 280-nm radiation can be studied. This transition showed no sign of population or coherence relaxations for times up to 550 s.[17]

The average number of photons scattered by an ion in

TABLE I. Predicted and observed values of the $1 \rightarrow 2$ and $2 \rightarrow 1$ transition probabilities for different values of the number of measurement pulses n. The uncertainties of the observed transition probabilities are about 0.02. The second column shows the transition probabilities that result from a simplified calculation, in which the measurement pulses are assumed to have zero duration and in which optical pumping is neglected.

		$1 \rightarrow 2$ transition		$2 \rightarrow 1$ transition	
n	$\frac{1}{2}[1-\cos^n(\pi/n)]$	Predicted	Observed	Predicted	Observed
1	1.0000	0.995	0.995	0.999	0.998
2	0.5000	0.497	0.500	0.501	0.496
4	0.3750	0.351	0.335	0.365	0.363
8	0.2346	0.201	0.194	0.217	0.209
16	0.1334	0.095	0.103	0.118	0.106
32	0.0716	0.034	0.013	0.073	0.061
64	0.0371	0.006	−0.006	0.080	0.075

level 1 during a single 313-nm pulse of length τ_p is approximately $\tau_p R_c/(\epsilon_d N)$, where R_c is the observed steady-state photon count rate, ϵ_d is the probability of detecting a scattered photon, and N is the total number of $^9Be^+$ ions. The photon detection efficiency ϵ_d was estimated from the solid angle of the lens system and the quantum efficiency of the detector to be about 2×10^{-4}. For typical experimental values $\tau_p = 2.4$ ms, $R_c = 30\,000$ s^{-1}, and $N = 5000$, the number of scattered photons per ion per pulse was therefore about 72, more than enough to cause the collapse of the wave function. We emphasize that it is the number of scattered photons which is important, not the number that can be detected by the apparatus. The number of photons detected per ion per pulse is much less than 1. As a further check that the pulses were long enough, some runs were taken with τ_p decreased to 1.4 ms (the shortest that the shutter could make). The results indicated that these pulses were still long enough to collapse the wave functions. These data are not reported here because the pulse shapes were not the same for different pulse repetition rates. This made quantitative interpretation of the data difficult.

With a faster optical shutter, such as an acousto-optic modulator, the 313-nm pulses could be decreased in length and still be long enough to collapse the wave functions. However, the minimum time required for a measurement pulse depends not only on the *average* photon scattering rate, but also on the time required to ensure that every ion will pass through the 313-nm beam. The $^9Be^+$ ions occupied a cylindrical volume with a height of about 1000 μm and a radius of about 350 μm. The 313-nm beam was focused to a radius of about 50 μm. It propagated perpendicular to the axis of the cylinder and intersected the $^9Be^+$ ions near the center of the volume. If the 313-nm beam were expanded radially and directed along the axis, so that it intersected the entire volume, this problem could be avoided.

IV. RESULTS

Table I shows the calculated and observed values of the probabilities of making the $1 \rightarrow 2$ and $2 \rightarrow 1$ transitions for values of $n = 1, 2, \ldots, 64$. The predicted and observed values agree within the measurement error of about 0.02 estimated from the scatter of the signal calibration data. The general decrease of the probabilities with n demonstrates the quantum Zeno effect. Probabilities must take values from 0 to 1. However, with our method of determining the transition probability, random fluctuations in the photon count rate can lead to an *apparent* transition probability which is less than zero or greater than 1. The value of −0.006 for the observed $1 \rightarrow 2$ transition probability for $n = 64$ just means that the number of photons detected was slightly higher than the number expected for a transition probability of 0. Figures 3 and 4 show the probabilities for the $1 \rightarrow 2$ and $2 \rightarrow 1$ transitions, respectively.

The assumptions made in the calculations are as follows: When the rf field is present and the 313-nm radiation is not, the transition between levels 1 and 2 is assumed to proceed without relaxations. During the 313-

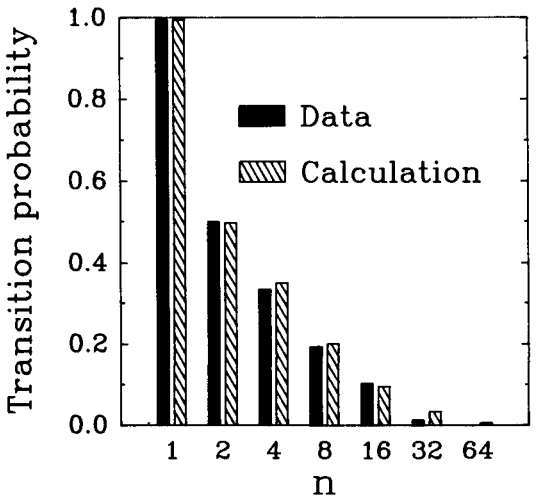

FIG. 3. Graph of the experimental and calculated $1 \rightarrow 2$ transition probabilities as a function of the number of measurement pulses n. The decrease of the transition probabilities with increasing n demonstrates the quantum Zeno effect.

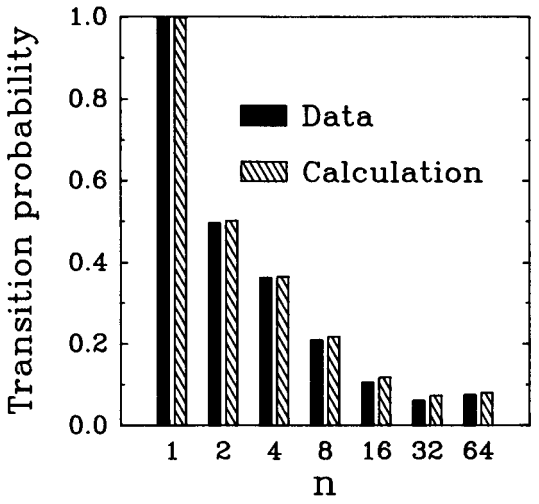

FIG. 4. Graph of the experimental and calculated $2 \rightarrow 1$ transition probabilities as a function of the number of measurement pulses n. The transition probabilities for $n = 32$ and $n = 64$ are higher than the corresponding ones for the $1 \rightarrow 2$ transition because of an optical pumping effect discussed in the text.

nm pulses, the coherence between levels 1 and 2 is assumed to be destroyed so quickly that the rf field can be ignored. The 313-nm radiation causes optical pumping from level 2 to level 1 with a time constant of about 1 s. This rate was measured by using an rf π pulse to prepare the ions in level 2, turning on the 313-nm radiation, and recording the 313-nm fluorescence as a function of time. Optical pumping by the 313-nm pulses can have an observable effect on the measured transition probabilities, especially for large n. This optical pumping causes a decrease in the $1 \rightarrow 2$ transition probability and an increase in the $2 \rightarrow 1$ transition probability. The decrease in the $1 \rightarrow 2$ transition probability is not noticeable in our data, since the transition probability is already small for large n. The increase in the $2 \rightarrow 1$ transition probability is noticeable for $n = 32$ and 64. The predicted transition probabilities shown in Table I and plotted in Figs. 3 and 4 take into account optical pumping, the finite 313-nm pulse durations, and the measured value of Ω. The measured value of Ω differed by less than 3% from the ideal value $\Omega = \pi/T$. For comparison, $\frac{1}{2}[1 - \cos^n(\pi/n)]$, the transition probability calculated if these effects are not included, is also shown in Table I.

For the larger values of n, the sum of the measurement periods, $n\tau_p$, is not negligible compared to T. Therefore, part of the decrease in the transition probability is due merely to the decrease in the time during which rf field can act. For the most extreme case ($n = 64$) $n\tau_p$ is 60% of T. However, even for this case, the decrease in the transition probability is much more than could be accounted for by the decrease in time. For $n = 16$, $n\tau_p$ is only 15% of T, but the transition probability is decreased by about 90%.

V. DISCUSSION

Cook[12] originally proposed an experiment with a single ion. Such an experiment should be feasible, since single ions have been observed in Penning traps[21,23] and in Paul traps.[24,25] The ensemble average, which is needed for comparison with calculations of the density matrix, would be obtained by repeating the experiment many times. In the present experiment, each measurement is an average over an ensemble of about 5000 independent ions, since their mutual interactions can be neglected. An experiment might be done with a single Hg^+ ion. Level 1 would be the ground $5d^{10}6s\,^2S_{1/2}$ state, level 2 would be the metastable $5d^96s^2\,^2D_{5/2}$ state, and level 3 would be the $5d^{10}6p\,^2P_{1/2}$ state. The $1 \rightarrow 2$ transition at 282 nm and the $1 \rightarrow 3$ transition at 194 nm have already been observed in a single Hg^+ ion.[25]

It might be argued that previous observations of effects such as collisional relaxation of rf transitions already contain the quantum Zeno effect. This is possible, but we know of no experiment in which the effect has been demonstrated simply and unambiguously. Collisions cannot usually be interpreted as quantum measurements. That is, they do not necessarily project a single quantum system, such as an atom, into one state or the other. Rather, in many cases, they perturb the phase of the coherence, represented by R_1 and R_2 in the vector model, for each system. For the ensemble average, R_1 and R_2 are driven to zero, just as in our experiment, but the underlying physics is different. Collisions may also perturb R_3, which is not desirable for a demonstration of the quantum Zeno effect.

Some experiments that involve continuous measurements have, in a sense, already demonstrated the quantum Zeno effect. Although the measurements are continuous, it takes a finite amount of time to make a measurement with a given degree of uncertainty. Thus a continuous measurement might be regarded as a series of measurements, one after the other. In such experiments, the measurement times are not separated from the free evolution periods, so the analysis is more difficult than for the present experiment. One example of such an experiment is the spin flip resonance of a single, trapped electron.[10] The spin state is detected by coupling the electron to an electronic circuit. As the time required to make a measurement is decreased by increasing the degree of coupling, noise broadens the spin flip resonance. This broadening decreases the rate of transitions induced by a weak microwave field. Another example is the three-level Hg^+ system described previously.[25] Radiation resonant with the $5d^{10}6s\,^2S_{1/2}$ to $5d^{10}6p\,^2P_{1/2}$ ($1 \rightarrow 3$) transition performs a continuous state measurement. Photons are not scattered if the ion is in the $5d^96s^2\,^2D_{5/2}$ state (level 2); otherwise they are. We have observed a decrease of the rate of the $1 \rightarrow 2$ transition, induced by a narrow-band laser, when radiation at the $1 \rightarrow 3$ transition frequency is applied.

Normally, the probability for spontaneous emission of

a photon by an atom grows quadratically only for extremely short times, approximately the inverse of the frequency of the emitted photon. However, it might be possible to increase this time by placing the atom inside a resonant cavity. Jaynes and Cummings[26] showed that a two-level atom coupled to a single mode of a resonant, lossless cavity oscillates between the ground and excited states. Suppose an excited atom is placed in a cavity that initially contains no photons. Then the probability for the atom to be in the excited state is $\cos^2(g\tau)$, where g is the coupling constant (the vacuum field Rabi frequency) and τ is the time that the atom has been in the cavity. The probability for the atom to be in the ground state is proportional to τ^2 for τ short compared to g^{-1}.

If the atom is coupled to a single *damped* cavity mode, the probability to be in the ground state is still proportional to τ^2, provided that τ is short compared to both g^{-1} and γ_c^{-1}, where γ_c is the dissipation rate of the cavity.[27] It might be possible to demonstrate the quantum Zeno effect on the decay of an atom in a cavity. This would not contradict the results of Ghirardi *et al.*,[3] since they did not consider such a system.

ACKNOWLEDGMENTS

This research was supported in part by the U. S. Air Force Office of Scientific Research and the Office of Naval Research. We thank Dr. S. L. Gilbert and Dr. M. G. Raizen for reading the manuscript.

[1] B. Misra and E. C. G. Sudarshan, J. Math. Phys. **18**, 756 (1977).
[2] C. B. Chiu, E. C. G. Sudarshan, and B. Misra, Phys. Rev. D **16**, 520 (1977).
[3] G. C. Ghirardi, C. Omero, T. Weber, and A. Rimini, Nuovo Cimento **52A**, 421 (1979).
[4] A. Peres, Am. J. Phys. **48**, 931 (1980).
[5] E. Joos, Phys. Rev. D **29**, 1626 (1984).
[6] K. Kraus, Found. Phys. **11**, 547 (1981).
[7] D. Home and M. A. B. Whitaker, J. Phys. A **19**, 1847 (1986).
[8] L. A. Khalfin, Zh. Eksp. Teor. Fiz. **33**, 1371 (1957) [Sov. Phys.—JETP **6**, 1053 (1958)]; R. G. Winter, Phys. Rev. **123**, 1503 (1961); W. Yourgrau, in *Problems in the Philosophy of Science*, edited by I. Lakatos and A. Musgrave (North-Holland, Amsterdam, 1968), pp. 191 and 192.
[9] E. B. Norman, S. B. Gazes, S. G. Crane, and D. A. Bennett, Phys. Rev. Lett. **60**, 2246 (1988).
[10] H. Dehmelt, Proc. Natl. Acad. Sci. U.S.A. **83**, 2291 (1986); **83**, 3074 (1986).
[11] G. J. Milburn, J. Opt. Soc. Am. B **5**, 1317 (1988).
[12] R. J. Cook, Phys. Scr. **T21**, 49 (1988).
[13] M. Porrati and S. Putterman, Phys. Rev. A **36**, 929 (1987).
[14] H. J. Carmichael, S. Singh, R. Vyas, and P. R. Rice, Phys. Rev. A **39**, 1200 (1989).
[15] I. I. Rabi, N. F. Ramsey, and J. Schwinger, Rev. Mod. Phys. **26**, 167 (1954); R. P. Feynman, F. L. Vernon, Jr. , and R. W. Hellwarth, J. Appl. Phys. **28**, 49 (1957).
[16] S. L. Gilbert, J. J. Bollinger, and D. J. Wineland, Phys. Rev. Lett. **60**, 2022 (1988); S. L. Gilbert, J. C. Bergquist, J. J. Bollinger, W. M. Itano, and D. J. Wineland, in *Atomic Physics 11*, Proceedings of the International Conference, Paris, 1988, edited by S. Haroche, J. C. Gay, and G. Grynberg (World Scientific, Singapore, 1989), p. 261.
[17] J. J. Bollinger, S. L. Gilbert, W. M. Itano, and D. J. Wineland, in *Frequency Standards and Metrology*, Proceedings of the Fourth Symposium, Ancona, Italy, 1988, edited by A. De Marchi (Springer-Verlag, Berlin, 1989), p. 319.
[18] J. J. Bollinger, D. J. Heinzen, W. M. Itano, S. L. Gilbert, and D. J. Wineland, Phys. Rev. Lett. **63**, 1031 (1989).
[19] D. J. Larson, J. C. Bergquist, J. J. Bollinger, W. M. Itano, and D. J. Wineland, Phys. Rev. Lett. **57**, 70 (1986).
[20] D. J. Wineland, J. C. Bergquist, W. M. Itano, and R. E. Drullinger, Opt. Lett. **5**, 245 (1980).
[21] R. G. Hulet, D. J. Wineland, J. C. Bergquist, and W. M. Itano, Phys. Rev. A **37**, 4544 (1988).
[22] L. R. Brewer, J. D. Prestage, J. J. Bollinger, W. M. Itano, D. J. Larson, and D. J. Wineland, Phys. Rev. A **38**, 859 (1988).
[23] D. J. Wineland and W. M. Itano, Phys. Lett. **82A**, 75 (1981).
[24] W. Neuhauser, M. Hohenstatt, and P. E. Toschek, Phys. Rev. A **22**, 1137 (1980); W. Nagourney, G. Janik, and H. Dehmelt, Proc. Natl. Acad. Sci. U.S.A. **80**, 643 (1983); F. Diedrich and H. Walther, Phys. Rev. Lett. **58**, 203 (1987); R. G. DeVoe, J. Hoffnagle, and R. G. Brewer, Phys. Rev. A **39**, 4362 (1989); J. D. Sankey and A. A. Madej, Appl. Phys. B **49**, 69 (1989).
[25] J. C. Bergquist, R. G. Hulet, W. M. Itano, and D. J. Wineland, Phys. Rev. Lett. **57**, 1699 (1986); J. C. Bergquist, W. M. Itano, and D. J. Wineland, Phys. Rev. A **36**, 428 (1987).
[26] E. T. Jaynes and F. W. Cummings, Proc. IEEE **51**, 89 (1963).
[27] S. Sachdev, Phys. Rev. A **29**, 2627 (1984).

Reply to "Comment on 'Quantum Zeno effect' "

Wayne M. Itano, D. J. Heinzen, J. J. Bollinger, and D. J. Wineland
Time and Frequency Division, National Institute of Standards and Technology, Boulder, Colorado 80303
(Received 12 November 1990)

Various interpretations of quantum mechanics are valid insofar as they predict the same experimental results. Some invoke "wave-function collapse" and some do not. An interpretation based on the collapse postulate provides a simple explanation for a recent experimental demonstration of the quantum Zeno effect [Itano *et al.*, Phys. Rev. A **41**, 2295 (1990)], but other interpretations are also valid.

The theory of quantum mechanics has the unusual property that, while there is general agreement on the experimental consequences, there is endless debate on matters of interpretation. The preceding Comment by Ballentine[1] on our article[2] illustrates this point.

The choice among interpretations that yield identical predictions, including the standard Copenhagen interpretation, the "statistical" or "ensemble" interpretation favored by Ballentine,[3] or even Everett's "relative-states" or "many-worlds" interpretation,[4] would seem to be a matter of personal taste. Ballentine states that "collapse of the wave function" is not necessary to quantum mechanics. We agree. However, we feel that the explanation given in our article, which invokes von Neumann's "collapse" postulate, is useful for giving a simple explanation of our experiment. Other situations may require a more elaborate treatment. One such case is the limit in which the optical "measurement" pulses are too weak to completely "collapse" the wave function. Peres and Ron[5] have carried out a calculation for this case.

We agree that the optical pulses perturb the atom, and we do not state otherwise in our article. However, we disagree with Ballentine's statement that the inhibition of the excitation is due to a strong perturbation *rather* than to a collapse of the wave function caused by measurement. We regard both statements as valid, under different interpretations of quantum mechanics.

Ballentine criticizes the phrase "wave-function collapse due to a null measurement," as being misleading. We used this term in the sense in which it was used by Porati and Putterman,[6] to mean that the nonemission of a photon during (or immediately subsequent to) the optical pulse is correlated with the atom being in the metastable state. We did not mean to imply that the optical pulses did not perturb the atom.

Ballentine objects to our use of the word "measurement" and quotes the *Oxford English Dictionary* to support his case. Dictionaries contain definitions of words like "energy," "force," or "work" that do not correspond to their meanings in physics. Therefore, one has to look at the way in which the words are used by physicists. It is true that the "measurement" pulses did not actually yield a detectable signal. Our usage of the word "measurement" in this case seems to be the same as that of Carmichael *et al.*[7] in their discussion of the theory of the detection of photons from resonance fluorescence. (This situation is very similar to that of an atom subjected to a measurement pulse.)

"The detector is not the agent *causing* state reduction. The atom collapses to its ground state due to its *irreversible* decay into the vacuum; the collapses proceed at an average rate given by the inverse atomic lifetime, quite indifferent to the successful or unsuccessful recording of the emitted photons." (Ref. 7, p. 1202.)

"... the source is an open system that loses energy *irreversibly* to the vacuum. The irreversibility effectively performs a continuous quantum measurement, without the need for a conscious observer to record the emitted photons." (Ref. 7, p. 1215.)

Ballentine carries out a simplified interpretation of our experiment. He calculates that the probability that each of a sequence of n optical "measurement" pulses results in the emission of a photon, leaving an atom in the ground state after the nth pulse, is $[\cos(\pi/2n)]^{2n}$. This calculation is correct, but is not particularly useful for comparison with our observable. Our experiment measures the total probability that an atom is left in the ground state after the nth pulse, regardless of whether or not each optical pulse resulted in the emission of a photon. This probability is, in our notation, $P_1(T) = 1 - P_2(T) = \frac{1}{2}[1+\cos^n(\pi/n)]$. This result comes from Eq. (7) of Ref. 2. (Here we neglect the duration of the optical pulses, as does Ballentine.) The two probabilities are not identical, because the rf field can drive the atom to the metastable state in one interval and return it to the ground state in a later interval. [Ballentine[1] states in his Ref. 10 that his method will also yield the proper value of $P_1(T)$, although he does not show this explicitly.]

In summary, quantum mechanics can be interpreted in different ways. In this case, interpretations with and without the collapse postulate correctly predict the experimental data. Therefore, the experiment neither verifies nor falsifies the notion of "wave-function collapse."

[1]L. E. Ballentine, preceding Comment, Phys. Rev. **43**, 5165 (1991).
[2]W. M. Itano, D. J. Heinzen, J. J. Bollinger, and D. J. Wineland, Phys. Rev. A **41**, 2295 (1990).
[3]L. E. Ballentine, Rev. Mod. Phys. **42**, 358 (1970).
[4]H. Everett, Rev. Mod. Phys. **29**, 454 (1957).
[5]A. Peres and A. Ron, Phys. Rev. A **42**, 5720 (1990).
[6]M. Porrati and S. Putterman, Phys. Rev. A **36**, 929 (1987).
[7]H. J. Carmichael, S. S. Singh, R. Vyas, and P. R. Rice, Phys. Rev. A **39**, 1200 (1989).

Search for Anomalous Spin-Dependent Forces Using Stored-Ion Spectroscopy

D. J. Wineland, J. J. Bollinger, D. J. Heinzen,[a] W. M. Itano, and M. G. Raizen
Time and Frequency Division, National Institute of Standards and Technology, Boulder, Colorado 80303
(Received 10 June 1991)

Resonances in atomic ions can be used to search for new, weak, spin-dependent interactions. Upper limits on anomalous dipole-monopole and dipole-dipole couplings for the neutron and electron are determined by examining hyperfine resonances in stored $^9Be^+$ ions. These experiments also place strict limits on anomalous weights of spinning gyroscopes.

PACS numbers: 42.50.Wm, 04.90.+e, 14.80.Gt, 32.80.Pj

The existence of weakly interacting bosons has been suggested previously [1–10]. Laboratory experiments might detect scalar or pseudoscalar couplings of such particles to photons [11–15] or matter [6,7,16–30]. In the latter case, new spin-dependent forces would occur. Here, we report the use of stored atomic ion spectroscopy to search for anomalous potentials having a dipole-monopole or dipole-dipole character. The first is expected to include terms like [7,9,16,31]

$$V_{AB}^{D}=\hbar^2 D\mathbf{S}_A\cdot\hat{\mathbf{r}}(1/\lambda_\phi r+1/r^2)\exp(-r/\lambda_\phi)\,, \tag{1}$$

where the spin $\mathbf{S}_A$ (in units of $\hbar$) of particle A couples to particle B, r is the distance between particles, λ_ϕ is the range of the force, and D is a coupling constant with units of (mass)$^{-1}$ [see Fig. 1(a)]. In 1968, observation of an interaction like Eq. (1) was reported [22] where particles A were proton spins and particles B comprised the Earth. Subsequent measurements [23,24] contradicted this measurement and found null results (see Table I).

A dipole-dipole interaction [Fig. 1(b)] would be expected to include terms like [7,16,31]

$$V_{AB}^{T}=(\hbar^3/c)T\exp(-r/\lambda_\phi)[(1/\lambda_\phi r^2+1/r^3)\mathbf{S}_A\cdot\mathbf{S}_B-(1/\lambda_\phi^2 r+3/\lambda_\phi r^2+3/r^3)(\mathbf{S}_A\cdot\hat{\mathbf{r}})(\mathbf{S}_B\cdot\hat{\mathbf{r}})]\,, \tag{2}$$

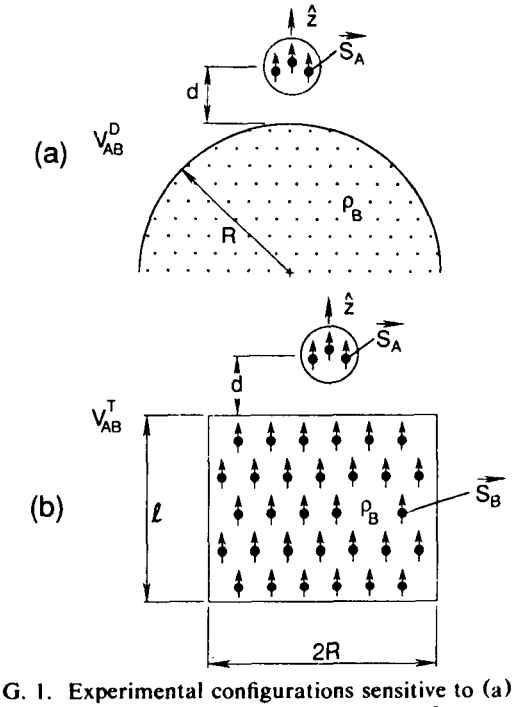

FIG. 1. Experimental configurations sensitive to (a) V_{AB}^{D} and (b) V_{AB}^{T} [refer to Eqs. (1) and (2) of the text]. In both parts, we assume the size of sample A is small compared to d, R, and l. In (a), B is assumed to be spherical with density of B particles ρ_B. In (b), B is assumed to be a cylinder of radius R and height l and spin density ρ_B. Experimentally, V_{AB}^{D} and V_{AB}^{T} are sensed as an anomalous change in energy when $\mathbf{S}_A\cdot\hat{\mathbf{z}}$ is changed. In the experiments reported here, $\mathbf{S}_A\cdot\hat{\mathbf{z}}$ for the electron and neutron are changed by driving a hyperfine transition in the ground state of atomic $^9Be^+$ ions.

where the spin of particle A interacts with that of particle B. T has units of (mass)$^{-2}$ and characterizes the strength of the interaction [see Fig. 1(b)]. This type of interaction is sought in acceleration [7,16,19,20], resonance [16,22–27,29], and induced magnetism [17,18] experiments.

Such forces mediated by axions [4] have received the most attention because the axion emerges in schemes attempting to resolve the strong CP problem [4,10]. The mass and coupling of axions and related particles to matter can be severely constrained by arguments based on observed energy-loss rates of stellar objects [32]. As discussed below, these constraints on axions appear to be much stronger than those derived from current laboratory experiments. Nevertheless, the laboratory experiments are still useful because they can search for interactions outside the scope of the axion-type models.

TABLE I. Values of the coupling strength D [Eq. (1)] evaluated from laboratory experiments. Here, we assume $\lambda_\phi \gg R = R_{\text{Earth}}$.

Experiment	Measured quantity	Result (kg^{-1})
Ref. [22]	D(proton)	$\simeq 0.02$
Ref. [23]	D(proton)	$<2\times10^{-4}$
Ref. [24]	D(deuteron)	$<6.7\times10^{-8}$
Ref. [28]	D(electron)	$<3.7\times10^{5}$
This work	$D(^9\text{Be})$	$<9.0\times10^{-9}$
This work	D(electron)	$<4.5\times10^{-5}$
This work	D(neutron)	$<2.7\times10^{-8}$
Ref. [30]	$D(^{201}\text{Hg})-D(^{199}\text{Hg})$	$\lesssim 3\times10^{-10}$

For the assumed configurations shown in Fig. 1, either V_{AB}^D or V_{AB}^T could be observed as an anomalous dependence of energy on $\mathbf{S}_A \cdot \hat{\mathbf{z}}$. In the experiments reported here, we looked for such a dependence in the energy $2\pi\hbar\nu_0$ of the atomic $^9Be^+$ $^2S_{1/2}$ ground-state $(F=1, m_F=0) \rightarrow (F=1, m_F=-1)$ hyperfine transition [33] in a magnetic field $B_0 \simeq 0.8194$ T (transition frequency $\nu_0 \simeq 303$ MHz). Here, m_F is the sum of the electron spin J $(=\frac{1}{2})$ and nuclear spin I $(=\frac{3}{2})$ projections along the magnetic-field axis, taken to be along $\hat{\mathbf{z}}$. Measurements of ν_0 were made on about 5000 $^9Be^+$ ions stored in a Penning ion trap [34]. The $^9Be^+$ ions are trapped and laser cooled (to reduce Doppler shifts), then optically pumped into the $(F=1, m_F=0)$ level using a combination of laser and radio-frequency (rf) radiation. Additional rf radiation is then used to drive the ion population from the $(F=1, m_F=0)$ to the $(F=1, m_F=-1)$ state. Changes in the population of the two states are sensed by looking for changes in laser light scattered by the ions [34]. The frequency ν_0 is the frequency of radiation which drives the above transition with maximum probability. The reference for ν_0 is an ensemble of hydrogen maser and cesium atomic clocks. Particles A are assumed to be either the ^9Be nucleus or the unpaired outer electron in $^9Be^+$. For the above hyperfine transition, the changes in $\mathbf{S}_A \cdot \hat{\mathbf{z}}$ are given by $|\Delta(\mathbf{S}_A \cdot \hat{\mathbf{z}})| \equiv |\Delta S_{Az}| \simeq 1$ or $|\Delta S_{Az}| \simeq 2\times10^{-4}$ for the ^9Be nuclear spin and electron spin, respectively. (We assume that V_{AB} affects either the electron or ^9Be nucleus but not both at the same time.)

In the search for V_{AB}^D, particles B were taken to be the nucleons in the Earth. We looked for a change in ν_0 between the cases where $\mathbf{B}_0$ was parallel or antiparallel to the vertical direction in the laboratory. (Since the hyperfine transition is a $|\Delta m_F|=1$ transition, we had to subtract the effects of the Earth's rotation.) In the search for V_{AB}^T, particles B were taken to be the electron spins in the iron pole faces of an electromagnet. We compared ν_0 when B_0 was created by this electromagnet with ν_0 when B_0 was created by a superconducting solenoid ($\mathbf{S}_B$ spins absent). The value of B_0 was chosen such that $\partial\nu_0/\partial B_0 = 0$. B_0 was set by measuring a magnetic-field-dependent transition in $^9Be^+$ [34]. (The inaccuracy in our measurement of B_0 due to V_{AB} is negligible on this field-dependent transition.) For $\partial\nu_0/\partial B_0 = 0$, we could rule out any positive results which might arise from small changes in B_0 between the different configurations. The largest systematic error in the experiment was due to a background-gas pressure shift of ν_0 [34].

For the geometries of Figs. 1(a) and 1(b) we integrate over the volumes containing the B particles to find the anomalous energy E_A of a single A particle. Assuming $\mathbf{S}_A = S_{Az}\hat{\mathbf{z}}$ and $\mathbf{S}_B = S_{Bz}\hat{\mathbf{z}}$, we find [Fig. 1(a)]

$$E_A^D = C^D L_D = C^D\lambda_\phi(R+d)^{-2}\{[R(R+d)+\lambda_\phi(2R+d)+\lambda_\phi^2]\exp[-(2R+d)/\lambda_\phi]+[R(R+d)-\lambda_\phi d-\lambda_\phi^2]\exp(-d/\lambda_\phi)\}$$
$$= 2C^D R^3/3(R+d)^2 \quad (\text{for } \lambda_\phi \gg R,d) \tag{3}$$

and [Fig. 1(b)]

$$E_A^T = C^T\xi_T = C^T\{(d/r_1)\exp(-r_1/\lambda_\phi) - [(d+l)/r_2]\exp(-r_2/\lambda_\phi) - \exp(-d/\lambda_\phi)+\exp[-(d+l)/\lambda_\phi]\}$$
$$= C^T\{d/r_1 - (d+l)/r_2\} \quad (\text{for } \lambda_\phi \gg R,d,l), \tag{4}$$

where $C^D = 2\pi\hbar^2 D\rho_B S_{Az}$, $C^T = 2\pi(\hbar^3/c)T\rho_B S_{Az}S_{Bz}$, $r_1 = (R^2+d^2)^{1/2}$, $r_2 = [R^2+(d+l)^2]^{1/2}$, and ρ_B is the number density of particles B (assumed here to be nucleons for V_{AB}^D and electron spins for V_{AB}^T).

In our experiment, we found the shift $\Delta\nu_0$ of ν_0 due to V_{AB}^D (where the magnetic field is upward) to be $\Delta\nu_0 = -6.4 \pm 2.9 \pm 6.4$ μHz for $d \simeq 1.5$ m [35]. The first error is the random uncertainty, the second, an estimate of the pressure shift variation between field-up and -down measurements. The estimate of the pressure shift variation was made by measuring the fluctuations in ν_0 over a period of many months with the magnetic field in one direction. Adding these errors in quadrature, we find $|\Delta\nu_0| < 13.4$ μHz ($< 5.5\times10^{-20}$ eV). Therefore we find for the coupling constant defined in Eq. (1), $D(^9Be) < 3.8/L_D$ kg^{-1} or $D(e^-) < 1.9\times10^4/L_D$ kg^{-1}, where L_D [Eq. (3)] is in centimeters. If we assume $\lambda_\phi \gg R,d$ and $R = R_{\text{Earth}} \simeq 6.36\times10^8$ cm [$\rho_B = \rho(\text{Earth}) \simeq 3.33\times10^{24}$ nucleons/cm^3] we can make the estimates of D shown in Table I. To obtain D(neutron) we argue as follows: In the simplest version of the shell model, the spin of the ^9Be nucleus is due to the odd neutron, which is in the $1p_{3/2}$ shell. In this model, the expectation value of a component of the neutron spin is $\frac{1}{3}$ of the expectation value of the corresponding component of the total nuclear spin. From this we obtain $D(\text{neutron}) < 2.7\times10^{-8}$ kg$^{-1} \simeq 4.8\times10^{-35}$ GeV^{-1}. This constrains one model proposed in Ref. [9] where D might be as large as 10^{-34} GeV^{-1}.

We also found $\Delta\nu_0 = -13 \pm 30 \pm 170$ μHz between ν_0 measured in an electromagnet [36] and a superconducting magnet system. The first error is the uncertainty in the reference oscillator for the time between measurements ($\simeq 5$ yr), the second, relatively large error is due to the uncertainty in an estimate of the pressure shift [34] in different apparatuses. Adding the errors in quadrature, we obtain $|\Delta\nu_0| < 186$ μHz ($< 7.7\times10^{-19}$ eV). For the electromagnet, $d = 2.7$ cm, $l = 33$ cm, $R = 15$ cm (V_{AB}^T is enhanced by 2 because of the two pole faces of the magnet). We neglect the magnet yoke which will increase the effects of V_{AB}^T slightly. From $\Delta\nu_0$ and Eq. (4), we can put an upper limit on T [Eq. (2)] for assumed values of λ_ϕ. Here, for brevity, we will assume that $\lambda_\phi \gg d,l,R$ in which case V_{AB}^T has the same form as normal magnetic coupling. In Table II, we list the ratio α of E_A^T [Eq. (4)] to the normal magnetic interaction for various experi-

TABLE II. Experimental determinations of $a(A,B)$, the ratio of E_A^T [Eq. (4)] to normal magnetic coupling for particles A and B as indicated in Fig. 1. Here, e^- denotes electron, p denotes proton, n denotes neutron, and d denotes deuteron.

Experiment	$a(A,B)$	Method
Ref. [25]	$a(p,p) < 5\times10^{-5}$	Molecular spectra
Ref. [26]	$a(^{201}\mathrm{Hg},e^-) < 10^{-10}$–$10^{-11}$	NMR
Ref. [26]	$a(^{199}\mathrm{Hg},e^-) < 10^{-10}$–$10^{-11}$	NMR
Ref. [27]	$a(p,e^-) - a(d,e^-) < 2\times10^{-10}$	NMR
Ref. [20]	$a(e^-,e^-) \lesssim 3\times10^{-10}$	Acceleration
Ref. [19]	$a(e^-,e^-) < 0.9\times10^{-11}$	Acceleration
Ref. [17]	$a(e^-,e^-) < 0.005\times10^{-11}$	Induced magnetism
Ref. [18]	$a(e^-,e^-) < 0.00085\times10^{-11}$	Induced magnetism
This work	$a(^9\mathrm{Be},e^-) < 3.8\times10^{-11}$	NMR
This work	$a(n,e^-) < 2.3\times10^{-11}$	NMR
This work	$a(e^-,e^-) < 4.1\times10^{-11}$	NMR

ments. From Ref. [32], $\lambda_\phi \simeq 10$ cm is within a "window" on the axion which has not been ruled out by stellar energy-loss rate arguments. If we take $T = g_A g_B/16\pi \times M_A M_B$, where g_A and g_B are coupling strengths and M_A and M_B are the masses of the elementary particles responsible for V_{AB}^T, then from Refs. [7] and [32] we estimate theoretically for axions $a(A,B) \approx 10^{-26}$ for $\lambda_\phi \simeq 10$ cm, considerably smaller than the sensitivity of the current laboratory experiments.

So far we have assumed that $\mathbf{S}_A$ is due to intrinsic spin. From Eq. (1), if $\mathbf{S}_A$ were orbital angular momentum rather than intrinsic spin, we would expect spinning gyroscopes to have a weight dependent on $\mathbf{S}_A \cdot \mathbf{g}/|\mathbf{g}|$, where $\mathbf{g}$ is the acceleration of gravity. Although an effect like this (for one sign of $\mathbf{S}_A \cdot \mathbf{g}$) has been reported [37], more accurate subsequent experiments [38–40] found a null result (an earlier experiment on the intrinsic spin of the neutron was reported in Ref. [21]). The authors of Ref. [40] found $\Delta m < 9\times10^{-8}$ kg for a 0.143 kg rotor whose angular momentum was approximately equal to $7.2 \times 10^{32}\hbar$. If we assume a gyroscopic weight is due to V_{AB}^D, and $\lambda_\phi \gg R_{\mathrm{Earth}}$, then the force derived from Eq. (3) gives $D < 4.0\times10^{-3}$ kg^{-1} for the experiment of Ref. [40]. In our experiment, if we consider the orbital motion of the unpaired neutron in ^{9}Be to act like a gyroscope with orbital angular momentum $\mathbf{L}$, we obtain $D < 5\times10^{-9}$ kg^{-1}, about 10^6 times more stringent a limit on an $\mathbf{S}_A \cdot \mathbf{g}/|\mathbf{g}|$ effect for angular momentum [4]. From Refs. [37–40], for our experiment, we might expect to replace $\mathbf{S}_A$ in Eq. (1) by $m_{\mathrm{neutron}} r_{\mathrm{eq}} \omega \simeq L/r_{\mathrm{eq}}$, where r_{eq} is defined in Ref. [37] (taken to be 10^{-13} cm here). If we assume $\lambda_\phi \gg R,d$ in Eq. (3), then the resonance test reported here is approximately 10^{18} times more sensitive than the acceleration test of Nitschke and Wilworth [40,41].

It is interesting to compare the sensitivity of resonance experiments (such as the type of experiment reported here) with acceleration tests. From Eqs. (3) and (4), we calculate the accelerations $a_D = -(\partial E_A^D/\partial d)/m_A$ and $a_T = -(\partial E_A^T/\partial d)/m_A$, where m_A is the unit of mass associated with each spin in A. If we use parameters of the current resonance and acceleration [16] experiments, the limits placed on C^D and C^T are roughly equal when λ_ϕ is on the order of the size of laboratory experiments. Resonance (acceleration) tests are more sensitive for larger (smaller) values of λ_ϕ.

Significant improvements in the sensitivity of the $^9\mathrm{Be}^+$ experiment could be expected. For 100% detection efficiency [34], a resonance time T_R (time taken to drive the ν_0 transition), N stored ions, and total measurement time τ, the statistical uncertainty in a frequency measurement is $\delta\nu = (4\pi^2 N T_R \tau)^{-1/2}$ [34]. In future experiments $N = 10^7$, $T_R = 100$ s, and $\tau = 30$ days do not seem unreasonable, whence $\delta\nu_0 \simeq 3\times10^{-9}$ Hz. In the $^9\mathrm{Be}^+$ experiments, the pressure shift can be made negligible by using cryogenic pumping. By operating on other field-independent transitions in $^9\mathrm{Be}^+$ or other ions, we could make $|\Delta\sigma_{S_z}| \simeq 1$ for the electron and be much more sensitive to anomalous couplings to electron spin. The characteristic dimensions of the ion experiments can also be made very small and therefore can investigate relatively short ranges ($\lambda_\phi < 1$ mm).

The authors gratefully acknowledge the support of ONR and AFOSR. We thank D. Bartlett and J. Gilligan for helpful suggestions on the manuscript.

[a]Present address: Department of Physics, University of Texas, Austin, TX 78712.

[1] J. Leitner and S. Okubo, Phys. Rev. **136**, B1542 (1964).

[2] L. B. Okun' and C. Rubbia, in *Proceedings of the International Conference on Elementary Particles, Heidelberg, 1967*, edited by H. Filthuta (North-Holland, Amsterdam, 1968), p. 338.

[3] N. D. Hari Dass, Phys. Rev. Lett. **36**, 393 (1976).

[4] S. Weinberg, Phys. Rev. Lett. **40**, 233 (1978); F. Wilczek, Phys. Rev. Lett. **40**, 279 (1978); M. Dine, W. Fischler, and M. Srednicki, Phys. Lett. **104B**, 1999 (1981); M. Shifman, A. Vainshtein, and V. Zakharov, Nucl. Phys. **B166**, 493 (1980); J. Kim, Phys. Rev. Lett. **43**, 103 (1979); H.-Y. Cheng, Mod. Phys. Lett. A **2**, 409 (1987).

[5] A. A. Ansel'm, Pis'ma Zh. Eksp. Teor. Fiz. **36**, 46 (1982)

[JETP Lett. **36**, 55 (1982)].
[6] G. B. Gelmini, S. Nussinov, and T. Yanagida, Nucl. Phys. **B219**, 31 (1983).
[7] J. E. Moody and F. Wilczek, Phys. Rev. D **30**, 130 (1984).
[8] T. Pradhan, R. P. Malik, and P. C. Naik, Pramana **24**, 77 (1985).
[9] D. Chang, R. N. Mohapatra, and S. Nussinov, Phys. Rev. Lett. **55**, 2835 (1985).
[10] R. Peccei and H. Quinn, Phys. Rev. Lett. **38**, 1440 (1977); Phys. Rev. D **16**, 1791 (1977).
[11] Y. Semertzidis *et al.*, Phys. Rev. Lett. **64**, 2988 (1990).
[12] W. U. Wuensch *et al.*, Phys. Rev. D **40**, 3153 (1989).
[13] A. A. Anselm, Phys. Rev. D **37**, 2001 (1988).
[14] A. A. Anselm, Yad. Fiz. **42**, 1480 (1985) [Sov. J. Nucl. Phys. **42**, 936 (1985)].
[15] K. Van Bibber, N. R. Dagdeviren, S. R. Koonin, A. K. Kerman, and H. N. Nelson, Phys. Rev. Lett. **59**, 759 (1987).
[16] "Fifth-force" experiments are briefly summarized by B. R. Heckel, E. G. Adelberger, C. W. Stubbs, Y. Su, H. E. Swanson, and G. Smith, Phys. Rev. Lett. **63**, 2705 (1989); spin-independent and spin-dependent fifth-force experiments are reviewed by E. G. Adelberger, B. R. Heckel, C. W. Stubbs, and W. F. Rogers (to be published).
[17] P. V. Vorobyov and Ya. I. Gitarts, Phys. Lett. B **208**, 146 (1988).
[18] V. F. Bobrakov, Yu. V. Borisov, M. S. Lasakov, A. P. Serebrov, R. R. Tal'daev, and A. S. Trofimova, Pis'ma Zh. Eksp. Teor. Fiz. **53**, 283 (1991) [JETP Lett. **53**, 294 (1991)].
[19] R. C. Ritter *et al.*, Phys. Rev. D **42**, 977 (1990).
[20] D. Graham and R. Newman, in *Proceedings of the Eleventh International Conference on General Relativity and Gravitation, Stockholm, Sweden, 1986*, edited by M. A. H. MacCullum (Cambridge Univ. Press, New York, 1987), p. 614.
[21] J. W. T. Dabbs, J. A. Harvey, D. Paya, and H. Horstmann, Phys. Rev. **139**, B756 (1965).
[22] G. E. Velyukhov, Zh. Eksp. Teor. Fiz. Pis'ma Red. **8**, 372 (1968) [Sov. Phys. JETP Lett. **8**, 229 (1968)].
[23] B. A. Young, Phys. Rev. Lett. **22**, 1445 (1969); B. V. Vasil'ev, Zh. Eksp. Teor. Fiz. Pis'ma Red. **9**, 299 (1969) [Sov. Phys. JETP Lett. **9**, 175 (1969)].
[24] D. J. Wineland and N. F. Ramsey, Phys. Rev. A **5**, 821 (1972).
[25] N. F. Ramsey, Physica (Amsterdam) **96A**, 285 (1979).
[26] E. B. Aleksandrov, A. A. Ansel'm, Yu. V. Pavlov, and R. M. Umarkhodzhaev, Zh. Eksp. Teor. Fiz. **85**, 1899 (1983) [Sov. Phys. JETP **58**, 1103 (1983)].
[27] A. A. Ansel'm and Yu. I. Neronov, Zh. Eksp. Teor. Fiz. **88**, 1946 (1985) [Sov. Phys. JETP **61**, 1154 (1985)].
[28] C.-H. Hsieh *et al.*, Mod. Phys. Lett. A **4**, 1597 (1989); Y. Chou, W.-T. Ni, and S.-L. Wang, *ibid.* **5**, 2297 (1990). From the first paper we estimate $m_A \simeq 800$ u (see discussion in text about acceleration tests).
[29] Preliminary reports of our work have been given in Proceedings of the Twelfth International Conference on General Relativity and Gravitation, Boulder, Colorado, 1989 (to be published) and in Proceedings of the Eleventh Moriond Workshop on Tests of Fundamental Laws in Physics, Les Arcs, Savoie, France, 1991 (to be published).
[30] B. Heckel *et al.*, in Proceedings of the Eleventh Moriond Workshop on Tests of Fundamental Laws in Physics (Ref. [29]) (final results of this work should appear at the same time as our report). See also S. K. Lamoreaux, J. P. Jacobs, B. R. Heckel, F. J. Raab, and E. N. Fortson, Phys. Rev. Lett. **57**, 3125 (1986).
[31] Moody and Wilczek's derivation (Ref. [7]) of the dipole-monopole and dipole-dipole potentials assumed that particles A and B have spin $\frac{1}{2}$. However, by use of the Wigner-Eckart theorem, we can show that for the conditions discussed in our paper Eqs. (1) and (2) are also valid for systems with higher spins, such as the spin-$\frac{3}{2}$ ^{9}Be nucleus.
[32] See recent reviews: M. S. Turner, Phys. Rep. **197**, 67 (1990); G. G. Raffelt, *ibid.* **198**, 1 (1990).
[33] We designate the states using the low- (magnetic-) field notation where the total atomic angular momentum **F** and projection m_F along the **B**-field axis are good quantum numbers. At higher fields, m_F is still a good quantum number.
[34] J. J. Bollinger, D. J. Heinzen, W. M. Itano, S. L. Gilbert, and D. J. Wineland, IEEE Trans. Instrum. Meas. **40**, 126 (1991); D. J. Wineland, J. C. Bergquist, J. J. Bollinger, W. M. Itano, D. J. Heinzen, S. L. Gilbert, C. H. Manney, and M. G. Raizen, IEEE Trans. Ultrasonics, Ferroelectrics, and Frequency Control **37**, 515 (1990).
[35] The $^9Be^+$ ions are located 1.5 m above a concrete foundation which rests on the ground. To a good approximation the experimental apparatus closer than 1.5 m to the ions is placed symmetrically around them. If a positive result was observed, the effects of the surrounding geometry would have to be studied in detail.
[36] J. J. Bollinger, J. D. Prestage, W. M. Itano, and D. J. Wineland, Phys. Rev. Lett. **54**, 1000 (1985).
[37] H. Hayasaka and S. Takeuchi, Phys. Rev. Lett. **63**, 2701 (1989).
[38] J. E. Faller, W. J. Hollander, P. G. Nelson, and M. P. McHugh, Phys. Rev. Lett. **64**, 825 (1990).
[39] T. J. Quinn and A. Picard, Nature (London) **343**, 732 (1990).
[40] J. M. Nitschke and P. A. Wilmarth, Phys. Rev. Lett. **64**, 2115 (1990).
[41] One might assume other forms of interaction such as (for $\lambda_\phi \to \infty$) $V_{AB} \propto \mathbf{S}_A \cdot \hat{\mathbf{r}}/r$. In this case also, the resonance tests are more stringent.

ATOMIC PHYSICS TESTS OF NONLINEAR QUANTUM MECHANICS*

J. J. Bollinger, D. J. Heinzen, Wayne M. Itano,
S. L. Gilbert, and D. J. Wineland
National Institute of Standards and Technology,
Boulder, Colorado 80303

ABSTRACT

Atomic physics experiments which test a nonlinear generalization of quantum mechanics recently formulated by Weinberg are described. The experiments search for a dependence of hyperfine transition frequencies or nuclear spin precession frequencies on the relative populations of the hyperfine or nuclear spin states. The experiments set limits less than 10 μHz on the size of the possible nonlinear contributions to these frequencies. In some cases this can be interpreted as a limit of less than ~ 10^{-26} on the fraction of binding energy per nucleon that could be due to a nonlinear correction to a nuclear Hamiltonian. The possibility that a nonlinear addition to quantum mechanics violates causality is discussed.

INTRODUCTION

Quantum mechanics has survived numerous tests since its inception in the 1920's. Many of these tests can be regarded as tests of a specific quantum-mechanical theory as well as tests of the basic formalism of quantum mechanics. For example, the fact that the measured energy levels of the hydrogen atom are in agreement with the predictions of quantum-mechanical theory is a test of both the formalism of quantum mechanics and the accuracy of the Hamiltonian for the hydrogen atom. However, this only tests quantum mechanics at the level we know the Hamiltonian is accurate. Because of its importance in modern physics, quantum mechanics should be tested independently of and, if possible, more precisely than any particular quantum-mechanical theory. Surprisingly few such tests exist. Some examples are the experiments [1] which have conclusively ruled out hidden variable theories in favor of quantum mechanics. These experiments, however, do not provide a test of quantum mechanics itself to much less than 1%.

The lack of precise, independent tests of quantum mechanics is at least partially due to the absence of generalized versions of quantum mechanics with which to plan or interpret an experimental test. Generalized versions of quantum mechanics which have a logically consistent interpretation have been difficult to construct. Recently, however, Weinberg has developed a formalism for introducing nonlinear corrections to quantum mechanics.[2,3] The size of the nonlinear corrections is determined by a parameter ϵ. In the limit that $\epsilon = 0$, Weinberg's nonlinear generalization reduces to ordinary

in Atomic Physics 12, (proc. of the 12th International Conference on Atomic Physics), ed. by Jens C. Zorn and Robert R. Lewis, (Amer. Inst. of Physics press, New York, 1991), p. 461.

linear quantum mechanics. This paper includes a discussion of atomic physics experiments[4-7] which search for nonlinear corrections permitted by Weinberg's formalism. The experiments completed to date have found null results which put upper bounds on the parameter ϵ. In some cases these bounds are 26 orders of magnitude smaller than the size of the ordinary, linear quantum-mechanical terms.

The following simple discussion gives an idea of how the atomic physics tests work. Consider a two-level system with energy eigenstates $|k\rangle$, $k = 1,2$ and energies $\hbar\omega_k$, with $\omega_1 > \omega_2$. The time evolution of these eigenstates is given by $e^{-i\omega_k t}|k\rangle$. Now suppose at time $t = 0$, the state

$$|\psi(0)\rangle = (1-a)^{\frac{1}{2}}|1\rangle + a^{\frac{1}{2}}|2\rangle \qquad (1)$$

is formed from a superposition of the two energy eigenstates. The linearity of quantum mechanics (specifically, the linearity of the Hamiltonian) requires that the time evolution of $|\psi(0)\rangle$ be given by

$$|\psi(t)\rangle = e^{-i\omega_1 t}[(1-a)^{\frac{1}{2}}|1\rangle + a^{\frac{1}{2}}e^{i(\omega_1-\omega_2)t}|2\rangle]. \qquad (2)$$

Except for an overall phase factor, the time evolution of the coherent superposition is determined by the frequency $\omega_p \equiv \omega_1 - \omega_2$, which is independent of the parameter a, the probability of finding the system in the eigenstate $|2\rangle$. This result can be stated graphically by using the mathematical equivalence between a two-level system and a system with a spin-½ particle in a magnetic field.[8] The eigenstates $|1\rangle$ and $|2\rangle$ correspond to spin states antiparallel and parallel to the magnetic field. The state $|\psi(0)\rangle$ corresponds to a state where the spin is tipped by an angle θ with respect to the magnetic field, where $\cos(\theta/2) = a^{\frac{1}{2}}$. The frequency ω_p is then the precession frequency of the spin about the magnetic field (or z axis). In the language of the equivalent spin-½ picture, the linearity of quantum mechanics requires that the precession frequency ω_p be independent of the tipping angle θ of the spin.

A test for a nonlinear addition to quantum mechanics can therefore be made by searching in a coherent superposition of states for a dependence of the frequency ω_p on the state probabilities (the parameter a). After a brief discussion of Weinberg's formalism, we will describe the different experimental tests. They include an ion trap experiment[4] which uses a ground-state hyperfine transition in $^9Be^+$, two different experiments[5,7] which use optical pumping techniques to polarize Ne and Hg nuclei in gas cells, and an experiment[6] which uses a hydrogen maser. The first three experiments may be viewed as tests of the linearity of quantum mechanics in a nuclear system. The hydrogen maser experiment may be viewed as a test of the linearity of quantum mechanics in an atomic system. In addition to the experimental tests, Weinberg's work has stimulated theoretical discussions[9-14] on the possibility of a nonlinear addition to quantum mechanics. In particular, a nonlinear addition to quantum mechanics may violate causality and make it

possible, at least in principle, to have arbitrarily fast communications.[11,12,14] We summarize this discussion and give an example of how a nonlinear correction to quantum mechanics in the Be^+ experiment could be used to communicate faster than the speed of light.

WEINBERG'S NONLINEAR QUANTUM MECHANICS

In order to help motivate tests of nonrelativistic quantum mechanics, Weinberg has developed a formalism[2,3] which generalizes quantum mechanics by permitting possible nonlinear terms. In this formalism, observables are represented as operators on a Hilbert space of states just as in ordinary quantum mechanics. The difference with ordinary quantum mechanics is that the operators no longer need be linear. In order to have a sensible physical interpretation, Weinberg requires that any nonlinear additions do not violate Galilean invariance. He shows that there is a possible class of such additions to the Hamiltonian describing the internal degrees of freedom of a particle with spin. This means that the time evolution of the wave function $\psi(t)$ is no longer given by a linear Schrödinger equation. Instead it takes the form

$$i\hbar\frac{d\psi_k}{dt} = \frac{\partial h(\psi,\psi^*)}{\partial \psi_k^*} \tag{3}$$

where $\psi_k = \langle k|\psi\rangle$ is the amplitude of state $|k\rangle$ ($k = -I, -I+1, .., I-1, I$ for a particle of spin I) and the Hamiltonian function $h(\psi,\psi^*)$ is a homogeneous function of ψ and ψ^* [$h(\lambda\psi,\psi^*) = h(\psi,\lambda\psi^*) = \lambda h(\psi,\psi^*)$ for any complex λ]. Homogeneity guarantees that if $\psi(t)$ is a solution of Eq. (3) then $\lambda\psi(t)$ is also a solution representing the same physical state. This ensures the proper treatment of physically separated and uncorrelated systems.[3] In general, $h(\psi,\psi^*)$ is not bilinear as it would be in ordinary quantum mechanics. A possible form of $h(\psi,\psi^*)$ which Weinberg has investigated is

$$h(\psi,\psi^*) = \sum_r \frac{h_r}{n^r}$$

$$= \sum_{k\ell} \psi_k^* H_{k\ell}\psi_\ell + \frac{1}{n}\sum_{k\ell mn} \psi_k^*\psi_\ell^* G_{k\ell mn}\psi_m\psi_n + \ldots \tag{4}$$

where the first term is the linear term which describes ordinary quantum mechanics, the second term is the lowest order nonlinear addition, and $n = \sum_k \psi_k^*\psi_k$. Galilean invariance puts restrictions on the coefficients $H_{k\ell}$, $G_{k\ell mn}$, ... If we ignore translational degrees of freedom, Galilean invariance reduces to rotational invariance. The Hamiltonian function must transform as a scalar under rotations. The only scalars that can be formed from the two components of a spin-½ wave function are functions of the norm n. Therefore, in the absence of external fields, the potential nonlinear contributions of Eq. (4) to the Hamiltonian function of a spin-½ particle are functions of the norm and have no effect other than to set the zero

of energy for the spin. Weinberg shows that in the presence of external fields (where the G_{klmn} transform according to the rotation properties of a tensor), a spin-½ particle can have a first-order quadrupole interaction. Particles with spin $I \geq 1$ can have a nonlinear contribution to the Hamiltonian function even in the absence of external fields. The lowest order nonlinear addition $h_{nl}(\equiv h_1/n)$ for a spin I = 3/2 can be written as[3]

$$h_{nl} = \frac{\epsilon}{n}\{|\sqrt{6}\psi_{3/2}\psi_{-\frac{1}{2}} - \sqrt{2}\psi_{\frac{1}{2}}\psi_{\frac{1}{2}}|^2 + |3\psi_{3/2}\psi_{-3/2} - \psi_{\frac{1}{2}}\psi_{-\frac{1}{2}}|^2 + |\sqrt{6}\psi_{-3/2}\psi_{\frac{1}{2}} - \sqrt{2}\psi_{-\frac{1}{2}}\psi_{-\frac{1}{2}}|^2\}. \quad (5)$$

For a nucleus with I = 3/2, Eq. (5) gives a possible nonlinear addition to the nuclear Hamiltonian. The parameter ϵ gives the strength of the nonlinear term. Weinberg does not make a prediction for a value of ϵ; he only constructs a theory in which $\epsilon \neq 0$ is allowed.

As a simple example, consider the two-level system consisting of the $m_I = -3/2$ and $-\frac{1}{2}$ states of a spin I = 3/2 nucleus. Let $|1\rangle \equiv |m_I = -3/2\rangle$ and $|2\rangle \equiv |m_I = -\frac{1}{2}\rangle$ and $h_0(\psi,\psi^*) = \hbar\omega_1\psi_1\psi_1^* + \hbar\omega_2\psi_2\psi_2^*$ denote the bilinear Hamiltonian function for the system. (Suppose the degeneracy of the levels is split by a magnetic field and that no population exists in the $+\frac{1}{2}$ and +3/2 sublevels.) The Hamiltonian function for the lowest order nonlinear contribution given by Eq. (5) reduces to

$$h_{nl} = n2\epsilon a^2, \quad (6)$$

where $a = |\psi_2|^2/n$ is the probability of finding the system in $|2\rangle$ and is identical to the parameter a in Eqs. (1) and (2). From Eq. (3) the time evolution of the superposition state $|\psi(0)\rangle$ from Eq. (1) is

$$|\psi(t)\rangle = e^{-i\omega_1(a)t}[(1-a)^{\frac{1}{2}}|1\rangle + a^{\frac{1}{2}}e^{i(\omega_1(a)-\omega_2(a))t}|2\rangle], \quad (7)$$

where $\omega_1(a) = \omega_1 - 2(\epsilon/\hbar)a^2$ and $\omega_2(a) = \omega_2 - 2(\epsilon/\hbar)a^2 + 4(\epsilon/\hbar)a$. The coherence frequency $\omega_p \equiv \omega_1(a) - \omega_2(a)$ now depends on the state probabilities according to

$$\begin{aligned}\omega_p &= \omega_0 - 4(\epsilon/\hbar)a \\ &= \omega_0 - 4(\epsilon/\hbar)\cos^2(\theta/2),\end{aligned} \quad (8)$$

where $\omega_0 \equiv \omega_1 - \omega_2$ is the transition frequency in the absence of nonlinearities. In the language of the equivalent spin-½ system, the precession frequency ω_p of the spin now depends on the tipping angle θ between the spin and the magnetic field. The equation of motion for a two-level system with the nonlinear addition given by Eq. (6) is formally identical to that of Jaynes' neoclassical theory of the interaction of the electromagnetic field with atoms.[15,16] However, the origin of the nonlinearity is quite different. In Jaynes' theory

the nonlinearity is due to a postulated radiation reaction of the atomic dipole on itself.

The frequency ω_p is the "instantaneous" transition frequency of the two-level system. That is, if an external field of frequency ω is used to induce transitions between the two states, this transition rate is maximized for $\omega = \omega_p$. Suppose all the population is initially in state $|1\rangle$. Application of an external field with frequency $\omega = \omega_0 = \omega_p(\pi)$ starts driving population from state $|1\rangle$ to state $|2\rangle$. If the Rabi frequency Ω due to the applied field is much smaller than the nonlinear correction ϵ [$\Omega \ll (\epsilon/\hbar)$], then the population can never be completely inverted. This is because the transition frequency given by ω_p is chirped as the state of the system evolves. Consequently, unless the frequency of the applied field is similarly chirped, a transfer of all the population to state $|2\rangle$ never occurs. Weinberg used this fact, along with the experimental observation that nuclear magnetic resonance transitions in $^9Be^+$ have been driven in times as long as 1 s to set a limit of $\sim 10^{-15}$ eV on the magnitude of a nonlinear correction to the energy of the ^{9}Be nucleus.[2]

Very few proposals for nonlinear terms in quantum mechanics have been made and experimentally tested. One proposal that has been experimentally tested is the addition of a logarithmic term $-b\psi(\vec{x})\ell n|\psi(\vec{x})|^2$ to the one-particle Schrödinger equation discussed by Bialynicki-Birula and Mycielski.[17] This nonlinear addition can be derived from a Hamiltonian function, but the Hamiltonian function is not homogeneous. Physically, it predicts that the time evolution of a wave function depends on its normalization, in contrast to Weinberg's theory. Nevertheless it gives a correct treatment of physically separated systems. Shimony[18] suggested an experimental test based on neutron interferometry for this nonlinear term. Experiments[19,20] have put a bound of 3×10^{-15} eV on the magnitude of the parameter b.

EXPERIMENTAL TESTS

Weinberg's generalization of quantum mechanics has motivated recent experimental tests which improve upon the limit set by Weinberg by more than 5 orders of magnitude. The first experiment to be described here was done at the National Institute of Standards and Technology and used ion storage techniques to measure the frequency of a hyperfine transition in $^9Be^+$ to high precision.[4] Trapped ions provide very clean systems for testing calculations of the dynamics of quantum transitions. The ions can be observed for long periods, relatively free from perturbations and relaxations. Their levels can be manipulated easily with rf and optical fields. This has led to their use in observing quantum effects such as quantum jumps, photon antibunching, sub-Poissonian statistics,[21] and the quantum Zeno effect[22]. In addition, trapped ions have been used to test the isotropy of space[23] and search for a spin-dependent fifth force.[24] For a test of nonlinear quantum mechanics, we searched

for a state population dependence (a θ dependence) of the $(m_I, m_J) = (-1/2, +1/2) \rightarrow (-3/2, +1/2)$ hyperfine transition at ~ 303 MHz in the ground state of $^9Be^+$ (see Fig. 1). At a magnetic field B of 0.8194 T, this transition, called the clock transition, depends only quadratically on magnetic field fluctuations. With $|1\rangle \equiv |-3/2, +1/2\rangle$ and $|2\rangle \equiv |-1/2, +1/2\rangle$, the lowest order nonbilinear addition to the Hamiltonian function of the free $^9Be^+$ nucleus for the two states is given by Eq. (6). Equation (8) then gives the dependence of the precession frequency ω_p on the tipping angle θ, which describes the relative amplitude admixture of the two states. A search for a nonlinear addition to quantum mechanics was made by measuring ω_p at two different tipping angles.

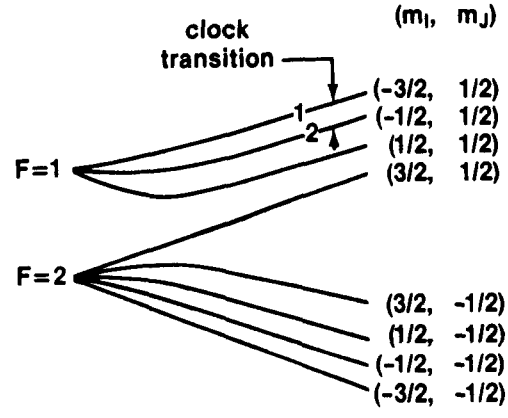

Fig. 1. Hyperfine energy levels (not drawn to scale) of the $^9Be^+$ 2s $^2S_{1/2}$ ground state as a function of magnetic field. At B = 0.8194 T the 303-MHz clock transition is independent of magnetic field to first order. (From Ref. 4)

Between 5000 and 10 000 $^9Be^+$ ions and 50 000 to 150 000 $^{26}Mg^+$ ions were simultaneously stored in a cylindrical Penning trap[25] with B ≃ 0.8194 T under conditions of high vacuum ($\lesssim 10^{-8}$ Pa). To minimize second-order Doppler shifts of the clock transition, the $^9Be^+$ ions were cooled to less than 250 mK by the following method. The $^{26}Mg^+$ ions were directly laser cooled[26] and the $^9Be^+$ ions were then sympathetically cooled[27] by their Coulomb interaction with the cold Mg^+ ions. Narrow-band 313-nm radiation was used to optically pump and detect the $^9Be^+$ ions. With the 313-nm source tuned to the 2s $^2S_{1/2}(3/2, 1/2)$ to 2p $^2P_{3/2}(3/2, 3/2)$ transition, 94% of the $^9Be^+$ ions were optically pumped into the 2s $^2S_{1/2}(3/2, 1/2)$ ground state.[28,29] The 313-nm source was then turned off to avoid optical pumping and ac Stark shifts.

The clock transition was detected by the following method. After the 313-nm source was turned off, the ions in the (3/2, 1/2) state were transferred to the (1/2, 1/2) state and then to the (-1/2, 1/2) state by two successive rf π pulses. The clock transition was then

driven by Ramsey's method of separated oscillatory fields[30] with rf pulses of about 1-s duration and a free-precession time on the order of 100 s. This transferred some of the ions from the (-1/2, 1/2) state to the (-3/2, 1/2) state. Those ions remaining in the (-1/2, 1/2) state were then transferred back to the (3/2, 1/2) state by reversing the order of the two rf π pulses. The 313-nm source was then turned back on, and the population of ions in the (-3/2, 1/2) state was registered as a decrease in the $^9Be^+$ fluorescence, relative to the steady-state fluorescence, during the first second that the 313-nm source was on. [The optical repumping time of the ions from the (-3/2, 1/2) state to the (3/2, 1/2) state was an order of magnitude longer than this.]

For the test of nonlinearities, Ramsey's method with unequal rf pulses was used to drive the clock transition and measure ω_0 for different values of θ. First an rf θ pulse of duration τ_θ was applied. This prepared the ions in a coherent superposition of states |1> and |2> of the clock transition given by Eq. (7) for a particular value of $a = \cos^2(\theta/2)$. After the rf θ pulse, the ions freely precessed for a time T. This was followed by an rf $\pi/2$ pulse, coherent with the first pulse, which completed the Ramsey excitation. In the limit that $T \gg \tau_\theta$, $T \gg \tau_{\pi/2}$, the Ramsey line shape (specifically, the number of ions remaining in the state |2> as a function of the rf frequency ω in the Ramsey excitation) is

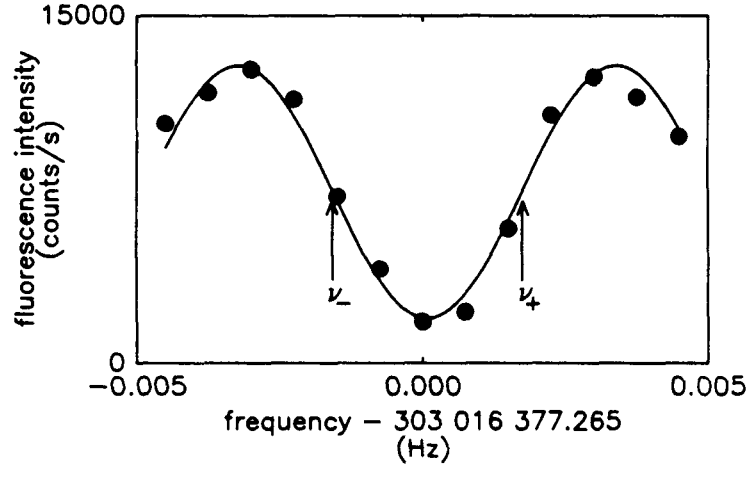

Fig. 2. Ramsey signal of the $^9Be^+$ clock transition with T = 150 s and $\theta = \pi/2$. The data are the result of one sweep (that is, one measurement per point). The sweep width is 9 mHz. The dots are experimental and the curve is a least-squares fit. The signal-to-noise ratio is limited by the frequency stability of the reference oscillator. The full-width-at-half-minimum frequencies are indicated by ν_+ and ν_-. (From Ref. 4)

proportional to

$$1 - \sin\theta\cos\{[\omega-\omega_p(\theta)]T\}, \qquad (9)$$

where $\omega_p(\theta)$ is given by Eq. (8). The center frequency of the Ramsey line shape is the precession frequency $\omega_p(\theta)$. Figure 2 shows a Ramsey signal obtained with T = 150 s and $\theta = \pi/2$.

Ramsey-signal measurements were taken near both of the full-width-at-half-minimum frequencies $\omega_+ \equiv 2\pi\nu_+$ and $\omega_- \equiv 2\pi\nu_-$, where ν_+ and ν_- are indicated in Fig. 2. The difference in the measured signal strengths on either side of the line center was used to electronically steer[28] the average frequency of a synthesized rf source to $\omega_p(\theta)$. Eight pairs of measurements were taken with an angle $\theta_A = 1.02$ rad followed by eight pairs of measurements with an angle $\theta_B = 2.12$ rad. This pattern was repeated for the length of an entire run as indicated in Fig. 3. The average frequency of the synthesizer for $\theta = \theta_A$ was then subtracted from the average frequency of the synthesizer for $\theta = \theta_B$. Runs were taken with free-precession periods of T = 30, 60, and 100 s. A weighted average of the synthesizer frequency differences for $\theta = \theta_A$ and $\theta = \theta_B$ from about 110 h of data gave a possible dependence of the precession frequency on θ of $[\omega_p(\theta_B) - \omega_p(\theta_A)]/2\pi = 3.8 \pm 8.3$ μHz. From Eq. (8) a value for the parameter ϵ of $\epsilon/(2\pi\hbar) = 1.8 \pm 4.0$ μHz is obtained. The uncertainty is expressed as a 1 standard deviation.

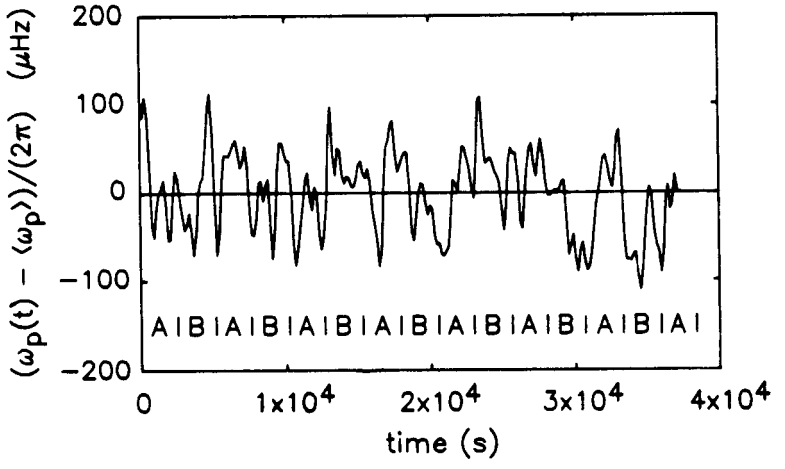

Fig. 3. $^9Be^+$ precession frequency $\omega_p(t)$ as a function of time for a single run with T = 100 s. The periods A(B) during which the initial Rabi pulse created a mixed state with angle $\theta_A = 1.02$ rad ($\theta_B = 2.12$ rad) are indicated. (From Ref. 4)

This sets an upper limit of $|\epsilon| < 2.4 \times 10^{-20}$ eV (5.8 μHz) for a nonlinear contribution to the $^9Be^+$ nuclear Hamiltonian. This is less than 4 parts in 10^{27} of the binding energy per nucleon of the $^9Be^+$ nucleus. Our experimental result is limited by statistical fluctuations due to the frequency instability of the reference oscillator used with the synthesizer (typically a commercial Cs atomic clock). The largest known systematic errors of our measurement of $\omega_p(\theta)$ are an apparent, surprisingly large pressure shift[31] of ~ 30 μHz and a second-order Doppler shift of ~ 3 μHz due to the $\vec{E}\times\vec{B}$ rotation of the ion cloud in the trap.[28] We believe both shifts are constant to better than 1 μHz over the time required to make a frequency difference measurement (about 40 min).

Experiments[5,7] with ^{21}Ne and ^{201}Hg nuclei have produced comparable results to the $^9Be^+$ experiment described above. All three experiments use spin-3/2 nuclei to test the linearity of quantum mechanics. In the ^{21}Ne and ^{201}Hg experiments, optical pumping techniques are used to polarize the nuclear spins of an atomic vapor along a weak magnetic field. Let $\hbar\omega_k$, k = +3/2, +1/2, -1/2, -3/2 denote the energies of the nuclear spin levels. In a coordinate system with the z axis along the polarization axis, the density matrix ρ describing the spin-3/2 state populations is diagonal and can be expressed[32] in terms of irreducible spherical tensors T_{L0} according to $\rho \equiv \sum_{L=0}^{3} \rho_{L0} T_{L0}$. The multipole polarizations

$\rho_{L0} \equiv \mathrm{Tr}(\rho T_{L0})$, L = 0,1,2,3 (the monopole, dipole, quadrupole, and octupole atomic polarizations) are given by

$$\begin{aligned}
\rho_{00} &= \tfrac{1}{4}\{\langle|\psi_{3/2}|^2\rangle + \langle|\psi_{\frac{1}{2}}|^2\rangle + \langle|\psi_{-\frac{1}{2}}|^2\rangle + \langle|\psi_{-3/2}|^2\rangle\},\\
\rho_{10} &= \frac{1}{2\sqrt{5}}\{3\langle|\psi_{3/2}|^2\rangle + \langle|\psi_{\frac{1}{2}}|^2\rangle - \langle|\psi_{-\frac{1}{2}}|^2\rangle - 3\langle|\psi_{-3/2}|^2\rangle\},\\
\rho_{20} &= \tfrac{1}{4}\{\langle|\psi_{3/2}|^2\rangle - \langle|\psi_{\frac{1}{2}}|^2\rangle - \langle|\psi_{-\frac{1}{2}}|^2\rangle + \langle|\psi_{-3/2}|^2\rangle\},\\
\rho_{30} &= \frac{1}{2\sqrt{5}}\{\langle|\psi_{3/2}|^2\rangle - 3\langle|\psi_{\frac{1}{2}}|^2\rangle + 3\langle|\psi_{-\frac{1}{2}}|^2\rangle - \langle|\psi_{-3/2}|^2\rangle\},
\end{aligned} \tag{10}$$

where $\langle\ \rangle$ denotes the ensemble average over the spin-3/2 state populations. A coherent superposition of all of the nuclear spin levels is created by tipping the polarized nuclear spins with respect to the magnetic field by an angle θ. The transverse polarizations of the nuclear spins then precess about the magnetic field at frequencies determined by the Zeeman frequency splittings. Measurement of these free precession frequencies as a function of the state populations provides a test of the linearity of quantum mechanics. The Zeeman frequencies ω_i, i = 1,2,3 are[33]

$$\begin{aligned}
\omega_1 &\equiv \omega_{3/2} - \omega_{\frac{1}{2}} = 2\pi(D + Q + \frac{13}{12}O),\\
\omega_2 &\equiv \omega_{\frac{1}{2}} - \omega_{-\frac{1}{2}} = 2\pi(D + \frac{1}{12}O),
\end{aligned} \tag{11}$$

$$\omega_3 \equiv \omega_{-\frac{1}{2}} - \omega_{-3/2} = 2\pi(D - Q + \frac{13}{12} O),$$

where D, Q, and O are the dipole, quadrupole, and octupole contributions to the splitting of the Zeeman levels. If the Zeeman frequencies are resolved (for example, if Q^{-1} is less than the relaxation time of the coherent superposition), Weinberg's nonlinear corrections to these frequencies from Eq. (5) can be expressed in terms of $\rho_{L0}(\theta)$, the multipole polarizations along the precession axis, where $\rho_{L0}(\theta) = \rho_{L0} P_L(\cos\theta)$ and $P_L(\cos\theta)$ is the L^{th}-order Legendre polynomial, according to[7]

$$\begin{aligned}
\delta\omega_1 &= \frac{\epsilon}{\hbar}\left[-\frac{9}{\sqrt{5}}\rho_{10}(\theta,t) + \rho_{20}(\theta,t) + \frac{12}{\sqrt{5}}\rho_{30}(\theta,t)\right] \\
\delta\omega_2 &= \frac{\epsilon}{\hbar}\left[-\frac{15}{\sqrt{5}}\rho_{10}(\theta,t) - \frac{15}{\sqrt{5}}\rho_{30}(\theta,t)\right] \qquad (12) \\
\delta\omega_3 &= \frac{\epsilon}{\hbar}\left[-\frac{9}{\sqrt{5}}\rho_{10}(\theta,t) - \rho_{20}(\theta,t) + \frac{12}{\sqrt{5}}\rho_{30}(\theta,t)\right].
\end{aligned}$$

The monopole component of the polarization has been omitted because it is unimportant to the discussion of these experiments. The variable t explicitly denotes the dependence of the multipole polarizations on time due to relaxation.

The precession frequencies in these experiments are relatively low (< 1 kHz) compared to the ~ 300 MHz frequency in the $^9Be^+$ experiment. In addition, the number of atoms used in these experiments is very large (10^{13} - 10^{19} atoms) compared with the number of ions (~ 5000) used in the $^9Be^+$ experiments. As a result, the second order Doppler shifts in these experiments are negligible and the signal-to-noise ratio is typically high enough to measure the precession frequencies to much better than 1 μHz. Time-dependent, systematic frequency shifts, however, typically limit the precision of the precession frequency measurements. In addition to the test of quantum mechanics discussed here, experiments like these have been used to test the isotropy of space[32-35] and to search for T-violating interactions.[36]

In the ^{201}Hg experiment done at the University of Washington,[7] circularly polarized light from a ^{198}Hg discharge lamp is used to optically pump about 10^{13} ^{201}Hg atoms contained in a quartz cell and polarize the ^{201}Hg nuclei along a few milligauss (1 mG = 10^{-7} T) magnetic field collinear with the light. A polarization of 45% of the value for a maximally polarized four-level system (all atoms in the m_I = +3/2 or -3/2) was obtained. After optical pumping, the polarized nuclear spins are adiabatically rotated by an angle ϕ by slowing rotating the magnetic field. The magnetic field is then suddenly changed to a direction perpendicular to the incident light and at an angle $\theta = 90° - \phi$ with respect to the polarized spins. By changing the angle θ the spin polarization moments given in Eq. (12) could be varied. The 2 Hz precession of the spins about the magnetic

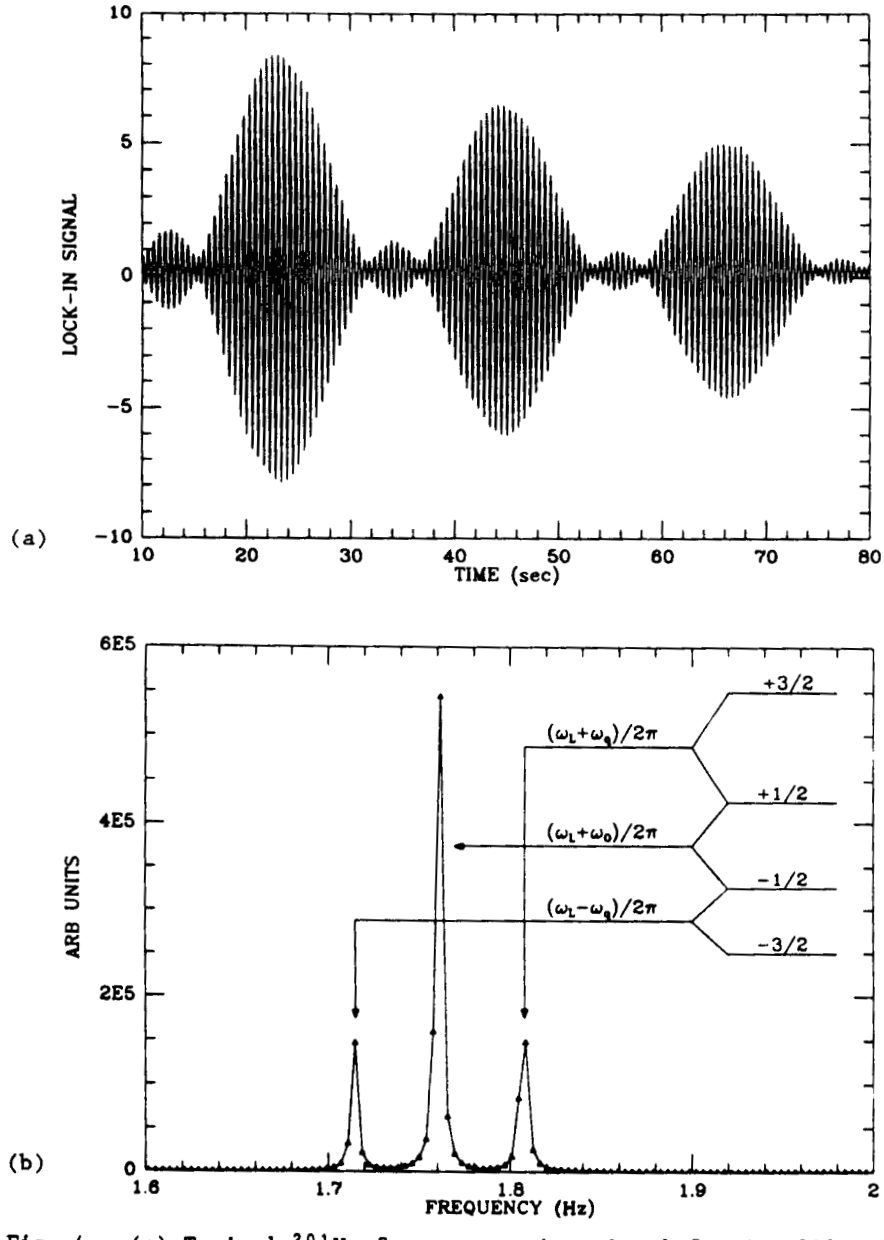

Fig. 4. (a) Typical ^{201}Hg free-precession signal for $\theta = 90°$. The signal-to-noise is photon shot-noise limited (roughly 500 to 1 here). (b) A fast Fourier transform power spectrum of the data in (a). Also shown are the relevant ^{201}Hg Zeeman levels and the parametrization of the three coherence frequencies used in Ref. 7. (From Ref. 7)

field is measured from a modulation of the light transmitted through the cell for about 240 s which is roughly 2.5 coherence lifetimes. The three precession frequencies are resolvable due to a Q = 50 mHz quadrupole interaction between the ^{201}Hg spins and the cell wall. A typical free precession signal and its fast Fourier transform are shown in Figs. 4a and 4b. In this experiment, the difference in the center frequency and the average of the outer two frequencies, $\omega_2 - (\omega_1 + \omega_3)/2$, was fitted for a possible dependence on the dipole and octupole polarization given by Eq. (12). This combination of frequencies is sensitive only to the octupole contribution [O in Eq. (11)] of the Zeeman splitting. This provides good isolation from possible systematic shifts; the only known octupole shift is due to a misalignment of the cell axis with the magnetic field and was measured to be small [$O \simeq 2.5 \pm 0.5$ μHz]. Furthermore, this octupole shift is independent of atomic polarization as well as precession angle θ. The result of several thousand 240-s runs taken at different precession angles θ between 15° and 45° is $\epsilon/(2\pi\hbar) = 1.1 \pm 2.7$ μHz. Thus the fraction of the binding energy per ^{201}Hg nucleon which could be due to nonlinear quantum mechanics is less than 2×10^{-27} (3.8 μHz).

In the ^{21}Ne experiment done at Harvard University,[5] ^{21}Ne and ^{3}He (about 2×10^{19} atoms of each) are contained in a sealed glass cell and polarized along a static 0.3 mT magnetic field by spin exchange with optically pumped Rb. The ^{21}Ne spins are then tipped by $\theta = 20°$ with respect to the static magnetic field axis by a pulse of oscillating magnetic field at the precession frequency. The free precession of the ^{21}Ne spins is then measured over a period of 4.5 h by monitoring the transverse magnetization with the voltage induced in a pickup coil. The ^{21}Ne spins remain coherent over the entire measurement. The ~ 995 Hz ^{21}Ne precession frequency is mixed with the ^{3}He precession frequency (~ 9600 Hz) divided by 9.649 to produce a ~ 1/60 Hz carrier frequency which is relatively free of the effects of magnetic field fluctuations. Figure 5 shows the ^{21}Ne precession data for one 4.5-h run. The three precession frequencies are resolvable due to the interaction of the electric quadrupole moment of the ^{21}Ne nucleus with the glass cell wall. The quadrupole contribution to the Zeeman splitting is Q ~ 240 μHz. Because the dipole component of the frequency splitting is sensitive to spin-exchange shifts, originally the quadrupole component of the Zeeman splitting was used to test the linearity of quantum mechanics.[5] Specifically the difference frequency $\omega_1 - \omega_3$ was extracted from the precession frequency data and fit for a possible dependence on the quadrupole polarization. The quadrupole polarization would decay during a run due to relaxation. The result of five 4.5 h runs is $\epsilon/(2\pi\hbar) = 12 \pm 19$ μHz. The upper limit on $|\epsilon/(2\pi\hbar)|$ of 31 μHz is 1.6×10^{-26} of the binding energy per nucleon of the ^{21}Ne nucleus. This measurement is limited at least in part by the small quadrupole polarization ($\rho_{20} \leq 0.025$). The quadrupole polarization is small since it arises only from quadrupole relaxation in the presence of spin exchange, where spin exchange is a dipole interaction that produces dominantly dipole polarization. Recently, these ^{21}Ne data

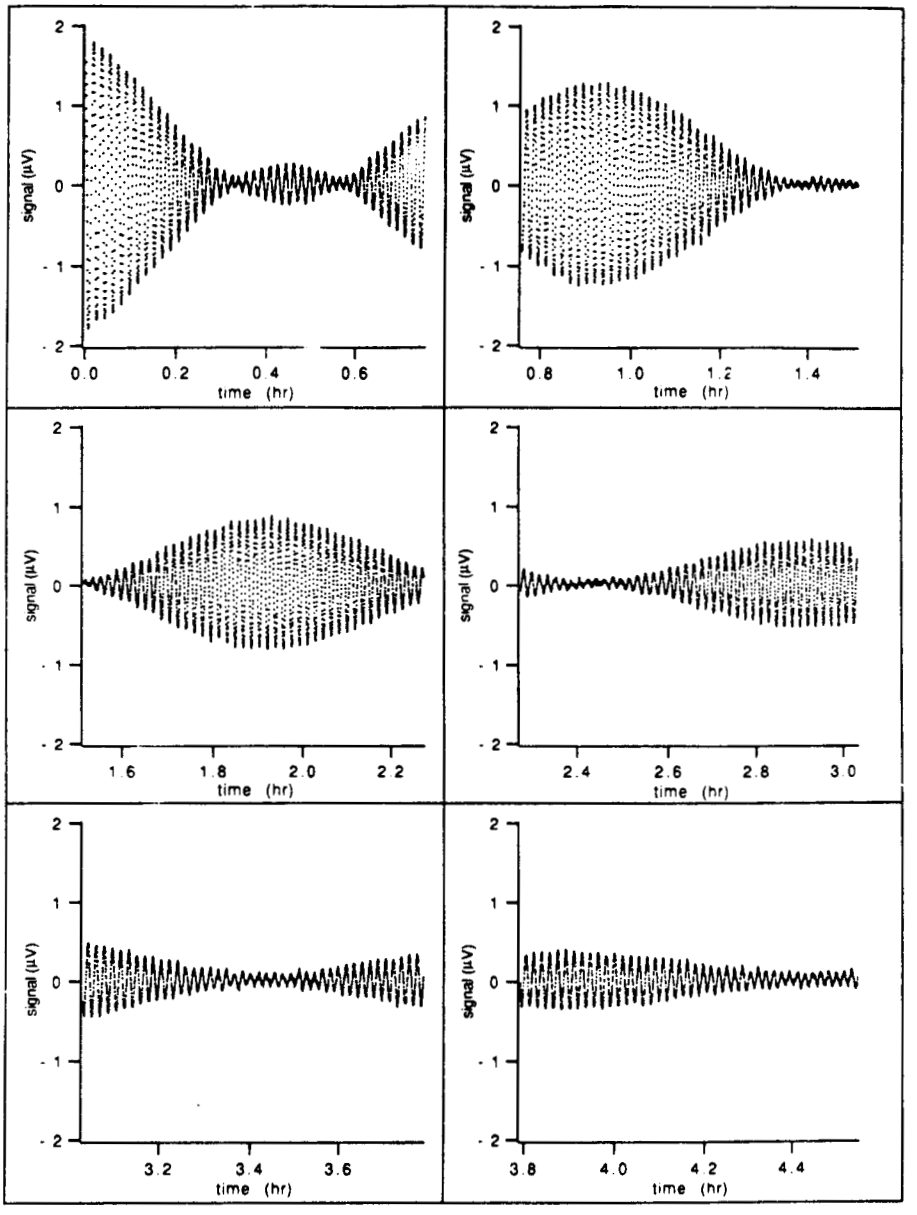

Fig. 5. Data for coherent free precession of ^{21}Ne over 4.5 h. Each panel represents a 45-min measurement of the beat frequency between the ^{21}Ne signals and a reference frequency derived from freely precessing ^{3}He. ^{3}He is not coherent from panel to panel; ^{21}Ne is. (From Ref. 5)

have been reanalyzed[37] by searching for a dipole and octopole polarization-dependent shift in the frequency component 0, similar to the technique developed by the University of Washington group in their ^{201}Hg experiment. The new limit on a possible nonlinear correction to the ^{21}Ne nuclear Hamiltonian of $|\epsilon|/(2\pi\hbar) < 1.5$ μHz is about a factor of 20 improvement over the previous limit.

In addition to these two experiments, a similar experiment[38] is planned which uses radioactive spin-3/2 ^{37}Ar nuclei ($t_{\frac{1}{2}}$ = 35 days) polarized by spin exchange with optically pumped Rb. The polarization of the ^{37}Ar is detected by observing the asymmetry in the emission of the internal bremsstrahlung accompanying the electron capture decay of ^{37}Ar to ^{37}Cl.

Hydrogen masers at the Smithsonian Astrophysical Observatory have also been used to search for a possible nonlinear correction to quantum mechanics.[6] The $(F,m_F) = (1,0) \rightarrow (0,0)$ clock transition in a hydrogen maser (see Fig. 6) is a transition between states of two coupled spin-½ particles. As noted earlier, a spin-½ particle cannot have a nonlinear correction to the Hamiltonian describing its internal degrees of freedom. However, the interaction between two spin-½ particles can. Walsworth and Silvera have determined the lowest order allowed nonlinear Hamiltonian function for the H ground-state hyperfine structure.[39] The resulting nonlinear contribution to the clock transition frequency ω_0 of the maser is

$$\delta\omega_0 = \left(\frac{\epsilon_1' + \epsilon_0'}{\hbar n} \right) (|\psi_1|^2 - |\psi_0|^2), \qquad (13)$$

where ψ_1 and ψ_0 are the amplitudes for the atom to be in the F = 1, m_F = 0 and F = 0, m_F = 0 states respectively, the nonlinearity parameters ϵ_1' and ϵ_0' include a possible dependence on the atom's state, and n is the norm. A test for a nonlinear correction to

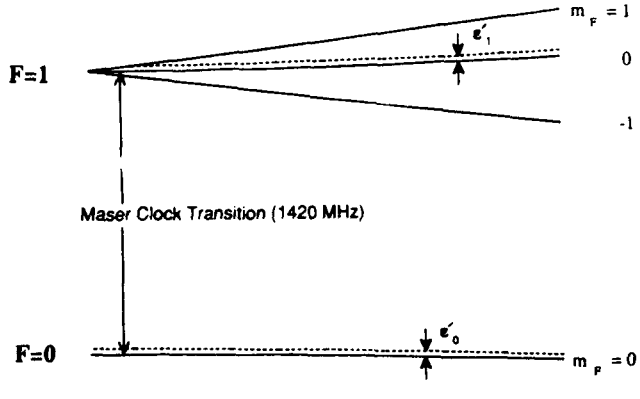

Fig. 6. Atomic hydrogen ground state hyperfine energy levels as a function of magnetic field, for fields < 0.02 T. Energy level shifts due to possible nonlinear effects are shown. (From Ref. 6)

quantum mechanics was made by searching for a dependence of the maser frequency on the relative populations of the clock states as shown in Fig. 7. The relative population of the two states was varied by changing the input H flux to the maser, and it was measured from the dependence of Q_l, the line Q of the maser signal, on the populations.[40] Increasing the H flux decreases both Q_l and the population difference between the states. The result of eight ~50 h runs searching for a dependence of the maser frequency on the state populations was $(\epsilon_1' + \epsilon_0')/(2\pi\hbar) = 1.5 \pm 7.4$ μHz. This limit is comparable in magnitude to the limits placed on nonlinear effects in a nuclear system described in three previous experiments. It sets an upper limit of 3×10^{-21} on the fraction of the 13.6 eV electronic binding energy that could be due to a nonlinear contribution to the atomic Hamiltonian of the hydrogen atom.

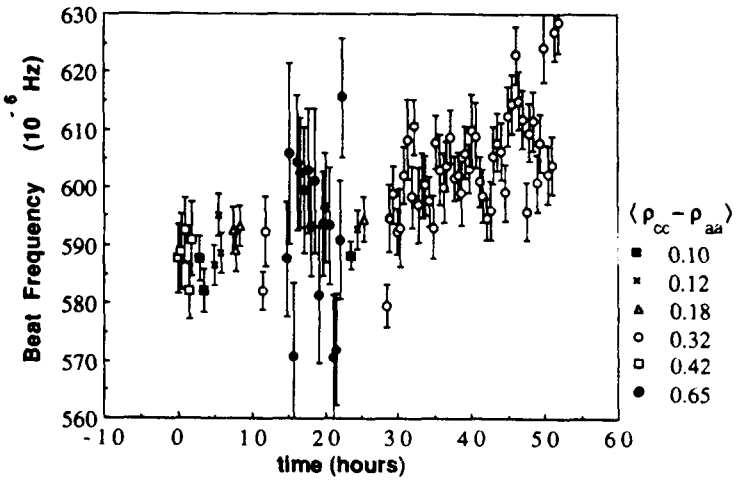

Fig. 7. The raw beat frequency data from a single run (#6). Six different H flux levels were used in this run. An overall linear frequency drift of ~ 6 μHz/day is evident in the data, due to the settling of the materials in the resonant cavity. (From Ref. 6)

Table I summarizes the experimental results. In the absence of a model which gives a specific prediction for ϵ, it is important to have experimental tests in several different systems. Limits have now been set at ~ 10 μHz or less in four different systems. This is 5 orders of magnitude smaller than experimental limits placed by neutron interferometry[19,20] on the size of a logarithmic addition to the one-particle Schrödinger equation. Three of the experiments can be interpreted as setting a fractional limit of better than 10^{-26} on a nonlinear addition to a nuclear Hamiltonian. The hydrogen maser experiment sets a fractional limit of 3×10^{-21} on a possible nonlinear contribution to an atomic Hamiltonian. All of the experiments are first attempts at measuring a nonlinear component of quantum mechanics and have the potential for an order of magnitude improvement in sensitivity.

Experiment	Limit on $\lvert\epsilon\rvert/(2\pi\hbar)$	Interpretation	Reference
^{9}Be	5.8 μHz	nuclear	4
^{201}Hg	3.8 μHz	nuclear	7
^{21}Ne	31 μHz	nuclear	5
	1.5 μHz		37
H	8.9 μHz	atomic	6

TABLE I. Summary of experimental tests for a nonlinear addition to quantum mechanics permitted by Weinberg's formalism. The interpretation column gives the type of Hamiltonian which the experiment is interpreted as testing. The limits are one standard deviation.

THEORETICAL DISCUSSIONS

In addition to motivating experimental tests, Weinberg's formalism for introducing nonlinear corrections to quantum mechanics has stimulated theoretical discussions.[9-14] These discussions center on whether there is any theoretical reason why quantum mechanics has to be linear. While the discussions do not rule out the possibility of a nonlinear component to quantum mechanics, they show the difficulty in constructing such a theory.

A. Peres has reported[9] that nonlinear variants of Schrödinger's equation violate the second law of thermodynamics. Weinberg's response[10] was that this may be true if entropy is defined as in ordinary quantum mechanics, but that is not an appropriate definition of entropy in a generalized version of quantum mechanics. An interesting question is how to generalize the concept of entropy in a generalized version of quantum mechanics.

Recently, A. Valentini has shown[13] that small nonlinearities of the Schrödinger equation lead to a violation of the wave-particle complementarity in quantum mechanics. Specifically, if the Schrödinger equation was nonlinear, a double slit experiment could be done where both an interference pattern and the slit the particle went through could be measured. Valentini points out that this does not necessarily rule out nonlinear theories, but that the wave-particle aspect of the physical interpretation of such theories must differ from that of standard quantum mechanics.

An interesting connection between nonlinear time evolution in quantum mechanics and causality has been discussed by

N. Gisin.[11,12] Gisin shows, by the example of an Einstein-Podolsky-Rosen (EPR) experiment consisting of pairs of correlated spin-½ particles traveling in opposite directions, that a nonlinear coupling between a spin-½ particle and an electric quadrupole field (permitted in Weinberg's formalism) would enable arbitrarily fast communications.[11] Gisin argues that the same conclusion follows for any nonlinear time evolution.[12] Gisin points out that there may be ways out of this dilemma by changing the usual interpretation of the EPR experiments. In addition, Weinberg's formalism generalizes nonrelativistic quantum mechanics only. As a nonrelativistic theory it may not necessarily give a correct description of causality. However, as Gisin points out, it does appear to create a problem where before there was none.

Following Gisin's example, we can show how a nonlinear contribution to the $^9Be^+$ clock experiment could result in communication faster than the speed of light. As before, let $|1\rangle$ and $|2\rangle$ denote the two states of the $^9Be^+$ clock transition. Let $|+\tfrac{1}{2}\rangle_z$ and $|-\tfrac{1}{2}\rangle_z$ denote the two states of a spin-½ particle, say an electron, along the same quantization axis (the z axis) as the $^9Be^+$ system. Suppose a source of correlated states,

$$\frac{1}{\sqrt{2}}(|1\rangle\,|-\tfrac{1}{2}\rangle_z - |2\rangle\,|+\tfrac{1}{2}\rangle_z), \tag{14}$$

is placed between two regions A and B in space. Assume the source continuously emits the correlated states with the electrons moving toward region A along the y axis and the $^9Be^+$ clock (the $^9Be^+$ ion in an 0.8194 T magnetic field) moving in the opposite direction toward region B. (If desired the $^9Be^+$ clock can be at rest and only the electron moves.) In region A an observer measures the spin of the electron in a Stern-Gerlach apparatus. In region B a different observer drives the clock transition and then measures the population of state $|2\rangle$. Specifically, a weak rf pulse (duration $\tau \gg (2\pi\hbar)/\epsilon$, Rabi frequency $\Omega \ll \epsilon/\hbar$) of frequency $\omega = \omega_p(\theta = \pi) = \omega_0$ is applied in region B. Due to the nonlinear contribution to the clock transition frequency, this applied field will start to drive a transition from a pure $|1\rangle$ state to state $|2\rangle$, but not from $|2\rangle$ to $|1\rangle$. After the applied rf pulse, the population of state $|2\rangle$ is measured as described in the previous section.

Suppose the observer in region A orients the Stern-Gerlach apparatus so that the z component of the electron spin is measured. This prepares the $^9Be^+$ clock in either the $|1\rangle$ state or the $|2\rangle$ state. The rf pulse takes the $|1\rangle$ state and puts it into a mixture of $|1\rangle$ and $|2\rangle$ but leaves the $|2\rangle$ state unchanged. Observer B will then measure on the average that state $|2\rangle$ has a population greater than ½. Now suppose the observer in region A rotates the Stern-Gerlach apparatus and measures the x component of the electron spin. The correlated state given by Eq. (14) can be written in terms of $|+\tfrac{1}{2}\rangle_x$ and $|-\tfrac{1}{2}\rangle_x$, the electron spin states along the x axis, as

$$\frac{1}{2}(|1\rangle - |2\rangle)|-\tfrac{1}{2}\rangle_x - \frac{1}{2}(|1\rangle + |2\rangle)|+\tfrac{1}{2}\rangle_x . \qquad (15)$$

According to the standard interpretation of the EPR experiments, when observer A measures the x component of the electron spin the $^9Be^+$ clock will be prepared in either the $(|1\rangle - |2\rangle)/\sqrt{2}$ state or the $(|1\rangle + |2\rangle)/\sqrt{2}$ state. Both of these states are described by $\theta = \pi/2$ and will not be affected by the rf pulse with frequency $\omega = \omega_p(\pi) \neq \omega_p(\pi/2)$. In this case, observer B will measure that state $|2\rangle$ has a population equal to ½. When observer A rotates the Stern-Gerlach apparatus, observer B instantly sees a change in the state $|2\rangle$ population. It will take observer B a time greater than $(2\pi\hbar)/\epsilon$ to measure this change, but since regions A and B are arbitrarily far apart, it appears that communication at arbitrarily fast speeds is possible.

Recently, Polchinski[14] has investigated whether nonlinear quantum mechanics necessarily violates causality by determining the constraints imposed on observables by the requirement that communication does not occur in EPR experiments. He shows that this leads to a different treatment of separated systems than that originally proposed by Weinberg, but that it is possible for quantum mechanics to be nonlinear without violating causality. However, he shows that this necessarily leads to another type of unusual communication: the communication between different branches of the wavefunction.[41] Polchinski points out that, in effect, this means the wavefunction is never reduced and that this may in turn lead to a dilution of any nonlinear effects.

Clearly a number of theoretical questions about nonlinear theories of quantum mechanics remain to be fully resolved. These questions at present may not prove that quantum mechanics must be linear, but they do point out some problems with the physical interpretation of a nonlinear theory. Experimental work to date has shown that a nonlinear component to quantum mechanics must be very small. In some cases, the nonlinear terms must be 26 orders of magnitude smaller than the linear terms. The theoretical discussion and the experimental tests given here, involve nonlinear generalizations of the Hamiltonian. A nonlinear version of quantum mechanics could possibly take a different form. For example, Weinberg's formalism allows the possibility that operators other than the Hamiltonian could be nonlinear.

The NIST work is supported by the U.S. Air Force Office of Scientific Research and the U.S. Office of Naval Research. We thank M. Raizen for carefully reading the manuscript and P. K. Majumder, S. K. Lamoreaux, R. L. Walsworth, and T. E. Chupp for their useful comments and help in understanding their experimental work.

REFERENCES

1. A. Aspect, P. Grangier, and G. Roger, Phys. Rev. Lett. 49, 91 (1982), and references therein.
2. S. Weinberg, Phys. Rev. Lett. 62, 485 (1989).
3. S. Weinberg, Ann. Phys. (N.Y.) 194, 336 (1989).
4. J. J. Bollinger, D. J. Heinzen, W. M. Itano, S. L. Gilbert and D. J. Wineland, Phys. Rev. Lett. 63, 1031 (1989).
5. T. E. Chupp and R. J. Hoare, Phys. Rev. Lett. 64, 2261 (1990).
6. R. L. Walsworth, I. F. Silvera, E. M. Mattison, and R. F. C. Vessot, Phys. Rev. Lett. 64, 2599 (1990).
7. P. K. Majumder, B. J. Venema, S. K. Lamoreaux, B. R. Heckel, and E. N. Fortson, submitted for publication.
8. R. P. Feynman, F. L. Vernon, Jr., and R. W. Hellwarth, J. Appl. Phys. 28, 49 (1957).
9. A. Peres, Phys. Rev. Lett. 63, 1114 (1989).
10. S. Weinberg, Phys. Rev. Lett. 63, 1115 (1989).
11. N. Gisin, Phys. Lett. A 143, 1 (1990).
12. N. Gisin, Helv. Phys. Acta 62, 363 (1989).
13. A. Valentini, Phys. Rev. A 42, 639 (1990).
14. J. Polchinski, submitted for publication.
15. M. O. Scully and K. Wodkiewicz, submitted for publication.
16. See for example C. R. Stroud, Jr. and E. T. Jaynes, Phys. Rev. A 1, 106 (1970).
17. I. Bialynicki-Birula and J. Mycielski, Ann. Phys. (N.Y.) 100, 62 (1976).
18. A. Shimony, Phys. Rev. A 20, 394 (1979).
19. C. G. Shull, D. K. Atwood, J. Arthur, and M. A. Horne, Phys. Rev. Lett. 44, 765 (1980).
20. R. Gahler, A. G. Klein, and A. Zeilinger, Phys. Rev. A 23, 1611 (1981).
21. W. Nagourney, J. Sandberg, and H. Dehmelt, Phys. Rev. Lett 56, 2797 (1986); Th. Sauter, W. Neuhauser, R. Blatt, and P. E. Toschek, ibid. 57, 1696 (1986); J. C. Bergquist, R. G. Hulet, W. M. Itano, and D. J. Wineland, ibid. 57, 1699 (1986); F. Diedrich and H. Walther, ibid. 58, 203 (1987); W. M. Itano, J. C. Bergquist and D. J. Wineland, Phys. Rev. A 38, 559 (1988); W. M. Itano, J. C. Bergquist, F. Diedrich, and D. J. Wineland, in Proceedings of the Sixth Rochester Conference on Coherence and Quantum Optics (Plenum Publishing Corp., N. Y.) in press.
22. W. M. Itano, D. J. Heinzen, J. J. Bollinger, and D. J. Wineland, Phy s. Rev. A 41, 2295 (1990).
23. J. D. Prestage, J. J. Bollinger, W. M. Itano, and D. J. Wineland, Phys. Rev. Lett. 54, 2387 (1985).
24. J. J. Bollinger, D. J. Heinzen, W. M. Itano, S. L. Gilbert, and D. J. Wineland, in Abstracts of the 12th International Conference on General Relativity and Gravitation, Boulder, CO, 1989, p. 500.
25. S. L. Gilbert, J. J. Bollinger, and D. J. Wineland, Phys. Rev. Lett. 60, 2022 (1988).

26. W. M. Itano and D. J. Wineland, Phys. Rev. A 24, 1364 (1981); W. M. Itano, L. R. Brewer, D. J. Larson, and D. J. Wineland, Phys. Rev. A 38, 5698 (1988).
27. D.J. Larson, J. C. Bergquist, J. J. Bollinger, W. M. Itano, and D. J. Wineland, Phys. Rev. Lett. 57, 70 (1986).
28. J. J. Bollinger, J. D. Prestage, W. M. Itano, and D. J. Wineland, Phys. Rev. Lett. 54, 1000 (1985).
29. L. R. Brewer, J. D. Prestage, J. J. Bollinger, W. M. Itano, D. J. Larson, and D. J. Wineland, Phys. Rev. A 38, 859 (1988).
30. N. F. Ramsey, Molecular Beams (Oxford Univ. Press, London, 1956).
31. D. J. Wineland, J. C. Bergquist, J. J. Bollinger, W. M. Itano, D. J. Heinzen, S. L. Gilbert, C. H. Manney, and M. G. Raizen, IEEE Trans. on Ultrasonics, Ferroelectrics, and Frequency Control, to be published.
32. S. K. Lamoreaux, J. P. Jacobs, B. R. Heckel, F. J. Raab, and E. N. Fortson, Phys. Rev. A 39, 1082 (1989).
33. T. E. Chupp, R. J. Hoare, R. A. Loveman, E. R. Oteiza, J. M. Richardson, M. E. Wagshul, and A. K. Thompson, Phys. Rev. Lett. 63, 1541 (1989).
34. T. E. Chupp, E. R. Oteiza, J. M. Richardson, and T. R. White, Phys. Rev. A38, 3998 (1988).
35. S. K. Lamoreaux, J. P. Jacobs, B. R. Heckel, F. J. Raab, and E. N. Fortson, Phys. Rev. Lett. 57, 3125 (1986).
36. S. K. Lamoreaux, J. P. Jacobs, B. R. Heckel, F. J. Raab, and E. N. Fortson, Phys. Rev. Lett. 59, 2275 (1987).
37. T. E. Chupp and R. J. Hoare, to be published.
38. M. L. Pitt and F. P. Calaprice, Phys. Dept., Princeton Univ., private communication.
39. R. L. Walsworth and I. F. Silvera, Phys. Rev. A 42, 63 (1990).
40. S. B. Crampton, Phys. Rev. 158, 57 (1967).
41. The Many-Worlds Interpretation of Quantum Mechanics, eds B. S. DeWitt and N. Graham (Princeton University Press, Princeton, 1973).

in: Proc. of the Workshop on Crystalline Ion Beams, Wertheim, W. Germany, Ed. by R. W. Hasse, I. Hofmann, D. Liese (GSI report GSI-89-10, ISSN 0170-4546), p. 241.

Coulomb Clusters of Ions in a Paul Trap*

Wayne M. Itano J. C. Bergquist D. J. Wineland

Time and Frequency Division
National Institute of Standards and Technology
(formerly National Bureau of Standards)
Boulder, Colorado 80303, U.S.A.

Abstract

Ordered structures of as many as 16 laser-cooled Hg^+ ions, confined in a Paul trap, have been observed. These structures, called Coulomb clusters, match those calculated by minimizing the effective potential energy of the system. The $5d^{10}6s\ ^2S_{1/2}$ to $5d^96s^2\ ^2D_{5/2}$ transition in Hg^+ has been observed by optical-optical double resonance. The resolution was high enough that Doppler-induced sidebands, due to the harmonic motion of a single ion in the trap, were clearly resolved. Additional sidebands, due to the relative vibration of two ions forming a pseudomolecule, have also been observed.

I. Introduction

A group of a few ions in a Paul (radiofrequency) trap is a system that can be modelled with simple calculations, but which still exhibits phenomena, such as spatial ordering and phase transitions, which are associated with condensed matter. Stimulated in part by recent theoretical predictions that systems of laser-cooled ions would form spatially ordered structures,[1–5] several experimental groups have produced and studied such structures.[6–11]

We have created systems of a few Hg^+ ions, which we call Coulomb clusters, in which the positions of the ions are approximately fixed relative to each other. These relative positions are determined by a balance between the confining forces of the trap and the mutual Coulomb repulsion of the ions. We have also observed a modification of the optical absorption spectrum of the ions by the harmonic vibration of two ions relative to each other. This vibration is an indication that the ions have formed a spatially ordered state. Direct evidence of spatial ordering has been obtained by two-dimensional imaging of the laser-induced fluorescence from the ions. Images of up to 16 ions have been recorded and compared with calculations. These clusters are a novel form of matter, in which the spacing between atoms is larger by about three orders of magnitude than in an ordinary crystal or molecule. Observations of similar structures of ions in a Penning trap have been made recently.[12] Those structures

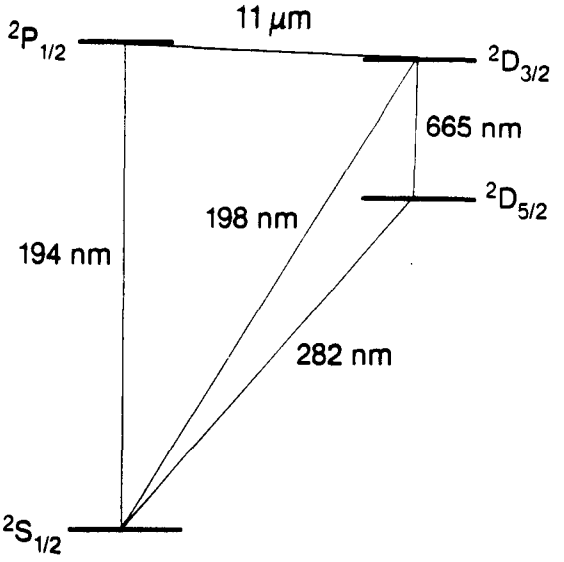

Figure 1: The lowest energy levels of Hg^+.

contained more ions than those described here (as many as 15 000). However, individual ions were not resolved in the Penning trap, as they were in the Paul trap. The smallest clusters studied in the Penning trap had about 20 ions, so that the two experiments taken together cover a range of ion numbers from one to 15 000. We have also observed Coulomb clusters of charged particles with diameters of several micrometers in a large Paul trap. Such clusters of mascroscopic particles are more easily produced and observed than ion clusters. However, the charge-to-mass ratio cannot be made as uniform as for ions. In Thomson's model of the atom, the potential energy function for the electrons was essentially the same as for the ions in a Paul trap. As a result, some of the cluster shapes that we observe are the same as those Thomson calculated for atomic electrons. Preliminary reports of this work have appeared elsewhere.[7,10]

II. Hg^+ levels

The lowest energy states of the mercury ion are shown in Fig. 1. The ground state is $^2S_{1/2}$, as in an alkali atom. The strong $^2S_{1/2}$ to $^2P_{1/2}$ electric dipole transition at 194 nm is used for the laser cooling and fluorescence detection. The lifetime of the $^2P_{1/2}$ state is about 2 ns. Usually, it decays directly back to the ground $^2S_{1/2}$ state. About once in 10^7 times, it decays instead to the metastable $^2D_{3/2}$ state, which has a lifetime of about 9 ms. If this happens the 194 nm fluorescence abruptly turns off. The $^2D_{3/2}$ state decays about half the time directly to the ground state and the rest of the time to the metastable $^2D_{5/2}$ state, which has a lifetime of about 86 ms. After the decay to the ground state the fluorescence turns on again. Thus, the 194 nm fluorescence from a single ion is bistable and switches randomly between zero and a steady level. The statistical properties of this bistable signal

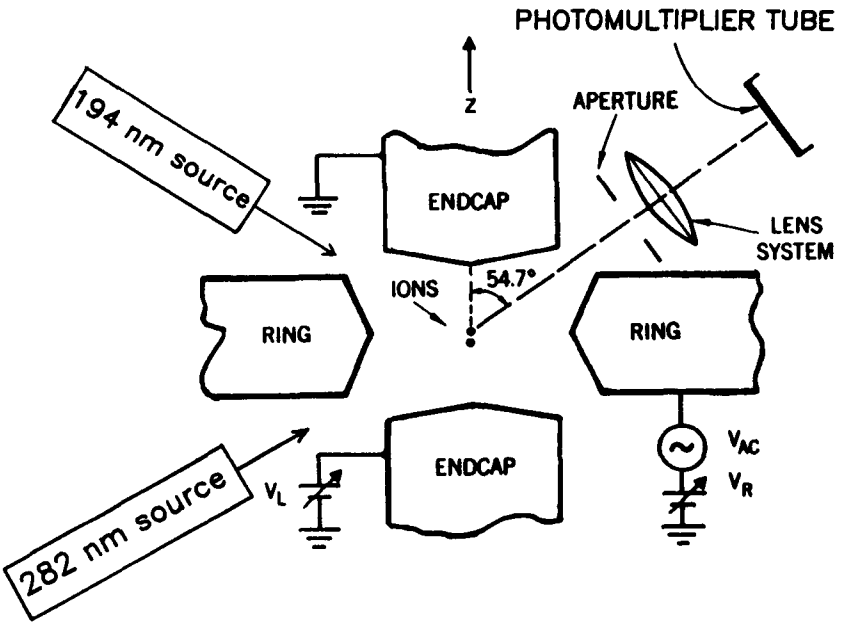

Figure 2: Schematic view of the apparatus. The separation between the endcap electrodes is approximately 625 μm. The inner diameter of the ring electrode is approximately 890 μm.

have been used to measure the decay rates of the metastable states.[13]

III. Apparatus

The experimental apparatus is shown schematically in Fig. 2. The electrodes of the Paul trap are shown in cross section. Radiofrequency and static voltages are applied between the electrodes to control the effective potential well for the ions. The 194 nm laser beam passes along a diagonal between the electrodes. The 194 nm source is required both for detecting the ions and for cooling them (by resonant radiation pressure). The 194 nm fluorescence is detected along another diagonal. For some experiments, the 194 nm detector is a photomultiplier tube. In other cases, a resistive-anode photomultiplier tube that provides two-dimensional positional information from single photoelectrons is used. For optical-optical double resonance experiments, 282 nm light from a frequency-doubled dye laser is focused on the ions.

A. Paul trap

The electric potential inside an ideal Paul trap is given by the expression,

$$\phi(x,y,z) = \frac{U_0 + V_0\cos(\Omega t)}{A^2}(x^2 + y^2 - 2z^2). \tag{1}$$

The potential V applied between the ring electrode and the two endcap electrodes is the sum of a static and a radiofrequency part: $V = U_0 + V_0\cos(\Omega t)$. The parameter A depends

on the geometry of the trap electrodes and has the dimensions of area. The radiofrequency voltage V_0 gives rise to an effective potential which confines in all directions. This potential is four times as strong in the axial (z) direction as in the radial (r) direction. The ratio of the axial to radial confining force can be changed by varying the static voltage U_0. The effective potential energy which governs the average motion, called the secular motion, is

$$q\phi_{\text{eff}}(x,y,z) = \left(\frac{q^2V_0^2}{m\Omega^2A^4} + \frac{qU_0}{A^2}\right)(x^2+y^2) + \left(\frac{4q^2V_0^2}{m\Omega^2A^4} - \frac{2qU_0}{A^2}\right)z^2 \quad (2)$$

$$= \frac{m\omega_r^2}{2}(x^2+y^2) + \frac{m\omega_z^2}{2}z^2. \quad (3)$$

We call the harmonic frequencies for the secular motion along the axial and radial directions ω_z and ω_r. The ion also oscillates at the frequency Ω of the applied field. This motion is called the micromotion. Under normal operating conditions, Ω is much greater than ω_z or ω_r. If there is a slight deviation from axial symmetry, we can describe the effective potential in terms of secular frequencies ω_x and ω_y, provided that we align the coordinate axes along the principal axes of the potential. The effective potential is

$$q\phi_{\text{eff}}(x,y,z) = \frac{m\omega_x^2}{2}x^2 + \frac{m\omega_y^2}{2}y^2 + \frac{m\omega_z^2}{2}z^2, \quad (4)$$

where $\omega_x \approx \omega_y$.

The trap used in these experiments has been described previously.[14] The electrodes were made of molybdenum. The design of the electrodes, which were machined with simple straight cuts, has been discussed in detail elsewhere.[15] The inside diameter of the ring electrode was less than 1 mm. This allowed very strong electric field gradients to be applied. The maximum value of V_0 was about 1 kV. The frequency $\Omega/2\pi$ was about 23 MHz. The ions were created inside the trap by electron impact ionization of isotopically purified ^{198}Hg.

B. Lasers

The cw, tunable 194 nm source has been described previously.[16] Radiation at 257 nm was generated by frequency doubling the output of a 515 nm single-mode cw argon ion laser in an ammonium dihydrogen phosphate crystal. This radiation was mixed with the output of a 792 nm cw dye laser in a potassium pentaborate crystal to generate the sum frequency at 194 nm. The efficiencies of the frequency doubling and mixing processes were enhanced by using ring buildup cavities to increase the powers of the input beams circulating through the crystals. About 5 μW were generated at 194 nm. The bandwidth was about 2 MHz.

The narrowband 282 nm source was obtained from a dye laser that was frequency doubled in a deuterated ammonium dihydrogen phosphate crystal. The bandwidth of the dye laser, which was stabilized to a Fabry-Perot cavity, was about 15 kHz for these experiments. Recently, the linewidth of this laser has been decreased further by stabilizing it to a higher-finesse cavity.

C. Photon imaging detection

A three-stage lens system projected an image of the ion fluorescence onto the photocathode of the position-sensitive photon counter with a magnification of about 180. The first stage

was an aberration-corrected multi-element lens with an f-number of 4.5. The positional information from single detected photons was available in either analog or digital form. Images could be observed in real time on an oscilloscope screen, using the analog pulses. The digital information went to a computer, in order to make time exposures. An image of a single ion in the trap, recorded with this apparatus, has been published previously.[17]

IV. High resolution optical spectroscopy

A. Optical-optical double resonance

We have observed the 282 nm $^2S_{1/2}$ to $^2D_{5/2}$ electric quadrupole transition with high resolution. The metastable $^2D_{5/2}$ state has a lifetime of about 86 ms, so the transition has a natural linewidth of about 2 Hz. It would be very difficult to observe this transition in a single ion by detecting the emitted 282 nm photons, since there would be at most about 11 photons per second. To increase the efficiency of observation, we use optical-optical double resonance with quantum amplification.[14,18,19] The method works in the following way. The 194 nm source is turned off and 282 nm source is turned on. Suppose the ion absorbs a 282 nm photon, and is put into the metastable state. When the 194 nm light is then turned on, no fluorescence is observed. If, on the other hand, the ion is still in the ground state when the 194 nm light is turned on, fluorescence is observed at the normal intensity (typically thousands of photons per second detected). After a few milliseconds, the state of the ion can be determined with almost complete certainty. This technique was developed with the goal of making an optical frequency standard. Here it is used to yield information about the temperature and mutual interactions of the trapped ions.

B. Single-ion motional sidebands

The Doppler broadening of an absorption resonance of an ion bound in a harmonic well is modified by the confinement.[20] Instead of a single, broadened resonance line, the spectrum takes the form of a series of discrete resonances, each having a width equal to the natural width of the resonance, which are separated by the frequency of harmonic motion.

Consider an ion moving in the x direction in a harmonic well with frequency ω_x and amplitude X_0, so that

$$x = X_0 \cos(\omega_x t). \tag{5}$$

Let it be irradiated by a monochromatic laser beam of frequency ω propagating along the x axis. The electric field $\vec{E}(x,t)$ of the laser beam is

$$\vec{E}(x,t) = \mathrm{Re}\ \vec{E}_0 e^{i(kx-\omega t)}, \tag{6}$$

where the symbol Re denotes the real part of a complex expression. In the frame of the ion, there is a frequency modulation of the laser field. The electric field in the ion's frame is obtained by substituting the expression for x given by Eq. (5) into Eq. (6):

$$\begin{aligned} \vec{E}(x,t) &= \mathrm{Re}\ \vec{E}_0 e^{i(kX_0 \cos\omega_x t - \omega t)} \\ &= \mathrm{Re}\ \vec{E}_0 \sum_{n=-\infty}^{+\infty} i^n J_n(kX_0) e^{-i(\omega - n\omega_x)t}. \end{aligned} \tag{7}$$

In addition to the carrier at ω, the ion sees sidebands, called motional sidebands, spaced by the harmonic oscillation frequency ω_x. The amplitudes of the sidebands are proportional to the Bessel functions J_n. The ion absorbs light when the laser frequency is equal to one of its resonance frequencies and also when one of the motional sidebands matches a resonance frequency.

The intensities of the sidebands can be used to measure the temperature of the ion. A quantum mechanical treatment, in which a thermal-state-probability distribution was assumed, has been given previously.[21] According to Eq. (44) of Ref. 21, the intensity of the nth sideband $\sigma(n)$, is

$$\sigma(n) = \sigma_0 \exp\left(\frac{n\hbar\omega_x}{2k_BT} - k^2\langle x^2\rangle\right) I_n\left(\exp\left(\frac{\hbar\omega_x}{k_BT}(kx_0)^2\langle n_x\rangle\right)\right). \tag{8}$$

In this notation, the intensity of the carrier is $\sigma(0)$, I_n is a modified Bessel function, and $\langle x^2\rangle$ is the mean squared displacement of the harmonic oscillator, given by

$$\langle x^2\rangle = \frac{\hbar}{m\omega_x}(\langle n_x\rangle + \tfrac{1}{2}) \equiv 2x_0^2(\langle n_x\rangle + \tfrac{1}{2}), \tag{9}$$

where m is the mass of the ion and $\langle n_x\rangle$ is the mean occupation number of the oscillator. The temperature T is related to $\langle n_x\rangle$ by

$$\langle n_x\rangle = \frac{1}{\exp\left(\frac{\hbar\omega_x}{k_BT}\right) - 1}. \tag{10}$$

Equation 8 can easily be generalized to cases where there are two or more distinct frequencies of motion and where the laser beam is not directed along one of the principal axes of the trap. We have measured the temperature of a single, laser-cooled Hg^+ ion from the motional sidebands of the $^2S_{1/2}$ to $^2D_{5/2}$ transition.[22] The measured temperature was about 2 mK, which agrees with theoretical predictions.[21]

Figure 3(a) shows the absorption spectrum of a single Hg^+ ion, observed by the optical-optical double resonance. The carrier (at optical frequency ν_0) and the motional sidebands above and below ν_0 are clearly resolved. The potentials U_0 and V_0 were adjusted so that $\nu_r \approx 2\nu_z \approx 473$ kHz, where $\nu_r \equiv \omega_r/2\pi$ and $\nu_z \equiv \omega_z/2\pi$. This condition helped to simplify the sideband spectrum. The frequencies ν_z and ν_r were determined experimentally by applying a radiofrequency voltage between the electrodes. When the frequency of the applied voltage matched one of the secular frequencies, the fluorescence decreased, due to heating of the ion. In our notation for the sidebands, $(3z, r+z)$, for example, denotes the two overlapping sidebands at the frequencies $\nu_0 + 3\nu_z$ and $\nu_0 + \nu_r + \nu_z$.

C. Two-ion motional sidebands

If $\nu_z < \nu_r$, two ions have the lowest possible potential energy when they are located on the z axis, at $z = \pm z_{\min}$, where $z_{\min} = (q^2/4m\omega_z^2)^{1/3}$. The normal-mode frequencies of vibration about the minimum of the potential have been calculated previously.[3,7,8] The center of mass of the two ions behaves like a particle of mass $2m$ and charge $2q$ and thus has the same

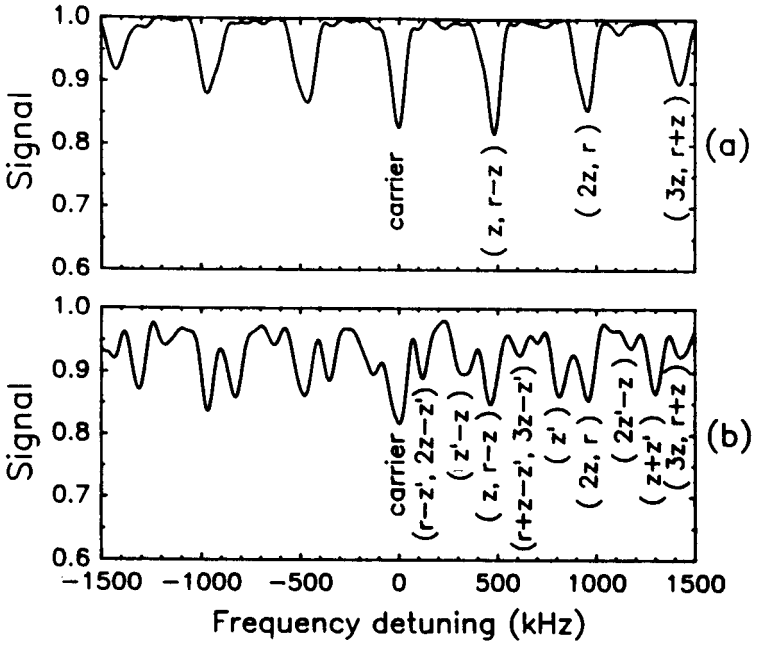

Figure 3: Absorption spectra of the $^2S_{1/2}(m_J = 1/2)$ to $^2D_{5/2}(m_J = -1/2)$ transition for (a) one Hg^+ ion and for (b) two Hg^+ ions. The carrier at optical frequency ν_0 (defined as zero frequency detuning) and the motional sidebands are clearly resolved. The sidebands are labeled in a notation that is explained in the text. The additional sidebands in (b) are due to the vibration of the two ions with respect to each other at frequency ν_z'.

frequencies of motion as a single ion. The frequency at which two ions vibrate with respect to each other along the z axis is $\nu_z' \equiv \sqrt{3}\nu_z$. This mode is like the stretch vibration of a diatomic molecule. The other vibrational frequency is $(\nu_r^2 - \nu_z^2)^{1/2}$, which, for $\nu_r = 2\nu_z$, is also equal to $\sqrt{3}\nu_z$. This vibration is a torsional motion in the x-z or y-z plane. Figure 3(b) shows an absorption spectrum taken with 2 ions in the trap. The trap potentials were the same as for the data of Fig. 3(a). The electronics of the position-sensitive photon detector were adjusted so that the fluorescence from only one of the two ions was detected. The motion of one ion is a superposition of harmonic motions at all of the normal-mode frequencies of the system. Therefore, all of the sidebands in Fig. 3(a) are also present in Fig. 3(b). The additional lines are due to the additional vibrational modes, at frequency ν_z', of the 2-ion pseudomolecule.

This kind of vibrational mode of two trapped ions has been observed by another method described in Ref. 9. Those workers applied a radiofrequency electric field between the trap electrodes, thus directly exciting the vibrational mode. When the frequency of the applied field matched the vibrational resonance, the fluorescence signal decreased.

V. Multi-ion cluster shapes

A. Calculations

The effective potential energy V_{eff} for a system of N ions of mass m and charge q is given by the expression,

$$V_{\text{eff}}(\{x_i, y_i, z_i\}) = \underbrace{\frac{m}{2}\sum_{i=1}^{N}(\omega_x^2 x_i^2 + \omega_y^2 y_i^2 + \omega_z^2 z_i^2)}_{\text{effective trap potential}} + \underbrace{\frac{1}{2}\sum_{i\neq j}\frac{q^2}{\mid \vec{r_i} - \vec{r_j} \mid}}_{\text{Coulomb repulsion}}. \tag{11}$$

Here, $\vec{r_i} = (x_i, y_i, z_i)$ is the position of the ith ion. The first term in Eq. (11) is the effective potential of the ions due to the trap fields. The second is the potential energy due to the Coulomb repulsion between the ions. The equilibrium configurations were calculated by finding the set of $3N$ ion coordinates that minimized the potential energy. A variable metric, or quasi-Newton, method was used to find the minimum, as in Ref. 3. We used the FORTRAN subroutine DFPMIN from Ref. 23. For a cylindrically symmetric Paul trap, there is an infinite set of solutions, since V_{eff} is unchanged by an arbitrary rotation about the z axis. To avoid possible convergence problems, and also to simulate the asymmetry of a real trap, ω_x and ω_y were assumed to differ by 0.2 %. Because of the remaining symmetry of the trap, there were in some cases several solutions, which were related by rotations and reflections. The algorithm sometimes converged to a minimum which was not the global minimum. In order to detect such false minima, at least 10 random initial configurations were used for each case. The solution with the lowest final value of V_{eff} was assumed to be a global minimum.

B. Observations

The ions were observed at an angle of approximately 54.7° with respect to the z axis of the trap. This allowed the three-dimensional structure of the clusters to be seen. In the apparatus of Ref. 6, the ions were observed along the z axis, so only the projection on the x-y plane could be seen. Figures 4-10 show the observed ion images and the corresponding calculated configurations. The magnification was the same for all of the experimental images. The scale of the experimental and calculated images is the same. The scale for the experimental images was determined from the separation between two ions, which is easily calculated. An approximate scale can be determined from the caption to Fig. 5. Experimental images of two, three, and four ions, obtained with less optical magnification, were published previously.[7]

Figure 4(a) shows five ions for $\nu_z = 0.308$ MHz and $\nu_r = 0.376$ MHz. Two of the ions lie along the z axis, symmetrically above and below the x-y plane. The other three ions circulate in the x-y plane about the z axis. They are not fixed in position, because the trap's effective potential is nearly cylindrically symmetric. Thus, the small, unintentional torque that the 194 nm beam applies to the system is enough to cause it to rotate. In this case, we determined the number of ions by reducing ν_z, relative to ν_r, until they were clearly separated in a chain along the z axis. Figure 4(b) shows the calculated ion positions for these

trap parameters. The circle in the calculated figure is obtained by rotating the configuration about the z axis.

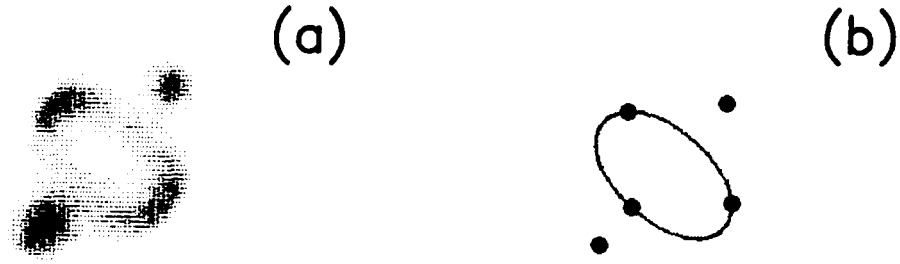

Figure 4: Nonplanar configuration of five ions for $\nu_z = 0.308$ MHz and $\nu_r = 0.376$ MHz. (a) Experimental data. (b) Calculation.

Figure 5 shows six ions for $\nu_z = 0.497$ MHz and $\nu_r = 0.256$ MHz. One is located at the origin. The other five circulate in the x-y plane. For these trap parameters, the configurations calculated for six, seven, and eight ions all have one ion at the origin and the rest in a ring in the x-y plane. In this case, we assume that there were six ions, because that number gives the best agreement between the observed and calculated ring sizes.

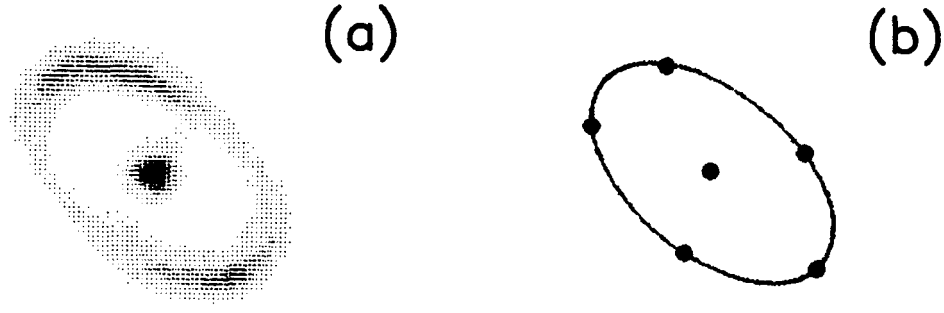

Figure 5: Planar configuration of six ions for $\nu_z = 0.497$ MHz and $\nu_r = 0.256$ MHz. The diameter of the ring is approximately 16 μm. (a) Experimental data. (b) Calculation.

Figure 6 shows six ions for $\nu_z = 0.780$ MHz and $\nu_r = 0.347$ MHz. One is at the origin, and four others lie at the vertices of a pentagon in the x-y plane. The fifth vertex of the pentagon appears to be vacant, but we assume that it is occupied by an ion which does not fluoresce. It may be a heavier isotope of mercury, such as $^{199}Hg^+$, or a molecular ion, such as $HgOH^+$, neither of which would fluoresce. If it had a higher charge-to-mass ratio than $^{198}Hg^+$, it would be more tightly bound to the trap, and would go the center. The additional asymmetry, due to the odd ion, keeps the configuration from rotating.

Figures 7 and 8 show two different configurations of the same nine ions. The secular frequencies for Fig. 7 were $\nu_z = 0.497$ MHz and $\nu_r = 0.256$ MHz; for Fig. 8, they were

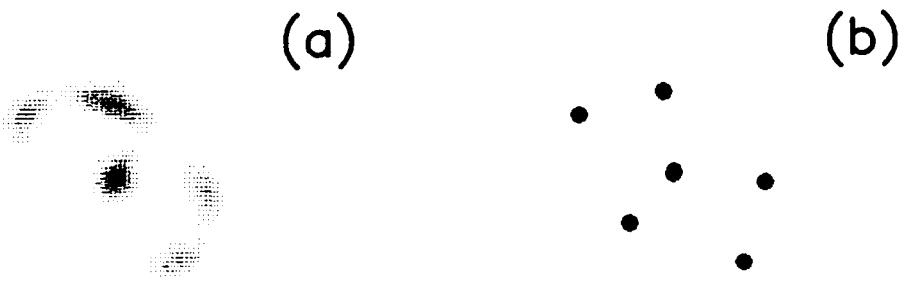

Figure 6: Planar configuration of six ions for $\nu_z = 0.780$ MHz and $\nu_r = 0.347$ MHz. Five ions are presumed to lie at the vertices of a pentagon in the x-y plane, but one does not fluoresce. Another one lies at the origin. (a) Experimental data. (b) Calculation.

$\nu_z = 0.439$ MHz and $\nu_r = 0.304$ MHz. The ions in Fig. 7 lie in the x-y plane. This configuration is the same as the calculated one shown in Fig. 1 of Ref. 3. The outer ring of the experimental image appears to be incomplete in this case because of nonuniform illumination of the cluster by the tightly focused 194 nm beam. In Fig. 8, two ions lie along the z axis, symmetrically above and below the x-y plane. The others form a ring in the x-y plane. The number of ions in Figs. 7 and 8 was determined uniquely from the observed configurations for the two different sets of conditions.

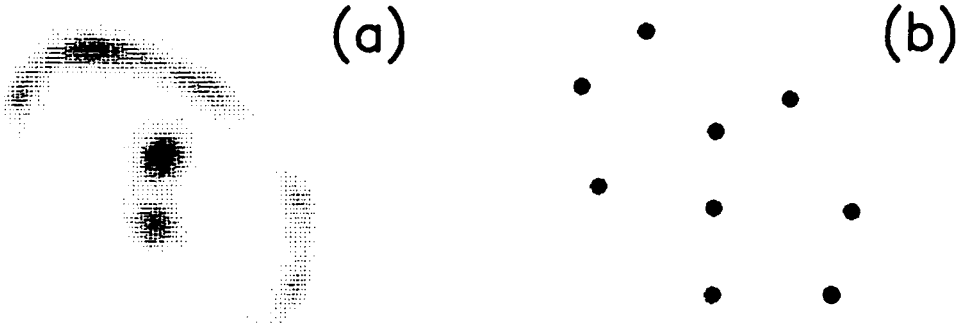

Figure 7: Planar configuration of nine ions for $\nu_z = 0.497$ MHz and $\nu_r = 0.256$ MHz. (a) Experimental data. (b) Calculation.

Figure 9 shows 15 ions for $\nu_z = 0.780$ MHz and $\nu_r = 0.347$ MHz. All of them lie in the x-y plane. Five form a pentagon, and the other ten form the outer ring. The observed pattern is only consistent with the one calculated for 15 ions.

Figure 10 shows 16 ions, for $\nu_z = 0.626$ MHz and $\nu_r = 0.479$ MHz. The large ring of eight ions lies nearly in the x-y plane. Two smaller rings of four ions each are displaced along the z axis, above and below the x-y plane. If another ion is added, at the same trap voltages, then, according to calculations, one ion goes to the center. By using data taken at another set of trap voltages, we could determine the number of ions. The 16 ions lie close to the surface of a spheroid. For larger numbers of ions, one would expect to see a

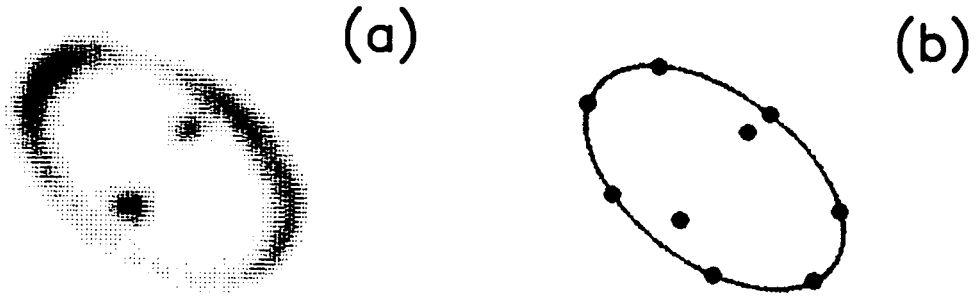

Figure 8: Nonplanar configuration of nine ions for $\nu_z = 0.439$ MHz and $\nu_r = 0.304$ MHz. Seven circulate in the x-y plane. The other two are displaced along the z axis. (a) Experimental data. (b) Calculation.

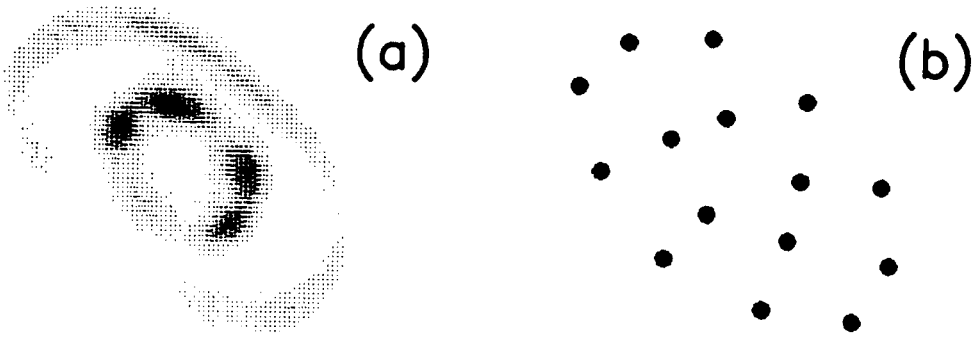

Figure 9: Planar configuration of 15 ions for $\nu_z = 0.780$ MHz and $\nu_r = 0.347$ MHz. (a) Experimental data. (b) Calculation.

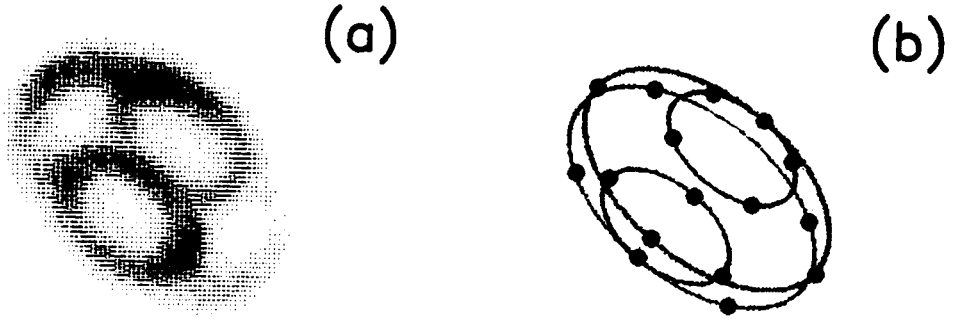

Figure 10: Nonplanar configuration of 16 ions for $\nu_z = 0.626$ MHz and $\nu_r = 0.479$ MHz. (a) Experimental data. (b) Calculation.

series of concentric spheroids like those which have been predicted and observed in Penning traps.[12,25]

VI. Related physical systems

A. Macroscopic particle traps

Perhaps the earliest studies of spatially ordered systems of charged particles in a Paul trap were made by Wuerker, Shelton, and Langmuir about 30 years ago.[24] In these studies, aluminum particles that had diameters of a few micrometers were suspended in a large Paul trap and cooled by collisions with gas molecules.

A similar trap has been built in our laboratory.[10] The inner diameter of the ring was about 2.5 cm. Typical trap parameters were $V_0 \approx 350$ V, $U_0 \approx 0$ V, and $\Omega/2\pi \approx 60$ Hz. Aluminum oxide particles of approximate mass 10^{-9} g and charge approximately 10^5 times the proton charge were trapped and observed to form ordered structures.

B. The Thomson model of the atom

In an early model for the atom, first suggested by Kelvin and later studied in detail by Thomson, electrons were assumed to be embedded in a uniform sphere of positive charge.[26] The potential energy of an electron inside the sphere due to the positive charge is proportional to $x^2 + y^2 + z^2$. Thus, the stable spatial configurations of the electrons in such a model are the same as for ions in a Paul trap with a spherically symmetric effective potential. Thomson's calculations of the minimum-energy configurations, which actually were done in two dimensions, showed patterns of concentric rings. He tabulated the configurations for up to 100 electrons. The 100-electron configuration contains seven rings. For $\nu_z > \nu_r$, the three-dimensional configurations for small numbers of particles are the same as for Thomson's two-dimensional calculations. For example, Thomson's 15-electron configuration has five in the inner ring and ten in the outer ring, like the data of Fig. 9. Thomson's calculations are perhaps the earliest predictions of layered structures in a bound Coulomb system. Such layered structures are predicted to occur in one-, two-, and three-dimensional systems[25] and have been observed in the Penning trap, a three-dimensional system.[12]

Thomson discussed experiments with floating magnets, which he used to verify his calculations of the two-dimensional configurations. For these experiments, equally magnetized needles, oriented in the same way, were pushed through corks and floated on water. An attractive force was produced by a large magnet placed above the surface of the water, the lower pole having the opposite sign to that of the upper poles of the floating magnets.

VII. Discussion

The equilibrium shapes of clusters that contain 16 ions or fewer and the intra-cluster vibrational frequencies can be calculated from the effective potential approximation. Other properties, however, such as the Doppler spectrum or the order-chaos transition, are affected by the micromotion, and require a more complete theoretical treatment.

Experiments with charged micrometer-sized particles in Paul traps might be useful in testing calculations, since they are relatively simple to perform, compared to experiments with ions. Large numbers of particles (on the order of 100) can be cooled and optically observed. The melting and freezing phase transitions have been observed previously.[24] Perhaps further experimental work could reveal details of the transition to chaotic behavior.[8,9] Other kinds of traps, with linear or "racetrack" geometries[27] might be useful in simulating ordered structures in ion storage rings. Such structures have been predicted, but not yet observed.[28]

Acknowledgments

We gratefully acknowledge support from the Air Force Office of Scientific Research and the Office of Naval Research.

References

1. J. Mostowski and M. Gajda, Acta Phys. Pol. **A67**, 783 (1985).
2. E. V. Baklanov and V. P. Chebotayev, Appl. Phys. B **39**, 179 (1986).
3. J. Javanainen, J. Opt. Soc. Am. B **5**, 73 (1988).
4. R. Casdorff and R. Blatt, Appl. Phys. B **45**, 175 (1988).
5. J. D. Prestage, M. J. Djomehri, and L. Maleki, Bull. Am. Phys, Soc. **33**, 914 (1988).
6. F. Diedrich, E. Peik, J. M. Chen, W. Quint, and H. Walther, Phys. Rev. Lett. **59**, 2931 (1987).
7. D. J. Wineland, J. C. Bergquist, W. M. Itano, J. J. Bollinger, and C. H. Manney, Phys. Rev. Lett. **59**, 2935 (1987).
8. J. Hoffnagle, R. G. DeVoe, L. Reyna, and R. G. Brewer, Phys. Rev. Lett. **61**, 255 (1988).
9. R. Blümel, J. M. Chen, E. Peik, W. Quint, W. Schleich, Y. R. Shen, and H. Walther, Nature **334**, 309 (1988).
10. D. J. Wineland, W. M. Itano, J. C. Bergquist, S. L. Gilbert, J. J. Bollinger, and F. Ascarrunz, in *Non-neutral Plasma Physics*, edited by C. W. Roberson and C. F. Driscoll, A. I. P. Conf. Proc. **175**, (Am. Inst. Phys., New York, 1988), p. 93.
11. P. Toschek et al., these Proceedings.
12. S. L. Gilbert, J. J. Bollinger, and D. J. Wineland, Phys. Rev. Lett. **60**, 2022 (1988).
13. W. M. Itano, J. C. Bergquist, R. G. Hulet, and D. J. Wineland, Phys. Rev. Lett. **59**, 2732 (1987).
14. J. C. Bergquist, D. J. Wineland, W. M. Itano, H. Hemmati, H.-U. Daniel, and G. Leuchs, Phys. Rev. Lett. **55**, 1567 (1985).

15. E. C. Beaty J. Appl. Phys. **61**, 2118 (1987).

16. H. Hemmati, J. C. Bergquist, and W. M. Itano, Opt. Lett. **8**, 73 (1983).

17. W. M. Itano, J. C. Bergquist, and D. J. Wineland, Science **237**, 612 (1987); D. J. Wineland and W. M. Itano, Phys. Today **40** No. 6, 34 (1987).

18. H. G. Dehmelt, Bull. Am. Phys. Soc. **20**, 60 (1975).

19. D. J. Wineland and W. M. Itano, Phys. Lett. **82A**, 75 (1981).

20. R. H. Dicke, Phys. Rev. **89**, 472 (1953).

21. D. J. Wineland and W. M. Itano, Phys. Rev. A **20**, 1521 (1979).

22. J. C. Bergquist, W. M. Itano, and D. J. Wineland, Phys. Rev. A **36**, 428 (1987).

23. W. H. Press, B. P. Flannery, S. A. Teukolsky, and W. T. Vetterling, *Numerical Recipes* (Cambridge Univ. Press, London, 1986).

24. R. F. Wuerker, H. Shelton, and R. V. Langmuir, J. Appl. Phys. **30**, 342 (1959).

25. A. Rahman and J. P. Schiffer, Phys. Rev. Lett. **57**, 1133 (1986); D. H. E. Dubin and T. M. O'Neil, *ibid.* **60**, 511 (1988); J. P. Schiffer, *ibid.* **61**, 1843 (1988).

26. J. J. Thomson, Phil. Mag. **7**, 237 (1904); *The Corpuscular Theory of Matter* (Scribner's Sons, New York, 1907).

27. D. A. Church, J. Appl. Phys. **40**, 3127 (1969).

28. J. P. Schiffer and P. Kienle, Z. Phys. A **321**, 181, (1985); J. P. Schiffer and O. Poulsen, Europhys. Lett. **1**, 55 (1986); D. Habs, in *Lecture Notes in Physics 296*, edited by M. Month and S. Turner (Springer-Verlag, Berlin, 1988), p. 310.

OBSERVATION OF CORRELATIONS IN FINITE, STRONGLY COUPLED ION PLASMAS*

J.J. BOLLINGER, S.L. GILBERT, D.J. HEINZEN, W.M. ITANO, and D.J. WINELAND

National Institute of Standards and Technology, 325 Broadway, Boulder, CO 80303

1. INTRODUCTION

We have observed[1] spatial correlations with up to 15 000 Be^+ ions in a Penning trap with a coupling (defined below) of $\Gamma > 100$. These correlations are strongly affected by the boundary conditions and take the form of concentric shells as predicted by computer simulations.[2-4] In this paper we briefly describe the experimental confinement geometry and the method of producing low temperature ions. The relatively large spacings between the ions (~ 20 μm) permit the shells to be directly viewed by imaging the Be^+ laser-induced fluorescence onto a photon-counting camera. Diagnostic techniques capable of measuring the ion diffusion are then discussed. Qualitative observations of the ion diffusion are compared with theoretical predictions.

2. CONFINEMENT GEOMETRY

The Penning trap uses a static, uniform magnetic field and a static, axially symmetric electric field for the confinement of charged particles. The magnetic field, which is directed along the z axis of the trap, provides confinement in the radial direction. The ions are prevented from leaving the trap along the z axis by the electric field. In the work described here, the electric field was provided by three cylindrical electrodes as shown in Fig. 1. The dimensions of the trap electrodes were chosen so that the first anharmonic term (i.e. fourth order term) in the expansion of the trapping potential was zero. Over the region near the trap center, the potential can be expressed (in cylindrical coordinates) as $\Phi \simeq AV_o(2z^2-r^2)$ where $A = 0.146$ cm^{-2}. A background pressure of 10^{-8} Pa($\approx 10^{-10}$ Torr) was maintained by a triode sputter-ion pump. The confinement geometry is similar to that used by the group of the University of California at San Diego (UCSD)[5] with the exception that our trap is smaller than the UCSD traps.

in Strongly Coupled Plasma Physics, ed. by S. Ichimaru, (Elsevier Science Publishers B.V. / Yamada Science Foundation, 1990) p. 177.

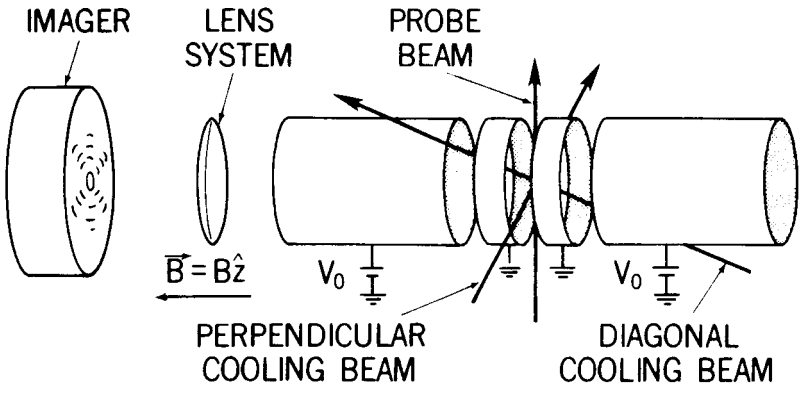

FIGURE 1
Schematic drawing of the trap electrodes, laser beams, and imaging system (not to scale). The overall length of the trap is 10.2 cm. The trap consists of two end cylinders and two electrically connected central cylinders with 2.5 cm inner diameters. Ion clouds are typically less than 1 mm in both diameter and axial length. The diagonal cooling beam crosses the cloud at an angle of 51° with respect to the z axis In the experiments, B = 1.92 T or 0.82 T and V_o ranged between 20 V and 200 V.

The stored ions can be characterized by a thermal distribution where the "parallel" (to the z axis) temperature $T_{\|}$ is approximately equal to the "perpendicular" temperature $T_{\perp}$. This thermal distribution is superimposed on a uniform rotation of the cloud[6-9] at frequency ω which, at the low temperatures of this experiment, is due to the $\vec{E}\times\vec{B}$ drift, where $\vec{E}$ is the electric field due to the trap voltage and the space charge of the ions. In a frame of reference rotating with the ions, the static thermodynamic properties of an ion cloud confined in a Penning trap are identical to those of a one-component plasma (OCP).[7] An OCP consists of a single species of charge embedded in a uniform-density background of opposite charge. For the system of ions in a Penning trap, the trapping fields play the role of the neutralizing background charge. An OCP is characterized by the Coulomb coupling constant,[7,10]

$$\Gamma \equiv q^2/(a_s k_B T),$$

which is a measure of the nearest-neighbor Coulomb energy divided by the thermal energy of a particle. The quantities q and T are the ion charge and temperature. The Wigner-Seitz radius a_s is defined by $4\pi a_s^3 n_0/3=1$, where $-qn_0$ is the charge density of the neutralizing background. In the Penning trap the

background density n_0 depends on the rotation frequency ω and the cyclotron frequency Ω and is given by[6-9]

$$n_0 = m\omega(\Omega-\omega)/(2\pi q^2). \quad (1)$$

3. LASER COOLING AND COMPRESSION

The ion density that can be achieved in a Penning trap is limited by the magnetic field strength that is available in the laboratory. Consequently to obtain large values of Γ and therefore strong couplings, a technique to obtain low ion temperatures is necessary. In our work, radiation pressure from lasers is used to reduce the temperature of the stored ions to less than 10 mK. This technique, known as laser cooling,[11-13] uses the resonant scattering of laser light by atomic particles. The laser is tuned to the red, or low-frequency side of the atomic "cooling transition" (typically an electric dipole transition like the D lines in sodium). Ions with a velocity component opposite to the laser beam propagation ($\vec{k}\cdot\vec{v} < 0$) will be Doppler shifted into resonance and absorb photons at a relatively high rate. Here, $\vec{k}$ is the photon wave vector ($|\vec{k}|=2\pi/\lambda$, where λ is the wavelength of the cooling radiation). For the opposite case ($\vec{k}\cdot\vec{v} > 0$), the ions will be Doppler shifted away from the resonance and the absorption rate will decrease. When an ion absorbs a photon, its velocity is changed by an amount $\Delta\vec{v} = \hbar\vec{k}/m$ due to momentum conservation. Here $\Delta\vec{v}$ is the change in the ion's velocity, m is the mass of the ion, and $2\pi\hbar$ is Planck's constant. The ion spontaneously reemits the photon symmetrically. In particular, when averaged over many scattering events, the reemission does not change the momentum of the ion. The net effect is that for each photon scattering event, the ion's average velocity is reduced by $\hbar\vec{k}/m$. To cool an atom from 300 K to millikelvin temperatures takes typically 10^4 scattering events but, since scatter rates can be 10^8/s, the cooling can be rapid.

In our work with Be^+, the $2s\ ^2S_{1/2} \rightarrow 2p\ ^2P_{3/2}$ "D_2" transition was used as the cooling transition as indicated in Fig. 2. Cooling laser beams were directed both perpendicularly and at an angle with respect to the magnetic field as indicated in Fig. 1. This enabled us to control the cloud size and obtain the lowest possible temperatures.[14,15] The 313 nm radiation required to drive this transition was obtained by frequency doubling the output of a continuous wave, narrow band (3 MHz) dye laser. The 313 nm power was typically 50 μW. The theoretical cooling limit, due to photon recoil effects,[11-13] is given by a temperature equal to $\hbar\gamma/(2k_B)$ where γ is the radiative linewidth of the atomic transition in angular frequency units. For the Be^+ cooling transition ($\gamma = 2\pi \times 19.4$ MHz), the theoretical minimum temperature is 0.5 mK.

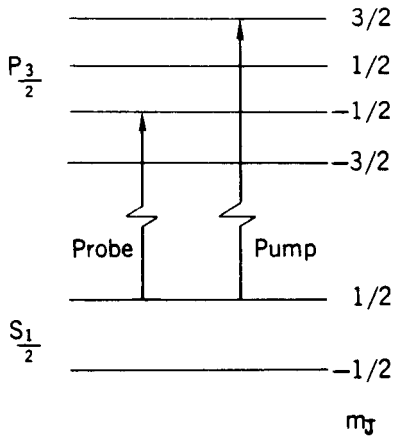

FIGURE 2

Energy level structure of the $^9Be^+$ $^2S_{1/2}$ ground state and the first excited $^2P_{3/2}$ state. The magnetic field splits each state into its m_J sublevels. The laser cooling (pump) and depopulation (probe) transitions are shown.

Laser scattering can also be used to change the angular momentum and compress the stored ion plasma.[8,9] The z component of the canonical angular momentum for an individual ion in the plasma is

$$\ell_z = mv_\theta r + \frac{qBr^2}{2c} . \tag{2}$$

The two terms in Eq. (2) are the ion's mechanical angular momentum and the field angular momentum. The total z component of the angular momentum of the plasma is

$$L_z = m(\Omega/2-\omega)N\langle r^2\rangle. \tag{3}$$

Here N is the total number of ions and $\langle r^2\rangle$ is the mean-squared radius of the plasma. For most of the work described in this paper $\omega \ll \Omega$ and

$$L_z \approx \frac{m\Omega N}{2}\langle r^2\rangle > 0. \tag{4}$$

Therefore the total angular momentum is dominated by the field angular momentum. Suppose the cooling laser beam is directed normal to the z axis but at the side of the plasma which is receding from the laser beam due to the plasma rotation. Because the rotation of the positive ions is in the $-\hat{\theta}$ direction, the torque of the laser on the ions will also be negative. Consequently, angular momentum is removed from the plasma and according to Eq. (4) the radius of the plasma must decrease. In general, the plasma is compressed until the torque due to the cooling laser is balanced by another

external torque. As the radius decreases, the density of the plasma increases.

Even in the absence of external torques, there is a limit to how far the plasma can be compressed. From Eq. (1), the maximum density, known as the Brillouin density, occurs when the rotation frequency $\omega = \Omega/2$. The Brillouin density is given by

$$n_{max} = \frac{m\Omega^2}{8\pi q^2} .$$

We have recently been able to achieve densities at or near the Brillouin limit. In fact we have also been able to achieve rotation frequencies $\omega > \Omega/2$ where according to Eq. (1) the ion density decreases. In these experiments, the temperature was not determined. At the magnetic field of 1.92 T used in some of the work discussed here, the Brillouin density is 1.1×10^9 cm^{-3}. This density with the theoretical minimum 0.5 mK temperature, results in a coupling $\Gamma \sim 5500$. For the work reported here, we have been able to obtain ion temperatures in the 1-10 mK range with densities 5-10 times less than the Brillouin density. This results in couplings Γ of a few hundred.

We measured[8,14,15] the ion density and temperature by using a second laser, called the probe laser, to drive the "depopulation" transition as indicated in Fig. 2. The cooling laser optically pumps the ions into the $^2S_{1/2}$ m_J=+1/2 state.[8] The resonance fluorescence (i.e. laser light scattered by the ions) from this transition is used as a measure of the ion population in the m_J=+1/2 state. The probe laser drives some of the ion population from the $^2S_{1/2}$ m_J=+1/2 state to the $^2P_{3/2}$ m_J=-1/2 state where the ions decay with 2/3 probability to the $^2S_{1/2}$ m_J=-1/2 state. This causes a decrease in the observed ion fluorescence because the $^2S_{1/2}$ m_J=-1/2 state is a "dark" state a (state which does not fluoresce in the cooling laser). The ion temperature is obtained from the Doppler broadening of the resonance lineshape when the probe laser is scanned through the depopulation transition. The ion rotation frequency is measured from the shift in the depopulation transition frequency as the probe laser is moved from the side of the plasma rotating into the laser beam to the side of the plasma rotating with the laser beam. From the measured rotation frequency, the density is calculated from Eq. (1). The measured density and temperature is used to calculate the coupling Γ.

4. OBSERVED CORRELATIONS

With measured couplings $\Gamma > 100$, we anticipate that the ions will exhibit correlated behavior. If the number of stored ions is large enough for

infinite volume behavior, the ions may be forming a bcc lattice.[10] Until now we have cooled and looked for spatial correlations with up to 15 000 Be^+ ions stored in the Penning trap of Fig. 1. A currently unanswered question is how many stored ions are required for infinite volume behavior, i.e. the appearance of a bcc lattice for $\Gamma > 178$. For a finite plasma consisting of a hundred to a few thousand ions, the boundary conditions are predicted to have a significant effect on the plasma state. Simulations involving these numbers of ions in a spherical trap potential predict that the ion cloud will separate into concentric spherical shells.[2-4] Instead of a sharp phase transition, the system is expected to evolve gradually from a liquid state characterized by short-range order and diffusion in all directions, to a state where there is diffusion within a shell but no diffusion between the shells (liquid within a shell, solid-like in the radial direction), and ultimately to an overall solid-like state.[4] These conclusions should apply to a nonspherical trap potential as well if the spherical shells are replaced with shells approximating spheroids. Independent theoretical investigations[16,17] of the nonspherical case support this conjecture.

We have observed shell structures with $^9Be^+$ ions stored in a Penning trap by imaging the laser induced fluorescence from the cooling transition. This technique is sensitive enough to observe the structures formed with only a few ions in a trap.[18-21] About 0.04% of the 313-nm fluorescence from the decay of the $^2P_{3/2}$ state was focused by f/10 optics onto the photocathode of a resistive-anode photon-counting imaging tube (see Fig. 1). The imager was located along the z axis, about 1 m from the ions. The imaging optics was composed of a three-stage lens system with overall magnification of 27 and a resolution (FWHM) of about 5 μm (specifically, the image of a point source when referred to the position of the ions was approximately 5 μm in diameter). Counting rates ranged from 2 to 15 kHz. Positions of the photons arriving at the imager were displayed in real time on an oscilloscope while being integrated by a computer. The probe laser could be tuned to the same transition as the cooling laser and was directed through the cloud perpendicularly to the magnetic field. With the probe laser turned on continuously, the cooling laser could be chopped at 2 kHz (50% duty cycle) and the image signal integrated only when the cooling laser was off. Different portions of the cloud could then be imaged by the translation of the probe beam, in a calibrated fashion, either parallel or perpendicular to the z axis. Images were also obtained from the ion fluorescence of all three laser beams.

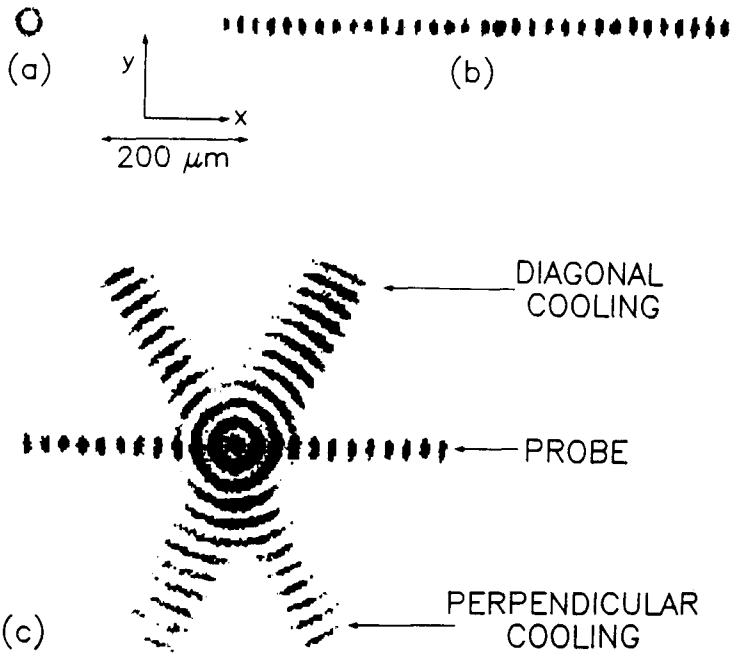

FIGURE 3
Images of shell structures obtained with B = 1.92 T. (a) A single shell in a cloud containing approximately 20 ions. Trap voltage V_0 = 14 V and cloud aspect ratio a_r (axial length/diameter) ≃ 6.5. This image was obtained from the ion fluorescence of the perpendicular and diagonal cooling beams. (b) Sixteen shells (probe-beam ion fluorescence only) in a cloud containing about 15 000 ions with V_0 = 100 V and a_r ≃ 0.8. (c) Eleven shells plus a center column in the same cloud as (b), with V_0 = 28 V and a_r ≃ 2.4. This image shows the ion fluorescence from all three laser beams. Integration times were about 100 s for all images.

We have observed shell structure in clouds containing as few as 20 ions (one shell) and as many as 15 000 ions (sixteen shells). Images covering this range are shown in Fig. 3. Even with 15 000 ions in the trap there is no evidence for infinite volume behavior. We measured the coupling constant Γ for several clouds containing about 1000 ions. Drift in the system parameters was checked by verifying that the same images were obtained before and after the cloud rotation frequency and ion temperatures were measured. Figure 4 shows examples of shell structures at two different values of Γ. The first image is an example of high coupling (Γ ≈ 180) and shows very good shell definition in an intensity plot across the cloud. The second image is an example of lower coupling (Γ ≈ 50) and was obtained with cooling only perpendicular to the magnetic field. Variations in peak intensities equidistant from the z axis are due to signal-to-noise limitations and imperfect alignment between the imager x axis and the probe beam.

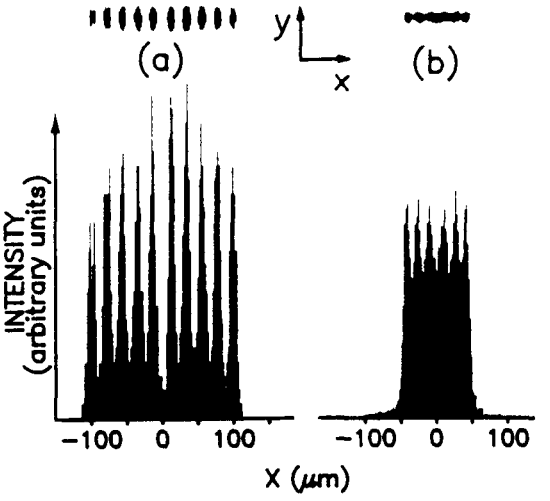

FIGURE 4
Intensity plots along the imager x axis (parallel to the probe beam) through the center of the ion cloud with corresponding images (above). (a) $\Gamma = 180^{+90}_{-70}$ ($T = 6\ ^{+4}_{-2}$ mK, $n_0 \simeq 7\times10^7$ ions cm^{-3}). Cloud aspect ratio $a_r \simeq 3.5$. (b) $\Gamma = 50^{+30}_{-20}$ ($T = 33^{+17}_{-13}$ mK, $n_0 = 2\times10^8$ ions cm^{-3}), $a_r \simeq 5$. The clouds contained about 1000 ions and B = 1.92 T in both cases.

We obtained three-dimensional information on the shell structure by taking probe images at different z positions; two types of shell structure were present under different circumstances. The first type showed shell curvature near the ends of the cloud, indicating that the shells may have been closed spheroids. Shell closure was difficult to verify because of a lack of sharp images near the ends of the cloud where the curvature was greatest. This may have been due to the averaging of the shells over the axial width of the probe beam. In the other type of shell structure, it was clear that the shells were concentric cylinders with progressively longer cylinders near the center. An example of these data is shown in Fig. 5. Other evidence for cylindrical shells was obtained from the observation that shells in the diagonal-beam images occurred at the same cylindrical radii as those from the perpendicular beams. This can be seen in the three-beam images such as that shown in Fig. 3(c). Systematic causes of these two different shell configurations have not yet been identified.

One comparison which can be made between the theoretical calculations and our experimental results is the relationship between the number of shells and the number of ions, N, in a cloud. For a spherical cloud, two independent approaches[2,22] estimate $(N/4)^{1/3}$ and $(3N/4\pi)^{1/3}$ shells. For the nearly spherical cloud of Fig. 3(b) ($N \simeq 15\ 000$), these formulae predict 15.5 and

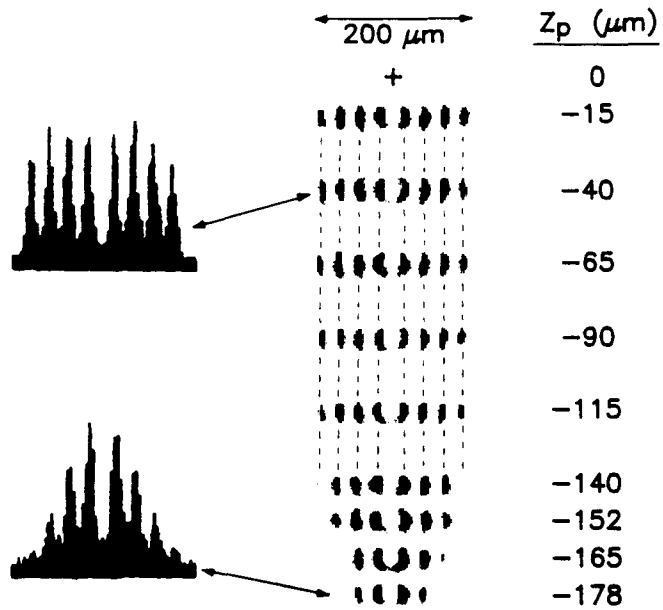

FIGURE 5
Data showing evidence for concentric cylindrical shells. On the right is a series of images obtained with the probe beam for different z positions z_p of the probe beam (lower half of the cloud only). Intensity plots for z_p = -40 μm and z_p = -178 μm are shown on the left. The cloud aspect ratio a_r was about 1.9 and B ≃ 1.92 T.

15.3 shells and we measure 16. At present, it is difficult to make further quantitative comparisons between our data and the theoretical calculations. For example, there is substantial uncertainty in our measurement of Γ due to uncertainty in the temperature measurement. Our data do agree qualitatively with the simulations with the exception, in some cases, of the presence of an open-cylinder shell structure as opposed to the predicted closed spheroids. Shear (that is, different rotation frequencies) between the shells could possibly account for this discrepancy. In our experiment, shear could be caused by differential laser torque or the presence of impurity ions.[8] For the data here, we have determined that the rotation frequency does not vary by more than 30% across the cloud.

5. ION DIFFUSION

The probe laser can be used to optically tag ions and observe the ion diffusion.[14] With the probe laser tuned to the depopulation transition (see Fig. 2), ions in the path of the probe laser beam are put into the "dark" m_J= -1/2 ground state. These ions will not fluoresce when they pass through the cooling laser until they are optically pumped back into the m_J=+1/2 ground state. This repumping time is typically on the order of 1.0 s. By pulsing the probe laser on and measuring the length of time it takes the dark ions to

diffuse from the probe beam to the cooling laser beam, it should be possible to measure the ion diffusion. By directing the probe laser beam to the radial edge of the plasma so that only the outer shell is intersected by the probe beam, it should be possible to observe the diffusion of ions in the radial direction or between shells. By directing the probe beam to the axial edge of the cloud it should be possible to observe the diffusion of the ions in the axial direction or within a shell. According to the simulations of Dubin and O'Neil,[4] for intermediate values of the coupling ($\Gamma \sim 100$) we expect to observe that the diffusion between shells is much slower than the ion diffusion within a shell (solid-like behavior between shells, liquid-like within a shell). As the temperature is lowered and the coupling Γ increases, the diffusion within a shell should smoothly slow down. At high enough couplings (i.e. $\Gamma > 400$) the diffusion should be very slow both between and within shells, indicative of solid-like behavior.

We have qualitatively observed the ion diffusion at intermediate values of Γ ($\Gamma \sim 100$-200). We observed that the diffusion of ions between shells is slow compared to the optical repumping time (~ 1 s) but that the diffusion within a shell (i.e. from the axial end of a shell to the $z = 0$ plane) is fast compared to this repumping time. We have also observed states with higher couplings (the couplings Γ were not measured) where the diffusion of ions both between and within a shell was slow compared to the optical repumping time. In the future we plan to make quantitative measurements of the ion diffusion.

ACKNOWLEDGEMENT

We gratefully acknowledge the support of the U.S. Office of Naval Research and the Air Force Office of Scientific Research. We thank M. Raizen and F. Moore for carefully reading the manuscript.

REFERENCES

1) S.L. Gilbert, J.J. Bollinger, and D.J. Wineland, Phys. Rev. Lett. 60 (1988) 2022.

2) A. Rahman and J.P. Schiffer, Phys. Rev. Lett. 57 (1986) 1133; J.P. Schiffer, Phys. Rev. Lett. 61 (1988) 1843.

3) H. Totsuji, in Strongly Coupled Plasma Physics, eds. F.J. Rogers and H.E. DeWitt (Plenum, New York, 1987) pp. 19-33.

4) D. Dubin and T. O'Neil, Phys. Rev. Lett. 60 (1988) 511.

5) C.F. Driscoll, J.H. Malmberg, and K.S. Fine, Phys. Rev. Lett. 60 (1988) 1290; J.H. Malmberg and J.S. deGrassie, Phys. Rev. Lett. 35, 577 (1975).

6) T.M. O'Neil, in Non-Neutral Plasma Physics, eds. C.W. Roberson and C.F. Driscoll (American Institute of Physics, New York, 1988) pp. 1-25.

7) J.H. Malmberg and T.M. O'Neil, Phys. Rev. Lett. 39 (1977) 1333.

8) L.R. Brewer, J.D. Prestage, J.J. Bollinger, W.M. Itano, D.J. Larson, and D.J. Wineland, Phys. Rev. A38 (1988) 859.

9) D.J. Wineland, J.J. Bollinger, W.M. Itano, and J.D. Prestage J. Opt. Soc. Am. B2 (1985) 1721.

10) S. Ichimaru, H. Iyetomi, and S. Tanaka, Phys. Rep. 149 (1987) 91 and references therein.

11) D.J. Wineland and W.M. Itano, Phys. Rev. A20 (1979) 1521.

12) W.M. Itano and D.J. Wineland, Phys. Rev. A25 (1982) 35.

13) D.J. Wineland and W.M. Itano, Phys. Today 40(6) (1987) 34; S. Stenholm, Rev. Mod. Phys. 58 (1986) 699.

14) L.R. Brewer, J.D. Prestage, J.J. Bollinger, and D.J. Wineland, in Ref. 3), pp. 53-64.

15) J.J. Bollinger and D.J. Wineland, Phys. Rev. Lett. 53 (1984) 348.

16) J.P. Schiffer, Argonne Natl. Lab., Argonne, IL, private communication.

17) D.H.E. Dubin, Dept. of Physics, UCSD, La Jolla, CA, private communication.

18) F. Diedrich, E. Peik, J.M. Chen, W. Quint, and H. Walther, Phys. Rev. Lett. 59 (1987) 2931.

19) D.J. Wineland, J.C. Bergquist, W.M. Itano, J.J. Bollinger, and C.H. Manney, Phys. Rev. Lett. 59 (1987) 2935; D.J. Wineland, W.M. Itano, J.C. Bergquist, S.L. Gilbert, J.J. Bollinger, and F. Ascarrunz, in Ref. 6), pp. 93-108.

20) J. Hoffnagle, R.G. DeVoe, L. Reyna, R.G. Brewer, Phys. Rev. Lett. 61 (1988) 255.

21) Th. Sauter, H. Gilhaus, I. Siemers, R. Blatt, W. Neuhauser, P.E. Toschek, Z. Phys. D10 (1988) 153.

22) D.H.E. Dubin, Phys. Rev. A40 (1988) 1140.

Microplasmas

Two or more atoms—stripped of their outer electrons, trapped by electromagnetic fields and cooled to temperatures near absolute zero—array themselves in structures that behave like both liquids and solids

by John J. Bollinger and David J. Wineland

In 1973 a container whose "walls" were built from electric and magnetic fields trapped a single electron. Then in 1980 a similar device confined a single atom. The technology enabled physicists to measure the properties of electrons and atoms in unprecedented detail. The workers who initiated these experiments, Hans G. Dehmelt of the University of Washington and Wolfgang Paul of the University of Bonn, shared the 1989 Nobel prize in physics. Employing the same control over the temperature and position of atoms, we and our colleagues are investigating fundamental theories of atomic structure by trapping as many as 15,000 ions (atoms stripped of one or more of their electrons). The result is called a microplasma, by extension from the large groups of ions and electrons known as plasmas.

A microplasma is made by first applying electromagnetic fields to confine the ions to a specified region of space. A technique called laser cooling can then cool the trapped ions to temperatures of less than a hundredth of a kelvin. Because microplasmas can be built up practically one ion at a time, they provide an excellent opportunity to explore mesoscopic systems, that is, collections of ions too small to behave like a familiar, macroscopic system and yet too complex to be identified with the behavior of a single ion. Furthermore, microplasmas can serve as models for the dense plasmas in stellar objects.

Like the atoms in liquids, the ions in some cold microplasmas can diffuse through a somewhat ordered state. In other cases, the ions can resemble the atoms in solids, diffusing very slowly through a crystal lattice. Yet the nature of microplasmas is quite different from that of conventional liquids and solids. Whereas common liquids and solids have densities of about 10^{23} atoms per cubic centimeter, microplasmas have concentrations of about 10^{8} ions per cubic centimeter. Consequently, the average distance that separates ions in a microplasma is about 100,000 times greater than the distance between atoms in common liquids or solids. Furthermore, whereas internal attractive forces between the atoms hold a conventional liquid or solid together, external electric and magnetic fields hold the trapped ion microplasmas together. Indeed, the ions, which all have the same charge, actually repel each other and tend to disperse the microplasma.

JOHN J. BOLLINGER and DAVID J. WINELAND are physicists at the National Institute of Standards and Technology in Boulder, Colo. Their work on microplasmas grew out of efforts to develop techniques for high-resolution spectroscopy of stored ions. Bollinger received a B.A. in physics from Cornell University and a Ph.D. from Harvard University in 1981. He enjoys playing volleyball and hiking in the Rocky Mountains. Wineland earned a B.A. in physics from the University of California, Berkeley, and a Ph.D. from Harvard University in 1970. He was a research associate at the University of Washington and joined the Institute in 1975. An avid bicyclist, Wineland "plans to race in the Tour de France in his next life."

The first investigations of these cold plasmas began more than a decade ago. In 1977 John H. Malmberg and Thomas M. O'Neil of the University of California at San Diego suggested that a collection of electrons or ions in an electromagnetic trap would resemble a type of matter known as a one-component plasma. In such a plasma, a rigid, uniform background of charge confines mobile, identical particles of opposite charge. The specific heat, melting point and other thermodynamic properties of a one-component plasma depend greatly on the density and the temperature of the mobile particles.

A single dimensionless parameter called the coupling, which can be derived from particle density and temperature, describes the thermodynamic properties of a one-component plasma by providing a measure of how strongly neighboring ions interact. The coupling is defined as the Coulomb potential energy between nearest neighboring ions divided by the kinetic energy of the ions. The Coulomb potential energy depends on both the average distance between the ions (a function of density) and the charge of the ion species. The kinetic energy is simply the temperature multiplied by a physical constant known as the Boltzmann constant.

When the Coulomb potential energy is less than the kinetic energy—that is, when the coupling is less than one—the one-component plasma should have no obvious structure and should behave like a gas. But a one-component plasma whose coupling is greater than one should show some spatial order. In such strongly coupled one-component plasmas, the ions should stay away from each other because the repulsive Coulomb forces are greater than the thermal forces. At couplings of two or more, a plasma should exhibit liquid behavior. At couplings near 180, a one-component plasma should change from a liquid to a solid phase, in which the ions are arranged in a body-centered cubic crystal.

These theoretical predictions for one-component plasmas pertain to "infinite" systems, ones whose macroscopic properties do not change when a large number of ions are added or subtracted. In addition, the predictions are valid as long as the ions in the plasma behave classically, that is, as long as the effects of quantum mechanics can be neglected. Under conditions of high density and low temperature, quantum mechanics can be important, as Eugene P. Wigner first investigated in 1934.

Examples of strongly coupled one-component plasmas can be found in

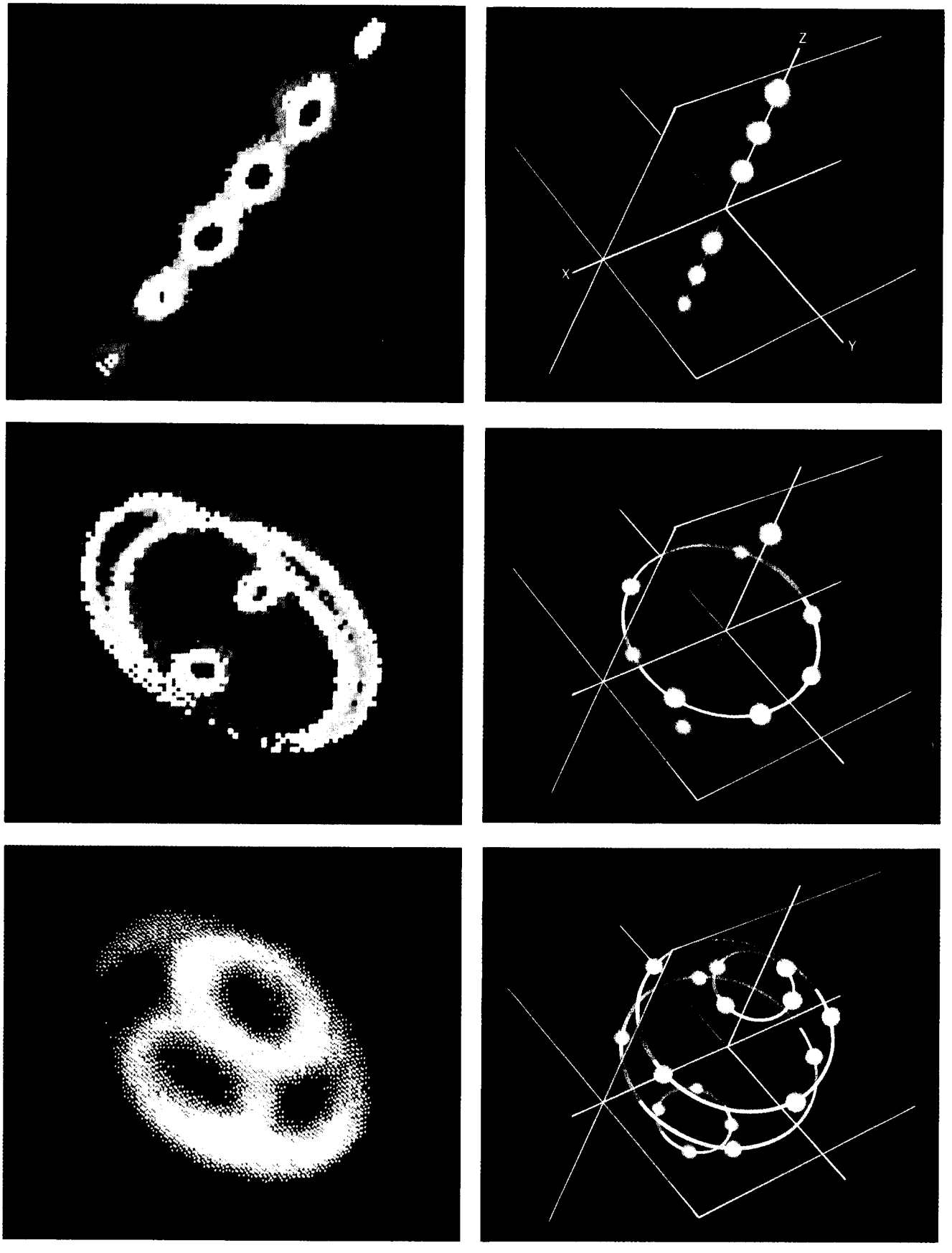

MICROPLASMAS composed of six, nine and 16 ions of mercury (*top, middle and bottom, respectively*) are held in a Paul trap. A structural diagram is shown next to each photograph. The diagrams are based on the predictions by Wayne Itano of the National Institute of Standards and Technology. Although the ions keep the same relative positions, they orbit around the *z* axis.

the universe, especially in dense stellar objects. The outer crust of a neutron star (the collapsed remnant of a large star that has exploded as a supernova) is expected to contain from 10^{26} to 10^{29} iron atoms per cubic centimeter—a density at least 1,000 times greater than anything on or within the earth. How does a strongly coupled one-component plasma form in this environment? The tremendous pressure in the star's crust breaks down the iron atoms into iron nuclei and free electrons. The iron nuclei behave classically: one positively charged nucleus simply repels its identical neighbors. On the other hand, the free electrons obey the laws of quantum mechanics, specifically the exclusion principle: every electron must occupy a different energy state. Because of the high density of electrons in a neutron star, the electrons are forced into very high energy states. The electrons are therefore unaffected by the motion of the much lower-energy iron nuclei. Hence, they form a uniform density background of negative charge. The mobile nuclei in the electron background form a one-component plasma whose coupling is estimated to range from 10 to 1,000.

To learn more about such natural plasmas, workers have attempted to generate a strongly coupled one-component plasma in the laboratory. Because the thermodynamic properties of a one-component plasma depend only on the coupling, a one-component plasma that is cool and diffuse can have the same properties as a one-component plasma that is hot and dense. Yet until recently one-component plasmas in the laboratory have not been dense enough or cool enough to become strongly coupled. In the outer crust of a neutron star, for example, the density of iron nuclei is roughly 20 orders of magnitude greater than the typical density of ions in the trap. To create a one-component plasma whose coupling matches that of a neutron star, workers must cool trapped, charged ions to a temperature that is roughly nine orders of magnitude less than that of the star. Attaining a high enough coupling demands temperatures well below one *kelvin*.

In addition to having a coupling equal to that of the natural system, the laboratory one-component plasma must include enough ions to reveal the behavior that is characteristic of the many ions in the natural system. Physicists have recently taken the first step and are now working on achieving the second.

Both efforts involve the technology of electromagnetic traps. The technology is roughly 30 years old: in 1959 Ralph F. Wuerker, Haywood Shelton and Robert V. Langmuir in the laboratory at Thompson Ramo-Wooldridge, Inc., in California tested an electromagnetic trap that confines charged metallic particles. This beautiful experiment demonstrates the effects caused by the strong coupling of the particles. At about the same time, workers began trapping electrons and ions [see "The Isolated Electron," by Philip Ekstrom and David Wineland; SCIENTIFIC AMERICAN, August, 1980].

In principle an electromagnetic trap can be nothing more than a sphere uniformly filled with negative charge. When a positively charged particle is released within the sphere, it is pulled toward the sphere's center by the uniformly distributed negative charge. Overshooting the center, the positive particle experiences a "restoring" force that is proportional to its distance from the center and eventually pulls it back toward the center again. As long as the particle is free to move through the sphere, it will oscillate about the center. If the positive particle is cooled gradually, however—that is, if its kinetic energy is decreased—it will oscillate over an ever smaller distance until it settles in the center.

Practical devices can approximate this ideal trap. Two types of electromagnetic traps in particular—the Paul trap and the Penning trap—can produce strongly coupled one-component plasmas.

The Paul trap consists of three metallic electrodes: a ring and two end caps [*see illustration on opposite page*]. The ring is wired to a generator whose voltage fluctuates sinusoidally at the so-called driving frequency. The electrodes are supported within a vacuum chamber to ensure that air molecules do not collide with the ions.

How does the Paul trap confine ions? The sinusoidal ring voltage produces a time-varying electric field between the ring and the end caps. The direction of the field alternates: half the time the ion is pushed toward the ring and pulled away from the end caps, and half the time the ion is pulled away from the ring and pushed toward the end caps. The ion wiggles sinusoidally at the driving frequency.

Because the driving force varies sinusoidally over time, one might expect the net force on the ion to be zero. In other words, one might think that the ion would move back and forth under the influence of the oscillating electric field but that the center of its oscillation would remain fixed over time. What, then, drives the ion toward the center of the trap?

The answer stems from the fact that because of the shape of the electrodes, the electric field is weaker at the center of the trap than it is near the electrodes. By considering a special case, one can gain a basic idea of how the spatial variation in the field affects an ion. Suppose that for a time the forced sinusoidal motion of an ion is centered closer to the top end cap than to the bottom end cap. When the ion is at the top of its oscillation, it encounters a strong force toward the center of the trap. When it is at the bottom of its oscillation, the force is toward the top end cap but is somewhat weaker. The ion therefore experiences a net force toward the center of the trap—the so-called ponderomotive force.

In the same way, the ion will experience a ponderomotive force that tends to drive it toward the center of the trap if it oscillates below the center or to either side. In the vertical direction the ponderomotive force is called the axial force; in the lateral direction it is called the radial force.

At all times, then, an ion in the trap experiences a driving force and a ponderomotive force. It turns out that the axial ponderomotive force is greater than the radial ponderomotive force. An ion therefore oscillates with three characteristic frequencies: driving, radial and axial. The trap is usually designed so that the radial and axial ponderomotive frequencies are about 10 times lower than the driving frequency. Hence, the motion caused by the driving force is a small, fast wiggle superposed on a large, slow oscillation about the center of the trap that is caused by the ponderomotive force.

If one disregards the smaller, faster oscillation caused by the driving force, an ion in the Paul trap moves in the same way it would inside a negatively charged sphere. Because the ponderomotive force differs in the axial direction, however, it is more appropriate to think of the Paul trap as a spheroid that is oblate (pancake-shaped) or prolate (cigar-shaped). To control the shape of the spheroid and the combined forces on the ions, one can apply an additional constant voltage between the ring and the end caps. When the overall radial force is greater than the axial force, the trap acts as a prolate spheroid. Conversely, when the radial force is less than the axial force, then the trap acts as an oblate spher-

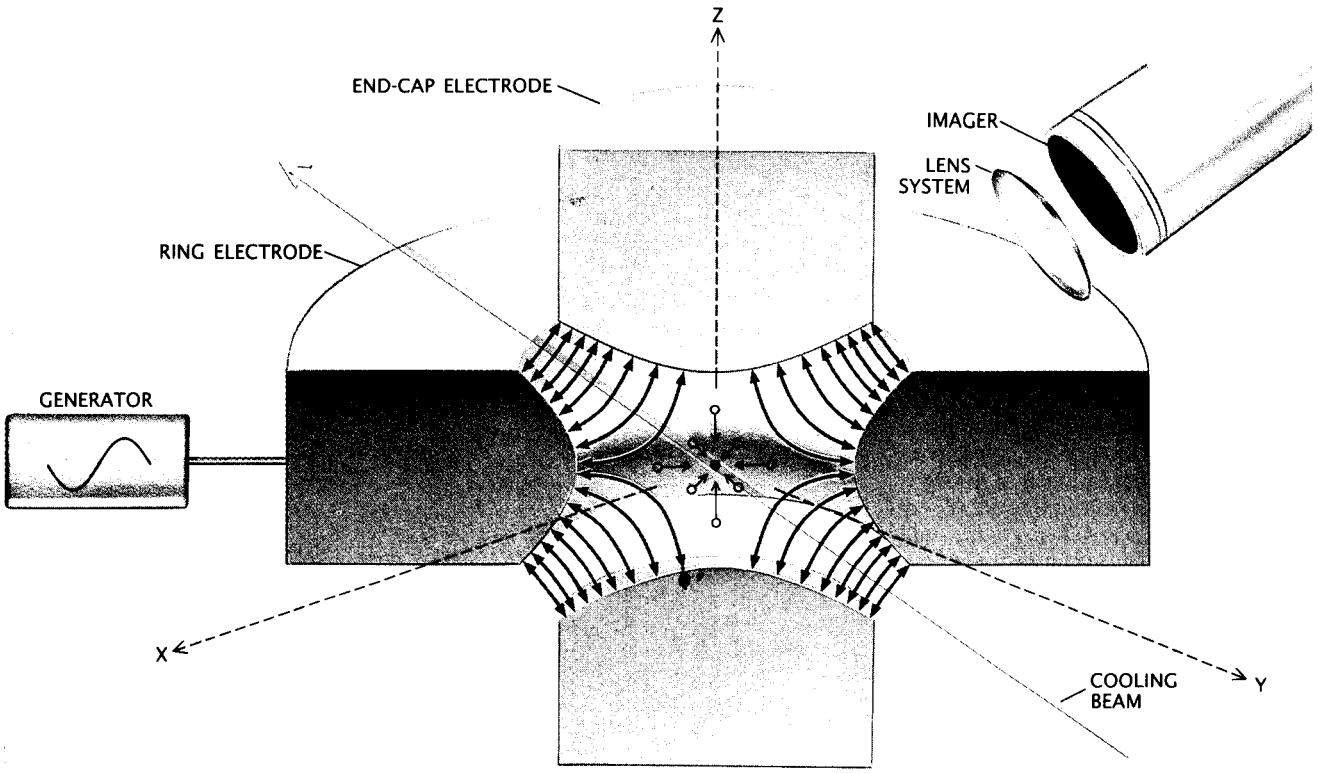

PAUL TRAP creates a time-varying electric field (*red lines*) between the electrodes. As a generator applies a changing voltage to the ring, the electric field changes strength and direction, but its shape stays constant. The resulting ponderomotive forces (*black arrows*) confine charged particles. A laser beam directed at the trap's center cools and probes the ions.

oid. Thus, the Paul trap can both confine the ions in the center and orient the collection in the axial or radial direction.

In 1987, working at the National Institute of Standards and Technology with James C. Bergquist, Wayne M. Itano and Charles H. Manney, we used a Paul trap to observe strongly coupled microplasmas of mercury ions. At the same time, groups led by Herbert Walther and Frank Diedrich of the Max Planck Institute for Quantum Optics in Garching, by Peter E. Toschek of the University of Hamburg and by Richard G. Brewer of the IBM Almaden Research Center in San Jose, Calif., were conducting similar experiments on various ion species.

At the start of our experiment, a small amount of mercury vapor was allowed to leak into the vacuum system containing the Paul trap. As the mercury atoms passed through the trap, they were bombarded with a beam of electrons. The electrons in the beam had just enough energy to knock a single electron out of any mercury atom they struck, thereby ionizing the atom.

To cool the ions, we relied on the technique of laser cooling [see "Cooling and Trapping Atoms," by William D. Phillips and Harold J. Metcalf; SCIENTIFIC AMERICAN, March, 1987]. We generated a laser beam at a frequency slightly below a frequency that the ions could easily absorb. The ions traveling toward the laser source, however, "saw" the frequency as being slightly increased because of the Doppler effect. These ions absorbed the light strongly and slowed down. The ions traveling away from the source encountered the light at a lowered frequency; as a result, they absorbed the light weakly and did not speed up much. Overall the average motion of the ions was reduced: the ions were cooled.

To observe the individual mercury ions and their spatial structures, we illuminated them with ultraviolet light, which mercury ions scatter strongly. An ultraviolet video camera recorded up to 100,000 photons of ultraviolet light per second and thereby generated a motion picture of the trapped ions. The camera could resolve details as small as one micron (one millionth of a meter).

At first we worked with only one mercury ion in the trap and cooled it to millikelvin temperatures. The ponderomotive force confined the ion to the center of the trap. When we allowed two ions into the trap, we discovered two possible configurations. If the radial ponderomotive force was stronger than the axial force, the two ions lined up in the axial direction, so that they were equidistant from the trap center. Conversely, if the radial ponderomotive force was weaker than the axial force, the ions lined up in the radial plane equidistant from the trap center. As we added more ions to the trap, our intuition about the locations of the ions became questionable. But, with the assistance of a computer to keep track of the many forces and ions, Itano simulated various conditions in the trap and accurately predicted the resulting configurations of ions.

By confining ions, we confirmed that a Paul trap could support a one-component plasma. Although the ions were strongly coupled, as the observed spatial structures demonstrated, we needed to calculate the coupling from measurements of density and temperature. We could easily determine the density of the ions from images, but we had to measure temperature indirectly. We observed (as have many other groups in other experiments) that the motion of the ions modified the absorption

spectrum associated with the ions. (The absorption spectrum of an atom or molecule reveals the frequencies of radiation absorbed most strongly by the atom or molecule.)

A collection of absolutely stationary ions would have a very sharp absorption spectrum, indicating absorption only at well-defined frequencies. On the other hand, if the ions moved around to some degree, the absorption spectrum would be blurred. The blurring results from the motion of the ions toward or away from the radiation source. From the perspective of the ions, however, it is the source that is moving toward or away from them, and so the frequency of the light is shifted by the Doppler effect. Thus, ions moving toward the source will be able to absorb radiation of slightly lower frequencies more effectively than motionless ions can, and ions moving away from the source will be able to absorb radiation of slightly higher frequencies. The combination of many ions moving in many directions has the effect of "smearing out" the spectrum, and the amount of smearing discloses the temperature of the ions. This technique proved that the temperature of the ions in our trap approached 10 millikelvins. The couplings, then, were as large as 500.

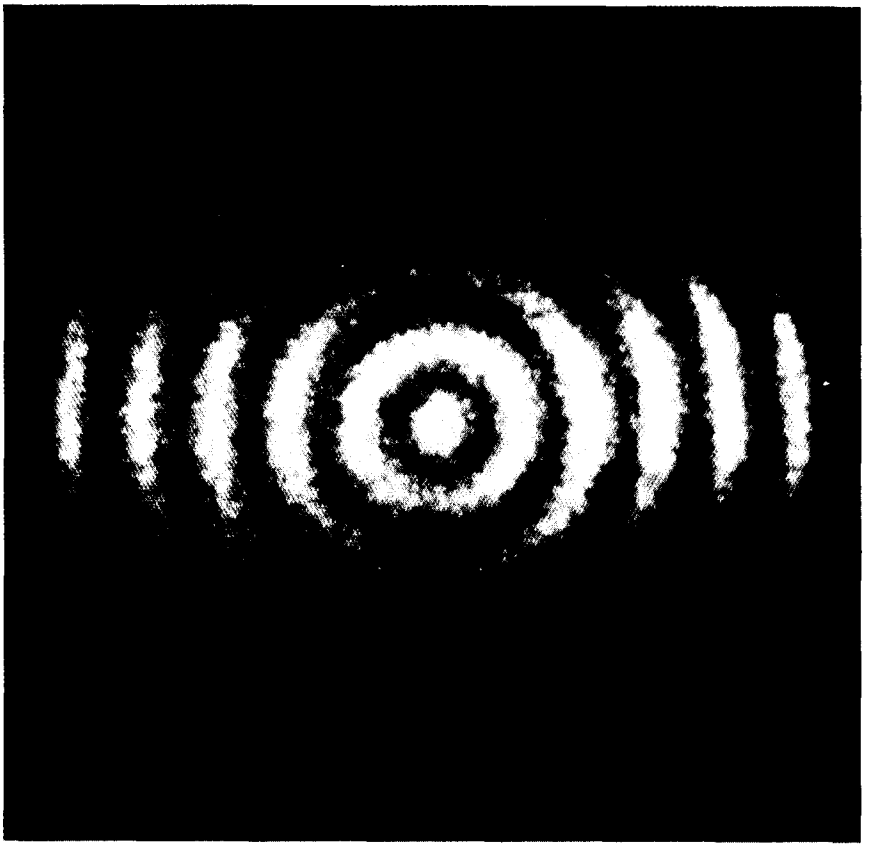

These measurements of the couplings, which indicated that the Paul trap could support a strongly coupled one-component plasma, were done with fewer than about 25 ions in the trap. We found it difficult to create similar solid states with more ions. The difficulty arose from the effects of the oscillation induced in the ions by the driving force. As an ion oscillates at the driving frequency, the repulsion between the ion and its neighbors enables it to influence the oscillations of the other ions. This additional perturbation can cause a plasma's structure to heat to a breaking point under certain operating conditions of the trap. The effect is known as radio-frequency heating, because the driving frequency for atomic ions is about the same as the frequency of radio waves. Radio-frequency heating was first observed in the experiments of Wuerker, Shelton and Langmuir.

More recently Reinhold Blümel and co-workers at the Max Planck Institute and John A. Hoffnagle and colleagues at the IBM Almaden Center have studied radio-frequency heating of atomic ions in great detail. These studies show that a small change in the system parameters of the Paul trap can cause a sudden transition between cold, crystalline states and hot, gaseous states. For example, the rate at which the ions are cooled is very sensitive to the frequency of the laser light employed for cooling. If the laser is tuned far below the optimal cooling frequency, radio-frequency heating transforms the ion plasma into a hot, disordered state. If the laser frequency is increased, the rate of laser cooling increases, until at a critical frequency the laser cools the ion plasma quickly enough, so that some order starts to appear. At that point the radio-frequency heating diminishes drastically, and the ion plasma suddenly freezes into an ordered state. This frozen state is quite stable and will persist even if the laser frequency is again decreased somewhat. The irregular nature of radio-frequency heating makes it difficult to study the liquid-to-solid phase transitions predicted for one-component plasmas.

The problem of radio-frequency heating grows as the number of ions in the trap increases. When many ions are in the trap, some are pushed toward the electrodes, where the driving force is stronger. Those ions then oscillate at the driving frequency with a large amplitude and thereby increase the effects of radio-frequency heating. These considerations have limited the number of ions that can be cooled at one time in a Paul trap to about 200. If the difficulties associated with radio-frequency heating can be overcome, the Paul trap should allow workers to study the liquid-to-solid phase transition as well as other properties of the "infinite" one-component plasma.

At present the Penning trap provides a more hospitable environment for experimenting with large strongly coupled one-component plasmas than the Paul trap does. Unlike the time-varying electric fields of the Paul trap, the electric and magnetic fields that confine charged particles in the Penning trap are static. In 1988, with Sarah L. Gilbert, we constructed a Penning trap to confine beryllium ions. Malmberg and colleagues have also employed a Penning-type trap to confine strongly coupled plasmas of electrons.

Our trap consisted of four cylindrical electrodes arranged end to end along a common axis [*see illustration on page 130*]. A positive voltage was applied to the two outer cylindrical electrodes. This voltage generated an electric field between each inner electrode and the adjacent outer electrode. These fields trapped the ions in the axial direction, near a plane between the inner electrodes.

A powerful magnet placed around the electrodes created a uniform mag-

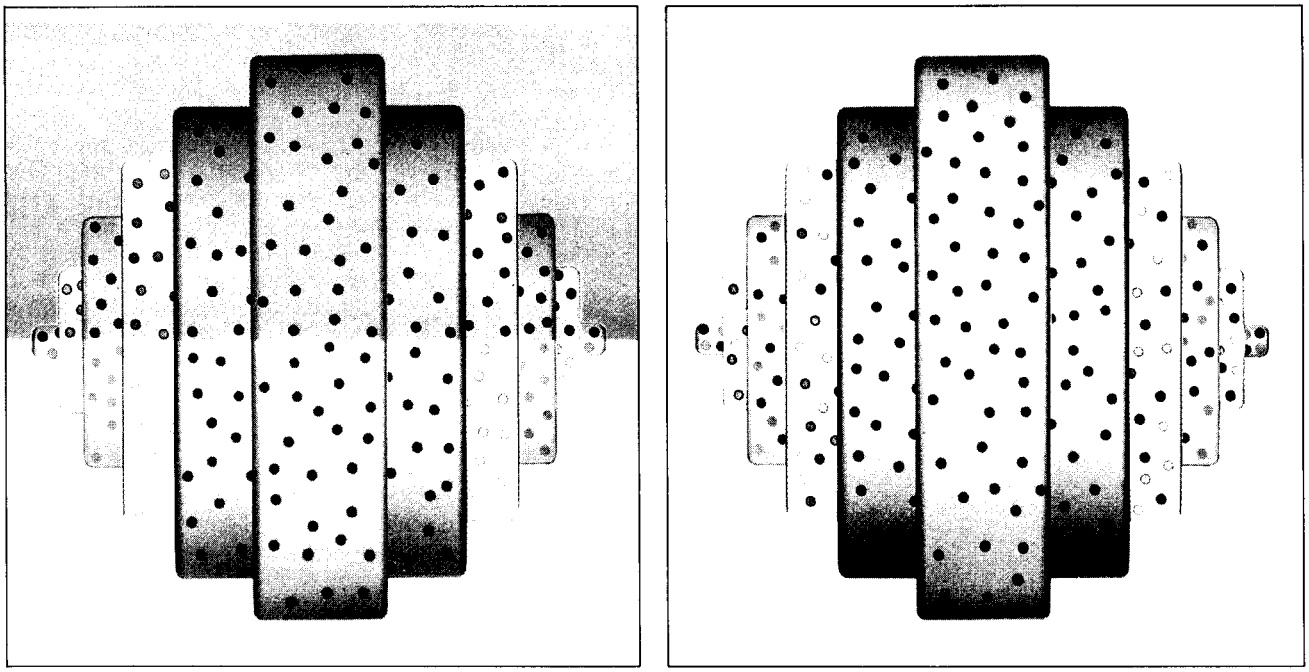

SHELL STRUCTURE of a microplasma consisting of about 1,000 beryllium ions is revealed in a photograph (*left*) made by shining a laser beam through the microplasma and recording the resulting fluorescence. The illustrations depict the complete shell structure as well as the diffusion of the beryllium ions from one moment (*center*) to the next (*right*). The microplasma behaves like both a solid and a liquid: the ions (*colored dots*) travel around within the shells but not between the shells.

netic field directed along the axis of the cylinders. The magnetic field prevented the ions from leaving the trap in the radial direction. The radial force of the electric field near the center of the trap is directed away from the trap center. This force combines with the axial magnetic field to cause the ions to orbit about the trap axis. As the orbiting ions pass through the magnetic field, they experience a Lorentz force that is directed radially inward. The Lorentz force is what confines the ions radially.

Except for this uniform rotation of the microplasma, the confining forces of the Penning trap are equivalent to the confining forces in the uniformly charged spheroid. Hence, even though ions in a Penning trap rotate, they behave like ions in a one-component plasma—in particular, they have the same thermodynamic properties.

To begin the experiment, we produced beryllium ions by a method similar to that described for making mercury ions in the Paul trap. The ions were cooled by two intersecting laser beams. A third laser beam, called the probe, was employed to measure the temperature of the ions. The light scattered by the ions was collected to make an absorption spectrum. As in the mercury-ion experiment, the temperature of the ions could be deduced from the blurring of certain features of the spectrum. This technique revealed that the ions had been cooled to below 10 millikelvins.

The rotation frequency of the beryllium microplasma could also be deduced from the spectrum. Beryllium ions circulated inside the trap at a rate of from 20,000 to 200,000 rotations per second. Because the rotation frequency is directly related to the radial electric fields, which are in turn related to the ion density, we were able to calculate that the ion density ranged from 50 to 300 million ions per cubic centimeter. From ultraviolet images of the plasmas we could determine the volume occupied by the trapped ions and therefore the number of trapped ions. The temperature and density measurements yielded couplings as large as 200 to 400 for less than about 15,000 ions in the trap.

We expect a phase transition from a liquidlike to a solidlike state to occur at a coupling of 180 for a one-component plasma with an infinite number of ions. Our measured values for the coupling indicate that the trapped ions should form a crystalline ion solid, if the trap contains enough ions. Should a system of 15,000 trapped ions, though, behave like an infinite system?

Recently some computer simulations have elucidated this question. The late Aneesur Rahman of the University of Minnesota at Minneapolis, John P. Schiffer of the Argonne National Laboratory, Hiroo Totsuji of Okayama University and Daniel H. E. Dubin and O'Neil of the University of California at San Diego have created simulations of a trapped plasma containing as many as several thousand ions. The simulations reveal several remarkable features. When the couplings exceed one, the ions are concentrated in concentric shells, which are spaced evenly. For couplings around 10, the shells are in a liquid state characterized by short-range order and diffusion in all directions. As the coupling increases, the shells become more clearly defined; the ions diffuse quickly within the shells and slowly between the shells. For high couplings (above 200), the diffusion of the ions within a shell slows down and the ions form a solidlike state. Instead of showing a sharp phase transition, the plasma evolves gradually from a liquidlike to a solidlike state.

Experiments have confirmed these predictions. Even though the plasma of beryllium ions rotates around the axis of the Penning trap, the shell structure is preserved in the radial direction. The scattered light from

a laser beam cutting across the plasma shows alternating bright and dark bands corresponding to the shells. We looked for shell structure in plasmas that contained as few as 20 ions and as many as 15,000 ions. In a plasma of 20 ions, a single shell was clearly observed. In a plasma of 15,000 ions, we could distinguish 16 shells. So far we have not detected any distinct structure within a shell because of the rotation of the plasma in the trap.

We were able to test predictions that for couplings around 100, the plasma will act like a liquid within a shell but like a solid between the shells. In particular, the ions should diffuse faster within shells than between shells. To demonstrate the effect, we optically "tagged" the ions by tuning the probe laser to a specific frequency. The probe laser suppresses the emission of light from the ions it strikes by placing them in a "dark" energy state in which they do not scatter light from the cooling laser beams.

First we darkened an outer shell of the plasma and measured the time required for the dark ions in the outer shell to move to the inner shells. Then we darkened part of the plasma across several shells and measured the time required for dark ions in one part of a shell to move to other parts of the same shell. These measurements verified that for moderate couplings the diffusion of ions between shells is more than 10 times slower than the diffusion of ions within a shell.

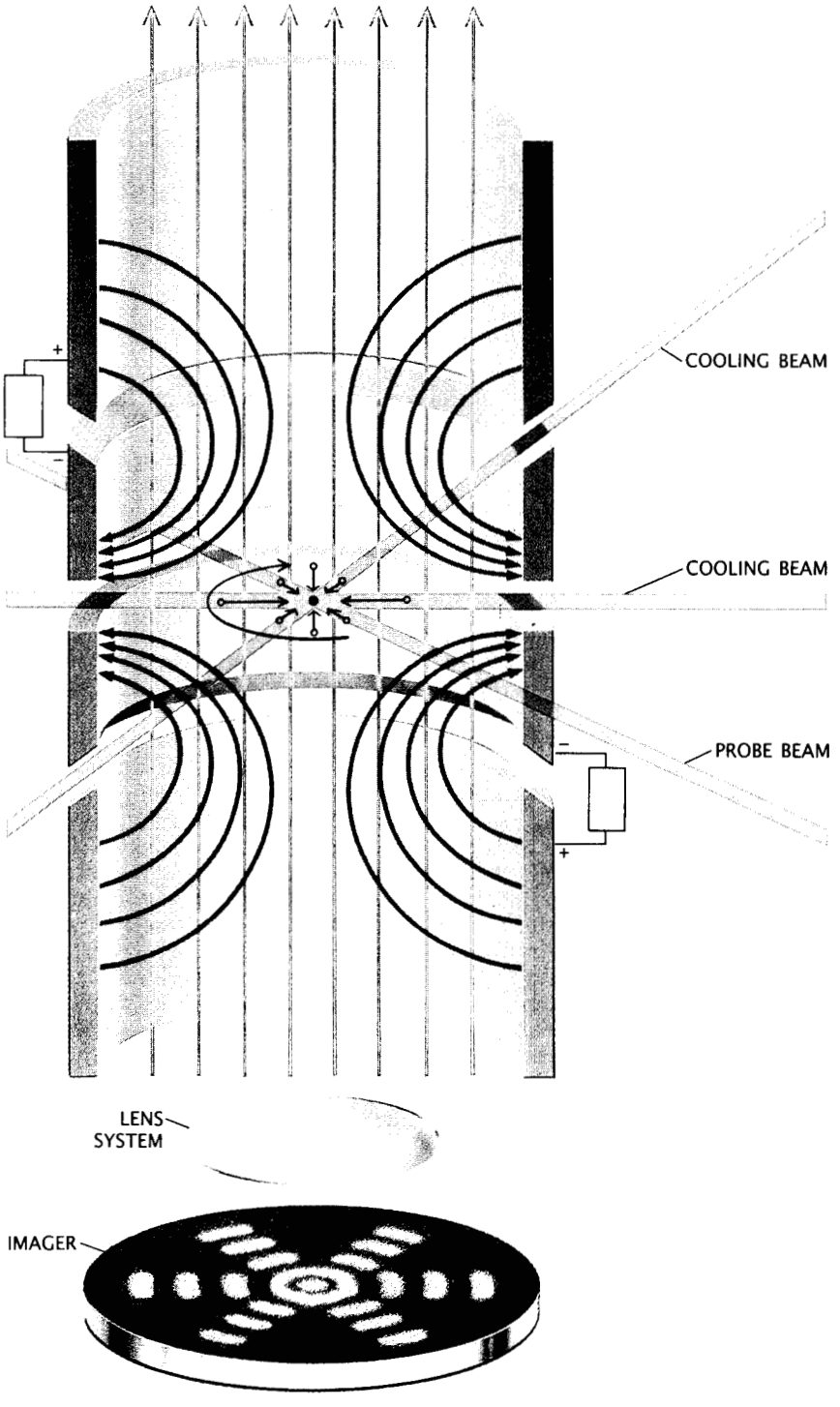

PENNING TRAP generates electric fields (*red lines*) and magnetic fields (*green lines*) to produce forces (*black arrows*) that confine charged particles. The electric and magnetic fields also cause the microplasma to rotate. Two laser beams cool the particles; a third serves as a probe for various experiments. The magnetic field arises from an electric current flowing through a solenoid (not shown) that encircles the trap.

Many questions about microplasmas are still unresolved. At what point will the behavior that is characteristic of an infinite system start to appear? How many ions are required for the system to exhibit a sharp phase transition? At what stage will the solid state become a body-centered cubic lattice rather than a collection of shells?

At present these questions are difficult to answer even in theory. Dubin predicts, however, that perhaps as many as 50 to 60 shells may be required before a body-centered cubic lattice would become an energetically favorable configuration. That would require about a million ions, more than 50 times the number of ions in the largest, strongly coupled microplasmas created so far. Current technology should be able to confine cold plasmas of this size. If couplings of 200 or more can be maintained for a plasma of a million ions, we may be able to visit the surface of a neutron star in a laboratory on the earth.

FURTHER READING

NON-NEUTRAL PLASMA PHYSICS. Edited by C. W. Roberson and C. F. Driscoll. AIP Conference Proceedings 175, American Institute of Physics, March, 1988.

PROCEEDINGS OF THE ELEVENTH INTERNATIONAL CONFERENCE ON ATOMIC PHYSICS, JULY 4-8, 1988, in *Atomic Physics 11*. Edited by S. Haroche, J. C. Gay and G. Grynberg. World Scientific Publishing Co., 1989.

PROCEEDINGS OF THE YAMADA CONFERENCE ON STRONGLY COUPLED PLASMA PHYSICS, AUGUST 29-SEPTEMBER 2, 1989. Edited by Setsuo Ichimaru. Elsevier Science Publishers, in press.

Rotational Equilibria and Low-Order Modes of a Non-Neutral Ion Plasma

D. J. Heinzen,[a] J. J. Bollinger, F. L. Moore, Wayne M. Itano, and D. J. Wineland

Time and Frequency Division, National Institute of Standards and Technology, Boulder, Colorado 80303

(Received 4 October 1990)

We study rotational equilibria and low-order electrostatic modes of a magnetically confined, non-neutral ion plasma. The plasma rotation rate is controlled with radiation pressure from a laser beam and is continuously varied over the entire allowed range, including Brillouin flow. Excitation of an asymmetric plasma mode by a static field asymmetry is observed. The symmetric quadrupole mode is also studied; its behavior is characteristic of a strongly magnetized plasma at low density, and of an unmagnetized plasma at Brillouin flow.

PACS numbers: 52.25.Wz, 32.80.Pj, 52.35.Fp

Recently, much attention has focused on the properties of plasmas containing charges with only one sign.[1] Such non-neutral plasmas are unusually simple both theoretically and experimentally, and are unique in that steady-state thermal equilibria are possible. Nevertheless, they exhibit a wide range of collective phenomena, such as Debye shielding and collective oscillations. Typically, non-neutral plasmas are confined radially by a uniform axial magnetic field $\mathbf{B}=B\hat{\mathbf{z}}$, and axially by an electrostatic potential.[2] Such a plasma may be characterized by a self-field parameter[3] $S=2\omega_p^2/\Omega^2$, where $\omega_p=(4\pi nq^3/m)^{1/2}$ is the plasma frequency, with n, q, and m are the particle density, charge, and mass, respectively, and $\Omega=qB/mc$ is the cyclotron frequency. Of particular theoretical[1,3] and practical[4] interest is the condition $S=1$, referred to as "Brillouin flow."[3] In this state the plasma rotates rapidly about the z axis at a frequency $\Omega/2$ and is compressed to its maximum possible density of $n_B=m\Omega^2/8\pi q^2$, the "Brillouin density." Near Brillouin flow, the plasma behaves in many ways like an unmagnetized plasma.[3] Values of S near unity have been obtained in only a few experiments[5,6] where the plasma confinement times were not long enough to reach thermal equilibrium.

This paper describes the use of laser-induced torques on a magnetically confined non-neutral $^9Be^+$ plasma to access the entire range of allowed rotational thermal equilibria including Brillouin flow. Geometrical errors in the trapping fields tended to limit the range of accessible rotational equilibria. A static, azimuthally asymmetric field error was observed to excite an asymmetric collective resonance and heat the plasma. When this asymmetry was eliminated, the techniques described here were used to study a symmetric quadrupole mode of the plasma over a wide range of conditions including Brillouin flow.

The experimental apparatus (Fig. 1) has been described previously.[7] Electroformed copper cylinders produce a trap with accurate cylindrical symmetry. A potential V_T of between 10 and 300 V, applied between the end and central electrodes, confines the ions axially. The potential near the trap center is

$$V(r,z)=\frac{V_T}{d_T^2}\left[z^2-\frac{r^2}{2}\right]=\frac{m\omega_z^2}{2q}\left[z^2-\frac{r^2}{2}\right], \quad (1)$$

where $d_T=1.85$ cm and ω_z is the frequency at which a single trapped ion oscillates along the z axis. The trap is placed in a uniform magnetic field $\mathbf{B}=B\hat{\mathbf{z}}$, with $B=0.8194$ T, which confines the ions radially. The $^9Be^+$ cyclotron frequency is $\Omega/2\pi=1.40$ MHz. Background gas pressure is approximately 10^{-8} Pa. For this work, between 1000 and 5000 $^9Be^+$ ions are confined in the trap for many hours. The plasma dimensions are typically less than 0.1 cm. We remove contaminant ions with a mass-to-charge ratio greater than $^9Be^+$ by raising V_T to $\sim$550 V ($\omega_z/\Omega\sim0.67$ for $^9Be^+$). Agreement between the predicted and observed mode frequencies is obtained only when the contaminant ions are removed.

The ion plasma evolves into a near-thermal equilibrium state characterized by a uniform rotation of the plasma about the z axis at frequency ω. Under the low-temperature conditions of this experiment, the density is

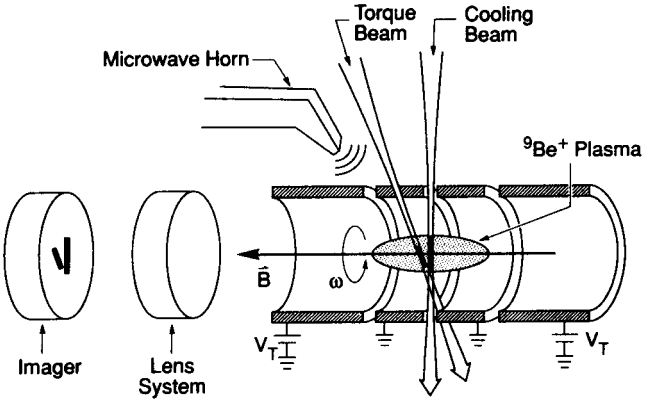

FIG. 1. Schematic drawing of the experimental apparatus. For clarity, the electrodes are shown in a cross-sectional view, and the diagonal laser beam is omitted. The size of the plasma is exaggerated.

uniform over length scales large compared to the interparticle spacing and the plasma frequency is given by $\omega_p^2 = 2\omega(\Omega - \omega)$.[8] The density falls to zero at the boundary of the plasma in a distance on the order of the Debye length,[9] which in our experiment is much less than the plasma dimensions. With the confining potential of Eq. (1), the plasma boundary is spheroidal with an aspect ratio $\alpha \equiv z_0/r_0$ determined by ω from the expression $\omega_z^2 = \omega_p^2 Q_1^0(\alpha/(\alpha^2-1)^{1/2})/(\alpha^2-1)$.[8] Here $2z_0$ and $2r_0$ are the maximum axial and radial extent of the plasma and Q_l^m is the associated Legendre function of the second kind. We neglect the effect of image charges because the plasma dimensions are much smaller than the trap dimensions.

The plasma density and temperature are controlled with radiation pressure from two cw laser beams nearly resonant with the $2s\,^2S_{1/2}(m_I = +\frac{3}{2}, m_J = +\frac{1}{2}) \rightarrow 2p\,^2P_{3/2}(+\frac{3}{2}, +\frac{3}{2})$ transition of $^9Be^+$ at frequency ω_0 ($\lambda \approx 313$ nm), where m_I and m_J are the nuclear- and electron-spin projections along $\hat{\mathbf{z}}$. One of these, the "cooling beam," is tuned 10–50 MHz below ω_0, has a power of 50–500 μW, and is directed through the plasma center in a direction perpendicular to the z axis. The second beam, the "torque beam," is directed perpendicularly to the z axis through the side of the plasma that recedes from the laser beam (Fig. 1). Its frequency ω_T is between 0 and 1500 MHz above ω_0 and its power is 1–3 μW. For some of the measurements, a third laser beam is directed diagonally through the plasma with a component along $\hat{\mathbf{z}}$, to provide additional laser cooling.[7] Each beam diameter is 25–50 μm, an order of magnitude less than the typical plasma diameter. The torque beam supplies energy to the plasma and provides a torque which changes the plasma angular momentum and increases ω. Equilibrium is maintained because the energy input by the torque beam is removed by the cooling beam,[10] and because the laser-beam torques and torques from static field asymmetries sum to zero.[11–13] Temperatures typically below 250 mK are obtained.

Light scattered from the ions is imaged by a lens system onto a photon-counting imaging tube.[7] A real-time display of the image is used to monitor the plasma kinetic energy; a hot plasma has a more diffuse boundary and less ion fluorescence. With this simple diagnostic we did not, in general, distinguish between an increase in the random thermal energy of the ions and the excitation of coherent modal motion of the ions. In order to measure the rotation frequency of the plasma, we drive the $(+\frac{3}{2}, +\frac{1}{2}) \rightarrow (+\frac{3}{2}, -\frac{1}{2})$ electron spin-flip transition of the $^9Be^+$ ground state at $\omega_s/2\pi \simeq 22$ GHz. The transition is observed as a decrease in the ion fluorescence.[14] Absorption at both the "carrier" frequency ω_s and the motional "sideband" frequencies $\omega_s \pm \omega$ are observed. These sidebands occur because the ions see the microwave field as being phase and amplitude modulated at frequency ω, due to the coherent rotational motion of the ions.[15] The rotation frequency $\omega/2\pi$ is determined to an accuracy of approximately 5 kHz.

With the two-laser-beam technique, we are able to establish a stable rotation frequency at any value in the allowed range from ω_m to $\Omega - \omega_m$, where $\omega_m = \Omega/2 - (\Omega^2/4 - \omega_z^2/2)^{1/2}$ is the single-ion magnetron frequency.[8] Initially, with ω small, the torque laser frequency ω_T is tuned near ω_0, and the torque beam induces very little fluorescence due to the rotation-induced Doppler shift. Then, as ω_T is slowly increased, the ion fluorescence and torque increase, and the plasma compresses and rotates faster. For $\omega < \Omega/2$, the plasma radius decreases and the aspect ratio α increases with increasing ω. A typical curve of rotation frequency versus torque laser tuning is shown in Fig. 2. At high rotation frequencies hysteresis occurs. On the lower branch (increasing ω_T), the plasma becomes much hotter and rotates at a nearly constant frequency, until an abrupt transition to a cold state of faster rotation occurs. With further increases in ω_T, the rotation frequency can be smoothly varied through Brillouin flow ($\omega = \Omega/2$) to frequencies slightly less than $\Omega - \omega_m$. For $\omega > \Omega/2$, the plasma radius increases and the aspect ratio decreases with increasing ω. On the upper branch of the hysteresis (decreasing ω_T), the rotation frequency decreases smoothly, and the plasma remains cold until some heating is again observed, at a rotation frequency slightly higher than that at which heating first occurred on the lower branch. The size of the hysteresis depended sensitively on the angle θ_0 between the trap symmetry axis and the magnetic field. For $\theta_0 > 0.1°$, the plasma rotation frequency could not be increased beyond the point at which heating first occurred. We could make $\theta_0 < 0.01°$ by searching for an alignment which gave no apparent heating or hysteresis.

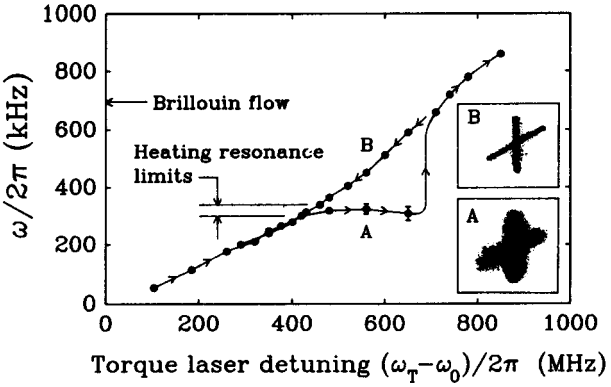

FIG. 2. Plasma rotation frequency as a function of torque laser frequency. Arrows indicate the direction of the frequency sweep. Insets *A* and *B* illustrate the appearance of hot and cold plasmas, respectively. Image *A* was recorded on the lower branch of the hysteresis, and image *B* on the upper. Bright fluorescence from the cooling and diagonal beams, and weak fluorescence from the torque beam, is visible.

The rotation frequency ω at which heating occurs for $\theta_0 \simeq 0.02°$ is shown in Fig. 3 as a function of ω_z. The lower bounds indicate where heating first occurs with increasing rotation frequency and the upper bounds indicate where heating first occurs with decreasing rotation frequency. We have identified this heating resonance as an excitation of a collective $(l,m)=(2,1)$ plasma mode by the static field asymmetry associated with the trap-magnetic-field misalignment. [The indices l and m refer to a description of the modes in spheroidal coordinates, with m describing the azimuthal (ϕ) variation, and l the variation along a spheroidal surface in the direction perpendicular to $\hat{\phi}$.] This mode is similar to an $m=1$ diocotron mode in a cylindrical plasma column with a wavelength equal to the plasma length.[16] In this mode the plasma density remains constant and the shape spheroidal, but the plasma symmetry axis is tilted with respect to the z axis and precesses backwards relative to the plasma rotation at frequency ω. That is, the mode frequency $\omega_{21}^{(\mathrm{rot})}$ in the rotating frame is negative. Therefore when $\omega_{21}^{(\mathrm{rot})}=-\omega$, the mode has frequency $\omega_{21}=0$ in the laboratory frame and may be excited by static field asymmetries.[11-13] We show as a solid line in Fig. 3 the calculated rotation frequency ω at which $\omega_{21}=0$. Excellent agreement between the predicted and observed rotation frequencies is obtained. We calculate[17] ω_{21} by considering small axial and radial displacements of the ions from their equilibrium positions consistent with a tilt of the plasma symmetry axis. A self-consistent calculation of the axial and radial restoring forces to first order gives two linear differential equations describing the motion of the axial and radial displacements. The requirement that the eigenfrequencies for these two equations be equal gives a cubic equation for ω_{21}.

A static field error cannot transfer energy to the plasma. However, it can convert potential energy to thermal energy by producing a radial expansion of the plasma. In our work, the laser beams are sources of strong torques and energy input as well as cooling. We have not attempted to model all of the energy input and torques and obtain a quantitative description of the radial transport and heating produced by the static (2,1) mode.

We have also measured the (2,0) axially symmetric quadrupole mode frequency of the plasma. This mode is similar to an $m=0$ plasma mode in a cylindrical plasma column with a wavelength equal to the plasma length. In this mode the plasma density remains uniform and the shape spheroidal, but the plasma aspect ratio α oscillates in time. The mode is excited with an oscillating potential applied between the trap's end and center electrodes and resonance is observed by a change in the ion fluorescence. Results are shown in Fig. 4 for two different trap potentials. The solid line shows the mode frequency ω_{20} calculated in a manner similar to the (2,1) mode and given by[17]

$$2\omega_{20}^2=\Omega_u^2+\omega_Q^2-\{(\Omega_u^2-\omega_Q^2)^2-4\Omega_v^2(\omega_z^2-\omega_Q^2/3)\}^{1/2}. \quad (2)$$

Here $\Omega_v=\Omega-2\omega$ is the vortex frequency, $\Omega_u=(\Omega_v^2+\omega_p^2)^{1/2}$ is the upper hybrid frequency, and $\omega_Q^2=\omega_p^2\times 3\alpha Q_2^0(\alpha/(\alpha^2-1)^{1/2})/(\alpha^2-1)^{3/2}$. The frequency ω_Q is the (2,0) mode frequency in the absence of a magnetic field (i.e., a plasma confined by a uniform background of opposite charge). Again, good agreement between the predicted and observed mode frequencies is obtained with no adjustable parameters. Independently, a more general calculation of spheroidal plasma mode frequencies has been recently carried out by Dubin.[18]

Figure 4 shows two additional calculations. In the

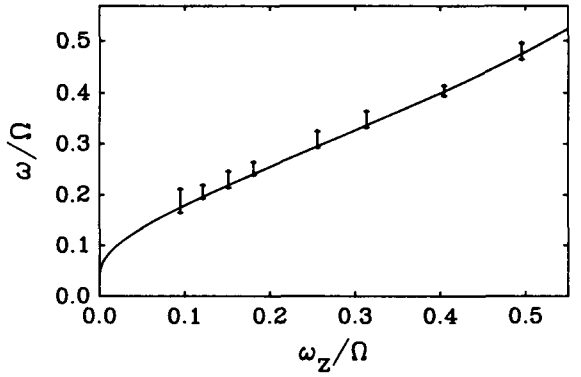

FIG. 3. Rotation frequency ω at which heating was observed as a function of the single-particle axial frequency ω_z. Both frequencies are expressed in units of the cyclotron frequency Ω. The error bars on the measurements are explained in the text. The solid line indicates the calculated rotation frequency ω at which $\omega_{21}=0$. This is a universal curve involving no adjustable parameters.

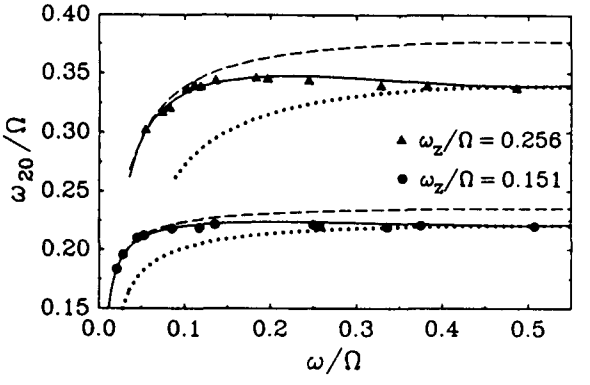

FIG. 4. Plasma quadrupole frequency ω_{20} as a function of rotation frequency ω for $\omega_z/\Omega=0.151$ ($V_T=28$ V) and $\omega_z/\Omega=0.256$ ($V_T=80$ V). All frequencies are expressed in units of the cyclotron frequency Ω. The circles and triangles give the experimental data. The solid lines give the cold-fluid model predictions for ω_{20}. The dashed and dotted lines give the high- and low-magnetic-field calculations for ω_{20}, respectively.

(Fig. 4 has been corrected as per erratum: Phys. Rev. Lett. 66, 3087 (1991).

first, shown as dashed lines, the magnetic field is assumed to be effectively infinite; that is, the ions are not allowed to move radially, and the mode frequency is calculated assuming a simple axial stretch of the charged spheroid. In the second, shown as dotted lines, the magnetic field is assumed to be effectively zero; that is, the curve shows ω_Q. The quadrupole mode frequency varies smoothly from the high-magnetic-field calculation at low rotation frequencies to the zero-magnetic-field calculation at the Brillouin limit.

We also studied plasmas containing about 40000 $^9Be^+$ ions at a magnetic field $B=6$ T ($n_B=1.1\times10^{10}$ cm^{-3}) and trap voltage $V_T=500$–1500 V. At this field, we were also able to obtain rotation frequencies throughout the allowed range. The (2,1) heating resonance was much stronger and more sensitive to the magnetic-field alignment. In addition, weaker heating resonances, which were also sensitive to the magnetic-field alignment, were observed at lower rotation frequencies than the (2,1) heating resonance. We were unable to remove contaminant ions from the plasma at this high magnetic field.

In conclusion, we have shown that the entire range of allowed rotational equilibria can be realized in a non-neutral ion plasma using laser-induced torques and by careful control of trap asymmetries. This should permit detailed investigations of non-neutral plasmas near Brillouin flow. Here we studied the excitation of an asymmetric tilt mode of the plasma by a static field asymmetry. This mode heated the plasma and tended to limit the plasma density. Observation of this mode allows the magnetic- and electric-field axes to be carefully aligned. We also studied a symmetric quadrupole mode and showed that the plasma exhibits unmagnetized behavior near Brillouin flow. Measurement of this mode frequency, perhaps through induced image currents in the trap electrodes,[19] could provide useful information on plasma rotation frequency, shape, and density when the plasma cannot be directly imaged.

We gratefully acknowledge the support of the Office of Naval Research. We also thank Dan Dubin and Fred Driscoll for stimulating conversations, and Sarah Gilbert and Jim Bergquist for their comments on the manuscript.

---

[a]Current address: Department of Physics, University of Texas, Austin, TX 78712.

[1]*Non-Neutral Plasma Physics,* Proceedings of the Symposium of Non-Neutral Plasma Physics, Washington, D.C., 1988, edited by C. W. Roberson and C. F. Driscoll, AIP Conf. Proc. No. 175 (AIP, New York, 1988).

[2]J. H. Malmberg and J. S. deGrassie, Phys. Rev. Lett. **35**, 577 (1975).

[3]R. C. Davidson, *Physics of Nonneutral Plasmas* (Addison-Wesley, Reading, MA, 1990); R. C. Davidson, in *Non-Neutral Plasma Physics* (Ref. 1).

[4]Wayne Vernon, in *Proceedings of the Workshop in Intense Positron Beams, Idaho Falls, Idaho, 1987,* edited by E. H. Ottewitte and W. Kells (World Scientific, Singapore, 1988), p. 135.

[5]A. J. Theiss, R. A. Mahaffey, and A. W. Trivelpiece, Phys. Rev. Lett. **35**, 1436 (1975).

[6]Guy Dimonte, Phys. Rev. Lett. **46**, 26 (1981).

[7]S. L. Gilbert, J. J. Bollinger, and D. J. Wineland, Phys. Rev. Lett. **60**, 2022 (1988).

[8]L. R. Brewer, J. D. Prestage, J. J. Bollinger, W. M. Itano, D. J. Larson, and D. J. Wineland, Phys. Rev. A **38**, 859 (1988).

[9]C. F. Driscoll, J. H. Malmberg, and K. S. Fine, Phys. Rev. Lett. **60**, 1290 (1988).

[10]W. M. Itano, L. R. Brewer, D. J. Larson, and D. J. Wineland, Phys. Rev. A **38**, 5698 (1988).

[11]Rhon Keinigs, Phys. Fluids **24**, 860 (1981); **27**, 1427 (1984).

[12]C. F. Driscoll and J. H. Malmberg, Phys. Rev. Lett. **50**, 167 (1983).

[13]D. L. Eggleston, T. M. O'Neil, and J. H. Malmberg, Phys. Rev. Lett. **53**, 982 (1984).

[14]D. J. Wineland, J. C. Bergquist, W. M. Itano, and R. E. Drullinger, Opt. Lett. **5**, 245 (1980).

[15]H. S. Lakkaraju and H. A. Schuessler, J. Appl. Phys. **53**, 3967 (1982).

[16]S. A. Prasad and T. M. O'Neil, Phys. Fluids **26**, 665 (1983).

[17]J. J. Bollinger *et al.* (to be published).

[18]D. Dubin, preceding Letter, Phys. Rev. Lett. **66**, 2076 (1991).

[19]D. J. Wineland and H. Dehmelt, Int. J. Mass Spectrom. Ion Phys. **16**, 338 (1975); **19**, 251 (1976).

Cooling methods in ion traps[1]

Wayne M. Itano, J. C. Bergquist, J. J. Bollinger, D. J. Wineland
Time and Frequency Division
National Institute of Standards and Technology
Boulder, Colorado 80303

I. Introduction

Trapping of ions is used to make measurements that are difficult or impossible to perform by other techniques, because the ions can be held for long periods in a well-controlled environment. Cooling of the ions has several beneficial effects for such experiments. First, it increases the time that the ions remain in the trap. Second, it can lead to increased precision for measurements of masses, magnetic moments, and optical or microwave spectra. Third, some phenomena, such as the formation of spatially ordered structures of ions, can be observed only at low temperatures.

We use the term "cooling" to mean a reduction in the velocities of the ions. Use of the term does not imply that the ions are in thermal equilibrium with each other nor that they have a well-defined temperature. The motional modes that are cooled may be random or coherent. The secular motion in a Paul (rf quadrupole) trap and the axial motion in a Penning trap are examples of random modes. The micromotion in a Paul trap and the magnetron rotation in a Penning trap are examples of coherent modes. Laser cooling is very effective and has been used to obtain temperatures much less than 1 K.[1],[2] However, since laser cooling depends on the energy level structure of the ions and on the availability of narrowband radiation sources matched to the level spacings, it has been applied only to a few kinds of ions. Other cooling methods are more generally applicable.[3],[4] Resistive cooling, active feedback cooling, or rf sideband cooling can be applied to all ions, since they depend only on the charge and mass of the ions. Collisional cooling is also widely applicable. Sympathetic cooling is the cooling of one ion species through Coulomb collisions with another, laser-cooled ion species. It has been demonstrated with ions in Penning traps[5],[6] and for (a few) ions in Paul traps.[7]

In spectroscopy the main reason for cooling ions is to reduce Doppler shifts. If the transition is broadened by the first-order Doppler shift, which is linear in velocity, cooling the random motion will reduce the observed linewidth. Methods other than cooling can eliminate the first-order Doppler shift. Dicke narrowing[8] and two-photon absorption[9] are two examples. Reduction of the second-order (time dilation) Doppler shift, however, requires cooling.

Dicke narrowing has been applied to many ion trap experiments. It occurs when the atoms or ions are confined to spatial dimensions less than about half the wavelength of the radiation that excites the transition. The lineshape contains a sharp component, which is free of the first-order Doppler effect. In addition, the lineshape contains a broad pedestal or a discrete series of sidebands, depending on whether the motion of the ions is random or periodic. The pedestal or sidebands are reduced in intensity as the spatial confinement is improved.

For radiofrequency or microwave transitions, this effect can be seen without any special cooling techniques. As long as the ions are confined in the trap, they are also confined to dimensions less than the wavelength. Hyperfine resonances a few hertzes wide (Q's of 10^9 to 10^{10}) were observed in early work with uncooled $^3He^+$ ions[10] and with $^{199}Hg^+$ ions.[11] For optical transitions, which have much shorter wavelengths, cooling to temperatures less than 1 K is required to obtain Dicke narrowing. A Dicke-narrowed optical spectrum has been observed in laser-cooled, trapped Ba^+ ions[12] and in Hg^+ ions.[13]

Precise measurements of masses and g-factors also benefit from cooling.[14]–[17] Reduction of the velocities lowers uncertainties due to the relativistic mass increase and due to anharmonicities of the electric potentials. Cooling the magnetron motion in a Penning trap confines ions to regions of smaller spatial extent. Over a small region, the magnetic field can be more uniform and the electric potential more nearly quadratic.

Cooling of trapped ions is also useful in studies of plasmas and ordered structures. With sufficient cooling so that the Coulomb potential energy between nearest neighbors is much greater than their average kinetic energy, the ions can form ordered structures. Ordered, crystal-like structures of highly-charged micrometer particles of aluminum in a Paul trap were observed when the particles were cooled with background gas.[18] Similar structures of a few laser-cooled atomic ions have recently been observed in Paul traps.[7],[19]–[21] A concentric shell structure of several thousand laser-cooled Be^+ ions has been observed in a Penning trap.[22]

II. Resistive cooling

Resistive cooling involves connecting the trap electrodes to an external circuit, so that the ions dissipate their energy by inducing electric currents in the circuit. If there are

no sources of heating besides the coupling to the external circuit, the ions come to equilibrium at the temperature of the external circuit. The method is, in principle, applicable to all ions.

The cooling time can be estimated from a simple model.[3] Consider a single ion of mass m and charge q. The ion is bound by a harmonic restoring force to the interior of a parallel plate capacitor. The separation between the plates is $2z_0$. The ion oscillates in the direction perpendicular to the plates (the z direction) at a frequency ω_z. The plates of the capacitor are connected by a resistor R. The capacitance C of the plates is assumed to be small, so that $R \ll 1/(\omega_z C)$. If the ion moves with a velocity v_z, electric charges are induced on the plates, and a current $i = qv_z/2z_0$ flows through R.[23] Let $W_z = m\langle v_z^2 \rangle$ be the total (kinetic plus potential) energy of the ion. The brackets denote a time average. The average rate at which the moving ion does work on the external circuit is

$$-\frac{dW_z}{dt} = \langle i^2 R \rangle = \frac{q^2 R W_z}{4mz_0^2}. \tag{1}$$

The energy is damped with a time constant equal to

$$t_0 = \frac{4mz_0^2}{q^2 R}. \tag{2}$$

This model can be applied to the axial (z) motion in either a Penning or a Paul trap. In those cases, the external circuit is connected between the two endcap electrodes. It could also be applied to the x or y mode in a Paul trap or the cyclotron mode in a Penning trap. In such a case, the ring electrode must be split, and the external circuit connected between the two halves. This method cannot be applied to the magnetron mode in a Penning trap, because the energy in the magnetron mode, which is mostly potential, *decreases* as the amplitude of the mode increases. Dissipation of energy leads to an increase in the diameter of the magnetron orbit and an increase in the magnetron velocity. As will be discussed in Section III, active feedback can be used to reverse this process.

In a real trap, as opposed to an infinite parallel plate capacitor, the expression for the induced current is $i = B_1 q v_z/(2z_0)$, where B_1 depends on the geometry of the electrodes. The cooling time t_0 is proportional to B_1^{-2}. Methods for calculating B_1 have appeared in the literature.[24],[25] For typical trap designs, $B_1 \approx 0.8$.

Equation (2) shows that resistive cooling is most effective for ions with high charge-to-mass ratios. For a given mass and charge, the cooling time can be reduced by decreasing z_0 or increasing R. In practice, the high value of R is usually obtained by using a parallel inductance L to cancel the reactance due to the capacitance C of the trap electrodes. The effective value of R is then $Q/(\omega_z C)$, where Q is the quality factor of the tuned circuit. Typically, $Q \approx 1000$. However, Cornell *et al.*[16] have used a superconducting tank circuit with $Q = 25\ 000$. This reduces the axial cooling time to 6 s for N_2^+ ions.

Consider N independent ions in a trap. Let $i = \sum_{j=1}^{N} i_j$ be the total current induced by the ions in the external circuit, where i_j is the current induced by the jth ion. Since the ions are assumed to be independent, $\langle i_j i_k \rangle = \delta_{jk} i_0^2$, where the brackets denote a time average and where i_0 is the rms current induced by a single ion. Thus, the total mean-squared induced current, and hence the rate of energy loss, is N times that of a single ion:

$$\langle i^2 \rangle = \sum_{j=1}^{N}\sum_{k=1}^{N}\langle i_j i_k \rangle = \sum_{j=1}^{N}\langle i_j^2 \rangle = N i_0^2. \tag{3}$$

The average energy of N ions is N times the average energy of a single ion. Thus, the time constant for damping the energy of N independent ions is the same as that for a single ion, provided that the relaxation of energy between the center-of-mass mode and the internal modes is fast. This is not necessarily the case, particularly if the trap potentials are very nearly harmonic.

Resistive cooling of the axial motion of a gas of electrons in a Penning trap was observed by Dehmelt and Walls.[26] The cooling time was about 0.1 s. Since there was very little heating from other sources, the temperature of the electrons could be brought down to the temperature of the external circuit. This system was studied in more detail by Wineland and Dehmelt.[27]

Resistive cooling of protons in a Paul trap was demonstrated by Church and Dehmelt.[28] The temperature without resistive cooling was about 12 000 K. Coupling to an external circuit reduced the temperature to 900 K and increased the storage time from 100 s to 3000 s. The cooling time was a few seconds. Heating caused by the rf trap fields ("rf heating") prevented cooling to the temperature of the external circuit.

Resistive destabilization (heating) of the magnetron motion of electrons in a Penning trap was observed experimentally by White, Malmberg, and Driscoll.[29] A resistance was connected between two sections of the cylindrical ring electrode. The magnetron mode is a displacement of the center of the electron plasma from the central axis of the trap. The magnetron mode is also called the $l = 1$, $k_z = 0$ diocotron mode, since it is an excitation that has an $e^{il\theta}$ azimuthal dependence, where $l = 1$, and no dependence on z. The displaced plasma rotates around the axis due to the drift caused by crossed electric and magnetic fields ($\vec{E} \times \vec{B}$ drift). This displacement grew exponentially with time. The observed variation of the growth rate with resistance was in agreement with theory.

III. Active-feedback cooling

Cooling trapped ions by negative electrical feedback has been discussed theoretically and demonstrated experimentally, though it has not yet been widely applied. Like resistive cooling, it can be applied to all ions.

Dehmelt *et al.*[30] have treated theoretically the case in which the feedback is applied continuously, to a single, harmonically bound ion. A displacement of the ion from its equilibrium position induces a signal on, for example, one of the endcap electrodes. Let this signal be amplified

by a factor g and fed back with reversed phase to the other endcap electrode. The fed-back signal forces the ion back toward the equilibrium position. The cooling time of the ion is $(1+g)$ times shorter than for ordinary resistive cooling. However, there is a trade-off between the cooling rate and the final temperature. The thermal noise voltage of the external circuit resistance is also amplified, so the final temperature is $(1+g)$ times higher than for resistive cooling. One potential problem with this method is that the correction signal can be picked up by the detector and interfere with the signal from the ion. This effect could be reduced by coupling part of the correction signal, with a phase reversal, to the detector. If there is more than one ion, the cooling is not as straightforward. To the extent that the electric field from the electrodes is uniform over the ion cloud, only the center of mass of the ions can be detected and corrected, not the deviations of the individual ions from the center of mass. Continuous feedback has been used to cool ions in Penning traps, but details have not been published. (See footnote 26 of Ref. [4].)

Resistive destabilization of the magnetron motion of an electron plasma in a Penning trap was described in Section II. The magnetron mode can be damped with active feedback similar to that described in the preceding paragraph. A signal is picked up on one section of the ring electrode and fed back on another section, with the proper gain and phase shift. Cooling of the magnetron mode by this method has been demonstrated experimentally.[31],[32] The magnetron mode is coherent; that is, the displacements of the individual ions have the same phase. Thus, the cooling of a plasma is similar to that for a single ion.

Stochastic cooling is a kind of negative feedback cooling which has successfully been applied to antiprotons in storage rings.[33] In stochastic cooling, a signal proportional to the average displacement of the particles is picked up on one section of the storage ring. It is amplified and fed back to a set of electrodes, called a kicker, at another section of the ring. The timing is adjusted so that the signal arrives at the electrodes at the same time as the particles. If there were only a single particle in the ring, its displacement from the desired orbit could be brought to zero by proper adjustment of the gain and phase of the amplifier. In practice, there are many particles, whose signals are not resolved. At best, only the center-of-mass deviation of a sample of particles can be brought to zero in a single application of feedback. Stochastic cooling depends on having a spread in the energies of the particles, so that, after a period of time, called the mixing time, the center-of-mass deviation again becomes nonzero and more energy can be extracted. This mixing time is analogous to the time required for coupling of energy between the center-of-mass and internal modes in an ion trap.

Stochastic cooling has been extended to traps by Beverini *et al.*[34]–[36] In a trap, the pick-up and kicker electrodes cannot be separated physically, as they can be in a storage ring. In order to avoid feed-through from the kicker to the pick-up, the detection and correction are separated in time from each other. The amplitude and phase of the center-of-mass motion is measured. Then a short electric pulse is applied, with the proper amplitude and phase to stop the center-of-mass motion. The process is then repeated.

To show that cooling can be obtained by this method, we consider a simplified model.[35] Consider N noninteracting ions, each oscillating at a fixed frequency ω_k $(k = 1, 2, \ldots, N)$. In the real case, there is a spread in frequencies due to space charge and the anharmonicity of the trap potential, but the frequency of a given ion is not fixed. The axial position of the kth ion is

$$Z_k = A_k \sin(\omega_k t + \phi_k). \tag{4}$$

The position of the center of mass is

$$Z_B = \frac{\sum_k A_k \sin(\omega_k t + \phi_k)}{N} \equiv A_B \sin(\omega_B t + \phi_B), \tag{5}$$

where A_B is the instantaneous center-of-mass amplitude.

We assume that the frequencies and amplitudes of the individual ions are distributed randomly. The time average of the square of the center-of-mass amplitude is then

$$\langle A_B^2 \rangle = \langle A^2 \rangle / N, \tag{6}$$

where $\langle A^2 \rangle$ is the ensemble average of the squared amplitude of a single ion. The instantaneous value of A_B^2 fluctuates around the mean value given by Eq. (6) as the phases of the ions change with respect to each other. Let σ_ω be the standard deviation of the ω_k's from their mean value ω_0. The time required for A_B^2 to change significantly (the mixing time) is on the order of $\tau_m = \sigma_\omega^{-1}$.

Suppose a short electric field pulse of amplitude E is applied to the ions at time t^*. The pulse duration τ is assumed to be much shorter than the oscillation period of the ions. Before the pulse, the position of the kth ion is

$$Z_k = A_k \sin(\omega_k t + \phi_k). \tag{7}$$

After the pulse, it is

$$Z_k' = A_k' \sin(\omega_k t + \phi_k'). \tag{8}$$

The change in the squared amplitudes is

$$A_k'^2 - A_k^2 = \left(\frac{qE\tau}{m\omega_k}\right)^2 + 2\frac{qE\tau}{m\omega_k} A_k \cos(\omega_k t^* + \phi_k), \tag{9}$$

where m and q are the mass and charge of an ion. The first term on the right side of Eq. (9) is positive and causes heating. The second term on the right side of Eq. (9) can be positive or negative, depending on the argument of the cosine.

Suppose that the amplitude of the applied field is

$$E = -g\frac{mA_B\omega_0}{q\tau}, \tag{10}$$

where g is the gain. The average change in the squared amplitudes of the particles is

$$\langle A'^2 \rangle - \langle A^2 \rangle = (g^2 - 2g)A_B^2. \tag{11}$$

The ions are cooled if $0 < g < 2$, which makes the right side of Eq. (11) negative. The optimum cooling is obtained for $g = 1$. For this case, we take a statistical average and use Eq. (11) to obtain

$$\langle A'^2 \rangle - \langle A^2 \rangle = -\langle A_B^2 \rangle = -\langle A^2 \rangle / N. \qquad (12)$$

The fractional change in $\langle A^2 \rangle$ is $1/N$ for one feedback pulse. Another pulse can be applied after a period of about τ_m. Thus, the optimum damping rate is approximately $1/(N\tau_m)$.

A more detailed calculation[35] shows that the energy per ion decreases to a limiting value $\epsilon_{\rm lim}$ which depends on the electrical noise and on the gain g. The cooling time $\tau_{\rm cool}$ also depends on g. There is no advantage to increasing g above about 0.5, since $\epsilon_{\rm lim}$ increases rapidly, while $\tau_{\rm cool}$ decreases slowly. For $g < 0.5$, there is a trade-off between $\epsilon_{\rm lim}$ and $\tau_{\rm cool}$, such that their product is approximately independent of g. If the electrical noise is due to thermal noise in the circuit,

$$\epsilon_{\rm lim}\tau_{\rm cool} \approx k_B T t_0, \qquad (13)$$

where k_B is Boltzmann's constant, T is the electrical noise temperature, and t_0 is the time constant for resistive cooling given by Eq. (2).

Beverini *et al.* have carried out an experimental demonstration of stochastic cooling of ions in a Penning trap.[36] The temperature was measured from the noise current induced on the trap electrodes by the ions. They measured a time constant for stochastic cooling of 55 ± 10 s, in good agreement with their calculation. The time constant for resistive cooling was about 160 s. The effectiveness of the cooling was verified by varying the phase of the feedback signal. For a 180° phase shift, heating occurred.

Stochastic cooling is most useful when the ions are initially at high energies. At low energies, the signal-to-noise ratio suffers, and stochastic cooling is less effective.

IV. Collisional cooling

Trapped ions can be cooled by collisions with charged or neutral particles which have lower temperatures. The collisions may lead to loss of the ions through charge-exchange or other reactions, or they may cause perturbations of the energy levels. However, in some cases the benefits of the cooling outweigh these disadvantages. One advantage of collisional cooling over resistive cooling is that it works with ions having a wide range of energies and oscillation frequencies. Because of the required high-Q tuned circuit, resistive cooling works for only a narrow range of oscillation frequencies. Two applications of collisional cooling will be given here: buffer gas cooling of ions in a Paul trap and electron cooling of antiprotons in a Penning trap. The latter is a form of sympathetic cooling (the cooling of one ion species by another). The case where one of the ion species is laser cooled is discussed in Section VI.

Consider collisions of ions in a Paul trap with neutral molecules which have lighter masses than the ions. Major and Dehmelt[37] showed that such collisions should damp the secular motion. The micromotion should not be much disrupted by a collision, but only slightly modified in amplitude and phase, so the trapping should not be affected. Other theoretical work on buffer gas cooling of ions in a Paul trap has been done by Blatt *et al.*[38] and Vedel *et al.*[39]

The final ion temperature results from a balance between heating and collisional cooling. Usually, rf heating[28] is the dominant source of heating. The mechanism of rf heating has recently been clarified. Computer simulations show that rf heating results from the existence of a chaotic regime for a system of many interacting ions in a Paul trap.[40] The chaos does not require stochastic forces. It results from the deterministic, classical dynamics of the coupled, nonlinear system. There are also crystalline or quasiperiodic states, in which the ions do not absorb energy from the rf trapping field. Chaos results in a continuous, rather than a discrete, power spectrum of the motion of the ions. This allows the ions to absorb energy from the rf field. If the density of the ions becomes low enough, their motions become nearly independent and are not chaotic. The rf heating then stops. This is why ions can be confined for long times even without cooling.

In an early experiment, Wuerker *et al.*[18] confined charged micrometer particles of aluminum in a Paul trap. The particle motions could be damped by background gas at a pressures up to 1.3 Pa (10^{-2} Torr). When the pressure was high enough, the particles crystallized into regular patterns. These patterns corresponded to the spatial configurations which minimized the effective potential energy of the system. The time required for the particles to crystallize, starting from a disordered state, increased as the pressure was reduced. An increase in the confinement time of heavy ions (Hg^+) by the introduction of a light buffer gas (Ne) was observed by Dawson and Whetton.[41] This increase in confinement time was interpreted as an effect of collisional cooling. However, the ion temperature was not measured directly.

Schaaf *et al.*[42] measured the temperature of Ba^+ ions confined in a Paul trap in the presence of He buffer gas. They measured the spatial density distribution of the ions by scanning a laser beam across the trap and observing the fluorescence. (Knight and Prior[43] had previously used a similar method to measure the density distribution of Li^+ ions in a Paul trap.) Schaaf *et al.* found the density distribution to be well described by a Gaussian in both the radial and axial directions. Since the strength of the confining potential was known, the ion temperature could be inferred from the width of the spatial distribution. The temperature of the ions decreased as the He pressure was increased. At a pressure of 5×10^{-4} Pa, the temperature was reduced by a factor of 3. At higher pressures, the ions were rapidly lost from the trap.

Cutler *et al.*[44],[45] have collisionally cooled $^{199}Hg^+$ ions with He for use in a microwave frequency standard. The frequency standard is based on measurements of the ground-state hyperfine separation, which is approximately

40.5 GHz. The ions are prepared in the ($F = 0$) ground-state hyperfine level by optical pumping with 194 nm radiation from a ^{202}Hg resonance lamp. This radiation is nearly resonant with the transition from the ($F = 1$) level of the ground state to the $6p\ ^2P_{1/2}$ state. If 40.5 GHz microwave radiation repopulates the $F = 1$ level, the trapped ions absorb and scatter radiation from the lamp, and the scattered radiation is detected by a photomultiplier tube.

The frequency of the hyperfine resonance increased rapidly, by about 5 parts in 10^{12}, as the He pressure was increased from 0 to about 1×10^{-4} Pa.[44] Cutler *et al.* interpreted this as a reduction of the second-order Doppler shift, due to collisional cooling of the secular motion. A slow, linear increase in frequency with pressure remained, which they interpreted as pressure shift of the hyperfine resonance. The fractional pressure shift was 4×10^{-11} Pa^{-1}. The maximum He pressure was approximately 10^{-3} Pa. The addition of He increased the ion storage time, increased the ion density, and stabilized the second-order Doppler shift. The storage time was 2.5×10^3 s.

The amplitude of the micromotion depends only on the intensity of the rf electric fields at the positions of the ions. The fields go to zero at the center of the trap and increase in all directions outward from the center. Hence, the second-order Doppler shift due to the micromotion depends on the spatial distribution of the ions in the trap. The spatial distribution depends on the number of ions, the temperature of the secular motion, and the trap parameters. The He collisions do not cool the micromotion directly, but by cooling the secular motion, they increase the ion density, so the ions are closer to the center of the trap. This reduces the micromotion second-order Doppler shift, since the rf electric fields sampled by the ions are reduced.

Cutler *et al.*[44] measured the second-order Doppler shift of the $^{199}Hg^+$ resonance. For 10^6 ions and typical trap parameters, it was -1.2×10^{-12} times the resonance frequency. An analysis of the sidebands of the Dicke-narrowed spectrum of the hyperfine resonance showed that the temperature of the secular motion was reduced to approximately 500 K by the He.[45] Without cooling the kinetic energy of the ions was about 2 eV, which corresponds to a temperature for the secular motion of 8000 K.

Neutral buffer gas cooling is not used in Penning traps, since such collisions would quickly drive the ions out of the trap. Unlike the Paul trap, which is stable in all directions, the Penning trap is unstable in the radial (x-y) direction. Although the particle orbits are stable in the absence of collisions, there is no restoring force in the radial direction. Rather, there is a balance between an electrostatic force directed away from the axis and a magnetic ($\vec{v} \times \vec{B}$) force directed toward the axis.

However, cooling of one ion species by another *charged* species is feasible in some cases in a Penning trap. The Penning trap can simultaneously hold ions of different charge-to-mass ratios. The stability of the trapping is not destroyed by collisions between the different kinds of ions. There must be some means of removing heat from the second species.

Electron cooling is used in storage rings to cool protons or other particles.[46] In this method, a beam of electrons is sent through a straight section of the storage ring, with a velocity that matches the average velocity of the circulating particles. In the frame moving with the average velocity of the ions, the ions lose energy to the electrons. Since the electrons pass through once and are dumped, they do not have to be cooled. Like stochastic cooling, electron cooling was first demonstrated in storage rings and has recently been adapted to ion traps.

Gabrielse *et al.*[47] have demonstrated cooling of trapped antiprotons by collisions with trapped electrons. Cold antiprotons can be applied to tests of CPT invariance (through measurements of their inertial mass) and to measurements of the gravitational force on antimatter.

In the experiment of Gabrielse *et al.*, pulses containing approximately 3×10^8 5.9 MeV antiprotons were extracted from a storage ring and directed toward the trap. After passing through a titanium window and an aluminum plate, some of the antiprotons were slowed down to 3 keV or less and were captured in a Penning trap. A maximum of about 60 000 antiprotons were captured. The Penning trap was made up of several cylinders, which can be held at different electric potentials. The magnetic field was 6 T.

The longitudinal energy distribution was measured by lowering the confining potential at one end of the trap, so that antiprotons that had an energy greater than the potential could escape. The antiprotons were annihilated when they struck the vacuum enclosure. The charged pions that were created were detected by scintillators. Soon after being trapped, the antiprotons had a broad energy distribution, about 2 keV wide. This distribution was almost unchanged after 2.7 d (in the absence of electron cooling).

Cooling of the antiprotons was observed when electrons were introduced to the trap. To improve the control and monitoring of the electron cooling, a small harmonic well was created inside the trap to hold the electrons. This was done by adjusting the potentials of five of the cylindrical electrodes to approximate a quadrupole potential over a short region. Approximately 10^7 electrons were loaded into the trap from a field-emission point. Since the electrons had low energies, they collected at the minimum of the harmonic well. The electrons cooled, by emitting synchrotron radiation, to the temperature of the surrounding apparatus (4.2 K) with a time constant of 0.1 s. The electrons induced a noise voltage across a parallel resonant circuit, which was connected between one of the electrodes and ground potential. This signal was used to determine the number of trapped electrons.[27]

If antiprotons were introduced after the electrons had been loaded and cooled, the voltage across the resonant circuit increased, due to heating of the electrons by the antiprotons. The time constant for cooling of the antiprotons was approximately 10 s. The energy distribution of the antiprotons was measured after cooling. Energy widths

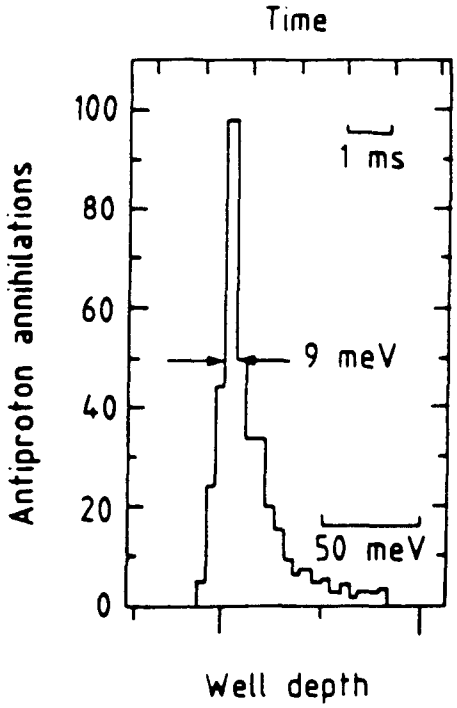

Figure 1: Graph of the number of antiprotons detected as a function of the well depth, which is reduced linearly in time. The width of this distribution reflects the energy distribution of the trapped antiprotons, which are cooled by electrons. (From Ref. [47].)

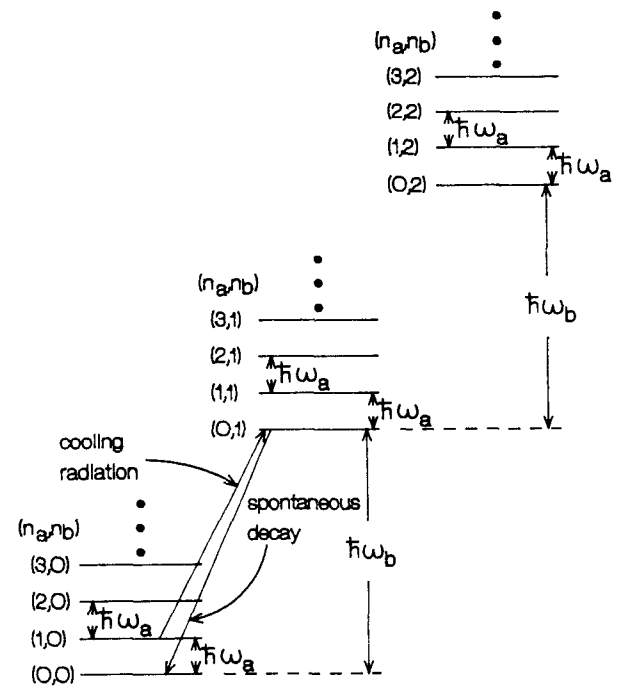

Figure 2: Energy level structure for a particle which is suitable for sideband cooling, having two modes, labeled a and b.

as small as 9 meV were observed (see Fig. 1). Part of this energy spread may have been due to conversion of the space charge potential energy to kinetic energy, as the antiprotons escaped from the trap. Thus, the actual energy spread of the kinetic energies of the antiprotons in the trap may have been even lower.

V. Sideband cooling

Rf sideband cooling and laser cooling (also known as optical sideband cooling) were developed for very different types of measurements. Rf sideband cooling was developed to improve measurements of elementary particle g-factors and of ion masses, by confining the particles to smaller spatial volumes.[48] Laser cooling was developed to reduce Doppler shifts in atomic spectroscopy.[49],[50] However, the two methods are fundamentally the same. Both can be described in terms of mode coupling by a parametric drive.

Figure 2 is a generalized diagram of the mode structure of the cooled system. The system contains two modes, represented by the subscripts a and b. We assume that $\omega_a \ll \omega_b$, so the energy levels separate into manifolds as shown. For simplicity, we assume the level separations in each manifold are the same, so that the energy is $\hbar(n_a\omega_a + n_b\omega_b)$, but this condition is not essential. The cooling relies on (1) parametric coupling of the two modes and (2) relaxation of the b mode by spontaneous decay at a rate γ_b. Spontaneous decay of the a mode is assumed to be negligible. Here, the a mode is a mode of oscillation of an ion, which is to be cooled. Figure 2 shows one part of the cooling process. The particle is initially in the state $(n_a = 1, n_b = 0)$. It absorbs a photon of energy $\hbar(\omega_b - \omega_a)$ from the externally applied field and is driven to the state $(n_a = 0, n_b = 1)$. The particle then spontaneously emits a photon of energy $\hbar\omega_b$ and makes a transition to the state $(n_a = 0, n_b = 0)$. In this process, system's energy is reduced by $\hbar\omega_a$. This is the basic idea of sideband cooling. Heating occurs if the coupling causes absorption of photons of energy $\hbar(\omega_b + \omega_a)$.

In general the process is more complicated. Other absorption processes of the form $(n_a, n_b) \rightarrow (n_a - 1, n_b + 1)$ can be driven by the same applied coupling. The entire distribution of n_a and n_b must be taken into account. Also, even when the coupling is tuned to resonance, other nonresonant transitions can occur, since the resonances are broadened by spontaneous emission.

For rf sideband cooling, ω_b and ω_a are rf frequencies. For example, the b mode might be the axial motion and the a mode might be the magnetron motion, in which case the a mode energy level structure is inverted. Cooling then occurs when the applied coupling is at frequency $(\omega_b + \omega_a)$.

For laser cooling, ω_b is an optical frequency. In this case, the b mode is just a two-level system ($n_b = 0$ or

1). The recoil of the cooled particle upon the spontaneous emission of a photon of frequency ω_b leads to heating. Let $\langle \Delta n_a \rangle$ be the average change in n_a per spontaneous emission. Then,

$$\hbar\omega_a \langle \Delta n_a \rangle = R \equiv (\hbar\omega_b)^2/2mc^2, \tag{14}$$

where R is the recoil energy (the kinetic energy of an initially stationary particle of mass m after emission of a photon of frequency ω_b). We assume that the photon is emitted into free space. That is, the emitted radiation is not influenced by cavity effects. Two cases of laser cooling will be treated separately: $\omega_a \ll \gamma_b$ (sidebands unresolved) and $\omega_a \gg \gamma_b$ (sidebands resolved).

Sideband cooling is closely related to methods of dynamic nuclear orientation.[51] The method of polarization by forbidden transitions is directly analogous to sideband cooling. In this method, an applied rf field drives transitions between states which differ in both the nuclear and electronic spin quantum numbers. This corresponds, for example, to the $(n_a = 1, n_b = 0) \longrightarrow (n_a = 0, n_b = 1)$ transition in Fig. 2. The electronic spin relaxes quickly $[(n_a = 0, n_b = 1) \longrightarrow (n_a = 0, n_b = 0)]$. The nuclear ($a$) mode reaches the same polarization as the electronic (b) mode.

Vyatchanin[52] has discussed, in general terms, the cooling of a quantum oscillator (or two-level system) by parametric coupling to another quantum oscillator (or two-level system) which is more strongly damped. This treatment is directly applicable to sideband cooling.

A. Rf sideband cooling

Rf sideband cooling has been used with great success, first on electrons stored in Penning traps[15] and more recently on atomic or molecular ions stored in Penning traps.[14],[16] It has been especially helpful in reducing the radii of the magnetron orbits of a few particles. Cooling of the magnetron motion is especially important, since most external perturbations, such as collisions with neutral gas, cause the magnetron radius to grow. Without cooling, the ions would eventually strike the ring electrode and be lost. With rf sideband cooling, the ions can be held in a Penning trap for as long as desired.

The case of rf sideband cooling which has received the most attention is when the a mode is the magnetron mode ($\omega_a = \omega_m$) and the b mode is the axial mode ($\omega_b = \omega_z$). This is similar to other cases. Since the a energy levels are inverted, the frequency of the applied drive is tuned to cause transitions of the form $(n_a, n_b) \longleftrightarrow (n_a + 1, n_b + 1)$. Spontaneous emission occurs at frequency ω_b, through coupling of the axial motion to a tuned circuit. We assume that damping of the magnetron motion, in the absence of sideband cooling, can be neglected. Finally, we assume that $\hbar\omega_z \ll k_B T_z$, where T_z is the temperature of the axial motion, and that the axial mode is nearly in thermal equilibrium with the external circuit. The average axial oscillation quantum number $\langle n_z \rangle$ is much greater than 1.

We wish to calculate the magnetron cooling rate. Let the ion be subjected to a parametric coupling in the form of a time-varying potential,[15],[17],[53]

$$V' = \frac{V_d}{d^2} xz\cos(\omega_d t), \tag{15}$$

where d has the dimensions of a length, and x and z are coordinates of the ion. Consider the case where $\omega_d = \omega_z + \omega_m$. The basic mechanism for cooling in this case is as follows: Suppose the x component of the magnetron motion is initially of the form $x = r_m \cos(\omega_m t)$. Substituting this expression for x into Eq. (15), we see that there is a z component of electric field ($-\partial V'/\partial z$) at frequency ω_z, which can excite the axial motion. The axial motion is then damped by the tuned circuit, at a rate γ_z. By this parametric process, the magnetron motion is transferred to the axial motion, which is then removed from the ion by the tuned circuit. We can show from Eq. (15) that the magnetron-induced axial motion gives rise to an electric field in the x direction, and that this field has frequency ω_m and the correct phase to damp the magnetron motion.[17],[53]

If saturation can be neglected, that is, if the axial damping is fast compared to the rate of energy transfer between the axial and magnetron modes, then the magnetron amplitude decays with a rate,[17],[53]

$$\gamma_m \approx \frac{q^2 V_d^2}{4m^2\omega_z\gamma_z(\omega_c - 2\omega_m)}. \tag{16}$$

Brown and Gabrielse[17] have considered a more general case, where saturation is allowed and where ω_d is not necessarily equal to $\omega_z + \omega_m$.

Figure 3 shows rf sideband heating and cooling of a single electron in a Penning trap. The magnetron radius r_m, plotted on the vertical axis, increases when the drive is applied at angular frequency ω_d equal to $\omega_z - \omega_m \equiv 2\pi(\nu_z - \nu_m)$. It shrinks when $\omega_d = \omega_z + \omega_m$.

If damping of both the axial and magnetron motions can be neglected, this type of parametric coupling leads to a sinusoidal exchange of the energies in the two modes. Parametric coupling of modes of ions in a Penning trap has been studied theoretically, for this case, by Cornell *et al.*[54]

The exchange of excitation between modes in a Penning trap, by coupling with a parametric drive, has been used to cool the cyclotron motion of ions in a recent experiment at MIT.[16] In this experiment, the ratio of the masses of CO^+ and N_2^+ was measured to an accuracy of 4×10^{-10}. This is the most accurate mass comparison to date. A short rf pulse of the appropriate amplitude and duration exchanges the phases and actions of the cyclotron and axial modes. The action of the rf pulse is mathematically like that of a π pulse applied to a two-level system. Since the axial motion is kept cold by resistive cooling, application of the π pulse cools the cyclotron motion. The axial motion is heated immediately after the pulse, but is cooled again resistively. Ordinary rf sideband cooling,

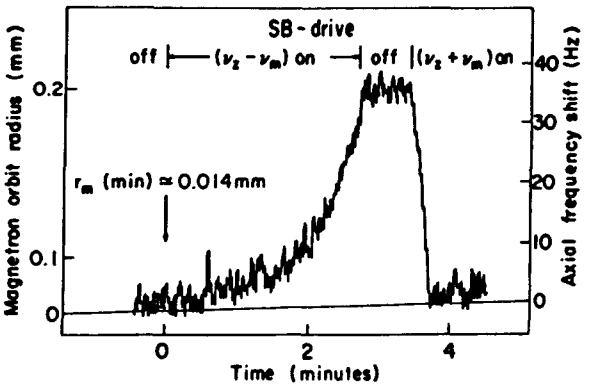

Figure 3: Rf sideband heating and cooling of the magnetron mode of a single electron in a Penning trap. The vertical scale is the axial oscillation frequency. This is related to the magnetron radius because of a deliberately applied magnetic inhomogeneity "bottle." (From Ref. [15].)

with cw excitation at frequency $\omega_z + \omega_m$ was used to cool the magnetron motion.

For both cw and pulsed parametric coupling, the minimum achievable temperature is determined by heating of the axial motion by thermal noise. When the axial motion is coupled to the tuned circuit, it has an amplitude due to random thermal noise. This causes a random excitation of the magnetron motion, given by Eq. (15), through the parametric coupling between the modes. The resulting noise excitation of the magnetron motion (or cyclotron motion in in the case of the MIT group) gives the limit for sideband cooling. This theoretical limit can be calculated from the equations of motion,[17],[53] by thermodynamic arguments,[55] or by detailed-balance arguments.[17] The result, for the case where $k_B T_b \gg \hbar\omega_b$, is

$$|T_a(\min)| = \frac{\omega_a}{\omega_b}|T_b|. \qquad (17)$$

Cooling is routinely observed in several experiments, but the temperatures achieved are somewhat higher than the limit given by Eq. (17).

B. Optical sideband cooling (resolved sidebands)

In optical sideband cooling, the b mode is an internal optical transition in a trapped particle. Generally, the transition is an electronic transition (at an optical frequency) which relaxes radiatively by spontaneous emission at the rate γ_b. The quantum number n_b takes only the values 0 and 1. Here we consider the resolved sideband case ($\gamma_b \ll \omega_a$), where ω_a is the oscillation frequency of the cooled mode of the bound particle. (The unresolved sideband case will be discussed in Section V. C.) Optical sideband cooling of trapped ions and neutral atoms has been an active field of research.[1],[2] New methods of laser cooling, which are distinct from optical sideband cooling, have recently been developed for neutral atoms.[56]–[59] These methods have not yet been applied to trapped ions.

The parametric coupling from the ground state vibrational manifold ($n_b = 0$) to the excited state vibrational manifold ($n_b = 1$) is done with narrowband radiation. The width $\Delta\omega_b$ of the radiation should be less than or on the order of γ_b for optimal cooling. It should be resonant with the first lower sideband at frequency $\omega_b - \omega_a$. If the recoil energy R [defined in Eq. (14)] is less than the vibrational energy $\hbar\omega_a$, then sideband cooling is possible. (Otherwise the cooling which results from the photon absorption is undone by the recoil from the photon emission.) An atom absorbs photons of energy $\hbar(\omega_b - \omega_a)$ and reemits photons of average energy $\hbar\omega_b$. Hence, on the average, each scattered photon reduces the atom's vibrational energy by $\hbar\omega_a$ and the atom's vibrational quantum number n_a by 1. In this way, it is possible to make the mean quantum number $\langle n_a \rangle$ much less than 1, provided that $R \ll \hbar\omega_a$. If $\langle n_a \rangle \ll 1$ for all motional degrees of freedom, then the atom resides in the ground state level of the confining potential most of the time.

Optical sideband cooling of the thermal degrees of freedom of many simultaneously trapped particles is possible in principle. However, the kinetic energy in coherent degrees of freedom usually limits the minimum attainable kinetic energy. The higher energies of the coherent motions in both the Penning trap and in the Paul trap are consequences of Coulomb repulsion.

In a Penning trap, any ion that does not lie on the symmetry axis of the trap rotates about the axis, due to crossed electric and magnetic fields ($\vec{E} \times \vec{B}$ drift). This rotation gives rise to a kinetic energy that depends quadratically on the radial distance of the ion from the trap axis. It might be possible for a few ions to lie along the symmetry axis. However, if there are many ions, the combined effects of the trapping fields and the mutual Coulomb repulsion of the ions will force some of the ions to lie at a finite distance from the axis.

In a Paul trap, the Coulomb repulsion between ions is balanced by a force from the trapping potential, directed toward the center of the trap. Only one ion can occupy the center of the trap, where the applied trap fields go to zero. Any offset of an ion from the trap center leads to micromotion of the particle at the frequency of the applied rf field. The kinetic energy in this nonthermal motion cannot be reduced by sideband cooling. So, although it is possible to reduce the kinetic energy of the secular motion for more than one ion, the kinetic energy in the micromotion remains undiminished and can be substantial. This limitation could be overcome in a Paul trap with linear geometry.[60]–[62] In such a trap, the magnitude of the rf field approaches zero on a line, rather than at a point.

Even for a single ion, optical sideband cooling in a Penning trap is difficult. The magnetron, cyclotron, and axial frequencies cannot be degenerate for stable trapping. This leads to a complicated sideband spectrum.[63] The spectrum contains sidebands not only at the fundamental motional frequencies (for example, $\omega_b \pm \omega_m$), but also all intermodulation products ($\omega_b + j\omega_c' + k\omega_z + \ell\omega_m$, where j, k, ℓ are any integers). At high temperatures this spec-

trum is nearly continuous. Therefore, precooling to near the Dicke limit ($x_{\rm rms} \ll \lambda/2$) is required before sideband cooling is done. Here, $x_{\rm rms}$ is the rms value of the x coordinate of the ion, and $\lambda = 2\pi c/\omega_b$)

Attaining the lowest vibrational energies (the minimum $\langle n_a \rangle$) for all degrees of freedom would require cooling with a laser tuned to an individual sideband for each of the three motional degrees of freedom. Finally, the condition that the recoil energy R be much less than any of the motional energies is more readily satisfied in the Paul trap than in the Penning trap.

For both Paul and Penning traps, the sideband cooling limit for a single ion is

$$\langle n_a \rangle = \frac{1}{4}\left(\alpha + \frac{1}{4}\right)(\gamma_b/\omega_a)^2, \tag{18}$$

where α depends on the angular distribution for photon emission and is of order 1. Equation (18) is valid when the intensity of the cooling radiation is below saturation and when $\gamma_b/\omega_a \ll 1$. The limit results from a balance between cooling and heating. The most important cooling process is on-resonance absorption of a photon on the lower sideband ($n_a \longrightarrow n_a - 1$), followed by emission on the carrier ($n_a \longrightarrow n_a$). (In the Dicke limit, almost all emission is on the carrier.) The most important heating processes are (1) off-resonance $n_a \longrightarrow n_a + 1$ transitions, followed by emission on the carrier, and (2) off-resonance $n_a \longrightarrow n_a$ transitions, followed by emission on the lower sideband ($n_a \longrightarrow n_a + 1$). This result was derived by Neuhauser *et al.*[64] and others.[55],[65] Wineland *et al.*[63] considered the effect of finite laser bandwidth and also explicitly treated resolved optical sideband cooling in a Penning trap.

Lindberg[66] and Javanainen *et al.*[67] have derived the steady-state energy of a single two-level atom, confined in a one-dimensional harmonic well of frequency ω_a, for arbitrary laser frequency, laser intensity, and γ_b/ω_a:

$$\langle E_a \rangle \equiv \hbar\omega_a\left(\langle n_a \rangle + \frac{1}{2}\right) = \tag{19}$$
$$\frac{\hbar}{-4\Delta}[\omega_a^2(\Delta^2 + \gamma_2^2 + 6\kappa^2) + 4\gamma_2^2(\Delta^2 + \gamma_2^2 + 2\kappa^2)]^{-1}$$
$$\times\{\alpha[\omega_a^2(\Delta^2 + 5\gamma_2^2 + 4\kappa^2 - \omega_a^2)^2$$
$$+4\gamma_2^2(\Delta^2 + \gamma_2^2 + 2\kappa^2 - 2\omega_a^2)^2]$$
$$+\omega_a^2(\Delta^2 + \gamma_2^2 + 2\kappa^2)(\Delta^2 + 5\gamma_2^2 + 8\kappa^2 + \omega_a^2)$$
$$+4\gamma_2^2[(\Delta^2 + \gamma_2^2 + 2\kappa^2)^2 + 2\kappa^2(\Delta^2 - 3\gamma_2^2 - 3\omega_a^2)]\}.$$

This result holds in the limit that $R/(\hbar\omega_a) \ll 1$. Here, κ is the Rabi frequency, which is proportional to the square root of the laser intensity, and $\gamma_2 \equiv \gamma_b/2$. The detuning Δ is defined as $\Delta \equiv \omega - \omega_b$, where ω is the laser frequency. It must be negative (laser frequency below resonance), or else there is no steady state. Equation (20) reduces to Eq. (18) in the limit $\kappa \to 0$, $\gamma_2/\omega_a \to 0$, and $\Delta \to -\omega_a$.

The value of $\langle n_a \rangle$ can be determined experimentally from the relative transition strengths for on-resonance absorption on the first lower and upper sidebands.[63],[68] When $\langle n_a \rangle \ll 1$, the strength of resonant absorption on the lower sideband ($\omega_b - \omega_a$), which is proportional to $\langle n_a \rangle$, approaches zero. When the ion is in the lowest kinetic energy state ($n_a = 0$), it is no longer possible to extract vibrational quanta from the ion. The strength of the upper sideband ($\omega_b + \omega_a$) is proportional to $\langle n_a \rangle + 1$. Thus, if the lower and upper sidebands are probed with saturating power, the ratio of their absorption strengths becomes independent of power and directly gives $\langle n_a \rangle$.

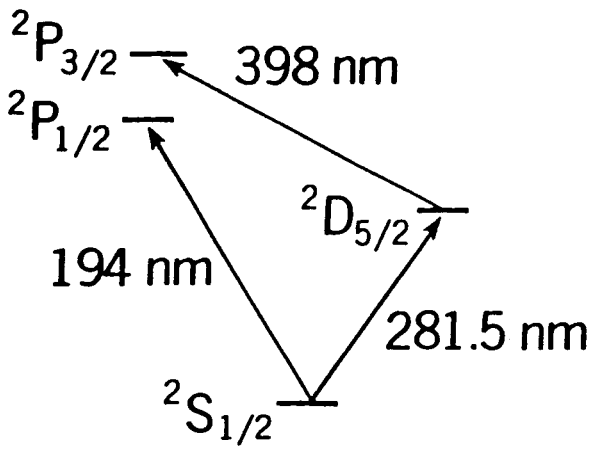

Figure 4: A simplified energy level diagram of Hg^+, showing the transitions used for optical sideband cooling. (From Ref. [68].)

A single $^{198}Hg^+$ ion, confined in a small Paul trap, has been laser-cooled, in the resolved sideband limit, to near the zero-point energy of motion.[68] The electronic energy levels of Hg^+ are shown in Fig. 4. The procedure was as follows: First, the ion was laser-cooled in the Doppler-cooling limit (discussed in Section V. C. 1.), by radiation scattered from the strongly allowed 194 nm first resonance line. This reduced the temperature to about 1.7 mK and the mean vibrational quantum number $\langle n_a \rangle$ to about 12. The secular frequency ($\omega_a/2\pi$) was about 3 MHz. Laser radiation, tuned to the first lower vibrational sideband of the narrow 282 nm $5d^{10}6s\ ^2S_{1/2}$-to-$5d^9 6s^2\ ^2D_{5/2}$ transition, was then applied to the ions. In order to speed the cooling process, 398 nm laser radiation was used to drive ions from the $^2D_{5/2}$ state to the $5d^{10}6p\ ^2P_{3/2}$ state, which decays rapidly to the ground $^2S_{1/2}$ state. This allowed the absorption of 282 nm photons to proceed faster than the 90 ms natural lifetime of the $^2D_{5/2}$ state would have allowed. After scattering enough photons to remove 12 vibrational quanta from the ion for each degree of freedom, laser radiation of saturating intensity probed the 282 nm sideband spectrum.

The results are shown in Fig. 5. The fact that the intensity of the lower sideband (S_L) is much less intense than the upper sideband (S_U) indicates that $\langle n_a \rangle \ll 1$. From these data, it was deduced that the ion was in the lowest vibrational quantum state, for the y and z degrees of freedom, 95% of the time. This corresponds to a temperature of 47 ± 3 μK. Since the 282 nm probe beam was

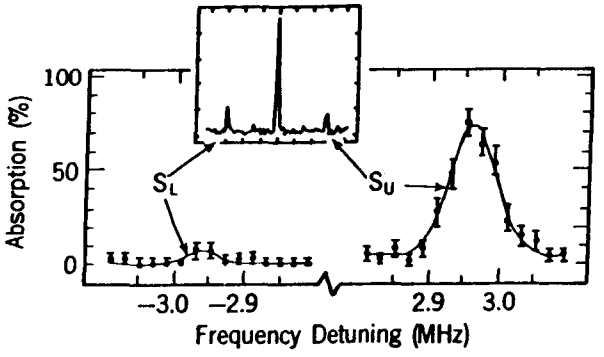

Figure 5: Absorption spectrum of the $^2S_{1/2}$-to-$^2D_{5/2}$ electric quadrupole transition. The vertical scale is the probability that the ion makes a $^2S_{1/2}$-to-$^2D_{5/2}$ transition when the probing 282 nm radiation is applied. The spectrum in the small inset was taken before the sideband cooling was applied. S_L is the first lower sideband (frequency $\omega_b - \omega_a$); S_U is the first upper sideband (frequency $\omega_b + \omega_a$). The asymmetry between S_U and S_L indicates that the average quantum number for the oscillation of the ion is much less than 1. (From Ref. [68].)

nearly orthogonal to the motion in the x direction, the measurement was not very sensitive to the energy in this degree of freedom. For this reason, a precise measurement of the x vibrational energy could not be made in this experiment. Cooling of all degrees of freedom could be done by orienting the 282 nm beam at a different angle with respect to the trap axes.

C. Optical sideband cooling (unresolved sidebands)

In most experiments on optical sideband cooling, a strongly allowed optical transition, which has a natural linewidth γ_b of approximately 20 MHz or more, is used. This is much greater than the motional frequencies of the trapped ion (typically 3 MHz or less). The sideband structure of the optical resonance is not resolved. It is then natural to treat the motion of the ion classically. The scattering of laser light by the ion leads to a force on the ion. The scattering takes place in a time of about γ_b^{-1}, much less than the orbital period, so it can be assumed to give an instantaneous impulse to the ion. In the low intensity limit, the average force on an atom is the product of the average momentum transfer per scattering (the photon momentum $\hbar\vec{k}$) and the scattering rate. The size of the force is maximized when the laser frequency, in the frame moving with the ion, is in resonance with the optical transition. Fluctuations in the force arise from (1) the randomness of the direction of the scattered photon and (2) the random time distribution of the scattering events. As an alternative to this semiclassical approach, the cooling can also be explained with the general concepts of sideband cooling.[55],[64] It is necessary, in this case, to include a large number of sidebands in the analysis.

1. Paul traps

An ion in a Paul trap can be treated, to a good approximation, as a particle in a three-dimensional harmonic potential, undergoing simple harmonic motion at the secular frequencies. The micromotion can be added by numerical simulation,[20],[40],[69] but is hard to treat analytically.

For simplicity, consider an ion moving in a harmonic well in the x direction, interacting with a laser beam propagating in the $+x$ direction. If the ion has a velocity v and the laser detuning is Δ, the average force is

$$\begin{aligned} F_{\rm av} &\approx \frac{I\sigma_0}{\hbar\omega}\frac{\gamma_2^2}{[(\Delta - kv)^2 + \gamma_2^2]}\hbar k \\ &\approx \frac{I\sigma_0\gamma_2^2}{\hbar\omega(\Delta^2+\gamma_2^2)}\left[1 + \frac{2\Delta kv}{\Delta^2+\gamma_2^2}\right]\hbar k \\ &\equiv F_0 - m\Gamma v, \end{aligned} \tag{20}$$

where I is the laser intensity, σ_0 is the resonant scattering cross-section, and m is the mass of the ion. The approximation holds for low intensities $[I\sigma_0/(\hbar\omega) \ll \gamma_2]$ and low velocities $(kv \ll \gamma_2)$.

In the last line of Eq. (20), F_0 is a velocity-independent force, which slightly displaces the equilibrium position of the ion, and $m\Gamma v$ is a damping force (for $\Delta \ll 0$), which leads to cooling. The fluctuations in the force, which are due to the discreteness of the photon scatterings, have properties similar to electronic shot noise.[70] The equation of motion for the ion position is the same as that of a series RCL (resistance-capacitance-inductance) circuit driven by a fluctuating emf. The steady-state energy of the ion can be calculated by methods analogous to those used to calculate noise in electronic circuits.[71]

The steady-state energy is

$$\langle E_a \rangle = \frac{(1+\alpha)\hbar(\gamma_2^2+\Delta^2)}{-4\Delta}. \tag{21}$$

This agrees with Eq. (20) in the limit where $\kappa \to 0$ and $\omega_a/\gamma_2 \to 0$. The lowest energy is obtained when $\Delta = -\gamma_2$:

$$\langle E_a \rangle = k_B T = \frac{(1+\alpha)\hbar\gamma_2}{2}. \tag{22}$$

For $\alpha \approx 1$, this yields the Doppler-cooling limit, $k_B T \approx \hbar\gamma_2 = \hbar\gamma_b/2$, which also holds, under suitable conditions, for free two-level atoms.[55],[64],[72] For typical cases, $T \approx 1$ mK.

Optical sideband cooling in a Paul trap was first demonstrated experimentally by Neuhauser *et al.*[64] They cooled Ba^+ ions, using the 493 nm, $6s\ ^2S_{1/2}$-to-$6p\ ^2P_{1/2}$ transition. One complication in the experiment was that the $6p\ ^2P_{1/2}$ state can decay to the metastable $5d\ ^2D_{3/2}$ state. A 650 nm laser beam drove the ions from the $5d\ ^2D_{3/2}$ state back to the $6p\ ^2P_{1/2}$ state, so that the cooling could continue. The effect of cooling was to increase the storage time of the ions in the trap. Figure 6 shows the effect of laser cooling when the 493 nm laser is tuned below the $6s\ ^2S_{1/2}$-to-$6p\ ^2P_{1/2}$ transition. Later,

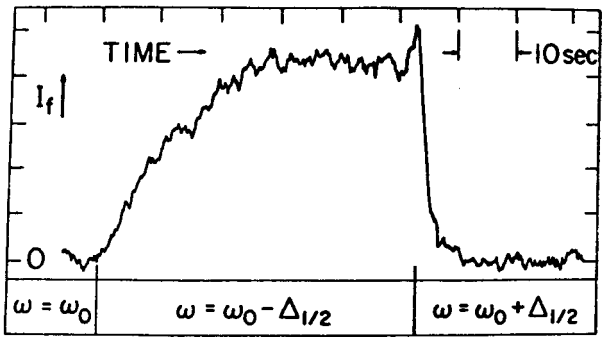

Figure 6: The first optical sideband cooling of ions in a Paul trap. The Ba^+ fluorescence intensity is plotted as a function of time. The trap is initially empty when the laser frequency ω is equal to the atomic resonance ω_0. The fluorescence increases when ω is tuned below the atomic resonance to $\omega_0 - \Delta_{1/2}$. It decreases rapidly when $\omega = \omega_0 + \Delta_{1/2}$. Here, $\Delta_{1/2}$ is the resonance half-width in the discharge tube used as a reference. (From Ref. [64].)

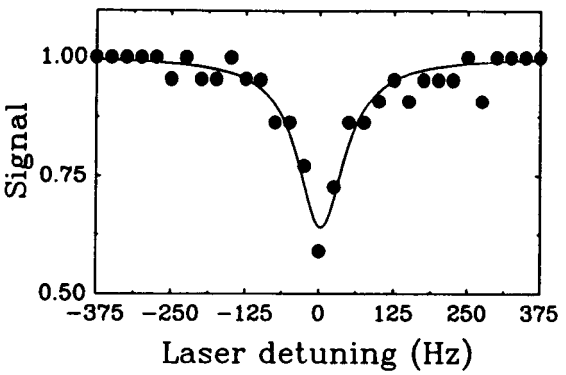

Figure 7: Absorption resonance for a single Zeeman-hyperfine component of the $5d^{10}6s\ ^2S_{1/2}$-to-$5d^96s^2\ ^2D_{5/2}$ transition in a single $^{199}Hg^+$ ion. The probability that the ion did not make a transition to the $^2D_{5/2}$ state is plotted on the vertical axis. The relative frequency of the 563 nm laser, which was frequency doubled to 282 nm, is plotted on the horizontal axis. The curve is a least-squares fit to a Lorentzian. The width of the Lorentzian is about 90 Hz. (From Ref. [74].)

Neuhauser *et al.* were able to estimate the temperature of a single ion to be less than 36 mK, from the size of its photographed image.[73]

Bergquist *et al.*[13] cooled a single Hg^+ ion, confined in a Paul trap, using the 194 nm $5d^{10}6s\ ^2S_{1/2}$ to $5d^{10}6p\ ^2P_{1/2}$ transition. The narrow 282 nm $5d^{10}6s\ ^2S_{1/2}$ to $5d^96s^2\ ^2D_{5/2}$ transition was used to determine the temperature. The relative intensities (transition probabilities) at the frequencies of the carrier (ω_b) and at the first sidebands ($\omega_b \pm \omega_a$) were measured. Equation (44) of Ref. [55] relates the relative intensities of the carrier and sidebands to the temperature. The measured temperature was 1.6 ± 0.5 mK, in good agreement with the Doppler-cooling limit of 1.7 mK. In later experiments with a single $^{199}Hg^+$ ion, the 282 nm carrier was observed with a linewidth of under 200 Hz ($Q \approx 5 \times 10^{12}$).[74] A typical resonance curve is shown in Fig. 7. Similar experiments have been done with a single Ba^+ ion by Nagourney *et al.*[75] They observed the 1.8 μm $6s\ ^2S_{1/2}$-to-$5d\ ^2D_{5/2}$ transition with a linewidth of about 40 kHz.

Optical sideband cooling of ions in Paul traps has been applied to other areas of physics. Radiative lifetimes have been measured in single, laser-cooled ions of Mg^+ (Ref. [76]), Ba^+ (Refs. [77] and [78]), and Hg^+ (Ref. [79]). Rates for quenching of a metastable state by various gases have been measured in single, laser-cooled Ba^+ ions.[78] The fluorescence from a single cooled ion can be easily observed. This has made it possible to observe certain inherently quantum properties of the electromagnetic field, such as photon antibunching[80]–[82] and quantum jumps.[77],[81],[83]

If several ions in a Paul trap are cooled to a low enough temperature, they arrange themselves into spatial configurations which minimize the potential energy. Such ordered patterns have been observed with laser cooled Mg^+ (Ref. [19]), Hg^+ (Ref. [7]), and Ba^+ (Refs. [20] and [21]). Phase transitions of these ions between ordered and disordered states have been studied, especially with regard to classical chaos.[19],[20],[40]

2. *Penning traps*

In some respects, optical sideband cooling of ions in Penning traps and Paul traps are similar. The axial and cyclotron modes are cooled if the laser is detuned below resonance. The differences arise from the $\vec{E} \times \vec{B}$ rotation of the ions around the trap axis. The rotation frequency of a single ion is the magnetron frequency ω_m. The rotation frequency of many ions is increased by electric fields caused by space charge.

Cooling of the rotation requires control of L_z, the z component of the canonical angular momentum of the ions.[84] For a single ion of charge q and mass m, the canonical angular momentum is $\vec{\ell} = \vec{r} \times \vec{p}$, where $\vec{r}$ and $\vec{p}$ are the position and the canonical momentum of the ion. The canonical momentum is defined as $\vec{p} \equiv m\vec{v} + (q/c)\vec{A}(\vec{r})$, where $\vec{v}$ is the velocity of the ion and $\vec{A}(\vec{r})$ is the vector potential at $\vec{r}$. For convenience, we choose the symmetric gauge, where $\vec{A}(\vec{r}) = \frac{1}{2}\vec{B} \times \vec{r}$ and $\vec{B}$ is the magnetic field. The z component of $\vec{\ell}$ is

$$\ell_z \equiv m v_\theta \rho + \frac{qB\rho^2}{2c}, \tag{23}$$

where v_θ and $\rho = (x^2+y^2)^{1/2}$ are the azimuthal component of the velocity and the cylindrical radius of the ion. For N identical ions of charge q and mass m,

$$L_z \equiv \sum_{i=1}^{N} \left(m v_{\theta,i} \rho_i + \frac{qB\rho_i^2}{2c} \right), \tag{24}$$

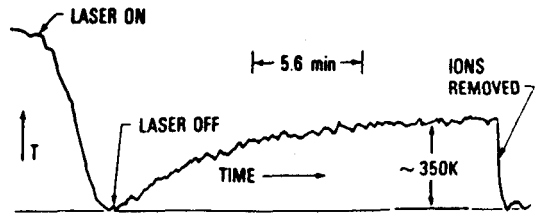

Figure 8: The first optical sideband cooling of ions in a Penning trap. The vertical scale is the axial temperature of the Mg^+ ions. The ions were heated by the laser before the beginning of the data. The laser was turned on with a frequency below the resonance frequency, cooling the ions to below 40 K. After the laser is turned off, the ions thermalize to the ambient temperature of 350 K. (From Ref. [87].)

where v_{θ_i} and ρ_i are the azimuthal component of the velocity and the cylindrical radius of the ith ion. If the trap has perfect axial symmetry and there are no interactions with the outside world, L_z is conserved. For the typical case, where the rotation frequency is much less than the cyclotron frequency $qB/(mc)$, the second term of Eq. (24) dominates. Conservation of L_z is then equivalent to conservation of the mean squared radius of the ion plasma. A more general proof of the fact that conservation of L_z leads to radial confinement has been given by O'Neil.[85]

There are confined thermal equilibria, whose properties are determined by the three conserved quantities: N, L_z, and the energy.[86] One property of these thermal equilibria is uniform rotation. That is, the velocity distribution, with respect to a rotating frame, is Maxwellian. In a continuous fluid model, the zero-temperature equilibria are uniformly rotating spheroids of uniform density.[84]

Asymmetries of the trap fields apply torques to the ions, so that L_z is not perfectly conserved. This leads to radial expansion. The light-scattering force from a laser beam can be used to apply a torque to the ions. This torque can be used to cancel the torques from the trap fields and establish radial confinement. Such a torque could also be applied with a neutral atomic beam.

The first experimental demonstration of optical sideband cooling in a Penning trap was made by Wineland *et al.*[87] Approximately 5×10^4 Mg^+ ions were cooled by a 280 nm laser beam tuned slightly lower in frequency than one Zeeman component of the $3s\ ^2S_{1/2}$-to-$3p\ ^2P_{3/2}$ transition. The temperature of the ions was determined from noise current induced on the electrodes. The ions were cooled below 40 K. This was the measurement limit set by the electronic noise. Figure 8 shows the decrease in temperature when the laser is turned on, with a frequency below the resonance frequency. Collisions with neutral gas molecules cause the ions to rethermalize after the laser is turned off. Optical sideband cooling of Mg^+ ions in Penning traps has also been observed by Plumelle *et al.*[88] and by Thompson *et al.*[89]

Drullinger *et al.*[5] laser-cooled Mg^+ ions to approximately 0.5 K. The temperature was determined from the Doppler width of the transition. They also demonstrated the connection between the plasma radius and the canonical angular momentum. Placing the laser beam on one side or the other of the axis exerted a torque on the ions, which caused radial expansion or contraction of the plasma.

If the cooling laser beam is perpendicular to the rotation axis, the steady state temperature can be calculated from the rotation frequency and the laser frequency and intensity profile.[90] The temperature is calculated from the requirement that the work done on the ions by the laser beam, averaged over the velocity distribution, be zero. The temperature increases with the rotation frequency, the distance between the axis and the laser beam, and the laser intensity. Itano *et al.*[90] obtained good agreement between the calculated and observed temperatures of Be^+ ions, over a wide range of experimental parameters.

In general, lower temperatures are obtained when the cooling laser beam is not perpendicular to the magnetic field. Brewer *et al.*[91] observed temperatures of Be^+ ions as low as 2 mK, when cooling beams were directed simultaneously at 90° and at 55° with respect to the magnetic field. They also confirmed experimentally the relationship between the rotation frequency and the shape of the ion plasma that was predicted in Ref. [84].

The reduction of Doppler shifts and the spatial confinement which results from the cooling has been useful for several experiments. Some examples are in mass spectroscopy[92] and in the observation of single-ion quantum jumps.[93] High-resolution optical spectra of Mg^+ (Ref. [5]) and Be^+ (Ref. [94]), have yielded hyperfine constants, fine structure separations, and isotope shifts. Rf–optical double resonance experiments have yielded ground-state hyperfine constants and g-factors of $^{25}Mg^+$ (Ref. [95]) and $^9Be^+$ (Ref. [92]).

A frequency standard, based on a 303 MHz ground-state hyperfine transition in laser cooled $^9Be^+$ ions, has been demonstrated.[96] The estimated error of this standard, about 1 part in 10^{13}, is comparable to that of primary cesium atomic beam standards. A search was made for any dependence of the frequency on the orientation of the magnetic field, with null results.[97] This is one of the most precise tests of local Lorentz invariance.

Ion plasmas which have high enough densities and low enough temperatures are called strongly coupled. In such plasmas, the positions of neighboring ions are correlated with each other, as in a liquid or a solid. Strongly coupled plasmas have been produced, by optical sideband cooling of ions in Penning traps.[98] Spatial ordering, in the form of concentric shells, has been directly observed by imaging of the resonance fluorescence.[22] Numerical simulations predict the existence of such shells.[99],[100]

VI. Sympathetic laser cooling

Because laser cooling depends on having a favorable energy level structure, it has been demonstrated on only a handful of different ion species (Be^+, Mg^+, Ba^+, Hg^+, and Yb^+). However, the technique of sympathetic laser cooling[6],[101] can be used to cool any ion species to sub-kelvin temperatures. In sympathetic laser cooling, two different ion species are loaded into a trap. One of the ion species is laser cooled. The other species is sympathetically cooled by its Coulomb interaction with the laser-cooled species. In a Penning trap, the sympathetically cooled species must have the same sign of charge as the laser-cooled ion species. Sympathetic laser cooling may enable the formation of cold, strongly coupled plasmas of positrons.[101]

In principle, sympathetic laser cooling can be done in either a Paul or a Penning trap. In a Paul trap, ordered, crystal-like structures in which at least one of the "lattice" sites was occupied by an impurity (perhaps another isotope) that was not directly laser-cooled have been observed.[7],[21],[102] These ions did not fluoresce, but their presence was detected by their effect on the positions of the other ions. This shows that at least a small number of ions can be sympathetically laser-cooled to sub-kelvin temperatures in a Paul trap. (If the nonfluorescing ions had not been cold, the ordered structures would not have formed.) In general, rf heating and the available cooling laser power limits the number of ions that can be sympathetically laser-cooled in a Paul trap. In the Penning trap, which is free of rf heating, experiments have demonstrated sympathetic laser cooling on much larger numbers of ions.[6],[103],[104] Sympathetic laser cooling is a form of collisional cooling between charged particles. However, the low temperatures that can be achieved with laser cooling produce some new features.

For simplicity, consider two ion species with like charges but different masses confined in the same Penning trap. The rotation of the ions about the magnetic field axis of the trap produces a centrifugal separation of the ion species.[105] For typical experimental conditions, where the rotation frequency is much less than the cyclotron frequency, the rotation frequency is nearly independent of ion mass. This is because the rotation is a circular $\vec{E} \times \vec{B}$ drift. The velocity for linear $\vec{E} \times \vec{B}$ drift is independent of mass. However, a more exact calculation shows that the higher mass ions rotate at a higher frequency than the lower mass ions, if they occupy they occupy the same volume in the trap, so that they are subjected to the same electric fields.

The equal and opposite momentum transfers due to the different rotation frequencies will cause the lighter ions to move in (toward the trap axis) and the heavier ions to move out. This separation of the ions continues until both species are rotating at the same frequency, as a result of the change in the space charge induced electric fields. Uniform rotation is one characteristic of thermal equilibrium of a nonneutral plasma.[105] In the low temperature limit, the separation is complete, and a gap forms between the ion species.[6],[101],[105] The higher mass ions form a "doughnut" around the lower mass ions. Although the separation of the ion species limits the thermal coupling between the species, sympathetic laser cooling has been demonstrated experimentally in a number of cases.[5],[6],[103]

The first temperature and density measurements on sympathetically cooled ions were done with Hg^+ ions, sympathetically cooled by laser-cooled Be^+ ions.[6] The ions were confined in a Penning trap. Up to 12 000 Be^+ ions, with temperatures less than 0.2 K, sympathetically cooled a larger number of Hg^+ ions to temperatures less than 1.8 K. As expected, Hg^+ ions were observed at larger distances from the trap axis than the Be^+. However, since the laser beams which probed the spatial distribution of the ions were perpendicular to the trap axis, not along the axis, complete separation could not be experimentally verified. The sympathetic cooling also prevented the radial diffusion of the Hg^+ ions. The Be^+ cooling laser applied a torque to the Be^+ ions, and this torque was transmitted by the Coulomb interaction to the Hg^+ ions. If the Be^+ cooling laser was blocked or tuned off resonance, the Hg^+ ions left the trap in several minutes. With sympathetic cooling, the Hg^+ ions were confined indefinitely.

In another Penning trap experiment, laser-cooled Mg^+ ions were used to sympathetically cool and radially confine Be^+ ions.[103],[104] The sympathetic cooling was used to improve the performance of the $^9Be^+$ frequency standard discussed in Section V. C. 2. In order to avoid ac Stark shifts, the laser used to cool and detect the Be^+ ions was turned off when the hyperfine transition was driven. With this laser off, the Be^+ plasma expanded radially, due to torques originating from trap asymmetries. The radial expansion releases electrostatic potential energy, leading to heating of the ions.[96] The expansion and subsequent heating were eliminated by using approximately 100 000 Mg^+ ions to sympathetically cool about 5000 Be^+ ions to temperatures less than 0.25 K. The ac Stark shift on the Be^+ hyperfine transition, due to the Mg^+ cooling laser, was estimated to be less than 1 part in 10^{15}. This could be neglected relative to other systematic shifts. The Mg^+ ions were observed, with an imaging photomultiplier tube, to form a doughnut around the Be^+ ions. The size of the gap between the two species could not be determined, because the optical system could not be focused at both wavelengths at the same time. In this way a cold, steady-state cloud of Be^+ ions was obtained, independent of the Be^+ cooling laser. The sympathetic cooling enabled long measurement periods (up to 550 s), free from the perturbing effects of the Be^+ cooling laser. The observed resonance linewidth is inversely proportional to the measurement time. For a measurement time of 550 s, 900 μHz linewidth was observed on the 303 MHz hyperfine transition.[103] A typical resonance curve is shown in Fig. 9.

The frequency standard based on this hyperfine transition was used to test the linearity of quantum mechanics.[104] A nonlinearity would have resulted in a dependence of the resonance frequency on the degree of

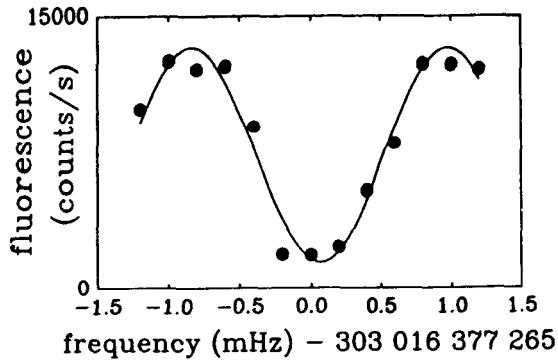

Figure 9: Resonance signal of the 303 MHz hyperfine transition of $^9Be^+$ at a magnetic field of 0.8194 T. A decrease in the fluorescence intensity corresponds to an increase in the transition probability. The width of the resonance is 900 μHz. (From Ref. [103].)

excitation of the transition, analogous to the frequency shift of an anharmonic oscillator with amplitude. An upper limit of 6 μHz was placed on a nonlinear correction to the Hamiltonian of the Be^+ nucleus.

References

[1] S. Stenholm, Rev. Mod. Phys. **58**, 699 (1986).

[2] D. J. Wineland and W. M. Itano, Phys. Today **40** (6), 34 (1987).

[3] H. G. Dehmelt, Adv. At. Mol. Phys. **5**, 109 (1969).

[4] M. H. Holzscheiter, Phys. Scripta **T22**, 73 (1988).

[5] R. E. Drullinger, D. J. Wineland, and J. C. Bergquist, Appl. Phys. **22**, 365 (1980).

[6] D. J. Larson, J. C. Bergquist, J. J. Bollinger, W. M. Itano, and D. J. Wineland, Phys. Rev. Lett. **57**, 70 (1986).

[7] D. J. Wineland, J. C. Bergquist, W. M. Itano, J. J. Bollinger, and C. H. Manney, Phys. Rev. Lett. **59**, 2935 (1987).

[8] R. H. Dicke, Phys. Rev. **89**, 472 (1953).

[9] J. C. Bergquist, D. J. Wineland, W. M. Itano, H. Hemmati, H.-U. Daniel, and G. Leuchs, Phys. Rev. Lett. **55**, 1567 (1985).

[10] E. N. Fortson, F. G. Major, and H. G. Dehmelt, Phys. Rev. Lett. **16**, 221 (1966).

[11] F. G. Major and G. Werth, Phys. Rev. Lett. **30**, 1155 (1973).

[12] G. Janik, W. Nagourney, and H. Dehmelt, J. Opt. Soc. Am. B **2**, 1251 (1985).

[13] J. C. Bergquist, W. M. Itano, and D. J. Wineland, Phys. Rev. A **36**, 428 (1987).

[14] R. S. Van Dyck, Jr., F. L. Moore, D. L. Farnham, and P. B. Schwinberg, Int. J. Mass Spectrom. Ion Processes **66**, 327 (1985).

[15] R. S. Van Dyck, Jr., P. B. Schwinberg, and H. G. Dehmelt, in *New Frontiers in High-Energy Physics*, edited by B. M. Kursunuglu, A. Perlmutter, and L. F. Scott (Plenum, New York, 1978), p. 159.

[16] E. A. Cornell, R. M. Weisskoff, K. R. Boyce, R. W. Flanagan, Jr., G. P. Lafyatis, and D. E. Pritchard, Phys. Rev. Lett. **63**, 1674 (1989).

[17] L. S. Brown and G. Gabrielse, Rev. Mod. Phys. **58**, 233 (1986).

[18] R. F. Wuerker, H. Shelton, and R. V. Langmuir, J. Appl. Phys. **30**, 342 (1959).

[19] F. Diedrich, E. Peik, J. M. Chen, W. Quint, and H. Walther, Phys. Rev. Lett. **59**, 2931 (1987).

[20] J. Hoffnagle, R. G. DeVoe, L. Reyna, and R. G. Brewer, Phys. Rev. Lett. **61**, 255 (1988).

[21] Th. Sauter, H. Gilhaus, I. Siemers, R. Blatt, W. Neuhauser, and P. E. Toschek, Z. Phys. D **10**, 153 (1988).

[22] S. L. Gilbert, J. J. Bollinger, and D. J. Wineland, Phys. Rev. Lett. **60**, 2022 (1988).

[23] W. Shockley, J. Appl. Phys. **9**, 635 (1938).

[24] G. Gabrielse, Phys. Rev. A **29**, 462 (1984).

[25] E. C. Beaty, Phys. Rev. A **33**, 3645 (1986).

[26] H. G. Dehmelt and F. L. Walls, Phys. Rev. Lett. **21**, 127 (1968).

[27] D. J. Wineland and H. G. Dehmelt, J. Appl. Phys. **46**, 919 (1975).

[28] D. A. Church and H. G. Dehmelt, J. Appl. Phys. **40**, 3421 (1969).

[29] W. D. White, J. H. Malmberg, and C. F. Driscoll, Phys. Rev. Lett. **49**, 1822 (1982).

[30] H. Dehmelt, W. Nagourney, and J. Sandberg, Proc. Nat. Acad. Sci. USA **83**, 5761 (1986).

[31] W. D. White and J. H. Malmberg, Bull. Am. Phys. Soc. **27**, 1031 (1982).

[32] K. S. Fine, Ph. D. thesis, Univ. Calif. San Diego, 1988.

[33] S. van der Meer, Rev. Mod. Phys. **57**, 689 (1985).

[34] N. Beverini, L. Bracci, G. Torelli, V. Lagomarsino, and G. Manuzio, Europhys. Lett. **1**, 435 (1986).

[35] N. Beverini, V. Lagomarsino, G. Manuzio, F. Scuri, G. Testera, and G. Torelli, Phys. Rev. A **38**, 107 (1988).

[36] N. Beverini, V. Lagomarsino, G. Manuzio, F. Scuri, G. Testera, and G. Torelli, Phys. Scripta **T22**, 238 (1988).

[37] F. G. Major and H. G. Dehmelt, Phys. Rev. **170**, 91 (1968).

[38] R. Blatt, P. Zoller, G. Holzmüller, and I. Siemers, Z. Phys. D **4**, 121 (1986).

[39] F. Vedel, J. André, M. Vedel, and G. Brincourt, Phys. Rev. A **27**, 2321 (1983) and references therein.

[40] R. Blümel, C. Kappler, W. Quint, and H. Walther, Phys. Rev. A **40**, 808 (1989).

[41] P. H. Dawson and N. R. Whetton, Naturwissenschaften **56**, 109 (1969).

[42] H. Schaaf, U. Schmeling, and G. Werth, Appl. Phys. **25**, 249 (1981).

[43] R. D. Knight and M. H. Prior, J. Appl. Phys. **50**, 3044 (1979).

[44] L. S. Cutler, R. P. Giffard, and M. D. McGuire, Appl. Phys. B **36**, 137 (1985).

[45] L. S. Cutler, C. A. Flory, R. P. Giffard, M. D. McGuire, Appl. Phys. B **39**, 251 (1986).

[46] A. Wolf, Phys. Scripta **T22**, 55 (1988).

[47] G. Gabrielse, X. Fei, L. A. Orozco, and R. L. Tjoelker, J. Haas, H. Kalinowsky, T. A. Trainor, and W. Kells, Phys. Rev. Lett. **63**, 1360 (1989).

[48] D. J. Wineland and H. Dehmelt, Int. J. Mass Spectrom. Ion Phys. **19**, 251 (1976).

[49] T. W. Hänsch and A. L. Schawlow, Opt. Commun. **13**, 68 (1975).

[50] D. J. Wineland and H. G. Dehmelt, Bull. Am. Phys. Soc. **20**, 637 (1975).

[51] C. P. Slichter, *Principles of Magnetic Resonance* (Springer-Verlag, Berlin, 1978), p. 217.

[52] S. P. Vyatchanin, Dokl. Akad. Nauk SSSR **234**, 1295 (1977) [Sov. Phys. Dokl. **22**, 321 (1977)].

[53] D. J. Wineland, J. Appl. Phys. **50**, 2528 (1979).

[54] E. A. Cornell, R. M. Weisskoff, K. R. Boyce, and D. E. Pritchard, Phys. Rev. A (in press).

[55] D. J. Wineland and W. M. Itano, Phys. Rev. A **20**, 1521 (1979).

[56] A. Aspect, A. Heidmann, C. Salomon, a and C. Cohen-Tannoudji, Phys. Rev. Lett. **57**, 1688 (1986).

[57] P. D. Lett, R. N. Watts, C. I. Westbrook, and W. D. Phillips, Phys. Rev. Lett. **61**, 169 (1988).

[58] A. Aspect, E. Arimondo, R. Kaiser, N. Vansteenkiste, and C. Cohen-Tannoudji, Phys. Rev. Lett. **61**, 826 (1988).

[59] Laser Cooling and Trapping of Atoms, edited by S. Chu and C. Wieman [J. Opt. Soc. Am. B **6**, No. 11 (1989)].

[60] H. Dehmelt, in *Frequency Standards and Metrology*, edited by A. De Marchi (Springer Verlag, Berlin, 1989), p. 286.

[61] J. D. Prestage, G. R. Janik, G. J. Dick, T. K. Tucker, and L. Maleki, in Proc. 43rd Annual Symposium on Frequency Control (IEEE, Piscataway, NJ, 1989), p. 135.

[62] D. J. Wineland, J. C. Bergquist, J. J. Bollinger, W. M. Itano, D. J. Heinzen, S. L. Gilbert, C. H. Manney, and C. S. Weimer, in Proc. 43rd Annual Symposium on Frequency Control (IEEE, Piscataway, NJ, 1989), p. 143.

[63] D. J. Wineland, W. M. Itano, J. C. Bergquist, and R. G. Hulet, Phys. Rev. A **36**, 2220 (1987).

[64] W. Neuhauser, M. Hohenstatt, P. Toschek, and H. Dehmelt, Phys. Rev. Lett. **41**, 233 (1978).

[65] J. Javanainen and S. Stenholm, Appl. Phys. **24**, 151 (1981).

[66] M. Lindberg, J. Phys. B **17**, 2129 (1984).

[67] J. Javanainen, M. Lindberg, and S. Stenholm, J. Opt. Soc. Am. B **1**, 111 (1984).

[68] F. Diedrich, J. C. Bergquist, W. M. Itano, and D. J. Wineland, Phys. Rev. Lett. **62**, 403 (1989).

[69] R. Casdorff and R. Blatt, Appl. Phys. B **45**, 175 (1988).

[70] S. O. Rice, Bell. Syst. Tech. J. **23**, 282 (1944); **24**, 46 (1945).

[71] W. M. Itano and D. J. Wineland, Phys. Rev. A **25**, 35 (1982).

[72] V. S. Letokhov, V. G. Minogin, and B. D. Pavlik, Zh. Eksp. Teor. Fiz. **72**, 1328 (1977) [Sov. Phys. JETP **45**, 698 (1977)].

[73] W. Neuhauser, M. Hohenstatt, P. Toschek, and H. Dehmelt, Phys. Rev. A **22**, 1137 (1980).

[74] J. C. Bergquist, F. Diedrich, W. M. Itano, and D. J. Wineland, in *Laser Spectroscopy IX*, edited by M. S. Feld, J. E. Thomas, and A. Mooradian (Academic, San Diego, 1989), p. 274.

[75] W. Nagourney, N. Yu, and H. Dehmelt, in *Frequency Standards and Metrology*, edited by A. De Marchi (Springer Verlag, Berlin, 1989), p. 312.

[76] W. Nagourney, G. Janik, and H. Dehmelt, Proc. Nat. Acad. Sci. USA **80**, 643 (1983).

[77] W. Nagourney, J. Sandberg, and H. Dehmelt, Phys. Rev. Lett. **56**, 2797 (1986).

[78] J. D. Sankey and A. A. Madej, in *Laser Spectroscopy IX*, edited by M. S. Feld, J. E. Thomas, and A. Mooradian (Academic, San Diego, 1989), p. 278.

[79] W. M. Itano, J. C. Bergquist, R. G. Hulet, and D. J. Wineland, Phys. Rev. Lett. **59**, 2732 (1987).

[80] F. Diedrich and H. Walther, Phys. Rev. Lett. **58**, 203 (1987).

[81] J. C. Bergquist, R. G. Hulet, W. M. Itano, and D. J. Wineland, Phys. Rev. Lett. **57**, 1699 (1986).

[82] W. M. Itano, J. C. Bergquist, and D. J. Wineland, Phys. Rev. A **38**, 559 (1988).

[83] Th. Sauter, W. Neuhauser, R. Blatt, and P. E. Toschek, Phys. Rev. Lett. **57**, 1696 (1986).

[84] D. J. Wineland, J. J. Bollinger, W. M. Itano, and J. D. Prestage, J. Opt. Soc. Am. B **2**, 1721 (1985).

[85] T. M. O'Neil, Phys. Fluids **23**, 2217 (1980).

[86] S. A. Prasad and T. M. O'Neil, Phys. Fluids **22**, 278 (1979).

[87] D. J. Wineland, R. E. Drullinger, and F. L. Walls, Phys. Rev. Lett. **40**, 1639 (1978).

[88] F. Plumelle, M. Desaintfuscien, M. Jardino, and P. Petit, Appl. Phys. B **41**, 183 (1986).

[89] R. C. Thompson, G. P. Barwood, and P. Gill, Appl. Phys. B **46**, 87 (1988).

[90] W. M. Itano, L. R. Brewer, D. J. Larson, and D. J. Wineland, Phys. Rev. A **38**, 5698 (1988).

[91] L. R. Brewer, J. D. Prestage, J. J. Bollinger, W. M. Itano, D. J. Larson, and D. J. Wineland, Phys. Rev. A **38**, 859 (1988).

[92] D. J. Wineland, J. J. Bollinger, and W. M. Itano, Phys. Rev. Lett. **50**, 628 (1983).

[93] R. G. Hulet, D. J. Wineland, J. C. Bergquist, and W. M. Itano, Phys. Rev. A **37**, 4544 (1988).

[94] J. J. Bollinger, J. S. Wells, D. J. Wineland, and W. M. Itano, Phys. Rev. A **31**, 2711 (1985).

[95] W. M. Itano and D. J. Wineland, Phys. Rev. A **24**, 1364 (1981).

[96] J. J. Bollinger, J. D. Prestage, W. M. Itano, and D. J. Wineland, Phys. Rev. Lett. **54**, 1000 (1985).

[97] J. D. Prestage, J. J. Bollinger, W. M. Itano, and D. J. Wineland, Phys. Rev. Lett. **54**, 2387 (1985).

[98] J. J. Bollinger and D. J. Wineland, Phys. Rev. Lett. **53**, 348 (1984).

[99] A. Rahman and J. P. Schiffer, Phys. Rev. Lett. **57**, 1133 (1986); J. P. Schiffer, Phys. Rev. Lett. **61**, 1843 (1988).

[100] D. H. E. Dubin and T. M. O'Neil, Phys. Rev. Lett. **60**, 511 (1988).

[101] J. J. Bollinger, L. R. Brewer, J. C. Bergquist, W. M. Itano, D. J. Larson, S. L. Gilbert, and D. J. Wineland, in *Intense Positron Beams*, edited by E. H. Ottewitte and W. Kells (World Scientific, Singapore, 1988), p. 63.

[102] W. M. Itano, J. C. Bergquist, and D. J. Wineland, in *Proc. Workshop on Crystalline Ion Beams*, edited by R. W. Hasse, I. Hofmann, and D. Liesen (Gesellschaft für Schwerionenforschung, Darmstadt, Federal Republic of Germany), p. 241.

[103] J. J. Bollinger, S. L. Gilbert, W. M. Itano, and D. J. Wineland, in *Frequency Standards and Metrology*, edited by A. De Marchi (Springer Verlag, Berlin, 1989), p. 319.

[104] J. J. Bollinger, D. J. Heinzen, W. M. Itano, S. L. Gilbert, and D. J. Wineland, Phys. Rev. Lett. **63**, 1031 (1989).

[105] T. M. O'Neil, Phys. Fluids **24**, 1447 (1981).

RECENT EXPERIMENTS ON TRAPPED IONS AT THE NATIONAL INSTITUTE OF STANDARDS AND TECHNOLOGY

D. J. Wineland, J. C. Bergquist, J. J. Bollinger, W. M. Itano,
F. L. Moore, J. M. Gilligan, M. G. Raizen, D. J. Heinzen,
C. S. Weimer, and C. H. Manney

Time and Frequency Division
National Institute of Standards and Technology
Boulder, Colorado 80303

INTRODUCTION

In these notes, we discuss recent experiments conducted by the ion storage group of the National Institute of Standards and Technology in Boulder, Colorado. The overall goal of this work has been the development of techniques for high resolution spectroscopy using stored ions. These techniques have also been applied to problems of practical and fundamental interest. In the following we summarize the work for the year preceding July, 1991.

(1) Be^+ Hyperfine pressure shift

In this experiment, an oscillator has been locked to the (m_I = -1/2, m_J = 1/2) $\longleftrightarrow$ (-3/2, 1/2) nuclear spin-flip, hyperfine, clock transition ($\omega_o/2\pi \simeq$ 303 MHz) in the ground state of $^9Be^+$ (Fig. 1). The details of this experiment have been described previously [1].

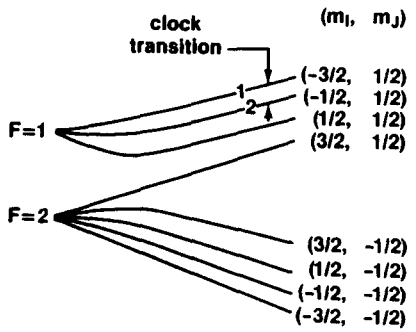

Fig. 1. Hyperfine energy levels (not drawn to scale) of the $^9Be^+$ 2s $^2S_{1/2}$ ground state as a function of magnetic field (horizontal axis). At B = 0.8194 T the 303 MHz clock transition is independent of magnetic field to first order.

A shift of the clock transition frequency, with an unexpectedly large value, was discovered when the background gas pressure was increased [1]. The background gas pressure could be increased by moving the magnet of the sputter ion pump (which evacuated the trap region) so that it overlapped fewer pumping cells and reduced the pumping speed. We checked to make sure the magnetic field at the site of the ions was not disturbed.

The composition of the gas was not known since the pressure was measured with a Bayard-

Proc. of the Enrico Fermi Summer School on "Laser manipulation of atoms and ions," ed. by E. Arimondo and W. D. Phillips, July, 1991, Varenna, Italy.

TN-182

Alpert gauge. It was difficult to install a residual gas analyzer on the system without a thorough reprocessing of the vacuum system. Therefore we opted to leak in various gases which are known to be present in high vacuum systems [2] that are similar to our $^9Be^+$ apparatus. We monitored the frequency of the oscillator that was locked to the clock transition as an increase in the background gas pressure was separately provided by the following gases: H_2, N_2, O_2, H_2O, CO, He, CH_4, and CO_2. The maximum pressure for any gas introduced into the system was around 4×10^{-7} Pa (3×10^{-9} Torr), and the base pressure of the system (as measured by a Bayard-Alpert gauge calibrated for N_2) was 1.3×10^{-8} Pa (1×10^{-10} Torr). (Below, we use pressure readings of the Bayard-Alpert gauge which was calibrated for N_2; the quoted results must be corrected for changes in sensitivity for the various gases.) The gases H_2, CO, H_2O, He, O_2 and N_2, gave no observable pressure shift. Specifically, the gases H_2, CO, and N_2 caused fractional frequency shifts of the $^9Be^+$ clock transition less than 1.5×10^{-6}/Pa ($2 \times 10^{-14}/10^{-10}$ Torr). Similarly, the gases H_2O, He, and O_2 caused fractional frequency shifts less than 3.8×10^{-7}/Pa ($5 \times 10^{-15}/10^{-10}$ Torr). The gas CH_4 gave a pressure shift of $(-1.7 \pm 0.4) \times 10^{-5}$/Pa ($(-2.2 \pm 0.5) \times 10^{-13}/10^{-10}$ Torr). When CO_2 was admitted to the system the hyperfine frequency slowly changed (over about one hour) as though CO_2 slowly reacted with some consituent inside the vacuum system and released a gas which caused a pressure shift of the clock transition.

The large difference between our data for CH_4 and the other gases we measured, and the difference between our data for CH_4 and ion hyperfine pressure shifts induced by inert gases which were measured by other groups [3,4], is not understood at this time. One possible explanation is suggested by studies [5] of radiative association of C^+ with H_2 to form CH_2^+. In the models of this process, it is assumed that the H_2 can stick to the C^+ for a long enough time to allow the C^+-H_2 complex to radiatively stabilize. This sticking is possible because the collision energy can be taken up by the internal degrees of freedom in the H_2 molecule or the H_2 - C^+ complex. The sticking time can be orders of magnitude longer than the interaction time during a simple elastic collision. If a similar sticking mechanism is active in CH_4 + Be^+ collisions, it may account for the apparent large pressure shift.

This pressure shift might affect all precision measurements of hyperfine structures of ions similarly. That is, we might expect the sticking time to depend only on the charge of the ion. In that case, it may be necessary to achieve significantly better vacuums by using cryopumping.

(2) Linear Paul Trap

The main advantage of using a single ion in a Paul quadrupole trap is that the kinetic energy of micromotion can be on the order of the secular motion energy. For a single $^{199}Hg^+$ ion cooled to the Doppler-cooling limit, the second-order Doppler shift would be [6,7] $\langle \Delta\nu_{D2}/\nu_o \rangle = -2.3 \times 10^{-18}$. In a quadrupole ion trap, two or more ions in the trap are pushed from the center of the trap by their mutual Coulomb repulsion. Therefore, the second-order Doppler shift is higher due to increased micromotion.

Consider the trap shown in Fig. 2. In this trap, the rf electric fields are transverse to the trap axis for the entire z extent of the trap. If a single string of ions is trapped along the z axis, the kinetic energy of micromotion is about equal to the kinetic energy in the secular motion. This kind of trap was first demonstrated for atomic ions by Drees and Paul [8]; lower temperatures were later obtained by Church [9]. Prestage et al. [10] have demonstrated a $^{199}Hg^+$ microwave clock with excellent short term stability ($\sigma_y(\tau) \simeq 1.6 \times 10^{-13}\, \tau^{-1/2}$) using a cloud of ions elongated in the z direction in a linear Paul trap. Dehmelt first suggested using a string of ions to suppress the second-order Doppler shift in such a trap [11]. Strings of atomic ions have been observed at Garching [12] and NIST [13].

In Fig. 3a, we show a string of $^{199}Hg^+$ ions confined in a linear trap that has rod diameters

1.60 mm and distance of the rod centers from the z axis of the trap equal to 1.55 mm. The spacing of the ions is approximately 20 μm.

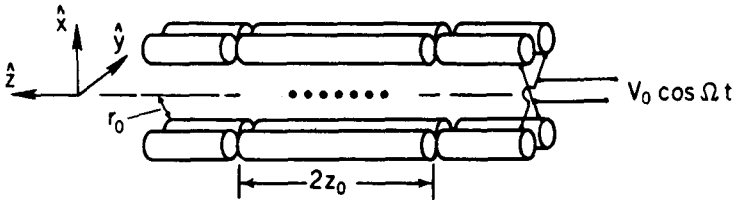

Fig. 2. Linear trap configuration. The alternating rf voltage $V_o \cos \Omega t$ is applied to diagonally opposing electrodes as shown. We assume the end portions of the electrodes are long enough that the resulting rf potential at the position of the ions is independent of z, so that the rf electric fields are parallel to the x-y plane. To trap ions along z, the center four electrodes are held at static ground potential and the two sets of four electrodes on either end are held at a static potential U_o ($U_o > 0$ to trap positive ions). The average position of the ions could be made to coincide with the rf electric field null by applying slightly different static potentials to the four central rods to correct for offsets from contact potentials or static charge on the electrode surfaces. This geometry allows laser beams to be directed along the z axis.

When the linear density of ions is increased by increasing the static voltage applied to the end sections of the rods, or when the x-y potential is weakened, zig-zag structures like those shown in Fig. 3b result. These structures are the lowest-energy configurations expected for a certain range of the ratio of z confining potential and x-y potential. They have been predicted to be the lowest energy configurations in ion storage rings [14].

Strings of ions should be useful for high resolution spectroscopy. If we use imaging techniques, each ion can be treated as an independent atomic clock where the clock transition could be detected with 100% efficiency (using Dehmelt's "electron shelving" scheme [6,15]). If we use 50 ions, a resonance frequency $\omega_o/2\pi$ = 40.5 GHz (the ground state hyperfine transition for $^{199}Hg^+$), and if we use the Ramsey method of interrogation where the free precession time is 100 s, the frequency stability of this clock "ensemble" should be $\sigma_y(\tau) = 5.5 \times 10^{-14}\tau^{-1/2}$. One or more ions whose positions are localized to less than $\lambda/2\pi$ are also interesting for experiments investigating interference, superradiance and subradiance, and cavity-QED.

(a)

(b)

Fig. 3. Images taken of crystallized structures of $^{199}Hg^+$ ions in a linear rf trap like the one of Fig. 2. In (a), 10 ions form into a string with length 220 μm. In (b), the the lowest energy configuration for 13 ions is a zig-zag structure. In (a) and (b), the trap conditions are different but the magnification is the same. (Ref. 13.)

The 40.5 GHz hyperfine resonance has been observed on a string of ions and also on a single ion using electron shelving. Currently, we are investigating the possibility of using cryogenic pumping to minimize ion loss due to $Hg^{+*} + Hg \rightarrow$ dimer formation and to minimize possible pressure shifts in the hyperfine resonance.

(3) Penning trap density limitations

We have discovered and investigated a particular limitation to the number and density of charged particles that can be stored in a Penning trap. The energy and angular momentum of a cloud of $^9Be^+$ ions were controlled with radiation pressure from two different lasers. One of the laser beams was directed through the radial edge of the ion cloud and supplied a radiation pressure torque which increased the $^9Be^+$ rotation frequency and density. We discovered that a slight misalignment of the trap symmetry axis with the magnetic field would heat the plasma when we attempted to increase the rotation frequency (or density) beyond a certain value [16]. With about 2000 $^9Be^+$ ions in the trap, we could use this heating to align the trap symmetry axis with the magnetic field to better than 0.01°. Larger ion clouds were even more sensitive to this misalignment. In fact, in this trap, all other known methods of alignment were less sensitive.

By measuring the rotation frequency where the heating occurred as a function of the trap voltage, we were able to associate this heating with the excitation of a collective mode of the plasma by the static field asymmetry produced by a misalignment of the trap electric field axis from the direction of the magnetic field [16]. The mode is called an $(\ell,m) = (2,1)$ mode. In a (2,1) mode the plasma tilts with respect to the magnetic field and precesses about the magnetic field axis. In a frame of reference rotating with the plasma, there is a particular (2,1) mode which precesses in a direction opposite to the rotation. For a particular value of the rotation frequency, this becomes a static mode (no time dependence in the lab frame) that can be excited by static asymmetries. It is this static (2,1) mode which we observed to limit the plasma density. While this is the lowest-order and therefore the strongest static mode that can be excited, other weaker heating resonances which tended to limit the plasma density to even lower values were observed. These weaker heating resonances are also due to the excitation of coherent modes by static field asymmetries. These static modes have important implications for experiments where storage of large number of charged particles is important. For example, they may provide a limit to the number of antiprotons or positrons which can be stored in a trap. The plasma modes also play an important role in the asymmetry-induced transport which occurs in a Penning trap even at low densities. An understanding of the modes may therefore improve the long term confinement of many ions in a Penning trap.

(4) Search for anomalous spin-dependent forces using $^9Be^+$ hyperfine spectroscopy

The existence of weakly interacting bosons (such as axions) has been suggested previously. Laboratory experiments might detect scalar or pseudoscalar couplings of such particles to matter in the form of new spin-dependent forces. We have used spectroscopy of $^9Be^+$ to search for anomalous potentials having a dipole-monopole or dipole-dipole character [17]. The first is expected to include terms like

$$V_{AB}^{D} = \hbar^2 D \vec{S}_A \cdot \hat{r} (1/\lambda_\phi r + 1/r^2) \exp(-r/\lambda_\phi), \qquad (1)$$

where the spin $\vec{S}_A$ (in units of $\hbar$) of particle A couples to particle B, r is the distance between particles, λ_ϕ is the range of the force, and D is a coupling constant with units of $(\text{mass})^{-1}$. A dipole-

dipole interaction would be expected to include terms like

$$V_{AB}^{T} = (\hbar^3/c)\, T \exp(-r/\lambda_\phi)[(1/\lambda_\phi r^2 + 1/r^3)\vec{S}_A \cdot \vec{S}_B$$

$$- (1/\lambda_\phi^2 r + 3/\lambda_\phi r^2 + 3/r^3)(\vec{S}_A \cdot \hat{r})(\vec{S}_B \cdot \hat{r})], \qquad (2)$$

where the spin of particle A interacts with that of particle B. T has units of (mass)$^{-2}$ and characterizes the strength of the interaction.

We have been able to place experimental limits on D and T by examining the $^9Be^+$ hyperfine "clock" transition frequency ν_0 under various conditions. Particles A are assumed to be either the ^9Be nucleus or the unpaired outer electron in $^9Be^+$. In the search for V_{AB}^{D}, particles B were taken to be the nucleons in the earth. We looked for a change in ν_0 between the cases where $\vec{B}_o$ was parallel or antiparallel to the vertical direction in the lab. In the search for V_{AB}^{T}, particles B were taken to be the electron spins in the iron pole faces of an electromagnet. We compared ν_0 when B_o was created by this electromagnet with ν_0 when B_o was created by a superconducting solenoid ($\vec{S}_B$ spins absent). From these data, upper limits on D and T for the electron and neutron have been established and compared to the results of others [17].

(5) Theory of Sisyphus cooling for a bound atom (ion)

Cooling that results from optical dipole forces has been considered for a bound atom (or trapped ion) [18]. Through optical pumping, the atom can be made to feel decelerating optical dipole forces more strongly than the accelerating optical dipole forces. This effect, which has previously been realized for free atoms, is called Sisyphus cooling [19]. A simple model for a bound atom is examined in order to reveal the basic aspects of cooling and heating when the atom is confined in the Lamb-Dicke regime. Results of semiclassical and quantum treatments show that the minimum energy achieved is near the zero-point energy and can be much lower than the Doppler cooling limit. Sisyphus cooling of trapped Mg^+ and Hg^+ have been examined theoretically.

(6) Observation of "atomic projection" noise

In spectroscopy, "technical noise," such as laser amplitude fluctuations caused by an unstable power supply, often dominates the noise. These sources of noise can be eliminated by careful engineering. Two examples of more fundamental noise sources are: (1) the detection shot noise in a laser absorption spectroscopy experiment and (2) the fluctuations in signal caused by the fluctuations in the number of atoms in an atomic beam experiment. These sources of noise can also be eliminated or significantly reduced. For example, laser shot noise can, in principle, be reduced by use of squeezed light [20].

In a stored-ion experiment, the number of ions can be held constant thereby reducing the atomic number fluctuations to zero. Also, when absorption is detected using electron shelving [6,15], the detection noise approaches zero since 100% detection efficiency is possible. Because of this immunity from some sources of noise, we have been able to observe, in a clear way, what might be called "quantum projection noise." Basically, this source of noise is caused by the statistical fluctuations in the number of atomic absorbers (ions in our case) which are observed to make the transition in an absorption spectroscopy experiment [21].

For simplicity, assume that the number N of atoms is fixed and the efficiency of detection of absorption by each atom is 100%. We also assume the resonance in question is driven using the Ramsey method in the time domain where the pulse times are much less than the free precession time

T and the lifetimes of both states involved in the transition are much greater than T. For optimum power, where the transition probability on resonance is unity, the probability of driving the absorber from one state to the other is given by[1,21]

$$p \simeq (1 + \cos(\omega - \omega_0)T)/2, \tag{3}$$

where ω_0 is the resonance frequency, and ω is the applied frequency. Upon detection, the average number of atoms that are observed to make the transition is pN and the rms fluctuations in the number of ions that are observed to make the transition is given by the dispersion of the binomial distribution

$$\Delta N = \sqrt{Np(1-p)}\ . \tag{4}$$

We call this the atomic projection noise because it arises from the fluctuations in the state the atom is projected into when a measurement is made. When no excitation occurs (p = 0), or when the atom is totally transferred into the other state (p = 1), this noise is zero. This is to be expected when the atom is in an eigenstate, since a measurement should always find the atom in that state. The noise is maximum for p = ½ which, for Ramsey excitation, is at the point of maximum slope of the resonance curve. Interestingly, we can show that, if this is the only source of noise, the sensitivity to frequency fluctuations is independent of where measurements are taken on the Ramsey curve (Eq. (3)). This is because the slope of the resonance curve, $\partial p/\partial\omega$, which gives frequency sensitivity (the signal), is proportional to ΔN as can be verified from Eqs. (3) and (4). Therefore the ratio of signal to noise is independent of ω. However, if there are any added sources of noise, it is more advantageous to measure at the points of maximum slope (the "half-power" points) for maximum frequency sensitivity.

In Fig. 4, we show the noise observed on a Ramsey resonance taken on the clock transition on approximately 20 $^9Be^+$ ions. The method for measuring the curve is described in Ref. 1. The qualitative evidence for the projection noise is the fact that the observed noise is larger on the sides of the Ramsey resonance than on the peaks and valleys of the curve.

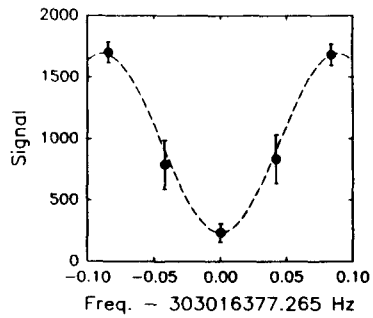

Fig. 4. A Ramsey resonance taken on the "clock" resonance of $^9Be^+$ ions in a Penning trap (refer to Fig. 1). The number of ions (approximately 20) was held fixed. At each rf frequency (horizontal scale), 30 measurements were made. The vertical scale is the number of detected photoelectron counts from the ions' fluorescence observed in a 1 second integration time [1]. The dots indicate the means of the measurements. The error bars indicate the standard deviations. We determined, by independent measurements, that the frequency fluctuations of the oscillator driving the clock transition caused a negligible contribution to the observed signal fluctuations. The fact that the standard deviations are higher on the sides of the resonance than at the peaks and valleys is a result of "atomic projection noise."

(7) Precision measurement of the g_J factor of Mg^+

Penning traps are well suited to precision measurements of g-factors of ions. The required magnetic field is already present. When the magnetic field is generated by a superconducting solenoid designed to have high homogeneity and stability, there is a potential for very high accuracy. Systematic errors can be well controlled because the ions occupy a small volume, over which the field can be very uniform. Further, the ion sample can be moved by adjusting the trap's electric potentials in order to map out the magnetic field variations.

Previously, we measured the g_J factor of the $^9Be^+$ ion [22]. This was done in a Penning trap that used a nonsuperconducting electromagnet. The frequencies of a magnetic-field-dependent hyperfine transition were measured at the same time as the ion cyclotron resonance and other motional resonances of the ions. From these measurements, and using the ratio of the ion mass to the electron mass, which was known from other experiments, we obtained $g_J(^9Be^+)$ to an accuracy of about 1.6 parts in 10^7. This measurement could be improved by the use of a superconducting magnet.

This year, we measured the ratio of the g_J factor of the $^{26}Mg^+$ ion to that of $^9Be^+$. The two types of ions were trapped and cooled simultaneously in nearly the same volume. (The higher-mass $^{26}Mg^+$ ions form a ring around the $^9Be^+$ ions [23].) A magnetic-field-dependent hyperfine transition in $^9Be^+$ and the electron spin-flip resonance in $^{26}Mg^+$ were measured, one after the other, by microwave-optical double resonance. From these measurements, we obtained the ratio $g_J(^{26}Mg^+)/g_J(^9Be^+)$ to an accuracy of 1.3 parts in 10^8. Combined with our previous measurement of $g_J(^9Be^+)$, we obtain $g_J(^{26}Mg^+)$ to an accuracy of about 1.6 parts in 10^7. This agrees with a Hartree-Fock calculation [24] to about 3 parts in 10^6. The deviation of $g_J(^{26}Mg^+)$ from the g factor of the free electron, which is the physically interesting quantity, is about 3 parts in 10^5. Our measurements already determine this deviation to about 0.5 %. The g_J factors of the neutral alkali atoms (Li, Na,...) are well known. Comparisons with the g_J factors of the isoelectronic positive ions (Be^+, Mg^+,...) may reveal systematic trends and lead to a better understanding of calculational methods.

(8) Subharmonic excitation of a single electron

A single electron in a magnetic field can have its cyclotron motion excited by an oscillating electric field. Similarly, a single electron in a Penning trap can have its cyclotron, magnetron, or axial motion excited by an oscillating electric field. Usually, the excitation of these motions is made at a frequency which coincides with the resonance frequency ω_0 of one of the motions of the electron, but excitation at a multiple of the motional frequency is also possible. This excitation of a single electron (whose orbit can be well controlled) is interesting because it is one of the simplest systems in which to study parametric and subharmonic excitation and because it should be possible to study these excitations in both the quantum mechanical and classical regimes in the same system.

We have recently studied excitation of the cyclotron and magnetron motions of a single trapped electron [27] by an electric field which we assume to be of the form

$$\vec{E} = \hat{y}\sum_{n=0}^{\infty} C_n x^n \cos\omega t \ . \qquad (5)$$

Because the field is spatially nonuniform (the x^n factors), excitation at some harmonic of the fundamental motional frequency is possible; that is, where $\omega \simeq n\omega_0$. This is called subharmonic excitation. One example of this process is subharmonic excitation of the magnetron motion of an electron. The magnetron orbit is first excited to a certain radius by a potential, oscillating at a frequency near ω_0, which is applied to one electrode of a split ring electrode of the Penning trap. Since the damping of the magnetron motion is extremely small, the orbit size is nearly constant after

this first drive is removed. The orbit size is observed as an anharmonic frequency shift of the axial resonance frequency [28]. Application of an electric field of frequency $\omega \simeq n\omega_0$ causes an excitation near ω_0 through the C_{n-1} and C_{n+1} terms in Eq. (5). In our experiment, this excitation was difficult to observe on the cyclotron motion because the stability of the magnet was poor and because the damping time of the cyclotron motion allowed initial excitation only due to thermal noise. Nevertheless, it was possible to observe excitation for $n = 3$ on the cyclotron motion ($\omega_0 \simeq 2.82$ GHz) and for $n = 9$ on the magnetron motion ($\omega_0 \simeq 47$ kHz).

One feature of this kind of system may be of practical importance. For example, if the subharmonic excitation can be detected by observing the motion of the electron at its fundamental frequency, the resulting device acts as a frequency divider [25,26]. That is, we inject a certain frequency into the device and measure a submultiple of the input frequency. For the electron, this parametric down-conversion process can, in principle, be extended to very high orders; that is, it should be possible to inject a laser frequency and read out a microwave frequency (the cyclotron frequency).

(9) Observation of time varying radiation pressure forces

This work arose out of attempts to observe the effects of optical dipole forces on trapped ions. One manifestation of dipole forces would be Sisyphus cooling (Section (5)). It should also be possible to observe the dipole force on ions without the effects of optical pumping (required for Sisyphus cooling). One way the dipole force could be observed is to modulate it at a frequency near a motional resonance frequency of the ions and observe the excitation as a change in fluorescence [22], or a change in the orbit size observed on an imaging device. Although not immediately apparent, this excitation has many similarities with the nonlinear excitation of a single electron (Section (8)).

One configuration for observing time-varying optical dipole forces is the following: Suppose we have a single ion localized near the center of the trap. We focus a Gaussian laser beam so that its waist coincides with the center of the trap along the direction of the beam, but we position the beam transversely so that the center of the trap coincides with the point of half intensity on the side of the beam. Specifically, assume the orgin of coordinates is at the trap center and the z axis is the trap symmetry axis. Assume the beam is incident along the y direction, and its center is in the $z = 0$ plane, but is located at a position $x = (\ln 2/2)^{1/2} w_0$, where w_0 is the Gaussian beam waist. The laser frequency ω is assumed to be detuned by an amount δ from a particular resonance transition frequency ω_0 of the ion ($\delta = \omega - \omega_0$). For $\delta > 0$ the dipole force [29] is in the minus-x direction; for $\delta < 0$, it is in the plus-x direction. If we now modulate the intensity of the laser we modulate the force in the x direction and can observe the corresponding excitation of the ion. A similar excitation occurs when we use two overlapping laser beams whose incident directions (taken to be along $\vec{k}_1$ and $\vec{k}_2$) are, in general, different. Assume the beams are plane waves. If the frequencies of the beams are the same, the intensity as a function of position goes as $\cos[(\vec{k}_1 - \vec{k}_2)\cdot\vec{r}]$. If we choose $\vec{k}_1 - \vec{k}_2$ along $\vec{x}$, then the intensity is spatially modulated in the x direction. If we now let the frequencies of the lasers ω_1 and ω_2 be different, then the dipole force in the x direction is modulated in time at the frequency $\omega_1 - \omega_2$. When $\omega_1 - \omega_2$ is adjusted near the motional resonance frequency of the ion, the orbit size will increase. This case is closely analogous to the excitation of a single electron by two laser beams [26].

For a traveling wave laser beam, the ion also feels the force along the direction of the beam due to the spontaneous scattering force. If the intensity of the laser is modulated, the spontaneous force is modulated and motional excitation will occur.

In order to see the dipole forces clearly, the effects of the spontaneous force (laser cooling and heating) must be suppressed. This requires that the laser intensity and detuning be sufficiently

large. In our preliminary experiments, our laser intensity was small enough that the spontaneous forces dominated. We were able to observe the axial and magnetron excitation of a small number of $^9Be^+$ ions in a Penning trap due to the modulated spontaneous force. A steady state excitation was observed because the spontanous force was balanced by laser cooling.

(10) Hg^+ optical spectroscopy

The basic idea for this experiment has been discussed previously [6]. The goal of the experiment is to lock a laser local oscillator to the 282 nm quadrupole transition in Hg^+. To obtain the best performance, it will be necessary to observe the linewidth of the quadrupole transition with a resolution near the natural linewidth of 2 Hz. The main problem in our experiment, as well as all other current optical frequency standard experiments, is to have the laser linewidth be narrower than the inverse of the time it takes to lock the laser to the resonance line.

By using a single, laser-cooled $^{199}Hg^+$ ion as an absolute frequency spectrum analyzer, we have measured a linewidth below 40 Hz for a ring dye laser (oscillating at $\sim 5.3 \times 10^{14}$ Hz) that was stabilized to an ultra-quiet reference cavity of high finesse [31]. This is the best absolute stability that has been demonstrated for an optical laser (as well as the highest atomic or molecular Q reported to date). If we try to improve the laser performance by using the spectrum of the single ion, we are limited by the low signal-to-noise ratio and by the lifetime of the ion in the trap.

To more easily study the performance of the cavity-stabilized laser, a second cavity was constructed on an independent optical table to which the frequency of a laser could be locked. A measurement of the noise fluctuations in the electronic error signals indicated that the laser frequency could be stabilized to each cavity to less than 30 mHz. In other words, the frequency of the stabilized laser tracked the resonance frequency of the reference cavity to within 30 mHz. Some authors claim this number to be their laser linewidth, but this is not the relevant linewidth for metrology. The dominating contribution to the laser linewidth comes from the length instability of the reference cavities.

The study was carried out by heterodyning the light from the two independently stabilized laser beams and analyzing the fluctuations in the power spectrum of the beat frequency. We have attempted to isolate the cavities thermally, barometrically, and mechanically. We begin with a cavity constructed from a cylindrical spacer made from an ultra-low expansion

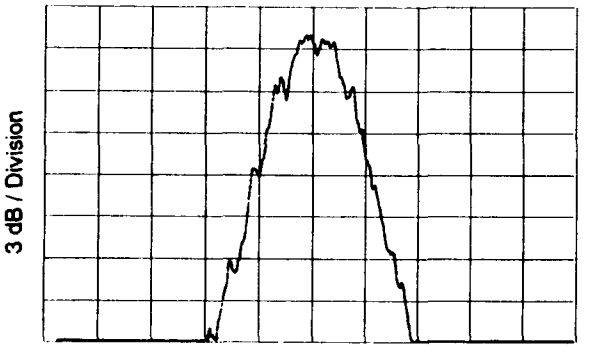

Fig. 5. Spectrum of the beat frequency between the two independent cavity-stabilized lasers discussed in the text. A linear, relative cavity drift is removed by mixing the beat note with the frequency from a synthesizer which is swept in time. The resolution bandwidth is 30 Hz. Total integration time for this data is 70 s. The 14.6 Hz sidebands are due to a floor vibration (indepedently detected with a seismometer). The apparent bandwidth is about 30 Hz; the bandwidth of the most stable laser of the two is at least $\sqrt{2}$ narrower.

material. The cavity is suspended by two thin wires in an aluminum vacuum chamber that is evacuated to about 10^{-6} Pa. ($\simeq 10^{-8}$ Torr). The walls of the vacuum vessel are temperature-regulated to better than 10 mK. The vacuum vessel is supported by, but thermally isolated from, a stiff surface plate. We have attempted several passive schemes to isolate the surface plates from seismic noise. The best isolation was achieved by supporting the surface plate from the ceiling with latex tubing. The vertical and horizontal resonant frequencies for the latex-support system were 0.33 Hz which is lower by more than a factor of 10 a brick, rubber pad, and sandbox support. The linewidth of the heterodyne signal between the laser radiation stabilized to the cavity supported by the latex tubing and the cavity supported on the sandbox table was approximately 30 Hz or less (Fig. 5). Presumably the width of the heterodyne signal is dominated by the stability of the cavity on the sandbox table. Currently, we are working to verify this and working to build better cavities (higher finesse, increased stiffness and lower sensitivity to temperature and aging).

ACKNOWLEDGEMENTS

We gratefully acknowledge the support of the U.S. Office of Naval Research and the U.S. Air Force Office of Scientific Research. We thank A. DeMarchi, R. Drullinger, H. Robinson and M. Young for helpful comments on the manuscript.

REFERENCES

1. J. J. Bollinger, D. J. Heinzen, W. M. Itano, S. L. Gilbert, and D. J. Wineland, Phys. Rev. Lett. 63, 1031 (1989); J. J. Bollinger, D. J. Heinzen, W. M. Itano, S. L. Gilbert, and D. J. Wineland, IEEE Trans. Instrum. and Meas., 40, 126 (1990); D. J. Wineland, J. C. Bergquist, J. J. Bollinger, W. M. Itano, D. J. Heinzen, S. L. Gilbert, C. H. Manney, and M. G. Raizen, IEEE Trans. on Ultrasonics, Ferroelectrics, and Frequency Control 37, 515 (1990).
2. The Physical Basis of Ultrahigh Vacuum, P. Redhead, J. P. Hobson, and E. V. Kornelsen (Chapman and Hall, London, 1968).
3. J. Vetter, M. Stuke, and E. W. Weber, Z. Phys. A273, 129 (1975).
4. L. S. Cutler, R. P. Giffard, and M. D. McGuire, Proc. 37th Ann. Symp. Freq. Control, 1983 (copies available from IEEE, 445 Hoes Lane, Piscataway, NJ 08854), p. 32.
5. E. Herbst, Astrophys. J. 252, 810 (1982), and references therein.
6. J. C. Bergquist, W. M. Itano, and D. J. Wineland, Phys. Rev. A36, 428 (1987).
7. D. J. Wineland, W. M. Itano, J. C. Bergquist, J. J. Bollinger, F. Diedrich, and S. L. Gilbert, in Frequency Standards and Metrology, Proc. 4th Symposium, ed. by A. DeMarchi, Ancona, Italy (Springer-Verlag, Berlin, Heidelberg, 1989) p. 71.
8. J. Drees and W. Paul, Z. Physik 180, 340 (1964).
9. D. A. Church, J. Appl. Phys. 40, 3127 (1969).
10. J. Prestage, G. J. Dick and L. Maleki, J. Applied Physics, 66, 1013 (1989); J. D. Prestage, G. J. Dick, and L. Maleki, IEEE Trans. Instrum. and Meas. 40, 132 (1991).
11. H. G. Dehmelt, in Frequency Standards and Metrology, Proc. 4th Symposium, ed. by A. DeMarchi, Ancona, Italy (Springer-Verlag, Berlin, Heidelberg) p. 286.
12. H. Walther in Light Induced Kinetic Effects on Atoms, Ions and Molecules, ed. by L. Moi, S. Gozzini, C. Gabbanini, E. Arimondo, and F. Strumia, (ETS Editrice, Pisa, 1991), p. 261;

G. Birkl, S. Kassner, W. Quint, H. Walther, private communication.
13. M. G. Raizen, J. C. Bergquist, J. M. Gilligan, W. M. Itano, and D. J. Wineland, J. Modern Optics, special issue on the Physics of Trapped Ions, ed. by R. Blatt, P. Gill, and R. C. Thompson, to be published.
14. See for example: R. W. Hasse and J. P. Schiffer, Proc. Workshop on Crystalline Ion Beams, Wertheim, W. Germany, ed. by R. W. Hasse, I. Hofmann, D. Liese (GSI report GSI-89-10, ISSN 0170-4546), p. 33; D. Habs, ibid, p. 43; R. W. Hasse and J. P. Schiffer, Ann. Phys. 203, 419 (1990).
15. W. Nagourney, J. Sandberg, and H. Dehmelt, Phys. Rev. Lett. 56, 2797 (1986).
16. D. J. Heinzen, J. J. Bollinger, F. L. Moore, W. M. Itano, and D. J. Wineland, Phys. Rev. Lett. 66, 2080 (1991).
17. D. J. Wineland, J. J. Bollinger, D. J. Heinzen, W. M. Itano, and M. G. Raizen, Phys. Rev. Lett. 67, 1735 (1991).
18. D. J. Wineland, J. Dalibard, C. Cohen-Tannoudji, J. Opt. Soc. Am. B9, 32 (1992).
19. C. Cohen-Tannoudji and W. D. Phillips, Physics Today, vol. 43, no. 10, 1990, p. 33.
20. B. Yurke and E. A. Whittaker, Optics Lett. 12, 236 (1987); A. Heidmann, R. J. Horowicz, S. Reynaud, E. Giacobino, C. Fabre, and G. Camy, Phys. Rev. Lett. 59, 2555 (1987).
21. D. J. Wineland, W. M. Itano, J. C. Bergquist, and F. L. Walls, Proc. 35th Ann. Symp. Freq. Control, Philadelphia, PA, May 1981, p. 602-611. (Copies available from: Annual Frequency Control Symposium, c/o Electronic Industries Assoc., 2001 Eye St., Washington, D. C., 20006.)
22. D.J. Wineland, J.J. Bollinger, and W.M. Itano, Phys. Rev. Lett. 50, 628 (1983).
23. D. J. Larson, J. C. Bergquist, J. J. Bollinger, W. M. Itano, and D. J. Wineland, Phys. Rev. Lett. 57, 70 (1986).
24. L. Veseth, Univ. of Oslo, unpublished calculations.
25. D. J. Wineland, J. Appl. Phys. 50, 2528 (1979).
26. Y. J. Ding and A. E. Kaplan J. Opt. Soc. Am. B6, 1299, (1989) and references therein.
27. C. Weimer, et al., in preparation.
28. F. L. Moore, D. L. Farnham, P. B. Schwinberg, and R. S. Van Dyck Jr., Nuclear Instruments and Methods in Physics Research B43, 425 (1989).
29. see for example: J. Dalibard and C. Cohen-Tannoudji, J. Opt. Soc. Am. B2, 1707 (1985).
30. D. J. Heinzen and D. J. Wineland, Phys. Rev. A42, 2977 (1990).
31. J. C. Bergquist, F. Diedrich, W. M. Itano, and D. J. Wineland, in Laser Spectroscopy IX, ed. by M. S. Feld, J. E. Thomas, and A. Mooradian (Academic, San Diego, 1989), p. 274; J. C. Bergquist, W. M. Itano, F. Elsner, M. G. Raizen, and D. J. Wineland, in Light Induced Kinetic Effects on Atoms, Ions and Molecules, ed. by L. Moi, S. Gozzini, C. Gabbanini, E. Arimondo, and F. Strumia, (ETS Editrice, Pisa, 1991), p. 291.

NIST Technical Publications

Periodical

Journal of Research of the National Institute of Standards and Technology—Reports NIST research and development in those disciplines of the physical and engineering sciences in which the Institute is active. These include physics, chemistry, engineering, mathematics, and computer sciences. Papers cover a broad range of subjects, with major emphasis on measurement methodology and the basic technology underlying standardization. Also included from time to time are survey articles on topics closely related to the Institute's technical and scientific programs. Issued six times a year.

Nonperiodicals

Monographs—Major contributions to the technical literature on various subjects related to the Institute's scientific and technical activities.

Handbooks—Recommended codes of engineering and industrial practice (including safety codes) developed in cooperation with interested industries, professional organizations, and regulatory bodies.

Special Publications—Include proceedings of conferences sponsored by NIST, NIST annual reports, and other special publications appropriate to this grouping such as wall charts, pocket cards, and bibliographies.

Applied Mathematics Series—Mathematical tables, manuals, and studies of special interest to physicists, engineers, chemists, biologists, mathematicians, computer programmers, and others engaged in scientific and technical work.

National Standard Reference Data Series—Provides quantitative data on the physical and chemical properties of materials, compiled from the world's literature and critically evaluated. Developed under a worldwide program coordinated by NIST under the authority of the National Standard Data Act (Public Law 90-396). NOTE: The Journal of Physical and Chemical Reference Data (JPCRD) is published quarterly for NIST by the American Chemical Society (ACS) and the American Institute of Physics (AIP). Subscriptions, reprints, and supplements are available from ACS, 1155 Sixteenth St., NW, Washington, DC 20056.

Building Science Series—Disseminates technical information developed at the Institute on building materials, components, systems, and whole structures. The series presents research results, test methods, and performance criteria related to the structural and environmental functions and the durability and safety characteristics of building elements and systems.

Technical Notes—Studies or reports which are complete in themselves but restrictive in their treatment of a subject. Analogous to monographs but not so comprehensive in scope or definitive in treatment of the subject area. Often serve as a vehicle for final reports of work performed at NIST under the sponsorship of other government agencies.

Voluntary Product Standards—Developed under procedures published by the Department of Commerce in Part 10, Title 15, of the Code of Federal Regulations. The standards establish nationally recognized requirements for products, and provide all concerned interests with a basis for common understanding of the characteristics of the products. NIST administers this program as a supplement to the activities of the private sector standardizing organizations.

Consumer Information Series—Practical information, based on NIST research and experience, covering areas of interest to the consumer. Easily understandable language and illustrations provide useful background knowledge for shopping in today's technological marketplace.
Order the **above** *NIST publications from: Superintendent of Documents, Government Printing Office, Washington, DC 20402.*
Order the **following** *NIST publications—FIPS and NISTIRs—from the National Technical Information Service, Springfield, VA 22161.*

Federal Information Processing Standards Publications (FIPS PUB)—Publications in this series collectively constitute the Federal Information Processing Standards Register. The Register serves as the official source of information in the Federal Government regarding standards issued by NIST pursuant to the Federal Property and Administrative Services Act of 1949 as amended, Public Law 89-306 (79 Stat. 1127), and as implemented by Executive Order 11717 (38 FR 12315, dated May 11, 1973) and Part 6 of Title 15 CFR (Code of Federal Regulations).

NIST Interagency Reports (NISTIR)—A special series of interim or final reports on work performed by NIST for outside sponsors (both government and non-government). In general, initial distribution is handled by the sponsor; public distribution is by the National Technical Information Service, Springfield, VA 22161, in paper copy or microfiche form.